

THE JOURNAL OF PHYSICAL CHEMISTRY

Registered in U. S. Patent Office © Copyright, 1966, by the American Chemical Society

VOLUME 70, NUMBER 7 JULY 15, 1966

Dissociation of Acetic Acid- d_4 in Deuterium Oxide from 5 to 50° and Related Isotope Effects

by Maya Paabo, Roger G. Bates, and R. A. Robinson

National Bureau of Standards, Washington, D. C. (Received February 23, 1966)

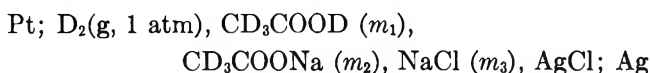
The dissociation constant of acetic acid- d_4 (CD_3COOD) in deuterium oxide (D_2O) has been determined by the emf method at ten temperatures from 5 to 50°. From the variation of the dissociation constant with temperature, the changes of enthalpy, entropy, and heat capacity have been derived. The four dissociation processes, namely those for ordinary acetic acid in ordinary water, for deuterioacetic acid in ordinary water, and for these two acids in deuterium oxide, are compared.

Introduction

The dissociation constant of protoacetic acid (CH_3COOH) in ordinary water has been determined using both the emf¹ and conductance² methods. In addition, the dissociation of protoacetic acid (CH_3COOD) in deuterium oxide³ and the dissociation of deuterioacetic acid (CD_3COOH) in ordinary water⁴ have been studied recently. The fourth dissociation process in this related series, namely that of deuterioacetic acid (CD_3COOD) in deuterium oxide, is the subject of the present study.

Procedures and Results

The cell used can be represented



The emf was measured at 5° intervals from 5 to 50°. The operation of the cell and the preparation of the materials, electrodes, and solutions followed the general procedures already described.³⁻⁶

The deuterium gas was found by mass spectroscopic examination to have an isotopic purity of better than 99.5%. The deuterioacetic acid (acetic acid- d_4) was obtained from two different commercial sources. The first lot was found to contain 0.88 atom % of H; gas chromatographic analysis showed it to consist only of acetic acid, acetic anhydride, and a trace of water. It was used without further purification. The other sample of material was purified by fractional distillation. Gas chromatographic examination of the fraction used revealed no impurities.

(1) H. S. Harned and R. W. Ehlers, *J. Am. Chem. Soc.*, **54**, 1350 (1932); **55**, 652 (1933).

(2) D. A. MacInnes and T. Shedlovsky, *ibid.*, **54**, 1429 (1932).

(3) R. Gary, R. G. Bates, and R. A. Robinson, *J. Phys. Chem.*, **69**, 2750 (1965).

(4) M. Paabo, R. G. Bates, and R. A. Robinson, *ibid.*, **70**, 540 (1966).

(5) R. Gary, R. G. Bates, and R. A. Robinson, *ibid.*, **68**, 1186 (1964).

(6) R. Gary, R. G. Bates, and R. A. Robinson, *ibid.*, **68**, 3806 (1964).

Table I: Emf of the Cell Pt; D₂ (g, 1 atm), CD₃COOD (*m*₁), CD₃COONa (*m*₂), NaCl (*m*₃), AgCl; Ag (in volts)

$\frac{m_1}{m_2} = \frac{m_1}{m_2}$	5°	10°	15°	20°	25°	30°	35°	40°	45°	50°
0.005261	0.64707	0.65103	0.65488	0.65881	0.66261	0.66636	0.67021	0.67401	0.67775	0.68142
0.007598	0.63805	0.64189	0.64564	0.64943	0.65305	0.65672	0.66048	0.66416
0.01010	0.63128	0.63504	0.63868	0.64226	0.64585	0.64936
0.01326	0.62485	0.62843	0.63195	0.63543	0.63889	0.64236	0.64578	0.64910	0.65245	0.65570
0.01680	0.61925	0.62269	0.62607	0.62947	0.63277	0.63606	0.63941	0.64264	0.64585	0.64904
0.02250	0.61234	0.61562	0.61890	0.62211	0.62534	0.62848	0.63166	0.63478	0.63786	0.64094
0.02637	...	0.61179	0.61508	0.61825	0.62134	0.62443	0.62744	0.63061	0.63366	0.63666
0.02957	0.61525	0.61837
0.02989	0.60550	0.60875	0.61188	0.61499	0.61806	0.62114	0.62419	0.62716	0.63015	0.63306
0.03273	0.60336	0.60656	0.60969	0.61273	0.61579	0.61885	0.62187	0.62479	0.62773	0.63060
0.03479	0.60204	0.60517	0.60824	0.61131	0.61429	0.61723	0.62025	0.62314	0.62602	0.62889
0.03873	0.59944	0.60248	0.60548	0.60846	0.61144	0.61434	0.61727	0.62015	0.62298	0.62581
0.04330	0.59673	0.59978	0.60276	0.60572	0.60860	0.61151	0.61440	0.61720	0.62003	0.62278
0.04535	0.59571	0.59870	0.60162	0.60442	0.60742	0.61027	0.61329
0.05008	0.59337	0.59632	0.59926	0.60214	0.60494	0.60779	0.61063	0.61335	0.61609	0.61878
0.05268	0.59216	0.59513	0.59806	0.60080	0.60368	0.60644	0.60925	0.61198	0.61468	0.61735

The measured values of the emf, corrected to 1 atm of deuterium gas, are given in Table I.

Calculations

The emf of the cell yields values of the acidity function $-\log(a_{D^+}\gamma_{Cl^-})$, with the aid of the equation

$$-\log(a_{D^+}\gamma_{Cl^-}) = (E - E^\circ)/k + \log m_3 \quad (1)$$

where *m* is molality, *E*^o is the standard emf of the cell,⁵ and *k* is written for $(RT \ln 10)/F$. Combination of this acidity function with the equation for the dissociation constant (*K*) of deuterioacetic acid, namely

$$K = a_{D^+} \frac{m_2 + m_{D^+} \gamma_{Ac^-}}{m_1 - m_{D^+} \gamma_{DAc}} \quad (2)$$

gives

$$pK' \equiv pK - \log \frac{\gamma_{Cl^-} \gamma_{DAc}}{\gamma_{Ac^-}} = \frac{(E - E^\circ)}{k} + \log m_3 + \log \frac{m_1 - m_{D^+}}{m_2 + m_{D^+}} \quad (3)$$

In all of the 16 cells measured, *m*₁ = *m*₂ = *m*₃, so that the last term of eq 3 becomes zero if *m*_{D⁺} makes a negligible contribution. Adoption of this simplification in procedure would result in values of *pK'* higher by only about 0.0007 at each temperature. It was nevertheless deemed worthwhile to make allowance for the small contribution of the *m*_{D⁺} term. For this purpose, a sufficient approximation to *m*_{D⁺} was obtained by the equation

$$-\log m_{D^+} = (E - E^\circ)/k + \log m_3 + 2 \log \gamma_{DCl}$$

where γ_{DCl} was taken as the activity coefficient of

deuterium chloride⁵ in its own solution at the same total ionic strength as that of the deuterioacetate buffer solution.

As for similar systems studied previously, the term $\log(\gamma_{Cl^-}\gamma_{DAc}/\gamma_{Ac^-})$ proved to be small, and almost horizontal straight-line plots of *pK'* vs. ionic strength were obtained. Extrapolation to zero ionic strength

Table II: Dissociation Constants of Acetic Acid

Temp, °C	pK in D ₂ O			$\Delta_1 pK^b$	pK CD ₃ COOH in H ₂ O	$\Delta_2 pK^c$
	CD ₃ COOD Obsd	CD ₃ COOD Calcd ^a	CH ₃ COOD			
0	4.795	...
5	5.360	5.360	5.347	0.013	4.784	0.576
10	5.348	5.348	5.334	0.014	4.778	0.570
15	5.338	5.338	5.324	0.014	4.774	0.564
20	5.331	5.330	5.317	0.013	4.772	0.558
25	5.325	5.326	5.312	0.014	4.771	0.553
30	5.323	5.324	5.310	0.014	4.773	0.551
35	5.323	5.324	5.310	0.014	4.777	0.547
40	5.326	5.326	5.313	0.013	4.783	0.543
45	5.330	5.330	5.317	0.013	4.790	0.540
50	5.336	5.337	5.324	0.013	4.799	0.538

^a Calculated from the equation $pK = 1278.92/T - 3.0490 + 0.013702T$. ^b $\Delta_1 pK = pK(\text{CD}_3\text{COOD in D}_2\text{O}) - pK(\text{CH}_3\text{COOD in D}_2\text{O})$. ^c $\Delta_2 pK = pK(\text{CD}_3\text{COOD in D}_2\text{O}) - pK(\text{CD}_3\text{COOH in H}_2\text{O})$.

was made by the method of least squares. Values of the intercepts (*pK*) obtained in this way are given in Table II. The standard deviations (σ_i) of the intercepts were less than 0.001 at each temperature.

Table III: Thermodynamic Quantities for the Dissociation of Protoacetic Acid and Deuterioacetic Acid in Water and in Deuterium Oxide^a

	CH ₃ COOH in H ₂ O	CD ₃ COOH in H ₂ O	CH ₃ COOD in D ₂ O	CD ₃ COOD in D ₂ O	Δ_1^b	Δ_2^c
ΔH° at 0°	+781	+735	+1192	+1174	-46	-18
25°	-98	-69	+275	+279	+29	-4
50°	-1047	-945	-730	-695	+102	+35
ΔS° at 0°	-18.8	-19.2	-20.2	-20.3	-0.4	-0.1
25°	-22.1	-22.1	-23.4	-23.4	0	0
50°	-25.1	-24.9	-26.6	-26.6	+0.2	0
ΔC_p° at 25°	-37	-34	-39	-38	+3	+1
t_{max} (°C)	22.4	22.9	32.0	32.4
$-\text{Log } K_{max}$	4.756	4.771	5.310	5.323

^a ΔH° in cal mole⁻¹; ΔS° and ΔC_p° in cal deg⁻¹ mole⁻¹. ^b Quantities in this column are for the exchange reaction: CD₃COOH + CH₃COO⁻ = CH₃COOH + CD₃COO⁻ in H₂O. ^c Quantities in this column are for the exchange reaction: CD₃COOD + CH₃COO⁻ = CH₃COOD + CD₃COO⁻ in D₂O.

Discussion

The values of pK obtained experimentally were fitted, by the method of least squares, to the equation⁷

$$pK = A_1/T - A_2 + A_3T \quad (4)$$

(0°C = 273.15°K) giving $A_1 = 1278.92$, $A_2 = 3.0490$, and $A_3 = 0.013702$. The pK values calculated from eq 4 are given in the third column of Table II. For comparison, pK values for protoacetic acid (CH₃COOD) in deuterium oxide³ are given in the fourth column.

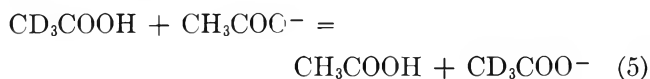
The fifth column of Table II gives the difference between the pK values of the two acids in deuterium oxide at each temperature. The difference is, within experimental error, independent of temperature between 5 and 50°. As we noted in an earlier paper,⁴ the difference in the pK values of protoacetic acid and deuterioacetic acid in ordinary water seems to diminish at 45 and 50°. As the pK values in ordinary water were determined by the same method, but in different laboratories, the slight variation in ΔpK may well be due to minor differences in technique. On the other hand, the comparison in Table II of the two forms of acetic acid in deuterium oxide is based on measurements made in the same laboratory. For this reason, we believe that the pK values differ by a constant amount over the temperature range 5 to 50°.

This constant difference is not displayed by the pK values of deuterioacetic acid in ordinary water and in deuterium oxide, as shown in the last column of Table II. The decrease from 0.576 at 5° to 0.538 at 50° is real and cannot be ascribed to experimental errors. It parallels very closely the decrease from 0.577 at 5° to 0.537 at 50° found for protoacetic acid in these two solvents.³

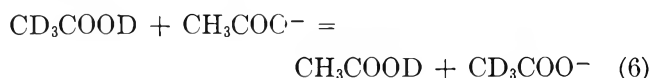
Equation 4, together with the numerical values of

A_1 , A_2 , and A_3 , permits a calculation of the enthalpy, entropy, and heat capacity changes on the dissociation of deuterioacetic acid (CD₃COOD) in deuterium oxide to be made. We can also calculate the temperature at which the dissociation constant has its maximum value and the pK value at this temperature. Data for the four related dissociation processes are compared in Table III; 1 cal is defined as 4.1840 joules.

The pK values of protoacetic acid and deuterioacetic acid are very similar in ordinary water, as they are in deuterium oxide. This similarity extends to some of the other thermodynamic properties. Thus there is little if any difference between the entropy changes on the dissociation of protoacetic acid (CH₃COOH) and deuterioacetic acid (CD₃COOH) in water; hence the entropy change for the exchange reaction



is effectively zero. This is also true for the exchange reaction



in deuterium oxide.

The enthalpy changes are, however, more considerable. For exchange reaction 5 in water, ΔH° increases from -46 cal mole⁻¹ at 0° to +102 cal mole⁻¹ at 50°, whereas for exchange reaction 6 the increase is only from -18 to +35 cal mole⁻¹ over this temperature interval. Correspondingly, the heat capacity change for reaction 5 is larger than that for reaction 6.

(7) H. S. Harned and R. A. Robinson, *Trans. Faraday Soc.*, **36**, 973 (1940).

In all of the work summarized in Tables II and III, concentrations were expressed on the molality (m) scale (moles per kilogram of solvent), and hence all values of K are based on the molal scale as well. This procedure has an arbitrary feature, in that a kilogram of ordinary water contains 55.51 moles of solvent, whereas a kilogram of deuterium oxide contains only 49.93 moles. A better comparison is obtained if dissociation constants expressed on the mole fraction (N) scale are used. The conversion is effected by means of the equation

$$pK_N = pK_m - \log(0.001W_s) \quad (7)$$

where W_s denotes the molecular weight of the solvent. Thus, the pK_N value is higher by 1.7444 than the pK_m when ordinary water is the solvent, while in deuterium oxide it is 1.6983 higher. Table IV summarizes the four sets of pK values on the mole fraction scale. It is evident that ΔpK ($\equiv pK$ in D_2O - pK in H_2O) is lower than it is when the molality scale is used, but it is still significantly large.

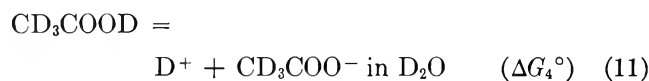
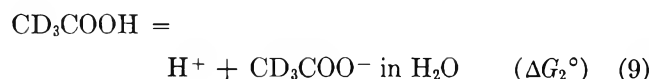
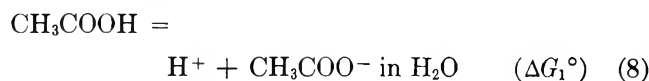
Table IV: Values of pK for the Dissociation of Protoacetic Acid and Deuterioacetic Acid in Deuterium Oxide and in Water (Mole Fraction Scale)

Temp., °C	Protoacetic acid			Deuterioacetic acid		
	CH ₃ - COOD in D ₂ O	CH ₃ - COOH in H ₂ O	Δ	CD ₃ - COOD in D ₂ O	CD ₃ - COOH in H ₂ O	Δ
0	...	6.524	6.539	...
5	7.046	6.514	0.532	7.058	6.528	0.530
10	7.032	6.507	0.525	7.046	6.522	0.524
15	7.022	6.502	0.520	7.036	6.518	0.518
20	7.015	6.500	0.515	7.028	6.516	0.512
25	7.010	6.500	0.510	7.024	6.515	0.509
30	7.008	6.502	0.506	7.022	6.517	0.505
35	7.008	6.506	0.502	7.022	6.521	0.501
40	7.011	6.513	0.498	7.024	6.527	0.497
45	7.015	6.521	0.494	7.028	6.534	0.494
50	7.022	6.531	0.491	7.035	6.543	0.492

It is important to inquire to what extent the thermodynamic quantities given in Table III are altered by such a change in scale of reference. The change in question is accomplished by decreasing the value of the A_2 parameter in eq 4 by 1.7444 when ordinary water is the solvent and by 1.6983 when the solvent is deuterium oxide, without modifying the A_1 and A_3 parameters. Consequently, ΔH° and ΔC_p° have the same values regardless of the scale of concentration used. However, ΔG° at 25° is higher by 2380 cal mole⁻¹ in ordinary water and by 2317 cal mole⁻¹ in deuterium oxide when the mole fraction scale is used in place of the

molality scale. Similarly, ΔS° is lower at 25° by 7.98 cal deg⁻¹ mole⁻¹ if water is the solvent and by 7.77 cal deg⁻¹ mole⁻¹ when the solvent is deuterium oxide.

It is clear that there are four dissociation constants corresponding to the dissociation of the two forms of acetic acid in the two solvents. Similarly, there are four changes in Gibbs energy corresponding to the four dissociation processes



The question may be asked whether there is a constant difference between the dissociation energies for a given acid in water and deuterium oxide, independent of the nature of the acid. This seems not to be so, as is evident from the following considerations.

Take two proto acids designated HA_1 and HA_2 . In water as solvent we have



and in deuterium oxide



Then if

$$\Delta G_1^\circ - \Delta G_3^\circ = \Delta G_2^\circ - \Delta G_4^\circ \quad (12)$$

the following relationship among the dissociation constants would hold

$$\frac{K_{\text{HA}_1}(\text{in H}_2\text{O})}{K_{\text{DA}_1}(\text{in D}_2\text{O})} = \frac{K_{\text{HA}_2}(\text{in H}_2\text{O})}{K_{\text{DA}_2}(\text{in D}_2\text{O})} \quad (13)$$

and the ratio of the dissociation constants of any given acid in the two solvents would be a constant.

Unfortunately, it is not known with certainty how this ratio varies with $pK(\text{in H}_2\text{O})$, although there is evidence that the difference, $pK(\text{in H}_2\text{O}) - pK(\text{in D}_2\text{O})$ increases more or less linearly with increase of pK .⁸ Consequently, it seems fairly certain that the

(8) R. P. Bell, "The Proton in Chemistry," Cornell University Press, Ithaca, N. Y., 1959, p 189, Figure 18.

relationship expressed by eq 13 is not generally true. We have confirmed this conclusion from our own measurements. Thus for protoacetic acid in water and in deuterium oxide at 25°, $\Delta pK = 0.556$, but for the second stage in the dissociation of phosphoric acid, $\Delta pK = 0.580$.

If, however, HA_1 and HA_2 are acids of nearly equal strength, we would expect eq 13 to be closely valid. When A_1 is CH_3COO and A_2 is CD_3COO , for example, it might be anticipated that eq 13 would be a very good approximation, though not necessarily exactly true. We have shown in an earlier paper³ that ΔpK

($\equiv pK$ in $D_2O - pK$ in H_2O) for protoacetic acid ranges from 0.577 at 5° to 0.537 at 50°. It is now found (Table II) that ΔpK for deuterioacetic acid in these two solvents ranges from 0.576 at 5° to 0.538 at 50°. Although eq 13 holds to a very good approximation in this instance, there is no apparent reason to expect it to be exactly valid.

Acknowledgment. The authors acknowledge gratefully the assistance of E. E. Hughes, who performed the mass spectrometric and gas chromatographic analyses, and of Dr. R. T. Leslie, who purified the deuterioacetic acid.

Adsorption Thermodynamics of the Interaction of Water and Various Silica Powders

by Donald E. Meyer and Norman Hackerman

Department of Chemistry, The University of Texas, Austin, Texas (Received February 8, 1965)

Free energies, heats and integral entropies, and enthalpies of adsorption are presented for powdered fused silica (0.056 to 13.58 m²/g) and powdered crystalline silica (0.11 to 5.65 m²/g). A volumetric adsorption system and a microcalorimeter were used. Both crystalline and amorphous silica were mechanically ground and separated by water sedimentation into several particle-size distributions. In addition, one sample of the ground crystalline silica was etched with varying amounts of dilute HF to yield a particle-size distribution. The effect of grinding and etching on the thermodynamic values of adsorption are reported, and the results are discussed on the basis of surface structure related to particle size and etching. Electron micrographs are also presented.

Introduction

Many investigators have considered the interaction of water with silica surfaces. Collectively, precision immersion calorimetry,¹⁻³ adsorption studies,^{4,5} and infrared studies^{6,7} have indicated that the energetics of water-silica interactions depend upon the presence and density of surface hydroxyl groups. Additional experimental evidence indicated that these surface OH groups participate in still another manner. Immersional heats⁸⁻¹⁰ and adsorption free energies¹⁰

normalized to unit surface area were found to vary with particle size for silica powders. Of the explana-

(1) A. C. Makrides and N. Hackerman, *J. Phys. Chem.*, **63**, 594 (1959).

(2) J. W. Whalen, *Advances in Chemistry Series*, No. 33, American Chemical Society, Washington, D. C., 1961, p 281.

(3) M. M. Egorov, V. G. Krasilnikov, and E. A. Sysoev, *Dokl. Akad. Nauk SSSR*, **108**, 103 (1956).

(4) N. Hackerman and A. C. Hall, *J. Phys. Chem.*, **62**, 1212 (1958).

(5) M. M. Egorov, V. F. Kiselev, and K. G. Krasil'nikov, *Russ. J. Phys. Chem.*, **33**, No. 10, 323 (1959).

tions for this particle size effect, the most generally accepted are based on evidence that structural order in the surface region of ground quartz powders decreases with decreasing particle size.

Crushing and grinding quartz crystals produces a less crystalline,^{11,12} more easily soluble^{13,14} surface region. Continued grinding produces smaller particles with a disturbed region descending deeper into the bulk. One explanation suggests that a less ordered (more amorphous) surface has a lower density of surface OH groups and thus exhibits a lower heat of wetting per unit area. The other explanation pictures the $\text{Si}^{4+}\text{O}^{2-}$ structure and the SiOH^{3+} grouping producing a surface electrostatic force field which interacts with the sorbate molecules. A more ordered SiO_2 surface structure would present a more ordered array of surface OH groups resulting in a stronger force field and greater interaction energies with water.

The object of this investigation was to obtain a systematic and detailed correlation between different surface structures (determined by type of silica, mechanical grinding, and chemical etching) and surface thermodynamics.

Experimental Section

Equipment. Specific surface areas (Σ) were determined by the BET method using either krypton, argon, or nitrogen. On samples where two or more of the gases were used, results were in good agreement. Excess surface free energies of adsorption (two-dimensional spreading pressures, π) were obtained from water adsorption isotherm data at $25 \pm 0.01^\circ$ and $15 \pm 0.02^\circ$. The volumetric adsorption apparatus was similar to the system previously reported¹⁰ except for two major modifications. Tandem bulb trains, allowing a selection of 35 volume combinations, were used which decreased the pressure surge when volume changes were made. A micrometer-U-tube assembly¹⁵ was found to be superior to cathetometric methods for measuring pressure changes. The adsorption system could be evacuated to 10^{-8} torr provided liquid nitrogen trapping was used. All samples were outgassed at $150 \pm 5^\circ$ for 48 hr at pressures below 10^{-6} torr.

Heats of immersion (ΔH_i) for certain of the SiO_2 samples were determined using the microcalorimeter and general procedures described previously.¹⁰ All measurements were at $25 \pm 0.1^\circ$, and the samples were outgassed at $150 \pm 5^\circ$ for 48 hr at 10^{-6} torr.

Using electron diffraction and electron microscopy, particle surface structures were obtained for many of the samples. The samples were pressed into a 200-mesh screen, and diffraction patterns were obtained by transmission at 50 kv (through edges of larger particles).

Electron micrographs of particle surfaces were obtained from preshadowed carbon replicas. A suspension of the powder in deionized water was spread over a glass microscope slide and allowed to dry. The particle-covered slide was placed in a vacuum evaporator and shadowed at 18° with a 80% Pt-20% Pd alloy. The slide was then coated with carbon at normal incidence.

The evaporated film was cut into $1/8$ -in. squares and floated free of the slide by immersion in HF. The films were then washed in water and mounted on 200-mesh electron microscope grids.

Materials. A billet of fused quartz, 99.97% pure, was obtained from General Electric Co., Willoughby Quartz Plant. Particles in the 100- to 300- μ range were produced using an iron jaw crusher and were treated with HCl to remove traces of iron. The fused quartz was further ground for 5 days in a water slurry using a motor driven agate mortar and pestle. The ground material was fractionated into particle size distributions by water sedimentation ranging from 5 min to 48 hr and then dried at 110° .

Ground 99.9% pure crystalline silica was supplied by Charles A. Wagner Co. of Philadelphia. The powder was washed in HCl and several times in distilled water and then stored in distilled water for 9 months. As a given amount was needed, it was taken from the bulk, fractionated into particle-size ranges, and air-dried at 110° .

A solution of 3% by weight HF in water was used to etch the ground crystalline silica. The extent of etching was controlled by the ratio of HF to silica. After allowing the powder to settle and decanting the liquid, HF was removed by NaOH washes of decreasing concentrations down to 0.001 *N*. This method of removal is similar to that reported by van Lier, *et al.*¹³ Extensive washings in boiling and cold distilled water were used to minimize the HF and NaOH contamination.

(6) R. S. McDonald, *J. Am. Chem. Soc.*, **79**, 850 (1957); *J. Phys. Chem.*, **62**, 1169 (1958).

(7) A. V. Kiselev and V. I. Lygin, *Kolloidn. Zh.*, **21**, 581 (1959).

(8) G. J. Young and T. P. Brush, *J. Colloid Sci.*, **15**, 361 (1960).

(9) W. H. Wade, R. L. Every, and N. Hackerman, *J. Phys. Chem.*, **64**, 355 (1960).

(10) R. L. Every, W. H. Wade, and N. Hackerman, *ibid.*, **65**, 25 (1961).

(11) D. D'Eustachio and S. Greenwalk, *Phys. Rev.*, **69**, 532 (1946); **70**, 522 (1946).

(12) D. W. Clelland and P. D. Ritchie, *J. Appl. Chem.*, **2**, 42 (1952).

(13) J. A. van Lier, P. L. de Bruyn, and J. Th. G. Overbeek, *J. Phys. Chem.*, **64**, 1675 (1960).

(14) I. Bergman and M. S. Paterson, *J. Appl. Chem.*, **11**, 369 (1961).

(15) D. E. Meyer and W. H. Wade, *Rev. Sci. Instr.*, **33**, 1283 (1962).

Calculations

Each isotherm was composed of from 30 to 50 points, usually half within the first monolayer. The free energy of adsorption (π) was calculated from a modification of the Gibbs equation by Bangham

$$\pi = (\gamma_s - \gamma_{sA}) = \frac{RT}{V\sigma} \int_{p=0}^{p=p^0} \frac{v}{p} dp \quad (1)$$

where γ_s and γ_{sA} are the surface tensions of a vacuum-baked surface and a surface following adsorption. Also, V = molar volume of the gas, σ = area for 1 g of solid, v = volume of sorbed gas per square meter of surface, and p = equilibrium pressure of the sorbing gas.

Graphical integration of eq 1 on the basis of Simpson's trapezoidal using a computer gave the integral free energy of adsorption as well as π as a function of coverage (θ). By applying Simpson's rule to isotherm data at 25 and 15°, the integral (constant free energy) enthalpies $[(H_G - H_s)_\pi]$ and entropies $[(S_G - S_s)_\pi]$ of adsorption were obtained using the equations of Hill¹⁶

$$(\partial \ln p / \partial T)_\pi = (S_G - S_s) / RT \quad (2)$$

and

$$(\partial \ln p / \partial T)_\pi = (H_G - H_s) / RT \quad (3)$$

where G corresponds to the gaseous state and S the sorbed state. These thermodynamic values were calculated by computer and expressed as a function of coverage (θ). Absolute entropies (S_s) were evaluated using water vapor at 25° and 1 atm as the standard state.

Heats of immersion (ΔH_i) yielded adsorption heats (ΔH_a) according to

$$\Delta H_a = \Delta H_c - 118.5 \text{ (ergs/cm}^2\text{)} \quad (4)$$

where 118.5 is the surface enthalpy of water. Heats of adsorption and corresponding values of π gave entropies of adsorption (ΔS_a) from

$$\Delta S_a = \frac{(\Delta H_a - \pi)}{T} \quad (5)$$

a modification of the Hill-Jura equation.¹⁷

Values of π , ΔH_a , and ΔS_a for only the amorphous samples were reported previously.¹⁸ Also, surface areas (Σ) used to calculate π values in this reference were in slight error. That there was no effect of particle size on π as reported¹⁸ for ground amorphous silica is in fact an error. The present work gives corrected π values and therefore corrected ΔS_a values (eq 5).

Results

Table I gives a comprehensive report of all the silica samples studied. Specific surface areas were averages of several runs usually differing less than 1%. Values of the heat of adsorption (ΔH_a) were averages of three or more measurements. All adsorption isotherms were duplicated at least twice and were found to be reproducible at relative pressures below 0.6. Small variances in isotherms of a given sample at higher relative pressures caused differences of less than 2% in calculated values of π .

Table I

Sample designation, description	Σ , m ² /g	ΔH_a , ergs/cm ²	π , ergs/cm ²	ΔS_a , ergs/cm ² /°C	ω , Å ²
Fused silica					
Sample A	0.056	372 ^a	139	0.78	17.6
Sample B	0.603	362 ^a	143	0.65	14.3
Sample C	1.81	378 ^a	151	0.84	18.4
Sample CLT ^b	1.81		155		
Sample D	7.46	345 ^a	176	0.57	14.4
Sample E	13.58	359 ^a	202	0.53	11.6
Sample E _{LT}	13.58		217		
Crystalline silica					
Sample F	0.112		48.6		48
Sample G	0.27	290	113.5	0.65	20.7
Sample G _{LT}	0.27		121.1		20.6
Sample H	1.34		122.4		18.5
Sample H _{LT}	1.34		127		18.0
Sample I	3.2		127		14.6
Sample J	5.65		122.5		20.6
Sample J _{LT}	5.85		127.4		20.4
Etched silica (crystalline)					
Sample K	0.136		135.5		15.9
Sample M	0.164		105.1		22.4
Sample M _{LT}	0.164		110		19.7
Sample N	0.364		86.8		24.8
Sample N _{LT}	0.364		99.3		24.4
Sample O	1.76		73.8		31.2
Sample P	0.185	385	101	0.95	
Sample Q	0.194	300	98	0.67	
Sample R	1.57	175	75	0.33	
Sample S	1.70	120	72	0.16	

^a See ref 18. ^b LT corresponds to 15° isotherm.

Absolute isotherms (amount adsorbed normalized to unit area) for various particle size distributions for the three types of silica studied are presented in Figures

(16) T. L. Hill, *Advan. Catalysis*, **4**, 242 (1952).

(17) G. Jura and T. L. Hill, *J. Am. Chem. Soc.*, **74**, 1598 (1952).

(18) W. H. Wade, H. D. Cole, D. E. Meyer, and N. Hackerman, *ref 2*, p 35.

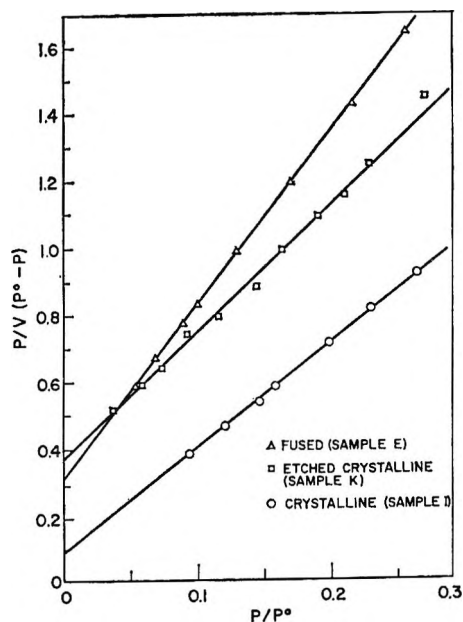


Figure 1. BET plots for three types of silica studied: 3.7-m²/g crystalline sample I, 0.136-m²/g etched sample K, 13.58-m²/g fused sample E (p = equilibrium pressure, p^0 = saturation pressure, and v = volume of gas adsorbed (cc at STP)).

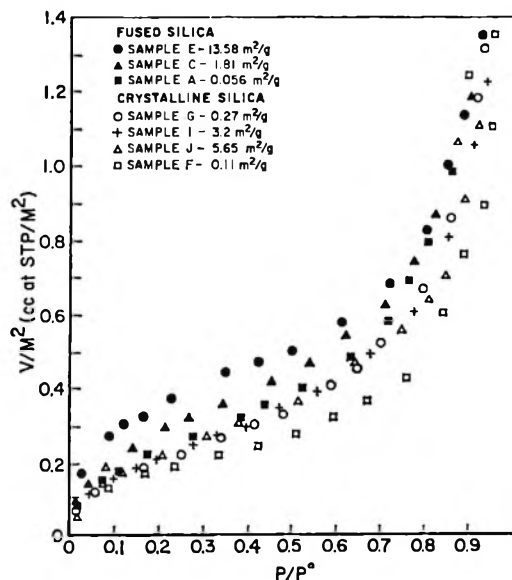


Figure 2. Absolute adsorption isotherms for fused and crystalline silicas of various specific surface areas.

1 and 2. The vertical displacement of any given isotherm is seen to depend upon the specific surface area (Σ) of the sample and the type of silica. In general, the relative vertical position of the isotherm determines π and ω . In determining the excess surface free energy using the Gibbs equation, extrapolations were made

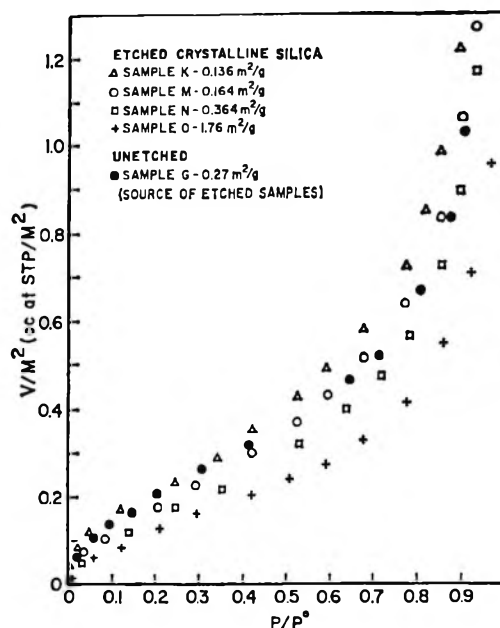


Figure 3. Absolute adsorption isotherms for several samples of etched crystalline silica and the parent sample, unetched sample G.

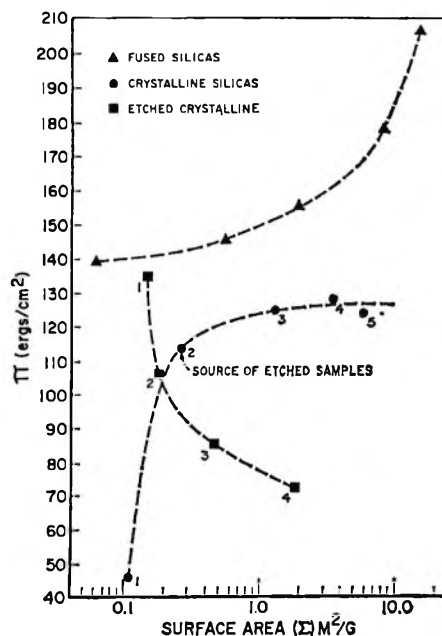


Figure 4. The free energy of adsorption (π) as a function of specific surface area for the three types of silicas studied.

from relative pressures (p/p^0) of 0.005 to 0 and above 0.96 to 1.0. The BET equation was also applied to the water adsorption data. Figure 3 gives representative linear BET plots for the three types of silica studied. Over the applicable pressure ranges, the water-silica adsorption data produced a straight-line

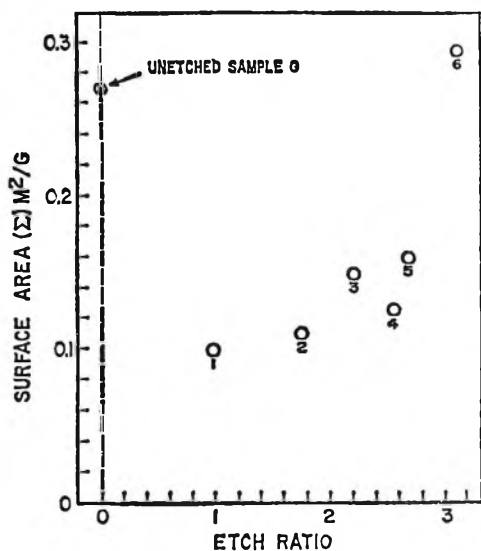


Figure 5. The change in specific surface area of sample G as a function of the etch ratio (volume of 3% HF to weight of SiO₂; sample 1 arbitrarily taken as unity). Increasing sample number corresponds to increased etching. Sample 2 is identical with sample K, Table I.

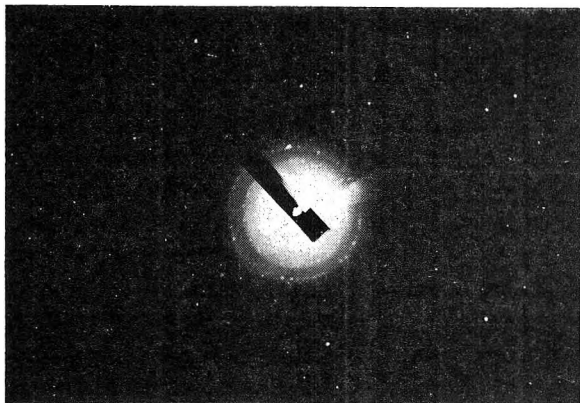


Figure 6. Transmission electron-diffraction pattern for crystalline silica before etching.

fit from which values for the effective area of an adsorbed water molecule (ω) were obtained.

In Figure 4 the dependence of π on Σ is demonstrated for all three types of silica samples. For the ground crystalline and particularly for the amorphous samples, π increased with Σ . In contrast, for the etched samples π decreased with increasing Σ . In Figure 4, squares numbered 1 through 4 correspond to samples from increased etching of crystalline sample G. The general effect of etching on Σ is shown in Figure 5. There is a rapid initial drop in Σ . This corresponds to the initial rise in π going from source sample (circle 2) to first etched sample (square 1) in Figure 4. Thereafter, Σ rises with increased etching and π drops. Time was



Figure 7a. Electron micrograph (23,000X) of surface region of a 50- μ crystalline particle.

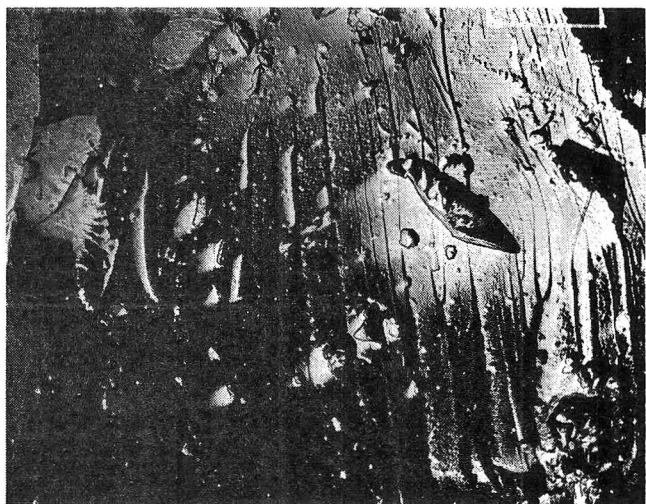


Figure 7b. Electron micrograph (35,000X) of crystalline particle.

not a factor in controlling etching, but the volume of 3% HF to weight of sample was. The ratio used to obtain the first sample (circle 1, Figure 5) was assigned a value of unity.

Both grinding and etching changed not only the surface structure but the particle-size distribution as well. Electron-diffraction patterns clearly indicated the presence of many crystallites on the ground crystalline particles before etching. The number of crystallites also appeared to vary with particle size. A diffraction pattern for sample G is shown in Figure 6. The dotted rings of the diffraction pattern apparently originates from the submicron particles on the surface of the larger particles (Figure 7). After slight etching, these particles practically disappear (Figure 8) and it

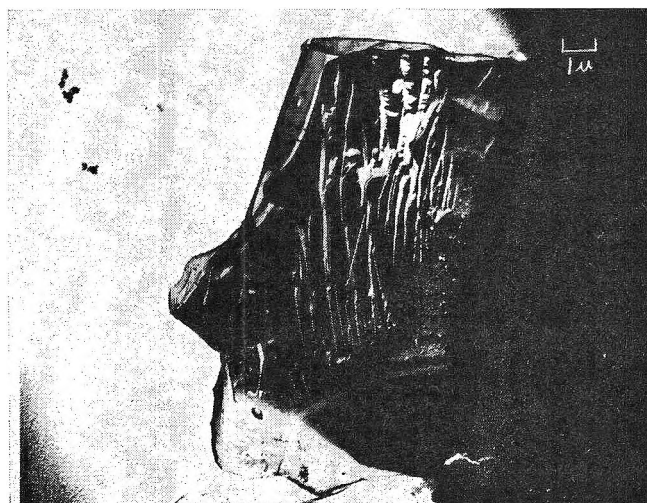


Figure 8a. Electron micrograph (18,000 \times) of an etched crystalline particle (sample M).



Figure 9. Electron micrograph (13,000 \times) of surface of a large amorphous silica particle.

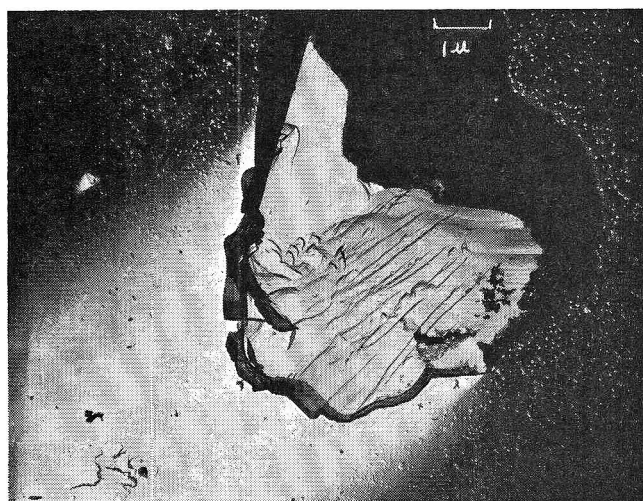


Figure 8b. Electron micrograph (23,000 \times) of crystalline particle more extensively etched (sample Q).

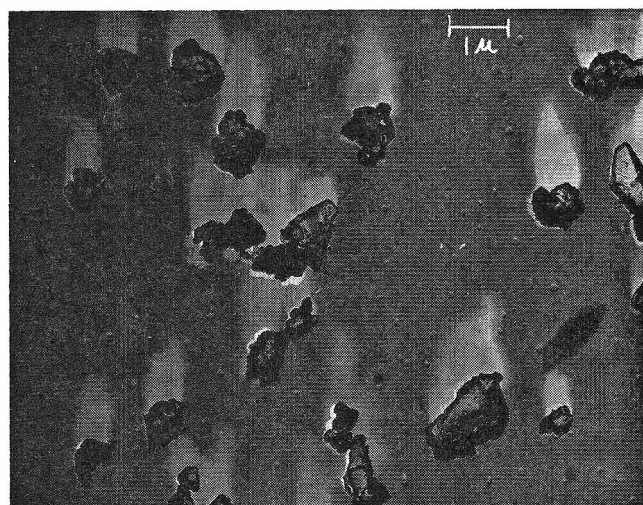


Figure 10a. Electron micrograph (22,000 \times) of ground amorphous silica particles.

was impossible to obtain this crystallite diffraction pattern.

Ground amorphous samples also showed submicron particles attached to the surface of larger particles (Figure 9); however, no diffraction patterns were observable. Electron diffraction studies gave no indication of devitrification as a result of prolonged grinding. Close observation of Figure 9, particularly the right side, reveals surface irregularities other than attached particles. This micrograph shows a particle (sample F, 0.11 m²/g) greater than 50 μ in size. A representative micrograph of particles of sample A, 13.58 m²/g, is presented in Figure 10a and a closeup of an individual particle in Figure 10b.

Using adsorption data from isotherms at 25 and 15 $^{\circ}$, adsorption thermodynamic values were obtained as a function of coverage (θ). As defined by Hill,¹⁶ the integral heats $(H_G - H_S)_\pi$, integral entropies $(S_G - S_S)_\pi$, and the absolute entropies are presented as a function of coverage in Figures 11 and 12. All three types of silica studied are represented, and there are significant variations related to particle size and type of silica at lower coverages. Even at higher coverages, several layers, there appears to be a particle size effect as the integral heats approach the heat of condensation in going from gas to liquid (Figure 11).

The absolute entropy of the sorbed water on various silica samples as a function of coverage is presented in Figure 12. At lower coverages the order of condensed

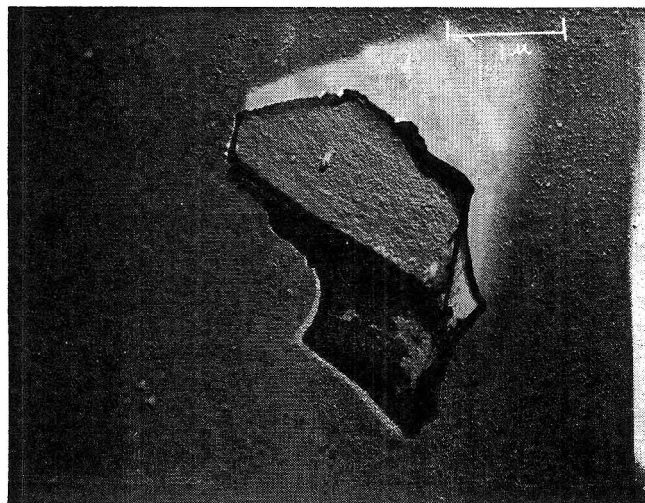


Figure 10b. Electron micrograph (44,000X) of an amorphous particle.

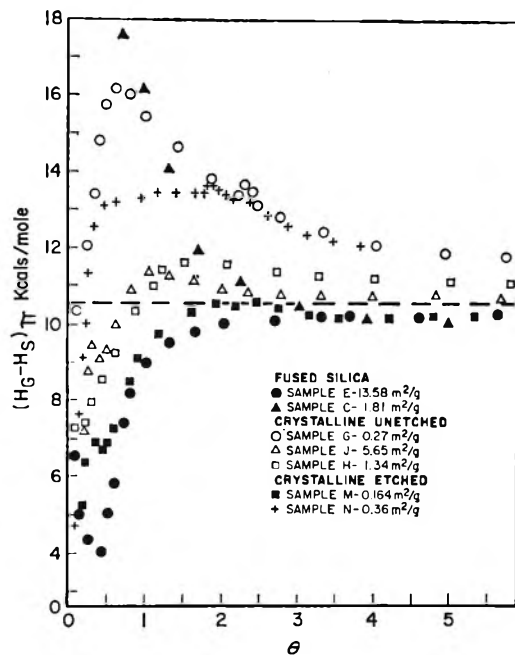


Figure 11. Integral heats of adsorption as a function of coverage for silica samples of differing histories and specific surface areas. Dashed line corresponds to the heat of condensation of water (H_G , enthalpy in gaseous state; H_S , enthalpy in sorbed state).

water on the largest crystalline particle sample (G) and an etched sample (N) was quite high. At higher coverages, S_S approached a value closer to that for the solid state than for the liquid state. For calculations of S_S , S_G was expressed in terms of $S^{\circ}_{298.16} = 45.106$ eu for water vapor at 1 atm.

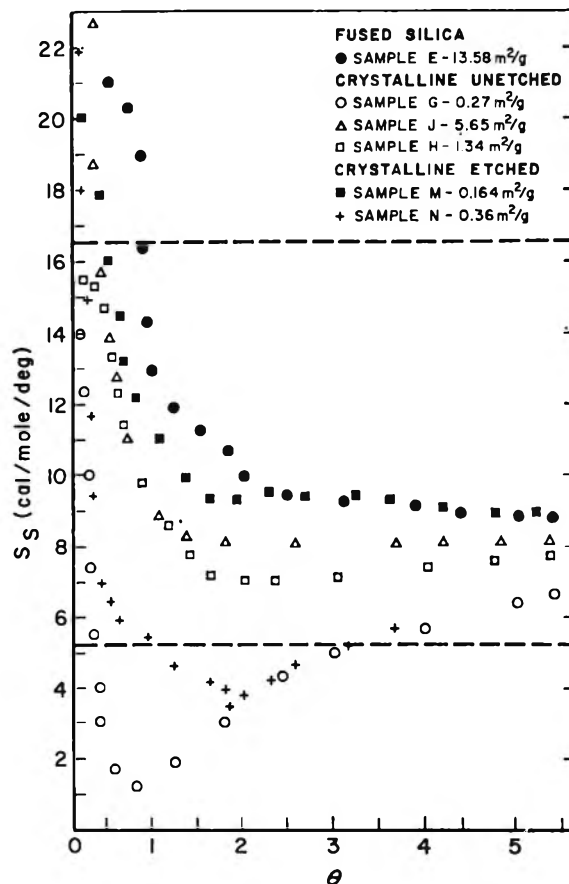


Figure 12. Absolute entropy of adsorption as a function of coverage. Lower dashed line corresponds to solid H_2O , upper dashed line to liquid H_2O .

Discussion

It has been shown that heats of immersion and free energies and entropies of adsorption for the water-silica powder system are dependent upon the specific surface area. One explanation suggests a correlation between particle size and crystalline surface order and between surface order and an electrostatic force field causing a greater polarization of surface hydroxyl groups. As a result, a ground crystalline silica sample of small specific surface area (Σ) and large particle size would possess a greater normalized energy of adsorption for water vapor. As this powder is ground, Σ increases, the heat of adsorption decreases, and the excess surface free energy increases.

Amorphous Silica. Amorphous silica ground into powder should not vary in crystallinity with particle size, and the normalized heats of immersion or free energies of adsorption should remain constant with changing Σ . As expected, ΔH_a was practically independent of Σ (Table I), which supports the particle size effect-crystallinity postulate. However, Figure

4 shows π to be dependent on Σ . It would seem that π is not influenced by the electrostatic force field and the polarity of the surface hydroxyl to the extent ΔH_a is.

The change in surface free energy for a silica particle interacting with water vapor appears to depend on the size of the particle. For Σ of 0.056 to 13.58 m²/g, π varied from 139 to 202 ergs/cm² at 25°. Since average particle size varied from approximately 50 to 1 μ , this apparent surface effect cannot be explained as directly as surface effects of particles 0.01 μ or less.

Several factors should be considered. Electron micrographs, Figures 7–10, showed submicron particles attached to the surfaces of larger particles. These smaller particles, together with other surface irregularities resulting from grinding damage, could affect the surface tension both before (γ_s) and after (γ_{sa}) adsorption and thus

$$\pi = (\gamma_s - \gamma_{sa})$$

The surface energy or surface tension is reportedly related directly to the tensile strength.¹⁹ Though it is somewhat more difficult to envision tensile strengths of various sized silica particles compared to various sized silica fibers or rods, there is apparently a difference in the change in tensile strength with adsorption on a larger particle (50 μ) compared to a smaller particle (1 μ). Stranski²⁰ found the tensile strength of ground rock salt to be a function of particle size, increasing as the dimensions decreased.

The tensile strength and, therefore, the surface energy depend upon the presence of surface cracks and fissures. Grinding is an important factor in affecting the tensile strength, and larger particles apparently have more surface damage of a nature affecting the tensile strength. Large particles would preferentially split into smaller particles along surface cracks and fissures.

Crystalline Silica. Every¹⁰ reported a particle size effect for both π and ΔH_a using the same crystalline powder from Charles A. Wagner Co. used in this work. No immersional heats were obtained on crystalline samples reported here, but the crystalline π values (Table I) increased with decreasing particle size just as Every observed.

The change in π with Σ differed for amorphous and crystalline silica, Figure 4, in an inverse fashion. For crystalline samples the greatest change occurred at low Σ and for amorphous samples at high Σ . There is an apparent correlation between these differences of π with Σ and the population of attached particles which decreased as the parent particles grew smaller (increased grinding, larger Σ). For crystalline powder,

electron micrographs showed that the greatest change in population took place between sample F (Figure 7a) and sample G (Figure 7b). This corresponds to the greatest change in π . Likewise for amorphous powder, there was a greater change in particle population between sample C (1.81 m²/g) and sample E (13.58 m²/g) than between sample C and sample A (0.056 m²/g). This was also true for the change in π for samples C, E, and A which tends to relate changes in π to these attached particles and thus suggesting their effect on the tensile strength and surface energy of the particles before and after adsorption of water vapor.

Cracks in the surface and smaller particles aggregated together on the surface of larger particles have been reported to effect adsorption properties of silica. Zhdanov²¹ suggested fissures in quartz produce an excess surface area available to an H₂O molecule but not to the larger N₂ molecule. Normalizing water isotherms for different samples with N₂ BET Σ values would lead to error. Egorov, *et al.*,⁵ found that grinding silica in air produced aggregations of particles which grinding in water does not. Again, crevices between particles would decrease the adsorptive capacity of N₂ relative to H₂O. Kiselev, *et al.*,²² provided further evidence supporting the theory that dry grinding results in particle aggregation and low N₂ specific surface areas. They pointed out that cracks or fissures, being the most probable place for cracking, should decrease with grinding. Thus particle aggregation rather than microfissures²¹ are responsible for the difference in areas "seen" by adsorbing N₂ compared to H₂O.

Several observations do not agree with the explanations given above. The amorphous samples were ground in a water slurry yet showed aggregation. Also, ΔH_a was constant with Σ , Table I, while π varied (Figure 4). If a difference existed between the total surface seen by the N₂ molecule (used to normalize ΔH_a and π) and between the total surface seen by the H₂O molecule, then ΔH_a should vary as did π . For the crystalline samples ΔH_a ¹⁰ decreased with increasing Σ while π increased. Particle aggregation must play some other role.

Stranski²⁰ observed that when ground rock salt was placed in a saturated solution small crystals formed on the surface of the larger particles accompanied by a lowering of their tensile strength. After the crystal-

(19) W. D. Harkins, "The Physical Chemistry of Surface Films," Reinhold Publishing Corp., New York, N. Y., 1952.

(20) I. N. Stranski, *Ber.*, **75b**, 1667 (1942).

(21) S. P. Zhdanov, *Dokl. Akad. Nauk SSSR*, **115**, 938 (1957).

(22) V. F. Kiselev, K. G. Krasil'nikov, and G. S. Khodakov, *ibid.*, **130**, 1273 (1960).

line silica powder used by Every¹⁰ was placed in water for several months, the values of π for the soaked samples (Table I and Figure 4) were lower by a factor of 2 to 3 over the π values for unsoaked samples.¹⁰ This suggests that the surface of the silica powder was altered in a manner that changed the tensile strength and surface energy.

Griot and Kitchener²³ found that silica powders underwent a slow change or "aging" effect which might explain the great difference in values of π for a given Σ reported here and π values reported previously on unsoaked samples.¹⁰

Etched Crystalline Silica. Etching with HF removed submicron surface particles as well as modified the larger particle surface structure depending upon the extent of etching. Gibb, *et al.*,²⁴ observed this also with electron-optical methods. In Figure 5, Σ drops with initial etching, and surface particles practically disappear (Figure 9). Corresponding to this initial etching where the particles disappear and Σ drops, π increases (Figure 4, circle 2 to square 1). This initial etching (sample G yielding sample M) apparently resulted in increased tensile strength and increased π . Plate glass is commonly treated with HF presumably to increase its tensile strength by removing surface irregularities. With continued etching, Σ increased (Figure 5) and π decreased (Figure 4). Perhaps the silica particles etched in 3% HF exhibited a decrease in π for the same reason the tensile strength of rock salt decreased when placed in a saturated salt solution. Smaller particles and higher Σ values would have resulted from further etching, but the powder sample was depleted after the fourth etch.

The effect of etching on ΔH_a was also significant. With amorphous and crystalline samples, while π increased with Σ , ΔH_a decreased. As noted in Figure 4 and Table I for the etched samples, π and ΔH_a both decreased with increasing Σ in much the same way. Both had increased in going from unetched sample G to etched sample M. Recalling the suggested mechanism for the particle size effect of ΔH_a with the water-silica system, the initial etching would be expected to remove disordered surface irregularities. This should increase surface electrostatic forces and increase surface-H₂O interaction heats.

Continued etching caused Σ to increase and ΔH_a to decrease. It might be expected that etching would leave a more crystalline surface region with a correspondingly higher electrostatic field. Then ΔH_a should increase with etching. Perhaps the dilute HF concentration did not etch to this extent. The etching did have the observable effect, Figure 9, of rounding sharp corners and steps which resulted from the

grinding. It is reasonable that sites, such as trenches and step edges, where the energy of water-surface hydroxyl interaction would be greatest would also be the sites most readily altered by etching. With continued etching by 3% HF, ΔH_a decreased. Circumstances did not permit continued etching of the sample originating from sample G, and higher Σ samples were not available. Presumably, ΔH_a would reach a constant value as Σ increased.

Thermodynamic Data. Integral heats, Figure 11, express the change in heat content going from the gaseous state to the sorbed state at a constant value for π . This change is dependent upon the extent of coverage, but as can be seen in Figure 11 the influence of coverage depends upon the specific surface area and type of sample.

At higher coverages the integral heats all tend to converge about the value for the heat of condensation. This is expected for interaction heats several layers removed from the sorbent surface. However, at lower coverages, particularly below the first monolayer, there were significant differences. Some trends are apparent.

Of the fused silica samples studied, only sample E (highest Σ) gave satisfactory integral heats. Adsorption isotherms at 15 and 25° were almost identical for sample A (0.056 m²/g). The same was true for the other amorphous samples such as sample C shown in Figure 11. Integral heats shown for sample C below $\theta = 2$ are doubtful because of this. At higher coverages sample E and sample C are almost identical. No explanation is available for the slight minima in the sample E curve at $\theta = 0.5$. Figure 11 shows that samples M and J also experienced slight minima at $\theta = 0.5$. Minima and maxima are not uncommon when expressing integral heats and entropies with coverage.²⁵

For any given coverage, integral heats decreased from the largest particle size crystalline sample to the smallest particle size amorphous sample. This trend is expected on the basis of the surface electrostatic field dependence on surface region crystallinity. For the same reason, the same trend was found with the integral entropies which indicate a change in order going from vapor to sorbed phase.

The absolute entropy, Figure 12, is perhaps most illustrative of the effect of particle size and type on adsorption thermodynamics. From the basis of deriva-

(23) O. Griot and J. A. Kitchener, *Nature*, **200**, 1004 (1963).

(24) J. G. Gibb, P. B. Ritchie, and J. W. Sharpe, *J. Appl. Chem.*, **3**, 213 (1953).

(25) J. W. Whalen, *J. Phys. Chem.*, **67**, 2114 (1963).

tion of the formulas¹⁶ the trend in S_s with θ is quite similar to that of the integral heat and entropy. Thus a high interaction energy between water molecules and the surface of sample G at about $\theta = 0.85$ corresponds to an extremely low sorbate entropy at the same coverage.

The sorbate entropy on the largest particle crystalline sample is about 1 cal/mole deg at $\theta = 0.85$. Whalen²⁵ observed the same degree of surface order for a similar silica surface using benzene at about the same coverage. The sorbed water molecule is almost immobile at this particular coverage. Even at much higher coverages sorbate entropy values predict a

molecular mobility much closer to that for ice than to that for liquid water.

Acknowledgment. This work is a contribution from Project 47D of the American Petroleum Institute at the Department of Chemistry, The University of Texas, and was also supported in part by a grant from the Robert A. Welch Foundation, Houston, Texas. The authors wish to take this opportunity to express their appreciation for the support and interest in this work. The authors also thank George A. Savanick of the Central Research Laboratories, Texas Instruments Incorporated, Dallas, Texas, for preparing the electron micrographs.

The Electronegativity of Multiply Bonded Groups

by James E. Huheey

*Division of Chemistry, Worcester Polytechnic Institute, Worcester, Massachusetts,
and the Department of Chemistry, University of Maryland, College Park, Maryland
(Received July 9, 1965)*

The electronegativities of 97 groups containing multiple bonds have been calculated by the method of electronegativity equalization. Although the values seem to be self-consistent, those of the more electronegative groups appear rather high in comparison with atomic electronegativities. This problem is discussed and it is concluded that the assumption of electronegativity equalizations is an oversimplified, though useful, description of the polarity within the group.

In a previous paper,¹ the assumption of electronegativity equalization was applied to the problem of the calculation of the electronegativity of σ -bonded groups. The method utilized was developed from recent work on variable electronegativity.² By treating the electronegativity as a linear function of charge, $\chi = a + b\delta$, it is possible to estimate the electronegativity of the central atom of a group as influenced by the electronegativities of its substituent atoms.

Most inorganic groups and many organic groups contain multiple bonds and were not treated previously. In the present paper, electronegativity equalization in multiply bonded groups is examined and previous

methods are extended to the calculation of the electronegativities of these groups.

Multivalent Groups. The question of the proper treatment of multivalent groups is not unique to multiply bonded groups, but assumes greater importance with respect to economy of effort in the calculations. It can be shown that a multivalent group such

(1) J. E. Huheey, *J. Phys. Chem.*, **69**, 3284 (1965).

(2) (a) J. Hinze and H. H. Jaffé, *J. Am. Chem. Soc.*, **84**, 540 (1962); (b) J. Hinze, M. A. Whitehead, and H. H. Jaffé, *ibid.*, **85**, 148 (1963); (c) J. Hinze and H. H. Jaffé, *J. Phys. Chem.*, **67**, 1501 (1963); (d) R. P. Iczkowski and J. L. Margrave, *J. Am. Chem. Soc.*, **83**, 3547 (1961); (e) R. T. Sanderson, "Chemical Periodicity," Reinhold Publishing Corp., New York, N. Y., 1960.

as the methylene group, $-\text{CH}_2-$, can be treated in much the same way as a multivalent atom. The equations developed previously¹ for univalent groups are equally applicable to multivalent groups. For example, consider the univalent group WXY. The electronegativity of this group is given by

$$\chi_{\text{WXY}} = \frac{a_{\text{W}}b_{\text{X}}b_{\text{Y}} + a_{\text{X}}b_{\text{W}}b_{\text{Y}} + a_{\text{Y}}b_{\text{W}}b_{\text{X}} + b_{\text{W}}b_{\text{X}}b_{\text{Y}}\delta_{\text{WXY}}}{b_{\text{W}} + b_{\text{X}} + b_{\text{Y}}} \quad (1)$$

where a represents the "inherent electronegativity" of an element (equivalent to Mulliken's definition³) and b is the coefficient of partial charge.¹ This group can now be treated as a combination of the divalent group $-\text{WX}-$ and the univalent atom Y. The electronegativity of $-\text{WX}-$ (assuming multivalent groups behave in the same way as univalent groups) is

$$\chi_{\text{WX}} = \frac{a_{\text{W}}b_{\text{X}} + a_{\text{X}}b_{\text{W}}}{b_{\text{X}} + b_{\text{W}}} + \frac{b_{\text{W}}b_{\text{X}}}{b_{\text{X}} + b_{\text{W}}}\delta_{\text{WX}} \quad (2)$$

where the first term represents a_{WX} and the second term is b_{WX} . Using a_{WX} , b_{WX} , a_{Y} , and b_{Y} to calculate the electronegativity as in any group composed of a divalent species and a univalent species, one obtains

$$\chi_{\text{WXY}} = \frac{a_{\text{WX}}b_{\text{Y}} + a_{\text{Y}}b_{\text{WX}}}{b_{\text{WX}} + b_{\text{Y}}} + \frac{b_{\text{WX}}b_{\text{Y}}}{b_{\text{WX}} + b_{\text{Y}}}\delta_{\text{WXY}} \quad (3)$$

Using the values of a_{WX} and b_{WX} obtained from eq 2 and substituting them into eq 3 yields eq 1 upon simplification. This indicates that the assumption of the behavior of multivalent groups is a valid one.

Multiple Bonds, σ - π Method. If one treats a double bond between atoms A and B under the assumption of electronegativity equalization, the following equations should hold

$$\chi_{\text{A}\sigma} = a_{\text{A}\sigma} + b_{\text{A}\sigma}\delta_{\text{A}} = \chi_{\text{B}\sigma} = a_{\text{B}\sigma} + b_{\text{B}\sigma}\delta_{\text{B}} \quad (4)$$

$$\chi_{\text{A}\pi} = a_{\text{A}\pi} + b_{\text{A}\pi}\delta_{\text{A}} = \chi_{\text{B}\pi} = a_{\text{B}\pi} + b_{\text{B}\pi}\delta_{\text{B}} \quad (5)$$

However, the values of the parameters a and b are such that in general eq 4 and 5 cannot both be satisfied by a single value of δ .

The partial charge residing in an orbital of an atom will affect the energies (and therefore the electronegativities) of the other orbitals of that atom.^{1,2a} In the case of a multiple bond, the σ and π orbitals link the same atoms and the values for δ in eq 4 and 5 must be the sum of all charges resulting from the polarity of σ and π bonds. This single value must satisfy the equation for both σ and π bonds. The fact that it may be mathematically impossible for it to do so reflects the fact that electronegativity equalization is

merely a convenient *approximation* as shown by Pritchard.⁴

Small deviations from electronegativity equalization can be expected as a result of the optimization of other energy terms, especially overlap. Actually, in the case of multiple bonds, we might expect the electronegativity equalization to be more nearly complete than in σ bonds alone because of the greater ability to adjust both charge transfer and overlap.

In order to test the ability to get consistent values for multiply bonded groups, two methods were used. One estimate (designated χ_{σ}) was made using σ values for all parameters and using the equations previously developed.⁵

The second method (designated χ_{π}) involves the use of the parameters a and b for π orbitals (Table I), derived from the work of Jaffé, *et al.*,^{2a} to calculate the polarity of the π system. Using the value of δ thus obtained, the electronegativity of the linking atom can now be calculated. The appropriate equations for these calculations are

$$\delta_{\text{A}} = \frac{a_{\text{B}\pi} - a_{\text{A}\pi}}{b_{\text{A}\pi} + b_{\text{B}\pi}} \quad (\text{for neutral group}) \quad (6)$$

$$\delta_{\text{A}} = \frac{a_{\text{B}\pi} - a_{\text{A}\pi} + b_{\text{B}\pi}}{b_{\text{A}\pi} + b_{\text{B}\pi}} \quad (\text{for cation}) \quad (7)$$

$$\chi_{\pi} = a_{\text{A}\sigma} + b_{\text{A}\sigma}\delta_{\text{A}} \quad (8)$$

The values of χ_{σ} and χ_{π} represent limiting values as estimated by use of parameters for σ and π systems. An average of these two values will probably be a fairly good estimate of the actual group electronegativity. Values of χ_{σ} and χ_{π} obtained by the above methods for three diatomic inorganic groups composed of elements from the second period are given in Table I. It

Table I: π Electronegativities

Element	Hybridization ^a	a^b	b^b
C	tr ¹ tr ¹ tr ¹ π^1	5.64	11.09
	di ¹ di ¹ π^1 π^1	5.60	11.13
N	tr ² tr ¹ tr ¹ π^1	7.95	12.34
	di ² di ¹ π^1 π^1	7.92	12.54
O	tr ² tr ² tr ¹ π^1	10.08	15.23
S	tr ² tr ² tr ¹ π^1	7.73	9.94

^a tr = sp², trigonal; di = sp, digonal. ^b Units are volts per electron corresponding to the Mulliken scale.

(3) R. S. Mulliken, *J. Chem. Phys.*, **2**, 782 (1934).

(4) H. P. Pritchard, *J. Am. Chem. Soc.*, **85**, 1876 (1963).

(5) The values of a and b for σ bonds are given in Table I of ref 1.

Table II: Comparison of Electronegativities Calculated by σ - π and Bent-Bond Methods

Group	Bcnd angle, deg	Valence ^a state	χ_{σ}		χ_{π}		χ	
			a	b	a	b	a	b
>C=O	120	trtrtr π	12.24	7.98	11.10	7.90	11.67	7.94
	120	trtrBB					11.73	7.95
	125.3	tetedi π	12.82	7.59	11.73	7.46	12.09	7.50
	125.3	tetetete					12.03	7.44
-N=O	120	trtrtr π	14.74	8.56	14.06	8.53	14.41	8.55
	120	trtrBB					14.49	8.56
	125.3	tetedi π	13.93	8.38	12.72	8.26	13.32	8.32
	125.3	tetetete					13.20	8.17
-C \equiv N	180	didi $\pi\pi$	12.82	7.59	11.73	7.46	12.09	7.59
	180	diBBB					12.03	7.44
	180	teS $\pi\pi$	10.22	6.98	9.25	7.04	9.57	7.02
	180	tetetete					9.66	6.98

^a te = tetrahedral, sp³; tr = trigonal, sp²; di = digonal, sp; B = 16.7% s-character for bent bond formation; S = 75% s-character.

appears that the values obtained by the two methods do not differ appreciably and that the average should approximate the group electronegativity fairly well.

Multiple Bonds, Bent Bond Method. Although it is customary to treat multiple bonds in terms of σ and π bonds, Pauling⁶ has suggested that they may be considered as bent bonds arising from the overlap of tetrahedral orbitals. Group electronegativities may be readily calculated assuming tetrahedral orbitals throughout. The results are given in Table II. In every case, these calculations yield electronegativities lower than those obtained by the previous method, but this is not unexpected since tetrahedral orbitals are less electronegative than orbitals containing more s-character.^{2a} To obtain valid comparisons, the same hybridization must be used. To do so results in unusual hybrids. For example, a bent bond description of the carbonyl group in which all bond angles are 120° (for comparison with the usual tr, tr, tr, π treatment) must utilize two trigonal orbitals for the substituents and two equivalent orbitals containing 16.7% s-character each for the bent multiple bonds. If the oxygen is hybridized in a similar manner (this will probably result in maximum overlap since the angle between the multiple-bonding orbitals will be the same in both atoms) the resultant calculated electronegativity is practically identical with that obtained by the σ - π treatment. Comparative values for carbonyl group and nitrosyl group, bonding through either trigonal or tetrahedral orbitals, are given in Table II. The values are comparable for either method and if one knows the bond angles involved, the appropriate hybridization may be employed.

The cyanide group is more difficult because no hint concerning the appropriate hybridization may be ob-

tained from the bond angles, all probable methods yielding 180°. The σ - π method predicts hybridization of di, di, π , π to a first approximation, whereas a simple bent-bond model may predict te, te, te, te, which gives quite different results as a result of the higher electronegativity of digonally hybridized atoms. Pauling⁷ has suggested the use of nontetrahedral orbitals in a bent-bond treatment of the nitrogen molecule. If the carbon and nitrogen of the cyanide group are assumed to be hybridized with 16.7% s-character in three orbitals forming bent bonds and 50% s-character in the remaining orbital, the result is very similar to that obtained by the σ - π method (*cf.* Table II).

Multiple Bonds Involving Elements of the Third Period. Difficulties are encountered in calculating the electronegativities of groups containing silicon, phosphorus, sulfur, and similar atoms because of the unavailability of data on *d* orbitals for these elements.^{2a} A further difficulty arises because multiple bonds such as those in the phosphoryl and sulfuryl groups are usually considered as a dative σ bond of a lone pair on the phosphorus (or sulfur) into an empty orbital of the oxygen and p_x - $d\pi$ backbonding from the oxygen to phosphorus (or sulfur). This can be symbolized as: (P = te²d⁰) + (O = tr⁰p²). This is certainly a useful point of view, but because of the difficulties attending the treatment of dative bonds, these bonds are here treated as two "normal" covalent bonds: (P = te¹d¹) + (O = tr¹p¹). Since the difference is merely a formalism, the results should be the same. In the absence of data

(6) L. Pauling, "The Nature of the Chemical Bond," 3rd ed, Cornell University Press, Ithaca, N. Y., 1960.

(7) L. Pauling, *Tetrahedron*, 17, 229 (1962).

on the electronegativity of d orbitals, it is impossible to calculate the polarity of the π system and to compute χ_π as above. However, since estimates of the electronegativities of these groups are highly desirable, estimates derived from χ_σ alone have been calculated. The assumption has been made that d_π - p_π systems will behave in a manner similar to that of p_π - p_π systems. Values given below for all groups containing an atom in the third period or greater should therefore be treated with some skepticism until further evidence can be gathered as to their validity.

Unsaturated Organic Systems. Systems composed of $-\text{CH}=\text{}$ units may be treated quite easily. The electronegativity of the trigonally hybridized $-\text{CH}=\text{}$ unit may be used to calculate the electronegativity of any system, $(-\text{CH}=\text{})_n$, by the equation

$$\chi = a_{\text{CH}} + \frac{b_{\text{CH}}}{n} \quad (9)$$

These methods may be readily extended to aromatic systems and to acetylenes.

Results and Discussion

Values for the electronegativities of various substituted inorganic, carbonyl, phenyl, vinyl, and acetylene groups are given in Table III. Comparison of these values with previous estimates indicates that the present values tend to be higher, especially for the more electronegative groups. There are probably two reasons for this. First, there seems to have been an inhibition against assigning values as high as 3.5–4.0 (the electronegativities of oxygen and fluorine) to groups composed largely of the less electronegative elements carbon, nitrogen, hydrogen, etc. However, this ignores the fact that the elements in these groups are often hybridized with a high per cent of s -character (sp^2 and sp) with a resultant increase in electronegativity.⁸ Secondly, the assumption of perfect electronegativity equalization gives equal "weight" to all atoms in the group. In reality, the electronegativity of a group always is influenced most by the atom which links the group to the remainder of the molecule. This explains the high values of such groups as cyanide, carboxyl, nitro, and thiocyanate. Supporting this viewpoint is the value of the acetoxy group which is lower (2.95) than a previous, experimentally obtained estimate (3.6). In this case the very low values of a and b of the methyl group reverse the situation described above and cause the group to have an unusually low calculated electronegativity.

A further example of this phenomenon is a comparison of the acetoxy and the carbomethoxy groups.

Since these two groups contain the same atoms in the same valence states, the present simplified procedure yields the same value, 2.95, for both groups. In contrast, the data of Allred and Rochow⁹ (chemical shifts of methyl hydrogens) may be used to obtain estimates of 3.52 and 2.54, respectively.

Values obtained for the charges in a pyridine π system obtained by Pritchard⁴ by a self-consistent molecular orbital method differ from those predicted by the assumption of electronegativity equalization by approximately 30%. Such deviations from 100% equalization will result in attenuation of polar effects. This problem is currently under study with a view toward compensating for this error.

The values for the organic groups are probably somewhat better than those of the more polar groups since the atoms which comprise the groups do not differ so much from one another in electronegativity. It should be pointed out that all values for aromatic groups are calculated solely on the basis of σ bonds between the group and substrate and do not include conjugative effects.

The extension of previous methods to multiply bonded groups is especially useful because few values are available for these groups. However, this very fact presents a difficulty in testing the validity of the results. In addition to values obtained from nmr data,⁹ there are a few data in the literature obtained from infrared¹⁰ or thermodynamic¹¹ data. These are listed in Table III for comparison.

The polar substituent constant, σ^* , has proved to be extremely useful in treating quantitatively polar effects in organic reactions. Group electronegativities reported here and previously¹ are found¹² to be consistent with previously reported¹³ values of σ^* if adjustments are made for imperfect equalization of electronegativity.

In addition to literature values, electronegativities calculated by the methods of Clifford¹⁴ and Sanderson^{2e} are given in Table III. It should be noted that

(8) This situation is not unique to π systems. The σ -bonded groups OH, OF, OCl, and OBr exhibit unexpectedly high electronegativities as a result of the large s -character of the oxygen (1).

(9) A. L. Allred and E. G. Rochow, unpublished results; doctoral dissertation, Harvard University, 1956.

(10) (a) J. K. Wilmshurst, *J. Chem. Phys.*, **26**, 425 (1957); (b) J. K. Wilmshurst, *ibid.*, **27**, 1129 (1957); (c) J. K. Wilmshurst, *ibid.*, **28**, 733 (1957); (d) J. K. Wilmshurst, *Can. J. Chem.*, **35**, 937 (1957).

(11) D. H. McDaniel and A. Yingst, *J. Am. Chem. Soc.*, **86**, 1334 (1964).

(12) J. E. Huheey, *J. Org. Chem.*, **31**, 2365 (1966).

(13) R. W. Taft in M. S. Newman, "Steric Effects in Organic Chemistry," John Wiley and Sons, Inc., New York, N. Y., 1956.

(14) A. F. Clifford, *J. Phys. Chem.*, **63**, 1227 (1959).

Table III^c

Group	Hybridization*	a	b	xP	xc ^b	xs ^b	Lit. values
Inorganic groups							
CN	di	12.06	7.47	3.84	4.17	4.08	3.11, ^c 3.22 ^d 3.27, ^e 3.3 ^f 3.17, ^g 2.50 ^h
CO	tr	11.70	7.94	3.72	4.14	3.90	2.78 ^e
C(O)H	tr	9.97	4.97	3.14			2.59 ^h
C(O)CH ₃	tr	8.63	2.30	2.69			} 2.97, ^c 2.88 ^e 2.84, ^g 3.50 ^h
C(O)OH	tr ⁱ	11.09	3.87	3.52			
	tr ^j	10.92	3.85	3.46			2.54 ^h
C(O)OCH ₃	tr	9.38	2.04	2.94			2.98, ^{c,d} 2.81 ^e
C(O)O	k	12.86	5.56	4.11			2.92 ^g
OC(O)O	k	13.49	4.28	4.33			3.60 ^h
OC(O)H	k	11.16	3.92	3.54			3.58 ^e
OC(O)CH ₃	k	9.40	2.05	2.95			3.6, ^f 3.52 ^h
OC(O)OCH ₃	k	10.02	1.84	3.17			
N ₃	l	13.77	5.26	4.42	4.31	4.17	
NO	tr	14.45	8.56	4.65			
	te	13.26	8.24	4.25			
NO ₂	tr	14.98	5.91	4.83			} 3.2, ^f 3.45 ^e 3.92 ^h
	te	13.83	5.65	4.33			
ONO	te	14.80	6.02	4.43			3.7 ^f
ONO ₂	te	14.24	4.33	4.58			
NCO	m	13.90	5.38	4.46			
OCN	n	14.50	5.91	4.66			
NCS	o	13.04	4.38	4.17			
SCN	p	12.27	4.29	3.91			3.1 ^f
PO	te, tr	11.94	7.12	3.8	4.2	3.9	
CH ₃ PO	te	9.95	2.23	3.1			
C ₆ H ₅ PO	te	8.60	1.03	2.7			
FPO	te	12.01	5.05	3.8			
ClPO	te	10.90	4.37	3.1			
BrPO	te	10.41	4.05	3.3			
(CH ₃) ₂ PO	te	8.22	1.32	2.6			
(C ₆ H ₅) ₂ PO	te	8.33	0.55	2.6			
F ₂ PO	te	12.05	3.91	3.8			
Cl ₂ PO	te	10.52	3.15	3.3			
Br ₂ PO	te	9.80	2.83	3.1			
HOPO	te	11.51	3.64	3.7			
(HO) ₂ PO	te	11.37	2.44	3.6			
PO ₄	te	13.72	3.28	4.5			
SO	te	12.63	6.88	4.0			
CH ₃ SO	te	9.05	2.20	2.8			
C ₆ H ₅ SO	te	8.75	1.03	2.7			
ClSO	te	11.40	4.27	3.6			
SO ₂	te	13.80	5.06	4.4			
CH ₃ SO ₂	te	9.88	1.97	3.1			
C ₆ H ₅ SO ₂	te	9.14	0.98	2.9			
HOSO ₂	te	12.70	3.01	4.1			
HSO ₄	te	12.88	2.59	4.1			
SO ₄	te	14.32	3.26	4.6			3.7, ^f 3.70 ^h
OCl	te ^q	13.69	4.96	4.4			
OCIO	te ^r	14.39	3.94	4.6			
OCIO ₂	te ^r	14.84	3.26	4.8			
OCIO ₃	te ^r	15.16	2.78	4.9			
Substituted phenyl groups							
C ₆ H ₅	tr	8.03	1.21	2.49			3.18, ^c 3.01, ^e 3.13 ^g

Table III (continued)

Group	Hybridization*	<i>a</i>	<i>b</i>	χ_P	χ_C^b	χ_S^b	Lit. values
Substituted phenyl groups							
CH ₃ C ₆ H ₄	tr	7.89	0.94	2.44			
(CH ₃) ₂ C ₆ H ₃	tr	7.82	0.77	2.42			
(CH ₃) ₃ C ₆ H ₂	tr	7.76	0.66	2.40			
(CH ₃) ₄ C ₆ H	tr	7.72	0.57	2.38			
(CH ₃) ₅ C ₆	tr	7.68	0.51	2.37			
FC ₆ H ₄	tr	8.41	1.24	2.55			
F ₂ C ₆ H ₃	tr	8.81	1.27	2.75			
F ₃ C ₆ H ₂	tr	9.23	1.30	2.89			
ClC ₆ H ₄	tr	8.25	1.19	2.56			
Cl ₂ C ₆ H ₃	tr	8.47	1.18	2.64			
Cl ₃ C ₆ H ₂	tr	8.68	1.16	2.71			
BrC ₆ H ₄	tr	8.15	1.17	2.53			
Br ₂ C ₆ H ₃	tr	8.27	1.13	2.57			
Br ₃ C ₆ H ₂	tr	8.38	1.09	2.61			
IC ₆ H ₄	tr	8.12	1.17	2.52			
I ₂ C ₆ H ₃	tr	8.20	1.12	2.55			
I ₃ C ₆ H ₂	tr	8.27	1.08	2.57			
O ₂ NC ₆ H ₄	tr	9.49	1.07	2.98			
(O ₂ N) ₂ C ₆ H ₃	tr	10.63	0.96	3.36			
(O ₂ N) ₃ C ₆ H ₂	tr	11.57	0.87	3.68			
C ₆ H ₆ O	^a	8.50	1.13	2.68			
Vinyl groups							
CH ₂ =CH	tr	7.79	2.63	2.41			3.12, ^c 2.97, ^a 3.08 ^d
CH ₂ =CH—CH ₂	te	7.66	1.64	2.37			
CH ₃ —CH=CH	tr	7.66	1.64	2.37			
C ₆ H ₅ CH=CH	tr	8.01	0.89	2.48			
CH ₃ C ₆ H ₄ CH=CH	tr	7.90	0.55	2.45			
(CH ₃) ₂ C ₆ H ₃ CH=CH—	tr	7.84	0.62	2.43			
(CH ₃) ₃ C ₆ H ₂ CH=CH—	tr	7.79	0.73	2.41			
(CH ₃) ₄ C ₆ HCH=CH—	tr	7.75	0.49	2.40			
(CH ₃) ₅ C ₆ CH=CH—	tr	7.71	0.44	2.38			
O ₂ NC ₆ H ₄ CH=CH	tr	9.11	0.69	2.85			
(O ₂ N) ₂ C ₆ H ₃ CH=CH—	tr	10.02	0.74	3.16			
(O ₂ N) ₃ C ₆ H ₂ CH=CH—	tr	10.82	0.81	3.56			
ClC ₆ H ₄ CH=CH—	tr	8.17	0.88	2.54			
Cl ₂ C ₆ H ₃ CH=CH—	tr	8.33	0.87	2.59			
Cl ₃ C ₆ H ₂ CH=CH—	tr	8.50	0.86	2.65			
Acetylene groups							
H—C≡C—	di	9.25	4.55	2.90			3.15, ^c 3.29 ^d
CH ₃ C≡C—	di	8.32	2.23	2.59			
C ₆ H ₅ C≡C—	di	8.38	1.03	2.61			
O ₂ NC ₆ H ₄ C≡C—	di	9.61	0.93	3.02			
(O ₂ N) ₂ C ₆ H ₃ C≡C—	di	10.60	0.84	3.35			
(O ₂ N) ₃ C ₆ H ₂ C≡C—	di	11.44	0.77	3.64			
CH ₃ C ₆ H ₄ C≡C—	di	8.18	0.83	2.57			
(CH ₃) ₂ C ₆ H ₃ C≡C—	di	8.07	0.69	2.50			
(CH ₃) ₃ C ₆ H ₂ C≡C—	di	7.99	0.60	2.48			
(CH ₃) ₄ C ₆ HC≡C—	di	7.92	0.53	2.45			
(CH ₃) ₅ C ₆ C≡C—	di	7.86	0.48	2.43			
ClC ₆ H ₄ C≡C—	di	8.56	1.02	2.67			

^a (Columns *a* and *b* list the inherent electronegativity and the charge coefficient in Mulliken units (volts per electron). The inherent electronegativity is given in Pauling units in the column headed χ_P . All hybridizations other than di, tr, and te, are based on bond angle values from L. E. Sutton, "Tables of Interatomic Distances and Configuration in Molecules and Ions," The Chemical Society, London, 1958, and computed by the method given by C. A. Coulson, "Valence," Oxford, England, 1952, p 193.) The asterisk, *, refers to the hybridization of the linking atoms unless otherwise noted. ^b Computed by the methods of Clifford¹⁴ and Sanderson,^{2a}

Table III (continued)

using appropriate valence state electronegativities of Jaffé.^{1a} ^c See ref 10a. ^d See ref 10d. ^e See ref 10c. ^f See ref 11. ^g See ref 10b. ^h See ref 9. ⁱ Hydroxyl oxygen hybridized 25% s-character. ^j Hydroxyl oxygen hybridized 20% s-character. ^k The linking oxygen atom is assumed to have 26.8% s-character corresponding to 111.5° bond angle, the average of values given by Sutton. ^l The nitrogen atoms are assumed to be hybridized tr, di, and tr, respectively. ^m Linked through the nitrogen; assumed to be hybridized tr, di, di. ⁿ Linked through the oxygen; assumed to be hybridized tr, di, di. ^o Linked through the nitrogen; assumed to be hybridized tr, di, di. ^p Linked through the sulfur; assumed to be hybridized tr, di, di. ^q Linked through the oxygen; both atoms assumed to be hybridized te. ^r Linked through the oxygen which is assumed to be hybridized te; all other oxygen atoms assumed to be hybridized tr.

in order to get comparable values by these methods, it is necessary to use the correct valence state atomic electronegativities^{1a} rather than the "average" values usually used.

Acknowledgment. The author wishes to thank Dr. H. H. Jaffé for suggesting the desirability of investigating the bent-bond treatment. Drs. W. D. Hobey and S. O. Grim offered helpful criticisms of the work.

The Pulse Radiolysis of Deaerated Aqueous Bromide Solutions¹

by M. S. Matheson, W. A. Mulac, J. L. Weeks, and J. Rabani²

Chemistry Division, Argonne National Laboratory, Argonne, Illinois 60439 (Received July 9, 1965)

The pulse radiolysis of deaerated aqueous KBr solutions in the pH range 5 to 9 yielded $k(\text{OH} + \text{Br}^-) = (1.2 \pm 0.15) \times 10^9 \text{ M}^{-1} \text{ sec}^{-1}$, $2k(\text{Br}_2^- + \text{Br}_2^-) = (3.3 \pm 1.0) \times 10^9 \text{ M}^{-1} \text{ sec}^{-1}$, and $k(\text{e}_{\text{aq}}^- + \text{Br}_2^-) = (1.3 \pm 0.5) \times 10^{10} \text{ M}^{-1} \text{ sec}^{-1}$. The value of $k(\text{OH} + \text{Br}^-)$ increases at low pH values and decreases markedly at high pH, indicating that the transition complex BrOH^- may react with H_3O^+ . The molar extinction coefficient of Br_2^- at 3650 Å is $7800 \pm 2000 \text{ M}^{-1} \text{ cm}^{-1}$. The $k(\text{OH} + \text{Br}^-)$ value has been compared with other rate constants for OH by means of rate constant ratios in the literature. Relative rate constants involving $k(\text{OH} + \text{Br}^-)$ must be used cautiously because of the pH sensitivity of this rate constant.

Introduction

A number of papers have been published concerning the steady radiolysis of aqueous bromide solutions. Hochanadel³ reported that a concentration of Br^- as low as 10^{-5} M was sufficient to protect H_2 from OH, indicating a high reactivity of OH radicals toward Br^- . The work of Linnenbom, *et al.*,⁴ showed that higher concentrations of Br^- were required to protect the H_2 as the pH was increased. Sworski⁵ interpreted the reduced yield of H_2O_2 obtained in aerated aqueous bromide solutions by a mechanism in which the "molec-

ular" yield of H_2O_2 is decreased by OH radicals reacting with Br^- in regions of high ionization density. On the other hand, over a wide range of concentrations Br^-

(1) Based on work performed under the auspices of the U. S. Atomic Energy Commission.

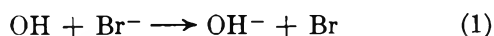
(2) The Hebrew University, Jerusalem, Israel.

(3) C. J. Hochanadel, *J. Phys. Chem.*, **56**, 587 (1952).

(4) V. J. Linnenbom, C. H. Cheek, and J. W. Swinnerton, *NRL Quarterly on Nuclear Science and Technology*, April 1962, p 46.

(5) T. J. Sworski, *J. Am. Chem. Soc.*, **76**, 4687 (1954).

does not affect the "molecular" yield of H_2 .^{3,6} Allen⁷ has pointed out that competitive scavenger studies yield values of the rate constant of (1) which disagree.



Results based on the competition of Br^- with ethanol⁸ and the comparison of ethanol with H_2O_2 through a series of competitions⁹ gave $k_1 = 1.35 \times 10^8 M^{-1} \text{sec}^{-1}$, while results based on direct competition of Br^- with H_2O_2 gave a value tenfold higher. In this paper, k_1 has been measured by the pulse radiolysis technique in order to resolve this discrepancy. Evidence concerning the mechanism of reaction 1 also has been obtained.

Experimental Section

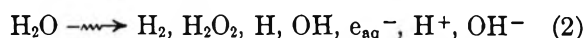
The experimental procedure has been described in a previous paper¹⁰ and the references cited therein. In the present work an 80-cm optical path length was used in the multiple reflection cell. The Br_2^- formation and decay were followed at 3650 Å using a 450-w xenon lamp and a Bausch and Lomb monochromator (Catalog No. 33-86-01). A Pyrex filter (no light below 2800 Å) between the light source and reaction cell minimized photochemical effects. The electron pulse of 0.4 μsec gave a dose of $\sim 1.1 \times 10^{19} \text{ev l.}^{-1}$ in most of the experiments. This dose was estimated in N_2O -free solutions by fitting experimental optical density vs. time curves with the aid of an IBM 1620 computer and assuming the molecular extinction coefficient of Br_2^- determined elsewhere in this paper.

Two sources of KBr were used: a KBr single crystal from Harshaw Chemical Co. and Mallinckrodt analytical reagent KBr. Both gave similar results. The KBr solutions were prepared and stored as argon-saturated (air-free) solutions using the syringe technique. Microsyringes fitted with drawn Kel-F capillary tubing were used for dilutions. All solutions were irradiated air-free at $\sim 23^\circ$ with special care to avoid air contamination.

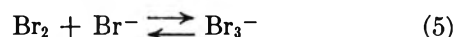
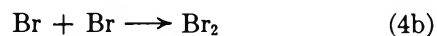
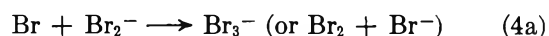
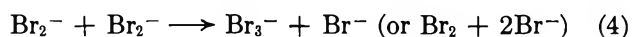
In some experiments the solutions to be irradiated were saturated with N_2O in order to convert e_{aq}^- to OH. Since, particularly in strongly alkaline solutions, small amounts of O_2 could scavenge $OH(O^-)$, the N_2O was passed through three separate gas bubblers containing pyrogallol-NaOH solution, then through aqueous NaOH and finally was condensed in a trap surrounded with liquid nitrogen. The trapped N_2O was then warmed, and the gas which boiled off was used to saturate the previously evacuated solutions. Less than 0.03% O_2 was found by mass spectrometric analysis in the gas samples taken from the N_2O -saturated solutions.

Results

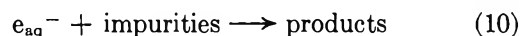
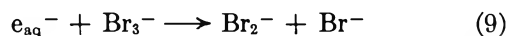
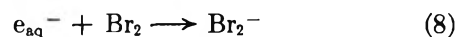
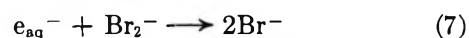
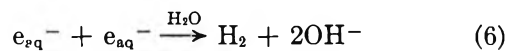
Pulse Radiolysis Mechanism in Aqueous Br^- Solutions. Grossweiner and Matheson¹¹ showed that the transient absorption bands near 3500 Å observed in the flash photolysis of deaerated aqueous solutions of halides (X^-) could be attributed to X_2^- (λ_{max} 3500 Å for Br_2^-). More recently, the Br_2^- absorption has been observed in the pulse radiolysis of deaerated¹² and aerated¹³ aqueous bromide solutions. A probable mechanism for the formation of Br_2^- in neutral solutions would consist of process 2 followed by reactions 1 and 3. By analogy with the I_2^- case,¹¹ the Br_2^-



ions would disappear as a result of reactions 4, 4a, and 4b, the 3 plus 3a equilibrium being maintained.



At the concentrations of Br^- used, all OH radicals will disappear by reaction 1. However, since e_{aq}^- and H may react to some extent with Br_2^- , Br_2 , and Br_3^- , reactions of these two species must be included.



(6) H. Fricke and E. J. Hart, *J. Chem. Phys.*, **3**, 596 (1935).

(7) A. O. Allen, *Radiation Res. Suppl.*, **4**, 54 (1964).

(8) A. Hummel and A. O. Allen, *Radiation Res.*, **17**, 302 (1962).

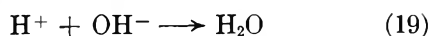
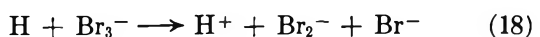
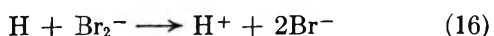
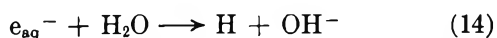
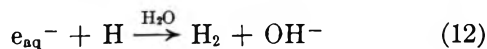
(9) J. Rabani and G. Stein, *Trans. Faraday Soc.*, **58**, 2150 (1962).

(10) J. Rabani, W. A. Mulac, and M. S. Matheson, *J. Phys. Chem.*, **69**, 53 (1965).

(11) L. I. Grossweiner and M. S. Matheson, *ibid.*, **61**, 1089 (1957).

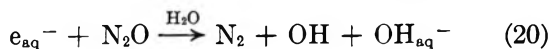
(12) L. M. Dorfman, I. A. Taub, and R. E. Bühler, *J. Chem. Phys.*, **36**, 3051 (1962).

(13) (a) B. Cercek, M. Ebert, J. P. Keene, and A. J. Swallow, *Science*, **145**, 919 (1964); (b) B. Cercek, M. Ebert, C. W. Gilbert, and A. J. Swallow, "Pulse Radiolysis," Pergamon Press, Inc., New York, N. Y., 1965, p 83; (c) H. C. Sutton, G. E. Adams, J. W. Boag, and B. D. Michael, *ibid.*, p 61. References 13b and c appeared after the present paper was submitted.



As will be seen, our experiments determining the extinction coefficient of Br_2^- indicate that under our conditions the steady state in (3) and (3a) greatly favors Br_2^- , so that (4a) and (4b) are not important and reactions of e_{aq}^- and H with Br have been omitted.

The above mechanism was assumed in the absence of N_2O . In N_2O -saturated solutions, reaction 20 occurs,¹⁴ suppressing reactions 6 to 14 inclusive, and



approximately doubling the initial yield of OH. N_2O reacts slowly with H atoms¹⁵ and may possibly affect reactions 15 to 18 inclusive. Since the H atom yield is



only about one-tenth the OH or Br_2^- yield in the presence of N_2O , and since only part of the H atoms will react in (21), the error introduced into $2k_4$ will be very small in neglecting (21).

The Change in Optical Density at 3650 Å with Time. In a typical N_2O -free experiment ($[\text{Br}^-] = 1.71 \times 10^{-4} M$), it was found that there is a small absorption, D , at the end of the electron pulse, and that the absorption increases to a maximum, D_{max} , and then decays away to zero. The formation and decay are not well separated in the time scales (Figure 1). The absorption at the end of the pulse is attributed to e_{aq}^- plus Br_2^- formed during the pulse with Br_2^- having a molar extinction coefficient at 3650 Å more than fivefold that of e_{aq}^- . The increase in optical density, D , is ascribed to (1) and (3), and the following decay principally at first to (7) and finally to (4). The final products do not absorb appreciably at 3650 Å.

When N_2O or H_3O^+ are present, e_{aq}^- is eliminated. The formation of the absorbing species becomes well separated in time from the decay. Again, the formation of Br by oxidation of Br^- , followed by reaction 3, is responsible for the increase. Since reaction 7 is eliminated, the decay is relatively slow.

The Molar Extinction Coefficient of Br_2^- (no N_2O).

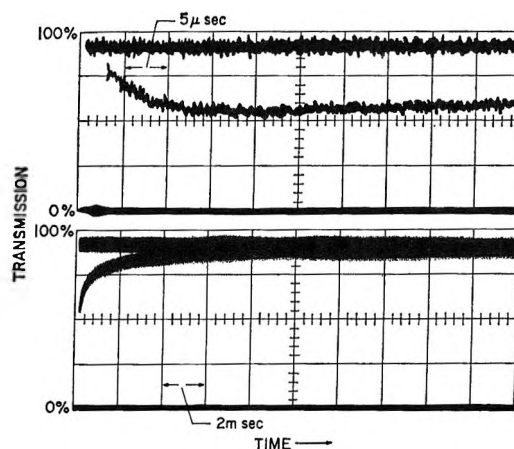


Figure 1. Oscilloscope traces showing the increase and decay of D^{3650} in $1.71 \times 10^{-4} M$ KBr: neutral aqueous solution, electron pulse delayed 2.5 μsec from beginning of trace.

The extinction coefficient of e_{aq}^- at 3650 Å has previously been determined,¹⁰ as $\epsilon_e^{3650} \approx 1400 M^{-1} \text{cm}^{-1}$. Two methods were used to estimate $\epsilon_{\text{Br}_2^-}^{3650}$, and both gave $7800 \pm 2000 M^{-1} \text{cm}^{-1}$. (1) The initial optical density at 5780 Å, D_0^{5780} , was measured for pulse-irradiated $1.71 \times 10^{-4} M$ KBr. The absorption at 5780 Å is due to e_{aq}^- only ($\epsilon_e^{5780} = 10,600 (\pm 10\%) M^{-1} \text{cm}^{-1}$).¹⁰ Then, using an equal electron pulse intensity, D_0^{3650} was measured in a solution of $1.62 \times 10^{-2} M$ KBr + $4 \times 10^{-3} M$ H_2O_2 . In this case the absorption at 3650 Å was due only to Br_2^- . The initial $[\text{Br}_2^-]$ was twice the initial $[e_{\text{aq}}^-]$ of the previous irradiation, assuming $G_e = G_{\text{OH}}$, since H_2O_2 converts e_{aq}^- to OH. Actually, the scavenging of OH by Br^- in "spurs"¹⁵ could increase initial $[\text{Br}_2^-]$ to ~ 2.16 times the initial $[e_{\text{aq}}^-]$, but this possibility was ignored. (2) The maximum D^{3650} in a pulse-irradiated $4 \times 10^{-4} M$ KBr solution was compared to D_0^{5780} in the same experiment. D_{max}^{3650} , which was due to absorption by Br_2^- and e_{aq}^- , was corrected for the small amounts of these species which reacted before the maximum was attained. Again D_0^{5780} was due only to e_{aq}^- absorption, and $G_e = G_{\text{OH}}$ was assumed.

The agreement in $\epsilon_{\text{Br}_2^-}^{3650}$ for these two experiments shows that practically all Br is tied up as Br_2^- , both at 1.62×10^{-2} and at $4 \times 10^{-4} M$ $[\text{Br}^-]$; otherwise the apparent $\epsilon_{\text{Br}_2^-}^{3650}$ would have been much lower for the low Br^- concentration than for the high. Our value of $\epsilon_{\text{Br}_2^-}^{3650} = 7800 \pm 2000 M^{-1} \text{cm}^{-1}$ observed in deaerated solutions agrees within experimental error with values obtained in aerated solutions, $\epsilon_{\text{Br}_2^-}^{3650} =$

(14) F. S. Dainton and D. B. Peterson, *Nature*, **186**, 878 (1960); *Proc. Roy. Soc. (London)*, **A267**, 443 (1962).

(15) F. S. Dainton and S. R. Logan, *Trans. Faraday Soc.*, **61**, 715 (1965).

$9600 \pm 800 M^{-1} \text{ cm}^{-1}$ by Cercek, *et al.*,^{13b} and $\epsilon_{\text{Br}_2^-}^{3600} = 8200$ by Sutton, *et al.*^{13c} This latter value was obtained by comparing the optical density of a neutral oxygenated solution of KBr and that of a neutral $\text{K}_4\text{Fe}(\text{CN})_6$ solution, both having been irradiated with equal pulses. Since the extinction coefficient of $\text{Fe}(\text{CN})_6^{4-}$ is known to a few per cent, the $\epsilon_{\text{Br}_2^-}^{3600}$ of Sutton, *et al.*, is probably the best value. The 9600 value depends upon the assumption of a high value for G_{OH} in 0.1 M KBr.

The Rate Constant ($2k_4$) for $\text{Br}_2^- + \text{Br}_2^-$ (no N_2O). The decay of Br_2^- , if due to reaction 4, should give a straight line plot of $1/D$ vs. time as expected for second-order reactions.¹¹ In Figure 2, $1/D$ vs. t is plotted for experiments with three different Br^- concentrations. After an initial curvature, straight lines are obtained with slopes (slope = $2k_4/\epsilon_{\text{Br}_2^-}^{3650}l$, where $l = 80$ cm) independent of $[\text{Br}^-]$. A salt effect would make k_4 somewhat higher at higher ionic strength, *i.e.*, higher KBr concentration. Possibly (4a) is faster than (4) and a small amount of (4a) occurs at the lower Br^- concentrations. The initial rapid decay is due to reactions of e_{aq}^- , especially (7). There is continued curvature after the disappearance of e_{aq}^- , and this is due to reactions of H atoms with Br_2^- , the H atoms having longer lifetimes than e_{aq}^- in these experiments. In Table I are listed values of $2k_4$ obtained from curves such as those in Figure 2, each value being the average of two or three experiments. Our average for $2k_4 = (3.3 \pm 1.0) \times 10^9 M^{-1} \text{ sec}^{-1}$ is in good agreement with recently published values^{13b,c} of $(3.6 \pm 0.6) \times 10^9$ and $(3.6 \pm 0.7) \times 10^9 M^{-1} \text{ sec}^{-1}$. For all experiments the pulse intensity was about $1.1 \times 10^{19} \text{ ev l}^{-1}$. The fact that k_4 is independent of $[\text{Br}^-]$ is further evidence that the equilibrium in (3) plus (3a) is displaced largely toward Br_2^- . In this we agree with Sutton, *et al.*,^{13c} but not with Cercek, *et al.*,^{13b} a point that will be discussed later. The rate constant for reaction of $\text{I}_2^- + \text{I}_2^-$ is 2.3-fold¹¹ that for $\text{Br}_2^- + \text{Br}_2^-$, which may indicate that the Br_2^- complex is more stable than the I_2^- .

The Rate Constant (k_7) for $e_{\text{aq}}^- + \text{Br}_2^-$ (no N_2O).

Table I: Rate Constant for $\text{Br}_2^- + \text{Br}_2^-$ ($2k_4$)

$[\text{Br}^-]$, $10^{-4} M$	$2k_4$, $10^9 M^{-1} \text{ sec}^{-1}$
1.20	3.0
1.71	4.2
2.21	3.2
4.60	3.2
106	3.0

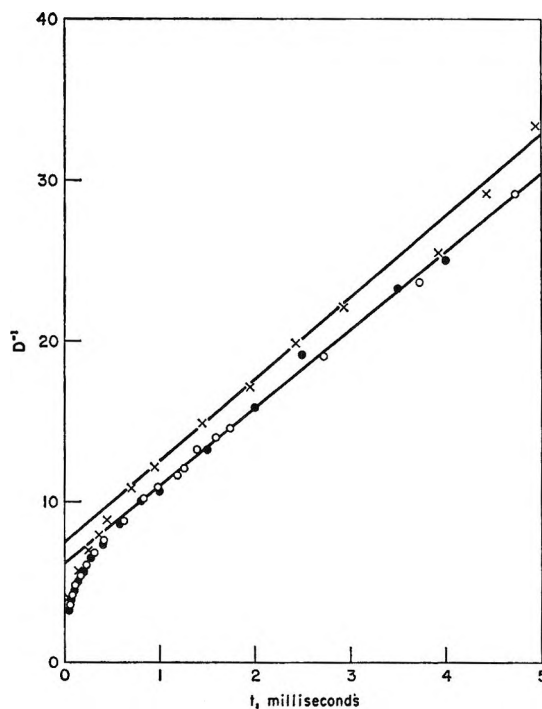


Figure 2. Decay at 3650 Å of optical density, D , vs. time, t , in neutral aqueous, N_2O -free Br^- solution: pulse intensity $\sim 1.1 \times 10^{19} \text{ ev/l}$. (slight variations between different experiments); optical path length 80 cm; \times , $1.20 \times 10^{-4} M$ KBr; \bullet , $4.60 \times 10^{-4} M$ KBr; \circ , $1.06 \times 10^{-2} M$ KBr.

At relatively high Br^- concentrations, Br_2^- forms rapidly and D_{max}^{3650} occurs near the end of the pulse. Under such conditions k_7 may be calculated since (7) is the most important reaction in the early decay of D . Many of the parallel reactions may be neglected. For fitting the $1/D$ vs. t curve by computer calculation, the same reactions were included as for the k_1 calculation (next section) plus (8) and (9). A value of $k_8 = k_9 = 1 \times 10^{10} M^{-1} \text{ sec}^{-1}$ was assumed, but (8) plus (9) is not important since (4) is so slow. The value obtained, $k_7 = 1.3 \times 10^{10} M^{-1} \text{ sec}^{-1}$, is not precise because there are many competing reactions.

The Rate Constant (k_1) for $\text{OH} + \text{Br}^-$ (in Neutral, N_2O -Free Solutions). If suitable concentrations of Br^- are used, the increase in D^{3650} can be conveniently followed after the electron pulse. The sequence of (1) followed by (3) is principally responsible for this increase. Since $k_3 \gg k_1$ in neutral solution (this point to be discussed later), reaction 1 is the rate-determining step in the formation of Br_2^- . Reactions 1, 4, 6, 7, 10-13, 16, and 19 were included in the computer calculations, the other reactions having a negligible effect. The rate constants k_4 and k_7 have been determined in this paper. Two rate constants were assumed: k_{16} was taken as $1 \times 10^{10} M^{-1} \text{ sec}^{-1}$ and has

little effect, while k_{10} was taken as $1.2 \times 10^4 \text{ sec}^{-1}$ because in earlier work using the same water purification such a value was found.¹⁶ The other k 's needed have been summarized elsewhere.¹⁶ The total correction on k_1 for all competing reactions does not exceed 20%, so that a precise value of k_1 is obtained in spite of the number of competing reactions. In Figure 3 a typical fit of a computer-calculated curve to experimental points is shown. From calculations such as those illustrated in Figure 3, the values in Table II were obtained.

Table II: Rate Constant for $\text{OH} + \text{Br}^-$ (k_1), Neutral Solution

$[\text{Br}^-]$, $10^{-4} M$	Dose, 10^{19} ev/l.	k_1 , $10^9 M^{-1} \text{ sec}^{-1}$
1.2	1.02	1.15
1.71	7.30	1.15
2.21	1.10	1.10
4.60	1.09	1.15

The Effect of pH on Br_2^- Formation and Decay (N_2O -Saturated). It is apparent that reaction 1 may be reversible at high pH and that it may be speeded up at high acid concentrations. To examine these possibilities, pulse radiolysis experiments of aqueous bromide solutions were carried out from pH 1.0 to 13.0. The experiments are summarized in Table III, and $(1/[\text{Br}^-])(d/dt)[\ln(D_{\text{max}} - D)]$ (which equals k_1 in neutral solutions) is plotted as a function of pH in Figure 4. Sutton^{13c} measured k_1 as 1×10^9 at neutral pH and as 5×10^9 at pH 2. These two points fall reasonably well on the curve of Figure 4. Two things are immediately evident from the curve. First, in neutral solution the value of $k_1 = 1.14 \times 10^9 M^{-1} \text{ sec}^{-1}$ in the absence of N_2O (Table II) is experimentally the same as that obtained, $1.30 \times 10^9 M^{-1} \text{ sec}^{-1}$, in the presence of N_2O (Table III), and the value of $2k_4$ is also experimentally the same in the absence of N_2O (Table I) and in the presence of N_2O (Table III). Second, the rate of formation of Br_2^- is faster in acid solution and slower in alkaline solution. Further, in the presence of N_2O , since, as indicated previously, most of the other reactions were eliminated, the formation of absorption and its decay were clearly separated in time.

The plots of $\ln(D_{\text{max}} - D)$ vs. time were always linear for growth of absorption. In Table III, $2k_4$ was obtained from plots of $1/D$ vs. t for decay of absorption. These plots were also linear except for the experiment at pH 11.08, which was calculated using

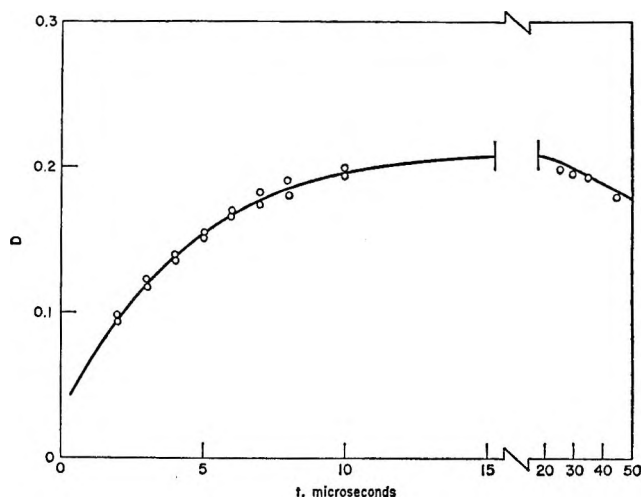


Figure 3. Change in optical density at 3650 Å with time: solid line, computer calculated curve; \circ , experimental points; $1.71 \times 10^{-4} M$ KBr; pulse, $0.4 \mu\text{sec}$, $1.82 \times 10^{26} \text{ ev l.}^{-1} \text{ sec}^{-1}$. Data for calculation: $G_{\text{H}^+} = G_{\text{OH}} = G_e = 2.6$, $G_{\text{H}} = 0.5$, $k_1 = 1.15 \times 10^9$, $k_4 = 1.8 \times 10^9$, $k_6 = 5 \times 10^9$, $k_7 = 1.3 \times 10^{10}$, $k_{11} = 1.2 \times 10^{10}$, $k_{12} = 2.5 \times 10^{10}$, $k_{13} = 2.2 \times 10^{10}$, $k_{16} = 1 \times 10^{10}$, $k_{19} = 1.4 \times 10^{11} M^{-1} \text{ sec}^{-1}$; $\tau_{1/2} = 58 \mu\text{sec}$ for (10) (pseudo-first-order).

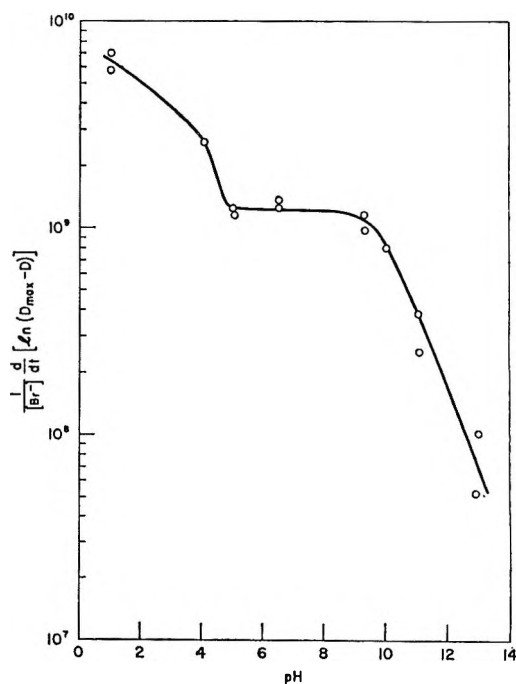


Figure 4. The pH dependence of the rate of formation of Br_2^- . In the pH range 5-9, $(1/[\text{Br}^-])(d/dt)[\ln(D_{\text{max}} - D)] = k(\text{OH} + \text{Br}^-)$. Data from Table III.

the initial slope. The identity of OH radical rate constants obtained in this system with and without N_2O

(16) M. S. Matheson and J. Rabani, *J. Phys. Chem.*, **69**, 1324 (1965).

Table III: Rates of Br_2^- Formation and Decay as a Function of pH^a

pH	$[\text{Br}^-]$, $10^{-4} M$	D_{max}	$\frac{1}{[\text{Br}^-]} \frac{d}{dt} [\ln (D_{\text{max}} - D)]$, $10^9 M^{-1} \text{sec}^{-1}$	$2k_4$, $10^9 M^{-1} \text{sec}^{-1}$
1.00	0.594	0.180	5.8	4.2
1.00	1.12	0.178	7.0	5.2
4.06	2.73	0.285	2.6	2.9
5.00	2.01	0.273	1.23	3.33
5.02	4.15	0.302	1.16	3.27
Neutral ^b	2.13	0.231	1.25	3.3
Neutral ^b	4.21	0.260	1.35	2.9
9.31	4.10	0.268	1.17	3.72
9.32	2.10	0.284	0.99	3.80
10.01	4.05	0.320	0.80	4.38
11.03	12.2	0.310	0.38	3.6
11.08	2.24	0.151	0.25	13
12.95	57.6	0.217	0.052	10
13.00	20.2	0.047	~0.1	~10

^a N_2O -saturated aqueous solutions of perchloric acid or 5% $\text{Ba}(\text{OH})_2 + 95\% \text{NaOH}$ were used. ^b Initial pH ~6.5 due to H^+ formed by pulse of radiation.

and the similar result obtained in the ferrocyanide system¹⁷ show that in our experiments if N_2O^- is an intermediate in (20) it behaves kinetically the same as OH does or else yields OH in less than 1 μsec .

It will be noted that $2k_4$ is faster in both strong acid and strong alkali. The increase at pH 1.0 may be due to the effect of ionic strength. More than just the effect of ionic strength appears to be involved at pH 11 and 13.

D_{max} is the maximum optical density attained after buildup of absorption and before appreciable decay (see Figure 3). D_{max} is a measure of pulse intensity, taking $l = 80 \text{ cm}$ and $\epsilon_{\text{Br}_2^-}^{3650} = 7800 M^{-1} \text{ cm}^{-1}$, except in strongly alkaline solutions, where reaction 1 is apparently incomplete especially at lower Br^- concentrations, and except at pH 1.0, where H^+ competes with N_2O for e_{aq}^- .

Discussion

The Value of k_1 . Our value of $k_1 = 1.20 (\pm 10\%) \times 10^9 M^{-1} \text{ sec}^{-1}$ in neutral solution agrees within experimental error with the value $k_1 = 1.35 \times 10^9$ estimated from competition of Br^- with H_2O_2 ⁷ taking $k(\text{OH} + \text{H}_2\text{O}_2)$ ¹⁸ as $4.5 \times 10^7 M^{-1} \text{ sec}^{-1}$. Our value does not agree with the tenfold lower value previously cited.⁷ In determining k_1 in neutral solutions, k_3 was ignored. This neglect is justified if $\exp(k_1 - k_3)t \ll 1$. In our experiments k_1 needs only a small correction (0 to 3% for the calculations made on our experiments)

if $k_3 \geq 6 \times 10^9 M^{-1} \text{ sec}^{-1}$. From Table III at pH 1.0 the average rate constant for formation of Br_2^- is 6.4×10^9 , which means that k_3 cannot be less than 6.4×10^9 and is probably $10^{10} M^{-1} \text{ sec}^{-1}$ or larger; therefore, negligible error is introduced by neglecting k_3 and setting $(1/[\text{Br}^-])(d/dt)[\ln(D_{\text{max}} - D)] = k_1$ in neutral solution. The value of k_1 is constant from pH 5 to pH 9.

Some Absolute Rate Constants for OH Radicals. Our value of $k_1 = 1.2 \times 10^9 M^{-1} \text{ sec}^{-1}$ plus $k(\text{OH} + \text{ferrocyanide})$ ¹⁹ = $1.07 \times 10^{10} M^{-1} \text{ sec}^{-1}$ and $k(\text{OH} + \text{H}_2\text{O}_2)$ ¹⁸ = $4.5 \times 10^7 M^{-1} \text{ sec}^{-1}$ were combined with rate constant ratios from the literature to determine whether a set of consistent OH rate constants could be obtained. The results are shown in Table IV.

Table IV: Rate Constants for Reaction of OH with Various Reactants

Reactant	Rate constant ^a	pH	Reference
Br^-	1.2 ^b	5-9	This work
	1.07	10	20
	0.95	9	21
	1.35	~7	7
	0.35	~7	7
$\text{Fe}(\text{CN})_6^{4-}$	10.7 ^b	3-10	19
	0.045	...	18
H_2O_2	1.4	10	20
	1.2	~7-10.5	9
$\text{C}_2\text{H}_5\text{OH}$	1.55	9	21
	2.0	~7	8
	1.1	7 and 10.7	22
	3.9	10	20
HCOO^-	2.7	4-10	9
	0.68	~2.5	9
HCOOH	0.13	0.4	24, 25
	4.3 ^b	~7	12
Benzene	3.3 ^b	3	23
	6.1	10	20

^a In units of $10^9 M^{-1} \text{ sec}^{-1}$. ^b Direct determination by pulse radiolysis.

At pH 10, Matthews and Sangster²⁰ found $k_1 = 1.07 \times 10^9$, $k(\text{OH} + \text{formate}) = 3.9 \times 10^9$, $k(\text{OH} + \text{ethanol}) = 1.4 \times 10^9$, and $k(\text{OH} + \text{benzene}) = 6.1 \times 10^9 M^{-1} \text{ sec}^{-1}$, all based on our value for $k(\text{OH} + \text{ferrocyanide})$.¹⁹ In Table IV it is seen that this k_1 agrees

(17) J. Rabani and M. S. Matheson, *J. Phys. Chem.*, **70**, 761 (1966).

(18) H. A. Schwarz, *ibid.*, **66**, 255 (1962).

(19) J. Rabani and M. S. Matheson, *J. Am. Chem. Soc.*, **86**, 3175 (1964).

(20) R. W. Matthews and D. F. Sangster, *J. Phys. Chem.*, **69**, 1938 (1965).

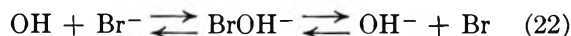
reasonably well with our result as well as does $k_1 = 0.95 \times 10^9$ estimated from the work of Kraljic and Trumbore²¹ (based on the k for ferrocyanide) and with Allen's value⁷ (based directly on Br^- competition with H_2O_2). The above value for ethanol agrees with rate constants based on $k(\text{OH} + \text{ferrocyanide})$ from Rabani and Stein,⁹ 1.2×10^9 , and from Kraljic and Trumbore,²¹ 1.55×10^9 , and is in fair agreement with results based on $k(\text{OH} + \text{Br}^-)$ from Hummel and Allen,⁸ 2.0×10^9 . Adams, *et al.*,²² using a competitive pulse-radiolytic method have measured $k(\text{OH} + \text{ethanol})$ as $1.1 \times 10^9 \text{ M}^{-1} \text{ sec}^{-1}$.

Dorfman, *et al.*,¹² reported a direct measurement from the pulse radiolysis of $k(\text{OH} + \text{benzene}) = 4.3 \times 10^9$, and later this value was revised²³ to $3.3 \times 10^9 \text{ M}^{-1} \text{ sec}^{-1}$. This latter value is about half the rate constant from Matthews and Sangster based on $k(\text{OH} + \text{ferrocyanide})$.

The rate constant for $\text{OH} + \text{formate}$, $2.7 \times 10^9 \text{ M}^{-1} \text{ sec}^{-1}$, from Rabani and Stein⁹ agrees reasonably well with the other values of Table IV, but other rate constants of these authors based on $k(\text{OH} + \text{H}_2\text{O}_2)$ are too low. (For example, note that the low value for k_1 in Table IV is based in part on Rabani and Stein's work.) They evaluated $k(\text{OH} + \text{HCO}_2^-)/k(\text{OH} + \text{HCO}_2\text{H})$ as 4. However, from Sworski,²⁴ $k(\text{OH} + \text{Ce}^{3+})/k(\text{OH} + \text{HCO}_2\text{H})$ is 1.70 in 0.8 *N* H_2SO_4 , and from Hochanadel and Boyle,²⁵ $k(\text{OH} + \text{Ce}^{3+})/k(\text{OH} + \text{H}_2)$ is 4.8, which yields $k(\text{OH} + \text{HCO}_2\text{H}) = 1.3 \times 10^9 \text{ M}^{-1} \text{ sec}^{-1}$, if $k(\text{OH} + \text{H}_2)$ ¹⁸ = $4.5 \times 10^7 \text{ M}^{-1} \text{ sec}^{-1}$. This rate constant for formic acid combined with the average of the two rate constants for formate in Table IV gives $k(\text{OH} + \text{HCO}_2^-)/k(\text{OH} + \text{HCOOH}) = 25$. Although this ratio is indirectly determined, it seems to be preferable to the directly determined ratio⁹ since it is consistent with other measurements of OH reactivity. The data of Hart²⁶ and of Weeks and Matheson²⁷ can be shown to be in agreement, if the new ratio is applied to their respective results. Except for the already discounted results in formate-formic acid, the intercomparison generally gives values consistent within a factor of 2, which is not bad considering that uncertainties in several different experiments are involved in combining directly measured k 's with ratios of k 's from competition studies. Further, in competition studies there is sometimes the possibility that one scavenger will react with OH to give an intermediate which can further react with the other scavenger.

The Effect of pH on $(1/[\text{Br}^-])(d/dt)[\ln(D_{\text{max}} - D)]$. As can be seen in Figure 4, $(1/[\text{Br}^-])(d/dt)[\ln(D_{\text{max}} - D)]$ is constant between about pH 5 and pH 9 (where it equals k_1) increases markedly below pH 5 and de-

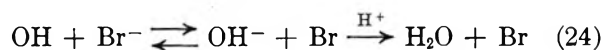
creases even more markedly above pH 9. These results are consistent with the equilibrium²⁸



The enhanced formation of Br_2^- at pH 4 and 1 as compared to neutral solutions is then due to the reaction



The removal of OH^- by H^+ , as in (24) cannot explain the constancy of $(1/[\text{Br}^-])(d/dt)[\ln(D_{\text{max}} - D)]$ between pH 5 and 9.



The effect of H^+ is, however, consistent with the existence of BrOH^- , and reaction 23 can account for the increase in $(1/[\text{Br}^-])(d/dt)[\ln(D_{\text{max}} - D)]$, if the lifetime of BrOH^- is long enough.

In alkaline solutions not only does the rate of Br_2^- formation decrease with increasing pH (Figure 4) but at pH 13 and at pH 11, with low Br^- the maximum yield of Br_2^- corresponding to $G_e + G_{\text{OH}}$, is not attained. This can be seen in the column entitled D_{max} in Table III since approximately equal pulse intensities were used in the experiments. Further, the yield is higher at pH 11 with higher $[\text{Br}^-]$, indicating that the scavenging of either Br and/or OH by Br^- helps to carry reaction 1 to completion.

These results are in agreement with the earlier observation of Linnenbom, Cheek, and Swinnerton,⁴ who suggested equilibrium 25 to account for their

(21) I. Kraljic and C. N. Trumbore, *J. Am. Chem. Soc.*, **87**, 2547 (1965).

(22) G. E. Adams, J. W. Boag, and B. D. Michael, *Trans. Faraday Soc.*, **61**, 1417 (1965).

(23) L. M. Dorfman, I. A. Taub, and D. A. Harter, *J. Chem. Phys.*, **41**, 2954 (1964).

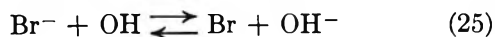
(24) T. J. Sworski, *J. Am. Chem. Soc.*, **78**, 1768 (1956).

(25) C. J. Hochanadel and J. W. Boyle, *Radiation Res.*, **9**, 129 (1958).

(26) E. J. Hart, *J. Am. Chem. Soc.*, **73**, 68 (1951).

(27) J. L. Weeks and M. S. Matheson, *ibid.*, **78**, 1273 (1956).

(28) It was suggested by one of the referees that our results could be satisfactorily explained by the "cage" mechanism (R. M. Noyes, *J. Am. Chem. Soc.*, **77**, 2042 (1955)). However, Noyes states that we cannot expect significant competition with geminate recombination unless a reactive scavenger is present at 0.01 *M* or greater. In Figure 4 it is seen that a significant effect is already observed at pH 4, *i.e.*, at a concentration of H^+ scavenger of only 10^{-4} *M*. Results of J. Jortner, M. Ottolenghi, and G. Stein, *J. Phys. Chem.*, **66**, 2029 (1962), would indicate that concentrations as low as 10^{-4} *M* could be effective in scavenging in the cage. More recently, F. S. Dainton and P. Fowles, *Proc. Roy. Soc. (London)*, **A287**, 312 (1965), have noted that there are some difficulties yet to be cleared up in applying the theory of the scavenging of geminate pairs to the work of Jortner, Ottolenghi, and Stein. The equilibrium in (22) seems to us the most likely explanation of the increase found at low pH in Figure 4.



alkaline Br^- results. The pH at which the decrease begins, and the apparent value of k_1 , will depend upon $[\text{Br}^-]$ through the effect of the scavenging reaction 3 on the equilibrium in (22).

If the equilibrium in (22) is assumed, the over-all rate of formation of Br in alkaline solutions (pH 9 to 11) is

$$d[\text{Br}]/dt = k_1[\text{OH}][\text{Br}^-] - k_{22b}[\text{OH}^-][\text{Br}] - k_3[\text{Br}][\text{Br}^-] \quad (26)$$

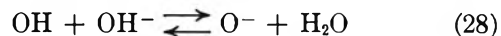
where k_1 is the value obtained in neutral solution. We have shown $k_3 > k_1$. Further, if k_1 (effective) increases several-fold in acid, because H^+ prevents the back dissociation of BrOH^- , then $k_{22b} > k_{22f} = k_1$. Since k_3 or $k_{22b} > k_1$, Br is in low concentration and the steady-state approximation may be applied.²⁹ It can then be shown that

$$\frac{k_1}{k_1(\text{effective})} - 1 = \frac{k_{22b}[\text{OH}^-]}{k_3[\text{Br}^-]} \quad (27)$$

This equation was applied to three experiments in Table III, those at pH 9.32, 10.01, and 11.03. These give 2.1, 2.0, and 2.5, respectively, for k_{22b}/k_3 . This calculated ratio must be viewed with reservations, however, since it is inherently assumed that $k(\text{H}^+ + \text{BrOH}^-)$ is large enough and the lifetime of BrOH^- long enough to give some scavenging of BrOH^- at $10^{-4}M \text{H}^+$, while at the same time $k(\text{OH}^- + \text{BrOH}^-)$

and $k(\text{Br}^- + \text{BrOH}^-)$ are smaller than $k(\text{H}^+ + \text{BrOH}^-)$ and the lifetime of BrOH^- is short enough so that OH^- or Br^- do not react with BrOH^- in these experiments.

Since the pK of OH (as defined in reaction 28) is 11.9,⁹ above pH 11 reaction 1 would be slowed still



further, because O^- is very likely to be less reactive than OH toward Br^- . Thus the situation in alkaline solution is quite complex, probably involving the equilibria 3 + 3a, 22, and 28, and therefore the results will depend upon both Br^- and OH^- concentrations.

The above discussion shows that the relative rate constants for the OH radical obtained in competition studies with Br^- must be used with great caution since the efficiency of Br^- in scavenging OH radicals is strongly pH dependent. Results in this laboratory show that $\text{OH} + \text{CO}_3^{2-}$ is another reaction whose rate constant varies with pH, and that competition studies with this reaction must also be interpreted cautiously.

Acknowledgment. We wish to acknowledge the careful Linac operation of Mr. Ed Backstrom and Mr. B. E. Clift and the technical assistance of Mr. Steve Petrek in maintaining the electronic equipment.

(29) A. A. Frost and R. G. Pearson, "Kinetics and Mechanism," John Wiley and Sons, Inc., New York, N. Y., 1953, p 181.

The Pulse Radiolysis of Deaerated Aqueous Carbonate Solutions. I. Transient Optical Spectrum and Mechanism. II. pK for OH Radicals¹

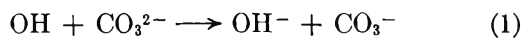
by James L. Weeks and Joseph Rabani

Chemistry Division, Argonne National Laboratory, Argonne, Illinois 60439 (Received January 3, 1966)

The pulse radiolysis of deaerated aqueous carbonate solutions in the neutral and alkaline pH was studied. A mechanism is presented, and several rate constants have been determined (all are in units of $M^{-1} \text{sec}^{-1}$): $k(\text{OH} + \text{CO}_3^{2-}) = 4.2 \times 10^8$, $k(\text{O}^- + \text{CO}_3^{2-}) < 10^7$, $2k(\text{CO}_3^- + \text{CO}_3^-) = 1.25 \times 10^7$ (zero ionic strength), and $k(\text{OH} + \text{HCO}_3^-) = 1.5 \times 10^7$. In the pulse radiolysis of carbonate solutions a transient optical absorption appears which is identified as the carbonate radical ion (CO_3^-). Its spectrum is reported and has a maximum extinction coefficient of $1860 \pm 160 M^{-1} \text{cm}^{-1}$ at 6000 Å. There is a pH dependency of the rate of CO_3^- formation, from which the pK for the ionic dissociation of OH radicals has been determined as 11.8 ± 0.2 , where pK is defined as $-\log \{ [\text{H}^+][\text{O}^-]/[\text{OH}] \}$. The results are compared with earlier work.

Introduction

A transient optical absorption at 5780 Å was reported by Gordon, *et al.*,² who assumed that carbonate radical ions, CO_3^- , are formed by



Adams and Boag³ used the absorption of CO_3^- to get relative rate constants of hydroxyl radicals with various solutes in aqueous solution. Adams, Boag, and Michael,⁴ using photographic plates, obtained the CO_3^- spectrum and reported a maximum absorption at 6000 Å, with an extinction coefficient, ϵ , equal to $1880 M^{-1} \text{cm}^{-1}$.

In the present work it seemed desirable to (a) extend the previous spectroscopic work to obtain a more precise spectrum of CO_3^- over a wider wavelength region, (b) study kinetics of the formation and decay of CO_3^- under various conditions, and (c) use the CO_3^- absorption to discriminate between OH and O_{aq}^- and the determination of the pK for the ionic dissociation of OH.

Experimental Section

The experimental procedure used in this work has been described previously.⁵ The preparation and handling of the solutions made use of a syringe technique.^{6,7} A multiple-reflection cell⁶ with a 4 cm long

optical cell gave an 80-cm light path. The formation and decay of CO_3^- was followed at 6000 Å using a 450-w xenon lamp, a Bausch and Lomb monochromator, a 1P28 photomultiplier, and a Tektronix oscilloscope with a Polaroid camera. A 0.4- μsec , 15-Mev electron pulse from a linear accelerator was used. Unless otherwise stated or indicated by the maximum optical density, the dose was about $2.5 \times 10^{19} \text{ev l.}^{-1}$ per pulse.

Using the above apparatus and varying the wavelength of the monochromator, the spectrum of CO_3^- was determined. No attempt was made to monitor the pulse intensity for the data taken between 2600 and 3300 Å. However, from 3250 to 6400 Å, the light beam was split, after passing through the cell, by means of a partially aluminized mirror. The reflected beam was used to obtain the relative pulse intensity at con-

(1) Based on work performed under the auspices of the U. S. Atomic Energy Commission.

(2) S. Gordon, E. J. Hart, M. S. Matheson, J. Rabani, and J. K. Thomas, *J. Am. Chem. Soc.*, **85**, 1375 (1963).

(3) G. E. Adams and J. W. Boag, *Proc. Chem. Soc.*, 112 (1964).

(4) G. E. Adams, J. W. Boag, and B. D. Michael, *Trans. Faraday Soc.*, **61**, 1674 (1965).

(5) J. Rabani, W. A. Mulac, and M. S. Matheson, *J. Phys. Chem.*, **69**, 53 (1965), and references cited therein.

(6) C. B. Senvar and E. J. Hart, *Proc. Intern. Conf. Peaceful Uses At. Energy, 2nd, Geneva*, **29**, 19 (1958).

(7) E. J. Hart, S. Gordon, and J. K. Thomas, *J. Phys. Chem.*, **68**, 1271 (1964).

stant wavelength, since the optical density of the pulsed solution is proportional to the pulse intensity. The data for the calculation of the extinction coefficient of CO_3^- at 6000 Å, based on the ϵ of $\text{Fe}(\text{CN})_6^{3-}$ at 4200 Å, were obtained using a spectrograph with photomultipliers at 6000 and 4200 Å, as previously described.⁵

Reagent grade chemicals were used for all of the experiments without further purification. J. T. Baker Chemical Co. sodium carbonate monohydrate and Mallinckrodt Chemical Works sodium hydroxide were used. Less than 0.5% carbonate was detected in the 1 M NaOH stock solutions. The kinetic results indicate that the carbonate impurity in the NaOH solutions was much lower and could be ignored. Where applicable, corrections were made for all concentrations of CO_3^{2-} and pH values for the equilibrium: $\text{H}_2\text{O} + \text{CO}_3^{2-} \rightleftharpoons \text{HCO}_3^- + \text{OH}^-$. Unless otherwise stated, 0.1 atm of N_2O was present in all of the solutions in order to convert e_{aq}^- to OH. The N_2O was passed through three alkaline pyrogallol solutions in order to eliminate small amounts of O_2 . With this procedure, N_2O containing 0.03% O_2 by volume was obtained and used without further purification. All experiments were carried out at room temperature (ca. 23°).

Results and Discussion

In the alkaline carbonate system, the effect of the following species produced during the electron pulse must be considered: H_2 , H_2O_2 , $(\text{H}_3\text{O})_{\text{aq}}^+$, $(\text{OH})_{\text{aq}}^-$, e_{aq}^- , H, OH.

H_2 does not react with carbonate ions. H_2O_2 decomposes slowly in alkaline carbonate solutions but has no effect on the carbonate ions. The properties of carbonate in solutions containing $(\text{H}_3\text{O})_{\text{aq}}^+$ and $(\text{OH})_{\text{aq}}^-$ are well known and need not be discussed here. Of the short-lived species, e_{aq}^- does not react with carbonate ions,⁸ although it may react with bicarbonate ions⁹ and is known to react very fast with CO_2 .¹⁰ H atoms may react with bicarbonate ions,⁹ but the reaction is very slow compared to other reactions of H atoms. The optical absorption with the peak at 6000 Å has also been obtained⁴ in the presence of O_2 , which is a known H atom scavenger. Thus, it seems evident that OH radicals are the main precursor and probably the only one for forming this absorption. This conclusion is confirmed by the effects of OH scavengers on the absorption^{2,3,11} at 6000 Å.

In order to investigate the carbonate radical ion, it is desirable to eliminate e_{aq}^- , since it still has a high absorption at 6000 Å (about 5 times more absorption^{2,5,8,12} than CO_3^-). Adams, Boag, and Michael¹¹

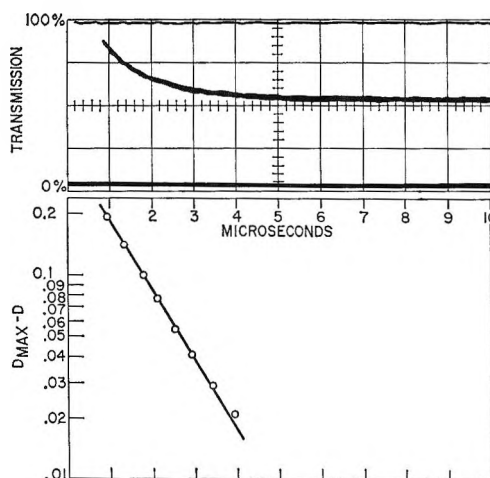
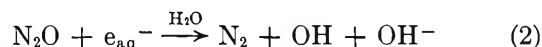


Figure 1. Formation of CO_3^- : upper, typical oscilloscope trace; lower, pseudo-first-order kinetics. Conditions: 1.97 mM CO_3^{2-} , 0.1 atm of N_2O , pH 10.76.

have used O_2 and N_2O in order to eliminate e_{aq}^- . However, since O_2 can react with O^- to form O_3^- at alkaline pH,¹³⁻¹⁵ the presence of oxygen was usually avoided in the present system. Most of these experiments have been carried out in the presence of N_2O , which, it is assumed, reacts rapidly with e_{aq}^- and forms¹⁶ OH or O^- , as in



This reaction has been discussed in earlier papers, and it has been concluded^{14,17} that, if N_2O^- is formed as an intermediate, it should live either less than 1 μsec , or else have the same properties as OH has in the ferrocyanide¹⁴ and bromide¹⁷ systems. As will be seen later, the present results with carbonate ions are consistent with the same conclusion.

- (8) E. J. Hart and J. W. Boag, *J. Am. Chem. Soc.*, **84**, 4090 (1962).
- (9) S. Nehari and J. Rabani, *J. Phys. Chem.*, **67**, 1609 (1963).
- (10) (a) L. M. Dorfman and M. S. Matheson, *Progr. Reaction Kinetics*, **3**, 237 (1965); (b) J. T. Allan, N. Getoff, H. P. Lehmann, K. E. Nixon, G. Scholes, and M. Simic, *J. Inorg. Nucl. Chem.*, **19**, 204 (1961).
- (11) G. E. Adams, J. W. Boag, and B. D. Michael, *Trans. Faraday Soc.*, **61**, 1417 (1965).
- (12) (a) L. M. Dorfman and I. A. Taub, *J. Am. Chem. Soc.*, **85**, 2370 (1963); (b) J. P. Keene, *Discussions Faraday Soc.*, **36**, 304 (1963).
- (13) G. Czapski and L. M. Dorfman, *J. Phys. Chem.*, **68**, 1169 (1964).
- (14) J. Rabani and M. S. Matheson, *ibid.*, **70**, 761 (1966).
- (15) G. E. Adams, J. W. Boag, and B. D. Michael, *Nature*, **205**, 898 (1965).
- (16) F. S. Dainton and D. B. Peterson, *Proc. Roy. Soc. (London)*, **A267**, 443 (1962).
- (17) M. S. Matheson, W. A. Mulac, J. L. Weeks, and J. Rabani, *J. Phys. Chem.*, **70**, 2092 (1966).

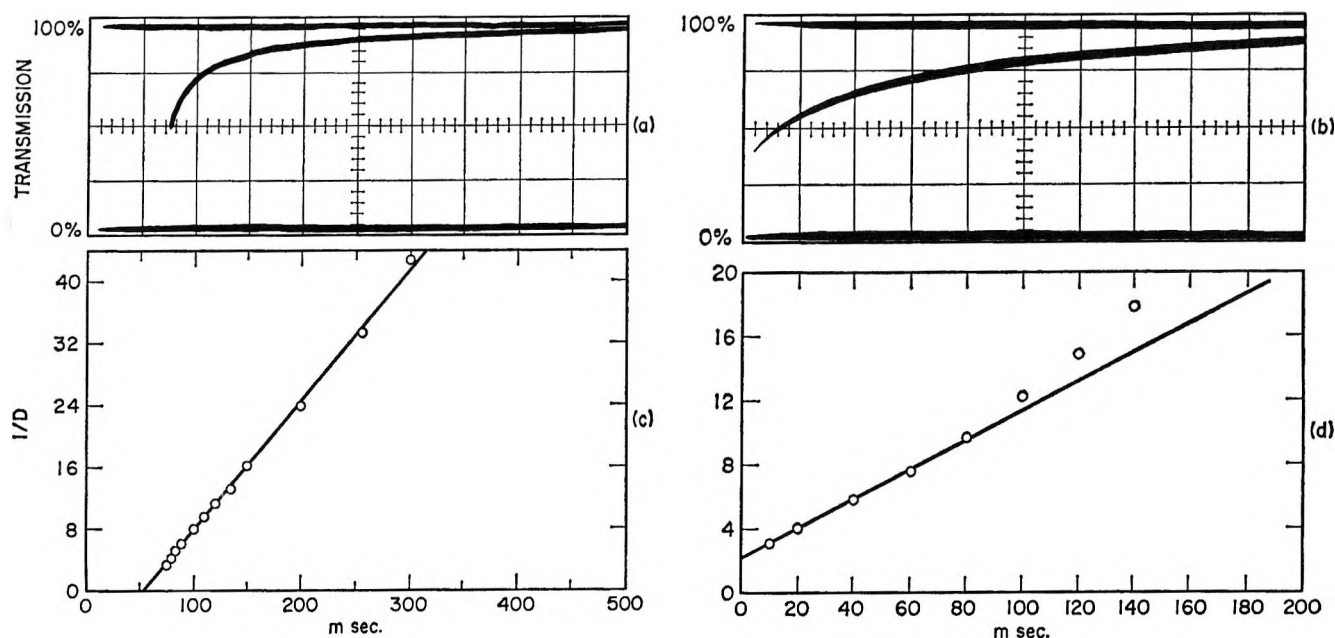


Figure 2. Carbonate radical decay curves and second-order plots. (a) 6.24 mM CO_3^{2-} , 0.1 atm of N_2O , pH 12.61. (b) 1.97 mM CO_3^{2-} , 0.1 atm of N_2O , pH 10.76. (c) Second-order plot for (a). (d) Second-order plot for (b).

The formation of the CO_3^- absorption in solutions containing N_2O is first order in both $[\text{OH}]$ and $[\text{CO}_3^{2-}]$. From the appropriate plots, a second-order rate constant " k_1 " has been calculated, defined as

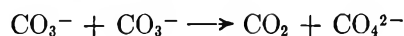
$$"k_1" = (1/[\text{CO}_3^{2-}]) \frac{d}{dt} \{ \ln (D_{\max} - D_t) \}$$

where D_{\max} is the maximum value of the optical density after all of the OH radicals have reacted and D_t is the optical density at time t . As will be seen later, " k_1 " is pH dependent, and only under certain specific conditions does " k_1 " = k_1 , where k_1 is the rate constant of reaction 1.

The buildup of optical density is followed by a slower decay, which is well separated in time from the formation. In Figure 1 a typical oscilloscope trace (upper part) for the formation of carbonate radical ions is presented. The straight line obtained (lower part of Figure 1), when $D_{\max} - D_t$ is plotted vs. time on a semilog scale, shows that the reaction is pseudo first order. The same result was obtained when either N_2O or CCl_4 was used to scavenge e_{aq}^- .

Figures 2a and 2b present typical oscilloscope traces for the decay of the transient absorption with time for solutions containing N_2O . A straight line is obtained when $1/D$ from Figure 2a is plotted vs. time in Figure 2c. In some experiments, deviations from linearity occurred (Figure 2d), indicating additional processes. It appears that there is a positive curvature (e.g., Figure

2d) at pH < 11.5, very little or no curvature (e.g., Figure 2c) at pH 12–13, and again positive curvature at pH 13.5. In most cases, however, the plots were linear within experimental errors until after 80% of the CO_3^- decayed away. The main reaction responsible for the decay is believed to be



or



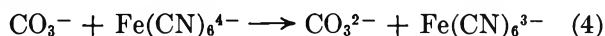
No explanation for the deviations from second order seems apparent. All of the rate constants reported in this paper for solutions containing N_2O are calculated from the initial slopes of the kinetic plots.

The Spectrum of CO_3^- . The spectrum of CO_3^- is given in Figure 3. In the ultraviolet region, optical absorption appears in the absence as well as in the presence of carbonate ions and/or bicarbonate ions. CO_3^- is probably responsible for the absorption in the presence of carbonate ions and bicarbonate ions. In the absence of these last ions, it may be due to OH in neutral and O_{aq}^- in alkaline solutions.¹⁸

The Extinction Coefficient of CO_3^- . *The Reaction of CO_3^- with Ferrocyanide.* The extinction coefficient of CO_3^- at 6000 Å, $\epsilon_{\text{CO}_3^-}^{6000}$, has been determined by a

(18) J. Rabani and M. S. Matheson, *J. Am. Chem. Soc.*, **86**, 3175 (1964).

method similar to that used before⁵ for $\epsilon_{\text{e}_{\text{aq}}^{\cdot-}}$.⁶⁷⁸⁰ It was found that CO_3^- oxidizes ferrocyanide by



Simultaneous traces at both 6000 and 4200 Å were obtained. In the presence of ferrocyanide, the decay of CO_3^- is enhanced owing to reaction 4. From pseudo-first-order plots, k_4 was calculated. Since $2k_3 \approx 10^7 \text{ M}^{-1} \text{ sec}^{-1}$, it is easy to choose high enough ferrocyanide concentrations so that no corrections for second-order decay⁵ are necessary. Reaction 4 is between two negatively charged species and is expected to be enhanced at higher ionic strengths. The values reported in Table I are for the actual ionic strengths and were not

Table I: Simultaneous Rates of Formation of $\text{Fe}(\text{CN})_6^{3-}$ at 4200 Å and Disappearance of CO_3^- at 6000 Å

pH	$[\text{Na}_2\text{CO}_3]^a$	$[\text{K}_4\text{Fe}(\text{CN})_6]^c$	D_{max}^b at 4200 Å	k_4^c at 4200 Å	k_4^c at 6000 Å
11.6	71	0.12	0.19	2.7	2.8
13.0	100	0.10	0.25	3.5	3.5
13.0	100	0.41	0.25	4.0	3.6

^a In units of mM. ^b D_{max} was constant by 100 μsec after pulse and was followed to at least 200 μsec . ^c In units of $10^8 \text{ M}^{-1} \text{ sec}^{-1}$. Each result is an average of at least two experiments.

calculated for zero ionic strength. The same rate constant is obtained at both 6000 and 4200 Å. A typical oscilloscope trace used for these calculations is shown in Figure 4. The initial absorption at 4200 Å is due to CO_3^- .

From traces such as shown in Figure 4, ΔD_{6000} values were plotted *vs.* ΔD_{4200} (see ref 5 for the definition of ΔD). The results are given in Figure 5 for pH 11.6. From the slope of Figure 5 and other similar plots, the ratio $\epsilon_r = \epsilon_{\text{CO}_3^-}^{6000} / \epsilon_{\text{Fe}(\text{CN})_6^{3-}}^{4200}$ can be calculated using⁵ $\epsilon_r = \text{slope} / (1 + A \times \text{slope})$, where $A = \epsilon_{\text{CO}_3^-}^{4200} / \epsilon_{\text{CO}_3^-}^{6000}$. The ratio A was calculated from simultaneous traces at 6000 and 4200 Å, using the spectrograph, in solutions containing carbonate in 0.1 atm of N_2O (no ferrocyanide). $A = 0.184 \pm 0.005$ (standard deviation) was obtained for 0.1 M NaOH, 0.1 atm of N_2O , and $3 \times 10^{-3} \text{ M Na}_2\text{CO}_3$, and $A = 0.182$ for $5 \times 10^{-3} \text{ M NaHCO}_3$ (near neutral pH) and 0.1 atm of N_2O . These results indicate that A is independent of whether CO_3^- is produced from carbonate ions or from bicarbonate ions. From Figure 5, and other such figures, $\epsilon_r = 1.78$ has been calculated for both pH 11.6 and 13.0. Other conditions for such calculations were the same as described in Table I.

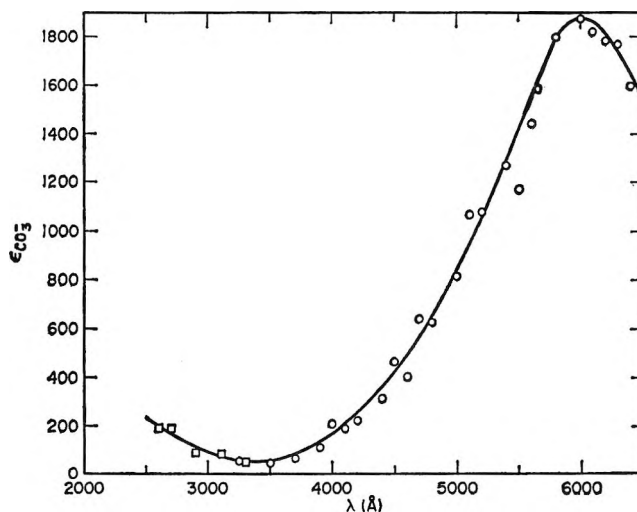


Figure 3. Spectrum of CO_3^- . Circles are values at pH 13 determined "point by point" using two monochromators (one used as pulse monitor); squares are values at pH 11 where no monitor monochromator was used.

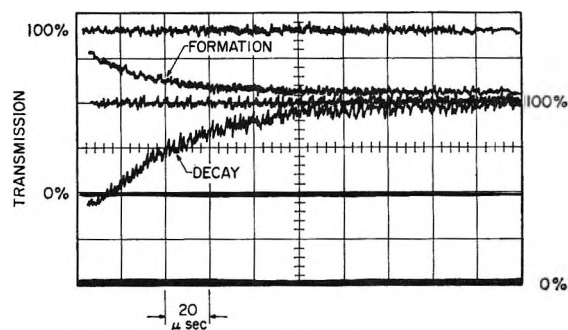


Figure 4. Simultaneous formation of $\text{Fe}(\text{CN})_6^{3-}$ at 4200 Å (upper set of curves) and decay of CO_3^{2-} at 6000 Å (lower set of curves). Conditions: 72 mM CO_3^{2-} , 0.122 mM $\text{Fe}(\text{CN})_6^{4-}$, 0.1 atm of N_2O , pH 11.6.

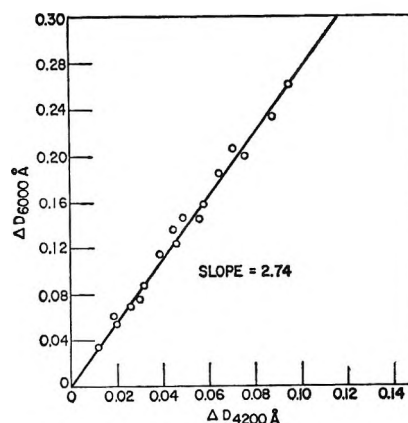


Figure 5. A typical comparison of ΔD at 6000 Å with that at 4200 Å for use in the calculation of $\epsilon_{\text{CO}_3^-}^{6000} / \epsilon_{\text{Fe}(\text{CN})_6^{3-}}^{4200}$. Conditions: 72 mM CO_3^{2-} , 0.122 mM $\text{Fe}(\text{CN})_6^{4-}$, 0.1 atm of N_2O , pH 11.6.

From Figure 3, $A = 0.135 \pm 0.015$, which yields $\epsilon_r = 1.95$. The difference between the results with the monochromator and spectrograph may be due in part to a difference in the effective wavelengths. Based on the average value of ϵ_r and $\epsilon_{Fe(CN)_6^{4-}} = 1000$, a value of $\epsilon_{CO_3^{2-}}^{6000} = 1860 \pm 160 M^{-1} cm^{-1}$ is obtained.

The Rate of Decay of CO_3^{2-} . As can be seen from Figures 2c and 2d, the initial decay of optical density in carbonate- N_2O solutions is closely second order. At the higher pH values, the rate of decay was some-

Table II: Rate of Formation and Decay of CO_3^{2-} in Solutions Containing 0.1 Atm of N_2O

(A) With No Added Salts						
pH	$[CO_3^{2-}]^a$	$D_{initial}$	D_{max}	% CO_3^{2-} decayed before non-linear ^b	" k_1 " ^c	$2k_3^d$
8.4	1.0 ^d	0.19	0.34	80	1.49	1.94
10.6	0.8	0.06	0.33	70	40.7	1.33
10.8	2.2	0.09	0.35	70	38.6	1.57
11.1	2.4	0.20	0.31	70	...	1.49
11.4	3.1	0.10	0.34	70	32.0	1.64
11.4	8.8	0.12	0.29	70	28.9	1.83
11.6	72	...	0.32	80	...	2.90
12.0	3.0	0.11	0.54	80	15.8	1.75
12.0	5.8	0.11	0.24	80	15.0	2.15
12.3	6.4	0.20	0.44	80	8.22	2.20
12.6	6.2	0.11	0.34	90	5.42	2.71
13.0	1.0	~0.01	0.40	80	3.20	3.93
13.0	3.2	~0.01	0.44	90	2.65	2.93
13.0	8.4	~0.01	0.46	90	2.68	2.25
13.0	15.0	0.14	0.62	90	3.18	2.23
13.0	15.0	0.12	0.35	90	2.31	3.33
13.0	100	0.29	0.49	80	...	3.69
13.0	109 ^e	...	~0.25	90	...	5.12
13.5	9.1	0.03	0.40	70	0.94	...
13.5	36	0.15	0.62	80	0.91	4.5

(B) With Added Na_2SO_4 or $NaClO_4$						
pH	$[CO_3^{2-}]^a$	Ionic strength, μ^a	$D_{initial}$	D_{max}	% CO_3^{2-} decayed before non-linear ^b	$2k_3^d$
10.6	0.8	18.2	0.05	0.34	70	1.54
10.6	0.8	31.9	0.04	0.27	70	1.76
10.5	0.8	91.2	0.04	0.23	80	2.30
10.6	0.8	123	0.06	0.33	80	1.98
10.5	0.7	327	0.06	0.33	80	2.79

^a In units of mM. ^b Measure of linearity on second-order plot of $1/D$ vs. t . ^c In units of $10^7 M^{-1} sec^{-1}$. ^d $[HCO_3^-]$. ^e Also contained 0.1 atm of air. Each result is an average of two to six experiments.

what faster and the scatter was larger. In Table II, the rate constants for the formation and decay of CO_3^{2-} are presented. Apart from the effect of the ionic strength (see Figure 6), $2k_3$ seems to be unaffected by the various pH values, carbonate ion concentrations, and intensities of the electron beam. The presence of 0.1 atm of air has little effect, if any, on the rate of CO_3^{2-} decay. Adams, Boag, and Michael⁵ reported an enhanced decay of CO_3^{2-} in the presence of O_2 , but in the absence of N_2O . This was interpreted⁴ as a reaction of CO_3^{2-} with O_2^- . In several of the experiments in the present work when both N_2O and air were present, most of the e_{aq}^- reacted with N_2O , and practically no O_2^- was formed.

In Figure 6, $\log 2k_{3,\mu}$, where $2k_{3,\mu}$ is $2k_3$ at ionic strength μ , has been plotted vs. $\mu^{1/2}/(1 + 0.4\mu^{1/2})$, using the values in Table II. The combination $\alpha = 0.4$ and a slope of 1.02 gave a good fit with the results. If $\alpha = 1.0$ were chosen, a slope of 1.3 would also give a good fit; however, the theory requires^{19,20} a slope of

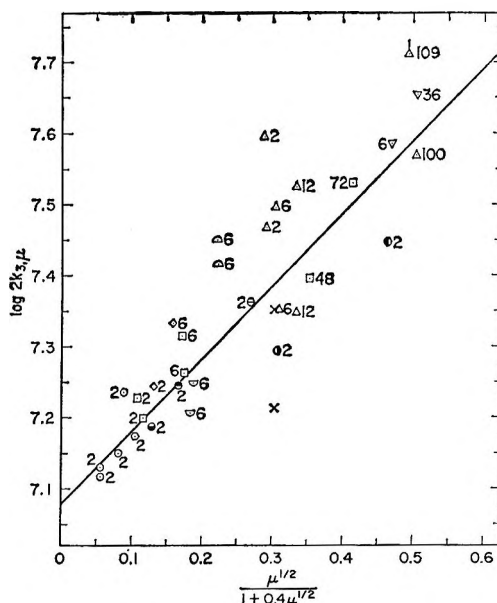


Figure 6. Ionic strength effect on k_3 . Conditions: all solutions contained 0.1 atm of N_2O . Numbers following symbols in the figure indicate approximate $[CO_3^{2-}]$ in mM: pH 8.4, \times , ~100 mM HCO_3^- ; pH 10.5–10.8, \circ , no added salt; pH 10.5–10.8, \ominus , 5 mM Na_2SO_4 ; pH 10.5–10.8, \bullet , 40 mM Na_2SO_4 ; pH 10.5–10.8, \odot , 108 mM Na_2SO_4 ; pH 10.5–10.8, \ominus , 29 mM $NaClO_4$; pH 10.5–10.8, \ominus , 89 mM $NaClO_4$; pH 11.1, \circ ; pH 11.3–11.6, \square ; pH 12.0, \diamond ; pH 12.3, ∇ ; pH 12.6, \triangle ; pH 13.0, Δ ; pH 13.0, Δ , also contained 0.1 atm of air; pH 13.5, ∇ .

(19) S. W. Benson, "The Foundations of Chemical Kinetics," McGraw-Hill Book Co., Inc., New York, N. Y., 1960, p 525.

(20) P. J. Durrant and B. Durrant, "Introduction to Advanced Inorganic Chemistry," John Wiley and Sons, Inc., New York, N. Y., 1962, p 319.

1.02 and $\alpha \approx 0.7$ to 0.8, assuming the C-O bond length in CO_3^- is the same²⁰ as in CO_3^{2-} .

Figure 6 demonstrates that the dependence of k_3 on pH is in fact a dependence on μ . Additionally, it shows that the decay of the transient absorption is mainly by a reaction of two species of the same charge. Reaction 3 appears to be the only one which can account for this observation. From Figure 6, $2k_3$ is $1.25 \times 10^7 \text{ M}^{-1} \text{ sec}^{-1}$ at zero ionic strength.

The Decay of CO_3^- in the Presence of CCl_4 . In some experiments CCl_4 was used to scavenge e_{aq}^- , as in reaction 5, instead of N_2O . This presence of CCl_4 did



not affect the rate of CO_3^- formation; however, the decay was different. Table III summarizes the results.

Table III: Rate of Formation and Decay of CO_3^- in Solutions Containing $\sim 0.5 \text{ mM CCl}_4$ (No N_2O)^e

pH	$[\text{CO}_3^{2-}]^a$	D_{initial}	D_{max}	" k_1 " ^b	$\frac{d}{dt} \left(\frac{1}{D} \right)_{\text{initial}} \times \epsilon \cdot d$
12.0	3.0	0.13	0.33	19.4	2.2
12.0	6.1	0.08	0.14	14.5	1.8
12.0	12.3	0.05	0.15	...	2.0
12.6	5.9	0.06	0.15	5.90	1.7
13.0	6.0	0.09	0.33	3.41	...
13.0	15.0	0.18	0.37	2.95	...
13.5	6.2	0.02	0.12	0.80	1.1
13.5	36.0	0.15	0.38	1.00	1.1

^a In units of mM. ^b In units of $10^7 \text{ M}^{-1} \text{ sec}^{-1}$. ^c In units of $10^9 \text{ M}^{-1} \text{ sec}^{-1}$. ^d l = light path, ϵ = extinction coefficient of CO_3^- at 6000 Å ($1.78 \times 10^8 \text{ M}^{-1} \text{ cm}^{-1}$). ^e Each result is an average of two to five experiments.

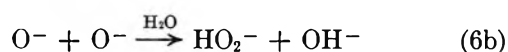
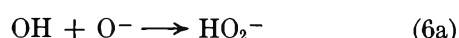
The decay of CO_3^- in CCl_4 solutions is much faster than in the N_2O solutions. Apparently, CO_3^- must react with CCl_4 or its products, but, at present, efforts to advance a full mechanism have not succeeded. D_{max} in CCl_4 is about one-half of D_{max} in N_2O , when the other conditions are the same.

The Effect of pH on the Formation of CO_3^- . Tables II and III present the effect of pH on " k_1 ". D_{max} can be used for the calculation of the electron beam intensity, since $G(\text{CO}_3^-)$, the yield of CO_3^- radicals per 100 ev, under these conditions, is known. The "linearity" is defined here as the percentage CO_3^- which has disappeared when the deviation from linearity just equals the error in $1/D$. D_{initial} is the optical density measured at the smallest t value. Some reaction takes place during the pulse and the electronic "noise"; the duration of both together is $\sim 1 \mu\text{sec}$.

From Table II it is seen that $k_{1a} \ll k_1$, where reaction 1a is

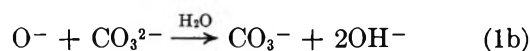


The reaction of OH with bicarbonate ions also produces CO_3^- , as indicated by the similar optical density in both bicarbonate and carbonate solutions, when irradiated with the same pulse intensity. Also, the rate of decay of the optical density is the same in both carbonate and bicarbonate solutions (see Figure 6). Small corrections have been made for the effect of reactions 6, 6a, and 6b



An effective " $2k_6$ " was taken from previous measurements or obtained by interpolation.¹⁴ The possible reactions of CCl_3 with OH or O^- were neglected because of lack of data.

A striking phenomenon is the pH dependency of " k_1 ". The carbonate ion reactivity toward OH and O^- parallels the reactivity of ferrocyanide.^{14,18} Reaction 1b can be neglected even at the highest pH used by us, since



$k_{1b} < 10^7 \text{ M}^{-1} \text{ sec}^{-1}$. Figure 7 shows a plot of $\log \left[\frac{k_1}{k_1'} - 1 \right]$ vs. pH. $k_1 = 4.2 \times 10^8 \text{ M}^{-1} \text{ sec}^{-1}$ has

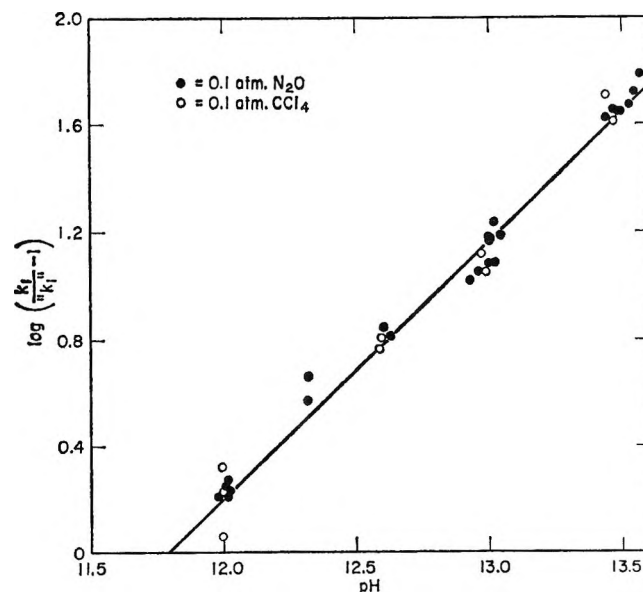


Figure 7. Determination of the ionic dissociation constant of OH radicals. The points are independent of $[\text{CO}_3^{2-}]$ in the range 1 to 50 mM.

been calculated from the results at $\text{pH} < 11.6$ by means of successive approximations, assuming that the $\text{p}K$ for OH radicals is higher than 11.5. Thus, our present determination of $\text{p}K_{\text{OH}}$ does not depend on the exact numerical value obtained previously.^{14,18} The results in both N_2O and CCl_4 solutions gave $\text{p}K_{\text{OH}} = 11.8 \pm 0.2$ (an error of ± 0.1 in the intercept of Figure 7 and an additional error of ± 0.1 due to k_1). This result is in excellent agreement with the value of 11.9 ± 0.2 which has been reported previously.^{14,18}

Conclusions

A mechanism which accounts for most of the observations in the pulse-irradiated carbonate solutions is given. The results are in very good agreement with previous work^{3,4,14,18} except for the value of k_1 . Adams, Boag, and Michael⁴ report $k_1 = 2 \times 10^8 \text{ M}^{-1} \text{ sec}^{-1}$ but mention certain difficulties in the measurements. A correction for the unreacted bicarbonate ions would raise their value a little. Since carbonate ions show a strong pH-dependent reactivity toward OH, it is not suitable as a reference system for competition reactions.

The constancy of k_3 (see Figure 6) and the similarity of the spectrum or optical density, in the whole pH

region investigated, indicates that only one form of carbonate radical was present in our systems. The ionic strength effect indicates that this form was CO_3^- and not HCO_3^- . Thus, HCO_3^- appears to be a stronger acid than HCO_3^- —a reasonable result.

The ionic dissociation constant for OH radicals was obtained again, in very good agreement with the previous value.^{14,18} The results show again that OH radicals produced from N_2O by reaction 2 reacted in our system in the same way as the primary OH radicals did. One must conclude that in this system $(\text{N}_2\text{O})_{\text{aq}}^-$ or N_2OH radicals, possible intermediates of reaction 2, are short-lived (less than 1 μsec) or else react in the same way and with the same rates as does OH, and have the same $\text{p}K$. The same conclusion was reached in two other systems.^{14,17,18}

Acknowledgment. It is a pleasure to acknowledge the invaluable assistance of W. A. Mulac in all phases of this work. We are indebted also to M. S. Matheson for his very helpful discussions. We wish to thank Ed Backstrom and B. E. Cliff for their careful operation of the linear accelerator and Steve Petrek for maintaining the electronic equipment.

Determination of the Roughness Factor of a Powdered Solid

by Sydney Ross and Ian J. Wiltshire

Department of Chemistry, Rensselaer Polytechnic Institute, Troy, New York (Received July 13, 1965)

A new method of determining the surface roughness of a powdered solid is described. The powdered solid is treated with various amounts of a nonvolatile oil, *i.e.*, tri-*o*-cresyl phosphate, to create a series of composite substrates. The surface area (and other adsorption parameters) of each of these samples is measured by argon adsorption, using the Ross-Olivier method of analyzing adsorption isotherms. The amount of oil that equals a close-packed monolayer of oil on the substrate is interpolated empirically. A value of the surface roughness can then be obtained from the ratio of the area of the original substrate to the area of the substrate after it has been covered with a monolayer of the much larger molecules of the nonvolatile oil. The fine-grained structure of the substrate is "perceived" by the argon molecule but is covered up by the larger molecule. The roughness factor of Graphon, a graphitized carbon black with a specific surface of 96 m²/g, is found to equal 1.6 by this method.

Introduction

The earliest determinations of the roughness of a solid surface were limited to solids with macroscopically rough surfaces, because of the lack of sufficiently sensitive devices. Wurth¹ determined the roughness of a surface by taking an impression with tin foil and painting the tin-foil model: from the quantity of paint used, the roughness of the surface was estimated. Reason² measured surface roughness by passing a stylus across the surface and thus obtaining a profile of its contour. Heyes and Lueg³ measured the roughness of plane and curved, polished or rough, surfaces by determining the ratio between the light thrown into the microscope objective by the surface under bright-field illumination and the same under dark-field illumination: the reciprocal value of this ratio was their suggested measure of surface roughness.

In a study of the spreading of liquids on solid surfaces, Bailey and Shuttleworth⁴ showed that the hysteresis of the contact angle is the result of the inescapable roughness of a solid surface. The polarization capacity of an electrode is proportional to its roughness and so can be used to determine the roughness of a metallic surface.⁵ Turpin and Testerman⁶ found that different surfaces give typical capacitance curves, which can be used to differentiate the respective surface roughnesses. The ferromagnetic resonance of polycrystalline ma-

terials is affected both by surface conditions and by the lattice defects of these substances. Biller⁷ investigated the separate contributions arising from these factors in a specimen of nickel.

Electron microscopy has recently come into use to study the surface topography of solids, powdered or massive.⁸ One method uses the long shadows cast by surface contours when a glancing electron beam is directed at the surface. A second method is to scan the object with a small electron beam, in a manner analogous to that of a television camera. Although pictures of the surface and its irregularities can be produced by each method, the interpretation in quantitative terms is tedious, as many pictures are required in order to evaluate the numerical roughness factor for the whole surface.

The transmitted electron beam can be used to de-

- (1) K. Wurth, *Farben-Ztg.*, **36**, 875 (1931).
- (2) Kapella Ltd. and R. E. Reason, British Patent 539,271 (1941).
- (3) J. Heyes and W. Lueg, *Mitt. Kaiser-Wilhelm-Inst. Eisenforsch. Dusseldorf*, **24**, No. 3, 31 (1942).
- (4) G. L. Bailey and R. Shuttleworth, *Discussions Faraday Soc.*, **3**, 16 (1948).
- (5) C. Wagner, *J. Electrochem. Soc.*, **97**, 71 (1950).
- (6) M. R. Turpin and M. K. Testerman, *ibid.*, **109**, 168 (1962).
- (7) E. Biller, *Z. Naturforsch.*, **17a**, 559 (1962).
- (8) S. P. Bowden and D. Tabor, "Friction and Lubrication of Solids," Vol. 2, Cambridge University Press, London, 1964.

termine indirectly the surface roughness of a solid. From pictures showing the shape of the particles, the specific surface area is calculated. This value is compared with the result of a gas-adsorption method that is capable of "seeing" more than the gross outline of the particles. A relatively narrow range of particle size and uniformity is required, which limits the scope of the method.

Any method of evaluating surface roughness of a powder involves either a detailed study of a large number of individual particles or the measurement of some macroscopic physical effect that depends on the extent of the submicroscopic surface. The present method falls into the latter category. A relatively large and nonvolatile molecule that is capable of covering up the fine-grained structure of the substrate is pre-adsorbed; its effect on the specific surface area is determined by gas adsorption, using argon or some other small molecule. The roughness factor that is evaluated depends essentially on determining how much of the fine-grained structure of the original substrate is denied to the argon by the presence of the larger molecule.

Materials and Methods

The solid used was a graphitized carbon black, Graphon, *i.e.*, Spheron 6 that had been heated in an inert atmosphere to 2700–3200°, provided by courtesy of Dr. W. R. Smith of Godfrey L. Cabot, Inc. The Graphon was first washed with ether in a Soxhlet extractor and degassed at 400° to 10⁻⁶ mm. Tri-*o*-cresyl phosphate (TCP) (K and K Laboratories, Inc.) was distilled *in vacuo* and used as the nonvolatile pre-adsorbed oil. Argon and helium (Air Reduction Co.) of assayed reagent grade were used for the adsorption measurements.

The various composite TCP-Graphon substrates were prepared by adding solutions of weighed amounts of TCP in benzene to known masses of clean Graphon. The mixtures were stirred vigorously as the benzene evaporated at room temperature, leaving the TCP dispersed over the various sample surfaces. The number of TCP-carbon substrates prepared in this way ranged in composition from zero to 30% by weight of TCP per gram of Graphon. Argon-adsorption isotherms at 77.5°K were measured for untreated Graphon and for all of the prepared substrates. The preliminary outgassing, consisting of exposure to vacuum (10⁻⁶ mm) for several hours, was ascertained to cause no loss of oil from the composite substrates. The TCP, therefore, would not reequilibrate with the adsorbent during the measurement of the argon-adsorption isotherm.

Results and Discussion

The argon-adsorption isotherms were analyzed by the Ross-Olivier technique⁹ to obtain (a) the monolayer capacity (V_β), (b) the average adsorptive potential (U_0'), and (c) the heterogeneity of the substrate (γ). The matching of the experimental curves to the computed model isotherms was made using a value for $2\alpha/RT\beta$ of 6.00 at 77.5°K, which is the value for argon, corrected for the surface electric field of graphite, as recommended by Ross and Olivier.⁹ The comparison of experimental adsorption isotherms (individual points) with the theoretical description of a mobile adsorbed film (solid line) is shown in Figure 1. Adsorption isotherms obtained from composite substrates containing more than 5% TCP are not matched in this way, because the log-log plots are linear, *i.e.*, Freundlich equation, for which the Ross-Olivier method is not applicable.

Following de Boer,¹⁰ the cross-sectional area of argon on these substrates is assumed to be equal to the two-dimensional van der Waals b constant, β , *i.e.*, 13.6 Å². The specific surface areas Σ of the composite substrates are calculated from V_β

$$\Sigma = \frac{6.023 \times 13.6 \times V_\beta}{22.4} = 3.66V_\beta \text{ m}^2/\text{g} \quad (1)$$

Values of Σ for the composite substrates are reported in Table I.

The theory of the Ross-Olivier method postulates that the adsorbed argon on each composite substrate behaves as a two-dimensional nonideal gas. On every

Table I: Parameters for Argon-Adsorption Isotherms at 77.5°K with Composite Substrates (TCP + Graphon)^a

Wt % of TCP/ g of Graphon	Σ , m ² /g of Graphon	γ , mole ² / kcal ²	$\pm r$, cal/ mole	K'	U_0' , kcal/ mole
0	96.0	70	57	1.83	2.25
1.32	78.0	70	57	2.13	2.23
2.58	60.0	70	57	2.13	2.23
3.86	50.0	20	107	2.74	2.19
5.08	41.3	10	151	4.35	2.12

^a The following additional composite substrates, expressed as % TCP/g of Graphon, were prepared and the adsorption isotherms were determined: 7.68, 9.96, 15.0, 20.0, and 30.0%. The parameters could not be determined by matching; the isotherms are reported in Figure 1.

(9) S. Ross and J. P. Olivier, "On Physical Adsorption," John Wiley and Sons, Inc., New York, N. Y., 1964.

(10) J. H. de Boer, "The Dynamical Character of Adsorption," Clarendon Press, Oxford, 1953.

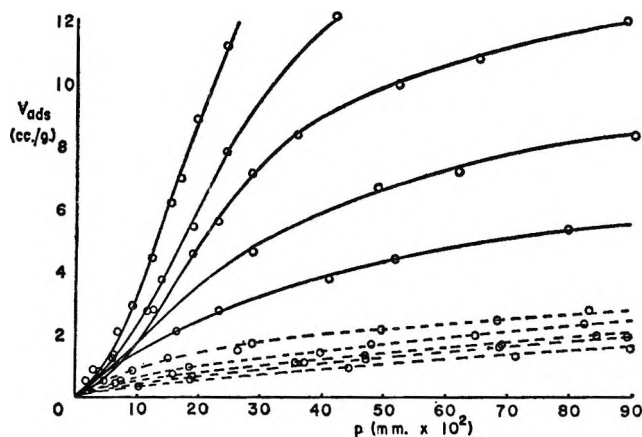


Figure 1. Adsorption isotherms of argon at 77.5°K on graphite-TCP composite substrates. The top five isotherms are matched with Ross-Olivier model isotherms (solid lines). The lower five isotherms (see footnote a, Table I) are not matched.

homotactic patch of the adsorbent, the adsorbate behavior is described by the Hill-de Boer equation

$$p = K_i \frac{\theta_i}{1 - \theta_i} \exp\left(\frac{\theta_i}{1 - \theta_i} - \frac{2\alpha\theta_i}{kT\beta}\right) \quad (2)$$

where θ_i is the surface concentration, in terms of degree of surface covered by adsorbate, of the i th patch at the equilibrium pressure p ; K_i is an adsorption parameter characteristic of the adsorptive energy, U_{0i} , of the i th patch, and related to it as

$$K_i = A^0 \exp(-U_{0i}/RT) \quad (3)$$

The term A^0 is a function of the changes in translation, rotation, and vibration that occur to the argon atom on adsorption. For a mobile adsorbed film, $\ln A^0$ is given by

$$\ln A^0 = -\frac{\Delta S_s^{tr}}{R} - \frac{\Delta S^{rot}}{R} + \frac{{}_a E^{vib} - {}_a E_0^{vib}}{RT} + \frac{\Delta E^{kin}}{RT} - \ln \frac{\theta_s}{1 - \theta_s} + \ln 760 \quad (4)$$

where the terms given refer to standard-state changes, on adsorption, of entropy, Gibbs function, and kinetic energy; θ_s is the surface concentration at the standard state of the adsorbed films ($\pi_s = 0.338$ dyne/cm) and 760 mm is the standard state of the gas. The term $\ln A^0$ describes in mathematical language the character of the adsorbed film, taking into account a new vibration, peculiar to the adsorbed state, of the molecule with respect to the substrate. The term has been evaluated experimentally⁹ for adsorbed argon at 77.5°K on a graphite substrate, where it has the value $A^0 = 4.07 \times 10^6$ mm. This value is used in the present work.

The composite substrates of the present investigation are not the same as the graphite substrate for which the evaluation was made, but there is no reason to anticipate that significant changes in the character of the two-dimensional adsorbed film, which determines the value of $\ln A^0$, would thereby occur. Actually, the Ross-Olivier theory likewise postulates the same value of $\ln A^0$ on every patch of a heterogeneous substrate, even where such patches are quite different in adsorptive energy from the crystallographic graphite substrate. The postulate is to be regarded, at present, as a convenient approximation.

The distribution of adsorptive potentials, which is the next factor to be considered, is probably not capable of any simple mathematical description, but a body of experimental evidence indicates that it can usually be approximated successfully by the equation for the gaussian distribution. Let df_i represent the fraction of the substrate that has adsorptive energies between U_{0i} and $U_{0i} + dU_0$, and let U_0' represent the average (most frequently occurring) adsorptive potential energy. The gaussian-distribution equation is

$$df_i = \frac{1}{n} \exp[-\gamma(U_0 - U_0')^2] dU_0 \quad (5)$$

where n is a normalizing factor required to make $\int_0^\infty df_i = 1$ and γ is a characteristic constant that describes the range of the distribution.

Using eq 2 as the "local isotherm equation" on each homotactic patch and eq 5 to describe the distribution of these patches on the total substrate, tables of computed model isotherms have been published for different values of the constants $2\alpha/RT\beta$ and γ . By suitable graphical devices, experimentally obtained adsorption isotherms can be matched against these model isotherms until the best match with the observed data is found. This match yields values for the constants γ , α/β , and U_0' that would therefore correspond to and describe the observed adsorption system in the terms of the assumed model. Arguments to justify the assumed model have been presented by Ross and Olivier.⁹ It must be admitted that opinions are not unanimous in accepting the validity of the Ross-Olivier model, but it has not been countered by any positive hypothesis that offers either a more probable model or an equally effective practical method of eliciting meaningful adsorption parameters. For the analysis of the present data, for example, we should have been at a loss if that method had not been available.

Graphon was selected as the adsorbent for this investigation because it provided a large specific surface

area, *i.e.*, 96 m²/g, and a relatively low heterogeneity of substrate, *i.e.*, $\gamma = 70$. The physical meaning of γ is best comprehended in terms of the adsorptive range ($U_0 \pm r$) within which one-half of the total surface lies. The degree of heterogeneity is then expressed by

$$r = 47/\sqrt{\gamma} \text{ cal/mole} \quad (6)$$

The adsorption isotherm reflects the character of the total substrate; therefore, the method of matching gives values of the adsorption parameters that pertain to the substrate as a whole. In the present work, TCP monolayers are spread over a relatively homogeneous graphite surface; the monolayers themselves would likewise be expected to provide another relatively homogeneous substrate. At concentrations of TCP less than monolayer coverage, both substrates are present; the adsorption parameters then refer to the average of the two substrates. The values of U_0' decrease slightly as the graphite substrate is increasingly covered with TCP, showing that TCP monolayers and, particularly, multilayers give rather less active substrates for adsorption than does graphite. That this should be so is not surprising, as the basal plane of graphite is known to be much more receptive to physical adsorption than most substrates.¹¹ For the composite substrate, the change in U_0' is linked with a change in the distribution of substrate heterogeneity, as measured by r in eq 6. If the two components of the substrate have values of U_0' that are sufficiently far apart, a bimodal distribution may be evident, but normally the composite distribution can still be described in terms of a single mode. When the two values of U_0' do not differ too much from one another, the sum of the distributions would produce a wider distribution than either one separately.

The TCP monolayer does not seem to differ much from graphite in affecting the adsorptive potential of argon. The polarity of the TCP molecule, no doubt, plays a part in transmitting the surface electric field of the underlying graphite substrate. At submonolayer concentrations of TCP, the decrease in U_0' , although observable, is not large enough to affect the experimental determination of r , which is more troublesome than U_0' to obtain precisely. In other words, the expected increase of heterogeneity is not manifest in the range of submonolayer coverage, *i.e.*, below about 2.5% TCP.

The second and succeeding layers of TCP, however, would not be expected to transmit the surface electric field so faithfully as the first layer, because the molecules would have more freedom to assume the mutual configurations normally found in the bulk liquid phase.

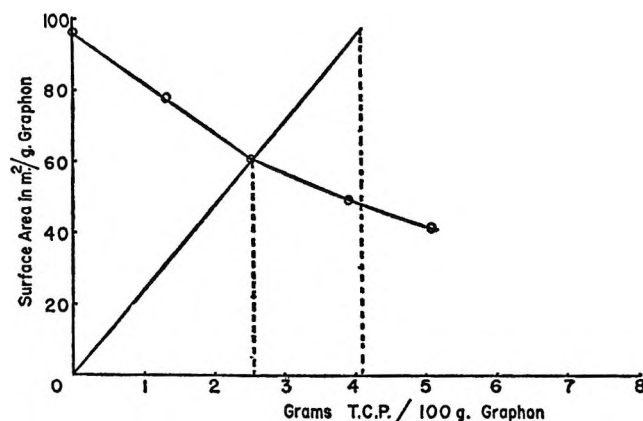


Figure 2. The decrease of available surface of the composite substrates as a function of TCP added. The straight line through the origin represents the area provided by the added TCP if extended as a close-packed planar monolayer. The point of intersection is at the saturated monolayer of TCP on Graphon. The separation of the two dotted vertical lines is a measure of the roughness of the substrate.

Accordingly, once the monolayer of TCP is completed and multilayers of TCP occur, the decrease of the average adsorptive potential (U_0') becomes more pronounced. The larger decrease of U_0' now begins to show its effect on the distribution of adsorptive potentials, which becomes wider. Ultimately, when more than two layers of molecules are present, the distribution of surface potentials is too wide to be measurable by the technique employed. Even when a substrate corresponding to bulk liquid is achieved by laying down a number of layers of TCP, the expected homogeneity of a liquid substrate would not be revealed by these measurements, which are carried out well below the freezing point of TCP. A polycrystalline layer of solid TCP would give a heterogeneous substrate for adsorption.

The specific surface area of the adsorbent decreases when a composite substrate is made by addition of even small quantities of TCP and the decrease is continuous with addition of TCP (Figure 2). The decrease in area is interpreted as evidence of surface roughness. If the surface of Graphon were ideally smooth, the addition of TCP or any nonvolatile liquid capable of spreading as a monolayer would not affect the specific surface area: adsorbed argon would lie indifferently on top of the solid substrate or on top of the preadsorbed monolayer.

Of the total surface area of the adsorbent, that portion consisting of the preadsorbed monolayer of TCP increases linearly with the quantity of TCP present on the surface. Simultaneously, the portion of the

(11) F. M. Fowkes, *Ind. Eng. Chem.*, **56**, No. 12, 40 (1964).

surface consisting of the bare carbon substrate decreases continuously and, for nearly homotactic substrates, almost linearly. Because of surface roughness, the loss in area of original bare substrate is greater than its replacement by substrate composed of preadsorbed liquid. At some point, the original substrate will be completely covered with a monolayer of nonvolatile oil; at that point, the area offered to the argon will be derived solely from a substrate composed of preadsorbed liquid. The point in question is determined experimentally by the intersection of the two curves shown in Figure 2. The linear curve is a calculation of the areas that would be extended by varying amounts of liquid TCP spread as a close-packed planar monolayer. This calculation is based on a "flat-on" projection of the TCP molecule, a value for which ($145 \text{ \AA}^2/\text{molecule}$) was found by means of a molecular model. The total specific surface area of the composite substrate, shown by the experimentally obtained curve of negative slope in Figure 2, intercepts the linear plot at a value of $59 \text{ m}^2/\text{g}$ and at 2.5% TCP in grams per gram of carbon. At this point, the area available to the argon molecules on the composite surface equals that provided by TCP molecules when extended as a planar monolayer. The $96 \text{ m}^2/\text{g}$ of Graphon has been covered with a layer of TCP that provides only $59 \text{ m}^2/\text{g}$ of available surface. This, therefore, is the empirical monolayer point of TCP on Graphon. It requires less TCP than the 4.1% calculated from the area of the bare solid substrate and that of the TCP molecule. The larger TCP molecule rests across ridges formed by the surface roughness, and thus preempts more area of the substrate than corresponds to its own cross-sectional area. The ratio of the two values is a measure of the surface roughness of the solid. From the data of the present experiments, the surface roughness of the solid is the ratio of 4.1 to 2.5, or 1.6, *i.e.*, the ratio of the calculated to the observed values of the amount of TCP for monolayer coverage. This value agrees well with a determination of the surface roughness of another sample of Graphon measured by Abram and Parfitt,¹² using the adsorption isotherm of Aerosol OT in aqueous solution. The result obtained for the roughness factor was 1.47. Abram and Parfitt used 55 \AA^2 for the cross-sectional area of the Aerosol OT molecule, so that their rather lower result for the

surface roughness (1.47 compared to 1.6) is reasonable, as the smaller molecule (Aerosol OT) would cover the roughness of the substrate less effectively than the larger molecule (TCP). However, the small magnitude of the difference is actually about equal to the possible error; hence, the effect of the molecular size of the adsorbate, as long as it is more than about 50 \AA^2 , is not really significant.

We have now to consider why the specific surface continues to decrease, albeit at a lower rate, beyond the value of 2.5 g of TCP/100 g of Graphon. The values of specific area for the composite substrates of composition more than 5% cannot be calculated by the Ross-Olivier technique, but inspection of the adsorption isotherms for these samples (Figure 2) indicates that the specific areas are decreasing, although more gradually. As more TCP is added to the substrate, larger irregularities of the composite surface are gradually filled in, until presumably the surface area is reduced to zero. These irregularities may be large pores in the particle or the interstitial spaces between the particles.

For general application, the present method of determining the surface roughness of a powdered solid need not depend on the use of the Ross-Olivier matched isotherms, although where they can be used one obtains more information about the system. For solids that offer too wide a range of substrate heterogeneity the Ross-Olivier method may be inapplicable, but since a determination of specific surface area is all that is required, the BET method, using either nitrogen or argon as an adsorbate at 77.5°K , could be used. A disadvantage of the present method of determining surface roughness is that the result depends on the size of the preadsorbed oil molecule. Irregularities of the substrate, of dimensions greater than those of the oil molecule, would not be "perceived" by the molecule and so would not be taken into account in the roughness factor obtained. The use of a larger preadsorbed molecule would avoid this difficulty.

Acknowledgment. The authors acknowledge a research grant, NSF-G19504, from the National Science Foundation, for the support of this work.

(12) J. C. Abram and G. D. Parfitt, "Proceedings of the Fifth Conference on Carbon," Pergamon Press Ltd., Oxford, 1962, pp 97-102.

The Vapor Pressure of Boron Oxide over the Range 1946–2419°K

by Frank T. Greene and John L. Margrave

Departments of Chemistry, University of Wisconsin, Madison, Wisconsin, and Rice University, Houston, Texas (Received August 18, 1965)

Direct boiling point and transpiration vapor pressure measurements on liquid B_2O_3 lead to the equation

$$\log p_{\text{atm}} = (7.124 \pm 0.064) - \frac{(1.763 \pm 0.055) \times 10^4}{T}$$

where $1946^\circ < T^\circ\text{K} < 2419^\circ$. Thus, $\Delta H^\circ_{2196^\circ\text{K}} = 80.2 \pm 2.5$ kcal mole⁻¹ and $\Delta S^\circ_{2196^\circ\text{K}} = 32.6 \pm 0.3$ cal deg⁻¹ mole⁻¹, but further interpretation of these data and an exact derivation of $\Delta H^\circ_{298^\circ\text{K}}$ are ambiguous because of the current uncertainty about the structure of $B_2O_3(\text{g})$.

Although the recent review of the vapor pressure of B_2O_3 presented in the "JANAF Tables"¹ cites 11 studies on this material,^{2–12} only one team of investigators worked at temperatures over 1650°K and none of the measurements extended into the pressure range of 10–760 mm. Interpretation of the data and calculation of a correct heat of vaporization are heavily dependent on the molecular structure and vibrational frequencies of the gaseous species (established mass spectrometrically as B_2O_3 monomer over the range 1300 to 1500°K) and on the thermodynamic properties of liquid B_2O_3 , which are extrapolated from data over the range 381–1777°K. This paper presents transpiration data and direct boiling point measurements over the range 1946–2419°K and establishes the normal boiling point of B_2O_3 as 2475°K.

Experimental Section

Previous studies on B_2O_3 have shown that there are two major obstacles which must be overcome in order to get reliable vapor pressure data. First, the sample must be absolutely free of water to eliminate interferences caused by gaseous hydroxides¹³ and, second, the sample must be free of dissolved oxygen to suppress the formation of gaseous BO_2 .¹⁴ In the present work, the volatile impurities were eliminated by rigorous degassing of the sample.

Crude boric oxide was first prepared by the dehydration of reagent grade boric acid in platinum crucibles open to the atmosphere. Samples of this crude boric

oxide were then transferred to crucibles of molybdenum, Al_2O_3 , or fused ZrO_2 and placed in the inductively heated vacuum furnace shown in Figure 1. The upper radiation shields were removed to permit direct observation of the boric oxide surface through a window on the top of the furnace. It was found that individual bubbles breaking the surface were clearly visible even

- (1) D. R. Stull, Ed., "JANAF Thermochemical Tables," Dow Chemical Co., Midland, Mich., Dec 31, 1964. Now available as document PB-168,370 from the Clearinghouse for Federal Scientific and Technical Information, Springfield, Va., 22151, Aug 1965.
- (2) S. S. Cole and N. W. Taylor, *J. Am. Ceram. Soc.*, **18**, 82 (1935).
- (3) R. Speiser, S. Naiditch, and H. L. Johnston, *J. Am. Chem. Soc.*, **72**, 2578 (1950).
- (4) J. R. Soulen, P. Sthapitanonda, and J. L. Margrave, *J. Phys. Chem.*, **59**, 132 (1955).
- (5) A. W. Searcy and C. E. Myers, *ibid.*, **61**, 957 (1957).
- (6) M. D. Sheer, *ibid.*, **61**, 1184 (1957).
- (7) A. N. Nesmeyanov and L. P. Firsova, *Russ. J. Phys. Chem.*, **34**, 490 (1960).
- (8) D. White, P. N. Walsh, H. W. Goldstein, and D. F. Dever, *J. Phys. Chem.*, **65**, 1404 (1961).
- (9) A. Sommer, Ph.D. Thesis, The Ohio State University, 1962.
- (10) P. E. Blackburn, "Research on Thermodynamics of the Al–B–O and Be–B–O Systems," Quarterly Report No. 4, Arthur D. Little, Inc., Mar 1–May 31, 1963, and following reports.
- (11) D. L. Hildenbrand, W. F. Hall, and N. D. Potter, *J. Chem. Phys.*, **39**, 296 (1963).
- (12) A. Buchler and J. B. Berkowitz-Mattuck, *ibid.*, **39**, 286 (1963).
- (13) (a) D. White, D. E. Mann, P. W. Walsh, and A. Sommer, *ibid.*, **32**, 488 (1960); (b) S. P. Randall and J. L. Margrave, *J. Inorg. Nucl. Chem.*, **16**, 29 (1960).
- (14) (a) W. E. Kaskan, J. D. MacKenzie, and R. C. Millikan, *J. Chem. Phys.*, **34**, 570 (1961); (b) J. W. C. Johns, *Can. J. Phys.*, **39**, 1738 (1961).

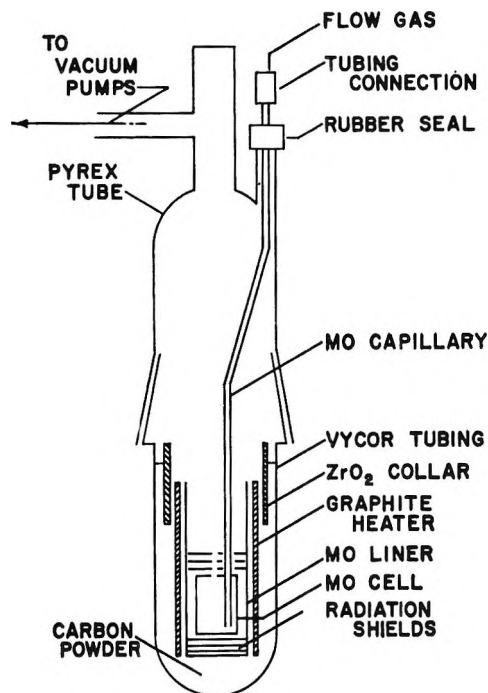


Figure 1. Transpiration vapor density apparatus.

at the highest temperatures. Temperatures were read from a blackbody hole formed by the crucible wall and the first radiation shield with a Leeds and Northrup optical pyrometer. A correction was made for the transmission of the window. Pressures were measured with a standard mercury manometer.

The sample was first outgassed at 1200° for a minimum of 6–8 hr. Argon, which had been purified by passage through a Dry Ice trap packed with silica gel and over copper turnings at 400° , was bled into the system and the temperature was raised. The pressure was then reduced until bubbling was observed, the pressure read, a few millimeters of argon introduced to stop the boiling, and the temperature reread. To determine when the sample was entirely degassed, the pressure was then reduced and the sample was allowed to boil vigorously for several minutes. Argon was then bled into the system and the boiling point was determined as before. This was repeated, with alternation of higher and lower temperatures, until reproducible pressures and temperatures were obtained.

The sample was observed to have a slight blue-green color after the runs which were made in molybdenum crucibles. This suggests that some molybdenum oxides had been dissolved in the sample. It does not follow, however, that there was a reaction between boric oxide and molybdenum since appreciable concentrations of oxygen, water, and BO_2 were present during the early outgassing steps, and could have been

dissolved in the sample then. In any case, the effect of the dissolved oxide was apparently unimportant since the observed boiling points (see Table II) were independent of the crucible material. Subsequent transpiration experiments were, for practical reasons, carried out in molybdenum containers.

The vapor density of gaseous boric oxide was also determined, using the transpiration technique. This technique has usually been limited to lower pressure-temperature combinations than were of interest in the present work by two problems.¹⁵ One is the large uncertainty in the correction for diffusion loss, which often becomes larger than the loss due to the action of the flow gas. The other is the difficulty in assuring saturation of the flow gas. It was found that these problems can be largely avoided if the sample is placed in a cell which is closed except for a capillary through which the flow gas is introduced and a small orifice through which the gases can escape. This arrangement facilitates saturation of the flow gas, since it may be bubbled through the sample or blown against the sample's surface to attain maximum gas-sample contact. With a relatively small orifice, the diffusion loss becomes both small and reproducible. This permits lower flow rates and better equilibration of the gas within the cell.

This modified technique was used to determine the vapor density of the boric oxide vapors above 1500° , providing simultaneously a test of the method and a check on the accuracy of the boiling point measurements. The apparatus is shown in Figure 1. The cell was constructed of molybdenum and the capillary was made by drilling a 0.0625-in. hole through the center of a 0.125-in. diameter molybdenum rod. Above the hot zone the molybdenum capillary was joined to stainless steel tubing. The orifice was 1 mm in diameter, and the temperature was read from it.

Boric oxide was placed in the molybdenum crucible and degassed to a constant boiling point as in the boiling point measurements. The cover was then added and the capillary inserted with its tip near the bottom of the crucible, so that the flow gas bubbled through the boric oxide sample.

The crucible was first heated under a dry argon atmosphere (with no flow gas) until a constant rate of weight loss was obtained. This weight loss due to diffusion was found to be a highly reproducible linear function of temperature over this limited temperature range.

(15) See, for example, J. L. Margrave in "Physico-Chemical Measurements at High Temperatures," J. O'M. Bockris, J. L. White, and J. D. MacKenzie, Ed., Butterworth and Co. Ltd., London, 1959, Chapter 10.

Four runs were made at two temperatures, using dried argon as the flow gas. The gas volume was measured by the displacement of water. The vapor density at a given temperature was calculated from the relation: $\rho = (R_T - R_D)/f$, where R_T is the average total rate of weight loss, R_D is the rate of weight loss due to diffusion, and f is the argon flow rate.

Results

The details of the transpiration measurements are presented in Table I. The relative lack of dependence of the vapor density on the flow rate indicates that saturation was approached. The pressures, calculated assuming vaporization to boric oxide monomer, are in good agreement with the pressures obtained from the direct boiling point measurement.

Table I: Vapor Density Measurements by the Transpiration Method

Run	Average flow rate, cc/min	Temp, °K	Vapor density, ^a g cc ⁻¹ × 10 ⁵	Calcd press., atm
1	21	1956	7.99	0.0147
2	23	2089	20.75	0.0511
3	39	2087	20.72	0.0511
4	11	2094	19.31	0.0477

^a Calculated assuming vaporization to B₂O₃ monomer.

The results from the direct boiling point and transpiration experiments are summarized in Table II. A least-squares treatment of the combined data yields the equation

$$\log P_{\text{atm}} = (7.124 \pm 0.064) - \frac{(1.763 \pm 0.055) \times 10^4}{T}$$

where 1946° < T °K < 2419°, giving an average value of the heat of vaporization over this temperature range of 80.2 ± 2.5 kcal mole⁻¹, an average entropy of vaporization of 32.6 ± 0.3 cal deg⁻¹ mole⁻¹ and an extrapolated boiling point of 2475 ± 50 °K.

The errors indicated above are standard deviations obtained from the least-squares calculation. The systematic errors were possibly much larger. It was not possible to measure the temperature gradients in the furnace with the crucible in place. Rough pyrometric measurements along the axis of the empty furnace revealed a temperature variation of 3–4%. Much more minor errors could arise from the optical pyrometer calibration, from the failure to obtain a perfect blackbody, and from scattering of the black-

Table II: Boiling Point and Transpiration Data for B₂O₃

Temp, °K	P, atm	$\Delta H^{\circ}_{298^{\circ}\text{K}}$, kcal mole ⁻¹	
		C _{2v} model	D _{3h} model
(a) Direct Boiling Point Data			
1946	1.48×10^{-2}	102.2	84.4
2026	2.69×10^{-2}	103.6	84.9
2068	4.58×10^{-2}	103.3	84.2
2083	5.62×10^{-2}	103.1	83.9
2154	7.08×10^{-2}	105.3	85.3
2172	1.07×10^{-1}	104.3	84.2
2176	1.66×10^{-1}	102.5	82.4
2218	1.78×10^{-1}	104.0	83.5
2273	2.46×10^{-1}	104.8	83.8
2342	4.17×10^{-1}	105.1	83.5
2381	5.79×10^{-1}	105.1	83.1
2419	7.94×10^{-1}	105.1	82.8
(b) Transpiration Data			
1956	1.47×10^{-2}	102.7	84.8
2089	5.11×10^{-2}	103.8	84.4
2087	5.11×10^{-2}	103.7	84.3
2094	4.77×10^{-2}	104.3	85.0
		Av 104.2	84.0

body radiation by condensing particles of boric oxide. The combined systematic error could be as great as 50° at the highest temperatures, which would give an error of 6–7 kcal mole⁻¹. The good agreement between the direct boiling point and transpiration measurements may therefore be misleading since the same furnace, crucibles, and geometry were used in both experiments. The temperature error, which is the major systematic error, probably contributed almost equally in the two experiments.

Discussion

One can compare these experimental results with the extrapolations and predictions made by past investigators but the interpretation of all of the data is complicated by uncertainties as to the correct structure for B₂O₃. For several years, all spectroscopic evidence was interpreted as supporting a bent C_{2v} configuration for the gaseous molecule. Derived second- and third-law heats of vaporization were reasonably consistent with this structure, although most investigators obtained lower second- than third-law values for $\Delta H^{\circ}_{298^{\circ}\text{K}}$. With this open model for B₂O₃, one predicts $\Delta S_{2000^{\circ}\text{K}} \approx 40 \pm 2$ cal deg⁻¹ mole⁻¹ for evaporation. Recently, however, Hanst, Early, and Klemperer¹⁶ reported new infrared and mass spectroscopic results which were inconsistent with a C_{2v} configuration and which supported

(16) L. Hanst, V. H. Early, and W. Klemperer, *J. Chem. Phys.*, **42**, 1097 (1965).

a structure with D_{3h} symmetry. The latter structure would give an entropy for gaseous B₂O₃ considerably smaller than for a C_{2v} structure¹⁷ and, if one accepts the JANAF data for liquid B₂O₃, predicts $\Delta S_{2000^\circ\text{K}} \approx 29 \pm 1 \text{ cal deg}^{-1} \text{ mole}^{-1}$.

The vapor pressure data obtained in this investigation have been treated using both the C_{2v} and D_{3h} models. The resulting third-law values for $\Delta H^\circ_{298^\circ\text{K}}$ are given in Table II. The free energy functions for the liquid phase and the C_{2v} model were taken from the JANAF tables; those for the D_{3h} model were taken from Kallman and Kreiger.¹⁷ These calculations yield a value for $\Delta H^\circ_{298^\circ\text{K}}$ of $104.2 \pm 2.0 \text{ kcal}$ for the C_{2v} model and $84.0 \pm 0.7 \text{ kcal mole}^{-1}$ for the D_{3h} model. Taking enthalpy data from the same sources, one obtains second-law values for $\Delta H^\circ_{298^\circ\text{K}}$ of 92 ± 3 and $93 \pm 3 \text{ kcal mole}^{-1}$ for the C_{2v} and D_{3h} models, respectively. The D_{3h} calculation is essentially that presented by Soulen and Margrave.¹⁸

Since the paper by Hanst, *et al.*,¹⁶ invalidates all the old ideas about vibrational frequencies for B₂O₃ except for features at $\sim 1300\text{--}1400 \text{ cm}^{-1}$ and since lower frequencies will play predominant roles in determining values for the thermodynamic functions, it is not possible to choose between the two proposed structures on the basis of available data. The vapor pressure data yield definite ΔH_T and ΔS_T values which are independent of guesses about the molecular structure. One has available the opportunity to test various estimated thermodynamic functions over a range of high

temperatures. If the C_{2v} model is correct, the discrepancy between the JANAF value for $\Delta H^\circ_{298^\circ\text{K}}$ of $100 \text{ kcal mole}^{-1}$ and that obtained here of $104 \text{ kcal mole}^{-1}$ indicates that the free energy functions in the range $1900\text{--}2500^\circ\text{K}$ should be revised by $1\text{--}2 \text{ cal deg}^{-1} \text{ mole}^{-1}$, either by making the gas functions less negative or the liquid functions more negative, or both. If, on the other hand, B₂O₃ has a structure with D_{3h} symmetry, the gas functions must be more negative than those of Kallman and Kreiger to be consistent with the value for $\Delta H_{298^\circ\text{K}}$ of $90\text{--}100 \text{ kcal mole}^{-1}$, indicated by the same second-law values.

Final conclusions about the absolute thermodynamic properties of B₂O₃(g) and B₂O₃(l) will have to await a definitive molecular structure determination, a reliable infrared study of gaseous B₂O₃, and a precise determination of enthalpy increments for liquid B₂O₃ up to 2000°K .

Acknowledgments. This work, taken in part from the Ph.D. thesis of F. T. Greene, was supported financially by the United States Navy and by the Advanced Research Projects Agency through funds administered by the Army Research Office, Durham, N. C.

(17) H. K. Kallman and F. J. Kreiger, "The Thermodynamic Properties of Boric Oxide and Aluminum Oxide in the Ideal Gaseous State," Rand Report P-120, The Rand Corp., Santa Monica, Calif., Feb 1949.

(18) (a) J. R. Soulen, Ph.D. Thesis, University of Wisconsin, 1956; (b) J. R. Soulen and J. L. Margrave, *J. Am. Chem. Soc.*, **78**, 2911 (1956).

The Rate of Reaction of Chloroacetate Ion with Thiocyanate in Concentrated Solutions

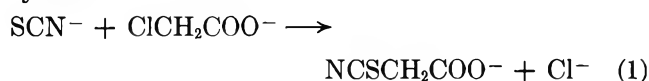
by Thomas I. Crowell, Jackson E. Hicks, and Ching Chih Lai

Cobb Chemical Laboratory, University of Virginia, Charlottesville, Virginia (Received August 19, 1965)

The S_N2 reaction of thiocyanate ion with chloroacetate ion was studied kinetically at 1:1 electrolyte molarities (*c*) of 0.0075–7.7 and at several temperatures. The rate constants for the potassium salts at 25° are correlated by the equation $6 + \log k (M^{-1} \text{ sec}^{-1}) = c^{1/2}/(1 + c^{1/2}) + 0.059c + 0.272$. The activation energy is 18.9 kcal/mole at both *c* = 2.1 and *c* = 5.5. Differences in the effects of the cations, K⁺ and Na⁺, or the anions, ClCH₂COO⁻, SCN⁻, and Cl⁻, are not large.

Introduction

The high nucleophilic reactivity of thiocyanate ion in solution together with the low melting point and high solubility of KSCN led us to believe that an organic displacement reaction could be studied over a wide range of concentrations, from dilute aqueous solution to the pure fused salt. Reasoning that the organic compounds most soluble in these media would be ionic,¹ we selected the reaction of chloroacetate ion with thiocyanate.



Although limited solubility of potassium chloroacetate at room temperature and rapid decomposition at high temperature discouraged measurements of the most concentrated solutions, we obtained data at ionic strengths up to 7.7 *M* and temperatures from 25 to 62.5°.

Experimental Section

Potassium chloroacetate and sodium chloroacetate were prepared by neutralizing reagent grade chloroacetic acid to the phenolphthalein end point with the corresponding hydroxide. Reaction mixtures were made up by conventional methods, titrated with iodate, and checked with silver nitrate as in previous studies with *n*-alkyl bromides.² In very dilute solutions, because of the difficulties previously encountered in studying the thiocyanate–bromoacetate reaction,³ reaction 1 was followed by analysis for chloride, in order

to eliminate all errors caused by interference of products with the iodate titration. A gravimetric modification of the method of Backer and Van Mels⁴ was used. A sample of the reaction mixture containing 0.5 mmole of SCN⁻ was acidified with nitric acid, and silver nitrate solution was added to precipitate silver chloride and silver thiocyanate. Chloroacetic acid did not react under these conditions. After collecting and washing the precipitate in a sintered-glass crucible, 15 ml of concentrated nitric acid was added, and the crucible was placed inside a covered beaker and warmed on the hot plate until oxidation of the silver thiocyanate was complete. The silver chloride remaining was washed, dried at 110° for 3 hr, and weighed.

In experiments run at higher temperatures, the reactants were pipeted into the compartments of a divided erlenmeyer flask,⁵ warmed in the thermostat, and mixed by swirling. After the desired time interval, the reaction mixture was cooled and titrated. The rate constant so obtained was multiplied by d_{25}/d_t to correct for the decrease in molarity caused by thermal expansion of the liquid.

(1) We now know that hydroxyl groups in sufficient number cause high solubility of organic compounds in fused KSCN (175°) or KSCN–NaSCN (130°); see T. I. Crowell and P. Hillery, *J. Org. Chem.*, **30**, 1339 (1965).

(2) T. I. Crowell, *J. Am. Chem. Soc.*, **75**, 6046 (1953).

(3) V. K. La Mer and J. Greenspan, *ibid.*, **54**, 2739 (1932).

(4) H. J. Backer and W. H. Van Mels, *Rec. Trav. Chim.*, **49**, 363 (1930).

(5) V. K. La Mer and M. E. Kamner, *J. Am. Chem. Soc.*, **57**, 2662 (1935).

In contrast to alkyl bromides, which consumed 99% of the theoretical quantity of thiocyanate ion,² chloroacetate ion appeared to proceed only about 97% to completion in the more concentrated potassium thiocyanate solutions where it was feasible to observe the final stages of the reaction. (The chloroacetic acid used yielded $99.9 \pm 0.3\%$ of theoretical chloride ion upon alkaline hydrolysis; hydrolysis in these kinetic runs was negligible.) It was found that the product, prepared as described below, reacted slightly with the titrating solution, causing a 1–4% error in the calculated thiocyanate concentration. This behavior of the reaction product is similar to that of the Bunte salt formed by the action of thiosulfate ion on alkyl halides, though error can be minimized in the latter case by avoiding an excess of iodine in the titration.⁶

The reaction product, potassium thiocanoacetate, was isolated by evaporating reaction mixtures to dryness and extracting with boiling methanol. The crystals so obtained showed a sharp infrared peak at 4.6μ . The compound was also prepared by dropwise addition of 50 g of ethyl chloroacetate to a boiling solution of 33 g of sodium thiocyanate in 150 ml of ethanol. The precipitated sodium chloride was filtered off, water was added to the filtrate, and the organic layer was separated and dried over magnesium sulfate. The ethyl thiocanoacetate fraction boiling at $117\text{--}119^\circ$ (12 mm) showed the sharp RSCN peak at 4.6μ . Rearrangement to ethyl isothiocanoacetate was effected in poor yield by heating 2.5 hr at 250° under an atmosphere of nitrogen. The product, bp $75\text{--}80^\circ$ (0.9 mm) showed a broad RNCS band at $4.6\text{--}4.9 \mu$. Both esters could be hydrolyzed by adding just enough potassium hydroxide solution to cause the compound to dissolve in boiling water. Evaporation of the solution obtained from the unrearranged ester produced crystals of potassium thiocanoacetate. The infrared spectrum of this solid was identical with that of the reaction product except for a small peak at 4.9μ .

Results

The second-order rate constants, k , are plotted logarithmically in Figure 1 against the square root of the electrolyte molarity, c . This electrolyte concentration was just that of the reactants except when potassium chloride or sodium chloride was added. Six categories are shown on the graph. The solid circles represent a set of runs⁷ in which the initial potassium chloroacetate concentration $[KA]$ was fixed at $0.1 M$ and the potassium thiocyanate concentration $[KSCN]$ was varied to give the c value shown. In the runs⁸ indicated by open circles, the concentration ranges of $[KA]$ and $[KSCN]$ were $0.390\text{--}1.608$ and $0.508\text{--}6.88 M$,

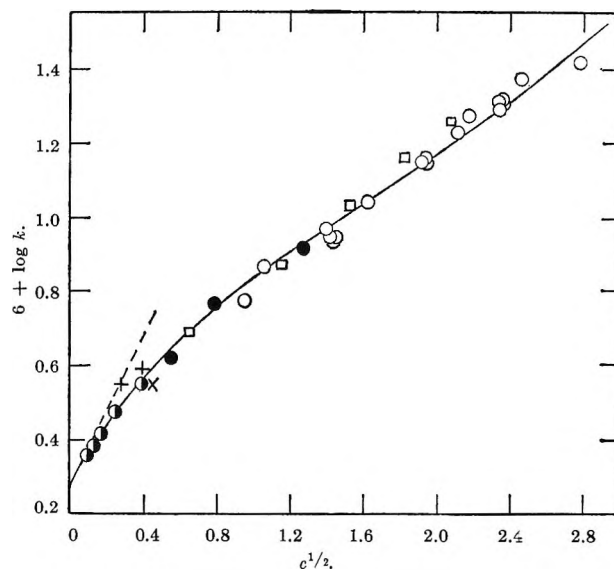


Figure 1. $\log k$ vs. $c^{1/2}$ at 25° . Experimental points as explained in the text. Curve calculated by eq 2.

respectively. The ratio $[KSCN]/[KA]$ varied from 1.2 to 8.2. A set of five experiments, starting with $[KA] = 0.131 M$, $[KSCN] = 0.202 M$, and $[KCl] = 0.1, 1.0, 2.0, 3.0,$ and $4.0 M$ is shown by squares. The reactions followed by gravimetric chloride analysis (Table I) are plotted as shaded circles \bullet in Figure 1. The k value reported⁴ for initially equal concentrations of KA and $KSCN$, $0.1 M$, is shown by \times . Two runs in this concentration range followed by iodate titration, uncorrected, are denoted by crosses $+$. The quantity c in Figure 1 is the total electrolyte molarity, which is equal to the molar ionic strength since only 1:1 electrolytes were employed.

Table I: Kinetic Runs in Dilute Solution

$[KA]_i$, M	$[KSCN]_i$, M	$10^4 k$, M^{-1} sec^{-1}	$10^4 k_{\text{cor}}$, $M^{-1} \text{sec}^{-1}$
0.00530	0.00215	2.9	2.25 ± 0.15
0.01059	0.00430	2.73	2.42 ± 0.10
0.02118	0.00860	2.76	2.60 ± 0.10
0.0424	0.0172	3.07	2.97 ± 0.10
0.1059	0.0430	3.58	3.55 ± 0.09

Although the hydrolysis of chloroacetate ion is very slow at 25° and pH 6 (1% complete in 3 months), it was appreciable in the reactions of Table I. The

(6) T. I. Crowell and L. P. Hammett, *J. Am. Chem. Soc.*, **70**, 3444 (1948).

(7) J. E. Hicks, M.S. Thesis, University of Virginia, 1960.

(8) C. C. Lai, M.S. Thesis, University of Virginia, 1965.

specific hydrolysis rate was determined to be $1.3 \pm 0.2 \times 10^{-9} \text{ sec}^{-1}$. The k values in Table I were corrected for this hydrolysis by subtracting from the measured chloride the quantity calculated to be formed by hydrolysis in that time interval. The corrected chloride concentration could be used in the simple second-order integrated rate equation because the runs with the larger corrections went only a few per cent toward completion. For example, after 3.69×10^6 sec, a 100-ml sample from the second run in Table I produced 6.1 mg of silver chloride, or 0.00043 mole/l. Hydrolysis accounted for 0.00005 mole/l., leaving 0.00038 M as the chloride concentration produced by thiocyanate displacement. The correct value of $[\text{KSCN}]$ at this time is then 0.00392, and to use $0.01059 - 0.00038 = 0.01021$ as $[\text{KA}]$ (rather than the correct value of $0.01059 - 0.00043 = 0.01016$) causes an error of only 0.5% and eliminates the necessity of using more elaborate differential equations.

Possibly the measured hydrolysis rate is that of a rate-controlling internal displacement to form the α -lactone. This species could react with thiocyanate, if present, adding a first-order component of $1.3 \times 10^{-9} \text{ sec}^{-1}$. The correction described above would, however, still yield the desired rate of the external $\text{S}_\text{N}2$ attack by thiocyanate.

The estimate of reliability of the runs of Table I, given in the last column, is based on the deviations from linearity in the second-order plots, weighing errors, and in the first run, the uncertainty in the rate constant for hydrolysis. The uncertainty in k above $c = 0.2$ is generally $\pm 5\%$. The rate constants for $c = 3.70$ and $c = 5.46$ were reproduced within 1% by different operators using new solutions. Because of the possible effect of the products on the titration, however, the error in these experiments is estimated at $\pm 2\%$. At the highest concentration, $c = 7.70$, the small change in thiocyanate ion concentration due to its eightfold excess caused a greater uncertainty.

The effect of temperature on reaction rate at two different ionic strengths is shown in the Arrhenius plots in Figure 2. The activation energy E_a calculated from the slopes is $18.9 \pm 0.3 \text{ kcal/mole}$ at both $c = 2.05$ and $c = 5.46$. (The respective rates at 25° are 8.6×10^{-6} and $2.08 \times 10^{-5} M^{-1} \text{ sec}^{-1}$ and the entropies of activation, calculated using the value $\Delta H^* = E_a - RT = 18.3 \text{ kcal/mole}$, are -20.3 and $-18.5 \text{ cal/deg mole}$.)

Discussion

The rate constants for reaction 1 of the potassium salts at 25° are correlated by eq 2. If b is set equal to 0.059, the curve drawn in Figure 1 is obtained. The

$$\log \frac{k}{k_0} = \frac{c^{1/2}}{1 + c^{1/2}} + bc \quad (2)$$

ordinate is chosen as $c^{1/2}$ in order to show both the approach to the Debye-Hückel limiting slope of 1.0 (dotted line) at low concentrations and the practically linear portion of the curve from $c^{1/2} = 1$ to 2.5. The average deviations of the points from the curve is 0.017 log unit, omitting the points at $c^{1/2} = 0.273$ and 7.70. The extrapolated value of $\log k$ in infinitely dilute solution is 0.272.

Figure 3 shows the correlation of $\log k$ with $c^{1/2}$.

In the absence of satisfactory activity coefficient data for the reactants and the activated complex, eq 2 is semiempirical. (It must be realized that at the highest concentrations studied, the average distance between centers of ions is about 5 Å; the radius of

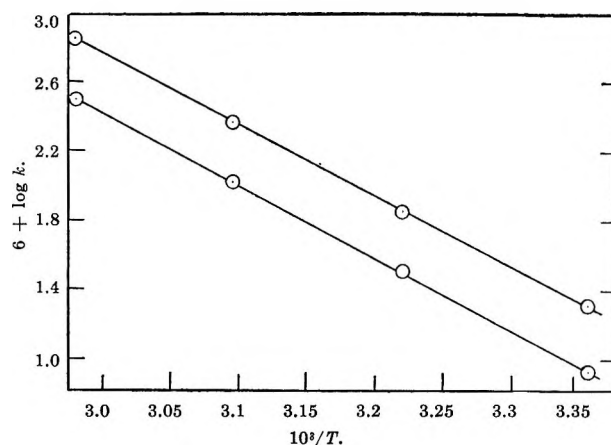


Figure 2. Arrhenius plots at $c = 2.05$ (lower line) and $c = 5.46$ (upper line).

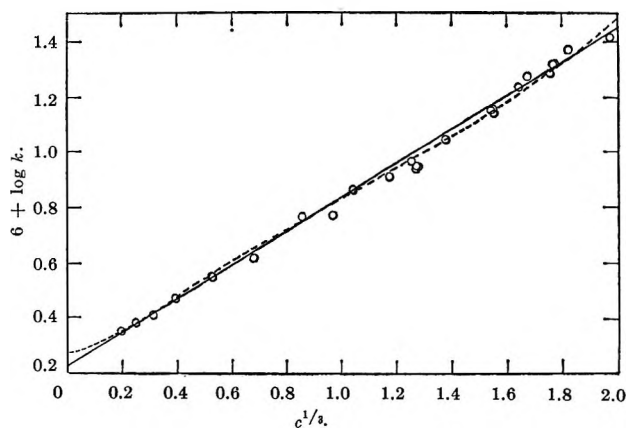


Figure 3. The experimental points are the same as in Figure 1 (omitting \square , $+$, and \times), and the values calculated by eq 2 (dotted line) are plotted against $c^{1/2}$, showing the degree to which they are approximated by $6 + \log k = 0.610c^{1/2} + 0.225$ (solid line).

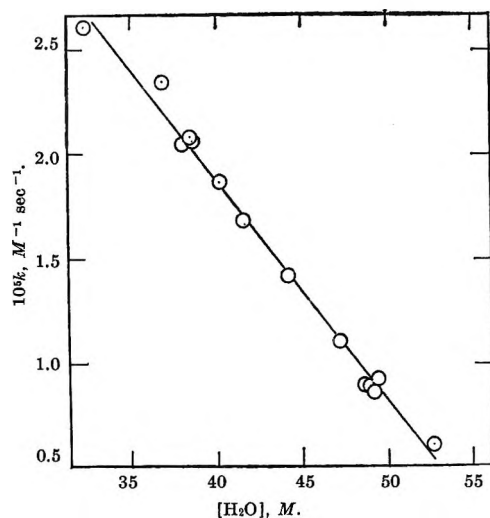


Figure 4. Correlation of rate with water concentration.

K^+ is 1.3 Å; SCN^- is about 7 Å; and there are only five H_2O molecules per positive ion.) However, in view of recent interest in kinetics in concentrated electrolyte solutions⁹ and the paucity of examples, it seems worthwhile to present the data even though complete theoretical interpretation is lacking.

The substitution of chloride for chloroacetate ion increases the rate constant only 5–8% in the higher concentration range, barely outside experimental error. This same substitution actually partially occurs during

the reaction and no general upward or downward trend in the second-order plots was observed. Preliminary results indicate that sodium ion depresses the rate about 10% in comparison with potassium.

The values of ΔH^* and ΔS^* show that there are no large parallel changes in these quantities in the medium concentration range. It would require more precise data to determine whether the increase in k with increasing electrolyte concentration is indeed chiefly associated with larger ΔS^* values. This is approximately the case in dilute solutions: differentiation of the ionic atmosphere part of ΔF^* predicts contributions to $\Delta S^*/R$ and $\Delta H^*/RT$ in the ratio 1.58/0.56 as the ionic strength is increased in water at 25°.¹⁰

Finally, we note that k increases linearly as the actual water concentration of the reaction mixtures decreases, as shown in Figure 4. The same relationship does not hold in the solutions containing KCl, however.

Acknowledgment. We are grateful for the support of the U. S. Army Research Office (Durham).

(9) (a) B. Perlmutter-Hayman and G. Stein, *J. Chem. Phys.*, **40**, 848 (1964); (b) B. Perlmutter-Hayman and Y. Weissmann, *J. Phys. Chem.*, **68**, 3307 (1964); (c) J. W. Gryder, *J. Chem. Phys.*, **37**, 718 (1962); C. W. Davies, *Progr. Reaction Kinetics*, **1**, 163 (1961).

(10) S. Glasstone, K. J. Laidler, and H. Eyring, "The Theory of Rate Processes," McGraw-Hill Book Co., Inc., New York, N. Y., 1941, pp 436, 437.

The Effect of Cyclic Oxygen Adsorption and Reduction on a Silver Surface

by A. W. Czanderna¹

*Union Carbide Corporation, Chemicals Division, Research and Development Department,
South Charleston, West Virginia (Received October 7, 1965)*

High-purity silver powder has been exposed cyclically to outgassing, oxygen adsorption, outgassing, and reduction with carbon monoxide or hydrogen (OAOR cycling) from 290 to 440°. Using a high-vacuum quartz ultramicrobalance, *in situ* measurements of the surface area, sample mass, and the rate and amount of adsorption, desorption, and reduction were carried out for numerous OAOR cycles. During cycling at the lower temperatures, a constant surface area is reached quickly, but changes in the other measurable parameters continue to occur for long periods of time. The OAOR cycling eventually produces a silver surface which has a constant surface area, sample mass, saturation oxygen uptake, and amount of desorbable oxygen and on which the rate of adsorption, desorption, and reduction can be reproduced for the same T , P , and θ conditions for many months. The rate at which the OAOR cycling produces a stable surface increases with increasing temperature. The changes in the measured parameters probably result from the elimination of the most active adsorption sites by rearrangement of silver surface atoms. This hypothesis requires that silver surface atoms have substantial mobility at the temperatures studied and/or that the surface mobility is enhanced by the presence of oxygen. It seems probable that low index plane facets are formed on an atomic scale as a result of OAOR cycling.

Introduction

In a recent study of the adsorption of oxygen on silver,² low-area silver powder and a vacuum microbalance were used to obtain maximum quantitative precision of the sorption parameters. Of the various methods of sample preparation and cleaning, the outgassing and chemical reduction technique was chosen.³ Before the adsorption study could be made, the effectiveness of the outgassing and reduction cleaning technique had to be established for silver powder. The usual disadvantages of this method of surface cleaning are these: the surface area may not become constant; the surface may be poisoned by diffusion from the bulk; the reducing gas and/or products may be chemisorbed on the surface; and finally, the chemisorption behavior of the cleaned surface may not be reproducible. The results of a study of these parameters are presented below. It was apparent that this type of study might also produce additional information about the relative importance of the adsorption, desorption, compound formation, and solubility processes that

are also possible during the interaction of oxygen with silver.

Experimental Section

The vacuum microbalance is one tool that is particularly adapted for studying the adsorption properties of low area materials over broad ranges of temperature and pressure.^{4,5} A detailed description of the operation of the balance, the vacuum system employed, the preparation of the gases used in this study, the techniques of study, and of the temperature control units has been reported before in some detail.² Surface areas were determined by nitrogen adsorption at 78°K as previously described.⁶

- (1) Clarkson College of Technology, Potsdam, N. Y. 13676.
- (2) A. W. Czanderna, *J. Phys. Chem.*, **68**, 2765 (1964).
- (3) B. M. W. Trapnell, "Chemisorption," Butterworth and Co. Ltd., London, 1955, p 16.
- (4) See ref 3, p 28 ff.
- (5) T. N. Rhodin, *Advan. Catalysis*, **5**, 55 (1953).
- (6) A. W. Czanderna and J. M. Honig, *J. Phys. Chem.*, **63**, 620 (1959).

The silver powder used in this study was Fisher reagent grade powder with a nominal purity of 99.97%. The major impurities included 0.02% sulfate and 0.005% chloride; minor metallic impurities were 0.002% lead, 0.001% copper, and 0.0005% iron. An aliquot of the powder was suspended from one side of the vacuum ultramicrobalance.

The vacuum system was used alternately to expose the sample to outgassing conditions, to oxygen for adsorption or incorporation, and to a reducing gas; the microbalance was used to monitor the mass changes that occurred in the sample during this repeated exposure to OAOR⁷ cycling. Once solubility and incorporation effects could be dismissed, it was evident that there were three important parameters that could be followed during OAOR cycling. These included the amount of mass gained by the sample during adsorption and the amount of mass lost by the sample during desorption and reduction, as shown schematically by 1, 2, and 3 of Figure 1. In addition, the rates attending the mass changes of 1, 2, and 3 also could be studied, although for the adsorption and desorption steps, it was found preferable to use lower temperatures in the later OAOR cycling stages in order to detect the subtle changes that were occurring.

Results and Discussion

The Outgassing of Silver Samples at Various Temperatures. The loss of mass by some of the silver samples studied during outgassing at different temperatures is shown in Figure 2. Here it is evident that, in general, progressively larger amounts of mass are lost at saturation as higher outgassing temperatures are employed. Silver powders exposed to temperatures higher than those shown in Figure 2 lose mass at progressively higher rates as the temperature is increased. This is oxygen that is soluble in silver which is difficult to remove even at temperatures near the melting point.⁸ However, unless contamination of the surface results from diffusion of the oxygen from the bulk to the surface, there is no apparent advantage to obtaining oxygen-free silver. It is of special interest that the amount of mass that is lost at 444° in a few hours (curve A, Figure 2) is also approached at temperatures significantly lower (curve B, Figure 2) in longer time intervals. This defines a relatively broad temperature range in which the relative amount of dissolved oxygen is not significantly different and is therefore an especially interesting region to study.

The Surface Area of Silver Powders. The effect of outgassing silver powders for 24 hr on the surface area is shown by the solid line in Figure 3. It is apparent from the shape of this line that sintering of the silver

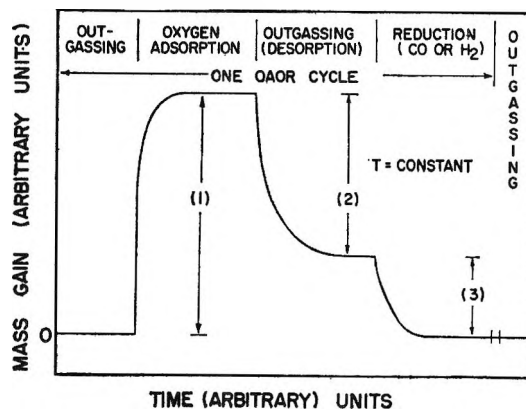


Figure 1. Schematic representation of mass changes by a silver powder in a typical OAOR cycle.

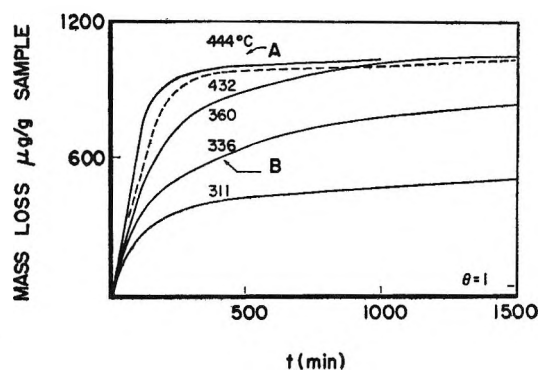


Figure 2. The outgassing of silver powders at various temperatures.

powder sets in at about 200°. Sintering of metal powders at one-half the Tammann temperature is not unexpected. Of much greater interest is the effect of OAOR cycling on the surface area as indicated by the other points shown in Figure 3. Several OAOR cycles with either carbon monoxide or hydrogen always produce a silver surface with an area of the order of 0.09 to 0.10 m²/g when the cycling is carried out between 300 and 400°.

The surface area, measured at pertinent intervals during OAOR cycling at a constant temperature, is shown in Figure 4. It is seen that after one OAOR cycle a surface is generated which remains resistant to further sintering through the five cycles shown in Figure 4. By further study, it was found that the surface area remains constant at a value of about 0.09

(7) OAOR cycling, repeated exposure of the sample to outgassing, oxygen adsorption, outgassing, and chemical reduction at a constant temperature using the same ambient pressure in each adsorption and reduction step.

(8) F. H. Buttner, E. R. Funk, and H. Udin, *J. Phys. Chem.*, 56, 657 (1952).

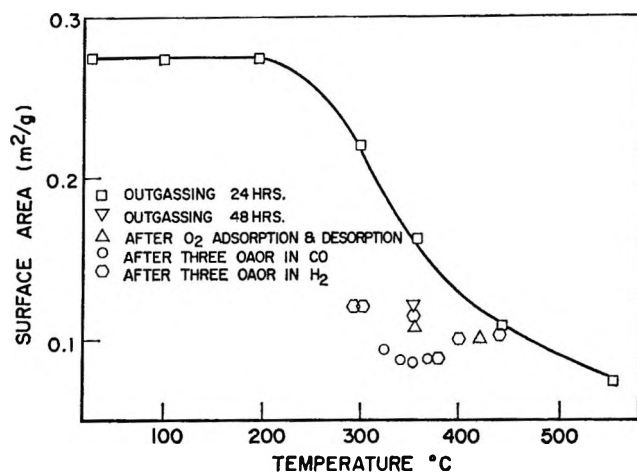


Figure 3. The surface area of silver powder after different thermochemical treatments.

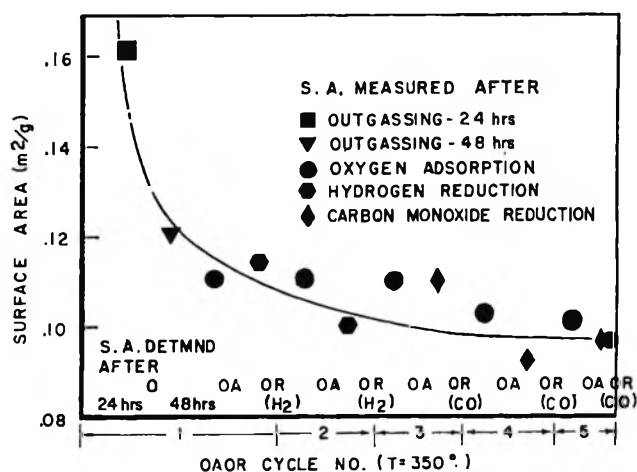


Figure 4. The surface area of silver powder at various stages of OAOR cycling.

m^2/g for over 100 OAOR cycles. During these cycles, the temperature and pressure were varied over extremely broad limits but the temperature did not exceed 400° at any time. Thus, the results shown by Figures 3 and 4 can be used to conclude that the silver surface area becomes and remains constant at an early stage of OAOR cycling at the temperatures studied.

Changes in the Chemisorption Behavior of Silver Powder During OAOR Cycling. While the sample obtained a constant surface area, the chemisorption behavior as a function of the adsorption reduction cycling continued to change. Both reproducibility of the rate of chemisorption and of the saturation uptake at the same temperature and pressure are included in the term chemisorption behavior. The changes that occur in the amount and rate of the parameters 1, 2, and 3 of Figure 1 and in the sample mass are

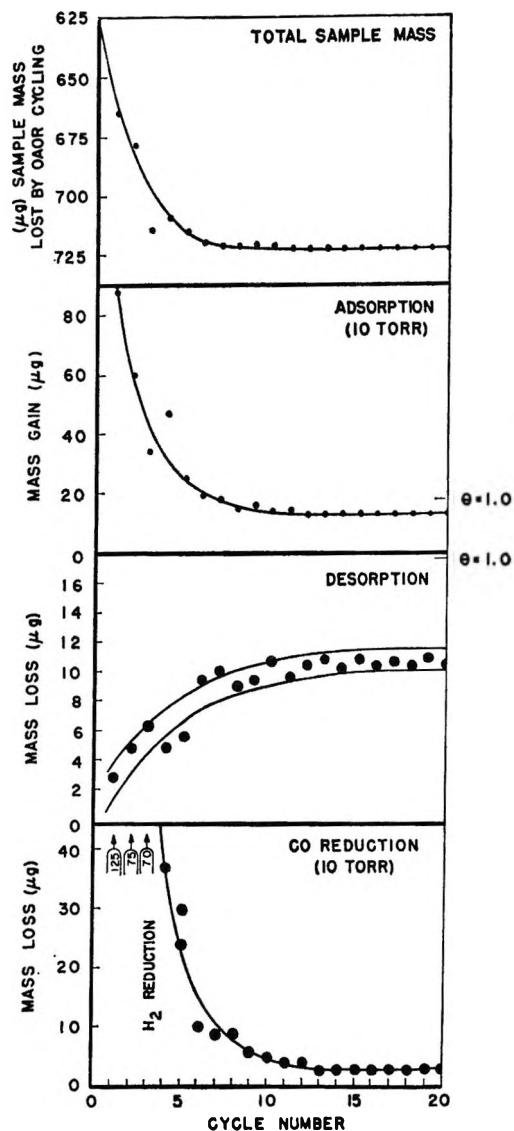


Figure 5. The effect of OAOR cycling on the total sample mass and amount of mass gained during adsorption, desorption, and reduction. Hydrogen reduction was used in the third cycle to remove chloride from the surface.

plotted for OAOR cycling at a temperature of 350° in Figures 5, 6, and 7. Here, it can be seen that the sample mass, saturation oxygen uptake, amount of desorbable oxygen, amount of mass that could be reduced from the surface, and the rate of adsorption and reduction all change gradually with the number of OAOR cycles. Ultimately, there is no measurable change in the rate or amount of these parameters with further OAOR cycling. At this time, it was found that the chemisorption behavior which is reproducible at the OAOR cycling temperature is also reproducible at all lower temperatures and at any pressure employed for oxygen adsorption up to 300 torr. Higher oxygen

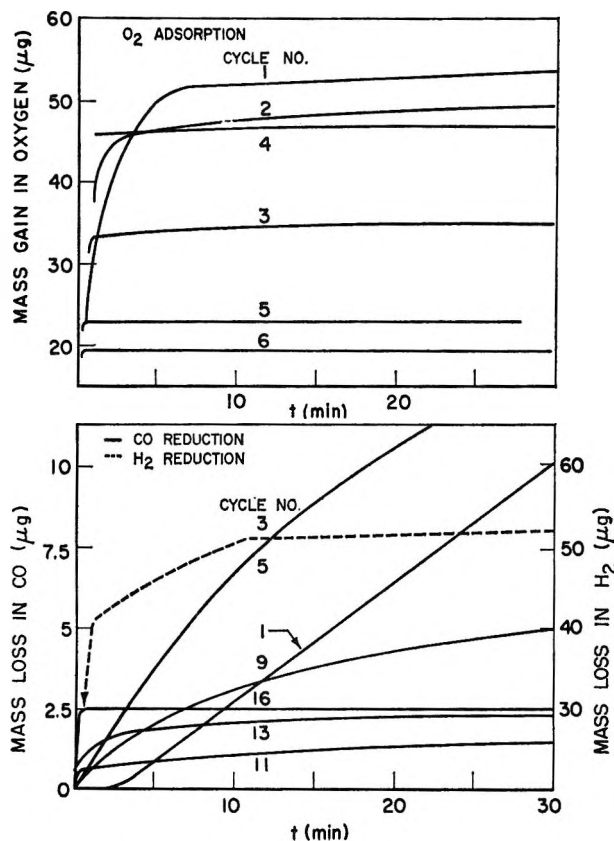


Figure 6. The mass change by a silver powder in 10 torr of CO or oxygen at various stages of OAOR cycling.

pressures were not employed. It was on this type reproducible surface that previous kinetic studies were carried out.²

The Effect of OAOR Cycling Temperatures on the Number of Cycles Required to Produce a Reproducible Chemisorption Behavior. The rate of attaining reproducible chemisorption behavior in terms of the number of OAOR cycles depends on the temperature as shown by Figure 8. To a first approximation, the number of cycles is directly related to time and, hence, when this is plotted as the ordinate of an Arrhenius plot, an activation energy of approximately 20 kcal/mole is obtained. Thus, the change in the silver surface that occurs to yield a reproducible chemisorption behavior is an activated process. The latter is more probably related to the surface diffusion of silver or a silver-oxygen complex during which the silver surface atoms are rearranged rather than the decomposition of an activated complex.

The Chemisorption of the Reducing Gases and the Poisoning of the "Cleaned" Surface by Bulk Diffusion. These possible objections to the chemical reduction cleaning technique were eliminated by carrying out the following experiments.

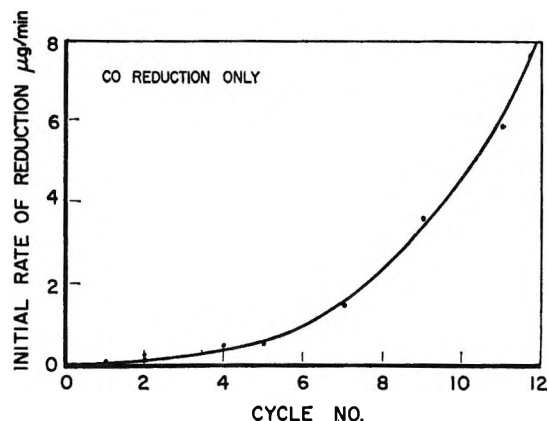


Figure 7. The initial rate of reduction in 10 torr of CO at various stages of OAOR cycling.

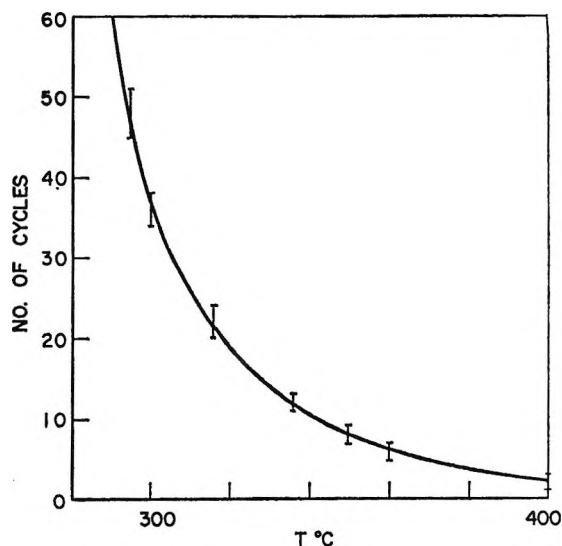


Figure 8. The temperature dependence of the number of cycles required to obtain reproducible chemisorption behavior on a silver powder.

The test for contamination of the cleaned surface from the bulk was carried out by exposing the reduced sample to carbon dioxide at temperatures ranging from -78 to 350° . No adsorption of carbon dioxide could be detected on the cleaned surface although carbon dioxide adsorption occurs on silver surfaces on which oxygen is preadsorbed.⁹

After the surface was reduced with carbon monoxide, the sample was exposed to prolonged outgassing for time intervals ranging from 5 min to several days at the reducing temperature (360°). Then, the sample was exposed to carbon dioxide at elevated temperatures and/or at room temperature. No adsorption

(9) A. W. Czanderna, *J. Colloid Interface Sci.*, in press.

was detected on any reduced surface. This demonstrates that no measurable poisoning of the reduced surface occurs by diffusion of dissolved oxygen atoms to the surface during the outgassing interval of this experiment. A similar confirmation was obtained by obtaining reproducible chemisorption of oxygen at the same temperature and pressure after prolonged outgassing of the reduced sample.

Nature of the Silver Surface. It is of interest to consider the change in the surface structure of the silver powder that is produced by OAOR cycling. Initially, the surface of the powder is probably polycrystalline because of the decomposition method of preparation. The results of the surface area studies indicate that a stable particle size is formed by the powder after about one OAOR cycle at temperatures of 350° or more. However, the chemisorption behavior does not become reproducible until after the sample has been repeatedly exposed to OAOR cycling. It is suspected from this result that a slow rearrangement of the silver surface atoms is taking place until finally a stable structure is obtained which is not altered by the action of oxygen, vacuum, or a reducing gas. Changes in silver surfaces in the presence of gases and vacuum have been discussed by others.¹⁰⁻²⁰ It is obviously impossible to deduce the structure of the new surface generated by OAOR cycling with the certainty of direct techniques such as field emission, low energy electron diffraction, and electron microscopy. However, it does not seem implausible to conclude that the adsorbed oxygen atom ions order the silver atoms into small stable arrays or facets in the chemisorptive rearrangement process. When the oxygen is removed, if the surface of the stable array is in a configuration of thermodynamic minimum free energy such as the 111 or 100 index plane of face-centered cubic silver, the structure of the surface will not change. The next cycle of oxygen chemisorption then produces further ordering of the surface until ultimately any changes taking place in the surface structure during chemisorption, desorption, and reduction are too small to be detected in the chemisorption behavior of the surface.

The driving force for the movement of the silver surface atoms is supplied by the strong bonding between silver and adsorbed oxygen. Mobility of the silver surface atoms is considerable even at temperatures as low as 200° as evidenced by the onset of sintering (Figure 3). There are indications that the mobility of the silver surface atoms is inhibited by the presence of oxygen,^{21,22} which would result if the surface bonds between silver and oxygen are stronger than for silver-silver. Hence, the chemisorption of oxygen could provide the driving force necessary to rearrange the

surface structure of silver particles that have achieved their gross geometrically stable size and shape.

The thermal etching of silver in oxygen at high temperatures to form macroscopically observable 111 and 100 index plane surfaces has been reported.^{16,17} It is known that the low index planes of silver are thermodynamically stable in oxygen at the temperatures and pressures employed in this investigation.²³ It has also been demonstrated that prolonged outgassing and annealing of field emitter tips made from face-centered cubic systems have produced surfaces which consist of about 90% low index planes. It has been observed by numerous investigators that the oxygen chemisorption is the weakest on the most densely packed index planes.

The progressive change in the amount of oxygen which can be desorbed and the increased ease of removal of the remaining oxygen by reduction both tend to indicate that the oxygen chemisorption bonds are becoming weaker on the silver surface as the OAOR cycling progresses. Thus, the gravimetric data provide indirect evidence that the process occurring on the surface is consistent with that expected for a surface experiencing an ordering process to low index planes during rearrangement. This conclusion does not necessarily contradict the results found by electron microscopy studies on the influence of catalytic reactions on silver single crystals.¹⁶ The exposure of the surface to simultaneous oxidizing and reducing conditions would not be expected to yield the same result as OAOR cycling. However, no direct evidence has been obtained to show that faceting is occurring on the silver surface in a manner similar to the copper system.²⁴

Conclusions

It is apparent from the reproducible chemisorption

- (10) L. Bagg and J. Bruce, *J. Catalysis*, **2**, 93 (1963).
- (11) E. Hondros and A. J. W. Moore, *Acta Met.*, **8**, 751 (1960).
- (12) W. W. Smeltzer, *Can. J. Chem.*, **34**, 1046 (1956).
- (13) E. Hondros, *J. Inst. Metals*, **88**, 275 (1960).
- (14) N. Suzuki, *J. Phys. Soc. Japan*, **24**, 2018 (1960).
- (15) J. N. Wilson, *et al.*, *J. Phys. Chem.*, **63**, 463 (1959).
- (16) A. J. W. Moore, *Acta Met.*, **6**, 293 (1958).
- (17) B. Chalmers, R. King, and R. Shuttleworth, *Proc. Roy. Soc. (London)*, **A192**, 465 (1948).
- (18) R. Echigoya and L. Osberg, *Can. J. Chem. Engr.*, **38**, 43 (1960).
- (19) K. Nakada, *J. Chem. Soc. Japan*, **32**, 1072 (1959).
- (20) R. G. Meisenheimer and J. N. Wilson, *J. Catalysis*, **1**, 151 (1962).
- (21) A. W. Smith, *J. Phys. Chem.*, **68**, 1465 (1964).
- (22) A. W. Czanderna, "On the Mobility of Silver in Thin Films," "Vacuum Microbalance Techniques," Vol. 5, Plenum Press, Inc., New York, N. Y., 1966.
- (23) G. E. Rhead and L. Mykura, *Acta Met.*, **10**, 843 (1962).
- (24) T. N. Rhodin, *Advan. Catalysis*, **5**, 70 (1953).

behavior which ultimately is attained from OAOR cycling that this is a suitable technique for cleaning silver powder for the purposes of quantitative measurements. The fact that the cleaned surface does not adsorb carbon dioxide or gases with similar chemisorptive properties at any of the temperatures studied indicates that the extent of surface cleaning is such that the amount of surface contamination remaining must either be very close to a coverage of zero, or the surface contamination is not sensitive to chemisorption of water and carbon dioxide. It seems unlikely that oxygen contamination of the surface would be of such a nature that it would not chemisorb carbon dioxide or water, whereas oxygen introduced to the

surface in measurable amounts does chemisorb these gases even though the chemisorption is weak and reversible. The reproducible surface generated by the OAOR cycling technique was employed for extensive kinetic studies of oxygen adsorption and desorption as has been reported previously.²

Acknowledgments. The author is grateful to Dean Henry Eyring and Drs. J. H. Block, H. C. Chitwood, T. H. George, P. O. Schissel, A. W. Smith, and F. G. Young for the numerous stimulating discussions about the results of this study. He is grateful to Miss L. I. Forrest for her due care in carrying out the measurements and assistance in reducing the data.

Interactions in Aqueous Nonelectrolyte Solutions. I.

Solute-Solvent Equilibria

by R. H. Stokes¹

Chemistry Department and Institute for Enzyme Research, University of Wisconsin, Madison, Wisconsin

and R. A. Robinson

National Bureau of Standards, Washington, D. C. (Received October 19, 1965)

Solutes which interact with the solvent by a series of solvation equilibria to form species which mix according to the ideal solution law are considered. General expressions relating the solvent activity to the molality and the equilibrium constants are given. Sucrose solutions can be described with considerable accuracy by the assumption of a number of possible solvation sites equal to the number of oxygen atoms in the solute molecule, with a single equilibrium constant given the same value for each site. Mixed solutions of several solutes conforming to this model are shown to obey very simple equations relating the molalities at isopiestic equilibrium between solutions of the separate and mixed solutes. A similar relation between the activity coefficients is given. Examples of systems which conform to these mixture relations are given, and it is suggested that cases of large departures from the relation may be taken as evidence of specific solute-solute interaction.

Introduction

While a rigorous treatment of concentrated aqueous solutions remains a distant goal of solution theory, there is great practical interest in such solutions, and some value in incomplete theoretical approaches in which certain major effects are singled out. In the present work we consider one such effect, that of interactions between solute and solvent which may be treated in terms of solvation equilibria. These are likely to be important in aqueous solutions of highly soluble nonelectrolytes such as sugars which have polar groups capable of hydrogen bonding with water molecules.

We shall use the concept of the semiideal (or species-ideal) solution introduced by Scatchard² and used earlier without this name by Dolezalek.³ Such a solution is one in which all the departures from ideal behavior are attributed to chemical reactions, and the activity of each actual species in the solution is equal to its actual mole fraction when the chemical reactions have reached equilibrium.

The Hildebrand-Scatchard⁴ theory of nonelectrolyte

solutions makes it clear that one may in general expect considerable departures from ideal behavior even when no specific interactions of a "chemical" kind are considered. Nevertheless, Saroléa-Mathot⁵ and McGlashan and Rastogi⁶ have successfully treated acetone-chloroform mixtures and dioxane-chloroform mixtures by the assumption of "semiideal" behavior. For aqueous solutions there are at least two other effects which may be of importance. One is the wide disparity in size between the molecules of water and the sugars which are our chief objects of interest. The other is the "structured" nature of liquid water. The main purpose of the present work is to obtain predictions of the activities in solutions of several solutes from known

(1) On leave from the University of New England, Armidale, N. S. W., Australia.

(2) G. Scatchard, *J. Am. Chem. Soc.*, **43**, 2387 (1921).

(3) F. Dolezalek, *Z. Physik. Chem.*, **64**, 727 (1908).

(4) J. H. Hildebrand and R. L. Scott, "The Solubility of Nonelectrolytes," Dover Publications, New York, N. Y., 1964.

(5) L. Saroléa-Mathot, *Trans. Faraday Soc.*, **49**, 8 (1953).

(6) M. L. McGlashan and R. P. Rastogi, *ibid.*, **54**, 496 (1958).

data for single solutes; it may be hoped that the ignored effects will to a large extent cancel between the several-solute and single-solute systems.

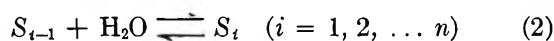
Solvation Equilibria and Average Hydration Numbers for One Solute and Several Solutes

Denote the anhydrous solute by S_0 , the monohydrate by S_1 , and so on. Let \bar{h} be the average hydration number, *i.e.*, the average number of molecules of bound solvent per solute molecule. This number will decrease with increasing concentration of solute. For semiideal solutions, Scatchard² has shown that \bar{h} is given by

$$\bar{h} = \frac{55.51}{m} - \frac{a_w}{1 - a_w} \quad (1)$$

where m is molality and a_w the water activity.

If we suppose that a solute molecule has n sites where a water molecule may be attached, the i th stepwise hydration equilibrium



has the equilibrium constant

$$K_i = N_i / (N_{i-1} a_w) \quad (3)$$

where N denotes mole fraction. Then by methods familiar from treatments of stepwise metal-ligand equilibria,⁷ we obtain

$$\bar{h} = \sigma / \Sigma \quad (4)$$

where

$$\Sigma = 1 + K_1 a_w + K_1 K_2 a_w^2 + \dots + K_1 K_2 \dots K_n a_w^n \quad (5)$$

$$\sigma = \frac{d\Sigma}{d \ln a_w} = K_1 a_w + 2K_1 K_2 a_w^2 + \dots + nK_1 K_2 \dots K_n a_w^n \quad (6)$$

It is important to note that according to eq 4, 5, and 6, \bar{h} depends only on the water activity. Now the study of solutions of several solutes is readily made by isopiestic vapor pressure measurements, in which by isothermal distillation a solution of the mixed solutes is brought to the same water activity as separate solutions of the single solutes.⁸ For a given water activity, a_w , let M_B be the molality of a solution of B alone, and M_C that of a solute C alone, while the mixture contains solute B at molality m_B and solute C at molality m_C . Then \bar{h}_B and \bar{h}_C will have the same values in the mixture as in the single solutions, since each is determined by the water activity.

We have, from eq 1

$$\frac{55.51}{M_B} = \frac{a_w}{1 - a_w} + \bar{h}_B \quad (7)$$

$$\frac{55.51}{M_C} = \frac{a_w}{1 - a_w} + \bar{h}_C \quad (8)$$

The corresponding result for the mixture is

$$\frac{55.51}{m_B + m_C} = \frac{a_w}{1 - a_w} + \frac{m_B \bar{h}_B + m_C \bar{h}_C}{m_B + m_C} \quad (9)$$

Multiplying eq 7 by m_B , eq 8 by m_C , adding, and using eq 9 gives

$$\frac{m_B}{M_B} + \frac{m_C}{M_C} = 1 \quad (10)$$

Equation 10 generalizes to any number of solutes

$$\sum_j \frac{m_j}{M_j} = 1 \quad (11)$$

Equation 10 is an alternative and neater expression for the situation discussed by Robinson and Bower⁹ where the isopiestic ratio, R , of the mixture, defined by

$$R = \frac{M_C}{m_B + m_C}$$

is linear in the fraction of B in the mixture, defined by

$$y_B = \frac{m_B}{m_B + m_C}$$

Where this linear relation, or eq 10, holds, the McKay-Perring¹⁰ equation for the activity coefficient of either solute in the ternary system can be shown to reduce to

$$\gamma_B = \frac{M_B \Gamma_B}{m_B + m_C} \quad (12)$$

where Γ_B is the molal activity coefficient of B in a solution of B alone having the same water activity as the mixed solution, and γ_B is the activity coefficient of solute B in the mixed solution. An equation similar to (12) of course holds for solute C. It can also be shown that subject to eq 11 holding, the activity coefficient of solute k in any mixture is

$$\gamma_k = \frac{M_k \Gamma_k}{\sum_j m_j} \quad (13)$$

(7) J. Bjerrum, "Metal Ammine Formation in Aqueous Solutions," P. Haase and Sons, Copenhagen, 1941.

(8) R. A. Robinson and R. H. Stokes, "Electrolyte Solutions," 2nd ed, Butterworth and Co. Ltd., London, 1959, Chapter 15.

(9) R. A. Robinson and V. E. Bower, *J. Res. Natl. Bur. Std.*, **69A**, 19 (1965).

(10) H. A. C. McKay and J. K. Perring, *Trans. Faraday Soc.*, **49**, 163 (1953).

Comparisons with Experiment

(a) *Single Sugar Solutions.* Equations 1 and 4-6 permit the calculation of the molality m corresponding to a chosen a_w if the K_i are known. This is of little value, since it seems likely that every oxygen atom in a sucrose molecule constitutes a possible hydration site. If we are free to assign 11 K_i values, we can be assured of a good fit to any reasonably simple experimental curve such as the osmotic coefficient of aqueous sucrose. Scatchard² chose the rather drastic course of assuming that only one hydrate (for preference, the hexahydrate) existed in significant amounts. A more acceptable simplifying assumption is to suppose that all the step-wise K_i are equal (though statistical objections can be raised against this assumption also). Then we obtain

$$\frac{55.51}{m} = \frac{a_w}{1 - a_w} + \frac{\sigma}{\Sigma} \quad (14)$$

where

$$\Sigma = 1 + Ka_w + \dots + (Ka_w)^n \quad (15)$$

$$\sigma = Ka_w + \dots + n(Ka_w)^n \quad (16)$$

are functions of a_w and the single equilibrium constant K . For sucrose solutions we put $n = 11$ and find that $K = 0.994$ gives a good fit to the osmotic coefficient data, as shown in Table I.¹¹

It is not advisable to attempt the calculation of a_w at a given value of m for any selected value of K and n . It is better to reverse the calculation to find m at a given value of a_w . The calculation is made as follows. First, a table is constructed of values of a_w , ranging from 0.98 to 0.84 at intervals of 0.02, and then of corresponding values of $a_w/(1 - a_w)$ and of $-55.51 \ln a_w (= m\varphi)$.

Table I: Osmotic Coefficients of Aqueous Sucrose Solutions at 25°

m	φ_{calcd}^a	φ_{exptl}^b
1	1.092	1.085
2	1.189	1.186
3	1.285	1.286
4	1.374	1.376
5	1.450	1.450
6	1.510	1.508

^a From eq 14-16 with $n = 11$, $K = 0.994$. ^b From isopiestic measurements (see ref 11)

$$\varphi = - (55.51/m) \ln a_w$$

A value of K is selected and the corresponding values of Σ , σ , and σ/Σ are calculated with the aid of tables. Knowing σ/Σ and $a_w/(1 - a_w)$, we calculate m by eq 1 with $\bar{h} = \sigma/\Sigma$. As m is known for each given a_w , we

can evaluate φ for each value of m . Graphical interpolation is then adequate to give values of φ at round values of m . The calculation is then repeated with different values of K until the best fit is found with the experimental data.

Other compounds of the sugar type for which isopiestic data exist are mannitol, glucose, and glycerol. The solubility of mannitol ($\sim 1.2 m$) is too limited to make a useful test of eq 14. For glucose, there is some difficulty in obtaining good isopiestic equilibrium at low concentrations, which may be connected with the mutarotation phenomenon. However, some results obtained by Dr. P. N. Henrion at the University of New England, probably reliable within 0.5% in the osmotic coefficient, are given in Table II. For glucose we put $n = 6$ and find that $K = 0.786$ gives a good representation of the results up to saturation. For glycerol, the isopiestic data of Scatchard, Hamer, and Wood¹² are available. Osmotic coefficients of glycerol derived therefrom have been calculated to conform with the reference data for sodium chloride¹³ so that the osmotic coefficients of glycerol are consistent with those of sucrose and glucose. For glycerol we put $n = 3$, since there are three oxygen sites, and obtain a good fit to 7 m with $K = 0.720$.

Table II: Osmotic Coefficients of Glucose and Glycerol Solutions at 25°

m	Glucose		Glycerol	
	Calcd ^a	Exptl	Calcd ^b	Exptl
1	1.028	1.020	1.011	1.012
2	1.054	1.050	1.021	1.023
3	1.080	1.079	1.031	1.033
4	1.105	1.105	1.039	1.043
5	1.128	1.128	1.047	1.050
6	1.147	1.149	1.055	1.055
7	1.166	1.166	1.062	1.060
7.5	1.175	1.173

^a Equations 14-16 with $n = 6$, $K = 0.786$. ^b Equations 14-16 with $n = 3$, $K = 0.720$.

The data for glucose show the same characteristic as those for sucrose, a slightly low osmotic coefficient in the region below 2 m but an excellent fit at the higher concentrations. In the case of sucrose, we have tried other values of the number of sites, n , and find that

(11) R. A. Robinson and R. H. Stokes, *J. Phys. Chem.*, **65**, 1954 (1961). [Note that in Table V of this paper the headings M_B and M_C in the first two columns should be interchanged.]

(12) G. Scatchard, W. J. Hamer, and S. E. Wood, *J. Am. Chem. Soc.*, **60**, 3061 (1938).

(13) See ref 8, p 476.

after choosing the best value of K the fit to the experimental data is definitely inferior to that in Table I. It is obviously preferable to fix n as equal to the number of oxygen atoms in the molecule, for then eq 14 becomes in effect a single-parameter equation.

It may well be asked why the equilibrium constant, K , should be noticeably lower for glucose and glycerol than for sucrose. A fairer question, in view of the extreme oversimplification of the argument, would be why the treatment works as well as it does. We have certainly neglected a great many effects which could be compensated by small variations in K .

(b) *Solutions of Several Solutes.* Equations 10-13 hold for solutions conforming to the present model irrespective of whether the equilibrium constants, K_i , are all the same or all different, known or unknown. Data have been published¹¹ for mixtures of sucrose and mannitol. Unfortunately, the limited solubility of mannitol means that direct tests of eq 10 must be confined to solutions of water activity greater than that of saturated mannitol solution. For more concentrated solutions, however, we can make the test by calculating from the data for mixtures and for sucrose alone, by eq 10, the value of M_C in a supersaturated solution of mannitol of the same water activity. The constancy of M_C obtained from several mixtures of the same water activity, shown in Table III, confirms relation 10.

Table III: Sucrose (B)-Mannitol (C) Mixtures^a

M_B	M_C	m_B	m_C	$(m_B/M_B) + (m_C/M_C)$
(a) Direct tests of eq 10				
0.7751	0.8197	0.6227	0.1604	0.9990
0.7751	0.8197	0.4597	0.3332	0.9996
0.7751	0.8197	0.3139	0.4880	1.0003
0.7751	0.8197	0.1555	0.6559	1.0008
0.9393	1.0046	0.7561	0.1947	0.9987
0.9393	1.0046	0.5594	0.4057	0.9993
0.9393	1.0046	0.3828	0.5953	1.0005
0.9393	1.0046	0.1900	0.8014	1.0000
(b) Indirect tests of eq 10				
2.8576	3.401	2.5321	0.3874	(1.000)
2.8576	3.390	2.2820	0.5756	(1.000)
2.8576	3.381	1.9707	1.9707	(1.000)
1.9123	2.180	1.5970	0.3594	(1.000)
1.9123	2.182	1.4767	0.4971	(1.000)
1.9123	2.184	1.1259	0.8979	(1.000)
5.497	7.14	5.2913	0.2669	(1.000)
5.497	7.08	5.1174	0.4889	(1.000)
5.497	7.13	4.9550	0.7051	(1.000)

^a Figures calculated from the equation are shown in boldface type.

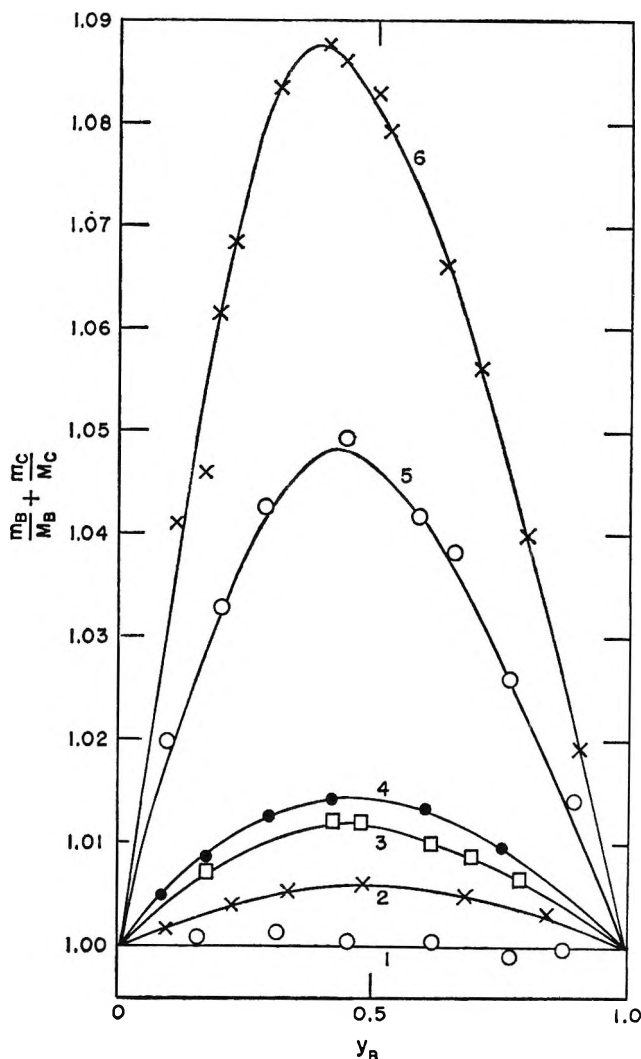


Figure 1. Plots of $(m_B/M_B) + (m_C/M_C)$ vs. $y_B = m_B/(m_B + m_C)$, where B = sucrose and C = a second solute: 1, sucrose-sorbitol; 2, sucrose-glucose; 3, sucrose-arabinose; 4, sucrose-glycerol; 5, sucrosetris(hydroxymethyl)aminomethane; 6, sucrose-urea.

Some further isopiestic experiments on mixed solutes have been made with sucrose (B) as one solute and one of the following: sorbitol, glucose, arabinose, glycerol, tris(hydroxymethyl)aminomethane, urea, as the second solute (C). The results are given in Table IV and plotted in Figure 1.

We do not claim that eq 10 will be valid for any pair of solutes. For it to hold, it is necessary that there be no interaction between the solutes themselves, although interaction between solute and solvent is permitted. Thus eq 10 describes a type of semiideal behavior to which some pairs of solutes may conform; a deviation does not mean a breakdown of eq 10 but does imply a departure from the semiideality symbolized by this

Table IV: Mixtures of Sucrose (B) and Other Substances (C)

M_B	M_C	m_B	m_C	$(m_B/M_B) + (m_C/M_C)$	M_B	M_C	m_B	m_C	$(m_B/M_B) + (m_C/M_C)$
Sucrose-sorbitol					Sucrose-tris(hydroxymethyl)aminomethane				
2.5881	3.0584	2.3125	0.3241	0.9995	2.4772	3.1036	2.0264	0.6385	1.0260
		1.6930	1.0593	1.0005			0.5808	2.4761	1.0329
		0.8984	2.0015	1.0015					
2.5974	3.0664	2.0678	0.6222	0.9990	2.4990	3.1095	1.6532	1.1837	1.0418
		1.2683	1.5709	1.0005			0.8438	2.1918	1.0426
		0.4604	2.5249	1.0008			0.2963	2.8023	1.0198
Sucrose-glucose					Sucrose-urea				
3.2588	3.8757	2.8039	0.5542	1.0034	2.7286	3.4372	2.5095	0.3243	1.0141
		2.3504	1.0996	1.0049			1.9921	1.0591	1.0382
		1.2166	2.4489	1.0052			1.4088	1.8323	1.0494
3.2916	3.9233	1.7391	1.8737	1.0060	2.1740	2.8645	0.4488	2.4058	1.0463
		0.8286	2.5903	1.0038					
		0.3648	3.4947	1.0016	2.1762	2.8659	1.8948	0.4851	1.0400
Sucrose-arabinose					Sucrose-urea				
2.5299	3.0535	2.0592	0.5885	1.0066	2.2143	2.9553	1.3823	1.2714	1.0788
		1.6592	1.0813	1.0099			0.6283	2.2345	1.0684
		1.1853	1.6606	1.0123			1.6317	0.9731	1.0662
							1.2148	1.5880	1.0859
2.5846	3.1370	1.9049	0.8524	1.0087	2.2596	3.0184	0.5438	2.4114	1.0616
		1.3632	1.5200	1.0119					
		0.5191	2.5289	1.0070			2.1232	0.2402	1.0192
Sucrose-glycerol					Sucrose-urea				
3.0975	3.8427	2.0405	1.3615	1.0131	2.2669	3.0317	1.8178	0.7704	1.0560
		1.0701	2.5640	1.0127			1.1582	1.7477	1.0874
		0.3278	3.4537	1.0046			0.3220	2.7258	1.0441
3.1193	3.8766	2.4640	0.8524	1.0098					
		1.5022	2.0650	1.0143					
		0.6493	3.1014	1.0082					

equation. An inspection of Figure 1 shows that sucrose and sorbitol conform to eq 10 as do sucrose and mannitol. But for mixtures of sucrose with glucose, arabinose, and glycerol there are small but significant departures from eq 10 amounting to a maximum of 1.5% in the case of sucrose-glycerol. With sucrose-urea, however, deviations amounting to almost 10% are found; this is not surprising, for urea itself gives a solution which is by no means ideal, since there are significant amounts of dimer formed.¹⁴ More surprising is the deviation shown in the sucrose-tris(hydroxymethyl)aminomethane system, for the latter has been shown¹⁵ to be almost ideal in its own solution. We suspect that the nearly ideal behavior of this solute is an accidental consequence of the near cancellation of two effects, a solvation which tends to increase the activity coefficient and a solute-solute association which tends to decrease the activity coefficient, *i.e.*, to a combination of the effects which characterize sucrose and urea in their separate solutions.

List of Symbols

- K_i Stepwise equilibrium constant for formation of S_i from S_{i-1}
 a_w Water activity
 $\Sigma = 1 + K_1 a_w + K_1 K_2 a_w^2 + \dots + K_1 K_2 \dots K_n a_w^n$
 $\sigma = K_1 a_w + 2K_1 K_2 a_w^2 + \dots + n K_1 K_2 \dots K_n a_w^n$
 $\varphi = -(55.51/m) \ln a_w$ (osmotic coefficient)
 \bar{h} Average hydration number = σ/Σ
 γ Stoichiometric molal activity coefficient of solute
 M_B, M_C Molalities of solutions of solutes, B or C, having the same water activity as the mixed solution
 m_B, m_C Molalities of solutes, B and C, in mixed solution
 Γ_B Stoichiometric activity coefficient (molal) of solute B alone at molality M_B
 $y_B = m_B/(m_B + m_C)$

Acknowledgments. Thanks are due to the National Science Foundation and to the University of Wisconsin

(14) R. H. Stokes, *J. Phys. Chem.*, **59**, 4012 (1965).

(15) R. A. Robinson and V. E. Bower, *J. Chem. Eng. Data*, **10**, 294 (1965).

for a Senior Foreign Scientist Fellowship award to R. H. S., during the tenure of which this work was done.

The Office of Saline Water also is thanked for a grant which assisted the experimental work.

Dissolution of Solid Oxides in Oxide Melts. The Rate of Dissolution of Solid Silica in $\text{Na}_2\text{O-SiO}_2$ and $\text{K}_2\text{O-SiO}_2$ Melts

by Klaus Schwerdtfeger

Edgar C. Bain Laboratory for Fundamental Research, United States Steel Corporation Research Center, Monroeville, Pennsylvania (Received October 26, 1965)

The rate of dissolution of solid silica in static sodium and potassium silicate melts was studied in the temperature ranges 1000–1400 and 1000–1200°, respectively, and in sodium silicate melt, stirred by a rotating silica disk, at 1400°. Concentration profiles obtained in the static melts were measured for selected slag composition and temperature. It is concluded from the experimental data that the dissolution process is controlled by mass transfer in the liquid. Interdiffusivities as calculated from the dissolution rates under static and stirred conditions and as determined from the concentration profiles are consistent with each other.

Introduction

The rates of dissolution of solid oxides in oxide melts are of considerable interest for numerous metallurgical and ceramic processes. In the present work, the rate of dissolution of solid silica in static sodium or potassium silicate melts was studied in the temperature ranges 1000–1400 and 1000–1200°, respectively, and in sodium silicate melts, stirred by a rotating silica disk, at 1400°.

Previous work on the dissolution of solid silica in liquid sodium metasilicate, as done by Shurygin, Barmin, and Esin¹ by using the rotating-disk method, revealed that the dissolution process was controlled by mass transport in the liquid. The authors, however, state that their data are only exact to the order of magnitude because of the experimental difficulties encountered in determining the corrosion rate accurately.

Experimental Section

Methods. Three different experimental methods were

employed for the dissolution of silica into static melts. (a) In the first method, silica was dissolved from silica plugs placed at the bottom of cylindrically shaped platinum crucibles. With this plug position, convection by density differences is assumed to be avoided since, according to data in the literature,^{2,3} the density is lowest in the silica-poorer slag at the top of the crucible. As an additional precaution to prevent convection currents, the crucible was suspended in a vertical tube furnace at the lower part of the hot zone so that the temperature at the top of the melt was about 3° higher than that at the bottom. After the experiment, the sample was rapidly cooled to room temperature. The platinum crucible was then sliced and the change in thickness of the plug was measured using a cathetometer. In order to have a reference point at the bottom of the plug for the length

(1) P. M. Shurygin, L. N. Barmin, and O. A. Esin, *Izv. Vysshikh. Uchebn. Zavedenii Chernaya Met.*, 5, 5 (1962).

(2) J. O'M. Bockris, J. W. Tomlinson, and J. L. White, *Trans. Faraday Soc.*, 52, 299 (1956).

(3) G. Heidtkamp and K. Eadell, *Glastech. Ber.*, 14, 89 (1936).

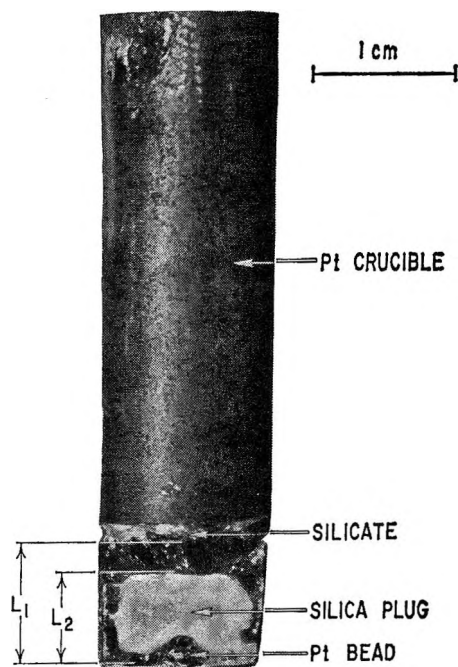


Figure 1. Specimen as used in this work; L_1 is the length of the silica plug at the start of the experiment; L_2 is the length of the silica plug at the end of the experiment; (corrosion $Y = L_2 - L_1$).

measurements, a platinum bead was embedded at the bottom of the silica plug. A sliced platinum crucible with plug and slag is shown in Figure 1. Since the plugs usually were more attacked at the side of the crucible, measurements were always taken at the center of the plug. (b) In the second method, silica was dissolved from cylindrical silica rods of 8 to 12-mm diameter and 20 to 25-mm length which were placed in the center of a silicate melt contained in a platinum crucible. The upper part of the rod was protected by a platinum foil to prevent the stronger corrosion at the slag-air interface. At low silica contents in the slag and at high temperatures this technique could be used only for limited dissolution times; at longer reaction times the corrosion of the rod became uneven over the length of the rod. (c) In the third technique, silica was dissolved from the walls of silica crucibles of ~ 10 -mm internal diameter. This technique was also used to determine the liquidus curve of SiO_2 in the Na_2O - SiO_2 system by equilibrating the melt with the crucible (equilibration time 2-12 weeks) and by analyzing the slag subsequently.

In some experiments done with technique a, the slag was drilled out of the crucible in layers and analyzed chemically for the determination of the concentration profile. Silica concentration near the silica-melt interface was determined using an electron microprobe

analyzer. The necessary electrical conductiveness of the specimen was obtained with a 100-Å thick coating of copper. It was found that the concentration in the silicate at the interface was 86 ± 4 wt % SiO_2 at 1400° , which is the equilibrium value (see next section, Figure 2).

In order to check the data of Shurygin, *et al.*,¹ some measurements were made with sodium silicate melts using the rotating-disk technique. The experiments were carried out in an apparatus which was similar in construction to that described elsewhere.⁴ The faces of silica rods, 1.3 cm in diameter, were used as disks. The sides of the rods were protected by a platinum foil. After the experiment, the adherent slag was easily dissolved in hot water, and the corrosion was determined by measuring the change in length of the rod with a cathetometer.

Temperature Control, Materials, and Analysis. The temperatures of all the furnaces used were controlled automatically in the usual manner. Temperatures were measured with a Pt-Pt-10% Rh thermocouple. The reported temperatures are accurate within $\pm 5^\circ$.

Starting materials for the slags were reagent grade sodium metasilicate, potassium hydroxide, silicic acid, and North Carolina quartz sand. The sodium silicates were prepared by first dehydrating the commercial sodium metasilicate which was then mixed with the desired amount of North Carolina quartz sand and fused. The potassium silicates were prepared by dissolving silicic acid in an aqueous potassium hydroxide solution and by evaporating the obtained solution to dryness. About half of the slag samples used were pre-melted under vacuum, although no difference in the results was found when such a treatment was not applied. In order to make slag and solid silica better distinguishable for the measurement of the corrosion thickness, the slags were colored blue with an addition of $\sim 0.1\%$ CoO .

The silica plugs and rods or crucibles were made from translucent quartz glass rod or tubing, respectively. During the experiment, the quartz glass crystallized to cristobalite (as identified by an X-ray test) in a layer adjacent to the slag.

The samples were analyzed for SiO_2 by the conventional dehydration method in the concentration range 50 to 65% SiO_2 with an accuracy of $\pm 1\%$. At higher SiO_2 contents, Na_2O or K_2O contents were analyzed by a modified technique, because of a decreased accuracy of the SiO_2 dehydration method. The procedure was first to evaporate all the silica with an HF - H_2SO_4 mix-

(4) R. G. Olsson, V. Koump, and T. F. Perzak, *Trans. Met. Soc. AIME*, in press.

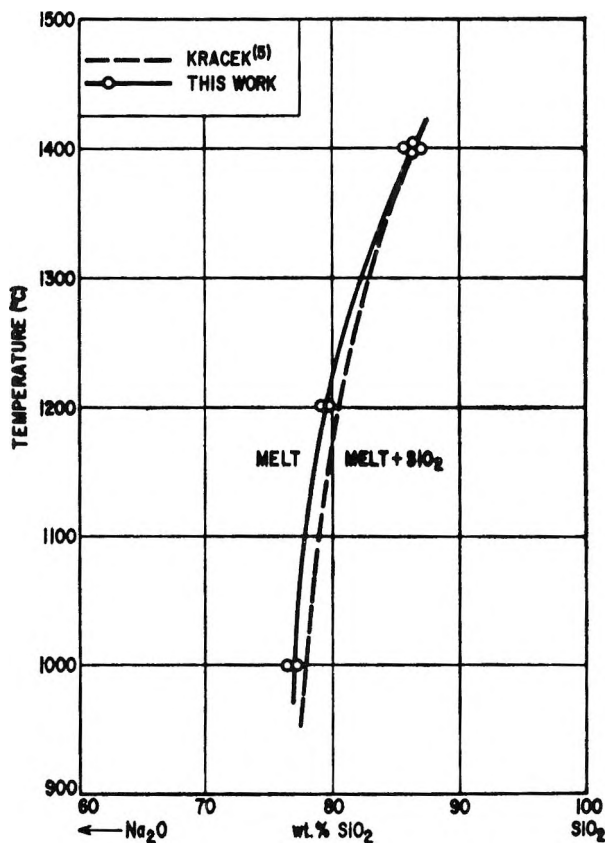


Figure 2. The liquidus curve of silica in the system Na₂O-SiO₂.

ture and then to convert the residue, by evaporating excess H₂SO₄ and H₂O, to Na₂SO₄ or K₂SO₄, which was determined gravimetrically. This method yielded a reproducibility of ±0.2% or better. Its reliability was checked with standard samples made up from Na₂CO₃, K₂CO₃, and North Carolina quartz sand.

Results and Discussion

Dissolution of Silica in a Static Semiinfinite Medium of Sodium or Potassium Silica Melt. Sodium Silicate Melts. Figure 2 shows the results of the equilibrium measurements to determine the liquidus curve of SiO₂ together with the same curve as obtained by Kracek.⁵ Good agreement exists between both curves within 1% or better. The results of the dissolution experiments are given in Figures 3, 4, and 5 where the change in the length (Y) of silica plug, the radius of silica rod, or the wall thickness of the silica crucible is plotted against the square root of reaction time for 1000, 1200, and 1400°, respectively. Within the limits of experimental error, the plots of distance Y vs. t^{1/2} may be taken to be linear, suggesting a diffusion-controlled rate of silica dissolution. Figure 6 shows the silica concentration profile in a selected slag at 1200° as a function of the

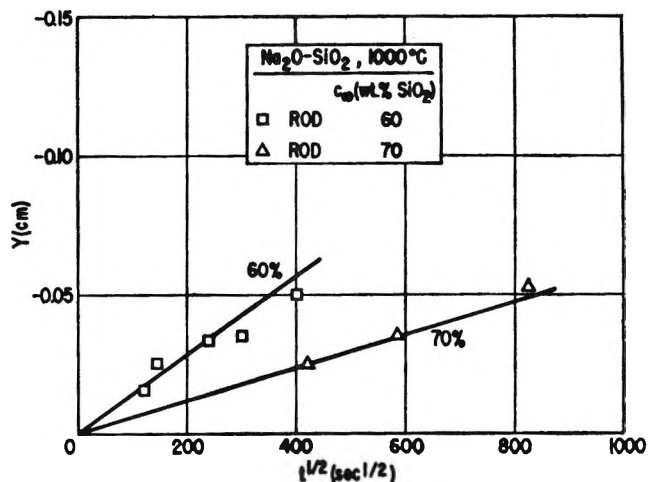


Figure 3. The dissolution of solid silica in static Na₂O-SiO₂ melts at 1000°.

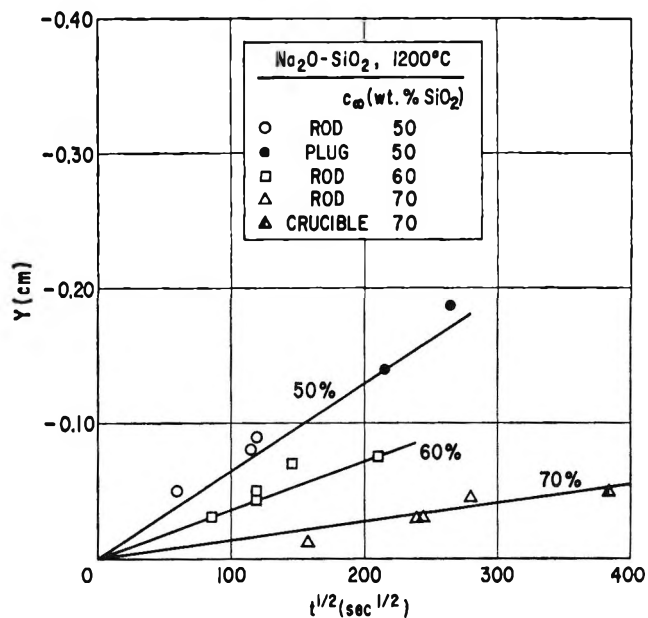


Figure 4. The dissolution of solid silica in static Na₂O-SiO₂ melts at 1200°.

parameter $y/t^{1/2}$, where y is the distance in the melt from the original position of the interface. The curve depicting the profile is drawn such that the shaded areas on either side of the initial interface are equal.

Interdiffusivities (D) may be calculated from the dissolution rate using expression 1 (Equation 1 is strictly valid only for diffusion into a semiinfinite medium with a plane source. However, if in the case of cylindrical sources (cylindrical rods, hollow cylinder) Y is small

(5) F. C. Kracek, *J. Phys. Chem.*, **34**, 1583 (1930); *J. Am. Chem. Soc.*, **61**, 2863 (1939).

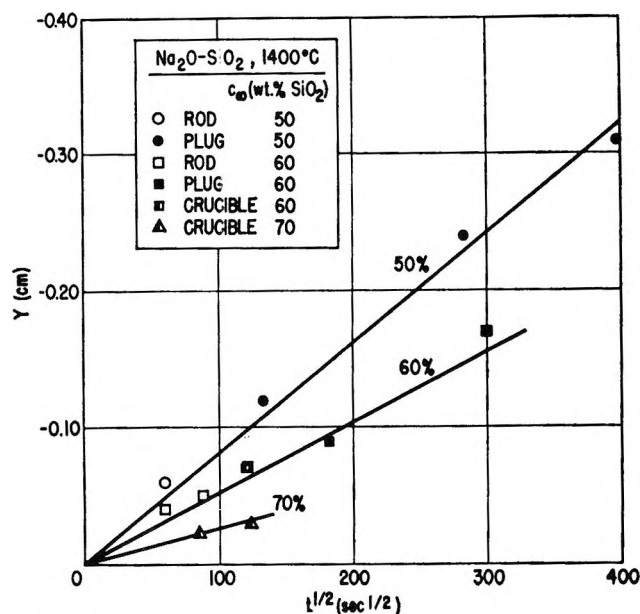


Figure 5. The dissolution of solid silica in static $\text{Na}_2\text{O-SiO}_2$ melts at 1400° .

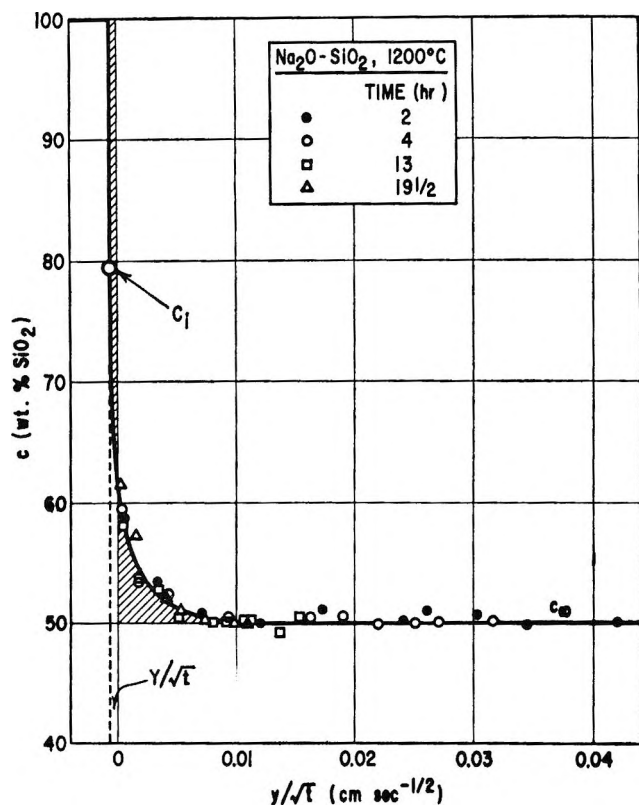


Figure 6. Concentration profile in static sodium silicate melt ($c_{\infty} = 50\%$ SiO_2 , 1200°).

compared to the radius, eq 1 is also a good approximation for these cases.)

$$\frac{c_i - c_{\infty}}{c_i - c_s} = ze^z \sqrt{\pi} (1 - \text{erf } z) \quad (1)$$

where $z = Y/2\sqrt{Dt}$, c_i is the concentration of silica at the interface (= equilibrium concentration), c_{∞} is the concentration of silica in the bulk melt, and c_s is the concentration of silica in solid silica. This equation may be derived for the present conditions from the general equations as given by Danckwerts⁶ for diffusion into a semiinfinite medium involving a moving phase boundary. Density differences^{2,3} in the melt and between melt and solid silica are small and may be neglected. All concentrations may be taken in wt %. Equation 1 applies for the case of concentration-independent interdiffusivity. Hence, if the interdiffusivity varies with concentration, D as obtained with (1) is an average interdiffusivity for the concentration range c_{∞} to c_i . An approximate interdiffusivity-concentration relationship may be obtained by relating D values obtained for various c_{∞} to the corresponding average compositions $c' = (c_{\infty} + c_i)/2$. Table I contains the obtained D values. As would be expected, D increases with decreasing silica content and increasing temperature. The accuracy of the reported log D values is in the order of ± 0.2 as was estimated from the uncertainties of the Y/\sqrt{t} values and from an assumed error of $\pm 1\%$ in the concentrations.

Table I: The Dissolution of Silica in Static $\text{Na}_2\text{O-SiO}_2$ Melts

Temp, $^\circ\text{C}$	c_i	c_{∞}	c'	Y/\sqrt{t} , cm sec ^{-1/2}	Log D , D in cm ² sec ⁻¹
1000	77.2	60.0	68.6	-1.4×10^{-4}	-7.25
		70.0	73.6	-0.6×10^{-4}	-7.40
1200	79.5	50.0	64.7	-6.4×10^{-4}	-6.30
		60.0	69.7	-3.5×10^{-4}	-6.59
		70.0	74.7	-1.3×10^{-4}	-7.00
1400	86.7	50.0	68.3	-8.1×10^{-4}	-6.39
		60.0	73.3	-5.2×10^{-4}	-6.64
		70.0	78.3	-2.6×10^{-4}	-7.00

^a c_i is the silica concentration in the melt at the interface (= equilibrium value). c_{∞} is the silica concentration in the bulk melt. $c' = (c_i + c_{\infty})/2$.

Interdiffusivities may be obtained from the concentration profile in the range 52–56% SiO_2 for 1200° (Figure 6) using the equation

(6) P. V. Danckwerts, *Trans. Faraday Soc.*, **46**, 701 (1950).

$$D = \frac{-1/2 \int_{c_\infty}^c \lambda dc}{\frac{dc}{d\lambda}} \quad (2)$$

in which

$$\lambda = \frac{y}{\sqrt{t}} \quad (2a)$$

An average value of $\log D = -5.4 \pm 0.2$ is obtained which is satisfactorily consistent with the data obtained with eq 1 (see Table I) if these values are related to the average concentration c' .

Potassium Silicate Melts. Figures 7 and 8 show the corrosion Y as a function of $t^{1/2}$ for various K_2O-SiO_2 melts. Calculated interdiffusivities are reported in Table II. The liquidus concentrations were used as given by Kracek, *et al.*⁷ The determination of the SiO_2 liquidus curve in the K_2O-SiO_2 system by equilibrating melts in a silica crucible, in the same way as for the Na_2O-SiO_2 system, is not possible within a reasonable period of time because of the much smaller interdiffusivity values near the liquidus concentrations.

Table II: The Dissolution of Silica in Static K_2O-SiO_2 Melts

Temp, °C	c_i	c_∞ wt % SiO_2^a	c'	Y/\sqrt{t} , cm sec ^{-1/2}	Log D , D in cm ² sec ⁻¹
1000	77.0	65.4	71.2	-4.5×10^{-5}	-7.97
		73.3	75.1	-1.0×10^{-5}	-8.44
1200	81.0	57.0	69.0	-12.5×10^{-5}	-7.65
		65.4	73.2	-7.5×10^{-5}	-7.84
		73.3	77.1	-3.7×10^{-5}	-7.99

^a See footnote in Table I.

Dissolution of Silica in Sodium Silicate Melt from a Rotating Silica Disk. Figure 9 shows the corrosion Y as a function of t (angular velocity $\omega = 131$ radians/sec) for the sodium silicate melt containing 51% SiO_2 at 1400° . Figure 10 shows dY/dt as a function of $\omega^{1/2}$. Included in this diagram is a corresponding curve for 1250° as obtained by Shurygin, *et al.*¹

As shown by Levich,⁸ the thickness of the diffusion boundary layer at a rotating disk is given by

$$\delta = 1.61 \left(\frac{D}{\nu} \right)^{1/2} \left(\frac{\nu}{\omega} \right)^{1/2} \quad (3)$$

when ν is the kinematic viscosity of the melt. Taking the moving phase boundary into account, the rate of

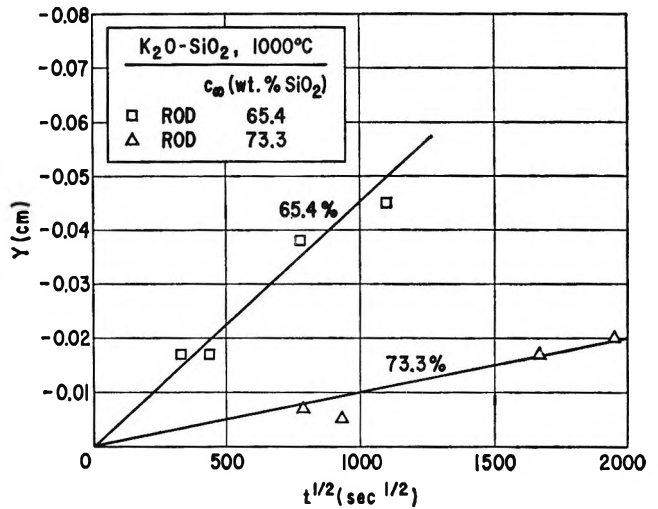


Figure 7. The dissolution of solid silica in static K_2O-SiO_2 melts at 1000° .

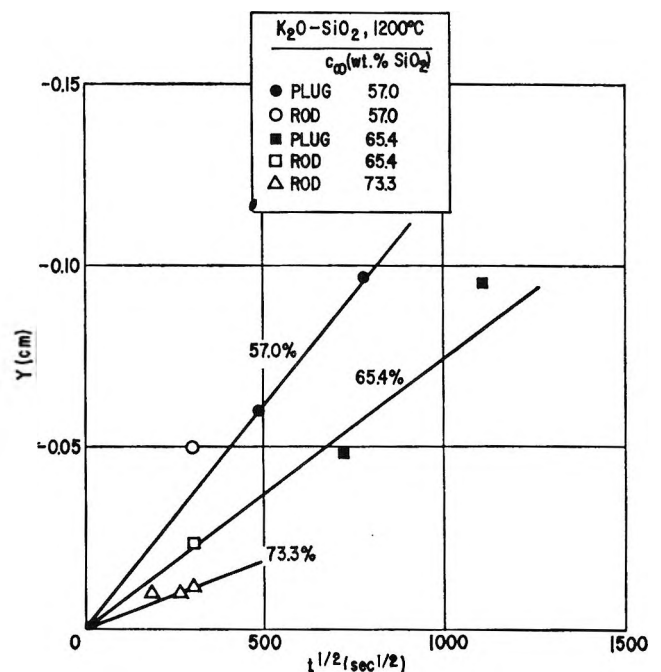


Figure 8. The dissolution of solid silica in static K_2O-SiO_2 melts at 1200° .

motion of the interface between solid and liquid is obtained as shown by Lommel and Chalmers⁹ from the expression (eq 4)

(7) F. C. Kracek, N. L. Bowen, and G. W. Morey, *J. Phys. Chem.*, **41**, 1188 (1937).
 (8) V. G. Levich, "Physicochemical Hydrodynamics," Prentice-Hall, Inc., Englewood Cliffs, N. J., 1962, pp 60-72.
 (9) J. M. Lommel and B. Chalmers, *Trans. Met. Soc. AIME*, **215**, 499 (1959); see also D. B. Spalding, "Convective Mass Transfer," McGraw-Hill Book Co. Inc., New York, N. Y., 1963, pp 184-186.

$$\frac{dY}{dt} = -\frac{D}{\delta} \ln \left[1 + \frac{c_i - c_\infty}{c_s - c_i} \right] \quad (4)$$

Inserting (3) into (4)

$$\frac{dY}{dt} = -0.62 D^{2/3} \nu^{-1/6} \omega^{1/2} \ln \left[1 + \frac{c_i - c_\infty}{c_s - c_i} \right] \quad (5)$$

Equation 5 is valid only for constant viscosity and interdiffusivity; however, eq 5 may be used for the present case to obtain an approximate value of D for an average melt composition. Average values of kine-

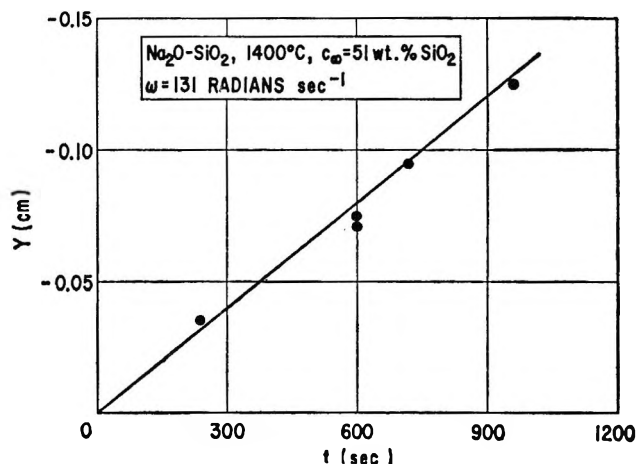


Figure 9. The dissolution of solid silica in liquid $\text{Na}_2\text{O-SiO}_2$ ($c_\infty = 51$ wt % SiO_2 , 1400°) at a rotating disk, as determined in this work.

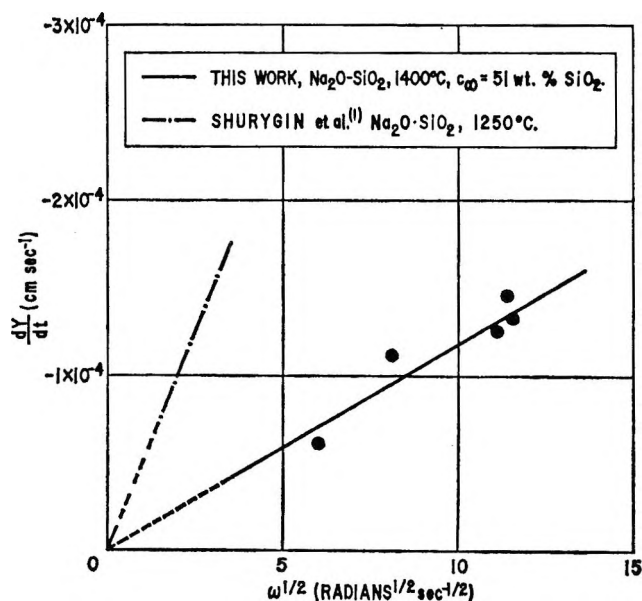


Figure 10. The rate of silica dissolution in $\text{Na}_2\text{O-SiO}_2$ melts at a rotating disk, as determined in this work and as reported by Shurygin, *et al.*¹

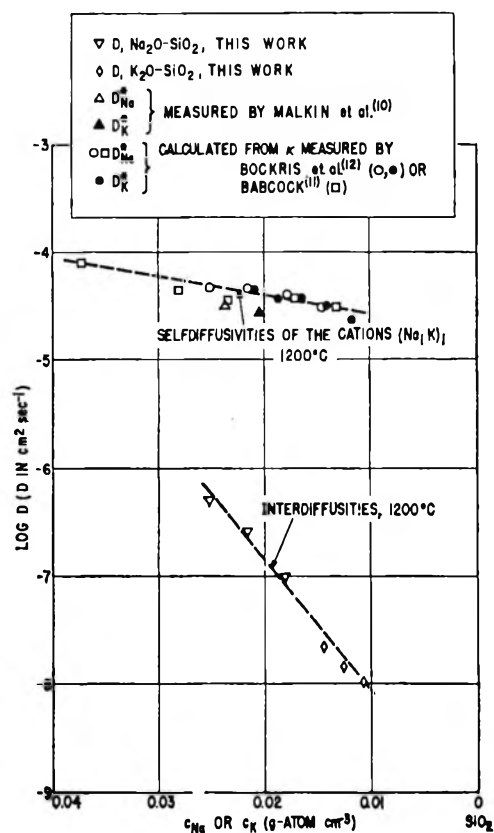


Figure 11. Interdiffusivities and self-diffusivities in $\text{Na}_2\text{O-SiO}_2$ and $\text{K}_2\text{O-SiO}_2$ melts at 1200° . The curve for the interdiffusivities is approximate (compare text).

matic viscosities were taken from the work of Heidtkamp and Endell.³ The value of D thus obtained from the present data is given in Table III. For the same average composition this value of D is somewhat smaller than that obtained by dissolution into a static melt (Table I). Considering, however, the experimental errors in both techniques and the approximations involved in using eq 1 and 5 for a system displaying the strong concentration dependence of diffusivity and viscosity, agreement may be regarded as satisfactory. Some source of error in the rotating disk method may also be due to the finite size of the disk diameter in comparison with the relatively large thickness of the hydrodynamic boundary layer established in the present system.

Comparison of Diffusivities in Sodium Silicate and Potassium Silicate Melts. Figure 11 shows interdiffusivities in $\text{Na}_2\text{O-SiO}_2$ and $\text{K}_2\text{O-SiO}_2$ melts, obtained from the dissolution rates of silica in the static melts, as a function of the average molar cation concentration in the melt at 1200° . It is seen that interdiffusivities in both systems can be represented essentially by one

Table III: The Dissolution of Silica in Na₂O-SiO₂ Melt, Stirred by a Rotating Disk

Temp, °C	c_i wt %	c_∞ % SiO ₂ ^a	c'	$(dY/dt)/\omega^{1/2}$, cm sec ^{-1/2} , rad ^{-1/2}	$\nu'^{-1/6}$, cm ^{-1/3} , sec ^{1/6} ^b	Log D , D in cm ² sec ⁻¹
(a) This work						
1400	86.7	51.0	68.8	-1.17×10^{-5}	0.43	-6.71
(b) From the work of Shurygin, Barmin, and Esin ^c						
1360	84.5	49.2	66.9	-7.7×10^{-5}	0.43	-5.42
1250	80.8	49.2	65.0	-4.8×10^{-5}	0.43	-5.60
1170	79.0	49.2	64.1	-2.1×10^{-5}	0.40	-6.03

^a See footnote in Table I. ^b $\nu' = (\nu_i + \nu_\infty)/2 \approx \nu_\infty/2$.
^c Shurygin, Barmin, and Esin¹ use a somewhat different equation than eq 5 with a wrong driving force to interpret their data. Log D values were therefore recalculated.

curve. Included in Figure 11 is a curve for the self-diffusivities D^*_{Na} , D^*_{K} of the cations Na or K at 1200°. These values were measured either directly with tracer methods¹⁰ or were calculated by the author from electrical conductivity data^{11,12} on the assumption that the

transport mechanism in electrical conduction is the same as that in diffusion. The oxide interdiffusivities are smaller at 1200° by two to three orders of magnitude than the above self-diffusivities. In the dissolution experiments, the transport of cations is accompanied by the movement of anions such that the electroneutrality is maintained. Since the anions have a much lower mobility than the cations,¹³ the oxide interdiffusivities are expected to be smaller than the cation self-diffusivities. A quantitative analysis of the present data with respect to self-diffusivities is not possible at present, because the self-diffusivities of O and Si are not known in these slags.

Acknowledgment. The author wishes to thank E. T. Turkdogan for fruitful discussion, R. G. Olsson for the use of the rotating apparatus, and C. W. Haworth for the microprobe analysis.

- (10) V. I. Malkin and B. M. Mogutnov, *Dokl. Akad. Nauk SSSR*, **141**, 1127 (1961); transl in *Proc. Acad. Sci. USSR*, **141**, 941 (1961).
(11) C. L. Babcock, *J. Am. Ceram. Soc.*, **17**, 329 (1934).
(12) J. O'M. Bockris, J. A. Kitchener, S. Ignatowicz, and J. W. Tomlinson, *Trans. Faraday Soc.*, **48**, 75 (1952).
(13) J. O'M. Bockris, J. A. Kitchener, and A. E. Davies, *ibid.*, **48**, 536 (1952).

Some Aspects of Interionic Charge-Transfer Interactions of Alkylpyridinium Ions in Ion Pairs and on Micelles¹

by Ashoka Ray and Pasupati Mukerjee²

Department of Physical Chemistry, Indian Association for the Cultivation of Science, Jadavpur, Calcutta 32, India (Received October 28, 1965)

The characteristic micellar absorption bands of long-chain alkylpyridinium (RPy⁺) iodides have been recently interpreted as charge-transfer (CT) bands. Similar absorption bands characteristic of interionic CT interactions are obtained on RPy⁺-type micelles in aqueous solution with Br⁻, S₂O₃²⁻, SO₃²⁻, and N₃⁻ also, but not with Cl⁻, SO₄²⁻, NO₃⁻, NO₂⁻, ClO₃⁻, BrO₃⁻, IO₃⁻, or formate. In the ion-pair form, in chloroform, RPy⁺ ions do show CT interactions with Cl⁻ but not with ClO₄⁻. The anions which show CT interactions with RPy⁺ ions also have absorptions characteristic of CT to the solvent. No evidence of any CT interactions with I⁻ or Br⁻ was found for tetraalkylammonium or trialkylphenylammonium ions in chloroform or at the surface of micelles. It is suggested that the planar geometry of the nitrogen charge center in RPy⁺ ions facilitates CT interactions. The effect of alkyl chain length on the CT band position in chloroform is negligible. The CT bands with I⁻ ions for both micelles and ion pairs in various solvent media have been found to have the same shape and half-width when plotted on a wavelength (λ) scale. The bands can thus be matched by shifting positions along the λ scale, and λ for maximum absorption for partially hidden bands can be determined. The average extinction coefficients for ion pairs of two pyridinium iodides in alcoholic solvent media have been estimated. The values are much smaller than the extinction coefficients of ion pairs in chloroform, suggesting that in different media different fractions of ion pairs are in the "contact" or "intimate" class. This approach is expected to be of some use in the study of the equilibrium between "intimate" and "solvent-sharing" or "solvent-separated" ion pairs.

Introduction

The two following papers in this series report the results of our investigations on the characteristic spectra exhibited by micelles of long-chain pyridinium iodides in water, which have recently been interpreted as charge-transfer (CT) bands,³ and the relation of these bands to the properties of the innermost part of the electrical double layer, the so-called Stern layer. The present paper deals with some problems of general interest concerning interionic CT interactions, particularly in alkylpyridinium salts, both as ion pairs in various solvents and at the surface of micelles.

The unusual spectra of alkylpyridinium iodides have been noticed by Hantzsch.⁴ Their interpretation has been possible only recently after the work of

Mulliken and others has clarified the essential features of the CT interactions in molecular complexes.⁵ Kosower and his co-workers⁶⁻⁹ have used these ideas

(1) Taken in part from the doctoral dissertation of A. Ray, Calcutta University, 1963.

(2) Chemistry Department, University of Southern California, Los Angeles, Calif. 90007. Requests for reprints should be sent to this address.

(3) P. Mukerjee and A. Ray, *J. Phys. Chem.*, **67**, 190 (1963).

(4) A. Hantzsch, *Ber.*, **44**, 1783 (1911).

(5) R. S. Mulliken, *J. Am. Chem. Soc.*, **74**, 811 (1952); *J. Phys. Chem.*, **56**, 801 (1952).

(6) (a) E. M. Kosower, *J. Am. Chem. Soc.*, **77**, 3883 (1955); (b) E. M. Kosower, *ibid.*, **78**, 3493 (1956).

(7) E. M. Kosower and J. C. Burbach, *ibid.*, **78**, 5838 (1956).

(8) E. M. Kosower, *ibid.*, **80**, 3253 (1958).

in their study of the spectra of alkylpyridinium iodides and have shown that most of their features can be understood in terms of interionic charge transfer. On the absorption of a photon, it is assumed that an electron from the iodide ion of the charged ground state of the alkylpyridinium ion pair is transferred to an orbital of the π -electron system of the pyridinium ion to produce a neutral excited state. The situation in this respect is the reverse of the charge transfer in molecular complexes for which the ground state is neutral. The interionic CT interactions thus exhibit some differences from CT interactions in molecular complexes.

Experimental Section

Materials. Two samples of dodecylpyridinium iodide (DPI) were used. One was prepared by heating stoichiometric amounts of pyridine (E. Merck, freshly distilled) and pure dodecyl iodide (Columbia Chemicals) in an evacuated and sealed tube in an oil bath at 80° for about 24 hr. The sample was recrystallized six times from a 1:6 mixture of absolute alcohol and absolute ether. The equivalent weight of the sample determined by ion-exchange analysis was 99.8% of theory. The critical micelle concentration (cmc) remained unchanged by two further recrystallizations. A second sample was prepared from dodecylpyridinium chloride supplied by Milton Industrial Chemicals, U. K. The chloride was washed with ether, recrystallized from dioxane, and precipitated twice from concentrated potassium iodide solutions, and finally recrystallized three times from water. The iodide was filtered in the cold, with as little passage of air as possible, washed with ice-cold water, and dried under vacuum. The two samples gave identical cmc's in 0.0001 M Na₂S₂O₃. The value of the cmc in water, $5.26 \times 10^{-3} M^{10}$ is about 5% higher than that obtained previously by the same method¹¹ and considerably higher than a conductometric value reported.¹² A light-scattering value of $5.60 \times 10^{-3} M^{13}$ is probably unreliable because high turbidities were observed below the cmc, suggesting impurities.

Dodecylpyridinium bromide (DPB) and myristylpyridinium chloride (MyPC) were gift samples from Diversey (U. K.) Ltd., and described as being of single chain length. The samples were slightly colored initially. They were treated with sugar charcoal in hot methanol for decolorization, followed by evaporation on a water bath and three recrystallizations from acetone. Dodecyltrimethylammonium bromide (DTAB) was supplied by Milton Industrial Chemicals Ltd., and was used after recrystallization from acetone. The ion-exchange analysis was 99.8% of theory.

The corresponding iodide (DTAI) was prepared from DTAB by precipitation with KI in aqueous solution and was recrystallized twice from water.

Myristylpyridinium perchlorate (MyPP) was prepared by precipitation from an aqueous solution of MyPC with excess KClO₄, filtration, repeated washing with KClO₄ solution and finally water, and drying under vacuum.

Methylpyridinium iodide (MePI) and ethylpyridinium iodide (EtPI) were prepared by refluxing pyridine (E. Merck, freshly distilled) and methyl or ethyl iodide (Riedel de Haen, Hanover, Germany, also distilled), taken in stoichiometric amounts, in absolute alcohol for 6 hr. The cooled mixtures were seeded with some previously prepared crystals. The solid materials were washed with alcohol and dried under vacuum. Ion-exchange analysis agreed to within 0.1% of theory. Phenyltrimethylammonium iodide (PhTAI) was obtained from the British Drug Houses, Ltd.

All inorganic salts used were of analytical reagent grade from E. Merck or the British Drug Houses, Ltd.

The methanol and ethanol used were dried over calcium oxide and distilled before use. E. Merck's pure variety ethylene glycol was dried with anhydrous Na₂SO₄ and distilled under vacuum just before use. The chloroform used was from E. Merck and contained a small amount of ethanol used as a preservative.

Apparatus. A Hilger Uvispek spectrophotometer was used for absorbance measurements. Silica cells were used throughout. The cell chamber was thermostated, when necessary, to within 0.2°. Solutions, in most cases, were prepared and diluted by weight.

Results and Discussion

The Effect of Alkyl Chain Length. For understanding the properties of the micelles of long-chain alkylpyridinium iodides in aqueous solution, it was necessary to investigate whether the long alkyl chains had any effect on the CT spectrum. The CT spectra of MePI, EtPI, and DPI in chloroform were found to be nearly identical in comparable concentrations, showing that the chain-length dependence of the position of the spectrum is very small as previously noted for methyl, ethyl, and isopropyl derivatives by Kosower.^{9b}

(9) (a) E. M. Kosower, J. A. Skorz, W. M. Schwartz, Jr., and J. W. Patton, *J. Am. Chem. Soc.*, **82**, 2188 (1960); (b) E. M. Kosower and J. A. Skorz, *ibid.*, **82**, 2195 (1960).

(10) P. Mukerjee and A. Ray, *J. Phys. Chem.*, **70**, 2150 (1966).

(11) W. D. Harkins, H. Krizek, and M. L. Corrin, *J. Colloid Sci.*, **6**, 576 (1951).

(12) K. Meguro and T. Kondo, *Nippon Kagaku Zasshi*, **80**, 818 (1959).

(13) H. C. Parreira, *Anais. Acad. Brasil. Cienc.*, **32**, 207 (1950).

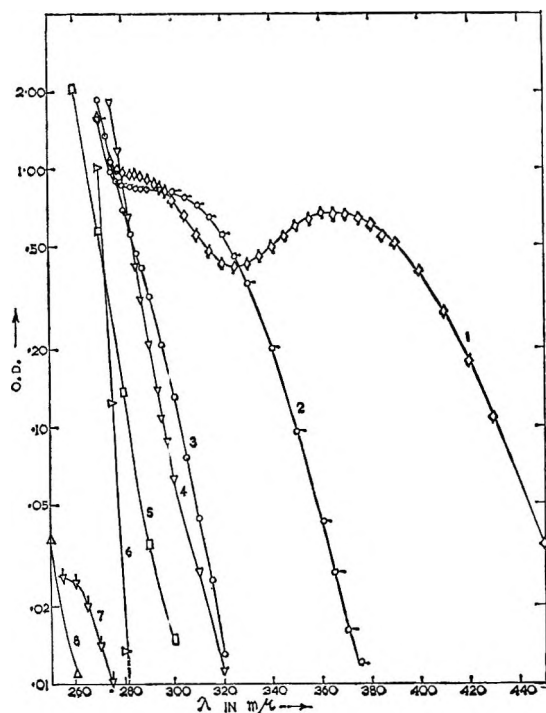


Figure 1. Absorption spectra in chloroform at 25°: (1) DPI, $5.89 \times 10^{-4} M$; (2) DPB, $8.5 \times 10^{-4} M$; (3) MyPC, $6.7 \times 10^{-4} M$; (4) PhTAI, $4.7 \times 10^{-3} M$; (5) DTAI, $6.8 \times 10^{-4} M$; (6) MyPP, $5.2 \times 10^{-4} M$; (7) KI, saturated solution; (8) DTAB, $8.4 \times 10^{-4} M$; DTAC at $6.0 \times 10^{-4} M$ has negligible absorption above 250 $m\mu$.

The Effect of Concentration. On changing the concentration of DPI in chloroform from 3.2×10^{-4} to 5.9×10^{-4} mole/l., we observed a slight blue shift of about 1 $m\mu$ of the band. Larger shifts have been observed by Kosower for more concentrated solutions of 1-ethyl-4-carbomethoxypyridinium iodide.⁸ No such shift was observed for alcoholic solutions. The blue shifts on changing the solvent medium are usually associated with increasing polarity.⁸ The same explanation may be advanced here as the effective polarity of a highly nonpolar medium is expected to increase with the concentration of dissolved electrolyte.¹⁴

Interionic Charge Transfer in Various Systems. Previous studies have been primarily concerned with iodide salts of alkylpyridinium ions. To investigate how general the CT interactions are, we have determined the spectra of a large number of salts.

Figure 1 shows some spectra in chloroform of several salts. All three of the alkylpyridinium halides undergo CT interactions, the bands appearing at higher wavelengths in the sequence $I^- > Br^- > Cl^-$. The I^- and Br^- bands are easily recognizable. For the chloride, the comparison of MyPC and MyPP shows the presence of CT interaction, since the absorbance of

Cl^- and ClO_4^- are negligible in this region. The perchlorate does not seem to undergo any CT interaction as the steep spectrum of MyPP seems to be due to the pyridinium ion. The quaternary ammonium and the quaternary anilinium iodides seem to show no CT interaction, their absorbances being due to that of I^- alone.^{15a} The absorbances of DTAB also seems to be due to that of Br^- alone.

It seems that the pyridinium moiety is particularly suited for CT interactions, presumably because of its geometry which allows the anions to come close to the positive charge center on nitrogen, as compared to substituted anilinium and tetraalkylammonium ions. However, in highly nonpolar solvents like CCl_4 , even the tetraalkylammonium iodides can undergo CT interactions as recent work has shown.^{15,16}

For aqueous micellar systems, we have studied the interactions of I^- , $S_2O_3^{2-}$, SO_3^{2-} , N_3^- , SO_4^{2-} , ClO_3^- , BrO_3^- , IO_3^- , formate, NO_3^- , NO_2^- , Br^- , and Cl^- with dodecyl- or myristylpyridinium ions. Positive evidence for CT interactions was obtained for I^- , $S_2O_3^{2-}$, SO_3^{2-} , and N_3^- (Figure 2) and for Br^- (Figure 3). The nearly flat part of the spectrum obtained at the higher wavelengths for Br^- (Figure 3), Cl^- , and other salts were ascribed to the scattering from the micelles, in view of their low intensities and the approximate dependence on λ^{-4} , but there is sufficiently strong absorption below 340 $m\mu$ for DPB (Figure 3) to show that the effects of CT interactions at the micelle surface are appreciable in this region, the absorptions of the individual ions being negligible. Indeed, the absorbance values can be used to determine the critical micelle concentration of DPB.¹⁰ No evidence of CT interactions was observed for SO_4^{2-} , ClO_3^- , BrO_3^- , IO_3^- , formate, NO_3^- , and NO_2^- .

The pyridinium thiosulfate band for micelles is extremely similar to the pyridinium iodide band, as far as the position and the shape are concerned. The similarity was also found in the ion-pair form in methanol.¹⁷

The extinction coefficient for the thiosulfate seems to be lower, however. Some unusual concentration dependence of absorption of tetramethylpyridinium iodide in ethanol obtained by Kosower in alcohol¹⁷ may have been due to a high concentration of $Li_2S_2O_3$ used, whose effect was not recognized.

As described in the following paper, there is no

(14) H. L. Friedman, *J. Phys. Chem.*, **66**, 1595 (1962).

(15) (a) T. R. Griffiths and M. C. R. Symons, *Mol. Phys.*, **3**, 90 (1960); (b) M. L. Blandamer, T. E. Gough, and M. C. R. Symons, *Trans. Faraday Soc.*, **60**, 488 (1964).

(16) F. S. Larkin, *ibid.*, **59**, 403 (1963).

(17) P. Mukerjee and A. Ray, *J. Phys. Chem.*, **70**, 2144 (1966).

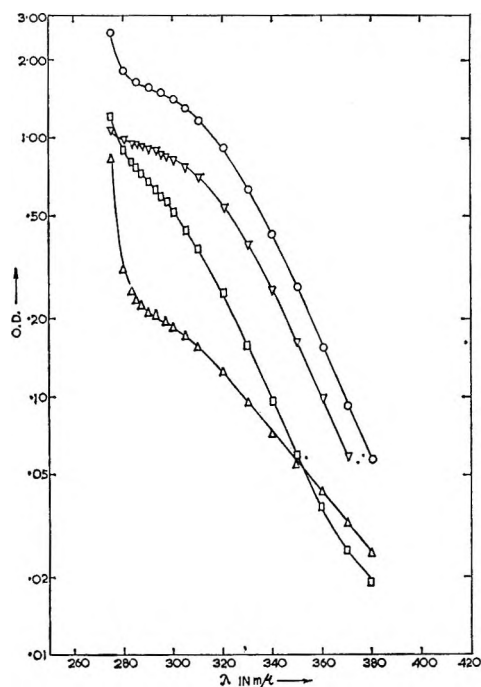


Figure 2. Absorption spectra at 25° in water: ▽, DPI, micellar difference spectrum, $6.57 \times 10^{-3} M$ against $5.76 \times 10^{-3} M$; ○, MyPC ($6.25 \times 10^{-3} M$) + $\text{Na}_2\text{S}_2\text{O}_3$ ($6.92 \times 10^{-3} M$) against water; □, MyPC ($3.13 \times 10^{-3} M$) + NaN_3 ($1.28 \times 10^{-2} M$) against water; Δ, MyPC ($6.25 \times 10^{-3} M$) + Na_2SO_3 ($8.08 \times 10^{-3} M$) against water.

evidence of CT interactions on the micelles of long-chain trimethylammonium iodides.

The above results establish the generality of CT interactions both in chloroform (as ion pairs) and on micelles (presumably at the surface) between alkylpyridinium ions and a variety of anions. The same anions, namely Cl^- , Br^- , I^- , $\text{S}_2\text{O}_3^{2-}$, N_3^- , and SO_3^{2-} , have absorptions in the ultraviolet in solution which have been attributed to charge transfer to the solvent.¹⁸⁻²¹ It is to be expected that CT interactions with pyridinium ions will be related to those with solvents, the main difference being the localized character of the acceptor for the former case. CT interactions with RPy^+ ions may be useful for diagnosing the existence of charge-transfer-to-solvent bands of anions and *vice versa*.

Comparison of CT Bands in Various Media and the Isolation of λ_{max} . The CT bands of pyridinium iodides on micelle surfaces are clearly seen to the extent of only about one-half of the band, on the long wavelength side. The other part is in the region of the very intense absorption of the pyridinium ions and partly the iodide ions themselves. For intercomparison of the bands in various media it was desirable to estimate

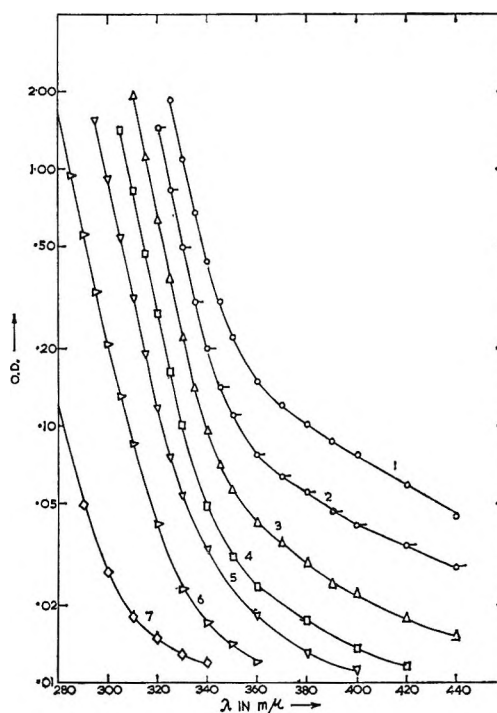


Figure 3. Absorbance data on DPB at 25° in water. Concentration: (1) 0.5037 M, (2) 0.2519 M, (3) 0.1260 M, (4) 0.0630 M, (5) 0.0315 M, (6) 0.01575 M, (7) 0.00788 M.

the wavelengths of these band maxima for these partly visible bands.

We attempted a gaussian analysis of the bands, but small deviations seem to occur from the strictly gaussian behavior so that, when the λ_{max} for a well-resolved band (in chloroform) was estimated from the long-wavelength half of the band alone and compared to the actual λ_{max} , the uncertainty was about 3 $m\mu$, which was unsatisfactory. Resolution of the partially visible band by correcting for the absorption of the individual ions did not prove satisfactory either.

The isolation of λ_{max} was achieved on the basis of an interesting observation on the shapes of the bands. When log OD is plotted against the wavelength, as in Figure 4, the effect of a different concentration of the absorbing species is a vertical parallel displacement of the whole curve. It was found empirically that the long-wavelength parts of the CT bands in micellar systems, and for ion pairs in various solvent media including chloroform, were very similar in shape in

(18) M. Smith and M. C. R. Symons, *Trans. Faraday Soc.*, **54**, 338 (1958).

(19) R. Sperling and A. Treinin, *J. Phys. Chem.*, **68**, 897 (1964).

(20) G. Stein and A. Treinin, *Trans. Faraday Soc.*, **55**, 1086, 1091 (1959).

(21) I. Burak and A. Treinin, *J. Chem. Phys.*, **39**, 189 (1963).

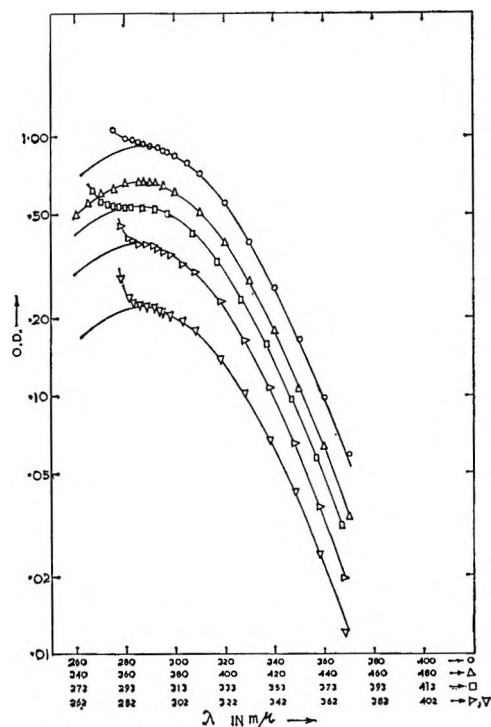


Figure 4. Matching of spectral shapes of DPI in different media at 25°: O, micellar difference spectrum in water; Δ , in CHCl_3 ; \square , in ethanol (100%); \triangleright , in ethanol-water (80:20 by weight); ∇ , in methanol-water (90:10 by weight).

such plots when data above 290 $m\mu$ were used and could be superposed on one another by a horizontal shift of the spectrum, *i.e.*, by a displacement along the wavelength coordinate, after a suitable vertical displacement to allow for differences in absorption intensities. This superposability, or the matching of band shapes, is satisfactory over a wide range of optical densities, about a factor of 10 from the band maximum.

Figure 4 shows examples of this matching of the spectra. Absorbance data for five systems are shown, including chloroform. The peaked continuous curves shown are all the same, however, namely the chloroform band, plotted after suitable vertical and horizontal displacements. The absorbance data in the long-wavelength region are clearly well represented by a single curve.

From such comparisons, λ_{max} for a partially resolved band can be estimated from the λ_{max} of the well-resolved band in chloroform. A stencil defining the shape of the long-wavelength half of the band in chloroform was found useful for such intercomparisons. The horizontal shift of the stencil which makes it match any band gives directly the difference between the λ_{max} of the band and that of chloroform. The uncertainty of these estimates of λ_{max} was about $\pm 1 m\mu$.

The above technique may be useful in extending the Z -value scale of the empirical measure of solvent polarities⁸ to solvents of high polarity, in which the band maxima cannot be directly isolated. For the Z -value scale, Kosower, *et al.*,⁸ used the λ_{max} values of 1-ethyl-4-carbomethoxypyridinium iodide, a system which shows much more pronounced effect of CT than an alkylpyridinium iodide. The λ_{max} values for this compound and those estimated by us for DPI show a fair linear correlation.

The observed matchability of the CT bands means that the width of the band $\Delta\lambda$, the difference between λ_{max} and $\lambda_{1/2}$, the wavelength at which the absorption is half that at the maximum, is constant. Its value is 39–40 $m\mu$ for the alkylpyridinium iodides. In terms of frequencies (ν), over limited variations in λ_{max} , the corresponding relation is $\nu_{\text{max}} - \nu_{1/2} = K\nu_{\text{max}}^2$, where K is a constant. Briegleb and Czekalla²² obtained a linear relation between $\nu_{\text{max}} - \nu_{1/2}$ and ν_{max} for intermolecular CT interactions of different donors and acceptors. The relationship observed here is probably characteristic of medium effects on CT interactions.

The Extinction Coefficients of CT Bands. It has been observed by Kosower⁸ that when the polarity of the medium increases, along with a blue shift of the CT band, the intensity at λ_{max} usually decreases when the concentration of the pyridinium iodides are kept constant. The most likely explanation, of course, is that the extent of ion pairing decreases. It is also likely, since CT interactions must involve short-range forces, that only a fraction of the ion pairs act as the absorber, the "contact" or "intimate" ion pairs, as compared to "solvent separated" or "solvent sharing" ion pairs,^{8,15} and the fraction is dependent on the medium. Because of the intrinsic interest of this question, and for comparisons with apparent intensities for micelles, we estimated the molar extinction coefficients of the CT bands for some ion pairs.

As the "intimate" ion pairs remain in equilibrium with the other types, they can be considered to be a constant fraction of all ion pairs, independent of concentration. The equilibria may be expressed as $(\text{RPy}+\text{I}^-)_{\text{intimate}} \rightleftharpoons (\text{RPy}+\text{I}^-)_{\text{solvent sharing}} \rightleftharpoons (\text{RPy}+\text{I}^-)_{\text{solvent separated}} \rightleftharpoons \text{RPy}^+ + \text{I}^-$.

If the total concentration of the salt is C and that of all ion pairs is C_2 , and if the absorbance is due entirely to the ion pairs and not the free ions, then from the definitions for the dissociation constant K_d [$K_d = (C - C_2)^2/C_2$] and the molar extinction coefficient ϵ averaged

(22) G. Briegleb and J. Czekalla, *Z. Physik. Chem. (Frankfurt)*, **24**, 37 (1960).

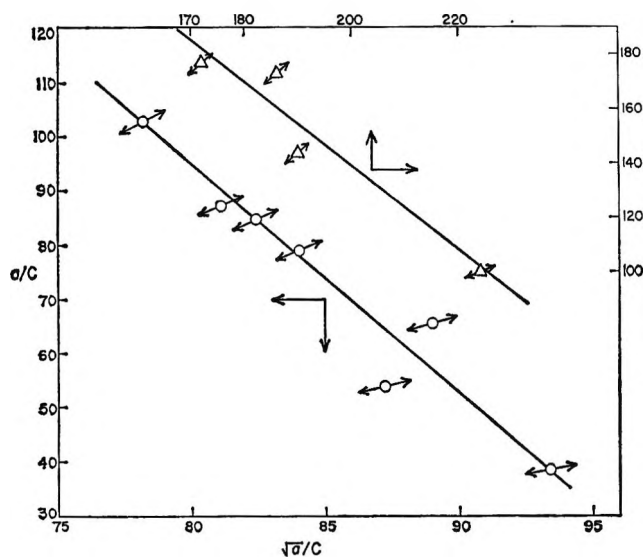


Figure 5. Plot of a/C against $a^{1/2}/C$: Δ , 1-ethyl-4-carbomethoxy-pyridinium iodide in ethanol, absorbance measurements at λ_{max} ; O , DPI in 80% methanol-water, absorbance measurements at 290 $m\mu$. Arrows indicate $\pm 2\%$ error in absorbance values.

over all ion pairs ($\epsilon = a/C_2$ where a is the absorbance for 1-cm path length), we obtain the relations

$$\frac{(K_d C_2)^{1/2}}{C} = 1 - \frac{C_2}{C} = 1 - \frac{a}{\epsilon C} = \frac{1}{C} \left(\frac{K_d a}{\epsilon} \right)^{1/2}$$

and

$$\frac{a}{C} = \epsilon - (K_d \epsilon)^{1/2} \frac{a^{1/2}}{C}$$

A plot of a/C against $a^{1/2}/C$ should give a straight line from the slope and intercept of which the ϵ and K_d values may be evaluated. For the approximate calculations involved here, the activity coefficients are considered to be unity.

Figure 5 shows plots of this type for DPI in 80% methanol-water (by weight) and 1-ethyl-4-carbomethoxy-pyridinium iodide in ethanol. The data for the second system were taken from ref 8. The estimated K_d values, 4.1×10^{-2} and 5.4×10^{-3} (mole/l.) for DPI and the carbomethoxy compound show the expected magnitude and trend for these solvent media. The corresponding ϵ values are only 430 and 450, much lower than the values of 1140 and 1200⁸ for chloroform. If the apparent oscillator strengths are estimated from a plot of a against ν , assuming symmetrical bands, the differences are reduced somewhat but still remain large. The most likely explanation seems to be that the fraction of the ion pairs exhibiting CT interactions, the "intimate" ion pairs, is much smaller in alcoholic solvents than in chloroform. This conclusion involves the assumption that the intrinsic oscillator strength of the CT band remains constant. It is expected that this approach will be of some use in investigating the equilibrium between "intimate" and other types of ion pairs, at least on a relative basis, as a function of the medium. The problem of estimating absolute fractions of "intimate" ion pairs would probably require some other approach. As discussed later,¹⁷ when micellar band intensities are compared to those of chloroform, it appears that not all ion pairs, even in such a nonpolar medium as chloroform with a dielectric constant of 5, are "intimate."^{15a} The high intensities, $\sim 10^4$, obtained for the tetraalkylammonium iodides in even less polar solvents such as carbon tetrachloride^{15b} seem to be in accord with this conclusion.

Acknowledgment. The writing of this paper was supported in part by PHS Research Grant GM 10961-01 from the division of General Medical Services, Public Health Service.

Charge-Transfer Interactions and the Polarity at the Surface of Micelles of Long-Chain Pyridinium Iodides¹

by Pasupati Mukerjee² and Ashoka Ray

*Department of Physical Chemistry, Indian Association for the Cultivation of Science,
Jadavpur, Calcutta 32, India (Received October 28, 1965)*

The absorption spectra of micelles of dodecylpyridinium iodides, characterized as charge transfer (CT) bands involving the interaction of pyridinium ions and iodide ions, provide an experimental probe for studying directly the innermost part of the electrical double layer or the Stern layer. These interionic CT bands are highly sensitive to the polarity of the environment. The micellar bands in water are found to be very different from the ion-pair bands in water. The difference is attributed to the reduced effective polarity at the micelle surface. Comparison of ion-pair bands in various solvents to the micellar band leads to an estimated "effective" dielectric constant of 36 for the micelle surface in water. Small shifts in the micellar band position for different environments produced by mixed counterions, added KI, and some other additives, including a nonionic association colloid, have been observed. The "effective" dielectric constant has been compared to theoretical expectations and agrees with some rough estimates made using Booth's theory of dielectric saturation or the effect of high concentrations in the Stern layer. The close similarity of the shape of the CT bands of micelles and ion pairs has been interpreted to show the essential homogeneity of the adsorption sites in the Stern layer.

Introduction

Perhaps the least understood region of micelles of association colloidal electrolytes, and highly charged colloids in general, is the so-called "Stern" layer, or the innermost part of the double layer. The characteristic distance of interaction here is more likely to be the average separation of charges (5–10 Å) rather than the Debye-Hückel thickness of the diffuse double layer and thus be comparable to the dimensions of ions and solvent molecules even when the concentration of small ions in the intermicellar fluid is small. This makes all continuum approximations in theories extremely hazardous. Short-range forces, usually of diverse origin and generally intractable, add to the difficulties.

On the experimental side, few approaches are available for investigating the Stern layer directly. The interesting optical absorptions characteristic of micelles of long-chain pyridinium iodides^{3–5} seem to be a very useful tool from this point of view. These micellar bands are very probably due to charge transfer (CT) interactions between alkylpyridinium and iodide ions.⁴

As these interactions must involve electronic orbitals, they must be of very short range. The study of the CT bands, therefore, provides an experimental probe for the innermost part of the double layer. The present paper is concerned with the interpretation of the position and shape of these bands for various micellar environments, as compared to bands due to ion pairs in various solvents.

Experimental Section

The materials used and the experimental procedures have been described previously.⁵

(1) Taken in part from the doctoral dissertation of A. Ray, Calcutta University, 1963.

(2) Department of Chemistry, University of Southern California, Los Angeles, Calif. 90007. Requests for reprints should be sent to this address.

(3) W. D. Harkins, H. Krizek, and M. L. Corrin, *J. Colloid Sci.*, **6**, 576 (1951).

(4) P. Mukerjee and A. Ray, *J. Phys. Chem.*, **67**, 190 (1963).

(5) A. Ray and P. Mukerjee, *ibid.*, **70**, 2138 (1966).

Results and Discussion

Qualitative Nature of the Micellar Band. The wavelength of maximum absorption (λ_{\max}) of the CT bands for dodecylpyridinium iodide (DPI) micelles in water at 25° has been estimated by the band-matching technique described previously⁵ to be 286 $m\mu$. In contrast, methylpyridinium iodide (MePI), which does not form micelles, gives in water a CT band due to ion pairs whose maximum lies too far into the ultraviolet to be directly determined.⁶ Kosower and Skorcz⁷ have been able to estimate λ_{\max} for MePI by an indirect method, namely by extrapolation of a plot of E_T vs. Z , where E_T and Z are transition energies, corresponding to band maxima, in kcal/mole, of MePI and a related standard compound, 1-ethyl-4-carbomethoxypyridinium iodide, respectively. The value so obtained is $256 \pm 1 m\mu$. This red shift of about 30 $m\mu$ of CT bands for DPI micelles as compared to MePI ion pairs, both in aqueous media, is of central interest to this paper.

Of the various alternative explanations possible, the possible effect of chain-length variation alone must be negligible since MePI, ethylpyridinium iodide, and DPI have CT bands in about the same position in chloroform.⁵ A second possibility arises from the consideration that the ion-pair bands are essentially due to 1:1 interactions between pyridinium and iodide ions, whereas on the surface of the micelle, containing a large number of monomers and a large fraction of the counterions, the ions are in close proximity. Although CT interactions must be of extremely short range, some cooperative effect involving several ions cannot be ruled out *a priori*.

This possibility was tested experimentally by absorbance measurements in mixed micelles. In the first experiment, the spectrum of a concentrated dodecyltrimethylammonium iodide (DTAI) solution well above the cmc was compared to a similar solution containing, in addition, 1 mole % of DPI. DTAI does not undergo any CT reaction, as is evident from the lower curve in Figure 1, where the longer wavelength absorbance is very small, considering the high concentration used, and is roughly proportional to λ^{-4} . It can, therefore, be ascribed entirely to scattering from micelles. On the other hand, the mixed micellar system containing 1 mole % of DPI has the characteristic micellar band, very similar in shape to the band obtained for DPI alone at 45°, but somewhat shifted toward the red (Figure 1). This experiment was performed at 45° because of the low solubility of DTAI at lower temperatures. Results of a similar experiment with myristylpyridinium chloride (MyPC), to which small amounts of KI were added, are shown in

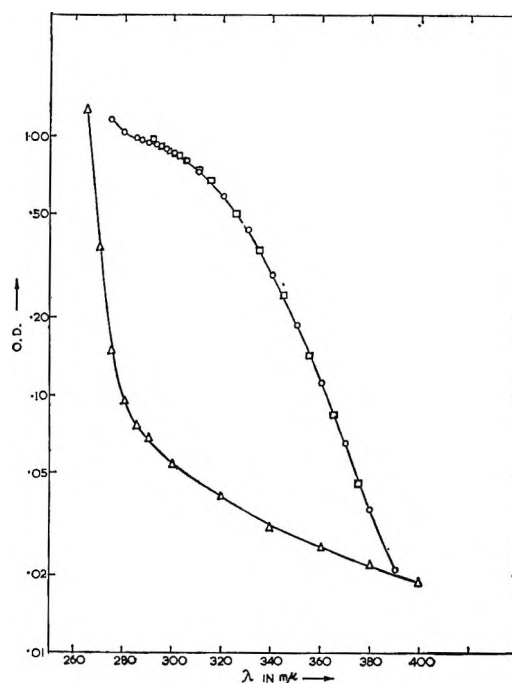


Figure 1. Absorbance data at 45°: Δ , $9.59 \times 10^{-2} M$ DTAI against water; O , $9.59 \times 10^{-2} M$ DTAI + $9.19 \times 10^{-4} M$ DPI against $9.59 \times 10^{-2} M$ DTAI; \square , micellar difference spectrum for DPI at 45°, after suitable vertical shift and a horizontal shift of 5 $m\mu$ toward the red.

Figure 2. Again, the micellar band is evident even when the Cl^-/I^- ratio is 75. We have thus no indication of any cooperative phenomenon involving either the pyridinium or the iodide ion.

The third and most likely possibility is that the band shift for micelles is due to a reduced polarity at the micelle surface. Kosower⁸ has shown that one of the characteristics of the pyridinium CT bands is their strong dependence on the solvent polarity, presumably because of the charged character of the ground state. A decrease in polarity causes a red shift of the band. A probable explanation is that the ground state is destabilized and thus brought closer to the essentially uncharged excited state. It is also generally recognized that at the surface of highly charged colloids, the polarity is reduced because of dielectric saturation,⁹ the high concentration of ions,¹⁰ and the proximity of the hydrocarbon core in the case of a micelle. Qualitatively, therefore, the position of the micellar band may be attributed to a combination of these factors.

(6) E. M. Kosower and P. E. Klinedinst, *J. Am. Chem. Soc.*, **78**, 3493 (1956).

(7) E. M. Kosower and J. A. Skorcz, *ibid.*, **82**, 2195 (1960).

(8) E. M. Kosower, *ibid.*, **80**, 3253 (1958).

(9) F. Booth, *J. Chem. Phys.*, **19**, 391, 1327, 1615 (1951).

(10) M. J. Sparnaay, *Rec. Trav. Chim.*, **77**, 872 (1958).

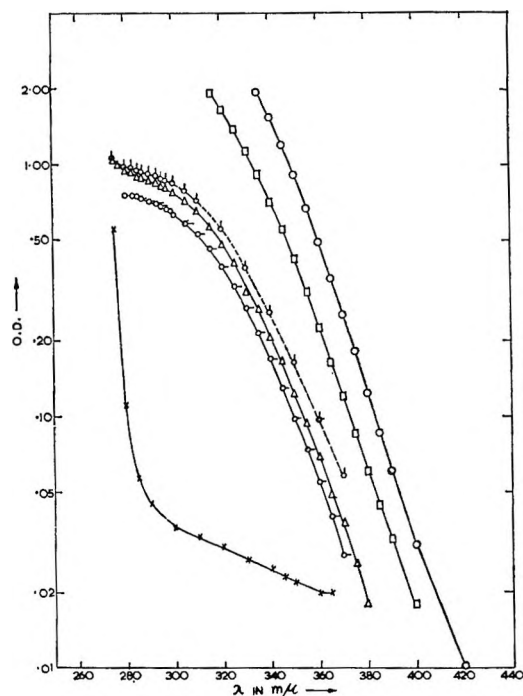


Figure 2. Absorbance data at 25°: \times , $6.12 \times 10^{-3} M$ MyPC against water; \circ , $3.58 \times 10^{-2} M$ MyPC + $4.41 \times 10^{-3} M$ KI against $3.58 \times 10^{-2} M$ MyPC; \square , $1.796 \times 10^{-2} M$ MyPC + $2.23 \times 10^{-3} M$ KI against $1.796 \times 10^{-2} M$ MyPC; Δ , $6.12 \times 10^{-3} M$ MyPC + $7.59 \times 10^{-4} M$ KI against $6.12 \times 10^{-3} M$ MyPC; \circ , $3.98 \times 10^{-2} M$ MyPC + $5.13 \times 10^{-4} M$ KI against $3.98 \times 10^{-2} M$ MyPC; δ , micellar difference spectrum for DPI at 25°.

Comparison of the Micellar Band with Ion-Pair Bands.

In order to make a more quantitative study of this effect, it was of interest to make a comparison of the micellar band position with the ion-pair bands in various solvent media of different dielectric constants. These positions have therefore been determined in solvent mixtures of methanol, ethanol, and ethylene glycol with water. The concentrations used were well below the estimated critical micelle concentrations in these media. Small amounts of sodium thiosulfate were added to all of these solvents to prevent any triiodide formation. It was found that the addition of the small amount of thiosulfate does not materially alter the shape or the position of the band because of the close similarity of the CT bands with thiosulfates and iodides. Figure 3 shows an example of the characteristic variation of the CT bands of the ion pairs of DPI in such solvent mixtures: the band always shifts toward the red with increasing concentration of the organic component. The shapes of the bands on the long wavelength side remain the same, however, and by matching these bands against

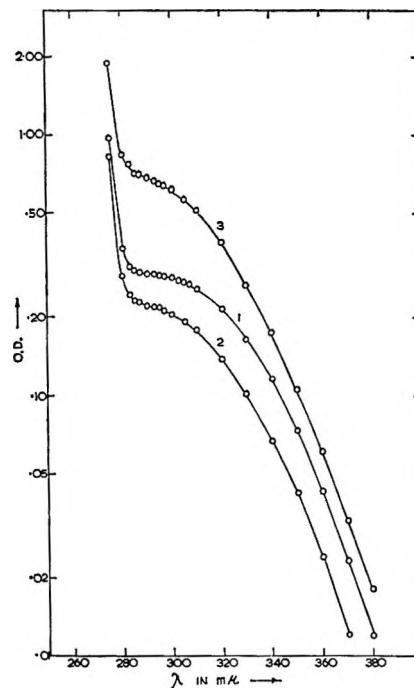


Figure 3. Absorbance data of DPI in methanol-water mixtures at 25°: (1) 100% methanol, $4.29 \times 10^{-3} M$ DPI + $3.0 \times 10^{-4} M$ $\text{Na}_2\text{S}_2\text{O}_3$; (2) 90% methanol, $4.40 \times 10^{-3} M$ DPI + $3.0 \times 10^{-4} M$ $\text{Na}_2\text{S}_2\text{O}_3$; (3) 80% methanol, $9.87 \times 10^{-3} M$ DPI + $3.3 \times 10^{-4} M$ $\text{Na}_2\text{S}_2\text{O}_3$. Measurements were made against the solvent; percentage of alcohol by weight.

the CT band in chloroform, as discussed previously,⁵ the λ_{max} values could be estimated.

A plot of these λ_{max} values against the dielectric constants (D) of the solvent mixtures is shown in Figure 4. For each solvent combination, λ_{max} varies smoothly with the dielectric constant D . The methanol-water and glycol-water curves overlap almost completely, and the ethanol-water curve lies close to them.

The micellar λ_{max} (286 $m\mu$) corresponds to dielectric constants of 36 ± 2 of these solvent mixtures, which is, therefore, the effective D at the micelle surface. This is unlikely, however, to be a true estimate of the polarity at the micelle surface, as discussed below, although it may be a close approximation. The important point is that even in an aqueous environment (of bulk $D = 79$) the CT band at the micelle surface corresponds to a macroscopic dielectric constant of 36. This provides very strong evidence of the reality of the dielectric saturation and other such polarity-reducing effects of highly charged surfaces. On the other hand, the reduction in D is not as excessive as is sometimes assumed.

The Polarity at the Micelle Surface. The uncertainty

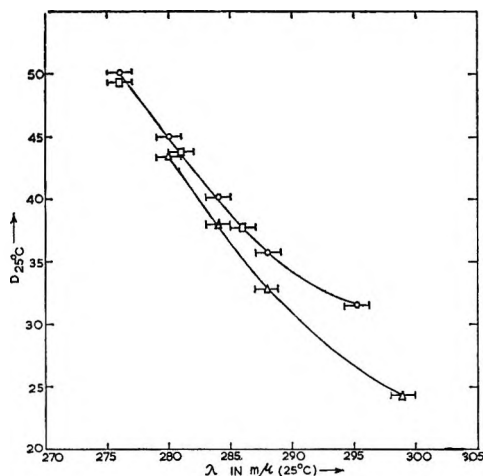


Figure 4. Plot of the dielectric constant of the solvent against λ_{\max} for DPI at 25°: \circ , methanol-water mixtures; Δ , ethanol-water mixtures; \square , glycol-water mixtures.

of the above estimated "effective" D at the micelle surface comes from two sources. First, the criticism can be made that in mixed solvents, fractionation of the solvent molecules may occur around an ion pair and, therefore, the bulk value of D is not representative of the microscopic value. However, in view of the close agreement of pure ethylene glycol ($D = 37.7$) with the other solvent mixtures, and the closeness of its λ_{\max} value to that of the micellar band, it seems that any preferential solvation effect is probably of little importance, at least in the systems considered here. More important, to accept the value of 36 for the micelle surface, we must neglect any dielectric saturation effect for the ion pair, *i.e.*, assume that the bulk D is identical with the microscopic D affecting the interactions of the ion pair. The neglect of this factor leads to an overestimate of D at the micelle surface. The error, however, is probably small. A recent estimate of D in water around a monovalent ion with a radius of 2 Å, comparable to the radius of 2.16 Å for I^- , shows that D increases rapidly between 2 and 3 Å from the center of the ion, and the value of D at 3.5 Å, the minimum distance of separation between the charges in the pyridinium iodide ion pair, is about 72.¹¹ In the mixed solvents, with lower D , the saturation effect is expected to be even smaller.

Environmental Effects on the Micellar Band Position.

If the positions of the CT bands on the micelle surface are truly indicative of the effective polarity, and the value of the effective D at the micelle surface is caused by the factors mentioned before, it would be expected that alterations of the surface conditions should affect the λ_{\max} of the CT bands. Small variations in λ_{\max} were indeed found. Thus, the CT band for trace

amounts of I^- on MyPCl micelles, shown in Figure 2, is shifted slightly toward the ultraviolet, as the comparison with the micellar band of DPI in water shows. The estimated shift in λ_{\max} is 3 $m\mu$. Since the specific interactions of I^- with pyridinium micelles is much stronger than that of Cl^- ,¹² the chloride micelles are expected to have a somewhat lower counterion concentration and field strength at the micelle surface than iodide micelles. Moreover, the concentration effect of Cl^- is less than that of iodide, the molar decrement in D of aqueous solutions being 11 and 15 for NaCl and NaI, respectively.¹³ It is thus expected that the effective polarity on the chloride micelle is higher, in agreement with the blue shift of the micellar band. Similar conclusions have been reached previously in a different connection.

Similarly, with increasing concentration of KI, as the micelle increases in size and charge density¹⁴ and there is a stronger specific adsorption of I^- ions,¹² the CT bands of DPI shift to higher wavelengths (Figure 5). The shift is small at 0.02 M KI, the estimated λ_{\max} being 288 $m\mu$ compared to 286 $m\mu$ for DPI micelles in water. At the higher concentration of KI, 0.1 M , the shift is more pronounced and the band actually crosses the bands of DPI in water and in 0.02 M KI. The estimated λ_{\max} here is 292 $m\mu$. The CT band for a trace of DPI in DTAI (Figure 1) is about 5 $m\mu$ toward the red as compared to the DPI micellar band in water at 45°, separately determined. Here again, the high concentration of DTAI used appears to be the main reason.

Some experiments were also performed using various additives. In the presence of $7.0 \times 10^{-4} M$ dodecylamine, the band position of $5.75 \times 10^{-3} M$ DPI was identical with that of DPI alone, but the intensity was about 55% higher than the value found for DPI alone, showing that micelle formation increased considerably, presumably because of induced micellization.¹⁵ When 5% by weight of ethanol was added to $6.55 \times 10^{-3} M$ DPI, the band shifted slightly toward the blue by about 2 $m\mu$. The intensity was about 24% lower than that for DPI alone, showing that micellization is decreased by the addition of ethanol. When a nonionic association colloid, Lubrol-W, was added, the characteristic micellar bands appeared when DPI concentrations well

(11) B. E. Conway, J. E. Desnoyers, and A. C. Smith, *Phil. Trans. Roy. Soc. (London)*, **A256**, 389 (1964).

(12) P. Mukerjee and A. Ray, *J. Phys. Chem.*, **70**, 2150 (1966).

(13) (a) J. B. Hasted, D. M. Ritson, and C. H. Collie, *J. Chem. Phys.*, **16**, 1 (1948); (b) P. Mukerjee and K. Banerjee, *J. Phys. Chem.*, **68**, 3567 (1964).

(14) H. C. Parreira, *Anais. Acad. Brasil. Cienc.*, **32**, 207 (1960).

(15) P. Mukerjee and K. J. Mysels, *J. Am. Chem. Soc.*, **77**, 2937 (1955).

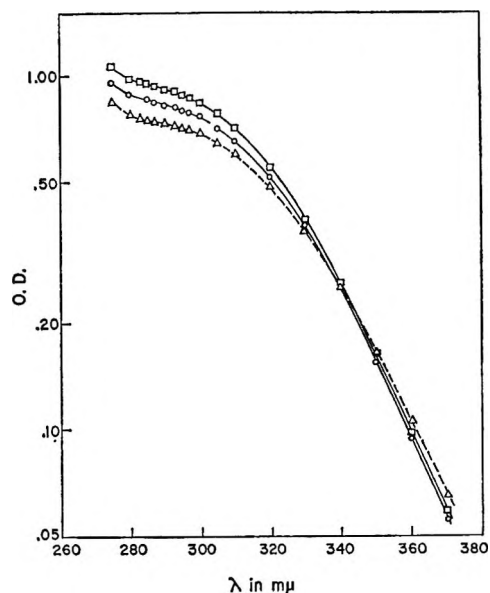


Figure 5. Difference micellar spectra of DPI at 25°C: □, in water, $6.57 \times 10^{-3} M$ DPI against $5.77 \times 10^{-3} M$; ○, $0.020 M$ KI, $3.066 \times 10^{-3} M$ DPI against $2.40 \times 10^{-3} M$; Δ, $0.100 M$ KI, $1.664 \times 10^{-3} M$ DPI against $1.175 \times 10^{-3} M$.

below the cmc were used, showing the formation of mixed micelles. On increasing the concentration of the nonionic detergent by a factor of 3, the intensity decreased by about 30%. This is probably due to the dilution of DPI, leading to lower charge densities on the micelles and thus lower binding of the counterions. Unexpectedly, however, the position of the band, as compared to DPI micelles in water, shifts toward the red by 4 and 6 $m\mu$ in 0.44 and 1.36% Lubrol-W, suggesting that the CT interaction centers are in an environment of a somewhat lower effective polarity, compared to DPI micelles in water, even when the nonionic fraction predominates in the mixed micelle. Lubrol-W contains polyethylene oxides as the head groups. It appears that these bulky head groups, which are, nevertheless, mainly organic in character, containing ether linkages, produce a region of low effective polarity at the micelle surface, a not unlikely result when it is remembered that ethyl ether has a dielectric constant as low as 4.3.

Comparison with Theory. Any detailed theory of the effective polarity at the micelle surface must include at least the three factors mentioned above: namely, the field-strength effect on dielectric saturation,⁹ the concentration effect,^{10,13} and the proximity of the hydrocarbon core. The factors, however, are not independent. The third factor can be evaluated separately, assuming its independence from the others.¹⁶ The calculated D depends critically on the assumed

position of the charges in relation to the hydrocarbon sphere, *i.e.*, whether the charges are considered to be just inside the surface of the sphere or just outside. In the former case, low effective D values are obtained, but in the latter case, using any reasonable geometry of charge separation and micelle radius, the effective D is only slightly lower than the medium value, not nearly enough to explain the observed value of 36. It seems to us that this latter assumption is physically more plausible and, therefore, the effect of the proximity of the hydrocarbon core is small.

The macroscopic dielectric saturation effect can be calculated on the basis of an average field strength on the basis of a continuum model. The Gouy-Chapman surface potential calculated for DPI micelles in water is about 200 mv. Considering the specific adsorption of I^- ions,¹² it is expected that the electrokinetic potential for DPI micelles should be considerably lower than those of micelles of sodium lauryl sulfate.¹⁷ Thus, a fall of approximately 100 mv for the Stern layer is unlikely to be an overestimate. In view of the expected roughness of the micelle surface,¹⁷ and the attendant snuggling of the counterions, the average separation between the surfaces describing the positive and negative charges on the micelle is certainly much less than the sum of the radii of I^- and of the nitrogen charge center of pyridine (3.5 Å). If we accept a reasonable value of 1.5 Å for this separation,¹⁷ the field strength is about 7×10^6 v/cm for which Booth's theory⁹ predicts a dielectric constant of 38. The excellent agreement with the experimental "effective" value is fortuitous, but it suggests that if the dielectric saturation approach is to be used,^{18,19} Booth's theory should be superior to the older theories of Debye and others, which, as treated by Conway, *et al.*,¹⁸ predict a value of only 16 for the above field strength.

Reasonable agreement with the experimental value can also be obtained using an estimate based on the concentration effect alone. The molar dielectric decrements are 11 and 15 for NaCl and NaI,¹³ and about 17 for tetraethylammonium chloride, as recently determined.²⁰ For the pyridinium iodide, the value should be in the range of 15–20. Assuming an average thickness of 4–5 Å for the Stern layer, its concentration is

(16) K. Lindström-Lang and S. O. Nielsen, "Electrophoresis," M. Bier, Ed., Academic Press Inc., New York, N. Y., 1959, Chapter II.

(17) D. Stigter and K. J. Mysels, *J. Phys. Chem.*, **59**, 45 (1955).

(18) B. E. Conway, J. O'M. Bockris, and I. A. Ammar, *Trans. Faraday Soc.*, **47**, 756 (1951).

(19) J. Lyklema and J. Th. G. Overbeek, *J. Colloid Sci.*, **16**, 501 (1961).

(20) W. D. Kraeft and E. Gerdes, *Z. Physik. Chem. (Leipzig)*, **228**, 331 (1965).

calculated to be 2-3 M , which is enough to account for the value of D at the micelle surface.

The fact that the two approaches are individually enough to explain the effective D , whereas the two factors should be additive, suggests the need for caution. It seems that the measured bulk dielectric constant of an ionic solution does not necessarily represent its value at the microscopic level, and the average field strengths calculated on the basis of a continuum model may be overestimated. The effect of high electrolyte concentrations on the positions of ion-pair bands should be of considerable interest, in this connection, to examine.

The Homogeneity of the Stern Layer. An important conclusion can be drawn regarding the Stern layer from the matchability of the CT bands⁵ of ion pairs and of micelles. Although the CT interaction is probably confined⁵ to the "intimate" ion pairs and is not exhibited by all ion pairs, there is no evidence of any heterogeneity of these "intimate" ion pairs; *i.e.*, to the best of our knowledge, all "intimate" ion pairs

involve the same interactions. Thus, the characteristic shape and width of the CT bands of ion pairs appear to correspond to a single class of absorbers. The same conclusion, therefore, follows for the micelle surface. Otherwise, if counterion adsorption sites of different energies or local environments with different effective polarities were present, it would be expected that the characteristic CT bands for the different kinds of sites would be differently placed along the wavelength axis, and the experimentally observed sum would be more diffuse and have a larger half-width than the ion-pair bands. It appears, therefore, that at least as far as the CT interaction centers are concerned, the Stern layer is quite homogeneous. It thus seems fairly safe to treat Stern layers as such in theoretical formulations.

Acknowledgment. The support of PHS Research Grant GM 10961-01 from the Division of General Medical Services, Public Health Service, during the preparation of this manuscript is gratefully acknowledged.

The Specificity of Counterion Adsorption to Micelles of Dodecylpyridinium Iodide and Their Critical Concentrations¹

by Pasupati Mukerjee² and Ashoka Ray

Department of Physical Chemistry, Indian Association for the Cultivation of Science, Jadavpur, Calcutta 32, India (Received October 28, 1966)

The critical micelle concentrations (cmc) of dodecylpyridinium iodide (DPI) have been determined at several temperatures and several concentrations of added potassium iodide at 30° from the ultraviolet absorbances of the self-indicating micelles. The technique is also applicable to the bromide, confirming the presence of charge-transfer interactions. The slope of the absorbance-concentration curve above the cmc measures the average extinction coefficient (ϵ') per equivalent of the long-chain ions in the micellar form. The absolute value of ϵ is surprisingly high; the effect is ascribed to the presence of the strong electric field at the micelle surface. The variation of ϵ' for DPI with added KI, temperature, and increasing micelle concentrations, as also some literature data on the micellar conductance of DPI and the corresponding bromide and the chloride, are in qualitative accord with the specificity of counterion adsorption for DPI micelles which is theoretically expected on the basis of the observed charge-transfer interactions. The effect of increasing micelle concentrations on ϵ' is contrary to the notion of "retrograde dissociation": it is concluded that because of the specificity of counterion interaction, DPI and also DPBr may be poor models for other micellar systems in this respect. Approximate estimates of the difference in the free energy of adsorption between chloride and iodide, obtained from the cmc and the selectivity of adsorption to micelles, give concordant results, the value being -1.7 ± 0.5 kcal/equiv. An approximate value of the enthalpy of specific adsorption for the iodide has also been derived. The variations of the cmc with temperature and added KI are also consistent with, and provide evidence for, a significant contribution of the specificity of counterion adsorption to the stability of micelles.

Introduction

The problem of the specificity of counterion adsorption on the surface of charged micelles and colloids in general is greatly complicated by the difficulty of separating any effect of short-range interactions from those of purely electrostatic interactions, which are as yet only imperfectly understood, and the paucity of experimental approaches for studying directly the innermost part of the electrical double layer, or the Stern layer. The previous paper³ has dealt with the effective polarity in the Stern layer as revealed by a study of the charge-transfer (CT) spectra characteristic of the micelles of dodecylpyridinium iodide (DPI). The short-range CT interactions involve some electronic interactions in the ground state. In Mulliken's

formulation of CT complexes,⁴ for example, it is assumed that the wave function of the excited state makes some contribution in the ground state. Since in interionic CT interactions the ground state is charged and the excited state is uncharged, an equivalent statement is that there is a weak contribution of covalent bonding in the ground state. Thus, excellent theoretical reasons exist, *a priori*, for expecting a speci-

(1) Taken in part from the doctoral dissertation of A. Ray, Calcutta University, 1963.

(2) Department of Chemistry, University of Southern California, Los Angeles, Calif. 90007. Requests for reprints should be sent to this address.

(3) P. Mukerjee and A. Ray, *J. Phys. Chem.*, **70**, 2144 (1966).

(4) R. S. Mulliken, *J. Am. Chem. Soc.*, **74**, 811 (1952); *J. Phys. Chem.*, **56**, 801 (1952).

ficity of interaction of iodide ions and pyridinium ions, *i.e.*, interactions over and above purely electrostatic interactions. Moreover, this interaction, as revealed in the CT bands, must be confined to the Stern layer, because of the short-range nature of CT interactions. It was thus expected that the intensity of the CT bands should reflect the extent of the specific adsorption. The present paper reports results on the variation of the CT band intensity of DPI micelles with counterion concentration, concentration of micelles, and temperature. Critical micelle concentrations (cmc), determined by the ultraviolet absorption method,^{5,6} as a function of the counterion concentration and temperature are also reported. The band intensities and the variations in the cmc are shown to be consistent with a significant specificity of adsorption.

Experimental Section

The materials used and the experimental methods have been described.⁷

Results

Critical Micelle Concentrations. The cmc's were determined from absorbance data at 290 m μ . Figure 1 shows the nature of the variation of the absorbance with concentration for DPI in water. The absorbance is appreciable at concentrations much below the cmc, presumably because of ion-pair formation of the iodide ion with the monomer, as is found for methylpyridinium iodide,⁸ and also, possibly, with the dimer of the long-chain ions.⁹ The absorbance increases nonlinearly as the cmc is approached until somewhat above the cmc, and then, in the micellar region, it increases rapidly but linearly with concentration. Any extrapolation from the curved region near the cmc is uncertain. We have, therefore, determined the cmc from the intersection of the straight lines through the absorbance data well below the cmc and those somewhat above.⁶ This procedure gives cmc values precise within 0.5–1% in water on duplicate measurements and on using different wavelengths for absorbance measurements. On the other hand, it seems to give a comparatively low estimate of the cmc. The cmc, of course, is always arbitrary to some extent, because it pinpoints one concentration from a range of concentrations. Different experimental methods lead to somewhat different estimates of the "break-point" of the "turn-away point," defined as the cmc, as some physical property of the solution is plotted against some function of the concentration. A consistent difference of about 3% is found even for such closely related plots, using the same basic experimental data, as equivalent

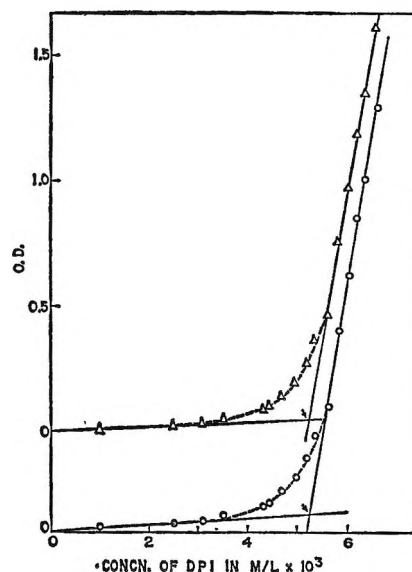


Figure 1. Absorbance data for DPI in water at 25°: O, 290 m μ ; Δ , 295 m μ .

conductance *vs.* the square root of concentration or specific conductance *vs.* the concentration, the latter giving the higher value of the cmc.^{10,11} Ideally, therefore, any cmc value determined should be associated with an estimate of the fraction micellized.¹² In our case, from a reasonable extrapolation of the absorbance data, due to nonmicellar material, well below the cmc, it appears that the micellar absorbance at the cmc corresponds to only about 1% of micellization in water. We thus expect that the cmc from ultraviolet absorbance data will have a slight, systematic bias toward lower values when compared to those determined from specific conductance data.

Our cmc value in water at 25°, $5.26 \times 10^{-3} M$, is some 5% higher than that previously obtained by the same method,⁵ and about 15% higher than one determined from specific conductance data.¹³ This suggests that our sample was purer than the previous ones.

The absorbance data for DPI at different tempera-

- (5) W. D. Harkins, H. Krizek, and M. L. Corrin, *J. Colloid Sci.*, **6**, 576 (1951).
- (6) P. Mukerjee and A. Ray, *J. Phys. Chem.*, **67**, 190 (1963).
- (7) A. Ray and P. Mukerjee, *ibid.*, **70**, 2138 (1966).
- (8) E. M. Kosower and P. E. Klinedinst, *J. Am. Chem. Soc.*, **78**, 3493 (1956).
- (9) P. Mukerjee, *J. Phys. Chem.*, **69**, 2821 (1965).
- (10) K. J. Mysels and P. Kapauan, *J. Colloid Sci.*, **16**, 481 (1961).
- (11) B. D. Flockhart, *ibid.*, **16**, 484 (1961).
- (12) R. J. Williams, J. N. Phillips, and K. J. Mysels, *Trans. Faraday Soc.*, **51**, 728 (1955).
- (13) K. Meguro and T. Kondo, *Nippon Kagaku Zasshi*, **80**, 818 (1959).

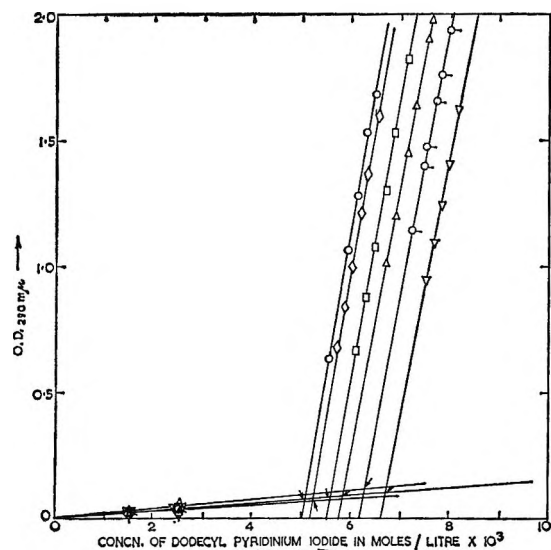


Figure 2. Absorbance data for DPI in water at different temperatures: \circ , 20.3°; \diamond , 24.9°; \square , 30.1°; Δ , 34.9°; ∇ , 40.0°; ∇ , 44.9° (cmc's indicated by arrows).

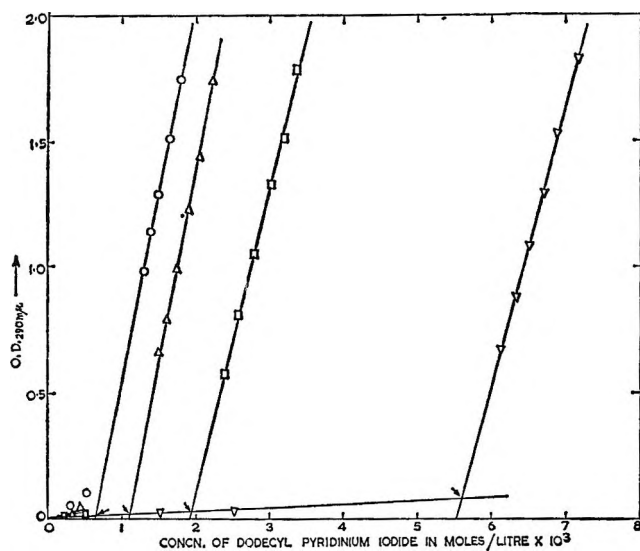


Figure 3. Absorbance data for DPI in KI solutions at 30°: ∇ , 0 M KI; \square , 0.0202 M KI; Δ , 0.0501 M KI; \circ , 0.1002 M KI (cmc's indicated by arrows).

tures are shown in Figure 2, and those at different concentrations of added KI are shown in Figure 3. The cmc data are collected in Table I.

Figure 4 shows absorbance data at three wavelengths⁷ for dodecylpyridinium bromide (DPBr) as a function of the concentration. The primary purpose here is to show that most of the absorbance at these wavelengths is characteristic of the micelles for the bromide also. The cmc estimated at 25°, $1.21 \times 10^{-2} M$,

Table I: Cmc Data for DPI

Temp, °C	Cmc in water $\times 10^4$, moles/l.	Concn of added KI, mole/l.	Cmc at 30° $\times 10^4$, moles/l.
20.3	5.10	0.0202	1.94
24.9	5.26	0.0501	1.12
30.1	5.60	0.1002	0.65
34.9	5.85		
40.0	6.30		
44.9	6.70		

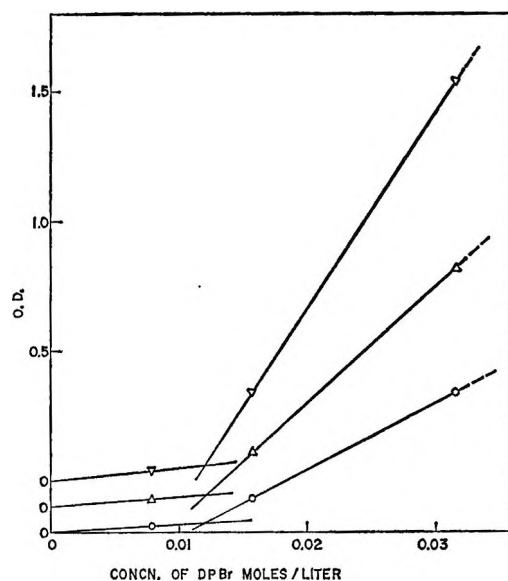


Figure 4. Absorbance data for DPBr in water at 25°: ∇ , 295 m μ ; Δ , 300 m μ ; \circ , 305 m μ .

agrees fairly well with a value of $1.14 \times 10^{-2} M$ obtained from specific conductance data.¹⁴

The slopes of the linear portion of the absorbance data above the cmc measure the apparent average extinction coefficient (ϵ') per equivalent of long-chain ion in the micellar form, on the assumption that the monomer concentration in this region remains constant. The error due to this assumption is probably small. The slopes were evaluated by linear regression analysis, and the results plotted later (Figures 5 and 6) contain the probable error. Because of the relatively rapid variation of the cmc of DPI with temperature, a part of the uncertainty of the ϵ' values arises from small temperature variations in the cell compartment, which alter the concentration of micelles.

Discussion

Extinction Coefficients of Micelles. The ϵ' value

(14) J. E. Adderson and H. Taylor, *J. Colloid Sci.*, 19, 495 (1964).

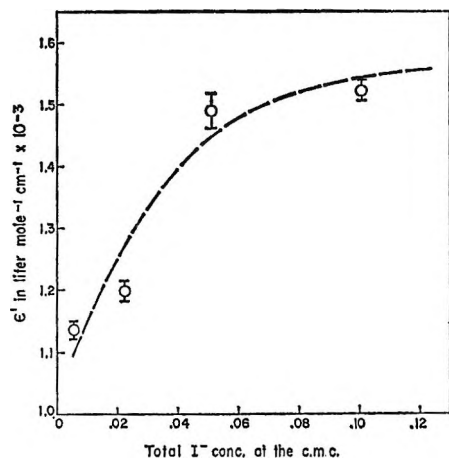


Figure 5. The variation in ϵ' for DPI micelles with total iodide concentration at the cmc at 30°.

calculated for DPI micelles in water at 25° is 1140 at 290 $m\mu$. It increases with added KI (Figure 5) to more than 1500, and a rough extrapolation gives the extinction coefficient per equivalent of iodide ion (ϵ) as about 1600. The value will be slightly higher at the estimated band maximum, λ_{max} of 286 $m\mu$.³ In comparison, the extinction coefficient of DPI ion pairs in chloroform, which has a dielectric constant of about 5, is 1140 at its long wavelength band maximum,⁷ whereas in solvents in which ion-pair bands have about the same λ_{max} as the DPI micelles in water, the average extinction coefficient for ion pairs is 400–450.⁷ It has been suggested that this low value is due to the fact that only a fraction of the ion pairs, the "intimate" ones, undergo CT interactions.⁷ The micellar ϵ is clearly very high. It suggests that the extent of "intimate" contacts between ions at the micelle surface is considerably higher than in ion pairs for the same effective polarity. This effect is probably due to the strong electric field created by the excess of positively charged ions around the individual CT sites on the micelles, which promotes desolvation of the solvent-separated or solvent-sharing ion pairs.⁷ The ϵ values for micelles are higher than even that for chloroform ion pairs. If the total oscillator strengths of the bands are estimated, by assuming a symmetrical band, the difference is magnified. It thus appears that the ion-pair band in chloroform cannot be used as a measure of the intrinsic oscillator strength of the CT band and that, even in chloroform, not all ion pairs are "intimate."

It is thus not possible, at present, to estimate the absolute fraction of counterions that are "intimately" bound to the micelle surface from the intensity of CT bands of model systems. However, if we make the

assumption that the "intimate" fraction of the bound iodide ions in the Stern layer remains constant, the relative intensities should indicate the variation of the extent of counterion binding on micelles.

Specificity of Pyridinium-Iodide Interaction on the Micelle. In the Introduction, theoretical reasons have been given for expecting some specificity in the interaction of iodide ions with pyridinium ions at the micelle surface. Any specific attractive interaction would result in greater "binding" of the counterions at the micelle surface than is possible from electrostatic interactions alone. Moreover, it would be predicted, theoretically, that the "binding" will increase with higher concentrations of counterions, and since the CT interactions should be exothermic, the "binding" should decrease with temperature. All of these and some other predictable results of the specificity of interaction were indeed found.

Micellar Conductance. That the iodide "binding" to the micelle surface is greater than that of the chloride or the bromide is shown by the conductance measurements of Meguro and Kondo.¹³ The rate of increase of specific conductance with concentration above the cmc, which is a measure of the conductance of the micelle and its counterions, is considerably greater for dodecylpyridinium chloride (DPCI) than the bromide and the iodide, the values being roughly in the ratio 1.9:1.2:1.0 for Cl^- , Br^- , and I^- , even though the ionic conductances of Br^- and I^- are slightly larger than that of the chloride. This shows a smaller percentage of free ions in the diffuse double layer for DPI and greater "binding" of the iodide ions in the Stern layer.

Effect of Added KI. Figure 5 shows the average ϵ' values, corrected for the small band shifts, as a function of the total concentration of iodide ions at the cmc as KI is added. There is a marked increase at first and a tendency to level off at high concentrations. This shows increased "binding" of the iodide ions at the micelle surface, with added KI. The shape of the curve suggests a close approach to saturation of the adsorption of iodide ions at the higher concentrations of KI. A rough extrapolation to a value of about 1600 for ϵ' corresponding to complete "binding" of the iodide ions does not seem unreasonable. This value, then, can be looked upon as the average ϵ for iodide ions.

It seems extremely likely from Figure 5 that at high concentrations of KI, the micelles of DPI will have a low charge. Electrophoretic mobility and conductance measurements to check this conclusion would be of great interest. It may be noted that Parreira found evidence for a rapid decrease in the charge of

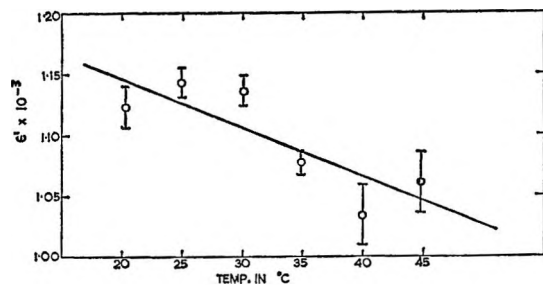


Figure 6. The variation in ϵ' for DPI micelles in water with temperature.

DPI micelles with added KI from light-scattering measurements.¹⁶

Effect of Temperature. Figure 6 shows the ϵ' values as a function of temperature. There is a significant decrease in ϵ' with rising temperature. These values were not corrected for the slight shift in the band position, about 2 $m\mu$ between 25 and 45°. The correction is small and would add slightly to the change shown in Figure 6.

The Effect of High Concentration of Micelles and the Problem of "Retrograde Dissociation." A long-standing puzzle for ionic association colloids is the problem of the increase in the equivalent conductance at high concentrations.^{16,17} One of the explanations suggested, originally by Hartley,¹⁶ is that the degree of dissociation of the counterions increases even as the concentrations of all ions increase. Hartley also suggested that the color of alkylpyridinium iodide micelles should be of some use in the study of this problem.¹⁸ Harkins, Krizek, and Corrin⁵ examined this suggestion and found that the intensity of the micellar absorption close to the band maximum varied linearly with concentration above the cmc up to 0.032 M , from which they concluded that the range of concentration was not sufficiently high to give any observable effect. In their experiments, the temperature variation was rather large, $\pm 2^\circ$, and different cells using different path lengths showed appreciable discrepancies. In our experiments, 10^{-4} M sodium thiosulfate was used to prevent any triiodide formation, and the absorbance measurements were made at 380 $m\mu$, enabling us to cover a concentration range up to 0.044 M . We corrected the observed absorbances for scattering from micelles, using turbidity data at 380 $m\mu$ for myristylpyridinium chloride (MyPCI).⁷ The myristyl compound was chosen rather than the dodecyl, because of the high cmc of the latter, 1.7×10^{-2} M ,¹³ and the low molecular weight of the micelles, 5300¹⁹ compared to 32,700 for DPI.¹⁶ It is expected that both in cmc and molecular weight, MyPCI is a

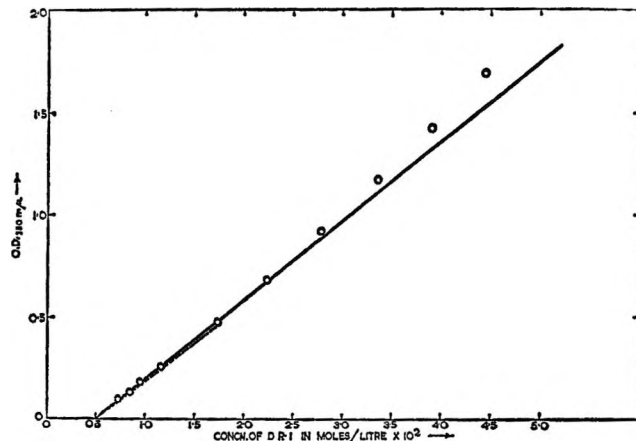


Figure 7. The variation of the absorbance at 25° with the concentration of DPI (absorbance measured at 380 $m\mu$ and corrected for turbidity).

better analog of DPI than DPCI. The maximum turbidity correction was only 0.044 in optical density.

Figure 7 shows the corrected absorbance data against the concentration of DPI. The slope of the line increases with concentration rather than decreases, contrary to what is expected from "retrograde dissociation." The initial slope, close to the cmc, determined from careful measurements of the micellar difference absorbance at 380 $m\mu$ and comparison to the more accurately determined slope at 290 $m\mu$, is shown by the dotted line.

Since small shifts in the micellar band positions may have occurred, the data at high concentrations should not be used quantitatively. The qualitative fact that the DPI system gives no evidence of "retrograde dissociation" is supported by the independent observations of Heckmann and Woodbridge.²⁰

Figure 8 shows similar measurements for DPB extended to very high concentrations. For this system, the turbidity corrections were made from optical densities at much longer wavelengths, using the λ^{-4} dependence. Here again, the evidence is for increased "binding" with concentration and, therefore, decreased dissociation.

On the other hand, the observed results are qualitatively in line with the specificity of interaction of the

(15) H. C. Parreira, *Anais. Acad. Brasil. Cienc.*, **32**, 207 (1960).

(16) G. S. Hartley, B. Collie, and C. S. Samis, *Trans. Faraday Soc.*, **32**, 795 (1936).

(17) K. J. Mysels and C. I. Dulin, *J. Colloid Sci.*, **10**, 461 (1955).

(18) G. S. Hartley, *Quart. Rev. (London)*, **2**, 152 (1948).

(19) R. H. Ottewill and H. C. Parreira, *J. Phys. Chem.*, **62**, 912 (1958).

(20) K. D. Heckmann and R. F. Woodbridge, *Proc. Intern. Congr. Surface Activity, 4th Brussels, 1964*, to be published.

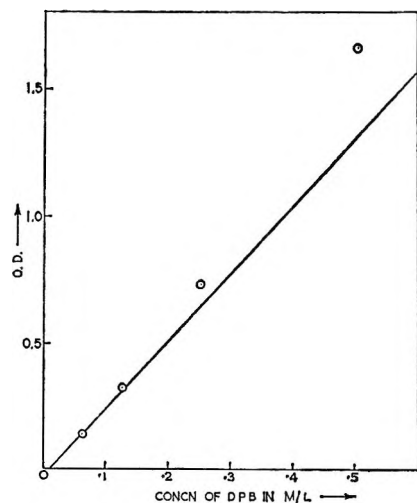


Figure 8. The variation of the absorbance at 25° with the concentration of DPB (absorbance measured at $325\text{ m}\mu$ and corrected for turbidity).

counterions. As the micelle concentration increases, the counterion concentration in the intermicellar fluid increases, leading to increased specific adsorption, as in the case of added KI (Figure 5). Thus the negative results obtained for DPI and DPB may have been caused by presence of short-range specific interactions. It should be of some interest to see if DPI shows any evidence of "retrograde dissociation" in conductance or transference measurements. We do not believe that our work precludes the reality of this phenomenon in systems where interionic interactions are primarily electrostatic.

Estimates of Specific Interaction Energy and Enthalpy. The quantitative treatment of specificity is complicated by the difficulty of separating the specific from the purely electrostatic interactions. Some rough but useful estimates of the specific interaction energy and enthalpy can be obtained nevertheless. The cmc of DPCl at 30° has been estimated¹³ as 1.74×10^{-2} compared to 5.60×10^{-3} for DPI. This difference by a factor of 3 corresponds to a difference of about -1.1 kcal in the free energy of micelle formation per equivalent of long-chain ion, that for the iodide being more negative. In this calculation, based on the mass-action model,²¹ no account has been taken of any dimerization,⁹ and it has been assumed that 70% of the counterions are bound to the micelle surface for both counterions. While the fraction bound, due to the combination of specific and electrical interactions, is expected to be less for the chloride, the correction for dimerization which reduces the monomer concentration at the cmc is expected to be much higher for the chloride because of its higher cmc. The

errors due to the neglect of the two factors are in the opposite direction and cancel in part. Considering that only about 70% of the counterions are bound to the DPI micelles, the free energy difference per equivalent of counterion, on the average, is about -1.6 kcal. This value is likely to be close to the total specific interaction energy of iodide ion itself, since that for the chloride is expected to be small on general grounds. The close similarity of the cmc of DPCl,¹³ $1.74 \times 10^{-2} M$ at 30° , and that of dodecyltrimethylammonium chloride,²² 1.72×10^{-2} at 25° , also argues for the absence of any strong specific interaction for DPCl.

Another estimate of the difference in the free energy of adsorption between chloride and the iodide can be obtained on the basis of the selectivity of the adsorption in systems with mixed counterions, assuming that the electrostatic interactions are identical for both ions. Absorption spectra of MyPCL in presence of small amounts of iodide are shown in Figure 2 of the previous paper. The intensities, corrected for the slight band shift observed, can be used to determine the fraction of the iodide ions in the Stern layer, using the value of $\epsilon' = 1600$ for the case of complete "binding." In $6.12 \times 10^{-3} M$ MyPCL containing $7.59 \times 10^{-4} M$ KI, the fraction of the iodide ions in the Stern layer thus evaluated is 0.72. The fraction of chloride ions in the Stern layer depends on some assumptions about the cmc and the total fraction of the micellar charge, α , neutralized by all counterions in the Stern layer. The estimated cmc of MyPCL is $4 \times 10^{-3} M$. For assumed α values of 0.60 and 0.70, the calculated fractions of all chloride ions in the Stern layer are 0.12 and 0.15, respectively. Thus iodide ions are adsorbed highly selectively. The selectivity factors f , given by the ratio of the concentration ratio of iodide to chloride ions in the Stern layer, and the same concentration ratio of the free ions in the bulk are 19 and 15, respectively, for assumed α values of 0.60 and 0.70. The difference in the free energy of adsorption of the two ions to the pyridinium micelles, given by $-RT \ln f$, where R is the molar gas constant and T is the absolute temperature, is -1.7 ± 0.5 kcal/equiv. The large estimated uncertainty includes the estimated uncertainty in the value of ϵ' for complete adsorption. The free energy difference agrees well with the estimate from the cmc data.

A rough estimate of the enthalpy of specific interaction of the counterions can be obtained from the temperature variation of ϵ' (Figure 6). In this case, the cmc and, therefore, the counterion concentration

(21) P. Mukerjee, *J. Phys. Chem.*, **66**, 1375 (1962).

(22) H. W. Hoyer and A. Marmo, *ibid.*, **65**, 1807 (1961).

close to the cmc, increases by about 30% between 20 and 40°. While this, by itself, should result in an increase in the binding of iodide ions, a part of this effect is cancelled by the decrease in the surface potential caused by this concentration increase. We therefore make the approximation that the effective concentration remains the same. Using the value of 1600 for complete "binding" and the experimental ϵ' , the fraction of the sites in the Stern layer to which counterions are bound, θ , can be calculated for each temperature. At the constant effective concentration assumed, $\theta/(1 - \theta)$ is a relative measure of the adsorption equilibrium between the bound and the unbound fraction. Plotting $\log \theta/(1 - \theta)$ against $1/T$, the enthalpy obtained from the slope is -2 ± 1 kcal/equiv, taking the uncertainty of the various factors into account. It seems probable that the specific interaction free energy consists primarily of enthalpy.

The surprisingly low values of the free energy of specific interaction of the counterions for DPI, for which the manifestations of the specificity are so pronounced, throws some doubts on occasional estimates of high specific interaction energies for many systems.²³

Interpretation of the Cmc Data. The variation of the cmc of DPI with temperature and counterion concentration shows some peculiarities, when compared with other similar systems. Figure 9 shows the linear dependence of \log cmc on the logarithm of the total counterion concentration. Such linear plots have been frequently demonstrated for a variety of ionic association colloids. The slope of the curve, -0.74 , is significantly different, however, from -0.679 for sodium lauryl sulfate¹² and -0.68 for dodecyltrimethylammonium chloride.²⁴ A large number of factors, such as dimerization,⁹ activity coefficient corrections, salting out of the long-chain ions,²⁵ and the variation of the micelle size, must be taken into account before a quantitative interpretation of these slopes can be given. Nevertheless, the slope of DPI is consistent with the idea that its absolute value represents the degree of association of the counterions.²⁶ Because of specific interactions, the degree of association of the counterions for DPI is expected to be greater.

The temperature dependence of the cmc of DPI, shown in Figure 10, is remarkable for its high magnitude over the range covered. Most ionic association colloids show a minimum in the cmc at 25–40°, and the variation of the cmc is much smaller than that of DPI.¹¹ The enthalpy of micelle formation, ΔH_m , can be calculated, using the phase-separation model,²⁷ from the equation

$$\Delta H_m = -RT^2 d \ln (\text{cmc})/dT \quad (1)$$

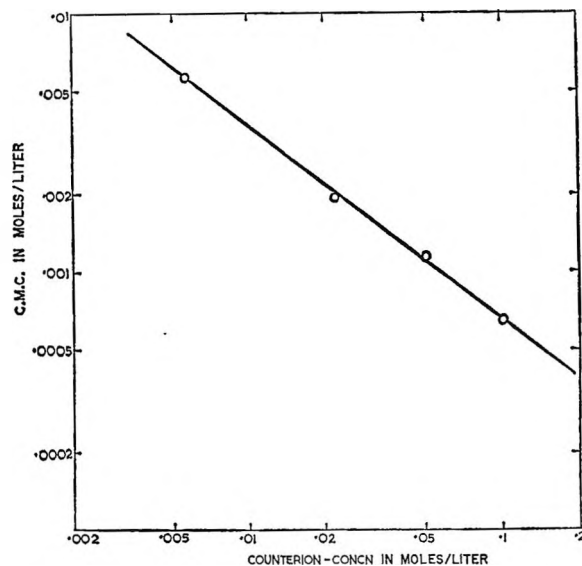


Figure 9. The variation of the cmc of DPI with the total counterion concentration at the cmc.

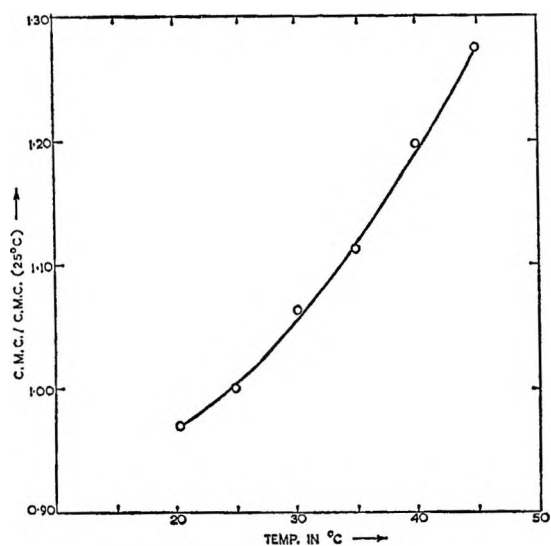


Figure 10. The variation of the cmc of DPI with temperature.

The estimated values of ΔH_m , in kcal/equiv for DPI, are -1.28 at 21°, -1.55 at 25°, -2.26 at 35°, and -3.01 at 45°. The phase-separation model is a poor model for micellar systems,²⁸ particularly for ther-

(23) J. T. Davies and E. K. Rideal, "Interfacial Phenomena," Academic Press Inc., New York, N. Y., 1961.

(24) L. M. Kushner, W. D. Hubbard, and R. A. Parker, *J. Res. Natl. Bur. Std.*, **59**, 113 (1957).

(25) P. Mukerjee, *J. Phys. Chem.*, **70**, 783 (1966).

(26) M. L. Corrin, *J. Colloid Sci.*, **3**, 333 (1948).

(27) G. Stainsby and A. E. Alexander, *Trans. Faraday Soc.*, **46**, 527 (1950).

(28) K. J. Mysels, P. Mukerjee, and M. Abu-Hamdiyyah, *J. Phys. Chem.*, **67**, 1943 (1963).

modynamic calculations.²¹ Unfortunately, other models, such as the chemical mass-action model, based on the idea of binding of counterions,²¹ or the more physical model based on the calculation of electrostatic free energies,²⁹ require many as yet undetermined parameters for the calculation of ΔH_m . It is to be expected, however, that the phase-separation model gives at least qualitative information about the variation of ΔH_m for related systems. Table II compares some ΔH_m values for some systems containing a dodecyl chain. The consistently more negative values for DPBr and DPI and the difference between the two argue for a significant contribution of the specific interaction of the counterions, increasing from the bromide to the iodide, to ΔH_m . Previous studies have indicated the absence of any strong specific interaction for the sulfonates and the sulfates.³⁰ The close similarity of the acid sulfonate and the sodium sulfate in their ΔH_m values (Table II) support this conclusion.

The cmc minimum for DPBr occurs at 15°, which is appreciably lower than the 25–30° range of the other systems of Table II excepting DPI. For the latter, an approximate estimate of the temperature of the minimum cmc can be obtained by plotting ΔH_m against

Table II: ΔH_m (Eq 1) Values for Some Association Colloids

Association colloid	$-\Delta H_m$, kcal/equiv	
	20°	40°
Sodium dodecyl sulfate ^a	0.4	-1.1
Dodecylsulfonic acid ^a	0.5	-1.1
Dodecylammonium chloride ^a	1.1	-2.0(50°)
Dodecylpyridinium bromide ^b	-0.55	-1.77
Dodecylpyridinium iodide ^c	-1.28(21°)	-2.63

^a Reference 11. ^b Reference 14. ^c This work.

temperature and extrapolating to a value of 0 for ΔH_m . The estimated temperature is close to 0°, which is in the expected direction.

Acknowledgment. The writing of this paper was supported in part by PHS Research Grant GM 10961-01 from the Division of General Medical Services, Public Health Service. We thank Professor Karol J. Mysels for helpful discussions.

(29) J. Th. G. Overbeek and D. Stigter, *Rec. Trav. Chim.*, **75**, 1264 (1956).

(30) P. Mukerjee, *J. Phys. Chem.*, **66**, 943 (1962).

A Study of Concentration-Dependent Three-Component Diffusion

by P. F. Mijnlieff and H. A. Vreedenberg

Koninklijke/Shell-Laboratorium, Amsterdam, Holland (Received November 23, 1965)

The continuity equations for isothermal and isopiestic diffusion in systems of three components, solutes I and II and a solvent, have been solved on an analog computer for the case of infinitely long diffusion cells ($-\infty < x < +\infty$). The concentration dependences of the four diffusion coefficients, D_{I-I} , D_{I-II} etc., were chosen such as to agree closely with those holding for aqueous solutions of two electrolytes with one common ion. The concentrations, $c_I(x,t)$ and $c_{II}(x,t)$, in the diffuse boundaries tend to become a function of x/\sqrt{t} only. The way in which c_I and c_{II} depend on this variable, once this situation has been reached, is determined by the particular functions $D_{I-I}(c_I, c_{II})$, $D_{I-II}(c_I, c_{II})$, etc., and by the values of c_I and c_{II} for $x \rightarrow -\infty$ and $x \rightarrow +\infty$, but not by the particular concentration distributions in the initial boundary layer. Three consequences of this behavior, to be generally expected in three-component diffusion, are discussed. The first concerns electromotive force measurements on galvanic cells with liquid junctions; as suggested by Guggenheim a long time ago, the liquid junctions should preferably be made in long capillaries. The second is that it proves possible to suggest a method for the determination of the values of all four diffusion coefficients, whether or not they are concentration dependent. Thirdly, the entropy produced per unit time in diffusion processes as considered here appears to become inversely proportional to the square root of time.

I. Introduction

The present paper deals with translational diffusion in liquids taking place isothermally and isopiastically in cells cylindrical along the x axis. We restrict ourselves to linear behavior. Then Fick's first law applies and in the one-dimensional case considered here it reads for a two-component system

$$J_{\text{diff}} = -D(c) \frac{\partial c}{\partial x} \quad (1)$$

In this equation, $D(c)$ is the diffusion coefficient, which quantity depends, in general, on concentration. J_{diff} denotes the diffusional mass flow, *i.e.*, the amount (we choose the mass) of one of the components (we take the solute, *i.e.*, the component with the lowest mass concentration) that passes per unit time through a plane of unit area perpendicular to the x axis. Further, c stands for the concentration of the component to which J_{diff} refers; in the present case, c is the mass of the solute per unit volume of solution. The above-mentioned plane is moving with a so-called reference velocity V_{ref} . A further discussion of this quantity

is postponed to section II (especially ref 12). Here it may suffice to say that, by introducing a reference velocity, it becomes possible to describe two-component diffusion with only one mass flow. In real diffusion processes a reference velocity equal or very nearly equal to zero (*viz.* the mean volume velocity) may be selected. We therefore discuss the equation of continuity that follows from eq 1 if the reference velocity is zero. It reads

$$\frac{\partial c}{\partial t} = -\frac{\partial}{\partial x} J_{\text{diff}} = \frac{\partial}{\partial x} \left\{ D(c) \frac{\partial c}{\partial x} \right\} \quad (2)$$

where t denotes time.

There are two main problems associated with concentration-dependent diffusion. The first one is to derive solutions of eq 2 for various types of concentration dependence of D and for boundary conditions and initial concentration distributions in conformity with the experimental setup. Then a rapid classification and evaluation of diffusion experiments becomes possible. Such solutions are available¹ for a few types of concentration dependence only.

The second problem is to determine, from diffusion

experiments, the course of D as a function of c without knowing, beforehand, anything about the way D depends on c . Of the methods used, that of Boltzmann² is best known. As much of the following is closely related to this method, we discuss it in some detail.

It is based on Boltzmann's statement that, irrespective of the way D depends on c , the concentration is a function of the single variable $x/\sqrt{t - t_{\text{sharp}}}$, provided

$$\left. \begin{aligned} c &= c_{0,-\infty} \text{ for } x < 0 \\ c &= c_{0,+\infty} \text{ for } x > 0 \end{aligned} \right\} \text{ at } t = t_{\text{sharp}} \text{ (step function)} \quad (3a)$$

$$\left. \begin{aligned} c &\rightarrow c_{0,-\infty} \text{ for } x \rightarrow -\infty \\ c &\rightarrow c_{0,+\infty} \text{ for } x \rightarrow +\infty \end{aligned} \right\} \text{ at } t \geq t_{\text{sharp}} \quad (3b)$$

where $c_{0,-\infty}$ and $c_{0,+\infty}$ are constants.

At these conditions each particular $D(c)$, say $D_{\text{part}}(c)$, gives rise to a particular concentration distribution

$$c(x,t) = c_{\text{part}}(x/\sqrt{t - t_{\text{sharp}}}) \quad (4)$$

Furthermore, each initial distribution given at $t = t_0$ by

$$c(x,t_0) = c_{\text{part}}(x/\sqrt{t_0 - t_{\text{sharp}}}) \quad (3c)$$

will, at $t \geq t_0$, result in the same distribution (4).

Experimentally supersharp (step-function) boundaries cannot be produced, and the creation of an initial distribution exactly equal to the distribution (3c) will be a matter of pure chance. Yet, in the general case that the initial distribution differs from the one described by eq 3c, it often appears (*viz.* in long diffusion cells and in the absence of a volume change on mixing) that $c(x,t)$, as diffusion proceeds, tends to become³ a function of the single independent variable $\zeta = x/\sqrt{t - t_0 + \Delta t}$, where Δt is a constant. Whether this situation exists or is being reached may be found out⁴ by plotting the square of the experimentally determined values of

$$A_{c_1}(t) \equiv \int_{-\infty}^{x_{c_1}} x \frac{\partial c}{\partial x} dx \quad (5a)$$

vs. $t - t_0$. If a straight line appears, extrapolation to $A_{c_1}(t) = 0$ and to $t - t_0 = 0$ produces the values of Δt and of D at $c = c_1$; x_{c_1} denotes the position in the diffusion cell at which $c = c_1$.

Essentially, this procedure means that, also for initial distributions which are not supersharp and even nonideal (*i.e.*, not in agreement with distribution (3c)), one may still indicate a moment t_{sharp} , *viz.* $t_{\text{sharp}} = t_0 - \Delta t$: the distribution $c(x,t)$ gradually approaches an "ideal" one, *i.e.*, one that would issue from a supersharp initial distribution, in this case supersharp at $t = t_0 - \Delta t$. Furthermore, the "ideal" distribution will be a function of the single variable ζ only if its virtual supersharp initial boundary is situated at $x = 0$.

The position of $x = 0$ may, if there is no volume change on mixing (as considered here), be determined⁵ from the condition

$$\int_{-\infty}^0 (c - c_{0,-\infty}) dx = \int_0^{+\infty} (c_{0,+\infty} - c) dx \quad (5b)$$

In finite diffusion cells the liquid column only extends from the cell bottom, at $x = x_{\text{lower}}$, to the meniscus, at $x = x_{\text{upper}}$. Concentration distributions depending on the single variable $x/\sqrt{t - t_0 + \Delta t}$ can then only exist as long as the concentrations at x_{lower} and x_{upper} have not yet changed. The boundaries $-\infty$ and $+\infty$ in the integrals (5) reduce in that case to x_{lower} and x_{upper} .

After this discussion of the Boltzmann method we just mention two other procedures for the determination of D as a function of c .

In the first one,⁶ D is calculated as the ratio of the experimentally found local values of J_{diff} and $-\partial c/\partial x$; it provides values of D at any concentration occurring in the diffusion boundary. Neither cell length nor initial concentration distributions come into play.

In the other one (differential diffusion), the total concentration difference across the diffusion boundary is chosen small enough⁷ for the diffusion coefficient to

(1) L. J. Gosting and H. Fujita, *J. Am. Chem. Soc.*, **79**, 1359 (1957); D. H. Clarke, *J. Chem. Phys.*, **27**, 29 (1957); E. Krücke and H. Ley, *Z. Physik. Chem. (Frankfurt)*, **26**, 187 (1960); J. Crank, "The Mathematics of Diffusion," Clarendon Press, Oxford, 1956, Chapter 9.

(2) (a) L. Boltzmann, *Ann. Physik*, [3], **53**, 959 (1894); (b) W. Jost, *Z. Physik*, **127**, 163 (1959); (c) see also: Y. Nishijima and G. Oster, *J. Chem. Phys.*, **27**, 269 (1957).

(3) For a constant diffusion coefficient this behavior follows from the general solution (see W. Jost, "Diffusion in Solids, Liquids, and Gases," Academic Press, Inc., New York, N. Y., 1952, eq 1.124) of the diffusion equation. For a diffusion coefficient depending on concentration in an arbitrary way, a derivation has not been given.

(4) On introducing the variable ζ , eq 2 transforms into

$$\frac{\partial c}{\partial \ln(t/t_0)} - 1/2\zeta \frac{\partial c}{\partial \zeta} = \frac{\partial}{\partial \zeta} \left(D \frac{\partial c}{\partial \zeta} \right)$$

As c becomes a function of ζ alone, the first term on the left-hand side disappears and integration over ζ gives

$$-1/2 \int_{-\infty}^{\zeta_{c_1}} \zeta \frac{\partial c}{\partial \zeta} d\zeta = -1/2 \frac{1}{\sqrt{t-t_0+\Delta t}} \int_{-\infty}^{x_{c_1}} x \frac{\partial c}{\partial x} dx = \left[D \frac{\partial c}{\partial \zeta} \right]_{\zeta=\zeta_{c_1}} \equiv K_{c_1}$$

in which K_{c_1} depends on c_1 only. This clarifies the above procedure.

(5) W. Jost, "Diffusion in Solids, Liquids, and Gases," Academic Press, Inc., New York, N. Y., 1952, pp 31, 32.

(6) (a) P. F. Mijnlieff in "Ultracentrifugal Analysis in Theory and Experiment," J. W. Williams, Ed., Academic Press, Inc., New York, N. Y., 1963, p 81 ff; (b) P. F. Mijnlieff, *Koninkl. Ned. Akad. Wetenschap., Proc.*, **B65**, 334 (1962).

(7) From diagrams at large concentration intervals a mean diffusion coefficient can be found by an elegant procedure recently proposed by H. Vink (*Nature*, **205**, 73 (1965)).

have effectively the same value everywhere in the boundary. The concentration distributions may then be analyzed by standard methods for concentration-independent diffusion. A series of experiments must be performed to find D as a function of c .

The problems in three-component diffusion are essentially similar to those encountered in two-component diffusion but more complicated. Equation 1 must now be extended to

$$J_{I,\text{diff}} = -D_{I-I} \frac{\partial c_I}{\partial x} - D_{I-II} \frac{\partial c_{II}}{\partial x}$$

$$J_{II,\text{diff}} = -D_{II-I} \frac{\partial c_I}{\partial x} - D_{II-II} \frac{\partial c_{II}}{\partial x}$$
(6)

where, in the general case, all four diffusion coefficients depend on c_I as well as on c_{II} ; I and II indicate two out of the three components, usually those with the lowest concentrations (the solutes). Roman numerals in subscripts refer to electroneutral solutes, whereas arabic ones, to be introduced later, refer to ions.

The continuity equations, again if V_{ref} is zero, become

$$\frac{\partial c_I}{\partial t} = -\frac{\partial}{\partial x} J_{I,\text{diff}}; \quad \frac{\partial c_{II}}{\partial t} = -\frac{\partial}{\partial x} J_{II,\text{diff}}$$
(7)

For diffusion coefficients that do depend on the concentrations, analytical solutions become very difficult, if not impossible.

The determination of the D values is difficult, too. This is apparent from the numerous experiments by Gosting and his co-workers,⁸ who, in the interpretation of the diffusion diagrams, had to start assuming all diffusion coefficients to be constant.

The present paper (section IV) proposes a method for the determination of all four diffusion coefficients, whether or not concentration dependent. Essentially, it is an extension of the Boltzmann method.

Most frequently, three-component diffusion problems are met in galvanic cells, *viz.*, in those containing so-called liquid junctions. This aspect is treated in section III. A closely related problem is the interpretation of Donnan potentials,⁹ for which detailed information on the liquid junctions involved is required.

The principal problem is that of the diffusion, in general a concentration-dependent diffusion, in three-component systems. We therefore determined $c_I(x,t)$ and $c_{II}(x,t)$ for some selected systems with the aid of an analog computer. These calculations are discussed in section II. Some remarks on the entropy production in diffusion are made in section V. The Appendix gives details of the analog computations and specific results for the electrolyte diffusion.

Attention has been paid to three-component diffusion in recent years;^{8,10} only Gose,¹¹ however, took the concentration dependence of the diffusion coefficients into account throughout his treatment.

II. Solution of the Diffusion Equations

We combine eq 6 and 7 into¹²

$$\frac{\partial c_I}{\partial t} = \frac{\partial}{\partial x} \left\{ D_{I-I} \frac{\partial c_I}{\partial x} \right\} + \frac{\partial}{\partial x} \left\{ D_{I-II} \frac{\partial c_{II}}{\partial x} \right\}$$

$$\frac{\partial c_{II}}{\partial t} = \frac{\partial}{\partial x} \left\{ D_{II-I} \frac{\partial c_I}{\partial x} \right\} + \frac{\partial}{\partial x} \left\{ D_{II-II} \frac{\partial c_{II}}{\partial x} \right\}$$
(8)

The degree of accuracy to which these equations can be solved depends on the boundary and initial conditions and on the way the diffusion coefficients depend on c_I and c_{II} .

We have solved them, on an analog computer, for the following initial concentration distributions and boundary conditions

$$\left. \begin{array}{l} c_i = c_{i,-\infty} \quad \text{for } -\infty < x \leq -x_b \\ \text{a smooth} \\ \text{(sigmoid)} \\ \text{symmetric} \\ \text{change of } c_i \end{array} \right\} \text{between } -x_b \text{ and } +x_b \left. \vphantom{\begin{array}{l} c_i = c_{i,-\infty} \\ \text{a smooth} \\ \text{(sigmoid)} \\ \text{symmetric} \\ \text{change of } c_i \end{array}} \right\} \text{at } t = t_0$$

$$c_i = c_{i,+\infty} \quad \text{for } +x_b \leq x < +\infty$$
(9a)

(8) (a) I. J. O'Donnell and L. J. Gosting in "The Structure of Electrolytic Solutions," W. J. Hamer, Ed., John Wiley and Sons, Inc., New York, N. Y., 1959, Chapter 11; (b) H. Fujita and L. J. Gosting, *J. Phys. Chem.*, **64**, 1256 (1960); (c) L. A. Woolf, D. G. Miller, and L. J. Gosting, *J. Am. Chem. Soc.*, **84**, 317 (1962); (d) L. A. Woolf, *J. Phys. Chem.*, **67**, 273 (1963).

(9) J. Th. G. Overbeek, *J. Colloid Sci.*, **8**, 593 (1953).

(10) (a) H. Fujita and L. J. Gosting, *J. Am. Chem. Soc.*, **78**, 1099 (1956); (b) H. Fujita, *J. Phys. Chem.*, **63**, 242 (1959); (c) L. O. Sundelöf and I. Södervi, *Arkiv Kemi*, **21**, No. 15 (1963); (d) H. Schönert, *Z. Physik. Chem. (Frankfurt)*, **42**, 247 (1964).

(11) E. E. Gose, *J. Chem. Phys.*, **39**, 735 (1963).

(12) The compactness of describing three-component diffusion with the aid of only two diffusional mass flows, as in eq 6, is arrived at (see S. R. de Groot and P. Mazur, "Non-equilibrium Thermodynamics," North-Holland Publishing Co., Amsterdam, 1962, pp 239, 240) by counting them with respect to some reference velocity V_{ref} . The latter is constructed as an average from the mass flows of all three components relative to the wall of the cell; the value of V_{ref} will, in general, vary with place and time. Unlike the mass flows in eq 6, however, those in the continuity equations of the form (7) are flows relative to the wall of the diffusion cell. Equations 8 are therefore correct only if V_{ref} is zero at any moment and any place in the cell. Solving diffusion equations as well as analyzing diffusion diagrams becomes extremely complicated (J. G. Kirkwood, *et al.*, *J. Chem. Phys.*, **33**, 1505 (1960); H. Fujita, *J. Am. Chem. Soc.*, **83**, 2862 (1961)) in the case of a nonzero, time- and place-dependent reference velocity.

Fortunately, the mean volume velocity (preferred for this reason as a reference velocity) is often very near, if not equal, to zero. So there is little loss of realism if V_{ref} is put equal to zero, as we will do here, thus obtaining eq 8. General conclusions arrived at later are only applicable therefore to diffusion processes in which a reference velocity that is equal to zero can be indicated.

$$\left. \begin{aligned} c_i &\rightarrow c_{i,-\infty} \text{ for } x \rightarrow -\infty \\ c_i &\rightarrow c_{i,+\infty} \text{ for } x \rightarrow +\infty \end{aligned} \right\} \text{at } t \geq t_0 \quad (9b)$$

where $c_{i,-\infty}$ and $c_{i,+\infty}$ are constants and where $i = \text{I, II}$.

A type of concentration dependence of the D values as may roughly be expected in the systems NaCl(I) + KCl(II) in water and HCl(I) + KCl(II) in water was selected on the basis of reasonable model assumptions discussed earlier.^{6a,13} They lead to the following simple expressions used already by Nernst¹⁴

$$\left. \begin{aligned} D_{\text{I-I}} &= D_1 - \tau_1(D_1 - D_2) \\ D_{\text{I-II}} &= -(M_{\text{I}}/M_{\text{II}})\tau_1(D_3 - D_2) \\ D_{\text{I-II}} &= -(M_{\text{II}}/M_{\text{I}})\tau_3(D_1 - D_2) \\ D_{\text{II-II}} &= D_3 - \tau_3(D_3 - D_2) \end{aligned} \right\} \quad (10)$$

These expressions¹⁵ apply to a thermodynamically ideal solution of two n - n electrolytes with one common ion. The "ionic diffusion coefficients" D_1 , D_2 , and D_3 , and therefore the frictional coefficients f_i (per gram) to which they are related by

$$D_i = RT/f_i M_i \quad (i = 1, 2, 3) \quad (11)$$

(where R is the gas constant) have been supposed not to depend on c_{I} and c_{II} . The discussion^{6a,13} on the validity of eq 11 and the constancy of the mobilities (inversely proportional to the frictional coefficients) is not repeated here. We would rather stress the fact that in general, owing to the dependence of the transference numbers τ_i on c_{I} and c_{II} , none of the four diffusion coefficients is constant or becomes constant at infinite dilution. This can be easily seen by introducing into eq 10 the definition¹³ of the transference number

$$\tau_i \equiv c_i e_i u_i / \sum_{i=1}^3 c_i e_i u_i$$

(e_i is the electrical charge per gram of the ions i , u_i their electrophoretic mobility in $\text{cm}^2/\text{v sec}$) and the relation¹³

$$u_i = e_i/f_i \quad (12)$$

between u_i and f_i . The result is

$$\left. \begin{aligned} D_{\text{I-I}} &= \frac{\alpha c_{\text{I}} + \beta c_{\text{II}}}{\gamma c_{\text{I}} + \beta c_{\text{II}}} D_1 \\ D_{\text{I-II}} &= -\frac{\delta c_{\text{I}}}{\gamma c_{\text{I}} + \beta c_{\text{II}}} (D_3 - D_2) \\ D_{\text{II-I}} &= -\frac{\epsilon c_{\text{II}}}{\gamma c_{\text{I}} + \beta c_{\text{II}}} (D_1 - D_2) \\ D_{\text{II-II}} &= \frac{\eta c_{\text{II}} + \gamma c_{\text{I}}}{\gamma c_{\text{I}} + \beta c_{\text{II}}} D_3 \end{aligned} \right\} \quad (13a)$$

where

$$\left. \begin{aligned} \alpha &\equiv 2D_2(M_2/M_{\text{I}}); \quad \delta \equiv D_1(M_2/M_{\text{II}}) \\ \beta &\equiv (D_3 + D_2)(M_2/M_{\text{II}}); \quad \epsilon \equiv D_3(M_2/M_{\text{I}}) \\ \gamma &\equiv (D_1 + D_2)(M_2/M_{\text{I}}); \quad \eta \equiv 2D_2(M_2/M_{\text{II}}) \end{aligned} \right\} \quad (13b)$$

The coefficients α , etc., are constants for a particular system considered.

Mainly in order to indicate their order of magnitude, the parameter values used have been collected in Tables I and II; D_1 etc., and α etc., are given in units $10^{-5} \text{ cm}^2 \text{ sec}^{-1}$; the values selected for D_1 , D_2 , and D_3 differ only slightly from the true ones derived in the well-known way¹⁶ from limiting equivalent conductivities. As $D_3 = D_2$, in both systems $D_{\text{I-II}} = 0$; furthermore $D_{\text{II-II}} = D_2$.

Equations 10 are based¹⁷ on the following simple

Table I

System	D_1	D_2	D_3	M_2/M_{I}	M_2/M_{II}
NaCl(I) + KCl(II)	1.33	1.98	1.98	0.607	0.476
HCl(I) + KCl(II)	9.29	1.98	1.98	0.973	0.476

picture. The ions are primarily moving at random. If concentration gradients are present, this random motion results in net displacements from higher to

(13) P. F. Mijnlieff and J. Th. G. Overbeek, *Koninkl. Ned. Akad. Wetenschap., Proc.*, **B65**, 221 (1962).

(14) W. Nernst, *Z. Physik. Chem.*, **2**, 613 (1888).

(15) They are easily derived from eq 13 of ref 13, *viz.* by realizing that the quantities $c_{\text{II}}/c_{\text{I}}$ and $c_{\text{I}}/c_{\text{I}}$ are, in a solution of two n - n electrolytes, equal to M_2/M_{II} and to M_2/M_{I} , respectively (M = molecular or ionic weight); they are equivalent to those given by L. J. Gosting, *Advan. Protein Chem.*, **11**, 429 (1956), eq 168-171.

(16) See, *e.g.*, H. S. Harned and B. B. Owen, "The Physical Chemistry of Electrolytic Solutions," Reinhold Publishing Co., 3rd ed, New York, N. Y., 1958, pp 231, 245.

(17) Formally, eq 10 or 13 can also be derived from irreversible thermodynamics, *viz.*, by introducing certain expressions (see ref 6) for the phenomenological coefficients, considering dilute solutions, admitting the model assumptions (11) and (12), and by inserting for $\partial \mu_i / \partial x$ and $\partial \mu_{\text{II}} / \partial x$ (occurring in the phenomenological equations for diffusion) the expressions applying to ideal electrolyte solutions. As mentioned earlier (ref 13), the expressions (10) and (13) are still consistent with the Onsager relation between the cross-phenomenological coefficients.

This fact reduces somewhat the significance of those experimental proofs (ref 8a-c; see also D. G. Miller, *J. Phys. Chem.*, **62**, 767 (1958)) of the Onsager relation that were based on measurements (ref 8a, b) of the four diffusion coefficients in systems like NaCl + KCl in water: even in concentrated solutions the simple physical picture (correct for very dilute solutions) already accounts for the major part of the cross-phenomenological coefficients; the merit of the Onsager relation is its prediction that the "remaining" parts (finding their origin in thermodynamic nonideality and in dependence of mobilities on concentrations, and coming into play at finite concentrations) are equal too; however, the experimental error in the measured values of the cross coefficients is sometimes larger than this "remaining" part. Fortunately, electrolyte solutions were not (ref 8c) the only ones from which the Onsager relations were shown to agree with experimental observations.

Table II

System	α	β	γ	δ	ϵ	η
NaCl(I) + KCl(II)	2.40	1.88	2.01	0.63	1.20	1.88
HCl(I) + KCl(II)	3.85	1.88	10.97	4.42	1.93	1.88

lower concentration regions; it is modified by an internal electric field with such a strength, everywhere in the cell, that there is nowhere a net transport of electrical charge.

Owing to the restrictions of the model underlying eq 10, the applicability of our computer results (see Appendix) on the electrolyte diffusion is limited to dilute solutions. Most of the conclusions, however, arrived at in this paper apply to concentration-dependent three-component diffusion in general.

We now return to the numerical solution of the diffusion equations (8). They have been solved for six initial distributions (indicated by a, b, etc.) of the type (9a); their characteristics are given in Table III. The possibility of gravitational instabilities¹⁸ has not been considered here, the development of the concentration profiles as far as resulting from diffusion alone having our primary interest.

Table III

Initial distribution	$c_{I,-\infty}$	$c_{II,-\infty}$	$c_{I,+\infty}$	$c_{II,+\infty}$
a	$1/50c_0$	0	c_0	0
b	0	$1/50c_0$	0	c_0
c	$1/50c_0$	c_0	c_0	c_0
d	c_0	$1/50c_0$	c_0	c_0
e	$1/50c_0$	c_0	c_0	$1/50c_0$
f	$1/50c_0$	$1/50c_0$	c_0	c_0

We introduced the new variables

$$\xi \equiv x/\sqrt{D'(t - t_{\text{ref}})};$$

$$\vartheta \equiv \ln \left\{ (t - t_{\text{ref}})/(t_0 - t_{\text{ref}}) \right\} \quad (14)$$

where D' is a diffusion coefficient which is conveniently chosen to be the largest ionic diffusion coefficient occurring in the system studied. Accordingly, in the system NaCl + KCl in water we chose $D' = D_3$, and in the system HCl + KCl in water we chose $D' = D_1$. The initial, sigmoid, boundary was taken to extend from $\xi = -2.0$ to $\xi = +2.0$; inspection of eq 9a and 14 then shows that

$$t_0 - t_{\text{ref}} = \frac{x_b^2}{4D'} \quad (15)$$

The meaning of t_{ref} is explained below.

With the new variables, eq 8 transforms into

$$\frac{\partial c_I}{\partial \vartheta} = \frac{1}{2} \xi \frac{\partial c_I}{\partial \xi} + \frac{1}{D'} \left[\frac{\partial}{\partial \xi} \left\{ D_{I-I} \frac{\partial c_I}{\partial \xi} \right\} + \frac{\partial}{\partial \xi} \left\{ D_{I-II} \frac{\partial c_{II}}{\partial \xi} \right\} \right] \quad (16)$$

$$\frac{\partial c_{II}}{\partial \vartheta} = \frac{1}{2} \xi \frac{\partial c_{II}}{\partial \xi} + \frac{1}{D'} \left[\frac{\partial}{\partial \xi} \left\{ D_{II-I} \frac{\partial c_I}{\partial \xi} \right\} + \frac{\partial}{\partial \xi} \left\{ D_{II-II} \frac{\partial c_{II}}{\partial \xi} \right\} \right]$$

The new boundary conditions follow from eq 9, 14, and 15.

After inserting expressions 13 and the data of Tables I and II into eq 16, they were solved on the analog computer; details on the method are given in the Appendix.

The solutions were produced as plots of c_I and c_{II} vs. ϑ for a number of selected ξ values. Figure 1 gives an example of such a plot.

According to these graphs (and to all other curves obtained), after some time c_I and c_{II} at fixed ξ become constant; in other words

$$c_I(\xi, \vartheta) \rightarrow c_I(\xi); \quad c_{II}(\xi, \vartheta) \rightarrow c_{II}(\xi) \quad (17)$$

as ϑ increases.

Functions $c_I(\xi)$ and $c_{II}(\xi)$ will be called "final distributions" in the following discussion.

If the initial distributions, c_I and c_{II} as functions of x at $t = t_0$, had been chosen in accordance with the final distribution, $(c_I)_\xi$ and $(c_{II})_\xi$ would have been constant from the very beginning. This is true for any $(t_0 - t_{\text{ref}}) > 0$, and the smaller $t_0 - t_{\text{ref}}$, the greater the resemblance of such an initial distribution to a super-sharp one. The supersharp distribution (step function) itself conforms with the (and with any) final distribution, for at $t_0 = t_{\text{ref}}$ all finite values of ξ are "compressed" at $x = 0$. The final distributions, therefore, are the solutions of eq 16 for the initial and boundary conditions: (with $i = I, II$)

$$\left. \begin{aligned} c_i &= c_{i,-\infty} \text{ for } x < 0 \\ c_i &= c_{i,+\infty} \text{ for } x > 0 \end{aligned} \right\} \text{ at } t = t_{\text{ref}} \quad (18a)$$

$$\left. \begin{aligned} c_i &\rightarrow c_{i,-\infty} \text{ for } x \rightarrow -\infty \\ c_i &\rightarrow c_{i,+\infty} \text{ for } x \rightarrow +\infty \end{aligned} \right\} \text{ at } t \geq t_{\text{ref}} \quad (18b)$$

and, naturally, for the particular functions $D_{I-I}(c_I, c_{II})$, etc. For the two-component case this was already stated by Boltzmann (see section I). Comparison of eq 18 and 3 shows that t_{ref} used here is identical with t_{sharp} used in section I.

If the distribution at $t = t_0$ differs from the one which would result, at $t = t_0$, from the initial distribution

(18) R. P. Wendt, *J. Phys. Chem.*, **66**, 1740 (1962).

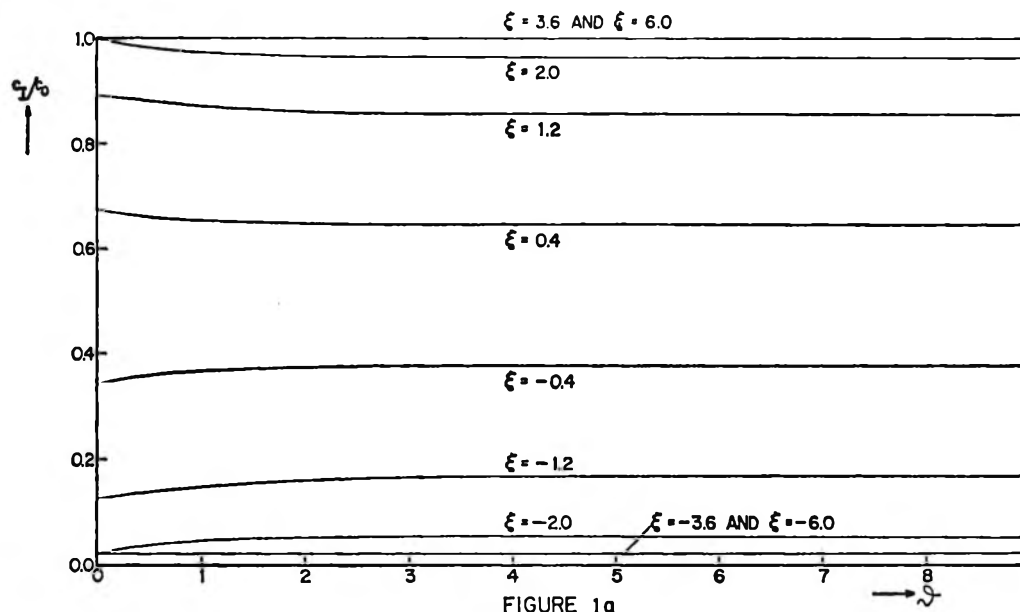


FIGURE 1a

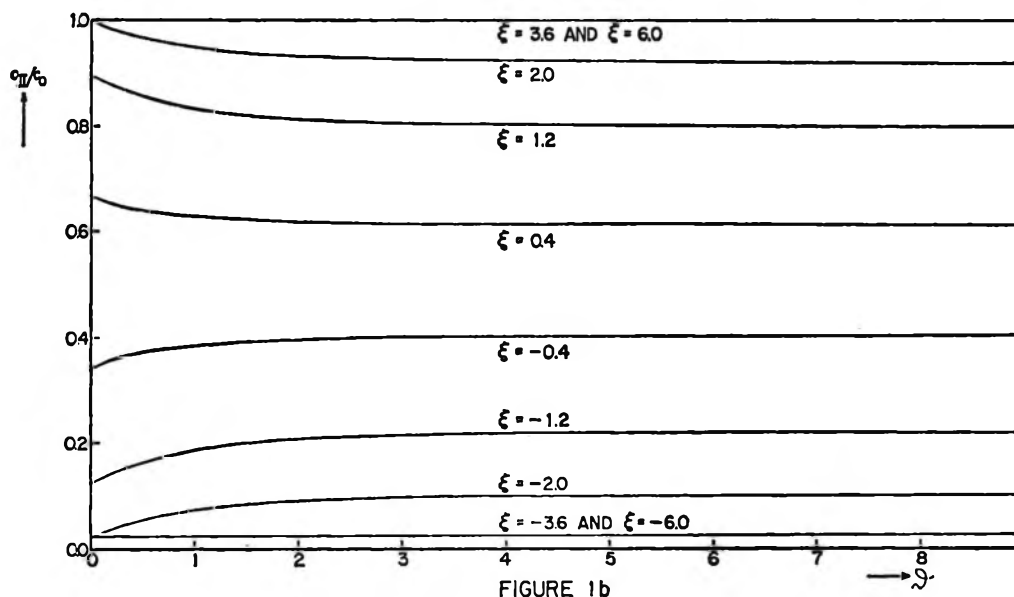


FIGURE 1b

Figure 1. Example of a solution of eq 16 with the analog computer. System: NaCl + KCl in water; initial distribution: f of Table III.

(18a), then according to the result (17), the system under investigation still “relaxes” to a distribution as would have issued from the initial conditions (18a).

The existence of final distributions in three-component systems was already recognized and used by Guggenheim.¹⁹ Probably, it will be difficult to furnish a rigorous mathematical proof²⁰ that the diffusion processes, whatever the initial concentration distributions and whatever the particular way the diffusion coefficients depend on c_I and c_{II} , relax automatically to final distributions solely determined by the values of $c_{I,-\infty}$ and $c_{I,+\infty}$ and by the way D_{I-I} etc.

depend on c_I and c_{II} . From a physical point of view, however, this result is plausible, for at $t = t_0$ the transition region (between $x = -x_b$ and $x = +x_b$) extends, relative to the length of the diffusion cell, over a very small distance only; its detailed structure will lose more and more influence as t increases. From now on we assume therefore that the behavior (17) is displayed in any real diffusion process, provided only that the dif-

(19) E. A. Guggenheim, *J. Am. Chem. Soc.*, **52**, 1315 (1930).

(20) Again (see ref 3), for constant diffusion coefficients, such proof is possible.

fusion cells are long enough to allow the final distributions to have been reached before the concentrations at the ends of the cell have changed perceptibly.

Finally, we ask how fast a given initial concentration distribution "relaxes" to a final one. This may be estimated from the curves of the type drawn in Figure 1. If the final distribution is observed to be attained at $\vartheta \approx \vartheta_{fin}$, then the time interval to which this corresponds can be calculated from

$$(t - t_{ref}) = (t_0 - t_{ref}) \exp(\vartheta_{fin}) = \frac{x_b^2}{4D'} \exp(\vartheta_{fin})$$

In our cases ϑ_{fin} varied between 3 and 6.

An exact calculation of the relaxation process will only be possible for constant diffusion coefficients; the equation already cited (ref 3) could then serve as a starting point. Guided by this equation we estimate that the relaxation may approximately be described by a relaxation time τ equal to

$$\tau = \frac{l^2}{4\pi^2 D} \quad (19)$$

where l is the width of the initial boundary (*i.e.*, $l = 2x_b$) and D is the smallest of the diagonal diffusion coefficients (in our case D_{I-I} or D_{II-II}).

In the present section we have confined ourselves to the more general aspects of concentration-dependent three-component diffusion. Some computer results for the specific cases of mixed electrolyte diffusion have been summarized in the Appendix.

III. Consequences for Galvanic Cells with Liquid Junctions

For a cell shown schematically in Figure 2, the electromotive force (emf) reads²¹

$$\text{emf} \equiv V_b - V_a = -\frac{1}{F} \int_{\text{left}}^{\text{right}} (\tau_1 d\mu_I + \tau_3 d\mu_{II}) \quad (20)$$

where subscripts I and II refer to electrolytes I and II, 1 and 3 indicating the noncommon ions (H^+ and Na^+) in I and II, respectively.

The chemical potentials, μ_I and μ_{II} , as well as τ_1 and τ_3 are functions of both c_I and c_{II} .

However, the knowledge of these four functions does not suffice to calculate the emf from eq 20. An additional piece of information, *viz.*, the whole set of corresponding values of c_I and c_{II} all across the diffuse boundary between solutions a and b, is required. This is seen by writing eq 20 as

$$\text{emf} = -\frac{1}{F} \int_{\text{left}}^{\text{right}} \left[\tau_1 \frac{\partial \mu_I}{\partial c_I} + \tau_3 \frac{\partial \mu_{II}}{\partial c_I} + \left\{ \tau_1 \frac{\partial \mu_I}{\partial c_{II}} + \tau_3 \frac{\partial \mu_{II}}{\partial c_{II}} \right\} \times \left\{ \left(\frac{\partial c_{II}}{\partial x} \right) / \left(\frac{\partial c_I}{\partial x} \right) \right\} \right] dc_I \quad (21)$$

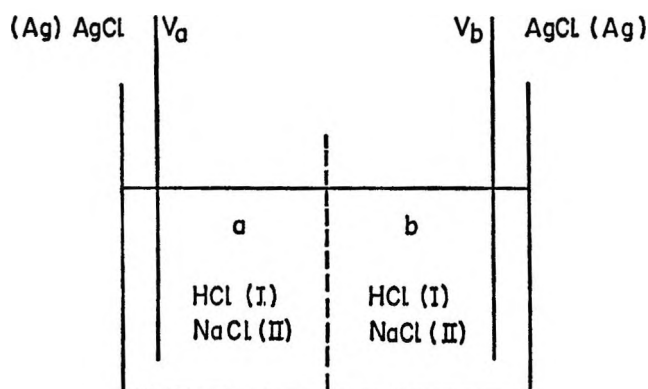


Figure 2. Scheme of a galvanic cell with a liquid junction. The dashed line indicates the position of the diffuse boundary (liquid junction) between the electrolyte solutions. The integration in eq 20 extends over the liquid junction from left to right.

The changes, caused by the diffusion, in the quantity $\{[\partial c_{II}/\partial x]_i / [\partial c_I/\partial x]_i\}$ with time give rise to a variation of the emf, a phenomenon frequently observed²² in experiments.²³

In the preceding section, however, we found—in agreement with Guggenheim's statement¹⁹ made long ago—that at constant ξ values c_I and c_{II} tend to become constant. This implies that then the integrand in the integral (21) may be treated as a function of c_I (or of c_{II}) only, the value of the integral thus becoming time-independent. This value can be predicted provided one knows: (a) the structure of the liquid junction, *i.e.*, the connection between c_I and c_{II} along the whole boundary; (b) the values of $\partial \mu_I/\partial c_I$, $\partial \mu_{II}/\partial c_{II}$, etc., and those of τ_1 and τ_3 at these particular combinations of c_I and c_{II} values.

As to (b), the precise values can only be provided by experiments; if, however, the values of one or more of the quantities considered are taken from a model theory, such a theory may be checked by comparing emf-values thus obtained with measured ones.

(21) P. B. Taylor, *J. Phys. Chem.*, **31**, 1478 (1927); see also ref 16, p 435 ff.

(22) See D. A. Mac-Innes, "The Principles of Electrochemistry," Reinhold Publishing Corp., New York, N. Y., 1939, p 229.

(23) These facts may disturb a comparison between predicted and measured emf values. For practical purposes, the time dependence of the emf is eliminated by continuously renewing ("flowing junction") the boundary between the two electrolyte solutions; the structure of the boundary is then assumed to be as calculated by M. Planck (*Ann. Physik*, [3], **39**, 161 (1890); [3], **40**, 561 (1890)), or, more frequently, as approximated by P. Henderson (*Z. Physik. Chem.*, **59**, 118 (1907); **63**, 325 (1908)). Although the agreement between prediction and experiment is often fairly good, the approximations used certainly become invalid for junctions between concentrated electrolyte solutions. Recently, the structure of this type of junction was calculated by Gose (ref 11). See also A. Ekman, *et al.*, *Nature*, **200**, 1071 (1963)).

As to (a), the safest way to obtain this information—certainly if the purpose is to check a model theory as referred to above—is from a diffusion experiment. This should be an experiment at boundary conditions (c_I and c_{II} at x_{lower} and x_{upper}) similar to those of the particular liquid junction investigated, warranting the final distributions to be identical. In the absence of such diffusion experiments the structure of the diffusion boundary must be calculated, for example, as described in section II, but in that case model assumptions cannot be avoided.

We agree with Guggenheim¹⁹ that exact information from emf data of cells with liquid junctions should be derived from measurements in the final situation (reached automatically) where the emf has become constant; only then is it certain that the structure of the liquid junction, to be formed in long capillaries, is identical with that in a diffusion experiment at similar boundary conditions. This is a useful application of diffusion measurements in three-component systems.

IV. Consequences for Three-Component Diffusion Experiments

In this section a method for the determination of the values of all four diffusion coefficients at known values of c_I and c_{II} is proposed.

We consider experiments in which the final distributions discussed in section II have been reached. In that case the relation between c_I and c_{II} along the boundary no longer changes with time. For example, at an initial distribution resembling type e of Table III, corresponding values of c_I and c_{II} lie on curve A of Figure 3, whereas at an initial distribution resembling type f of Table III they lie on curve B.

We now suppose to have the disposal of c_I and c_{II} as a function²⁴ of x for two diffusion experiments (A and B) of the type mentioned above (ways to find c_I and c_{II} separately are discussed below). These data may be converted²⁵ into curves of c_I and c_{II} vs. $x/\sqrt{t} \equiv \xi'$. Furthermore, the same data enable us to construct two curves (A and B) like those shown in Figure 3.

The point of intersection of curves A and B indicates the only combination of c_I and c_{II} values that occurs in both experiments. In addition, it provides us with the ξ' values, to be called ξ'_A ξ'_B , at which this combination is situated in experiments A and B, respectively.

By virtue of the property (17), eq 16 reduces to

$$\begin{aligned}
 -1/2 \xi' \frac{dc_I}{d\xi'} &= \frac{d}{d\xi'} \left(D_{I-I} \frac{dc_I}{d\xi'} \right) + \frac{d}{d\xi'} \left(D_{I-II} \frac{dc_{II}}{d\xi'} \right) \\
 -1/2 \xi' \frac{dc_{II}}{d\xi'} &= \frac{d}{d\xi'} \left(D_{II-I} \frac{dc_I}{d\xi'} \right) + \frac{d}{d\xi'} \left(D_{II-II} \frac{dc_{II}}{d\xi'} \right)
 \end{aligned}$$

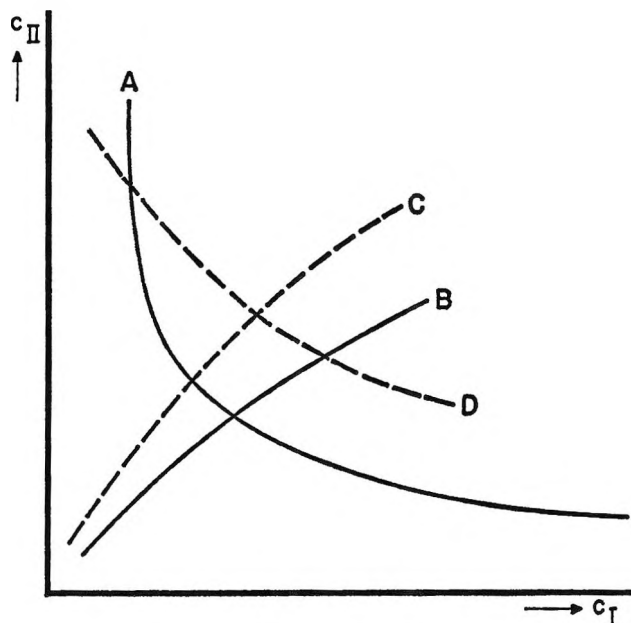


Figure 3. Combinations of c_I and c_{II} values as expected qualitatively in various diffusion experiments.

The left-hand sides of these equations are known from the graphs of c_I and c_{II} vs. ξ' , and may be integrated numerically. Integration between $\xi' = -\infty$ and $\xi' = \xi'_A$ in experiment A and between $\xi' = -\infty$ and $\xi' = \xi'_B$ in experiment B leads to

$$\left. \begin{aligned}
 -1/2 \int_{-\infty}^{\xi'_A} \xi' \frac{dc_I}{d\xi'} d\xi' &= \left\{ D_{I-I} \frac{dc_I}{d\xi'} + D_{I-II} \frac{dc_{II}}{d\xi'} \right\}_{\text{at } \xi'_A} \\
 -1/2 \int_{-\infty}^{\xi'_A} \xi' \frac{dc_{II}}{d\xi'} d\xi' &= \left\{ D_{II-I} \frac{dc_I}{d\xi'} + D_{II-II} \frac{dc_{II}}{d\xi'} \right\}_{\text{at } \xi'_A}
 \end{aligned} \right\} \quad (22a)$$

$$\left. \begin{aligned}
 -1/2 \int_{-\infty}^{\xi'_B} \xi' \frac{dc_I}{d\xi'} d\xi' &= \left\{ D_{I-I} \frac{dc_I}{d\xi'} + D_{I-II} \frac{dc_{II}}{d\xi'} \right\}_{\text{at } \xi'_B} \\
 -1/2 \int_{-\infty}^{\xi'_B} \xi' \frac{dc_{II}}{d\xi'} d\xi' &= \left\{ D_{II-I} \frac{dc_I}{d\xi'} + D_{II-II} \frac{dc_{II}}{d\xi'} \right\}_{\text{at } \xi'_B}
 \end{aligned} \right\} \quad (22b)$$

(24) The position of $x = 0$ may be determined with the aid of eq 5b' to be applied to $c_I(x)$ or to $c_{II}(x)$. We consider the instance that the mean volume velocity is the reference velocity that is equal to zero (cf. ref 12). In that case the positions of $x = 0$, as derived from $c_I(x)$ and $c_{II}(x)$, will not move. If they do not coincide, their difference, Δx , leads to an uncertainty $\Delta x/\sqrt{t}$ in $\xi' \equiv x/\sqrt{t}$. Only after this uncertainty, by the increase of time, has become negligible, the check on the attainment of final distributions may lead to a positive answer. The way in which initial boundaries are formed in all usual experiments will keep the Δx values negligibly small.

(25) In the final distribution state, curves pertaining to different times coincide provided that t is counted with respect to the virtual time, t_{sharp} , at which the concentration distributions (c_I and c_{II} as a function of x) would have been infinitely sharp. We attribute to t_{sharp} its proper value in the same way as in the case of a two-component system, explained in section I.

Table IV

System (soln in water at 18°)	$\lambda_p, \text{Å}$	$\lambda_q, \text{Å}$	$R_{I,p}$	$R_{I,q}$	$R_{II,p}$	$R_{II,q}$
LiCNS(I) + LiCl(II)	2749	3612	0.3846	0.3020	0.2833	0.2517
LiBr(I) + RbBr(II)	2502	4601	0.4307	0.2800	0.1435	0.0969
NaCl(I) + NaI(II)	2749	4601	0.2310	0.1890	0.2549	0.1600

where D_{I-I} in eq 22a is equal to D_{I-I} in eq 22b etc., because $\{c_I\}_{\text{at } \xi'_A} = \{c_I\}_{\text{at } \xi'_B}$ and $\{c_{II}\}_{\text{at } \xi'_A} = \{c_{II}\}_{\text{at } \xi'_B}$. Equations 22 may be solved, thus providing us with the values of the four diffusion coefficients at $c_I = \{c_I\}_{\text{at } \xi'_A} = \{c_I\}_{\text{at } \xi'_B}$ and $c_{II} = \{c_{II}\}_{\text{at } \xi'_A} = \{c_{II}\}_{\text{at } \xi'_B}$.

Additional experiments, C, D, etc., giving rise to curves C, D, etc. (see Figure 3), produce values at other combinations of c_I and c_{II} .

The procedure suggested is an extension of Boltzmann's method² to three-component diffusion. We see no way, however, of extending the method correspondingly to systems of four components, for there is no general reason why, even at an infinite number of diffusion experiments, a single combination of the concentrations of the *three* solutes should occur twice.

A practical difficulty is to find c_I and c_{II} separately.

One way would be by chemical analysis of the contents of sections into which the diffusion cell is broken up after sufficient time of diffusion; this method goes back to Schuhmeister.²⁶ It does not take advantage of the fact (which increases the accuracy) that measurements at different times reduce to identical c - ξ' curves.

The most usual method to follow diffusion is by Philpot-Svensson schlieren or Rayleigh interference optics. These two methods give, in principle, the same information, so we confine ourselves to the first one. Here the refractive index gradient, dn/dx , is recorded as a function of x . In a three-component system dn/dx contains the contributions of the concentration gradients of both I and II

$$\frac{dn}{dx} = \frac{\partial n}{\partial c_I} \frac{dc_I}{dx} + \frac{\partial n}{\partial c_{II}} \frac{dc_{II}}{dx} \equiv R_I \frac{dc_I}{dx} + R_{II} \frac{dc_{II}}{dx}$$

We will only consider cases where the refractive increments R_I and R_{II} are concentration independent.

Though R_I and R_{II} are known (measurable in separate experiments), the measured dn/dx does not give us the separate values of dc_I/dx and dc_{II}/dx . For that purpose we need additional information, which might be provided by a light-absorption measurement in case there is specific absorption by one of the solutes.

Another possibility would be to measure dn/dx for two different wavelengths, λ_p and λ_q , chosen such that

$$\frac{R_{I,p}}{R_{I,q}} \neq \frac{R_{II,p}}{R_{II,q}}$$

For some combinations of electrolytes values²⁷ of R_I and R_{II} (in cubic centimeters per gram) have been collected in Table IV. Only a few systems lend themselves to such an analysis and the experiments will be tedious; often quartz optics will be required and optical distances must be readjusted when switching from one wavelength to another.

V. The Entropy Production in Diffusion

As before, we consider a system in which one-dimensional diffusion takes place in a cylindrical cell, with a cross section of unit area. Pressure and temperature are assumed to be uniform and constant; the constancy of temperature is thought to be effected by appropriate heat exchanges through the walls of the cell.

The difference between the increase, per unit time, of the entropy of the total system and the increase corresponding to heat exchanged with the surroundings will be called the total entropy production, to be indicated by σ_{tot} . From irreversible thermodynamics²⁸ the following expression for σ_{tot} may be derived

$$T\sigma_{\text{tot}} = \sum_{j=1}^{n-1} \int J_{j,\text{diff}} \left\{ \frac{\partial \mu_j}{\partial x} \right\}_t dx$$

The integration extends over the total length of the cell; the summation over all components j , except for the last one, n . The term for component n , for which, in general, the solvent is taken, was eliminated in a way indicated in ref 12.

For three-component systems, the equation for σ_{tot} reduces to

$$T\sigma_{\text{tot}} = \int J_{I,\text{diff}} \frac{\partial \mu_I}{\partial x} dx + \int J_{II,\text{diff}} \frac{\partial \mu_{II}}{\partial x} dx \quad (23)$$

For linear behavior, the diffusional mass flows may be decomposed into

(26) J. Schuhmeister, *Sitzungsber. Wien. Akad.*, **79** (II), 603 (1879).

(27) C. Lubden, *Ann. Physik*, [4], **44**, 977 (1914); A. Heydweiller and O. Grube, *ibid.*, **49**, 653 (1916).

(28) S. R. de Groot and P. Mazur, "Non-equilibrium Thermodynamics," North-Holland Publishing Co., Amsterdam, 1962, p 241.

$$J_{I,diff} = A_{I-I} \frac{\partial \mu_I}{\partial x} + A_{I-II} \frac{\partial \mu_{II}}{\partial x}$$

$$J_{II,diff} = A_{II-I} \frac{\partial \mu_I}{\partial x} + A_{II-II} \frac{\partial \mu_{II}}{\partial x}$$

where the coefficients A_{I-I} etc. are functions of c_I and c_{II} .

For $\partial \mu_I / \partial x$ and $\partial \mu_{II} / \partial x$ one may write

$$\frac{\partial \mu_I}{\partial x} = \frac{\partial \mu_I}{\partial c_I} \frac{\partial c_I}{\partial x} + \frac{\partial \mu_I}{\partial c_{II}} \frac{\partial c_{II}}{\partial x}$$

$$\frac{\partial \mu_{II}}{\partial x} = \frac{\partial \mu_{II}}{\partial c_I} \frac{\partial c_I}{\partial x} + \frac{\partial \mu_{II}}{\partial c_{II}} \frac{\partial c_{II}}{\partial x}$$

where the factors $\partial \mu_I / \partial c_I$ etc. are again functions of c_I and c_{II} .

The integrands in eq 23 are therefore quadratic expressions in the concentration gradients ($\partial c_i / \partial x$), where $i = I, II$, with coefficients depending on c_I and c_{II} only. In the "final-distribution state," c_I and c_{II} depend on $\xi' = x/\sqrt{t}$ only.²⁹ After replacing the variable x by ξ' , eq 23 transforms into

$$T\sigma_{tot} = \frac{1}{\sqrt{t}} \int_{-\infty}^{+\infty} F(\xi') d\xi' = \frac{\text{constant}}{\sqrt{t}} \quad (24)$$

where $F(\xi')$ is a function of ξ' only.

The result (24) seems worth mentioning because it is valid for a three- and even multi-component diffusion process, whatever the particular way the diffusion coefficients depend on the concentrations. It applies to the "final-distribution state." As was stressed before, this is the state approached in a system containing concentration gradients. Whether or not it is ever reached in an actual diffusion experiment depends on the length of the diffusion cell and on the nature of the deviations of the initial distribution, at $t = t_0$, from the distribution that (at the same moment $t = t_0$) corresponds to the final distribution. Once the concentrations at the ends of the diffusion cell start to change, σ_{tot} will decrease faster with time than described by eq 24, e.g., according to

$$\sigma_{tot} \sim t^{-m} \quad (m > 1)$$

for the total increase of the entropy of a finite system remains finite. However, as long as the "final distribution" exists, eq 24 prevails and as such provides an answer, albeit a partial one, to questions³⁰ on the way in which nonequilibrium systems "move" toward equilibrium.

We note that the inverse proportionality with the square root of time is a property of the total entropy production σ_{tot} , obtaining as soon as the concentra-

tions have become functions of ξ' only. In the same stage, the local entropy production σ , the quantity usually considered in irreversible thermodynamics, does not behave in such a simple way.

Finally, the fundamental stage in which relation 24 is obeyed should be well distinguished from that³¹ of "minimum entropy production," characterized by

$$\sigma_{tot} = \text{constant}$$

as realized in constrained, constant concentration gradients.

Addendum

After the manuscript of this paper had been submitted for publication, two papers on related subjects appeared.

Hafeman³² has calculated the time necessary for a liquid-junction potential to be built up. This process is shown to be finished after some nanoseconds, after which the condition of zero electric current, underlying the diffusion expressions (10), may be applied.

Duda and Vrentas³³ have solved the equations for multicomponent concentration-dependent diffusion by rigorous mathematical treatment, admitting volume changes on mixing. Even then the concentrations appear to be functions of x/\sqrt{t} only. The authors confined the treatment to step-function initial concentration distributions; the "relaxation" toward the "final distributions" was therefore not considered.

Appendix

Details of Analog Computation and Some Specific Results. In the analog computation, the continuous independent variable was chosen to be ϑ . Differential quotients with respect to ξ were replaced by difference quotients in the points $\xi_1 = -6.0$, $\xi_2 = -5.2$, $\xi_3 = -4.4$, . . . , $\xi_{15} = 5.2$, $\xi_{16} = 6.0$. Thus, the first of eq 16 transforms, after substitution of (13), into

$$\begin{aligned} \frac{dc_{I,n}}{d\vartheta} = & (c_{I,n+1} - c_{I,n}) \left\{ \frac{\xi_n}{4\Delta} + \frac{\alpha D_1}{\gamma D' \Delta^2} - \right. \\ & \left. \frac{(\alpha - \gamma)\beta D_1}{2\gamma \Delta^2 D'} (\Gamma_{II,n+1} + \Gamma_{II,n}) \right\} + (c_{I,n} - c_{I,n-1}) \times \\ & \left\{ -\frac{\xi_n}{4\Delta} + \frac{\alpha D_1}{\gamma D' \Delta^2} - \frac{(\alpha - \gamma)\beta D_1}{2\gamma \Delta^2 D'} (\Gamma_{II,n} + \Gamma_{II,n-1}) \right\} + \\ & (c_{II,n+1} - c_{II,n}) \frac{\delta(D_2 - D_3)}{2\Delta^2 D'} (\Gamma_{I,n+1} + \Gamma_{I,n}) + \\ & (c_{II,n} - c_{II,n-1}) \frac{\delta(D_2 - D_3)}{2\Delta^2 D'} (\Gamma_{I,n} + \Gamma_{I,n-1}) \end{aligned}$$

(29) For the value to be attributed to t see ref 25.

(30) G. V. Chester, *Rept. Progr. Phys.*, **26**, 411 (1963).

(31) See ref 28, Chapter 5.

for $n = 1, 2, \dots, 16$. In this formula

$$\Gamma_{i,n} = \frac{c_{i,n}}{\gamma c_{I,n} + \beta c_{II,n}}$$

where $i = I, II$; $c_{I,n}$ and $c_{II,n}$ are the values of c_I and c_{II} pertaining to $\xi = \xi_n$; $\Delta = \xi_n - \xi_{n-1} = 0.8$.

The second eq 16 yields a similar result. The quantities $c_{i,0}$ and $c_{i,17}$ which occur in the equations for $n = 1$ and $n = 16$ can be eliminated by means of the boundary conditions

$$c_{i,0} = c_{i,2}; c_{i,17} = c_{i,15} \quad (A1)$$

where $i = I, II$.

For a chosen initial distribution of c_I and c_{II} all the 32 quantities $c_{I,n}/c_0$ and $\beta c_{II,n}/\gamma c_0$ were simultaneously generated as functions of ϑ .

At $\xi_n = \pm 6.0$, c_I and c_{II} were always found to be independent of ϑ . Thus it was justified to restrict the computation to the range $|\xi| \leq 6$ with the aid of the boundary conditions (A1).

According to the above procedure, difference equations instead of differential equations were solved on the computer. The accuracy of these solutions was high; for concentration-independent two-component diffusion the difference equation can also be solved by hand, and the computer values of c/c_0 (at selected ξ values, for $\vartheta >$ about 6) for such a case agreed within 0.001 with those of the solution obtained by hand.

The comparison, for the same simple case, between the solution of the difference equation and the physically sound differential equation was less favorable. This is demonstrated in Table V.

Table V: Solution of the Difference Equation and the Differential Equation for NaCl in Water

ξ	c/c_0 as the solution of		ξ	c/c_0 as the solution of	
	Difference equation	Differential equation (error function)		Difference equation	Differential equation (error function)
-6.0	0.020	0.020	0.4	0.635	0.632
-5.2	0.020	0.020	1.2	0.841	0.832
-4.4	0.020	0.020	2.0	0.955	0.944
-3.6	0.020	0.022	2.8	0.992	0.987
-2.8	0.027	0.033	3.6	0.999	0.998
-2.0	0.063	0.076	4.4	1.000	1.000
-1.2	0.176	0.188	5.2	1.000	1.000
-0.4	0.382	0.388	6.0	1.000	1.000

The discrepancies shown in this table will decrease the closer the ξ values selected are and the larger their number is. If one were interested in solutions nearer

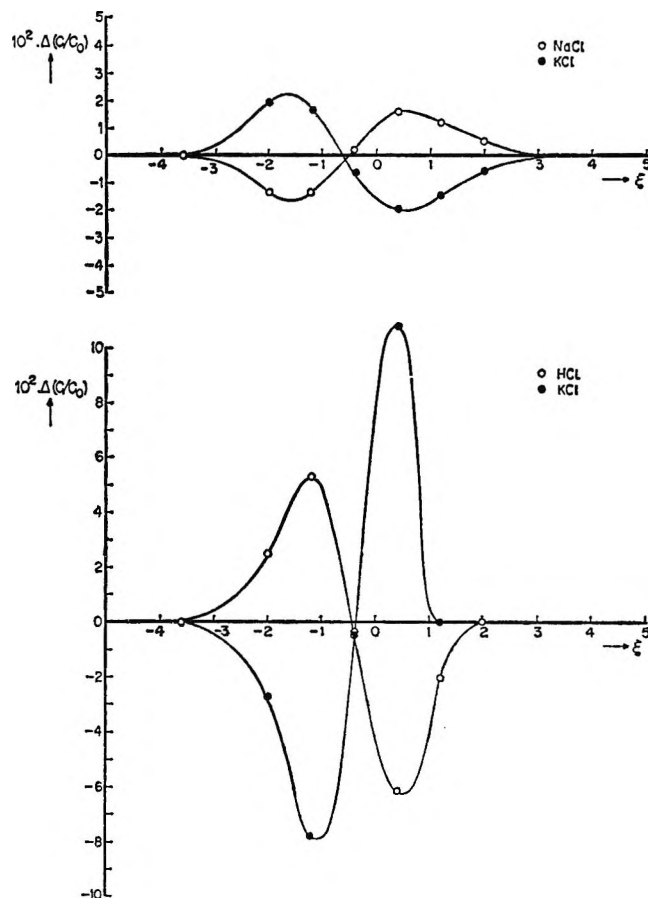


Figure 4. $\Delta(c_I/c_0)$ and $\Delta(c_{II}/c_0)$ (see text) as a function of ξ for initial distribution e of Table III.

to those of the differential equations, the analog computer should be used in a different way or a digital computer could be used. There the limitation with regard to the number and distance of ξ values, inherent in the analog computation outlined above, hardly exists.

Nevertheless, the influences of the concentrations and the concentration gradients of the two electrolytes on each other's diffusion manifest themselves clearly in the solutions of the difference equations. They result in differences, at corresponding ξ values

$$\Delta(c_i/c_0) \equiv (c_i/c_0)_{\text{real}} - (c_i/c_0)_{\text{indep}} \quad (i = I, II)$$

where $(c_i/c_0)_{\text{real}}$ indicates the computer solutions (derived from plots of the type of Figure 1, for $\vartheta >$ about 6) for the realistic case of coupled concentration-dependent diffusion (initial distributions c, d, e, and f of Table III therefore), while $(c_i/c_0)_{\text{indep}}$ denotes the computer solutions for the imaginary case that I and

(32) D. R. Hafeman, *J. Phys. Chem.*, **69**, 4226 (1965).

(33) J. L. Duda and J. S. Vrentas, *ibid.*, **69**, 3305 (1965).

II, though present together, diffuse independently; in the latter process the diffusion coefficients would be

$$D_{I-II} = D_{II-I} = 0; \quad D_{I-I} = \frac{\alpha}{\gamma} D_1; \quad D_{II-II} = \frac{\eta}{\beta} D_3 \quad (\text{A2})$$

The solutions of the difference equations are then either equal to those for initial distributions a and b of Table III, or constant. For one initial distribution the values of $\Delta(c_i/c_0)$ have been plotted in Figure 4.

The general character of the results for the initial distributions c and f is the same. At least as far as

their sign is concerned, the results are as can be expected qualitatively from eq 13 and Tables I and II. In agreement with qualitative and quantitative expectations, $\Delta(c_i/c_0)$ for initial distribution d came out to be zero for all ξ .

It might well be, therefore, that the influences of I and II on each other's diffusion are adequately described by the $\Delta(c_i/c_0)$ as found with the computer. If so, the complete distributions, (c_i/c_0) at chosen ξ values and at $t \rightarrow \infty$, should be found by adding these $\Delta(c_i/c_0)$ values to the exact solutions for independent diffusion (preferably to be derived from error functions, using D_{I-I} and D_{II-II} , as given in eq A2).

Heats of Immersion in Water of Characterized Silicas of Varying

Specific Surface Area

by J. A. G. Taylor¹ and J. A. Hockey

Chemistry Department, Faculty of Technology, University of Manchester, Manchester, England
(Received November 29, 1965)

The heat of immersion (ΔH_I) in water of annealed, fully hydroxylated amorphous silica is 160 ± 3 ergs/cm². This value is independent of the specific surface area in the range 8.5–147.5 m²/g. Higher values were obtained for samples containing microporous defects.

Introduction

Although absolute values for the surface energy of solids cannot be obtained from heat of immersion (ΔH_I) studies, this technique has been widely used in recent years to measure variations between surfaces of differing structure.²⁻⁷ The results obtained have in some cases been interpreted in terms of the crystallinity of the solid. It has been suggested that as the particle size of the solid increases, the surface corresponds more closely to that of the pure crystalline material and so the energy change on formation of the solid-liquid interface increases. This hypothesis has been used to interpret the marked increase in ΔH_I on passing from high to low surface area solids.² In

the present work, values for ΔH_I in water of well-characterized silicas of similar surface properties but varying particle size have been determined.

(1) Chemical Physics Division, Unilever Research Laboratory, Port Sunlight, Cheshire, England.

(2) W. H. Wade, H. D. Cole, D. E. Meyer, and N. Hackerman, *Advances in Chemistry Series*, No. 33, American Chemical Society, Washington, D. C., 1961, p 35.

(3) (a) A. C. Makrides and N. Hackerman, *J. Phys. Chem.*, **63**, 594 (1959); (b) W. H. Wade, R. L. Every, and N. Hackerman, *ibid.*, **64**, 355 (1960).

(4) R. L. Venables, W. H. Wade, and N. Hackerman, *ibid.*, **69**, 317 (1965).

(5) J. W. Whalen, ref 2, p 281.

(6) M. M. Egorov and V. F. Kiselev, *Zh. Fiz. Khim.*, **36**, 158 (1962).

(7) D. Kolar, *Croat. Chem. Acta*, **35**, 123, 289 (1963).

Table I: Characteristics of the Silica Samples

Sample no.	Preparation	Specific surface area, m ² /g	Initial N _{OH}	Micro-porosity, ml/g	ΔH_1 , ergs/cm ²	
					Set A ^a	Set B ^b
1	Heated at 700° for 48 hr	147.5	4.71	0.006	165	170
2	Heated at 940° for 4 hr	99.3	4.61	0.005	158	154
3	Heated to 940° for 16 hr	87.1	4.64	0.004	158	144
4	Heated to 980° for 4 hr	79.0	4.62	...	158	160
5	Heated to 980° for 16 hr	64.7	4.68	...	153	159
6	Heated to 1040° for 16 hr	29.9	4.31	0.005	155	...
7	Heated to 1060° for 4 hr	8.2	163	173
8	Heated to 1040° for 4 hr	35.5	5.50	0.018	186	177
9	Prepared by precipitation	47.1	>8.0	0.110	1330	1320

^a A: heated in air at 115° for 6 hr. ^b B: heated *in vacuo* at 115° for 6 hr.

Experimental Section

1. *Apparatus.* ΔH_1 values were determined at $27.0 \pm 0.05^\circ$ by means of a differential calorimeter mounted in an ethylene glycol-water bath thermostated to $\pm 0.002^\circ$ during the experimental run. Up to three sample bulbs could be mounted in each calorimetric vessel, where the temperature changes were measured to $\pm 5 \times 10^{-5}^\circ$ by means of two 10^5 -ohm thermistors mounted in opposing arms of a Wheatstone bridge circuit. At least two electrical calibrations were performed after each experiment, the agreement between these pairs always being better than 0.3%. All the values for ΔH_1 in Table I are the result of at least two independent determinations. The 3- to 15-g samples were contained in thin-walled Pyrex glass bulbs, 22 mm in diameter and 50 mm long, which had an exothermic heat of bulb breaking of 0.22 ± 0.05 cal. A correction of 0.0075 cal/g of sample, calculated from the heat of vaporization of water, was applied to the experimentally determined heats to allow for the change in the free volume available for evaporation. The bulbs were completely shattered to ensure rapid and complete dispersion of the solid. In an experimental determination, the heat liberated varied from 3 to 15 cal; this corresponded to a $1-5 \times 10^{-2}^\circ$ temperature rise. The accuracy of the data is $\pm 3\%$ for the lowest surface area sample but considerably better in the other cases.

2. *Materials.* Samples 1-8 (see Table I) were all derived from a 2-kg batch of "Aerosil" (from Degussa) which had been rehydrated by heating in liquid water at 95° for 5 hr and then dried at 115° in air.⁸ This material (coded R.A.2) had a specific surface area (ssa) of 158 m²/g and a surface hydroxyl population of 6.25 groups per 100 Å², *i.e.*, $N_{OH} = 6.25$. Sample 1 was prepared by heating a portion of this material at 700° for 48 hr; it was then rehydrated and dried

as described above. There was little change in the surface area ($ssa = 147.5$ m²/g) as a result of this treatment, but the N_{OH} value fell to 4.71. This N_{OH} value corresponds closely with that expected for one hydroxyl group per silicon atom in a β -cristobalite or β -tridymite structure. Samples 2-8 of varying particle size were obtained by heating portions of R.A.2 for differing lengths of time at temperatures between 940 and 1060° (see Table I), then rehydrating and drying, as described above. Sample 9 was a highly microporous precipitated silica which was used, after drying, without further rehydration. Finally the bulbs were loaded, weighed, and glass-blown onto a vacuum line separated by means of a liquid nitrogen trap from any portion of the system having greased joints. One set (A) was heated in air at 115° for 16 hr, followed by evacuation to a pressure of $<10^{-5}$ mm at room temperature for a further 16 hr. A second set (B) was heated *in vacuo* at 115° for 16 hr. The bulbs were sealed off under vacuum. Control experiments demonstrated that such treatments gave reproducible surface properties.

The ssa values (Table I) were determined by application of the BET equation to the adsorption of nitrogen at 77°K. A surface area of 16.2 Å² was assigned to the nitrogen molecule.

Distilled water was passed through a bed of "Biode-minrolit" mixed-bed ion-exchange resin, distilled from dilute alkaline permanganate solution and then finally distilled in a previously steamed Pyrex still.

The microporosities (Table I) were calculated from the difference in apparent densities of samples immersed in water and carbon tetrachloride. The samples were loaded into a previously calibrated dilatometer, then

(8) J. A. G. Taylor, J. A. Hockey, and B. A. Pethica, *Proc. Brit. Ceram. Soc.*, **5**, 133 (1966).

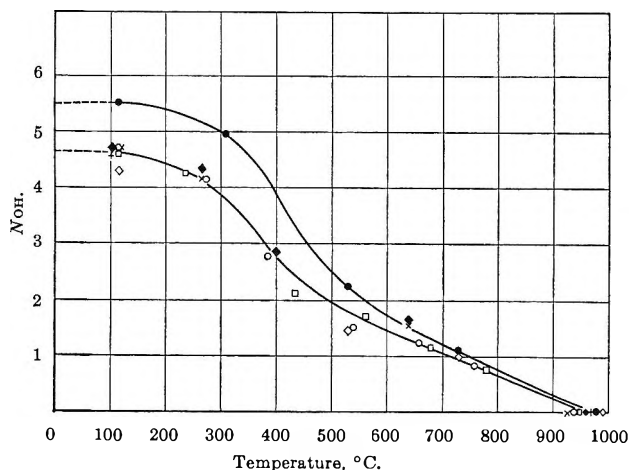


Figure 1. Dehydration curves for the various surface area silicas (sample no. in parentheses): O (1), □ (2), × (3), + (4), ◆ (5), ◇ (6), ● (8).

evacuated as described above for set B; the outgassed liquids were then distilled into the dilatometer under reduced pressure. Control experiments with a flame sphericalized silica ("Fransil," Fransol S.A.) demonstrated that changes in the molar volumes of the liquids were negligible under the experimental conditions used and confirm that this method gives a meaningful indication, though not necessarily an absolute measurement, of the microporosity.⁹⁻¹¹ N_{OH} values were determined from the weight lost on heating samples from 115 to 1100°. ¹²

Results and Discussion

Figure 1 compares the thermal dehydration characteristics of the samples and gives the equilibrium N_{OH} values as a function of ignition temperature under virtually identical atmospheric conditions. Previous workers^{12,13} have suggested that this dehydration process reflects the loss of water by elimination between pairs of adjacent surface hydroxyls; the governing factor in the dehydration is therefore the initial steric arrangement of the surface hydroxyl groups. The close similarity of the curves in Figure 1 therefore supports the assertion that samples 1-7 have virtually identical surface properties and vary only in particle size. de Boer¹² has shown that silicas heated above ca. 700° and then rehydrated have a limiting N_{OH} value of 4.6-4.7. Thus samples 8 and 9, which have higher N_{OH} values, presumably contain a portion of their surface unavailable to nitrogen. This view is confirmed by the presence of microporous defects accessible to molecules of water but not to those of carbon tetrachloride.

Figure 2 shows values of ΔH_I for the silicas 1-7 and

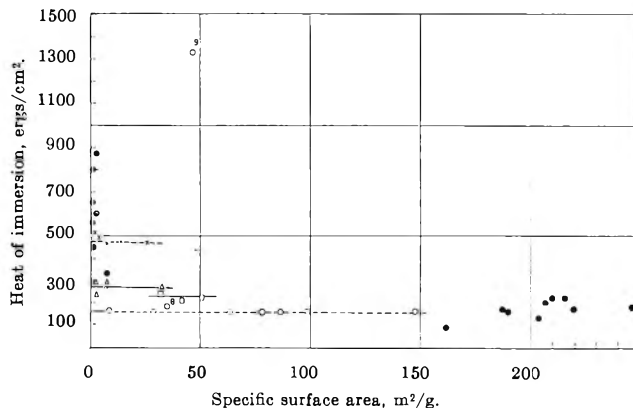


Figure 2. Variation in ΔH_I in water with specific surface area: O, this work, heated at 115°; ×, Wade, *et al.*;² Δ, Paterson and Wheatley,¹⁴ heated at 250°; □, Egrov and Kiselev,⁹ heated at 200°; ●, miscellaneous other studies heated at 115-150°.

the two microporous silicas 8 and 9 together with the data of previous workers^{2,6,14} as a function of ssa.

It has previously been reported that ΔH_I of SiO_2 ,^{3a} TiO_2 ,¹⁵ and Al_2O_3 ¹⁶ in water increases as the particle size increases. The data given in Figure 2 from this study and that of certain other workers^{2,6,14} clearly show that there is no variation in the ΔH_I of SiO_2 in water with variation in particle size as such. Similarly, a recent study by Kolar⁷ shows that for UO_2 ΔH_I in water is independent of particle size over the range 1-9 m²/g. However, there is a wealth of contradictory data, and it is pertinent to consider why this is so. In a previous paper⁸ we summarized the parameters which must be defined to make heat of immersion results meaningful. Unfortunately, many studies have been performed on insufficiently characterized systems, and hence valid comparisons between the results obtained by different workers often cannot be made. The four sets of internally consistent data given in Figure 2 differ from each other. It is possible that these differences reflect changes in the crystallinity of the solid as suggested by Wade and Hackerman.² As large particles are generally associated with a

(9) C. Okkerse, Ph.D. Thesis, Delft, 1961.

(10) S. C. Bright, unpublished data.

(11) D. Dollimore and G. R. Heal, *Trans. Faraday Soc.*, **59**, 2386 (1963).

(12) J. H. de Boer, M. E. A. Hermans, and J. M. Vleeskens, *Koninkl. Ned. Akad. Wetenschap., Proc.*, **B60**, 45 (1957).

(13) J. A. Hockey and B. A. Pethica, *Trans. Faraday Soc.*, **57**, 2247 (1961).

(14) M. S. Paterson and K. Wheatley, *J. Appl. Chem.*, **9**, 231 (1959).

(15) W. H. Wade and N. Hackerman, *J. Phys. Chem.*, **65**, 1681 (1961).

(16) W. H. Wade and N. Hackerman, *ibid.*, **64**, 1196 (1960).

higher degree of crystallinity, ΔH_I per unit surface area would appear, at first sight, to be a function of the particle size, *i.e.*, specific surface area.

Some reported ΔH_I values are significantly higher than any of the values given in the four sets of internally consistent data illustrated in Figure 2, *e.g.*, 892 ergs/cm² obtained by Wade, *et al.*^{3b} It is noteworthy in this context that samples 8 and 9 which have a microporous nature and higher N_{OH} values exhibit higher ΔH_I values. The presence of pores of diameter less than *ca.* 7 Å leads to a spuriously low value for the ssa as measured with N₂ by the normal BET method and hence to too high a value for ΔH_I and N_{OH} . Also, in such small pores where "persorption" can occur, the heat of adsorption of water is greater than for a planar surface. The presence of such micropores may account for the report that N_{OH} values, based on the N₂ surface areas, increase significantly when the surface area decreases.¹⁷ The presence of such structural defects in large particles of quartz has already been suggested,¹⁸ but, owing to the experimental problems involved, unambiguous verification is difficult. When such particles are ground to produce higher surface area samples, it is likely that fracture will occur at these defects; thus ΔH_I , N_{OH} , and, probably, the microporosity will decrease. This hypothesis may explain much of the variability of previously published data, but unfortunately the lack of information on N_{OH} values and possible structural defects does not allow this view to be checked. Hence, the findings of Wade and Hackerman, who in one study¹⁹ report a decrease in ΔH_I with decreasing particle size for a number of fractionated samples derived by grinding a low surface area quartz, but in another study,² following a similar procedure, note no change, are understandable if the first sample contained such defects but the latter did not. The proposal of Egorov and Kiselev⁶ that variations result from the creation of porosity on dry grinding is directly opposed to the experimental ΔH_I data as this would give rise to an *increase* in ΔH_I as the particle size decreases.

The presence of micropores would also account for the findings of Holmes and Secoy,²⁰ who show for four samples of ThO₂ having ssa's of 2–15 m²/g that, with one exception, ΔH_I increases as the ssa increases. The samples were all prepared from the same batch of thorium oxalate by thermal decomposition at

various temperatures. Surface areas calculated from crystallite dimensions (determined by X-ray line broadening) were always higher than the measured BET value. The greatest discrepancy between the two was noted for the sample having the anomalously high ΔH_I value (see Table II). Winfield²¹ has noted that the surface area calculated for ThO₂ from H₂O isotherms was *ca.* twice that calculated from the nitrogen isotherms. Again, the results could be explained by the presence of microporosity in these samples.

Table II: Properties of the ThO₂ Samples^a

	N ₂ surface area, m ² /g	Calcd surface area, m ² /g	Ratio	ΔH_I^b
A	14.7	32.1	2.18	500
B	11.5	27.7	2.40	570
C	5.64	8.92	1.58	530
D	2.20	3.58	1.63	430

^a See ref 20. ^b *In vacuo*, 115°.

Conclusions

(1) There is no variation in the ΔH_I per unit surface area of silica in water with particle size. (2) ΔH_I in water of crystalline modifications of silica is probably higher than that of amorphous silica. (3) Microporous silicas exhibit higher values of ΔH_I and N_{OH} than do nonmicroporous silicas when these values are based on the N₂ surface area determined by the normal BET method.

Acknowledgments. The authors express their thanks to Dr. B. A. Pethica for his interest, encouragement, and useful suggestions and to Mr. S. C. Bright for determining the microporosities. This work was carried out while J. A. G. T. was on secondment from Unilever Research Laboratory, Port Sunlight.

(17) M. M. Egorov, V. F. Kiselev, and K. G. Krasil'nikov, *Zh. Fiz. Khim.*, **35**, 2031 (1961).

(18) S. P. Zhdanov, *Dokl. Akad. Nauk SSSR*, **120**, 103 (1958).

(19) W. H. Wade and N. Hackerman, *Advances in Chemistry Series*, No. 43, American Chemical Society, Washington, D. C., 1964, p 222.

(20) H. F. Holmes and C. H. Secoy, *J. Phys. Chem.*, **69**, 151 (1965).

(21) M. E. Winfield, *Australian J. Sci. Res.*, **A3**, 290 (1950).

The Promotion of a Nickel Catalyst by Electronic Interaction with Germanium Supports

by Raymond F. Baddour and Max C. Deibert

*Department of Chemical Engineering, Massachusetts Institute of Technology, Cambridge, Massachusetts
(Received December 7, 1965)*

The activity of nickel deposited on carefully prepared germanium supports for the decomposition of formic acid was studied as a function of the electronic properties of the germanium. It was concluded that electronic interaction between the germanium supports and the nickel has a strong promoting effect, increasing the catalytic activity by a factor of 1.33–3 for as few as one electron transferred per 10,000 nickel atoms in the catalyst layer.

I. Introduction

The properties of supported catalysts are highly dependent on the properties of the supporting material, especially those properties which influence the surface area, and accessibility of the active catalyst. It has been demonstrated that the specific activity of the exposed surface of supported metal catalysts is also dependent on the chemical nature of the support.^{1,2} The source of this dependence may be indicated by the results of measurements of the infrared spectra of species chemisorbed on supported metals.^{3,4} These investigations revealed that the properties of chemisorption bonds are influenced by type of material used as the support for the metals. This influence of support on chemisorption bonds, if extended to the properties of chemisorbed intermediates in a catalytic reaction mechanism, would be expected to affect the activity of a supported catalyst.

The mechanism by which a support can influence the properties of chemisorption bonds may be by altering the electronegativity of the metal through the electronic interaction at the metal-support interface. If the metallic deposit on the support surface is sufficiently thin, or if the ratio of the support-metal interfacial area to the volume of the metal is sufficiently high, any charge transfer at the support interface may alter the concentration and energy of the electrons on the active catalyst surface. Since the strength of a chemisorption bond should depend on the difference in electronegativity of the chemisorbed species and the solid

surface, the alteration of the electronic, and therefore the chemical, nature of the catalyst surface may have been the source of the effects noted earlier.¹⁻⁴

In addition to the influence of support-catalyst interphase electronic interaction on the properties of supported catalyst, the support may alter the rate or course of a catalytic reaction in other ways.⁵ These influences may result from the contribution of impurities to the catalyst from the support, through the modification of the particle size and crystal orientation of the supported catalyst, or through contribution of catalytic properties of the support surface itself to alter the course of a reaction. In this latter case, interphase electronic effects may exert an important influence if interphase surface diffusion is a step in the catalytic mechanism, as has been indicated for certain reactions in recent studies.⁶ The interphase potential between the catalyst and support could influence the rate of this diffusion.

The promoting effect of interphase electronic interaction has been investigated previously⁷⁻⁹ using nickel

(1) E. B. Maxted and S. I. Ali, *J. Chem. Soc.*, 4137 (1961).

(2) D. J. C. Yates, W. F. Taylor, and J. H. Sinfelt, *J. Am. Chem. Soc.*, **86**, 2996 (1964).

(3) R. P. Eischens and W. A. Pliskin, *Advan. Catalysis*, **10**, 1 (1958).

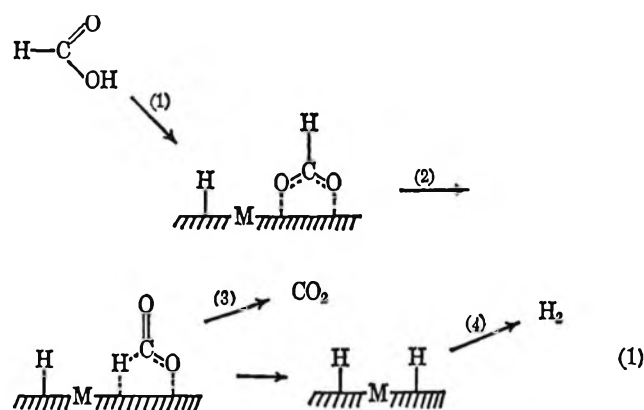
(4) C. E. O'Neill and D. J. C. Yates, *J. Phys. Chem.*, **65**, 901 (1961).

(5) R. P. Eischens, "Surface Chemistry of Metals and Semiconductors," H. C. Gatos, Ed., John Wiley and Sons, Inc., New York, N. Y., 1959, p 421.

(6) P. J. Lucchesi, J. L. Carter, and J. H. Sinfelt, *J. Am. Chem. Soc.*, **86**, 1494 (1964).

catalysts supported on variously doped refractory oxide supports (Al_2O_3 , NiO , Cr_2O_3 , and TiO). All of these studies revealed an increase in the activation energy for formic acid decomposition on the nickel catalysts as the electron concentration in the supports was increased.

Previous evidence indicates that a possible rate-limiting step of the zero-order decomposition of formic acid on nickel involves replacing an oxygen-catalyst bond with a hydrogen-catalyst bond in an adsorbed formate group.¹⁰



In the rotation of the adsorbed formate group (step 2), electronic charge will be transferred from the formate group to the catalyst surface since the electronegative oxygen is replaced by a hydrogen atom adjacent to the surface.

Increasing the electron concentration in the refractory oxide supports may, through the interphase charge transfer, have increased the electron concentration in the supported nickel. These added electrons could have made the transfer of charge from the decomposing formate groups more difficult, thus increasing the activation energy and decreasing the reaction rate. The specific activity of the supported nickel catalysts was not reported,⁷⁻⁹ so there is no assurance that the activity decreased with increasing activation energy. The consistent increase in the activation energy with the electron concentration in the supports is evidence, however, that the interphase electronic interaction does influence the catalytic properties of nickel for formic acid decomposition.

A quantitative estimate of the magnitude of the electronic interaction between these supports and the nickel catalysts cannot be made since the refractory oxides are poorly characterized semiconductors whose surface properties are not well understood.

The purpose of this investigation was to demonstrate quantitatively the promoting effect of support-catalyst electronic interaction. A series of supported

catalysts were prepared using materials and methods designed to yield predictable variations in the magnitude of the electronic interaction between the catalyst and its support. The catalysts consisted of nickel deposited on various types of powdered germanium supports. The germanium supports were prepared from single-crystal germanium samples containing differing quantities and types of impurities. Variations in the impurities produced measured variation in the electronic properties of the germanium and predictable changes in the magnitude of electronic interaction at the germanium-nickel interface in the catalysts. The influence of these changes in interphase electronic interaction on the catalytic properties of the nickel was detected by measuring and comparing the activity of the catalysts for formic acid dehydrogenation.

II. Theory

If the electronic properties of a semiconductor are well characterized and its surface properties are closely controlled, the magnitude of the equilibrium interfacial electronic interaction between the semiconductor and a metal whose work function is known can be predicted from the Schottky theory of metal-semiconductor contact.¹¹⁻¹³ Although this theory is currently under attack, it is apparently the best available at present for the estimation of these effects.

The magnitude of the equilibrium potential difference (Volta potential) can be varied by an amount equal to the maximum variation in the Fermi energy of the semiconductor, which is approximately equal to the width of the forbidden energy gap between its valence and conduction bands. It has been demonstrated that the measured potential difference at carefully prepared contacts between silicon and various metals can be predicted with fair accuracy by this method.¹⁴ The germanium-metal contact should also be amenable to analysis by the Schottky theory.

The potential difference (V_D) which is established between a metal and a semiconductor in contact at thermal equilibrium is given by¹³ relationship 2

(7) G.-M. Schwab, J. Block, and D. Schultze, *Angew. Chem.*, **71**, 101 (1959).

(8) G.-M. Schwab, *ibid.*, **73**, 399 (1961).

(9) Z. G. Szabó and F. Solymosi, *Actes Congr. Intern. Catalyse*, **2°**, Paris, 1960, **2**, 1627 (1961).

(10) P. Mars, J. J. F. Scholten, and P. Zwietering, *Advan. Catalysis*, **14**, 35 (1963).

(11) W. Schottky, *Z. Physik*, **113**, 367 (1939).

(12) N. F. Mott, *Proc. Roy. Soc. (London)*, **A171**, 25, 281 (1939).

(13) E. Spence, "Electronic Semiconductors," McGraw-Hill Book Co., Inc., New York, N. Y., 1958.

(14) R. J. Archer and M. M. Atalla, *Ann. N. Y. Acad. Sci.*, **101**, 697 (1963).

$$V_D = -kT/e \ln \left(\frac{n_s}{n_B} \right) \quad (2)$$

where n_s and n_B are the concentration of conduction electrons (electrons/cm³) in the bulk of the semiconductor and immediately adjacent to the metal interface, respectively. The boundary electron concentration, n_B , is a constant independent of n_s for a given metal-semiconductor pair. It depends on the work function of the metal, ψ_m , the electron affinity of the semiconductor, E_c , which is the electron energy at the bottom of its conduction band, and the magnitude of any interfacial potential barrier resulting from impurities and lattice interruptions at the interface, ψ_B , according to the equation

$$n_B = N_c \exp \left(-\frac{\psi_m - E_c - \psi_B}{kT} \right) \quad (2a)$$

where

$$N_c = 2.5 \times 10^{19} \left(\frac{m_{eff}}{m} \right)^{3/2} \left(\frac{T}{300^\circ \text{K}} \right)^{3/2} / \text{cm}^3 \quad (2b)$$

The quantity (m_{eff}/m) which is of the order of magnitude of unity, is the ratio of the effective mass of an electron at the bottom of the conduction band of the semiconductor to the mass of a free electron.

The work function of nickel has been measured to be 4.96 eV.¹⁵ The electron affinity of germanium is 4.49 eV, as derived from the work function ψ_{Si} of intrinsic germanium, 4.78 eV,¹⁶ and the width of its forbidden energy gap ($E_c - E_v$) of 0.582 eV at 240° (the reference temperature of this study) by the equation

$$E_c = \psi_{Si} - 1/2(E_c - E_v) \quad (2c)$$

Substituting these values into eq 2a yields a value of 1.41×10^{15} for n_B at the germanium-nickel interface at 240°.

The potential difference between nickel and germanium at 240° (calculated from eq 2) is plotted in Figure 1 as a function of the conduction electron concentration in the germanium. Also shown are the interphase potential differences predicted when an impurity potential barrier of ± 0.10 v is present. The calculated potential difference between germanium and nickel changes by about 0.1 v when the conduction electron concentration is changed by a factor of 10.

The magnitude of the charge transfer between nickel and germanium is given by¹⁷

$$\sigma/e = \frac{\epsilon\epsilon_0}{2\pi e} (n_s)^{1/2} (-V_D)^{1/2} \text{ electrons/cm}^2 \quad (3)$$

when $n_s > 10n_B$, and

$$\sigma/e = -\frac{\epsilon\epsilon_0}{2\pi e} (n_p)^{1/2} (V_D)^{1/2} \text{ electrons/cm}^2 \quad (4)$$

when $n_s < n_B/10$.

These equations are plotted in Figure 2 as a function of the conduction electron concentration. Also shown in Figure 2 is the interphase electronic interchange predicted when an impurity potential of ± 0.10 v is present. Increasing the conduction electron concentration by a factor of 10 increases the interphase charge transfer by a factor of about 4. The charge transfer for very heavily doped germanium, $n_s = 10^{20}/\text{cm}^3$ for n-type or $10^{12}/\text{cm}^3$ for p-type, is about 10^{13}

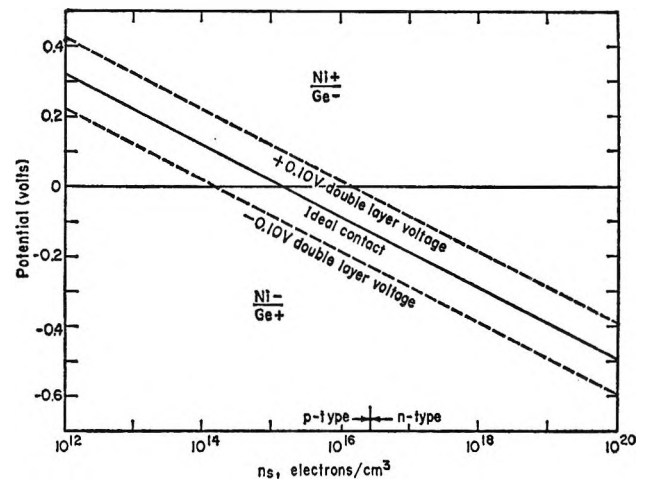


Figure 1. Volta potential difference at a germanium-nickel interface at 240°.

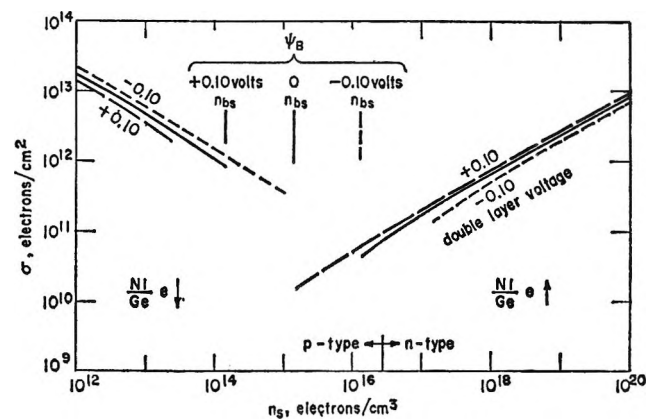


Figure 2. Charge transfer at a germanium-nickel interface at 240°.

(15) A. J. Decker, "Solid State Physics," Prentice-Hall, Inc., Englewood Cliffs, N. J., 1957, p 223.

(16) H. E. Farnsworth and J. Dillon, *J. Appl. Phys.*, **28**, 174 (1957).

(17) H. K. Henish, "Rectifying Semi-conductor Contacts," Oxford University Press, London, 1957, pp 177-182.

electrons/cm², or about 1 electron per 1000 Å². The effect of an interfacial potential barrier on the charge transfer is small.

The conduction electron concentration in germanium can be varied between about 10¹²/cm³ and 10²⁰/cm³ at 240° with variations of the type and concentration of impurities dissolved in the germanium. The maximum concentration of these impurities is about 0.01%. There is, thus, little variation in the chemical nature of the germanium while the electronic properties of the germanium-supported nickel catalysts vary over wide limits. The concentration of lattice defects in germanium crystals generally increases with increases in the concentration of dissolved impurities. This may result in an increase in the magnitude of the double-layer voltage, ψ_B , at the germanium-nickel interface at high impurity contents, but should not substantially affect the magnitude of interphase charge transfer, as shown in Figure 2. Thus, any regular variation in the catalytic properties of a series of catalysts prepared from these materials would most probably result from variations in their electronic properties.

The possibility that nickel from the catalyst layer or hydrogen from the catalytic reaction might diffuse into the germanium supports and alter their electronic properties is unlikely because of the extremely low solubility of these materials in germanium under the conditions to which the catalysts were exposed. The solubility of nickel in germanium is given by¹⁸

$$S = 1.9 \times 10^{23} \exp(-39,500/RT) \text{ atom/cm}^3$$

This equation was calculated from solubility data obtained between 700 and 920°, where the solubility is on the order of 10¹⁴ to 10¹⁵ nickel atoms/cm³. Extrapolation of this solubility equation to 300°, the maximum temperature encountered by any of the catalysts, yields a maximum solubility of nickel in these supports of less than 10⁹ atoms/cm³. This is well below the concentration of about 10¹³ atoms/cm³ at which it is felt that dissolved nickel would significantly influence the electrical properties of the catalysts. The solubility of hydrogen in germanium is given by¹⁹

$$S = 1.60 \times 10^{24} \exp(-52,800/RT) \text{ atoms/cm}^3$$

This equation was developed from solubility data taken between 800 and 910°. Extrapolation of this equation to 300° yields a value below 10⁵ hydrogen atoms/cm³, again well below an electronically significant level.

The solution of germanium in the nickel might influence its catalytic properties. The solubility of germanium in nickel is probably quite low at tempera-

tures below 300°, however, and should be identical for all the catalysts studied.

It has recently been demonstrated in this laboratory that the surface of vacuum-crushed germanium is oxidized to some extent by oxygen-free ethanol vapors.²⁰ The reaction products, in addition to germanium oxide, are hydrogen and ethylene. It is most probable that any uncovered germanium surfaces in the catalysts prepared for this study were oxidized by the formic acid vapor in the catalytic reactor. This surface oxide should not extend to the germanium-nickel interface and should influence the interphase electronic interaction only near the edges of nickel deposits on the germanium surface. The catalytic reaction was conducted at temperatures above 200° since under those conditions nickel surfaces are not oxidized by formic acid vapor.²¹

III. Experimental Section

A diagram of the catalyst preparation equipment is shown in Figure 3. A major problem of this research was the preparation of the germanium-supported nickel catalysts by a procedure which potentially yields clean and reproducible electrical contact between the two materials. Any impurity on the germanium surface, such as the oxide film which readily forms, would effectively insulate the nickel from the germanium. Uncontaminated germanium surfaces were created by crushing germanium chips into a fine powder under ultrahigh vacuum by the technique of Rosenberg, *et al.*²²

In preparing a batch of germanium powder support, approximately 10 g of germanium chips, 1–3 mm in size, was sealed into the side arm on the crushing apparatus. These chips were obtained from a single crystal of germanium which had been electrically characterized by the Hall technique to determine its conductivity (σ), the sign of the majority charge carriers (electrons or holes), and their mobility (u_n or u_p). The concentration of the majority charge carrier was determined from the equation

$$\sigma = e(u_n n_s + u_p n_p)$$

where $\sigma \cong eu_n n_s$ when $n_s \gg n_p$, *i.e.*, n-type semi-

(18) F. van der Maesen and J. A. Brenkman, *Philips Res. Rept.*, **9**, 225 (1954).

(19) R. C. Frank and J. E. Thomas, Jr., *Phys. Chem. Solids*, **16**, 144 (1960).

(20) C. W. Selvidge, Sc.D. Thesis, Chemical Engineering Department, MIT, 1966.

(21) R. E. Eischens and W. A. Pliskin, *Actes Congr. Intern. Catalyse*, **2^o**, Paris, 1960, 1, 789 (1961).

(22) A. J. Rosenberg, P. H. Robinson, and H. C. Gatos, *J. Appl. Phys.*, **29**, 771 (1958).

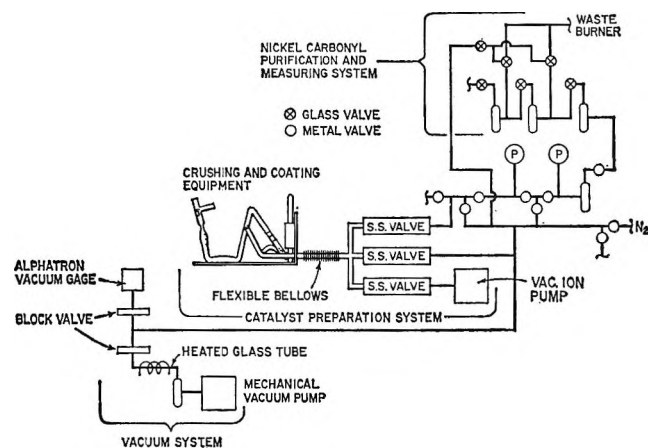


Figure 3. Catalyst preparation equipment.

conductor, and $\sigma \cong eu_p n_p$ when $n_p \gg n_s$, i.e., p-type semiconductor. The electron or hole concentration and the impurity element contained in the three types of germanium supports used in this study are indicated in Table I.

Table I: Electronic Properties of Germanium Supports

Ge-type	Conduction electron concn at 240° n_p , electrons/cm ³	Equilibrium charge transfer at Ge-Ni interface ^a σ , electrons/cm ²
p-Type		
Zn doped	3×10^{18} ^b	7.3×10^{10} to Ni
n-Type		
Sb doped	3.4×10^{17}	5.3×10^{11} to Ni
As doped	2.4×10^{19}	3.7×10^{12} to Ni

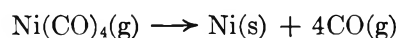
^a From Figure 2. ^b For Ge at 240° ($n_s n_p$)^{1/2} = 3.46×10^{16} .

After sealing the germanium chips into the catalyst preparation unit, it was evacuated first with a roughing pump and then with a Vac-Ion ion-trap pump, until a pressure as low as 10^{-8} torr was obtained. It was necessary to bake the unit out at 450° to attain this pressure. Generally a pressure of about 10^{-9} torr was maintained in the apparatus during crushing.

Crushing was accomplished by dropping a stainless steel hammer, enclosed in the crushing tube, repeatedly onto individual batches of about 0.5 g of chips. Hammer movement was activated by a solenoid coil placed outside the crushing tube to which a pulsed dc current was supplied. Chips were added to the crushing tube and crushed powder was removed by tipping the apparatus up or down through the flexible coupling in the vacuum manifold. The crushed powder was held in the quartz irradiating dish.

Nickel was deposited on the germanium powder supports by the decomposition of rigorously purified nickel carbonyl vapor. Since it was desired that the interphase charge-transfer influence the electrical properties of the nickel exposed to the chemical reaction, the average thickness of the nickel deposit was no more than a few atomic layers.

The nickel carbonyl was initially purified by two trap-to-trap distillations, discarding both the initial and final 25% portions of the distillate from each trap. This partially purified nickel carbonyl was stored as the liquid at room temperature in a storage trap. Prior to the use of a portion of this initially purified carbonyl for catalyst coating, it was further treated by repeated freeze-evacuation-sublimation cycles to remove traces of dissolved gases, together with any CO formed by the autodecomposition of the carbonyl in the storage trap. A portion of the purified carbonyl vapor was then added to the crushing and coating apparatus, which had been isolated from the high-vacuum pump and opened to a 0–20-mm absolute pressure gauge. The germanium powder was then heated with infrared radiation, while cooling the outside of the quartz dish with air streams. The carbonyl vapor decomposed on the heated powder by the reaction²³



The carbon monoxide does not irreversibly adsorb on the germanium surface.²⁴ The amount of nickel deposited was calculated from the pressure increase indicated on the absolute pressure gauge and the known volume and temperature of the system. Uniform heating and nickel deposition on the germanium powder was encouraged by mixing the powder through the vibration and occasional tipping of the crushing and coating system. Since the carbon monoxide formed tended to purge the carbonyl vapor out of the dish, it was sometimes necessary to evacuate and recharge the system repeatedly with fresh carbonyl vapor until the total pressure increase in all runs indicated that the desired quantity of nickel had been deposited. The pressure increase corresponding to the deposition of 1 m² of a monolayer of nickel was about 1.75 torr in this system. In the absence of germanium powder, only slight pressure rises were noted in the system when the carbonyl vapor was admitted to it, indicating that very little decomposition occurred on the inner surface of the apparatus during the catalyst-coating process.

Following the nickel deposition, the catalyst was

(23) R. K. Chan and R. McIntosh, *Can. J. Chem.*, **40**, 845 (1962).

(24) H. C. Gatos, personal communication, 1962.

Table II: Catalytic Properties of the Germanium-Nickel and Pure Nickel Catalysts for Formic Acid Dehydrogenation at 240° and 19.5 mm

Catalog no.	Ge-type	Surface area, cm ² /g	Average nickel layer thickness, atomic layers	Initial activity, moles/m ² hr	Activation energy, kcal/mole	A frequency factor, moles/m ² hr	Apparent reaction order
3 ^a	n-Type Sb doped	680	1.0	None			
4		658	None	2.4×10^{-4}			
9a		961	1.0	3.4×10^{-4}			
9b		961	3.1	7.8×10^{-4}			
10a		812	6.2	14.2×10^{-4}	17.0-18.9	7.1×10^4	0.97
10b		812	18.5	23.7×10^{-4}	10.6-11.0	9.6×10^1	0.89
11a	p-Type Zn doped	1143	4.4	2.9×10^{-4}	33.6	6.0×10^{10}	0.85
11b		1143	13.1	7.9×10^{-4}	10.0	1.46×10^1	0.85
12c	n-Type As doped	936	10.7	25.4×10^{-4}	13.8	1.9×10^3	0.83
7b	Pure Ni	122		1.54 ± 0.06	28.7 ± 1.1	2.2×10^{12}	0.15

^a Not outgassed to remove carbon monoxide.

baked out and evacuated in the quartz dish until no more adsorbed CO could be removed from the nickel. This condition was assumed when the pressure had reached 10^{-8} torr while the catalyst temperature was at 250°. Approximately one-fifth of the catalyst was then removed from the system in one of the two break-seals on the quartz dish. The remaining catalyst was then, generally, coated with additional nickel by the procedure outlined above. After a sample of this catalyst was taken in a break-seal, the remaining nickel-coated germanium powder, about 6 g, was removed from the system for BET surface area measurements. The results of these measurements are indicated in Table II for the catalysts prepared. The surface area varied from 658 to 1143 cm²/g.

It was assumed in calculating the activity of the catalysts that the surface area of the air-exposed germanium-nickel powder was the same as that of the break-seal-sampled catalysts which were not exposed to air. It was also assumed that the nickel deposition did not change the area of the catalysts, so that the same surface area could be used to calculate the specific activity of both catalysts prepared from a single germanium crushing. The average thickness of the nickel deposit on each catalyst, as indicated in Table II, was calculated under the same assumptions from the BET surface areas and the measured amount of carbonyl decompositions. Except for a single catalyst, which was sampled before nickel deposition, the nickel deposits on the nine catalysts prepared and

tested ranged in average thickness from 1.0 to 18.5 atomic layers.

Nickel powder catalysts were also prepared by reducing slightly oxidized commercial nickel powder, supplied by Federal-Mogal-Bower Bearings, Inc., with hydrogen in the catalyst preparation unit. The reduced powder was heated to 450° under a pressure, lowered to 10^{-8} torr, in an attempt to remove the dissolved hydrogen. It was sampled under vacuum in break-seals.

The activity of the germanium-nickel catalysts for formic acid dehydrogenation was measured in a single-pass, continuous-flow reactor, to which carefully purified formic acid vapor was fed. A diagram of the reactor system is shown in Figure 4.

The formic acid feed was purified by repeated distillations in which the distillate was collected as a solid in a continuously evacuated flask or trap. Water was removed by storing the formic acid over anhydrous copper sulfate in the first distillation flask and by passing the vapor through a bed of the same material in the first distillation step. After the second distillation step the formic acid was purged with nitrogen to remove the last traces of dissolved gases, especially oxygen. All traces of oxygen were removed from the nitrogen purge gas by passing it through a bed of hot, freshly reduced copper powder. The formic acid was stored in the third distillation flask at -78° under vacuum.

Prior to the initiation of a kinetic run a portion of the

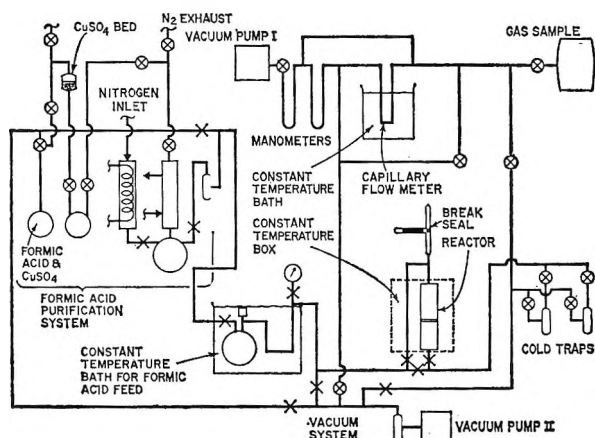


Figure 4. Formic acid decomposition reactor system.

stored formic acid was distilled into a feed flask. Included in this transfer step were two condensations of the formic acid vapor into the solid in continuously evacuated flasks, the second evacuated condensation being in the feed flask. The feed flask was immersed in a constant-temperature bath maintained at $35.0 \pm 0.1^\circ$ during a kinetic run. The formic acid feed rate was established by the setting on a fine metering valve above the feed flask and the reading on a 0–20-mm absolute pressure gauge on the feed line downstream of the metering valve. The feed pressure was maintained at 19.5 mm except during tests of reaction order, when lower pressures were used.

The reactor was a vertical glass tube 3 cm in diameter, containing a glass frit to support the catalysts and thermowell above and below the frit to measure the reaction temperature. The reactor was contained in a thermostated box capable of maintaining constant reaction temperatures between room temperature and about 400° . All kinetic runs were initiated at 240° , with the activation energy determined by temperature cycles within 30° of that point. The direction of the temperature cycle depended on the magnitude of the activity at 240° . Following the reaction, the unreacted formic acid vapor was removed from the product stream in cold traps. The composition of the uncondensed gases was measured by gas chromatography and the flow rate of these gases determined by measuring the absolute pressure upstream of and the pressure drop across a capillary flow meter. The reaction gases were finally removed from the system through a vacuum pump.

After initiation of the formic acid feed, measurements were made to ensure the absence of inert gases in the feed and to determine the activity of the empty reactor (usually negligible). After the formic acid flow was established and the reactor had reached a steady

240° , the evacuated break-seal was opened to add the catalyst to the reactor. After the activity at 240° was determined, the temperature and then the pressure were cycled to obtain activation energy and reaction order data. These latter data were not taken on the earlier tests.

IV. Results

The kinetic data collected on the pure nickel catalysts and the germanium–nickel catalysts are indicated in Table II. The activities listed are those initially obtained on the catalyst; in all cases only hydrogen and carbon dioxide were detected in the product gas, indicating that the nickel catalyst promoted only the dehydrogenation reaction, as reported elsewhere.²⁵ As noted above, total BET surface areas were used to calculate specific activities. The possible presence of uncovered germanium surface in some of the catalysts may make the calculated specific activities a little low. The character of deposits containing similar quantities of nickel should not be substantially different on the various germanium supports. For this reason, and others to be noted later, only catalysts containing similar quantities of supported nickel are compared to determine the influence of interphase charge transfer.

Seven kinetic tests were made on separate 1.0-g samples of the reduced nickel powder catalyst. These tests were interspersed with the kinetic tests on the germanium–nickel catalysts. The reaction rate decreased with time, as shown in Figure 5, for one of the tests. The initial activity of the seven nickel powder catalysts at 240° and 19.5 torr was 1.54 ± 0.06 moles/hr m^2 . After 130 min the rates decreased to 0.396 ± 0.041 mole/hr m^2 . Thus, although the rates were time dependent, they were reproducible on a time-dependent basis. In separate kinetic tests in which less than 1 g of the reduced nickel powder was used, the initial activities were approximately equivalent to those ob-

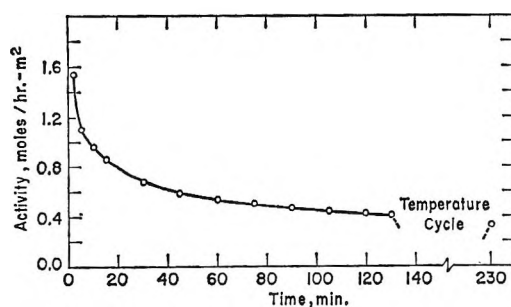


Figure 5. Variation of catalyst activity with time: 1 g of nickel powder catalyst, $122 \text{ cm}^3/\text{g}$, 240° , 19.5 torr (run 49).

(25) G. C. Bond, "Catalysis by Metals," Academic Press Inc., New York, N. Y., 1962.

tained for 1 g of catalyst, while the reaction rates decreased more rapidly with time. Thus in tests using 0.41, 0.73, and 1.3 g of nickel powder, the percentage decrease in the reaction rate during 130 min of testing was 85, 81, and 74%, respectively. It appears that the catalyst poisoning may have been caused either by an impurity in the formic acid feed or by trace quantities of water and carbon monoxide produced by the decomposition of formic acid on the glass walls of the reactor.

Activation energy data were obtained by cycling the temperature after 130 min of reaction. A linear decrease in catalytic activity was assumed during the period of temperature cycling in the calculation of activation energy, which was found to be 28.7 ± 1.1 kcal/mole. The reaction rate on the reduced nickel catalysts showed only a slight pressure dependence, varying as the 0.15 power of the pressure of the formic acid feed to the reactor. The reaction rate was shown to be essentially independent of formic acid flow rate at constant pressure.

The activity of the germanium-nickel catalysts generally also decreased with time, although to a much smaller extent than did that of reduced nickel powder catalysts. Typical time-dependent reaction-rate data for these catalysts are shown in Figure 6 for catalyst 12c. The activities reported in Table II are the maximum activities obtained before the initial temperature cycle, except for catalyst 11b for which a higher activity obtained after the temperature cycle was reported.

The slower deactivation of the germanium-nickel catalyst may possibly be explained by the larger surface areas of these catalysts. The surface areas of the germanium-nickel catalyst test samples were about 20 times those of the nickel powder catalysts. If a constant amount of catalyst poison was exposed to the catalyst bed in all tests, this should have produced a smaller effect on the higher surface catalysts.

The specific activities of the germanium-supported nickel catalysts are on the order of 0.1% of the activities on the nickel powder catalysts. The specific rates of formic acid decomposition on five previously investigated nickel catalysts, as summarized by Bond,²⁶ vary by about two orders of magnitude. The decomposition rate on the most active of these nickel catalysts corresponds closely to that of the presently investigated nickel powder catalyst, and all investigators indicated that the reaction was zero order in formic acid pressure. The difference of nearly an order of magnitude in the specific activity of the least active, previously reported nickel catalyst and the germanium-supported nickel catalysts indicates that the

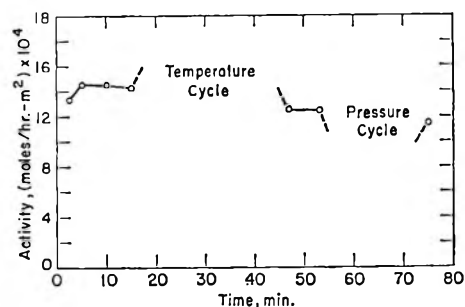


Figure 6. Variations of activity of catalyst 12c with time: 240° and 19.5 torr HCOOH pressure.

latter are significantly different from other nickel catalysts. This difference is also indicated by the higher pressure sensitivity of the reaction on the germanium-nickel catalysts. The source of this difference is not clear. It may arise from the poisoning of the nickel by germanium, or from the character of the deposit formed by nickel carbonyl decomposition on germanium. Although this difference is real, it should not affect the significance of the results of this study, since the nickel deposits should have similar catalytic properties apart from the electronic influence of the germanium supports.

The activation energies of the catalysts with nickel deposits averaging 18.5 atomic layers on the Sb-doped support and 13.1 atomic layers on the Zn-doped support were about 10 kcal/mole, while that on the As-doped support containing an average of 10.7 atomic layers was 13.8 kcal/mole. The catalysts with nickel deposits averaging 6.2 atomic layers on the Sb-doped support and 4.4 atomic layers on the Zn-doped support had higher activation energies, about 18 and 34 kcal/mole, respectively. There appears to be a general increase in the activation energy, with a decrease in average nickel layer thicknesses. Variations in the Arrhenius frequency factors compensate for the wide variations in the activation energies to give specific rates of the same order of magnitude.

The reaction was slightly less than first order in the upstream formic acid pressure, varying from 0.83 to 0.97 in the five tests conducted. Since the average pressure in the catalyst bed varied less than linearly with the upstream pressure, the actual order of the reaction was probably closer to first order than the data indicate.

V. Discussion

The relationship between the specific activity and the average thickness of the nickel deposits on the three germanium-support materials is shown in Figure 7. The activities of the catalysts supported on the Sb-

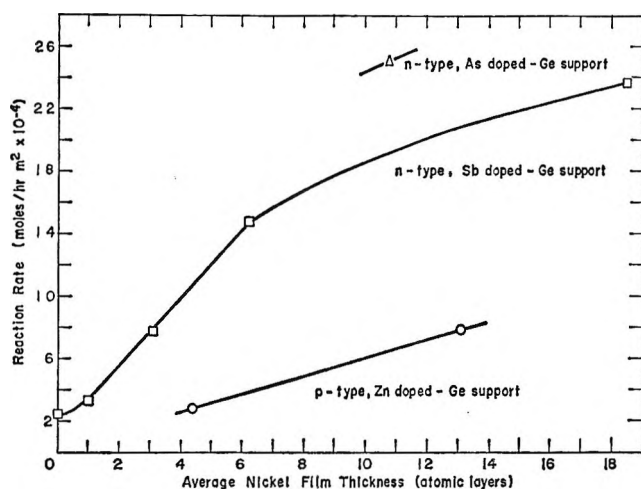


Figure 7. Activity of germanium-supported nickel catalysts for formic acid dehydrogenation at 240°.

doped and Zn-doped germanium samples increase as the average thickness of the nickel deposit increases. Interpolating the curves drawn on Figure 7, the relative specific activities of catalysts with nickel deposits averaging 10.7 atomic layers on the Zn-doped, Sb-doped, and As-doped germanium supports are in the ratio 1:3:4. The ratio of 1:3 in the activity of the catalysts containing Zn-doped and Sb-doped germanium, respectively, holds quite closely for catalysts containing 4.4 and 13.1 atomic layer quantities of nickel.

The nearly linear increases in the activity of the catalysts containing Sb-doped germanium, with the average thickness of the nickel layer from 0 to 6.2 atomic layers, indicate that the nickel may have been present in clumps or islands which increase in number as more nickel was added to the catalysts. The activity of the catalyst containing an 18.1 atomic layer quantity of nickel was well below a continuation of the initial straight-line position of the curve, indicating that the clumps may have grown together by that point. As noted above, there is a sharp decrease in the activation energy in going from catalysts containing less than about 10 atomic layers of nickel to those containing more. This may be the result of a changing character of the nickel deposit, *i.e.*, a growing together of clumps of nickel and a thickening of the nickel deposit. Deposits containing similar quantities of nickel on the separate supports should have similar physical character, however, and be amenable to comparison to determine the effect of interphase electronic interaction.

Increasing the interphase charge transfer from the germanium supports to catalyst deposits containing an average of 10.7 atomic layers of nickel from $7.3 \times$

10^{10} to 5.3×10^{11} and then to 3.7×10^{12} electrons/cm² promoted an increase in activity in the ratio of 1:3:4. The number of nickel atoms in films containing 10.7 atomic layers is about 1.8×10^{16} atoms/cm². Thus, an average of only about 2.5×10^{-5} and 1.8×10^{-4} electrons were added per nickel atom in going from the Zn-doped to the Sb-doped germanium and from the Sb-doped to the As-doped germanium. A similar effect is noted for the influence of interphase charge transfer to nickel layers of about 4 and 13 atomic layers in average thickness on the Zn-doped and Sb-doped supports. These nickel deposits contain about 6.4×10^{15} and 22.4×10^{15} nickel atoms/cm², respectively. Thus a variation of only about 7×10^{-5} and 2×10^{-5} electrons/nickel atom in the interphase charge transfer results in a tripling in the catalytic activity of the nickel. This fraction was a great deal smaller for the surface nickel atoms several atomic layers from the germanium interface, where the catalytic reaction may occur. This small variation in the excess charge associated with the nickel catalyst layers definitely appears to be catalytically significant.

The increase in the activity of the nickel catalysts with increasing concentrations of excess charge in the catalyst layers may be explained by the mechanism indicated in eq 1. The rate-limiting step in the first-order decomposition of formic acid is probably the dissociative adsorption of the acid, step 1. In this step, there is a transfer of charge from the catalyst surface to the adsorbed formate group. Increasing the concentration of electrons in the catalyst should make this charge transfer easier. The results of this investigation indicate that easing this charge transfer increases the reaction rate.

VI. Conclusions

The activity of nickel catalysts for formic acid decomposition can apparently be increased by a factor of 1.33–3 by transferring from a germanium support as little as one electron for every 10^5 nickel atoms. Interphase charge transfer from a support can thus be an important factor in determining the activity of industrial catalysts.

Acknowledgment. This work was supported by the National Science Foundation under Grant No. GP-607. The authors are grateful to Professor H. C. Gatos of MIT for his useful discussions on the properties of germanium, to Dr. Allen Strauss of the Lincoln Laboratory of MIT for conducting the Hall measurements on the germanium crystals, and to Norman Davis of Union Carbide Development Co. for his suggestions on the nickel carbonyl decomposition procedure.

The Viscosity of Water under Pressure

by R. A. Horne and D. S. Johnson

Arthur D. Little, Inc., Cambridge, Massachusetts (Received December 15, 1965)

The effect of hydrostatic pressure on the viscosity of pure water has been measured with a rolling-ball type of viscometer over the pressure and temperature ranges of 1–2000 kg/cm² and 2–20°. The application of pressure tends to destroy the structured regions in liquid water.

Introduction

Over the past few years we have been concerned with the electrical conductivity of aqueous electrolytic solutions, including sea water, under high hydrostatic pressure.^{1–4} A modified Walden's rule has been proposed relating empirically the conductivity with the viscosity under pressure.^{5,6} The viscosity of water, relative to 1 atm, exhibits a minimum at about 1000 kg/cm²,⁷ and this anomaly has been attributed to the breakup of the rarified regions of structure in liquid water.⁸ At somewhat higher pressure (about 2000 kg/cm²), the relative conductances of aqueous solutions of strong 1:1 salts exhibit maxima, the activation energies of such transport processes exhibit minima,³ and the "mixture effect" in mixed electrolytic solutions exhibits inflections.⁴ Presumably the same pressure-induced structural changes in liquid water are responsible for these phenomena even though the mechanism of electrical conductivity and viscous flow in water are not identical.⁹

Reliable data on the viscosity of aqueous solutions under pressure are needed for purposes of interpreting conductivity data and for correlating the structural changes that have been indicated by the changes in the activation energies of conduction.

Unfortunately, although the earlier work of Bridgman,¹⁰ Tammann and Rabe,¹¹ and Lederer¹² for the viscosity of pure water under pressure appear to be in agreement at 30°, at lower temperatures significant discrepancies are apparent (see Figure 1). Recent new measurements by Bett and Cappi¹³ and Weber¹⁴ are in disagreement with the earlier work of Bridgman, Tammann and Rabe, and Lederer at 30° (Figure 1). Although the discrepancies in the relative viscosity (Figure 1) are appreciable, it should be remembered that the differences in absolute viscosity are quite small.

Experimental Section

The details of the thermostat and the high-pressure producing and measuring equipment are described elsewhere.¹ The rolling-ball type of viscometer, while it may not be as accurate at 1 atm as other types, lends itself so easily to high-pressure work that, although other types of high-pressure viscometers have been developed,¹⁵ it has been used by a majority of investigators of the viscosity of fluids under high hydrostatic pressures.^{16–29}

- (1) R. A. Horne and G. R. Frylinger, *J. Geophys. Res.*, **68**, 1967 (1963).
- (2) R. A. Horne, W. J. Bannon, E. Sullivan, and G. R. Frylinger, *J. Electrochem. Soc.*, **110**, 1282 (1963).
- (3) R. A. Horne, B. R. Myers, and G. R. Frylinger, *J. Chem. Phys.*, **39**, 2666 (1963).
- (4) R. A. Horne and R. A. Courant, *J. Chem. Soc.*, 3548 (1964).
- (5) R. A. Horne, *Nature*, **200**, 418 (1963).
- (6) R. A. Horne and R. A. Courant, *J. Geophys. Res.*, **69**, 1971 (1964).
- (7) R. Cohen, *Ann. Phys.*, **45**, 666 (1892).
- (8) S. D. Hamann, "Physico-Chemical Effects of Pressure," Butterworth and Co. Ltd., London, 1957, p 82.
- (9) R. A. Horne, R. A. Courant, D. S. Johnson, and F. F. Margosian, *J. Phys. Chem.*, **69**, 3988 (1965).
- (10) P. W. Bridgman, *Proc. Am. Acad. Arts Sci.*, **61**, 57 (1926); *Proc. Natl. Acad. Sci.*, **11**, 603 (1925).
- (11) G. Tammann and H. Rabe, *Z. Anorg. Allgem. Chem.*, **168**, 73 (1927).
- (12) E. L. Lederer, *Kolloid-Beihfte*, **34**, 270 (1932).
- (13) K. E. Bett and J. B. Cappi, *Nature*, **207**, 620 (1965).
- (14) W. Weber, *Z. Angew. Phys.*, **15**, 342 (1963).
- (15) See, for example, M. M. Kusakov, L. A. Konovalova, and A. A. Konstantinov, *Chem. Abstr.*, **61**, 6417d (1964).
- (16) A. E. Flowers, *Proc. Am. Soc. Testing Materials*, **14**, 565 (1914).
- (17) M. D. Hersey, *J. Wash. Acad. Sci.*, **6**, 525 (1916).
- (18) M. D. Hersey and H. Shore, *Mech. Eng.*, **50**, 221 (1928).
- (19) B. H. Sage, *Ind. Eng. Chem., Anal. Ed.*, **5**, 261 (1933).
- (20) F. Hoespler, *Z. Tech. Physik*, **14**, 165 (1933).

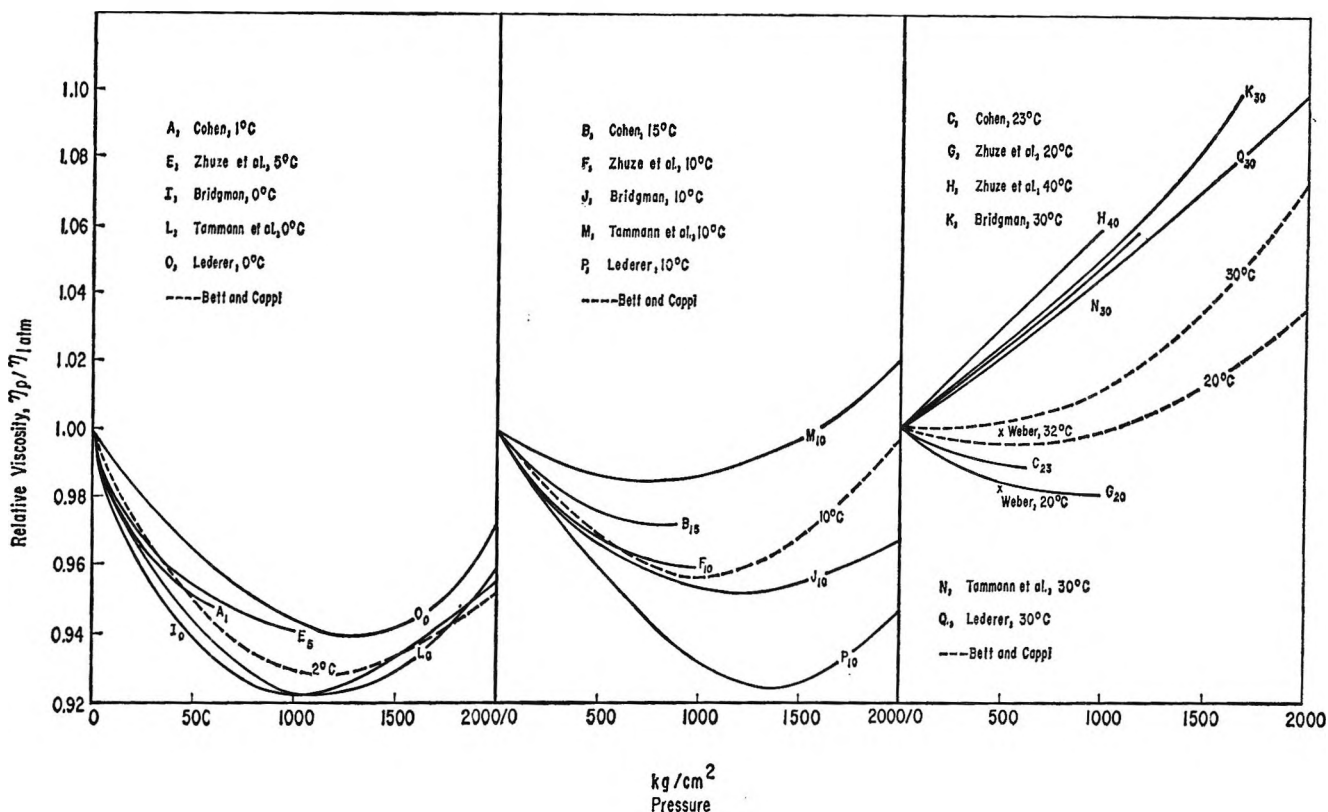


Figure 1. Comparison of literature values for the relative viscosity of pure water as a function of temperature and pressure.

Although the literature contains many descriptions of high-pressure, rolling-ball type of viscometers,¹⁶⁻²⁹ inasmuch as the discrepancies mentioned above probably arise from differences in apparatus and experimental technique, a detailed description of the present experiment is necessary.

The high-pressure, rolling-ball viscometer consists of a length of $\frac{3}{8}$ -in. o.d., $\frac{1}{8}$ -in. i.d. stainless steel, nonmagnetic tubing, 30 in. in length and closed at one end with a dead-end plug. The viscometer is enclosed in a Lucite jacket through which transformer oil circulates. Thermocouple probes measure the temperature at both of the pickup coils.

The viscometer design incorporates one important innovation. The ball rolls, not along the inside of the high-pressure tubing itself, but rather along a loose-fitting inner lining consisting of thin-wall stainless steel tubing, 0.0955-in. i.d., slightly crimped near the lower end to stop the ball's descent. Pressure forces the walls of the high-pressure tubing outward, thereby increasing the inside diameter, but there is no pressure differential across the walls of the inner liner; thus the ball moves in a tube of essentially constant diameter and, inasmuch as the compressibility of the ball is very small, there is no significant correction factor with

increasing pressure. We feel that the present measurements are more accurate than those previously reported largely because the uncertainties of a pressure-deformation correction have been thus avoided.

In order to avoid corrosion, initially the 0.0625-in. diameter balls were nickel struck and gold plated. After a short time, the fall time of these balls became erratic and tended to increase. Microscopic examination revealed that the gold plate had blistered. Nickel-plated balls were substituted. These performed satisfactorily and were quite corrosion resistant. The balls were very uniform; no differences among the balls were detectable from viscometer fall times at 1 atm

(21) B. H. Sage and W. N. Lacey, *Am. Inst. Mining Met. Engrs., Tech. Pub.*, 845 (1937).

(22) B. H. Sage and W. N. Lacey, *Ind. Eng. Chem.*, **30**, 829 (1938).

(23) R. B. Block, *J. Appl. Phys.*, **11**, 635 (1940).

(24) B. H. Sage and W. N. Lacey, *Ind. Eng. Chem.*, **32**, 587 (1940).

(25) R. M. Hubbard and G. G. Brown, *Ind. Eng. Chem., Anal. Ed.*, **15**, 212 (1943).

(26) E. M. Griest, W. Webb, and R. W. Schiessler, *J. Chem. Phys.*, **29**, 711 (1958).

(27) S. E. Babb, Jr., and G. J. Scott, *ibid.*, **40**, 3666 (1964).

(28) G. E. McDuffie, Jr., and M. V. Kelly, *ibid.*, **41**, 2666 (1964).

(29) D. E. Harrison and R. B. Grosser, *Rev. Sci. Instr.*, **36**, 1840 (1965).

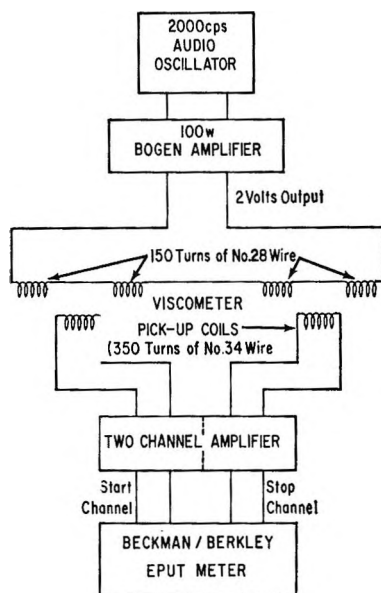


Figure 2. Viscometer circuit diagram.

and a given temperature, weightings, or diameters as measured with a micrometer.

The angle used was 30° , this optimum value being determined by trial and error. A more steep inclination sacrificed a significant figure in the fall time, while less steep inclinations tended to give erratic fall times. The latter was probably due to the greater likelihood of a very slowly moving ball getting retarded by dust motes or slight inhomogeneities on the inner surface of the liner.

The rolling-ball viscometer timing circuit is shown in Figure 2. Using a magnet, the steel ball is brought to the top of the inclined viscometer. When the magnet is withdrawn, the ball rolls down the inclined section, and its fall time between the two pickup coils is measured.

Two sets of coils are arranged a fixed distance apart (approximately 26 cm) along the viscometer. Each set of coils contains two primary sections, wound in series opposition, and a centrally located pickup coil. The primaries are energized by an audio oscillator feeding 2000 c to a 100-w amplifier. The amplifier is adjusted so as to put out a 2-v signal. (The dc resistance of each coil is approximately 6 ohms.) In the absence of the steel ball, the effect of the two primary sections on the pickup coil cancels out, and the output voltage should be zero. Although each section of the primary coils has been designed to be exactly the same, a 10-mv background signal remains in each pair of coils owing to residual unbalance in the mutual inductance. This is caused by slight differences in geometry when the coils are wound.

The EPUT meter contains a precision quartz crystal controlled clock. As the ball passes through the first set of coils, it produces a gross imbalance in the coupling and thus induces a voltage in the pickup coil. This signal is amplified and fed into the start channel of the EPUT meter. It triggers the start channel and actuates the running-time readout. As the ball passes through the second set of coils, the process is repeated except that the amplified signal is fed into the stop channel of the EPUT meter and terminates the readout of the elapsed time. The interval of time between the start and stop signals is read directly off the digital display on the EPUT meter. Since the distance between the two pairs of coils is known and the time for the ball to roll between the two pairs of coils is measured, the velocity of the rolling ball can be calculated.

Immediately prior to a run the viscometer is disassembled, and the high-pressure tube and its stainless steel liner are rinsed successively with washes of (1) acetone, (2) distilled water, and (3) the solution to be studied. The liner is next inserted and the viscometer filled. The liquid in the viscometer is subjected to a mild vacuum to remove the gases and the ball carefully inserted with the tube enclosed in such a manner as to minimize gas entrainment. The viscometer is loosely connected to the high-pressure system and a slight pressure applied until the escape of hydraulic fluid through the loose coupling indicates that the air space between the fluid to be studied and the hydraulic fluid is removed. The proper angle of the viscometer is checked with a special level, the connection tightened, and the level checked again. The angle is also checked in the course of the experiment since it is very critical.

The hydraulic fluid used was Esso Univis P-38. The electrical conductivity of aqueous solutions is very sensitive to molecular and especially ionic contamination. Conductivity measurements on aqueous electrolytic solutions in direct contact with Univis P-38 before, during, and after pressurization and over extended periods of time (weeks) at 1 atm showed that, in the absence of strong acids or bases, water is not significantly contaminated by this hydraulic fluid. As a further check on water purity, following each pressurization series the sample was immediately returned to 1 atm and its viscosity remeasured.

Following each pressure increment the apparatus is allowed to stand from 10 to 15 min in order that the temperature increase resulting from adiabatic compression be dissipated. This equilibration time was determined experimentally and is quite small as a result of the relatively large surface-to-volume ratio of the "sample" (about 32 in.^{-1}). The ball is raised to the top of the viscometer by hand with a 2495-gauss mag-

Table I: Relative Viscosity of Compressed Water

Pressure, kg/cm ²	Rel viscosity, $\eta_P/\eta_1 \text{ atm}$	Pressure, kg/cm ²	Rel viscosity, $\eta_P/\eta_1 \text{ atm}$	Pressure, kg/cm ²	Rel viscosity, $\eta_P/\eta_1 \text{ atm}$	Pressure, kg/cm ²	Rel viscosity, $\eta_P/\eta_1 \text{ atm}$
At 2.252 ± 0.073°				At 6.241 ± 0.053°			
70	0.9938	844	0.9370	492	0.9898	1828	0.9954
141	0.9875	844	0.9358	562	0.9889	2109	1.001
141	0.9869	844	0.9353	562	0.9880		
141	0.9838	984	0.9358	633	0.9865		
281	0.9708	984	0.9349	633	0.9875		
281	0.9713	984	0.9343				
281	0.9702	984	0.9352				
281	0.9689	1125	0.9326	211	0.9960	984	0.9901
281	0.9688	1195	0.9346	281	0.9955	984	0.9911
422	0.9539	1125	0.9350	281	0.9952	984	0.9901
562	0.9457	1406	0.9382	562	0.9908	1265	0.9938
562	0.9434	1406	0.9373	562	0.9917	1265	0.9938
633	0.9420	1406	0.9369	633	0.9895	1265	0.9929
633	0.9417	1547	0.9383	703	0.9906	1547	0.9977
703	0.9403	1547	0.9394	703	0.9896	1898	1.0039
703	0.9392	1547	0.9388	703	0.9906	1898	1.0060
703	0.9396	1828	0.9425	703	0.9910	2109	1.0086
773	0.9318	1968	0.9455	844	0.9894	2109	1.0091
773	0.9322			844	0.9894	2109	1.0089
				844	0.9889		
At 4.009 ± 0.015°				At 15.112 ± 0.085°			
70	0.9985	703	0.9765				
70	0.9976	703	0.9750	70	0.9990	1406	1.0036
141	0.9938	703	0.9745	211	0.9985	1406	1.0045
141	0.9942	844	0.9726	422	0.9974	1758	0.0125
141	0.9933	844	0.9765	703	0.9968	1758	1.0130
281	0.9889	844	0.9748	1055	0.9994	2109	1.0216
281	0.9875	844	0.9748	1055	0.9985	2109	1.0210
281	0.9884	984	0.9745	1406	1.0050		
423	0.9839	1265	0.9775				
423	0.9814	1265	0.9781				
562	0.9775	1476	0.9800	141	0.9992	1055	1.0024
562	0.9786	1547	0.9818	211	0.9990	1055	1.0026
633	0.9777	1828	0.9876	281	0.9986	1055	1.0034
633	0.9749	1828	0.9861	422	0.9982	1406	1.0096
				562	0.9979	1406	1.0092
				562	0.9981	1406	1.0089
				703	0.9993	1406	1.0081
				703	0.9988	1758	1.0181
				703	0.9984	1758	1.0176
At 6.241 ± 0.053°				At 20.359 ± 0.183°			
70	0.9986	703	0.9865				
352	0.9930	844	0.9850				
352	0.9922	984	0.9855				
422	0.9902	984	0.9850				
422	0.9907	1195	0.9875				
422	0.9911	1265	0.9852				

net with a 3.5-cm gap. The ball is held at the top about 4–5 cm above the first pickup coil for about 30 sec (longer for more viscous solutions). If this precaution is not taken, the roll times tend to be erratic and not reproducible. Apparently this pause allows eddies set up by raising the ball to die away. The ball is then released and its fall time between the two pickup coils measured. The procedure is then repeated.

The initial position of the ball at the top of its roll is crucial. If the ball is too close to the top coil, it may

still be accelerating while in the timed zone between the two coils. On the other hand, if it is too near the top of the viscometer, it may come in contact with the interface between the fluids. Fortunately, when the ball does accidentally come in contact with the interface, erratic results obtain so the difficulty is easily recognized.

At a given temperature and pressure an experiment was repeated from four to as many as ten times. In the course of a given series of runs, the measured

average deviation of the temperatures of the viscometer ranged from ± 0.005 (for temperatures near room temperature) to as much as $\pm 0.02^\circ$ (for the lowest temperatures). The larger temperature deviations listed in Table I are averaged over series of series.

The ball-roll time is read to four significant figures and the roll times range from 5 to 10 sec. The average deviation in the measured roll time is about 0.10%.

Over the temperature interval 0–10°, thermal expansion of the vitreous silica spacer between the pickup coils increases the distance between them and thus the roll time by approximately 0.008%. The diameter of the rolling ball increases by about 0.034%, but the effect of this increase is partially compensated by an approximately 0.018% increase in the diameter of the inner tube in which the ball rolls. These effects of thermal expansion are well within the measured average deviation of 0.10%; therefore no attempt is made to apply corrections for them. However, the temperature dependencies of the densities of the ball and of the fluid are taken into consideration (see below).

The pickup coil spacer is not exposed to pressure, and the application of pressure does not appreciably alter the inside diameter, D_T , of the liner, and its effect on the diameter of the ball, D_B , is slight. The expressions derived by Hubbard and Brown,²⁵ contain the terms D_B/D_T and $(D_T + D_B)$, and over the pressure range 1–10,000 kg/cm² they change by only 0.02 and 0.06%, respectively. However, again, the pressure dependencies of the densities of the ball, ρ_B , and of the fluid, ρ_F , are taken into consideration.

In the present work the simplified relation developed by Sage¹⁹ was used

$$\eta = Ct(\rho_B - \rho_F) \quad (1)$$

where η is the viscosity, C is a constant, and t is the roll time. Over the temperature and pressure ranges involved, the density of the steel ball is very nearly a constant, but the density of water and thus of $(\rho_B - \rho_F)$ varies significantly. The density of steel, ρ_{Fe} , was calculated from the expression

$$\rho_B = \rho_{Fe} = 7.8835 / (1 + 3.5 \times 10^{-5}T) \times (1 - 6.1 \times 10^{-7}[P - 1]) \quad (2)$$

where T is the centigrade temperature, P is the hydrostatic pressure in atmospheres, and the constants are based on the densities, compressibilities, and coefficients of cubic thermal expansion from "The International Critical Tables."

Up to about 2500 kg/cm² there is good agreement in the density of water as reported by Amagat³⁰ and Bridgman.³¹ In view of this agreement, reliance was placed on Dorsey's compilation of specific volumes,³²

and, for a given P and T , densities were calculated from specific volumes read or interpolated from Dorsey's Table 95.

A calibration curve of the viscosity *vs.* $t(\rho_B - \rho_F)$ for aqueous NaCl solutions (using data of Sheely³³) and water-sucrose solutions (using data of Bingham and Jackson³⁴ and more recent data of Swindells, Snyder, Hardy, and Golden³⁵) shows that in the region of interest in the present experiments the curve is linear; thus eq 1 is applicable, and the following useful relationship is valid.

$$\eta_P / \eta_{1 \text{ atm}} = t_P(\rho_B - \rho_F)_P / t_{1 \text{ atm}}(\rho_B - \rho_F)_{1 \text{ atm}} \quad (3)$$

Earlier viscosity measurement made on pure water and sea water at 1 atm⁹ with this same viscometer yielded values in good agreement with those compiled by Dorsey.³² Deionized and degassed water was used.

Results

The effect of pressure on the absolute viscosity at a given temperature is quite small (Figure 3); therefore a much more meaningful way of reporting the results is in terms of the viscosity at pressures relative to the viscosity at 1 atm and the same temperature. The observed temperature and pressure dependencies of the relative viscosity of pure water are summarized in Table I and Figure 4. Absolute viscosities may be obtained by multiplying the relative viscosity given in Table I by the 1-atm viscosity for the corresponding temperature obtained from Figure 1 or Figure 2 in Horne, Courant, Johnson, and Margosian,⁹ or the tables in Dorsey.³²

Discussion

Qualitatively the present results show the same features as revealed by earlier studies, namely an initial decrease in the relative viscosity as pressure is applied followed by an increase, the minima in the relative viscosity becoming more shallow and gradually disappearing as the temperature increases (Figure 4). Quantitatively, however, the agreement among the values obtained by different experimentalists is poor (*cf.* Figures 1 and 4). In particular, the present results are not in agreement with the older values of

(30) E. H. Amagat, *Ann. Chim. Phys.*, **29**, 68, 505 (1893).

(31) P. W. Bridgman, *Proc. Am. Acad. Arts Sci.*, **48**, 307 (1913).

(32) N. E. Dorsey, "Properties of Ordinary Water-Substance," Reinhold Publishing Corp., New York, N. Y., 1940, pp 182–189.

(33) M. L. Sheely, *Ind. Eng. Chem.*, **24**, 1060 (1932).

(34) E. C. Bingham and R. F. Jackson, *Bull. Natl. Bur. Std.*, **14**, 59 (1918).

(35) J. F. Swindells, C. F. Snyder, R. C. Hardy, and P. E. Golden, National Bureau of Standards Circular 440, Supplement, U. S. Government Printing Office, Washington, D. C., July 31, 1958.

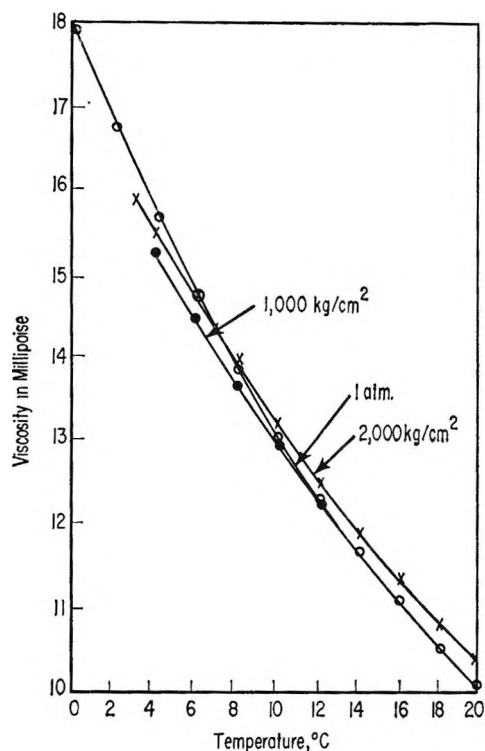


Figure 3. Absolute viscosity of pure water as a function of temperature and pressure.

Bridgman¹⁰ as quoted by Dorsey.³² Bridgman's values of $\eta_P/\eta_{1 \text{ atm}}$ at 30° appear much too high compared with the present 20° values, while his values at 10° appear much too low. Tammann and Rabe¹¹ have criticized Bridgman's results, and the present values at 2 or 10° appear to be in fair agreement with their 0 and 10° values, respectively, as quoted by Dorsey.³² Although the values of Zhuze, Sergeevich, and Chestnov at 40°, as quoted by Richardson, *et al.*,³⁶ and Tammann and Rabe¹¹ at 30° as quoted by Dorsey appear to be in agreement with Bridgman,¹⁰ the more recent work of Weber¹⁴ at 32° and Bett and Cappi¹³ at 30° indicate that Bridgman's values are much too high and seem to be in better harmony with our values at 20°, yet Weber's values at 20° appear to be considerably less than our values and those of Bett and Cappi¹³ at the same temperature. At temperatures close to 0° the present values and those of Cohen,⁷ Bridgman,¹⁰ Tammann and Rabe,¹¹ and Lederer¹² are in fair agreement. Reading values from the small graphs published by Bett and Cappi¹³ is difficult, yet their values and the present ones appear to be in good agreement at 2 and 20°, but in poor agreement at 10°.

In summary, the present results are in agreement with the recent results of Bett and Cappi;¹³ however, by making many measurements over a rather narrow

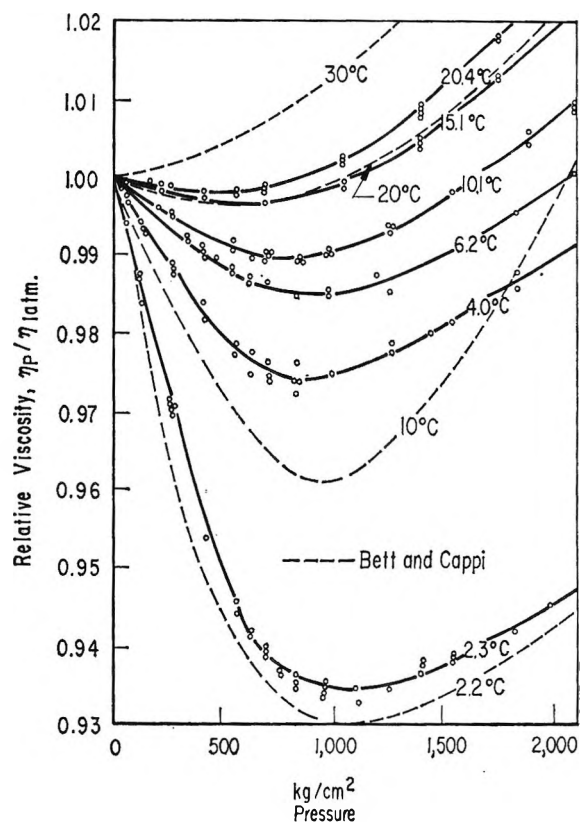


Figure 4. Relative viscosity of pure water as a function of temperature and pressure.

temperature region the present results give evidence of phenomena which escaped the notice of Bett and Cappi.¹³

The structured regions in liquid water are less dense than the "free" water; thus cluster breakup results in a volume decrease and is therefore enhanced by the application of pressure. The thermal destruction of the clusters superimposed on the "normal" thermal expansion of the "free" water gives rise to the well-known maximum in the density of pure water near 4°. If the data in Figure 4 are plotted isobarically *vs.* temperature (Figure 5), two significant features become clear: (1) the isobars exhibit inflections in the form of an abrupt change in slope near 4° and (2) isobars above and below 1000 kg/cm² appear to form two distinct families of curves. As mentioned in the Introduction, this pressure appears to have considerable structural significance. Above 1000 kg/cm² and 4°, Figure 5 suggests that the dominant effect is an increase in relative viscosity with increasing pres-

(36) J. L. Richardson, P. Bergsteinson, R. J. Getz, D. L. Peters, and R. W. Sprague, "Sea Water Mass Diffusion Coefficient Studies," Philco Corp. Publication No. U-3021 (Feb 26, 1961), Office of Naval Research Contract No. Nonr-4061(00).

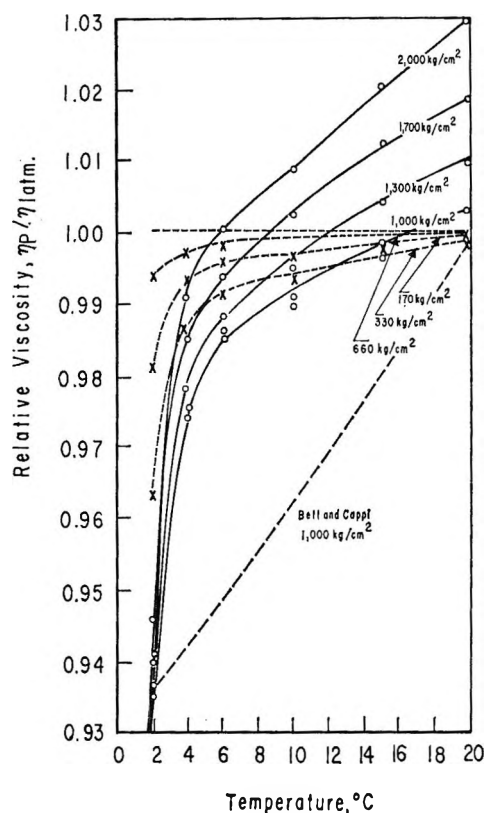


Figure 5. The effect of temperature on relative viscosity isobars.

sure as the water molecules are crowded closer together, the effect becoming more marked with increasing temperature. The pressure-induced destruction of the water clusters is greatest in the region below 4° , where the clusters are largest, and, as a result, a given relative viscosity isobar drops off very abruptly as the temperature is lowered below 4° . The data of Bett and Coppi¹³ when plotted isobarically (Figure 5) give no hint of these phenomena.

Pressure is a water structure-breaking influence; thus one expects the low-temperature structural transition in water and hence its temperature of maximum density to be displaced by the application of pressure.

Nemethy and Scheraga³⁷ have estimated that in going from 0 to 100° the average cluster size decreases from 90.6 to 21.0 molecules, while the fraction of unbroken H bonds decreases from 0.529 to 0.325. Although transport processes such as electrical conductivity and viscous flow correlate nicely with this estimate of cluster size,³⁸ the phenomenological transitions in viscosity (Figure 5) and conductivity^{3,38,39} at 4° are so sharply defined and abrupt that one is somewhat at a loss to account for them in terms of the more or less gradual cluster breakup, and one is tempted to revert

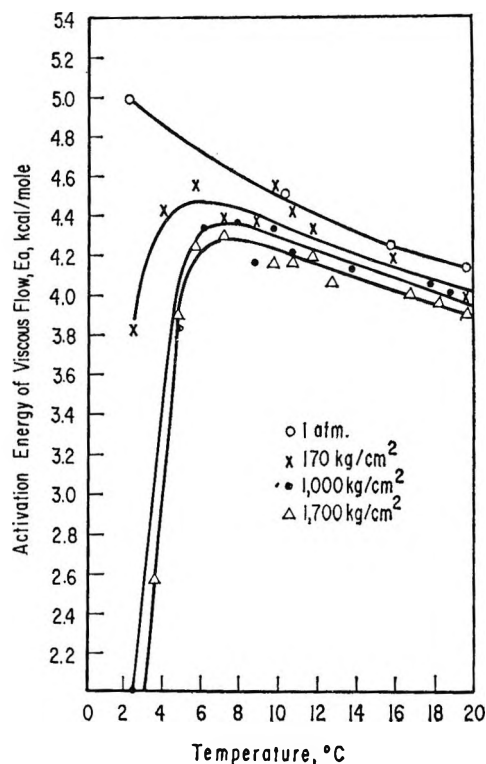


Figure 6. The temperature dependence of the activation energy of viscous flow of pure water under pressure.

to a more radical structural transition such as that postulated in the classical paper of Bernal and Fowler.⁴⁰ The greater elegance of the Frank-Wen-Nemethy-Scheraga model for liquid water is very much to its credit; however, this model may be a more serious oversimplification than presently realized.

The pressure at which the relative viscosity is at its minimum is decreased with increasing temperature. The qualitative conclusions to be drawn from this are in harmony with experience: as the freezing temperature is approached, very high pressures are necessary to destroy the structure, while at temperatures above about $40\text{--}50^\circ$ there is so little structure that the effect of pressure is slight and the relative viscosity *vs.* pressure isotherms cease to exhibit minima. The pressure at which the relative viscosity is again equal to unity also increases with decreasing temperature, the rate of increase becoming very great as the freezing temperature is approached.

(37) G. Nemethy and H. A. Scheraga, *J. Chem. Phys.*, **36**, 3382 (1962).

(38) R. A. Horne and R. A. Courant, *J. Phys. Chem.*, **68**, 1258 (1964).

(39) R. A. Horne and R. A. Courant, *J. Geophys. Res.*, **69**, 1152 (1964).

(40) J. D. Bernal and R. H. Fowler, *J. Chem. Phys.*, **1**, 515 (1933).

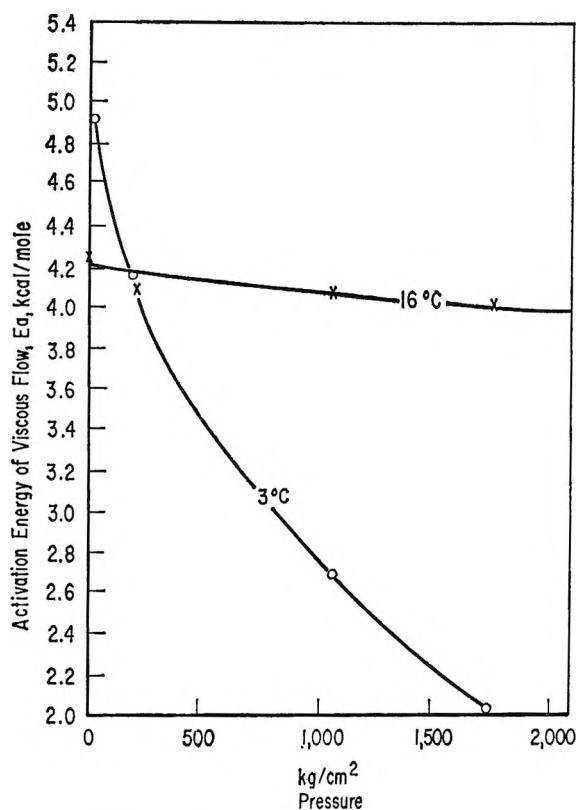


Figure 7. The pressure dependence of the activation energy of viscous flow of pure water.

Viscous flow can be treated as a rate process and activation energies, E_a , calculated from the integrated form of the Arrhenius equation. At 1 atm the Arrhenius activation energy of viscous flow of pure water, unlike the activation energy of electrical conductance in water, continues to increase with decreasing temperature.⁹ However, under hydrostatic pressure a maximum appears in the temperature dependence of E_a (Figure 6), and the value of E_a appears to be related to T_{max} , the temperature at which the maximum occurs, in a very simple way

$$(E_a)_{max} = 5.2 - 0.126T_{max} \quad (4)$$

The rapid decrease in E_a with decreasing temperatures in the low-temperature region at a given pressure was not expected, and its explanation is not clear at this time. However, the pressure dependence of E_a for a given temperature (Figure 7) is as anticipated: at 3°, where water structure is extensive, increasing the pressure destroys this structure and E_a decreases accordingly, but at 16° where there is less water structure the effect of pressure is correspondingly less and E_a decreases much more slowly with increasing pressure.

Finally, returning now to Figure 4, at some pressure below 1000 kg/cm² the relative viscosity of water goes

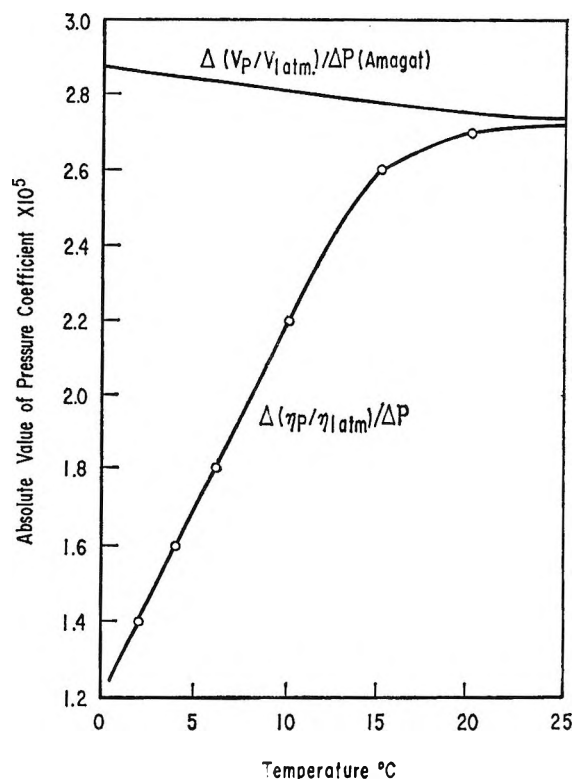


Figure 8. Pressure coefficients of specific volume and viscosity.

through a minimum and then begins to increase with increasing pressure as a "normal" unassociated liquid. Does this observation imply that by the time such pressures have been reached, all of the structure in liquid water has been destroyed and water has become a "simple," unassociated fluid? If such is the case, then pressure is indeed a powerful structure-breaking influence, for, as we have seen above, even at 100° the fraction of unbroken H bonds in water is still as high as 0.325. Unfortunately, highly specific molecular interactions strongly dependent on molecular structure appear to be important in determining the viscous properties of fluids under high pressure;⁴¹ hence there is little point in trying to compare water's behavior with that of other "simple" liquids. However, at 20° above 1500 kg/cm² the $\eta_P/\eta_{1 atm}$ vs. P curve (Figure 4) is linear and its slope corresponds to a pressure coefficient $\Delta(\eta_P/\eta_{1 atm})/\Delta P$ of $+2.7 \times 10^{-5}$ cm²/kg. At 20° the pressure coefficient of the specific volume of water, $\Delta(V_P/V_{1 atm})/\Delta P$, calculated from Dorsey's compilation of data of Amagat,³⁰ is -2.75×10^{-5} cm²/kg. Thus the viscosity at this temperature and these pressures appears to depend only on the reciprocal of the specific volume (Figure 8). Whether the water molecules

(41) See ref 8, pp 81-84.

would cease behaving as compact spheres upon further crowding at even greater pressures remains to be seen; but, if the present finding is not fortuitous, then the state of affairs in liquid water above moderate temperatures and pressures may be incredibly simple.

Acknowledgment. The authors are indebted to Dr. I. Simon and Mr. F. F. Margosian for the design, construction, and testing of the high-pressure viscometer. This work was supported in part by the Office of Naval Research.

Reactions of the Ethyl Radical. VIII. A Molecular Orbital Approach to the Energetics of the Addition Reaction

by J. E. Bloor,

Department of Chemistry, University of Virginia, Charlottesville, Virginia

A. C. R. Brown,

Petrochemical and Polymer Laboratory, Imperial Chemical Industries Limited, Runcorn, Cheshire, England

and D. G. L. James

Department of Chemistry, University of Aberdeen, Old Aberdeen, Scotland (Received December 16, 1965)

The atom localization energy and maximum free valence have been calculated for a diverse selection of olefins, cyclic polyenes, and vinyl monomers. A simple LCAO molecular orbital method was used in which allowance for the effects of differences in bond length, interaction between nonbonded atoms, and hyperconjugation was made. The activation energy for the addition of the ethyl radical to these diverse substrates shows significant correlation with the atom localization energy, but no appreciable correlation with the maximum free valence was found. A similar correlation energy was also found for the rates of methyl radical addition with atom localization energy, but not with free valence. A deviation was observed with cyclooctatetraene and was linked with flattening of the molecule during the formation of the activated complex. An alternative correlation with the incremental conjugation stabilization energy of the transition state succeeds to a similar degree; the linearly related experimental quantity $\log Q'$ shows greater correlation, where Q' is an intrinsic reactivity parameter based upon styrene with $Q' = 1.00$ and $e' = 0.00$. These four parameters are critically examined as indices of reactivity toward radical addition, and we conclude that the atom localization energy offers the greatest promise at the simple computational level.

Introduction

The selection of an appropriate molecular property as an index for the reactivity of unsaturated molecules toward the addition of free radicals continues to provoke discussion as the variety of kinetic data increases. Ten years ago the only comprehensive body of such data was a list of relative rate constants for the addition of the methyl radical to a series of aromatic hydrocarbons and closely related compounds in isooctane solution at 65°. Localization energy,² free valence,^{1,2} singlet-triplet excitation energy,¹ electron affinity,³ and ionization energy³ each gave linear correlation with the logarithm of the relative rate constant divided by the

number of equivalent reactive sites in the molecule. Each of these molecular properties is therefore suitable as an index of reactivity of aromatic compounds toward the addition of free radicals. The generality of these correlations arises from two characteristics of this class of substrate: (a) the linear correlation of all such electronic properties of the molecule and (b) the steric equivalence of the most reactive sites of all substrates. Such generality limits the degree to which the study of aromatic systems can increase our

(1) M. Levy and M. Szwarc, *J. Am. Chem. Soc.*, **77**, 1949 (1955).

(2) C. A. Coulson, *J. Chem. Soc.*, 1435 (1955).

(3) F. A. Matsen, *J. Chem. Phys.*, **24**, 602 (1956).

understanding of the radical addition process, but this limit is removed when olefins and their derivatives are employed as substrates. Among this wide class of compounds the electronic properties of the molecule are no longer so simply related, and the steric equivalence of the most reactive sites may be destroyed by successive substitution at the carbon atoms of the double bond. This loss of steric equivalence has proved a serious obstacle to the interpretation of the available kinetic data, which are normally limited to a set of rate constants at a single temperature. To plot the logarithms of such rate constants against, for example, the corresponding localization energies is to attempt a correlation between free energy and internal energy, and a uniformity of the entropy factor is implied. This severely limits the generality of our methods of correlation. The values of entropy of activation should be reasonably uniform for the addition of a given radical to a series of molecules having an identical pattern of substitution at the carbon atoms of the double bond. If the pattern of substitution is varied, however, we may expect an associated change in the preexponential factor,⁴ which would render dubious any correlation based upon the logarithm of the rate constant. Recognition of this difficulty has led Jennings and Cvetanović⁵ to employ the hydrogen atom as the attacking radical in the expectation that the variation of the steric factor with the degree of substitution would be insufficient to invalidate such a correlation; they found evidence for correlation with atom localization energy, but not with free valence. Clearly a more satisfactory resolution of the difficulty lies in the correlation of the energy of activation for the addition reaction with the appropriate molecular property. Yang⁶ has applied this approach to the addition of the hydrogen atom to a range of hydrocarbons similar to those chosen by Jennings and Cvetanović and has confirmed their conclusions by finding a reasonable correlation of the energy of activation with the atom localization energy, but not with the free valence.

In this present investigation we have extended this approach to our own experimental results on the ethyl radical as attacking radical and to selected data taken from the extensive collection of Szwarc and his collaborators^{1,4,7-10} on the methyl radical as attacking agent. The molecular orbital calculations were carried out on a much wider variety of olefinic derivatives than in previous studies.

Correlations are attempted between the activation energy for addition (ethyl radical only) and the β -carbon atom localization energy, the maximum free valence, the incremental stabilization energy of the react-

ing species in the transition state,¹¹ and the revised expressions^{12,13} of the Alfrey-Price intrinsic reactivity parameter Q .¹⁴ The molecular orbital calculations were designed to recognize any interaction between the formally nonbonded carbon atoms of the cyclic polyenes by including an appropriate bond integral in the calculation.

The Method of Calculation

The simple LCAO molecular orbital method was improved in a manner appropriate to the wide variety of the substrates. The variation of the bond integral with internuclear separation was included as in the comparable calculations of Binks and Szwarc⁴ and Sato and Cvetanović;¹⁵ moreover, it was extended to encompass interaction between nonneighboring atoms, so that possible transannular interaction in the molecules of cyclic polyenes should not be neglected. The effect of hyperconjugation was treated according to the conjugation model.¹⁶ Pure overlap integrals were omitted from the secular matrix, as in the method of Binks and Szwarc;⁴ their inclusion merely raises the values of the resonance energies uniformly¹⁷ and would scarcely affect the validity of any linear correlation discovered. Ethylene is used as a reference molecule; the carbon atoms are assigned a Coulomb integral of α_0 , and the carbon-carbon double bond is assigned a bond integral of β_0 , corresponding to a bond length of 1.335 Å. Bond integrals for other internuclear distances were assumed to be directly proportional to the overlap integral in coplanar π -electron systems and expressed in terms of β_0 , using the tables of Kopineck¹⁸ and Mulliken, *et al.*¹⁹ The corresponding inter-

- (4) J. H. Binks and M. Szwarc, *J. Chem. Phys.*, **30**, 1494 (1959).
- (5) K. R. Jennings and R. J. Cvetanović, *ibid.*, **35**, 1233 (1961).
- (6) K. Yang, *J. Am. Chem. Soc.*, **84**, 3795 (1962).
- (7) R. P. Buckley and M. Szwarc, *Proc. Roy. Soc. (London)*, **A240**, 396 (1957).
- (8) A. Rajbenbach and M. Szwarc, *ibid.*, **A251**, 1266 (1959).
- (9) J. Gresser, A. Rajbenbach, and M. Szwarc, *J. Am. Chem. Soc.*, **83**, 3005 (1961).
- (10) L. Herk, A. Stefani, and M. Szwarc, *ibid.*, **83**, 3008 (1961).
- (11) K. Hayashi, T. Yonezawa, S. Lkamura, and K. Fukui, *J. Polymer Sci.*, **A1**, 1405 (1963).
- (12) N. Kawabata, T. Tsuruta, and J. Furukawa, *Makromol. Chem.*, **51**, 70 (1962).
- (13) R. D. Burkhart and N. L. Zutty, *J. Polymer Sci.*, **A1**, 1137 (1963).
- (14) T. Alfrey and C. C. Price, *ibid.*, **2**, 101 (1947).
- (15) S. Sato and R. J. Cvetanović, *J. Am. Chem. Soc.*, **81**, 3223 (1959).
- (16) A. Streitwieser, Jr., "Molecular Orbital Theory for Organic Chemists," John Wiley and Sons, Inc., New York, N. Y., 1961, p 131.
- (17) R. S. Mulliken and C. A. Rieke, *J. Am. Chem. Soc.*, **63**, 1770 (1941).
- (18) H. J. Kopineck, *Z. Naturforsch.*, **A5**, 420 (1950).

nuclear distances were calculated from the values selected by Lide²⁰ wherever direct measurements had not been made. The π -electron system of cyclohexadiene-1,3 was assumed to be coplanar.²¹ The molecular parameters for cycloheptatriene-1,3,5,²² cyclooctatetraene-1,3,5,7,²³ and bicyclo[2.2.1]heptadiene-2,5²⁴ are all known, and the bond integrals were corrected for deviations from coplanarity wherever appropriate. The Coulomb integrals of the heteroatoms were taken as $\alpha_0 + k_X\beta$, where β is the bond integral for the carbon-carbon bond of benzene and is equal to $0.914\beta_0$; k_X was assigned the value of 1 for both ethereal oxygen and nitrilic nitrogen. Vinyl acetate was treated as a conjugated system comprising the two carbon atoms of the vinyl group and the directly attached oxygen atom only; for the latter the factor k_X was assigned a value of 2 to compensate for the large electron-withdrawing capacity of the acetyl group. Each carbon atom bonded to a heteroatom was assigned a Coulomb integral of $\alpha_0 + 0.1k_X\beta$.²⁵ The effect of hyperconjugation was treated¹⁶ by assigning the following parameters to the CH_3 and CH_2 groups: $\alpha_C = \alpha_0 - 0.1\beta$, $\alpha_H = \alpha_0 - 0.5\beta$, $\beta_{C-C} = 0.8\beta$, $\beta_{C-H} = 3.0\beta$; and the Coulomb integral of a carbon atom attached to a hyperconjugative group was taken as $\alpha_0 - 0.1\beta$.

Results and Discussion

Ethyl Radical Addition. The calculated values of atom localization energy and maximum free valence for 14 unsaturated compounds (B) are given in Table I, with the corresponding experimental values of activation energies, preexponential factors, and rate constants at 100° .²⁶⁻³¹ The subscripts refer to the reactions



Where appropriate the rate constants have been divided by n , the number of equivalent most reactive sites in the molecule of the substrate. Limits of error are given at the 5% probability level. Figures 1 to 4 show attempts to correlate the localization energy or the maximum free valence with the activation energy or with the statistically corrected rate constant at 100° . Localization energy is clearly the more promising index of reactivity. The points for seven hydrocarbons lie very close to the reference straight line drawn in Figure 1 for the correlation between corrected rate constants and localization energy. Marked deviation from this line is shown by the points for the nitriles, cyclooctatetraene, and 2,5-dimethylhexadiene-2,4. A similar pattern of correlation is shown for the

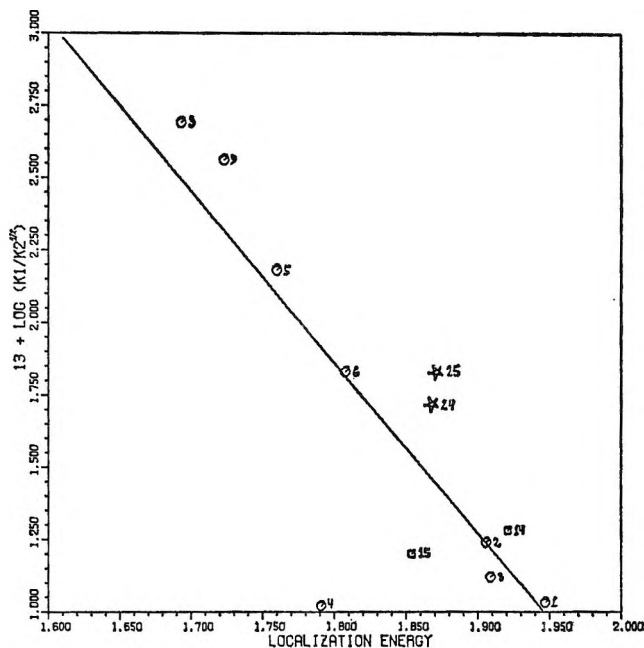


Figure 1. Correlation of rates of ethyl radical addition with localization energies: circles represent hydrocarbons; squares, ethers and esters; and stars, nitriles (on this and all subsequent figures).

activation energies in Figure 2, except that the deviation for 2,5-dimethylhexadiene-2,4 is much less pronounced.

The general pattern of correlation shown by Figures 1 to 4 parallels the conclusion of Binks and Szwarc⁴ on methyl radical addition, and of Jennings and Cvetanović⁵ and Yang⁶ on hydrogen atom addition. The significance of this pattern of correlation was reviewed by Fueno.³² The atom localization energy is the energy required to disengage one electron from the

(19) R. S. Mulliken, C. A. Rieke, D. Orloff, and H. Orloff, *J. Chem. Phys.*, **17**, 1248 (1949).

(20) D. R. Lide, Jr., *Tetrahedron*, **17**, 125 (1962).

(21) B. Franzus, *J. Org. Chem.*, **28**, 2954 (1963).

(22) M. Traetteberg, *J. Am. Chem. Soc.*, **86**, 4265 (1964).

(23) O. Bastiansen, L. Hedberg, and K. Hedberg, *J. Chem. Phys.*, **27**, 1311 (1957).

(24) C. F. Wilcox, Jr., S. Winstein, and W. G. McMillan, *J. Am. Chem. Soc.*, **82**, 5450 (1960).

(25) T. Fueno, T. Tsuruta, and J. Furukawa, *J. Polymer Sci.*, **40**, 487 (1959).

(26) D. G. L. James and D. MacCallum, *Can. J. Chem.*, **43**, 633 (1965).

(27) D. G. L. James and T. Ogawa, *ibid.*, **43**, 640 (1965).

(28) A. C. R. Brown and D. G. L. James, *ibid.*, **43**, 1102 (1965).

(29) A. C. R. Brown and D. G. L. James, *ibid.*, **43**, 1110 (1965).

(30) D. G. L. James and G. E. Troughton, *J. Polymer Sci.*, **A3**, 75 (1965).

(31) D. G. L. James and S. M. Kambanis, unpublished results.

(32) T. Fueno, *Ann. Rev. Phys. Chem.*, **12**, 303 (1961).

Table I: Kinetic Data for the Addition of the Ethyl Radical to Various Substrates (B) Compared with the Corresponding Values of Atom Localization Energy and Free^a Valence

No.	Substrate (B)	Ref	$13 + \log k_1/nk_2^{1/2}$ (at 100°)	$13 + \log A_1/nA_2^{1/2}$	$E_1 - 1/2E_2$, kcal/mole	Localization energy, $-\beta$	Max free valence
1	Octene-1	23	1.03 ± 0.03	5.5 ± 0.1	7.6 ± 0.2	1.947	0.754
2	2-Methylpentene-1	23	1.24 ± 0.03	5.5 ± 0.2	7.3 ± 0.3	1.906	0.776
3	2,3-Dimethylbutadiene-1,3	24	2.69 ± 0.06	5.3 ± 0.2	4.5 ± 0.2	1.693	0.808
4	2,5-Dimethylhexadiene-2,4	24	1.02 ± 0.04	4.9 ± 0.2	6.6 ± 0.3	$\begin{cases} 1.791 C_2 \\ 2.136 C_3 \end{cases}$	$\begin{cases} 0.435 \\ 0.485 \end{cases}$
5	Cyclohexadiene-1,3	24	2.18 ± 0.04	5.2 ± 0.2	5.2 ± 0.3	1.760	0.615
6	Cycloheptatriene	25	1.83 ± 0.04	5.6 ± 0.2	6.4 ± 0.2	1.808	0.691
7	Cyclooctatetraene	25	1.11 ± 0.07	4.4 ± 0.2	5.6 ± 0.6	2.014	0.561
8	Bicycloheptadiene	25	1.12 ± 0.02	5.2 ± 0.1	7.0 ± 0.1	1.909	0.732
9	Styrene	22	2.56 ± 0.15	5.0 ± 0.3	4.1 ± 0.6	1.723	0.796
14	Vinyl acetate	22	1.28 ± 0.12	5.3 ± 0.3	6.9 ± 0.5	1.921	0.774
15	Vinyl <i>n</i> -butyl ether	22	1.20 ± 0.12	4.8 ± 0.3	6.1 ± 0.5	1.854	0.838
23	Acrylonitrile	22	3.17 ± 0.17	5.2 ± 0.3	3.4 ± 0.4	1.769	0.860
24	<i>cis</i> -Crotonitrile	23	1.72 ± 0.12	4.6 ± 0.3	5.0 ± 0.5	1.866	0.687
25	<i>trans</i> -Crotonitrile	23	1.83 ± 0.15	4.9 ± 0.3	5.2 ± 0.6	1.869	0.685

^a The units of k_1 and k_2 are $\text{cm}^3/\text{molecule sec}$; n denotes the number of equivalent most reactive sites for addition; limits of error are given at the 5% probability level.

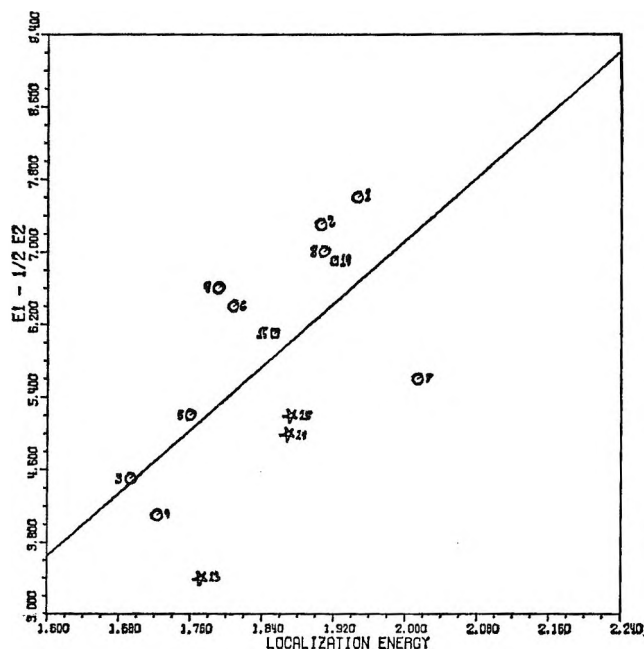


Figure 2. Correlation of activation energies for ethyl radical addition with localization energies.

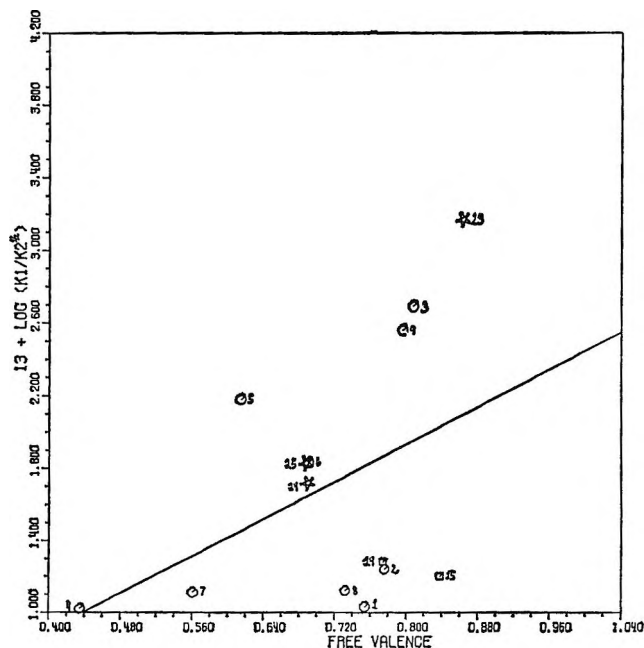


Figure 3. Correlation of rate of ethyl radical addition with free valences.

system and localize it at the chosen carbon atom. The localized species resembles the electron density pattern at an advanced stage in the reaction (certainly later than the transition state) at which incipient bond formation is largely completed. In contrast, free valence is an index of reactivity which describes the state of the reactants before mutual interaction has become

appreciable. Neither index is accurately matched to the configuration of the transition state, so that only approximate correlation should be expected at all. Nevertheless, the relative success of localization energy as an index indicates that the transition state resembles the products more closely than the reactants, for the addition of radicals of low electron affinity. Calcula-

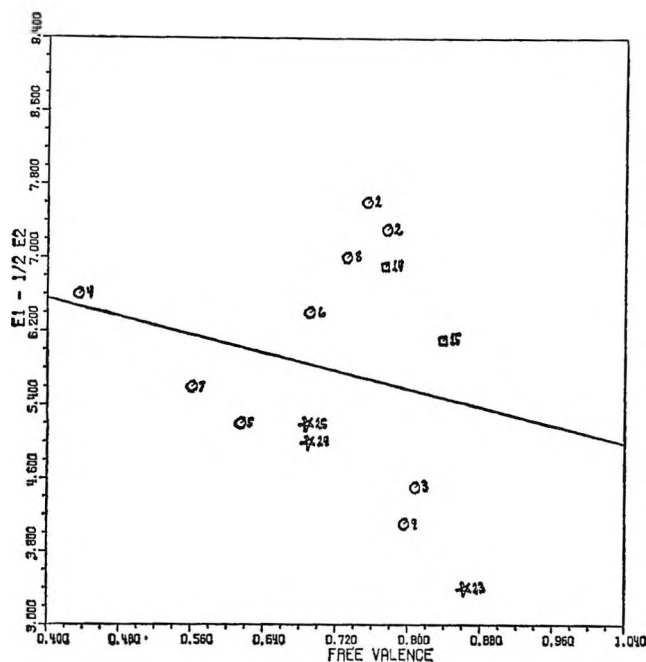


Figure 4. Correlation of activation energies for ethyl radical addition with free valences.

tions based upon an index of reactivity more appropriate to the transition state might seem to have a greater hope of success. The incremental stabilization energy of the transition state is such an index, and will be discussed below. First we shall enquire why the localization energy fails even as an approximate index of reactivity for certain substrates.

Each of the deviations of the hydrocarbons of Figures 1 and 2 may be rationalized. Cyclooctatetraene shows the greatest deviation; the molecule has equilibrium dihedral angles of 42.3° which severely restrict the extent of conjugation.^{22,23} The method of calculation requires that the geometry of the substrate should be unchanged in the transition state except at the reaction center. Any reduction in the dihedral angles during the formation of the transition state should increase the extent of conjugation and thereby reduce the observed activation energy below the predicted value, and indeed this is the direction of the observed deviation. Furthermore, cyclooctatetraene possesses a remarkably high electron affinity, and a planar configuration for the radical anion is consistent with the electron spin resonance spectral parameters, with the position of the disproportionation equilibrium, and with the rates of the electron exchange reactions.³³ Accordingly, any polar contribution to the transition state should also reduce the activation energy below the predicted value.

The deviation of the point for 2,5-dimethylhexadiene-2,4 is much smaller in Figure 2 than in Figure 1, indi-

cating a low preexponential factor for the addition. This is consistent with addition at either of the highly shielded equivalent atoms C_2 and C_5 , at which the localization energy is 1.791β . Pullman has suggested³⁴ that addition occurs preferentially at C_3 and C_4 , but the localization energy at these atoms is much greater at 2.136β , corresponding to an even greater deviation in the opposite direction. The observed deviations may be rationalized either (a) by accepting exclusive addition at C_2 and C_5 with an increment in the energy of activation associated with the penetration of the ethyl radical between the ethyl groups to the site of reaction or (b) by accepting simultaneous addition at C_3 and C_4 , C_2 and C_5 with a composite rate constant and an apparent intermediate energy of activation.

The parameters used for ethereal oxygen lead to a satisfactory degree of correlation for vinyl *n*-butyl ether and vinyl acetate, but there are considerable deviations for the nitriles. The fair correlation between the rate of methyl radical attack and localization energy for nitriles discussed in the next section indicate that the course of these deviations is not in the choice of theoretical parameters.

Methyl Radical Addition. Szwarc and his collaborators⁷⁻¹⁰ have compiled a large number of rate constants

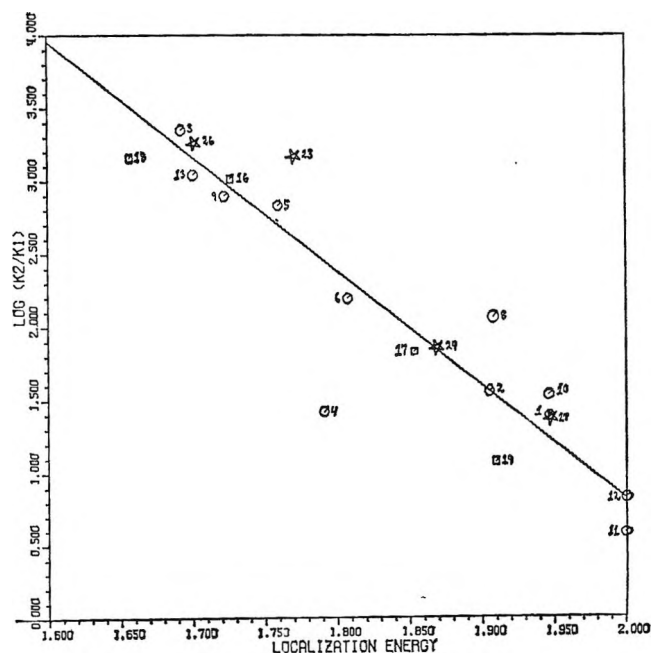


Figure 5. Correlation of methyl radical addition rates with localization energies.

(33) H. L. Strauss, T. J. Katz, and G. K. Fraenkel, *J. Am. Chem. Soc.*, **85**, 2360 (1963).

(34) B. Pullman, *J. Chim. Phys.*, **55**, 790 (1958).

for the addition of methyl radicals to conjugated systems. We have extended our calculations on the molecules of Table I to include four more olefins, four methyl esters, and two nitriles. The results for the localization energies, free valencies, and the experimental $\log k_2/k_1$ values are given in Table II. Our correlations between experiment and theory for these 24 substances are shown graphically in Figures 5 to 7. Comparison of Figures 5 and 7 shows clearly that the rate data correlates much better with localization energy than with free valence in accordance with our findings for the ethyl radical. The points for cyclooctatetraene, bicycloheptadiene, and 2,5-dimethylhexadiene-2,4 also behave, as for ethyl radical attack, in that they deviate from the best straight line, probably because of steric effects which are apparently more important than potential energy affects for these molecules.

Table II: Kinetic Data for the Addition of the Methyl Radical to Various Substrates and the Atom Localization Energies and Free Valences

No.	Substrate	Log k_2/k_1	Localization energy, $-\beta$	Free valence
1	Octene-1	1.389	1.947	0.754
2	2-Methylpentene-1	1.556 ^a	1.906	0.776
3	2,3-Dimethyl-1,3-butadiene	3.348	1.693	0.808
4	2,5-Dimethyl-2,4-hexadiene	1.431	1.791 C ₂ 2.136 C ₃	0.435 0.485
5	Cyclohexadiene-1,3	2.830	1.760	0.615
6	Cycloheptatriene	2.193	1.808	0.691
7	Cyclooctatetraene	1.908	2.014	0.561
8	Bicycloheptadiene	2.060	1.909	0.732
9	Styrene	2.899	1.723	0.796
10	Propylene	1.530	1.947	0.754
11	cis-2-Butene	0.580	2.000	0.574
12	trans-2-Butene	0.826	2.000	0.574
13	1,3-Butadiene	3.043	1.701	0.813
16	Methyl acrylate	3.013	1.727	0.875
17	Methyl crotonate	1.830	1.854	0.719
18	Methyl methacrylate	3.158	1.657	0.890
19	Methyl β,β -dimethylacrylate	1.077	1.910	0.529
23	Acrylonitrile	3.170	1.769	0.860
24	cis-Crotonitrile	1.860	1.866	0.687
25	trans-Crotonitrile		1.869	0.685
26	Methacrylonitrile	3.263	1.700	0.868
27	β,β -Dimethylacrylonitrile	1.371	1.946	0.507

^a Isobutene.

In Figure 7 we have compared the log of the relative rate constants for the ethyl radical attack with the corresponding quantities for methyl radical attack. Sev-

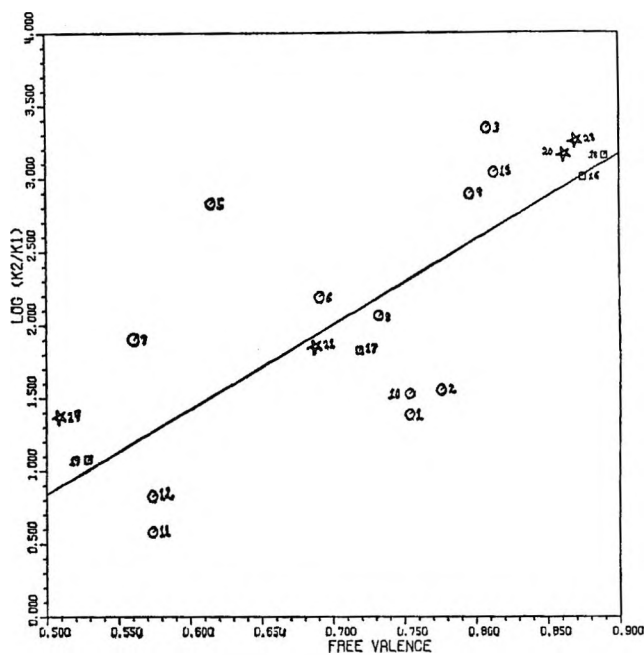


Figure 6. Correlation of methyl radical addition rates with free valences.

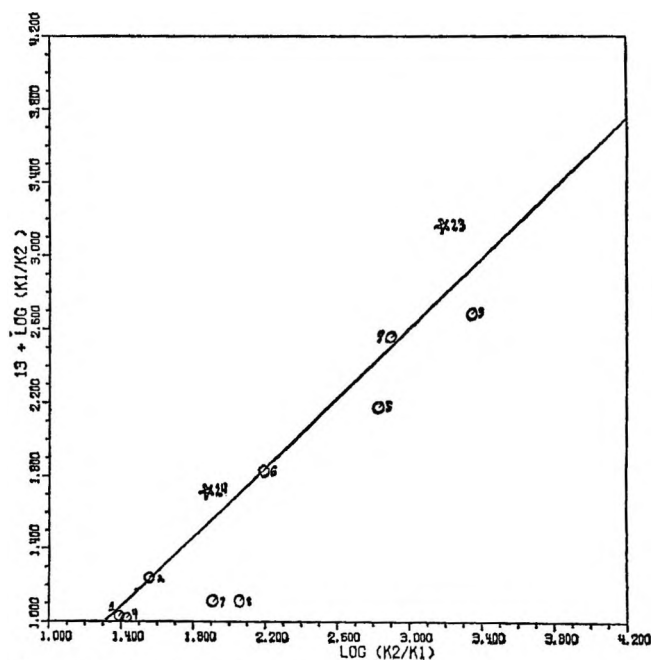


Figure 7. Correlation between rates of addition of methyl and ethyl radicals.

eral points deviate considerably from the regression line. The most serious deviations are for cyclooctatetraene and bicycloheptadiene, deviations which may be rationalized in terms of the different steric requirements in the transition state for ethyl and methyl radical attack. However, for the deviations of acrylonitrile,

cyclohexadiene-1,3, and 2,3-dimethylbutadiene, we can offer no explanation except to remark that the deviation is beyond that expected from the reported errors in the experimental measures. It is unfortunate that for molecules containing heteroatoms only acrylonitrile is common to both sets of data.

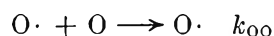
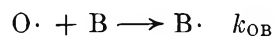
The data for methyl radical attack on conjugated nitriles and on acrylic methyl esters are fairly close to the regression line in Figure 6, implying that the poor fit for nitriles in the case of ethyl radical attack is not due entirely to a poor choice of parameters in the calculation of the localization energies. However, our choice of parameters is not an entirely happy one because they predict the nitriles to be slightly less reactive than the corresponding methyl esters whereas the experimental rate constants of Table II show the opposite trend. Nevertheless, the difference is very small and considering the crudeness of our adopted model we do think that the results are satisfactory and do not warrant further refinement.

Related Correlations. The ethyl radical, the methyl radical, and the hydrogen atom belong to a class of radical having low electron affinity and high ionization energy. The results of three other investigations⁴⁻⁶ support the conclusion of this study that localization energy is a much better index than free valence for the reactivity of olefinic compounds toward the addition of this class of free radical. However, Sato and Cvetic¹⁵ have presented evidence for the linear correlation of the logarithms of corrected relative rate constants for radical addition with the free valences of the olefins attacked. The apparent success of their graphical correlation should be accepted with reserve. First, the failure of the correlation with localization energy may arise from the comparison of a free energy term ($\log k$) with an internal energy term. The substrates are classified according to the degree of substitution at the carbon atoms of the double bond, and all degrees from 0 to 4 are represented. The attacking radicals are $\text{CH}_3\cdot$, $\text{CCl}_3\cdot$, and $\text{CH}_3\text{CH}_2\cdot$, and a considerable range of steric factors is certain.³⁵ Secondly, the correlation claimed for the addition of the ethyl radical is illusory, as the critical points for vicinal disubstituted ethylenes represent merely the maximum values which the rate constants could possess under the conditions prevailing in systems where *no* addition was detected.³⁵ Thirdly, the support lent by the behavior of the trichloromethyl radical may be ambiguous as it is an electrophilic radical, and the indices of reactivity appropriate to electrophilic reagents appear to be distinct from those appropriate to radicals of low electron affinity.¹⁵ The case for free valence must therefore depend upon the behavior of the methyl radical, and this behavior has

been interpreted as evidence for localization energy as an index of reactivity.⁴

We conclude that the atom localization energy is the index appropriate to the addition of alkyl radicals to olefinic compounds.

Radical Polymerization. The calculation of reactivity ratios r_0 for the radical copolymerization of ethylene (O) with a series of vinyl monomers (B) is closely related to the main theme of this investigation. With the usual assumption that the reactivity of a polymer radical is determined solely by its terminal unit, all polymer radicals terminating in an ethylene unit may be represented as $\text{O}\cdot$, and their propagation reactions written in the simple form



The ethyl radical is then a particular form of the polyethylene-type radical $\text{O}\cdot$, and the addition reaction



emerges as a particular example of the cross-propagation reaction given above. The reactivity ratio r_0 is defined as $k_{\text{OO}}/k_{\text{OB}}$, and we may expect a linear correlation between k_1 and $1/r_0$ at a common temperature. We have previously demonstrated this correlation for a diverse set of twelve monomers at 60°;²⁷ a line of unit gradient was fitted to a graph of $\log(1/r_0)$ against $\log(k_1 k_2^{1/2})$, and the degree of scatter of the points about the line is small although the magnitudes of the values span a range of 200:1.

The temperature dependence of the reactivity ratio is given by the equation.

$$r_0 = (A_{\text{OO}}/A_{\text{OB}}) \exp(E_{\text{OB}} - E_{\text{OO}})/RT \quad (3)$$

We shall show below that the activation energy term $E_{\text{OB}} - E_{\text{OO}}$ may be calculated, while experiment yields the corresponding term $E_1 - 1/2 E_2$. We can therefore attempt a more significant form of the correlation mentioned above by comparing the activation energies E_1 and E_{OB} .

Molecular orbital theory has been applied in two different forms to the calculation of reactivity ratios for the radical copolymerization of vinyl monomers. The β -carbon atom localization energy was chosen as a suitable index for the reactivity of a monomer by Fueno, *et al.*²⁴ The calculations of localization energy were less detailed than our own as the variation of the bond integral with bond length was not introduced, but the success of their correlation of the addition rate

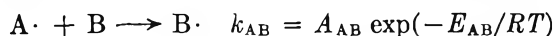
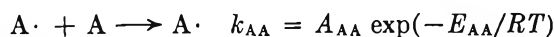
(35) D. G. L. James and E. W. R. Steacie, *Proc. Roy. Soc. (London)*, **A244**, 297 (1958).

constants with the localization energy parallels the conclusions of this paper.

The transition state is not accurately portrayed by models based upon localization energy or free valence as indices of reactivity. Recognition of this anomaly led to the adoption of a model based directly upon the transition state by Yonezawa, *et al.*,³⁶ and by Levinson.³⁷ These authors propose that conjugation occurs between the π -electron systems of the unsaturated molecule and the attacking radical in the transition state and that the activation energy of the addition reaction is simply related to the magnitude of the associated stabilization energy. In general the activation energy E may be expressed by the equation

$$E = C + \Delta E_{\sigma} + \Delta E_{\pi} \quad (4)$$

where C is a constant, and ΔE_{σ} and ΔE_{π} are increments associated with the systems of σ and π electrons, respectively. In a binary copolymerizing system of monomers A and B, the polymer radicals may be designated simply as $A\cdot$ and $B\cdot$. Four propagation reactions are possible, but the reactivity ratio r_A is defined as the ratio of the rate constant of two of them.



$$r_A = k_{AA}/k_{AB} = (A_{AA}/A_{AB}) \exp(E_{AB} - E_{AA})/RT \quad (5)$$

For such reactions, the activation energy may be rewritten in a simple generalized form, for example

$$E_{AB} = E_K - E_{AB}^* \quad (6)$$

The term E_K has a common value for all such reactions and includes the terms $C + \Delta E_{\sigma}$ of the equation above. The decrement E_{AB}^* has a specific value for each system and represents the stabilization energy due to conjugation of the π -electron systems of the radical and the monomer in the transition state. This stabilization energy E_{AB}^* is equal to the difference in the energy of the system $A\cdot + B$ when the exchange integral between the carbon atoms which ultimately form the new bond has a value appropriate to the transition state and when it has the value of 0 appropriate to separated reactants. The reactivity ratio r_A may therefore be related to the difference in the corresponding stabilization energies by the equation

$$-RT \ln r_A = E_{AB}^* - E_{AA}^* \quad (7)$$

if we may assume that $(A_{AA}/A_{AB}) = 1$. The validity of this relationship has been confirmed graphically in the form indicated by the equation, using experimental values of r_A ; the points showed only small deviations from a linear relationship. Yonezawa, *et al.*,¹¹ have

calculated the stabilization energies by the second-order perturbation method. Levinson³⁷ has applied simple molecular orbital theory to the calculation by assigning a value of 0.4β to the bond integral of the incipient bond in the transition state. The accuracy of the latter method was tested by comparing calculated and experimental reactivity ratios for 38 systems of fully representative diversity. Although the reactivity ratios span a range of 2000:1, the greatest error in the predicted values is a factor of only 3. The close correlation observed for both methods of calculation indicates that each provides a reasonably satisfactory model for the transition state.

Further progress³⁸ resulted from the adoption of ethylene (O) as the reference monomer and the separation of the general stabilization energy E_{AB}^* into four separate terms

$$E_{AB}^* = E_{OO}^* + \Delta E_{AO}^* + \Delta E_{OB}^* + \Delta E_{AB}^{\circ} \quad (8)$$

The term E_{OO}^* is the stabilization energy for the system $O\cdot + O$, ΔE_{AO}^* is the increment of this stabilization energy for the system $A\cdot + O$, and ΔE_{OB}^* is the corresponding increment for the system $O\cdot + B$. These increments were associated³⁸ with the parameters of the revised¹² Q - e scheme

$$\ln(Q_A'/Q_B') = (\Delta E_{OA}^* - \Delta E_{OB}^*)/RT \quad (9)$$

$$\ln(P_A'/P_B') = (\Delta E_{AO}^* - \Delta E_{BO}^*)/RT \quad (10)$$

This revised scheme is based upon the values $Q' = 1.00$ and $e' = 0.00$ for styrene; the constancy of the parameters P' and Q' for a particular monomer in a variety of systems was established on this basis. The fourth term ΔE_{AB}° has been called the "surplus stabilization energy" and is related to the revised composite polarity term e_{AB} by the equation^{8,39}

$$\Delta E_{AB}^{\circ} = -RTe_{AB}'$$

The stabilization energy for the addition of a polymer radical terminating in an ethylene unit ($O\cdot$) to a monomer molecule (B) is given by the simplified equation

$$E_{OB} = E_{OO}^* + \Delta E_{OB}^* \quad (11)$$

in which the surplus stabilization energy ΔE_{OB}° is 0.³⁶ The activation energy for this class of reaction may therefore be written in the form of relationship 12

(36) K. Hayashi, T. Yonezawa, C. Nagata, S. Okamura, and K. Fukui, *J. Polymer Sci.*, **20**, 537 (1956).

(37) G. S. Levinson, *ibid.*, **60**, 43 (1962).

(38) N. Kawabata, T. Tsuruta, and J. Furukawa, *Makromol. Chem.*, **51**, 80 (1962).

(39) N. Kawabata, T. Fueno, T. Tsuruta, and J. Furukawa, *Bull. Chem. Soc. Japan*, **36**, 1168 (1963).

$$E_{OB} = E_K + E_{OB}^* = E_{KO} + \Delta E_{OB}^* \quad (12)$$

where E_{KO} has a common value for all systems of the type $O \cdot + B$. Simple copolymerization theory allows us to treat the ethyl radical as a particular example of the radical class $O \cdot$. Equation 12 may then be applied to systems of the type $CH_3CH_2 \cdot + B$, and we may expect $E_1 - 1/2E_2$ to be linearly related to ΔE_{OB}^* . Figure 8 presents a test of this relationship. The values of ΔE_{OB}^* were calculated³⁶ by a simple LCAO molecular orbital method and are given in Table III. The degree of correlation found in Figure 8 is not appreciably greater than that found in Figure 2, although the structural diversity of the substrates of Figure 2 is much greater. This is perhaps surprising, as the method underlying Figure 8 alone treats the transition state directly. We may infer that the inadequacies of our own model, based upon localization energy, are of secondary importance.

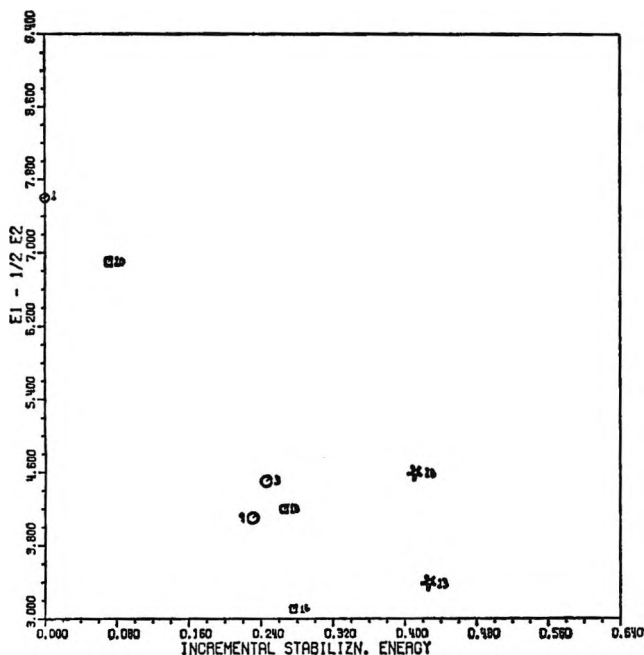


Figure 8. Correlation between activation energy for ethyl radical addition and incremental stabilization energy ΔE_{OB}^* of the transition state, in units of $-(\Delta\beta)^2/\beta$.

The revised intrinsic reactivity parameter Q_B' is related to ΔE_{OB}^* by the equation

$$\log Q_B' = \log Q_0' + \Delta E_{OB}^*/2.3RT \quad (13)$$

which is obtained from 9 by using the definition $\Delta E_{OO}^* = 0$. We may therefore devise a test of the proposed linear relationship between ΔE_{OB}^* and $E_1 - 1/2E_2$ which is independent of the choice of parameters for

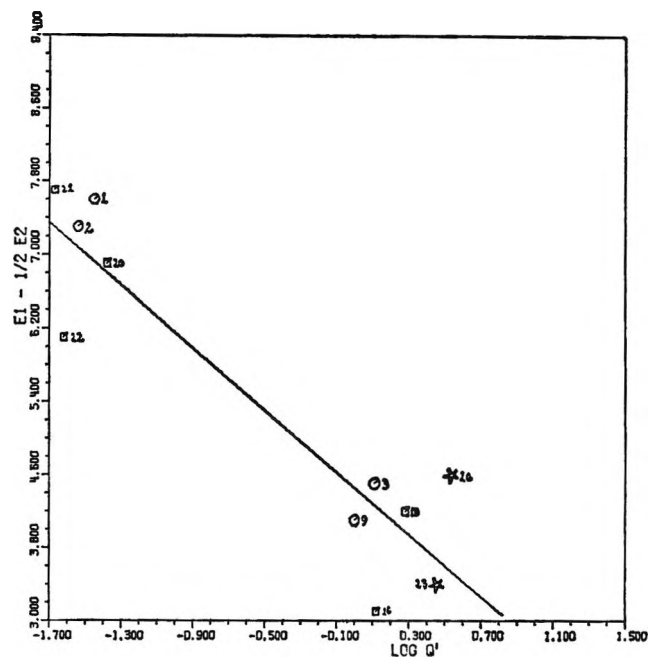


Figure 9. Correlation between the activation energy for ethyl radical addition and the intrinsic reactivity parameter Q' . The reference is styrene ($Q' = 1.00$, $e' = 0.00$).

heteroatoms. This is shown in Figure 9, which is a plot of $E_1 - 1/2E_2$ against $\log Q_B'$. For common substrates the degree of correlation is greater than in Figure 8, suggesting that inadequate parameters for heteroatoms cause the main deviations found in that diagram. Figure 9 reveals a reasonably good general correlation between the activation energy E_1 and the experimental intrinsic reactivity parameter Q_B' .

Burkhart and Zutty have proposed^{13,40} a revision of the Q - e scheme based upon ethylene as the reference monomer with $Q_0^0 = 1.00$ and $e_0^0 = 0.00$. In principle the activation energy $E_1 - 1/2E_2$ should show greater correlation with $\log Q_B^0$ than with $\log Q_B'$, but Figure 10 is no better than Figure 9. This is not remarkable as nearly all the values of Q_B^0 used in Figure 10 are determined indirectly and are subject to larger error. When directly determined values of Q_B^0 are available we may expect Figure 10 to show the greater correlation.

Figure 11 shows that $E_1 - 1/2E_2$ is poorly correlated with $\log Q_B$, where Q_B is the original Alfrey-Price parameter based upon styrene as a reference monomer with $Q = 1.00$ and $e = -0.80$. A comparison of Figures 9 and 11 lends very little support to the view that Q_B' is the better index of reactivity and that a system based upon styrene with $Q' = 1.00$ and $e' =$

(40) R. D. Burkhart and N. L. Zutty, *Makromol. Chem.*, **67**, 219 (1963).

Table III: The Activation Energy for the Addition of the Ethyl Radical to Various Substrates (B) Compared with the Increment of Conjugation Stabilization Energy in the Transition State and Various Forms of the Intrinsic Reactivity Parameter of Copolymerization Theory

No.	Substrate (B)	Ref	$E_1 - 1/2E_2$, kcal/mole	ΔE_{OB}^* , $-(\Delta\beta)^2/\beta$	Log Q'	Log Q^0	Log Q
1	Octene-1	23	7.6 ± 0.2	0.000 ^a	$\bar{2}.55^c$	$\bar{1}.83^c$	$\bar{2}.28^c$
2	2-Methylpentene-1	23	7.3 ± 0.3	...	$\bar{2}.46^d$	$\bar{1}.94^d$	$\bar{2}.52^d$
3	2,3-Dimethylbutadiene-1,3	24	4.5 ± 0.2	0.246 ^b	0.11 ^b	1.78 ^b	0.38 ^b
9	Styrene	22	4.1 ± 0.6	0.231	0.00	1.45	0.00
14	Vinyl acetate	22	6.9 ± 0.5	0.071	$\bar{2}.62$	$\bar{1}.97$	$\bar{2}.42$
6	Allyl acetate	31	7.7 ± 0.5	...	$\bar{2}.33$	$\bar{1}.84$	$\bar{2}.45$
15	Vinyl <i>n</i> -butyl ether	22	6.1 ± 0.5	...	$\bar{2}.38^e$	$\bar{1}.89^e$	$\bar{2}.50^e$
23	Acrylonitrile	22	3.4 ± 0.4	0.424	0.44	1.57	$\bar{1}.76$
26	Methylacrylonitrile	23	4.6 ± 0.7	0.409	0.52	1.72	$\bar{1}.91$
16	Methyl acrylate	30	3.1 ± 0.3	0.276	0.12	1.35	$\bar{1}.64$
18	Methyl methacrylate	30	4.2 ± 0.3	0.266	0.28	1.55	$\bar{1}.88$

^a Ethylene. ^b Butadiene-1,3. ^c Hexene-1. ^d Isobutene. ^e Vinyl ethyl ether.

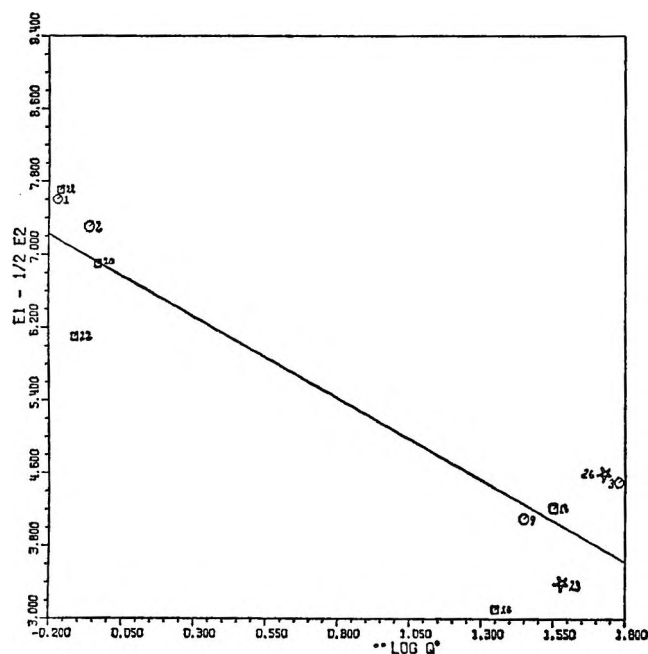


Figure 10. Correlation between the activation energy for ethyl radical addition and the intrinsic reactivity parameter Q^0 . The reference is ethylene ($Q^0 = 1.00$, $e' = 0.00$).

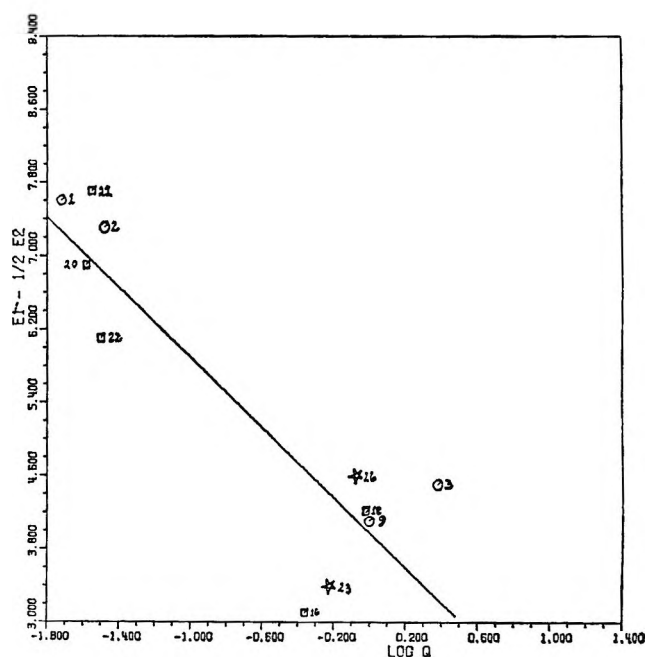


Figure 11. Correlation between the activation energy for ethyl radical addition and the intrinsic reactivity parameter Q . The reference is styrene ($Q = 1.00$, $e = -0.80$).

0.00 has inherent advantages, but this may be due to paucity of data.

The validity of Q' as an index of reactivity depends upon a simple relationship with the incremental stabilization energy such as that expressed in eq 9 and 13. The derivation of these equations depends in turn upon a uniformity of the preexponential factors of the appropriate addition reactions. This limits the usefulness of Q' to correlations involving substrates having a simi-

lar pattern of substitution at the double bond, and indeed the substrates of Table II are all unsubstituted at the terminal carbon atom. As an index of reactivity Q' therefore shares the limitations of K_1/n and lacks the generality of ΔE_{OB}^* or E_1 .

Each of the theoretical indices of reactivity suffers a common disadvantage when applied to the conjugated nitriles as the treatment commonly employed for the nitrile group is inadequate. The special theoretical

advantage of using a model for the addition reaction based upon the transition state appears to be lost in the process of calculation. We conclude that the model based upon localization energy seems in its simplicity to offer the greatest promise for the calculation of an index of reactivity of a molecule toward the addition of free radicals.

Acknowledgments. We wish to thank Dr. P. N. Daykin of the British Columbia Research Council and Miss M. R. O'Donnell and Mr. D. Lee of the Mond Division of Imperial Chemical Industries Limited for performing part of the computation, and the National Research Council of Canada for financial assistance and a studentship to A. C. R. B.

Triplet State Zero-Field Splittings of Some Structurally Related Aromatic Hydrocarbon and Heterocyclic Molecules¹

by Seymour Siegel and Henry S. Judeikis

Aerospace Corporation, El Segundo, California (Received December 21, 1966)

The triplet state zero-field splitting parameters D and E have been determined from the $\Delta m = \pm 1$ epr spectra of the photoexcited triplet states of several structurally related aromatic hydrocarbons and aromatic heterocyclic molecules, using diethyl ether glasses at 77°K. The values of the splitting parameters in cm^{-1} for the various molecules are as follows: biphenyl, $D = 0.1092$, $E = 0.0036$; fluorene, $D = 0.1075$, $E = 0.0033$; carbazole, $D = 0.1022$, $E = 0.0066$; dibenzofuran, $D = 0.1071$, $E = 0.0092$; dibenzothiophen, $D = 0.1130$, $E = 0.0021$. The uncertainties in these numbers are ± 0.2 mK for D and ± 0.1 mK for E . Lifetimes of the triplet states were also determined. A discussion of the results in terms of conjugation of the heteroatom with the aromatic rings is given. Also, the results are compared to the published values of D and E for phenanthrene. It is found that biphenyl is a better hydrocarbon model than phenanthrene for the heterocyclics investigated in this paper.

I. Introduction

The utility of electron paramagnetic resonance (epr) spectroscopy for studying triplet state molecules was considerably increased by the observation that the epr spectra of randomly oriented triplet state molecules gave special significance to those molecules where the principal axes of the electron dipolar spin-spin interaction tensor were parallel to the direction of the applied magnetic field.² It was no longer necessary to have single crystal hosts to determine the separation of the magnetic sublevels of the triplet state experimentally. The data obtained when using noncrystal-

line rigid media are not as accurate as that obtained when using appropriate single crystals; however, the number of suitable host single crystals available is small, and the accuracy of the glass or plastic technique is sufficient for many purposes. The major drawback of using noncrystalline host media is that it is not usually possible to determine the hyperfine interaction energies between the triplet state electrons and the

(1) This work was supported by the U. S. Air Force under Contract No. AF 04(695)-669.

(2) W. A. Yager, E. Wasserman, and R. M. R. Cramer, *J. Chem. Phys.*, **37**, 1148 (1962).

various nuclear magnetic moments present in the molecule.

The effective spin Hamiltonian for a triplet state molecule in a magnetic field may be written as

$$\mathcal{H} = \beta \vec{H} \cdot \vec{g} \cdot \vec{S} + DS_z^2 + E(S_x^2 - S_y^2) - \frac{2}{3}D \quad (1)$$

where the constants D and E can be obtained directly from the $\Delta m = \pm 1$ epr spectra and x , y , and z are a principal axes coordinate system. The constants are the zero-field splitting parameters and are related to the spatial distribution of the two triplet electrons over the molecule. For two electrons, when we consider mutual dipolar interactions and ignore spin-orbit interactions, the zero-field parameters can be expressed as

$$D = \frac{3}{4}g_e\beta^2 \langle \varphi(1,2) | r_{12}^{-2} - 3z_{12}^2 | \varphi(1,2) \rangle \quad (2)$$

$$E = \frac{3}{4}g_e\beta^2 \langle \varphi(1,2) | y_{12}^2 - x_{12}^2 | \varphi(1,2) \rangle$$

where g_e is the free electron "g" value and the quantities in brackets are averages of the interelectronic distances, and corresponding vector components in the principal axes system, taken over the antisymmetric spatial portion of the two-electron wave function.³ The particular labeling of the molecular axes is somewhat arbitrary. However, for molecules of sufficient symmetry, a natural choice usually presents itself. For planar molecules, z is usually chosen parallel to the normal to the molecular plane.

This paper presents the results of the experimental determination of the values of zero-field parameters for the photoexcited, lowest triplet states of the structurally related molecules shown in Figure 1. The particular assignment of a molecular axes system used in the analysis is also given in Figure 1. Assignment of the epr spectral transitions to the correct molecular axes was made with the aid of the optical polarization effects discussed in the following paper. Similarities between the ultraviolet absorption spectra of the heterocyclics in Figure 1 and that of phenanthrene (R = —HC=CH—) has been discussed in several places.^{4,5} The equivalence of the heteroatom to a —HC=CH— group instead of CH₂ group has been emphasized.⁵ The results of the D and E determinations are discussed in terms of this postulated equivalence; it will be shown that, for triplet states, biphenyl is a better hydrocarbon model molecule than phenanthrene for the heterocyclics.

II. Experimental Details and Results

A Varian X-band epr spectrometer was used to observe the $\Delta m = \pm 1$ and ± 2 transitions of the photoexcited triplet state molecules. Details of the epr spectrometer and optical excitation configuration

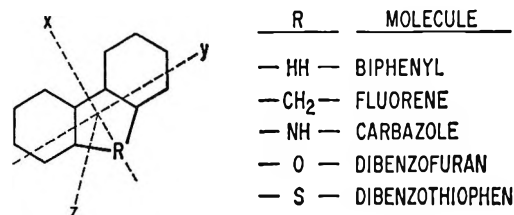


Figure 1. Molecules studied and principal axes system used in analysis.

are given elsewhere.⁶ The lifetimes of the triplet state molecules were measured by observing the dark decay of the phosphorescent optical emission and the $\Delta m = \pm 2$ epr transition intensities. All measurements were made at 77°K, using 10^{-2} M solutions of the aromatic molecules dissolved in Baker Analyzed reagent grade diethyl ether; the solutes were either Eastman White Label or Chemical Procurement Laboratories research quality chemicals. Magnetic field measurements were made with a Numar Model M-2 nmr precision gaussmeter, an HP Model 524C electronic counter, and an HP Model 525A frequency converter plug-in unit. Approximate measurement of the epr klystron frequency was obtained with an HP Model X532B frequency meter; an HP Model 540B transfer oscillator and the electronic counter with an HP Model 525B plug-in unit were used for accurate klystron frequency determinations.

The values of the zero-field splitting constants D and E , as well as the values of g_{xx} , g_{yy} , g_{zz} where g_{ii} is the component of the g tensor in eq 1 along the i th principal axis, were determined using the equations developed by Wasserman, Snyder, and Yager.⁷ Determination of g_{xx} , g_{yy} , and g_{zz} gave values in the range 2.0023 to 2.0035 with an experimental uncertainty of ± 0.0015 in each g value. Therefore, within the experimental uncertainty, the g tensor is isotropic, and there was no evidence of contributions from spin-orbital interactions to the g values for these molecules. The experimentally determined values of D and E are given in Table I; the experimental precision indicated in the table arises mainly from the large line widths of the epr lines which preclude the determination of

(3) J. H. van der Waals and M. S. de Groot, *Mol. Phys.*, **2**, 333 (1959); **3**, 190 (1960).

(4) G. M. Badger and B. J. Christie, *J. Chem. Soc.*, 3438 (1956).

(5) H. H. Jaffé and M. Orchin, "Theory and Applications of Ultraviolet Spectroscopy," John Wiley and Sons, Inc., New York, N. Y., 1962, pp 353-361.

(6) (a) S. Siegel and H. S. Judeikis, *J. Chem. Phys.*, **41**, 648 (1964);

(b) S. Siegel and K. B. Eisenthal, *ibid.*, **42**, 2494 (1965).

(7) E. Wasserman, L. C. Snyder, and W. A. Yager, *ibid.*, **41**, 1763 (1964).

specific line shape positions to better than ± 0.5 gauss. Also included in Table I are the results of the lifetime measurements. Both the phosphorescent emission and epr ($\Delta m = \pm 2$ transitions) dark decay curves were found to be exponential, and the lifetimes derived from both techniques were equivalent (within experimental error). Most of the lifetimes have been reported elsewhere^{8,9} and are in good agreement with the present results.

Table I: Zero-Field Splitting Parameters and Lifetimes

Molecule	D, cm^{-1} ($\pm 0.2 \text{ mK}$) ^a	E, cm^{-1} ($\pm 0.1 \text{ mK}$) ^a	τ, sec ($\pm 0.2 \text{ sec}$) ^b
Phenanthrene	0.10044	0.04657	3.7
Biphenyl	0.1092	0.0036	4.4
Fluorene	0.1075	0.0033	6.3
Carbazole	0.1022	0.0066	7.7
Dibenzofuran	0.1071	0.0092	5.9
Dibenzothiophen	0.1130	0.0021	1.3

^a The phenanthrene data were taken from the literature (an certainty $\pm 0.02 \text{ mK}$ is given) and were obtained using a biphenyl single crystal as a host. (See R. W. Brandon, R. E. Gerkin, and C. A. Hutchison, Jr., *J. Chem. Phys.*, **37**, 447 (1962); **41**, 3717 (1964).) With the axis labeling in Figure 1, D and E for phenanthrene are both positive since D is positive and E negative if x and y are interchanged. (See Brandon, *et al.*) The other values of D and E are absolute values because the sign of the parameters cannot be obtained from glass data at 77°K ; however, there is no reason to assume any change from phenanthrene; therefore, D and E are most likely both positive in this axis system for all the molecules studied here. ^b The phosphorescent emission lifetimes are given; however, the lifetimes derived from the epr data are identical, within experimental error.

From the $\Delta m = \pm 2$ transitions, only a combination of the zero-field parameters³ can be determined directly for these molecules, *i.e.*, $D^* = (D^2 + 3E^2)^{1/2}$. The values of D^* , determined directly from the $\Delta m = \pm 2$ transitions, are given in Table II; values of D^* , determined from the values of D and E in Table I, are also given in Table II. There seems to be a systematic discrepancy in the results obtained by the two methods, with the values obtained from the $\Delta m = \pm 2$ transitions being uniformly larger by 1.0 to 1.5 mK. This discrepancy could arise, in part, from experimental measurement error; however, the uniformity of the trend indicates that the specific choice of the maximum of the derivative line shape of the $\Delta m = \pm 2$ transition or that another more fundamental cause may also be involved.

III. Discussion

The assignment of the ultraviolet absorption bands

of the heterocyclic molecules discussed here to π, π^* transitions have been made in various places^{4,10} (including ref 11) by analogy to the spectra of the aromatic hydrocarbons. Similar arguments have been used to assign the phosphorescent triplet-singlet emission for the heterocyclics to π, π^* transitions.¹⁰ The data in Table I agree with the π, π^* assignments for the triplet state of these molecules, considering the general similarity of the values of D and E for the hydrocarbons and heterocyclics. The magnetic z direction is shown to be perpendicular to the molecular plane, as is expected for π, π^* triplet states. The long lifetimes shown in Table I are also consistent with π, π^* triplet state assignments.

The most striking aspect of the values of D and E is the large differences between the symmetry of the electron spin distribution in phenanthrene and the symmetry in the heterocyclic aromatics, as reflected by the large differences in the E values. Alternatively, the electronic distributions in the heterocyclic aromatics are very similar to those in biphenyl and fluorene. From the conclusion that the triplet states of the heterocyclics are very similar to the triplet state of biphenyl and quite different from that of phenanthrene, as far as the electronic spatial distribution is concerned, it can be further concluded that the heteroatoms do not enter into any appreciable degree of conjugation with the aromatic rings. In fact, the small value of E observed for dibenzothiophen indicates that sulfur is least effective in introducing added conjugation. The latter conclusion is opposite to that which one would predict on the basis of the relative electronegativities of the heteroatoms. Sulfur has essentially the same electronegativity as carbon and has d orbitals available for partial double bonding; therefore, sulfur might be expected to have the most conjugation. However, sulfur is a large atom and the resultant strain on the molecule may change the geometry sufficiently so that conjugation is minimized. Also, sulfur does not form double bonds easily.

The trend in the values of D given in Table I also indicates that there is the least conjugation in the thiophen because it has the largest value of D . The large value of D reflects a greater concentration of electron density in the two rings, thereby decreasing the average value of r_{12} and increasing the value of the dipolar interaction. Therefore, the geometry of the

(8) D. S. McClure, *J. Chem. Phys.*, **17**, 905 (1949).

(9) A. N. Terenin and V. L. Ermolaev, *Izv. Akad. Nauk SSSR Ser. Fiz.*, **26**, 21 (1962).

(10) R. N. Nurmukhametov and G. V. Gobov, *Opt. i Spektroskopia*, **18**, 227 (1965).

(11) S. Siegel and H. S. Judeikis, *J. Phys. Chem.*, **70**, 2205 (1966).

Table II: Magnitude of $D^* = (D^2 + 3E^2)^{1/2}$

Molecule	D_1^* , cm ^{-1a}		D_2^* , cm ^{-1b}			$D_2^* - D_1^*$, mK
	This work (±0.2 mK)	Brandon ^c (±.04 mK)	This work (±0.1 mK)	Smaller ^d (±1.5 mK)	Thomson ^e (±0.4 mK)	This work (±0.3 mK)
Phenanthrene	...	0.12882	...	0.1335	0.1336	...
Biphenyl	0.1094	...	0.1107	0.1130	0.1111	1.3
Fluorene	0.1076	...	0.1092	0.1096	0.1088	1.6
Carbazole	0.1028	...	0.1043	0.1044	0.1063	1.5
Dibenzofuran	0.1082	...	0.1092	1.0
Dibenzothiophen	0.1131	...	0.1144	1.3

^a D_1^* calculated using D and E values in Table I. ^b D_2^* calculated from $D_2^* = (1/hc)[(\delta/4)(h\nu)^2 - 3(g\beta H_m)^2]^{1/2}$ where ν is the klystron frequency and H_m is the field position of the low-field maximum of the $\Delta m = \pm 2$ epr transition derivative spectrum (see ref 3). ^c See Brandon, *et al.*, ref *a* in Table I. ^d Methanol or EPA at 77°K used as the host medium. See B. Smaller, *J. Chem. Phys.*, **37**, 1578 (1962). ^e Poly(methyl methacrylate) used as the host medium. See C. Thomson, *ibid.*, **41**, 1 (1964).

triplet state of the dibenzothiophen must be such that the two rings are somewhat nonplanar or the C-C bond between rings is somewhat bent compared to that in biphenyl and the other heterocyclics. Ordering of the molecules in Figure 1 according to the increasing degree of conjugation, as reflected by the magnitude of D , can be given as dibenzothiophen, biphenyl, fluorene, dibenzofuran, carbazole, and phenanthrene.

It must be emphasized that this discussion is based on a simple model of a pure π, π^* electronic distribution. More subtle effects such as configuration interactions are, by necessity, completely neglected. Also, more

obvious effects such as geometry and symmetry changes in the triplet states of these molecules as the nature of the R group changes have not been considered since these geometries are not available. However, within the limitations of the simple model, the data presented here indicate that biphenyl is a better hydrocarbon model molecule than phenanthrene for the discussion of the absorption spectra of the heterocyclic aromatics. This conclusion is in agreement with that made by Nurmukhametov and Gobov on the basis of their recent detailed studies of the fluorescence and phosphorescence spectra¹⁰ of these molecules.

A Magnetophotoselection Study of the Polarizations of the Absorption Bands of Some Structurally Related Hydrocarbons and Heterocyclic Molecules¹

by Seymour Siegel and Henry S. Judeikis

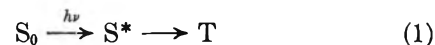
Aerospace Corporation, El Segundo, California (Received December 21, 1965)

The polarizations of the long wavelength electronic absorption bands of the molecules phenanthrene, biphenyl, fluorene, carbazole, dibenzofuran, and dibenzothiophen have been determined by the method of magnetophotoselection. Also, the polarizations of the next higher absorption bands have been estimated for phenanthrene, carbazole, and dibenzothiophen. In general, the results agree with theory. The bands belonging to the heterocyclic molecules have been assigned to ¹L_a and ¹L_b designations on the basis of the polarization results. The results are discussed briefly.

I. Introduction

The electronic absorption and emission spectra of many molecules containing one or more benzene rings fused to a five-membered heterocyclic system have been reported.²⁻⁴ However, the interpretation and correlation of the heterocyclic spectra have been quite difficult. In general, only qualitative trends have been obtained, and assignments of the spectra to π, π^* transitions have been made by analogy with the spectra of structurally similar aromatic hydrocarbon molecules. In this paper, the method of magnetophotoselection⁵⁻⁷ is used to determine the polarization of the long wavelength electronic absorption bands of several structurally related aromatic hydrocarbons and heterocyclic molecules. The molecules studied are given in Figure 1 along with the axis system used in the analysis. For some of the molecules, estimates are also given of the polarizations of the next highest transitions. The molecules studied are the same ones for which the zero-field splitting parameters of the triplet states were determined in the preceding paper.⁸

The advantage of using the magnetophotoselection method is that the $\Delta m = \pm 1$ electron paramagnetic resonance (epr) spectrum of triplet-state molecules dissolved in a rigid glass gives overwhelming prominence to the molecules oriented so that one of the principal axes of the electron spin-spin dipolar coupling tensor is parallel to the applied magnetic field.^{9,10} For the experiments in this study, the triplet states are populated by the intramolecular sequence



If polarized light is used to excite the populating $S_0 \rightarrow S^*$ transition, the relative intensities of the epr transitions will be directly related to the fraction of the polarization of the optical transition carried along each molecular axis if certain conditions are satisfied.^{7,11} The necessary conditions which concern intra- and intermolecular processes, molecular symmetry, and molecular motions are given in a previous paper,⁷ and these conditions were met to a satisfactory approximation in the experiments being described here. When the polarization of the electric vector E of the exciting light is parallel to the direction of the external magnetic

(1) This work was supported by the U. S. Air Force under Contract No. AF 04(695)-669.

(2) R. N. Nurmukhametov and G. V. Gobov, *Opt. i Spektroskopia*, **18**, 227 (1965).

(3) G. M. Badger and B. J. Christie, *J. Chem. Soc.*, 3438 (1956).

(4) H. H. Jaffé and M. Orchin, "Theory and Applications of Ultraviolet Spectroscopy," John Wiley and Sons, Inc., New York, N. Y., 1962, pp 347-361.

(5) M. A. El-Sayed and S. Siegel, *J. Chem. Phys.*, **44**, 1416 (1966).

(6) S. Siegel and L. Goldstein, *ibid.*, **43**, 4185 (1965).

(7) S. Siegel and L. Goldstein, "A Study of Triplet-Triplet Transfer by the Method of Magnetophotoselection: II. Concentration Depolarization," Aerospace Corp. Report No. TDR-669(6250-20)-2, Dec 1965; also *J. Chem. Phys.*, in press.

(8) S. Siegel and H. S. Judeikis, *J. Phys. Chem.*, **70**, 22C1 (1966).

(9) E. Wasserman, L. Snyder, and W. A. Yager, *J. Chem. Phys.*, **41**, 1763 (1964).

(10) P. Kottis and R. Lefebvre, *ibid.*, **41**, 379 (1964).

(11) P. Kottis and R. Lefebvre, *ibid.*, **41**, 3660 (1964).

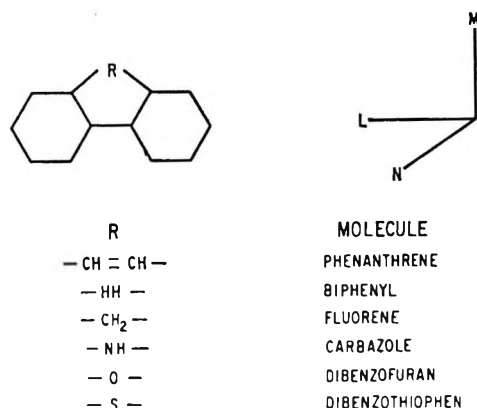


Figure 1. Molecules studied and principal axes system used in analysis.

field H , the intensity I_i of the $\Delta m = \pm 1$ epr transition corresponding to any one of the three canonical orientations is proportional to the number of excited triplet state molecules $N_i^\delta(\parallel)$ which have their i th molecular axis at the correct observational angle $\theta_{iH} \leq \delta$. Because the i th axis must be essentially parallel⁹ to H for its corresponding epr transition to be observed in the usual derivative epr spectrum, the magnitude of δ must be very small (*i.e.*, $\theta_{iH} \approx 0$). When the assumption that the probability of observation is unity for $\theta_{iH} \leq \delta$ and zero for all other values of δ is used, expressions are derived in the Appendix for $N_i^\delta(\parallel)$ and $N_i^\delta(\perp)$ (where the latter term is the number of excited molecules with $\theta_{iH} \leq \delta$ and $H \perp E$).

If the magnitudes of the incident light intensity are equal in the two polarization directions, then the use of eq A5 and A6 yields an expression for the usual polarization ratio P_i as follows

$$P_i = \frac{N_i^\delta(\parallel) - N_i^\delta(\perp)}{N_i^\delta(\parallel) + N_i^\delta(\perp)} = \frac{I_i(\parallel) - I_i(\perp)}{I_i(\parallel) + I_i(\perp)} = \frac{3r_i - 1}{1 + 4/3k + r_i} \quad (2)$$

where M , N , and L are the molecular axes defined in Figure 1, r_i is the component of the polarization of the optical populating transition carried along the i th molecular axis, and k is a constant introduced to include the percentage of depolarized (*i.e.*, isotropic) light present or other depolarizing effects. The data will be analyzed in terms of eq 2.

II. Experimental Section

The epr spectrometer and optical excitation configuration used in this study have been described elsewhere.^{5,12} The sample container consisted of a 4-mm o.d. quartz tube that had been flattened at one end to an

approximate rectangular shape. This crudely fashioned cell was found to be adequate for this study. The tube was placed in a quartz liquid nitrogen dewar with an unsilvered tip directly in the epr cavity. All measurements were made at 77°K. Solutions were prepared from Baker Analyzed reagent grade diethyl ether, and the solutes were either Eastman White Label or Chemical Procurement Laboratories research quality chemicals.

The concentrations used were all 0.003 M (room-temperature concentrations). This concentration was sufficiently high, because of the long triplet state lifetimes involved,⁸ to permit accurate measurements of the $\Delta m = \pm 1$ epr lines; it was also high enough to avoid uncertainties arising from photochemical effects related to sensitized solvent decomposition.¹³ Yet, the concentration used was sufficiently low to avoid complications from intermolecular triplet-triplet energy transfer.⁷

The transmission characteristics of the filter combinations used between the exciting lamp (PEK-500 high-pressure mercury arc) and the sample were determined with the use of a Cary 15 spectrophotometer and are given in Figure 2. The absorption spectra of the solutes in ether solution at room temperature were determined on the spectrophotometer and are given by the solid curves in Figure 3. Also given in Figure 2 is the relative spectral output (manufacturer's specifications) of the PEK-500 lamp. It was found that the broad output of the lamp in the 230–250- $m\mu$ region was of minor importance in populating the triplet states under the experimental conditions used in this study. This conclusion is based on a series of measurements on the triplet state epr intensity of a solution of dibenzofuran, using several sharp-cut filters (some of which are given in Figure 2). The results of these measurements indicate an appreciable dependence of the triplet state population (monitored by means of the $\Delta m = \pm 2$ epr transitions) on the cutoff wavelength of the filter in the wavelength region $\lambda > 260 m\mu$, but a minor or negligible dependence in the region $\lambda < 260 m\mu$.

The remaining curves in Figure 3 represent the wavelength dependence of the light absorbed by the solutes I_A when the samples were exposed to the unfiltered (dashed curve) and filtered (dotted curve) lamp outputs. The I_A curves were constructed using the expression

$$I_A(\lambda) = I_0(\lambda)T(\lambda)[1 - \exp(-\epsilon_\lambda lc)] \quad (3)$$

where $I_0(\lambda)$ is the unfiltered lamp output, $T(\lambda)$ is the

(12) S. Siegel and H. S. Judeikis, *J. Chem. Phys.*, **41**, 648 (1964).

(13) S. Siegel and K. B. Eisenthal, *ibid.*, **42**, 2494 (1965).

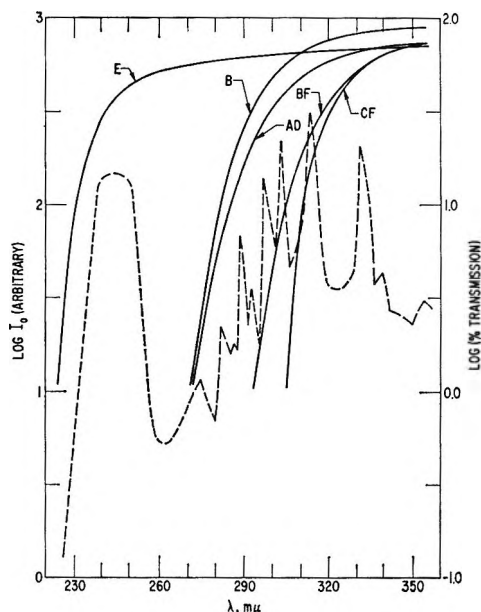


Figure 2. Lamp output (---) and filter transmissions (—). Filter used: phenanthrene (Filter CF), biphenyl (Filter E), fluorene (Filter B), carbazole (Filter CF), dibenzofuran (Filter AD), dibenzothiophen (Filter BF).

fraction of light transmitted by the filter at wavelength λ , ϵ_λ is the appropriate molar extinction coefficient, and l and c are the path length and concentration, respectively. A value of $l = 0.1$ cm was used because this is the approximate width of the sample cell; also, a value of $c = 0.0036$ was used to account for the volume contraction of the solvent at 77°K compared to room temperature. The contributions from wavelengths below 260 $m\mu$ were neglected when constructing the I_A curves in Figure 3 because of the reasons discussed above. This neglect of the shorter wavelengths will be continued, for the most part, in the subsequent analysis. Although this neglect may have some slight bearing on the results obtained using the full lamp output, it will not affect the results of the filtered experiments because the filters do not transmit appreciably below 260 $m\mu$. The only exception to this conclusion may be the case of biphenyl because it does not absorb appreciably above 260 $m\mu$, as is discussed subsequently.

A glan prism was used to polarize the exciting light. Moreover, great care was taken to minimize or eliminate such depolarizing effects as ice formation in the liquid nitrogen dewar or cracking of the low-temperature glasses. Also, the mutual alignment of sample tube, dewar, and polarizer was kept as reproducible as possible. However, some variations in the geometry of the optical train did occur from one experiment to the next. These resulted mainly from slight changes in the positioning of the lamp, filters, or polarizer. To

compensate for these variations and for the effects of different amounts of light reaching the sample in the two polarizer positions used (*i.e.*, H parallel to or perpendicular to E), all data for a given solute were normalized by assuming that, first, the intensity of a $\Delta m = \pm 2$ transition is proportional to the light intensity incident upon the sample, and, second, the intensity of the $\Delta m = \pm 2$ transition is isotropic with respect to the polarization of the incident optical radiation. The first assumption was verified experimentally by using calibrated wire screens to reduce the incident light intensity in steps. The second assumption was verified by simultaneous measurements of the $\Delta m = \pm 2$ epr transition intensity and the phosphorescent emission intensity. To well within experimental error, the ratio of the results of these latter measurements was found to be independent of the polarization of the exciting light. Normalization of the $\Delta m = \pm 2$ intensities led to reproducible results between separate experiments to well within the experimental uncertainties of a single experiment.

III. Results

The experimentally determined values of P_i are given in Table I. They represent the average of the values determined independently for the high- and low-field transitions of the pair of $\Delta m = \pm 1$ transitions corresponding to each canonical orientation.^{5,9,10} To well within experimental error, the values of P_i derived from

Table I: Experimental Values of the Polarization Ratios P_i^a

Molecule	Filtered excitation ^b		
	P_M^c	P_L^c	P_N^d
Phenanthrene	+0.27	+0.15	-0.74
Biphenyl	-0.64	+0.82	... ^e
Fluorene	-0.32	+0.48	-0.42
Carbazole	+0.42	-0.17	-0.51
Dibenzofuran	+0.44	-0.08	-0.67
Dibenzothiophen	+0.75	-0.39	-0.63
Unfiltered excitation ^b			
Phenanthrene	-0.32	+0.49	-0.65
Biphenyl	-0.39	+0.63	-0.77
Fluorene	-0.30	+0.49	-0.48
Carbazole	+0.01	+0.27	-0.59
Dibenzofuran	+0.27	-0.06	-0.63
Dibenzothiophen	+0.48	-0.18	-0.78

^a Defined by eq 2. ^b For light absorbed with filtered and unfiltered excitation; see Figure 3. ^c Experimental precision was ± 0.05 except for biphenyl where the precision was ± 0.10 . ^d Experimental precision was ± 0.15 for filtered excitation and ± 0.08 for unfiltered excitation. ^e Signal was too weak to make meaningful determination.

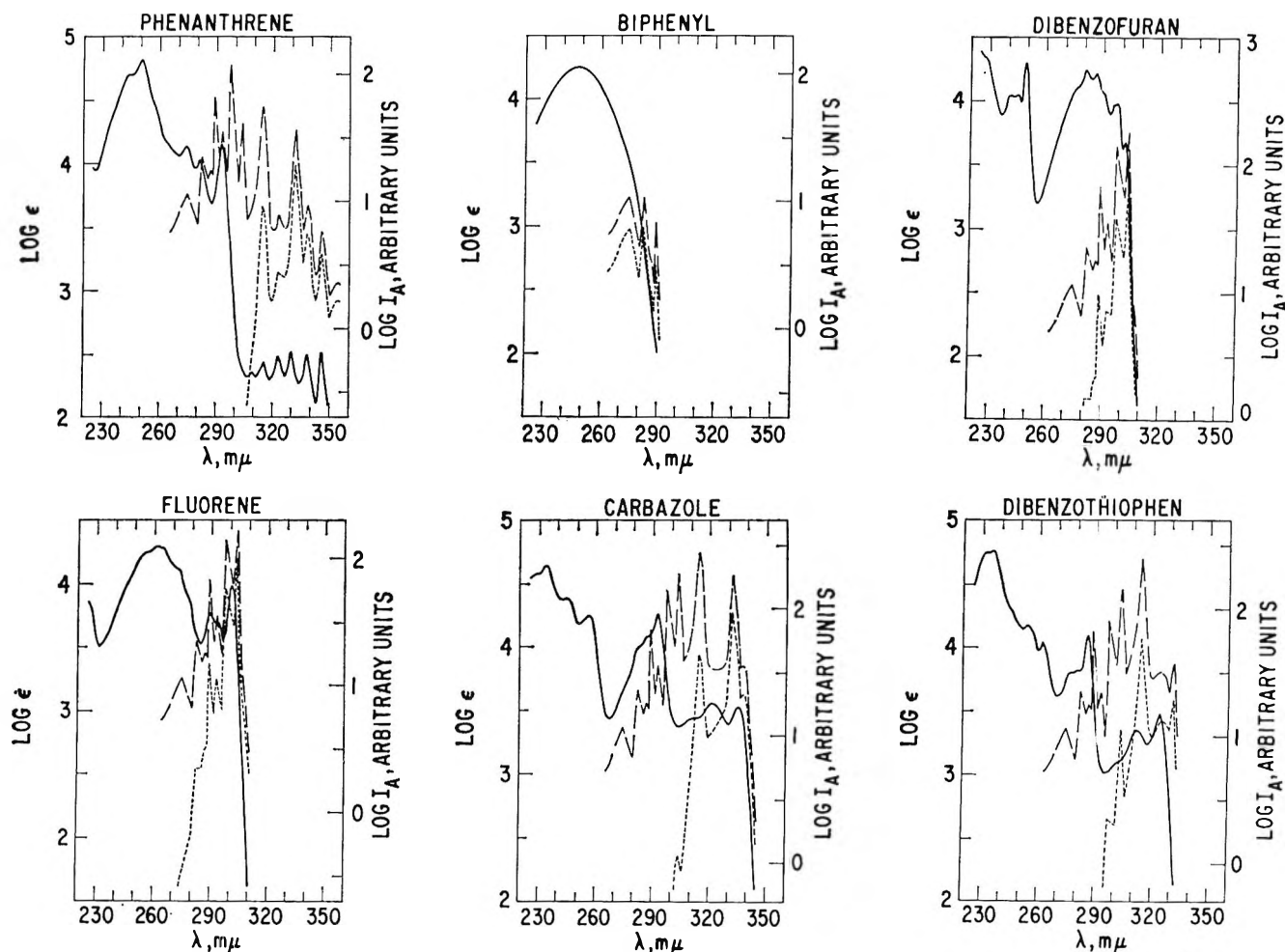


Figure 3. Absorption curves of molecules studied. Absorption spectrum in diethyl ether (—). Light absorbed by sample when unfiltered lamp output is used (---). Light absorbed by sample when exposed to filter lamp output (....); (see Table I and Figure 2 for filter used). The molar extinction coefficient is ϵ ; the light absorbed as calculated from eq 3 is I_A .

the low-field components were equal to those found for the high-field components. The experimental uncertainties are also given in Table I; for most cases, we have based these uncertainties on the liberal side. The large values of the uncertainties in P_N arise because the intensity of the corresponding epr transitions are usually the weakest of the set. Differences in the excitation bands with the filtered and unfiltered PEK-500 output can be estimated by using Figure 3.

In theory, the use of eq 2 together with the relationship

$$r_M + r_L + r_N = 1 \quad (4)$$

should allow the determination of the values of all three components of the polarization and the value of k , directly from the experimental data. Unfortunately, the experimental precision is not sufficient to produce a meaningful value of k by this procedure. The simplest

method of estimating k is to assume that $r_N = 0$ for the hydrocarbons phenanthrene and biphenyl because π, π^* transitions are expected to be polarized in the molecular plane. This assumption leads to a value of $k = 0.27 \pm 0.07$, which corresponds to approximately 20% unpolarized excitation. In general, the determination of the values of r_M and r_L is not too sensitive to the choice of k over a range of $\pm 50\%$; the experimental precision is the dominant source of uncertainty in these determinations. For r_N , the choice of the value of k is critical, and thus very little confidence should be placed in these values. A liberal estimate of $k = 0.35$ is used in the following analysis and calculations; therefore, the derived values of r_N should be considered as lower limits.

The values of r_t from the filtered excitation experiments were calculated using a reorganized form of eq 2 and the data in Table I; the results are given in Table II. The sum of r_M and r_L is also given in Table II. If

Table II: Components of the Polarization of the Long Wavelength Absorption Bands (*i.e.*, Filtered Excitation Absorption)^a

Molecule	r_M	r_L	r_N	$r_M + r_L$	Assignment
Phenanthrene	0.51 ± 0.04	0.43 ± 0.03	0.01 ± 0.01^b	0.94 ± 0.07	1L_b
Biphenyl	0.03 ± 0.03^b	0.96 ± 0.04^b	<i>c</i>	0.99 ± 0.07	1L_a
Fluorene	0.15 ± 0.02	0.68 ± 0.04	0.11 ± 0.07	0.83 ± 0.06	1L_a
Carbazole	0.63 ± 0.04	0.23 ± 0.02	0.06 ± 0.06	0.86 ± 0.06	1L_b
Dibenzofuran	0.65 ± 0.04	0.28 ± 0.02	0.03 ± 0.03^b	0.93 ± 0.06	1L_b
Dibenzothiophen	0.94 ± 0.05	0.12 ± 0.02	0.03 ± 0.03^b	1.06 ± 0.02	1L_b

^a The equation $r_i = [P_i(1.50) + 1]/(3 - P_i)$ was used in the calculations; a liberal value of $k = 0.35$ was used in all calculations; therefore, the calculated numbers are probably lower limits. ^b Negative values of r_i and values of r_i greater than unity were rejected. In these cases, the actual results are as follows: phenanthrene, $r_N = -0.03 \pm 0.05$; biphenyl, $r_M = 0.01 \pm 0.05$; dibenzofuran, $r_N = 0.00 \pm 0.06$; and dibenzothiophen, $r_N = 0.01 \pm 0.06$. ^c No data are available because of large experimental uncertainty.

Table III: Components of the Polarization of Short Wavelength Bands^{a,b}

Molecule	r_M	r_L	$r_M + r_L$	f_λ^c (λ)	Assignment
Phenanthrene	0.02 ± 0.02	0.99 ± 0.01	1.01 ± 0.03	0.6 (306)	1L_a
Carbazole	0.02 ± 0.02	1.00 ± 0.01	1.01 ± 0.03	2 (304)	1L_a
Dibenzothiophen	0.08 ± 0.08	0.85 ± 0.15	0.93 ± 0.23	5 (296)	1L_a

^a Calculated using eq 2 and 6. ^b Negative values of r_i and values of r_i greater than unity were rejected. For example, when a result $r_i = 1.10 \pm 0.15$ was obtained, the result was listed as $r_i = 0.97 \pm 0.03$. Therefore, the actual uncertainty in the absolute values of r_i was greater than listed. ^c The ratio of the amount of light absorbed in band 1 compared to that absorbed in band 2 is f , and λ is the wavelength chosen to separate the two bands. The values of f_λ were obtained by integrating the dashed curves in Figure 3; this determination is probably the greatest source of error in the calculation.

$r_N = 0$, then $r_M + r_L = 1$ by eq 4. Analysis of the data in Table II indicates that only two molecules, *i.e.*, fluorene and carbazole, have components of the polarization perpendicular to the LM plane which are outside of experimental uncertainty. The uncertainty is too large for the other molecules for one to make any definite statements about their r_N components. Analysis of the P_N data from the unfiltered excitation experiments also shows an r_N component for fluorene and carbazole. Whether the out-of-plane component arises from mixing of energy states or from a nonplanar geometry cannot readily be determined from these data.

The data from the unfiltered experiments were analyzed by assuming that all the absorption occurs in two bands and that the absorption in the filtered experiments occurs in one band. If the long wavelength band is labeled band 1 and the short wavelength band is labeled band 2, then the observed value of P_i from the unfiltered experiments can be expressed as

$$P_i(\text{obsd}) = \frac{fP_i^1}{1+f} + \frac{P_i^2}{1+f} \quad (5)$$

where P_i^1 and P_i^2 are the polarization ratios of band 1 and band 2, respectively, and $f = I_A^1/I_A^2$. To deter-

mine P_i^2 from the experimental data, one can rearrange eq 5 to

$$P_i^2 = (1+f)P_i(\text{obsd}) - fP_i^1 \pm \Delta(2f+1) \quad (6)$$

where Δ is the essentially constant experimental uncertainty in $P(\text{obsd})$ and P_i^1 .

Magnitudes of the ratio f can be estimated by integration of the dashed curves given in Figure 3. Estimates for the values of r_M and r_L for the short wavelength band of three of the molecules which had well-defined bands were determined using eq 6, and the results are given in Table III. The estimates of f , together with the wavelengths arbitrarily chosen to separate bands 1 and 2, are also given in Table III. The values of r_N for band 2 are assumed to be equal to those given in Table II because there are no real differences, outside of experimental precision, observed in the values of P_N obtained with the filtered and unfiltered excitation. For fluorene, the same band is excited both with and without the use of filters, as can be seen from Figure 3; the results in Table I confirm this conclusion because no changes were observed in the values of P_i . The changes observed in the values of P_M for dibenzofuran are very small and are negligible for P_L ; there-

fore, because it is difficult to resolve bands, no calculations were attempted for this molecule.

The results for biphenyl seem to indicate small changes in the values of P_M and P_L going from the filtered to the unfiltered excitation. However, a detailed analysis of the biphenyl absorption curves in Figure 3 indicates that any changes which take place must occur in the I_A band at 240 m μ . Because biphenyl does not absorb much above 260 m μ , any small amount of light from the short wavelength source would have considerably more influence for biphenyl than for any other molecule. However, the observed changes are so small that no effort was made to determine the small contributions from this short wavelength band except that it can be seen that the polarization is opposed to the polarization of the long wavelength band.

IV. Discussion

The broad-band technique used in this study does not allow for the separation of the polarizations of the individual vibronic subbands. Therefore, the values of P_i or r_i obtained from this technique are averages over all the vibronic subbands. Also, the averages are non-weighted averages because the entire electronic band did not contribute equally to the populating of the triplet state, and no attempt was made to correct for this fact. Estimates of this effect could be made by reference to the I_A curves in Figure 3. With a suitable monochromator, this technique can be made easily into a narrow-band method.

The result for the shorter wavelength 1L_a band of phenanthrene agrees with theoretical predictions^{14,15} that it should be long-axis polarized. Theory predicts that the long wavelength 1L_b band of phenanthrene should be short-axis polarized, while the results in Table II give $r_M/r_L \approx 1$. However, the prediction applies to a pure electron system where no vibronic perturbations are present. Therefore, the experimental result indicates that substantial vibronic coupling exists between the 1L_b and higher states (probably the 1L_a state).

The long wavelength absorption band of biphenyl peaking at 250 m μ has been assigned to the 1L_a transition, while the 1L_b band is probably lost in the long wavelength tail of this strong band.¹⁵⁻¹⁷ The result in Table II agrees with this prediction because the 1L_a band should be long-axis polarized. However, the long wavelength band of fluorene (which can be considered as a 2,2'-disubstituted biphenyl) is assumed to be the 1L_b band shifted to the red in this molecule. If this assignment is correct, the polarization result $r_L/r_M \approx 4$ indicates that the absorption intensity arises mainly from vibronic coupling with the 1L_a transition. The polarization results also indicate that there is an

appreciable out-of-plane component to the polarization. It is probable that this component also arises from some vibronic coupling with a higher electronic state which has out-of-plane polarization. It is unlikely that the out-of-plane contributions come from interactions with the solvent.

The assignments in Table II and III of the heterocyclic absorption bands to 1L_a or 1L_b have been made by analogy with the polarization results from the aromatic hydrocarbons; *i.e.*, 1L_a is long-axis polarized and 1L_b is both long- and short-axis polarized. If the mixed polarization in the 1L_b bands arises from vibronic coupling between electronic states, then the data in Table II indicate that dibenzothiophen has the least degree of coupling and the 1L_b band for this molecule is nearly a pure electronic band. As indicated previously, the carbazole data indicate the presence of components of the polarization of the 1L_b and 1L_a bands which are out of plane. Therefore, some small coupling must exist between the π, π^* states and a higher n, π^* or σ, π^* state.

Finally, a word of caution must be raised in regard to the discussion given here. If the geometry and symmetry of the triplet state is sufficiently different from that of the ground state of the molecule in question, then the magnetic axes do not necessarily coincide with the ground state symmetry axes. Therefore, one must consider the projections of the polarization components upon the magnetic axes. The out-of-plane components discussed above may arise from this cause.

Appendix

The probability of absorption P_A for any molecule excited with light polarized parallel to H is

$$P_A = r_M \cos^2 \theta_{MH} + r_L \cos^2 \theta_{LH} + r_N \cos^2 \theta_{NH}$$

where r_i is the component of the polarization carried along each axis ($\sum_i r_i = 1$) and θ_{iH} is the angle between the molecular axis and the magnetic field. The fraction of excited molecules ρ_i with $\theta_{iH} \leq \delta$ for a random distribution of originally unexcited molecules is

$$\rho_i = \frac{r_i \int_0^\delta \cos^2 \theta_{iH} \sin \theta_{iH} d\theta_{iH}}{\int_0^{\pi/2} \cos^2 \theta_{iH} \sin \theta_{iH} d\theta_{iH}} \quad (\text{A1})$$

Because only excited molecules which have essentially canonical orientations^{9,10} are observed in the derivative epr spectra in glasses, δ , the angle of observation, is

(14) R. Parriser, *J. Chem. Phys.*, **24**, 250 (1956).

(15) J. R. Platt, *ibid.*, **19**, 1418 (1951).

(16) A. Wentzel, *ibid.*, **21**, 403 (1953).

(17) I. B. Berlman and O. J. Steingraber, *ibid.*, **43**, 2140 (1965).

very small. It is assumed that the probability of observation is unity if $\theta_{iH} \leq \delta$ and zero for $\theta_{iH} > \delta$. Evaluation of eq A1 yields

$$\rho_i \text{ (for small } \delta) = \frac{3}{2}\delta^2 r_i \quad (\text{A2})$$

The fraction of *all* molecules ρ' with $\theta_{iH} \leq \delta$ is

$$\rho' = \frac{\delta^2}{2} \quad (\text{A3})$$

for all three axes. If all the exciting light is polarized, then the number of excited molecules with the observation angles $\theta_{iH} \leq \delta$ is equal to $\rho_i N_{\text{EX}}$, where N_{EX} is the total number of excited molecules present.

However, if the incident optical excitation has a depolarized isotropic component because of light scattering or other physical depolarizing causes, the excited molecules present will have $N_{\text{EX}}(\text{p})$ molecules excited by the polarized excitation and $N_{\text{EX}}(\text{np})$ molecules excited by the nonpolarized component. The number of excited molecules with $\theta_{iH} \leq \delta$ when E is parallel to H can be written as

$$N_i^\delta(\parallel) = N_{\text{EX}}(\text{p})\rho_i + N_{\text{EX}}(\text{np})\rho' \quad (\text{A4})$$

If it is assumed that the ratio $N_{\text{EX}}(\text{np})/N_{\text{EX}}(\text{p}) = k$ is a constant, then

$$N_i^\delta(\parallel) = N_{\text{EX}}(\text{p})\left(\frac{\delta^2}{2}\right)(3r_i + k) \quad (\text{A5})$$

When E is polarized perpendicular to H , then only molecules excited along the other components ($j \neq i$) of the molecular polarization will contribute to $N_i^\delta(\perp)$ and

$$N_i^\delta(\perp) = N_{\text{EX}}(\text{p})\rho'(1 - r_i) + N_{\text{EX}}(\text{np})\rho' = N_{\text{EX}}(\text{p})\left(\frac{\delta^2}{2}\right)\left[\frac{3}{2}(1 - r_i) + k\right] \quad (\text{A6})$$

since the probability of absorption along an axis other than i must be averaged over all values of $\cos^2 \theta_{jH}$.

If it is assumed that photoexcited molecules with the canonical orientation $\theta_{iH} \leq \delta$ have unit probability of being observed and those with $\theta_{iH} > \delta$ have zero observational probability, the intensity of the epr transition I_i is proportional to $N_i^\delta(\parallel)$ or $N_i^\delta(\perp)$ when E is parallel to or perpendicular to H , respectively.

A Study of Some Free-Radical Reactions in Aqueous γ Radiolysis by Direct Measurements of Cu^+ Intermediates during Irradiation

by Olga Mičić and Ivan Draganić

Boris Kidrič Institute of Nuclear Sciences, Vinča, Yugoslavia (Received December 27, 1965)

Changes in potential and limiting currents on a rotating platinum electrode were studied directly and continuously during irradiation of aqueous solutions of cupric sulfate and sulfuric acid, with and without ethanol. Conditions under which Cu^+ intermediates may be directly measured are demonstrated. Measurements were made at pH values ranging from 1.5 to 4.5 and for different scavenger concentrations. Dependent on the experimental conditions, the limiting current was a measure of the primary reducing short-lived species or of the total free-radical yield. It made possible calculation of the primary radical product yields in water radiolysis in the pH region studied, $G_{\text{H}} + G_{\text{e}_{\text{aq}}^-}$ and $G_{\text{OH}\cdot}$. By measuring competition reactions we found that $k_{\text{H,Cu}^{2+}}/k_{\text{H,C}_2\text{H}_4\text{OH}} = 2.64 \pm 0.06$ and $k_{\text{e}_{\text{aq}}^-, \text{Cu}^{2+}}/k_{\text{e}_{\text{aq}}^-, \text{H}^+} = 1.64 \pm 0.03$. From these measurements we also derived that at pH 3.6–4.8, $G_{\text{e}_{\text{aq}}^-} = 2.3 \pm 0.1$. Variation of the sulfate ion concentration in the solutions studied confirms that dissociated as well as undissociated forms of copper act as efficient scavengers.

It is generally accepted that the yields of primary radical products of water radiolysis decrease when the pH of the solution changes from acid to neutral. Data available in the literature report a sharp decrease after pH 2, which stops at about pH 4. On the other hand, Draganić, *et al.*,¹ found that this decrease is fairly slow and continuous in the oxalic acid–oxygen system. The values given in this report for acid and neutral media are in agreement with the generally adopted values, but are different in the transient region between pH 2 and 5. This difference seemed fairly significant to us, and we tried to check these observations by means of an inorganic system. The hydrolysis of radiolytic products at higher pH makes the choice very limited. Some preliminary experiments suggested that we select cupric sulfate. In this case, one has a suitable solubility product of hydroxides of cuprous and cupric ions, as well as a suitable method of measurement.

From thermodynamical data² it may be seen that cuprous ions are unstable and disproportionate to metallic copper and cupric ions. However, preliminary measurements made by one of the present authors suggested the possibility of direct observation of the

Cu^+ intermediate with electrochemical measurements during irradiations.³

Evidence for Cu^+ ions found in the literature has been obtained from kinetic considerations only by using the data of stable products measurements. This was just the reason why we were particularly interested in the possibility of direct observation of short-lived Cu^+ intermediates during irradiation. It should be pointed out that electrochemical measurements have been used earlier to follow intermediates; Miller and Veselovski⁴ measured pentavalent uranium, an intermediate in the radiolysis of aqueous solutions of quadri- and hexavalent uranium.

Hart and Walsh⁵ have shown that in irradiated cupric ion aqueous solutions Cu^+ intermediates are formed in reactions with short-lived reducing species.

(1) Z. D. Draganić, I. G. Draganić, and M. M. Kosanić, *J. Phys. Chem.*, **68**, 2085 (1964).

(2) A. N. Frumkin, "Kinetika elektrodnih processov," Academy of Sciences of the USSR, Moscow, 1955; W. M. Latimer, "Oxidation Potentials," Prentice-Hall Inc., New York, N. Y., 1952.

(3) C. I. Zalkind and O. I. Mičić, unpublished data.

(4) N. B. Miller and V. I. Veselovski, *Tr. 2-g. Ves. Soveshch. po Radiats. Khim. Akad. Nauk SSSR, Otd. Khim. Nauk, Moscow*, (1962).

(5) E. J. Hart and P. D. Walsh, *Radiation Res.*, **1**, 498 (1954).

Schwarz⁶ has studied the scavenging efficiency of Cu^{2+} ions on molecular hydrogen yields and considered the dissociated cupric ions to be responsible for these reactions.

Experiments with pulsed electron beams have shown that cupric ions are among the most efficient scavengers for solvated electrons. There is some disagreement between the data on the reaction rate constants for copper sulfate and H atoms. From some observations⁷ one may conclude that the reaction rates of cupric ions with solvated electrons and with hydrogen atoms are of the same order of magnitude, while from some other data the reaction of atomic hydrogen should be slower by a factor of 10,⁸ or even 1000.⁹

Today it is generally accepted that solvated electrons and H atoms are the primary short-lived reducing species in acid and neutral media. A disagreement does exist in the radiation yields. Until recently the generally accepted yield for solvated electrons has been 2.8. Today, there are some published data indicating that the yield could be lower.^{10,11} The simplicity of the measurements and of the reaction scheme for the systems we studied also provided information in this respect.

Experimental Section

Solutions. The chemicals $\text{CuSO}_4 \cdot 5\text{H}_2\text{O}$, Na_2SO_4 , and H_2SO_4 were all AR Merck products. The ethanol was a BDH AR grade product. The cupric sulfate concentration was determined by the conventional polarographic procedure using a solution made up by dissolving metallic copper (Merck).

The solutions were made up with water of a purity usually requested in radiation chemistry. The pH of the solution was adjusted by sulfuric acid. Sodium sulfate was added in order to secure that the ionic strength of the solution was always the same (0.15). All measurements were made in a nitrogen gas atmosphere. The nitrogen was previously purified.¹²

Irradiation Cell. The irradiation cell was a cylindrical glass vessel fitted with ground-glass inlet tubes for the working, polarizing, and reference electrodes as well as gas inlet and outlet tubes for nitrogen supply. The volume of the solution was about 5 ml. A rotating platinum electrode was used in standard experimental conditions; detailed description of the irradiation cell, including data on the electrode treatment, is given elsewhere.¹² To reduce the residual current to several tenths of a microampere, it was sufficient to keep the electrode at the working potential for 15 min.

A hydrogen electrode in a 0.1 N H_2SO_4 solution, whose potential was 0.08 v in comparison with the

normal hydrogen electrode, was used as reference electrode. For some comparative measurements we used a rotating gold electrode¹³ which, by suitable treatment, was adjusted so that molecular hydrogen was not oxidized on it.

Measurement of the Change in Potential and in Limiting Current. All measurements, except in blank tests, were performed while the sample was simultaneously irradiated. Changes in the potential were determined by measuring the electromotive force of the working and reference electrode with a Tacussel Model SGE cathode voltmeter, and a Beckman Model G pH meter. The precision of the measurements was ± 2 mv.

The limiting current at anodic polarization, on a platinum electrode, was measured at 0.5 v against the hydrogen electrode in 0.1 N H_2SO_4 . The working potential of the electrode was kept constant by means of a Tacussel Model PRT potentiostat with an accuracy of ± 5 mv. The current was measured with a Safram Model TLVA 3 galvanometer, with a sensitivity of 1.5×10^{-9} amp. During irradiation the current was read every 6 sec.

Irradiation. Irradiations were performed in a 2000-curie cobalt source.¹⁴ The dose rate was 1.02×10^{17} ev $\text{ml}^{-1} \text{min}^{-1}$ as determined with the Fricke dosimeter and assuming $G(\text{Fe}^{3+}) = 15.5$. The temperature of the room (17°) in which the ^{60}Co source was located varied during a series of irradiations only within $\pm 1^\circ$ and the irradiation cell was therefore not temperature controlled.

Determination of Molecular Hydrogen.¹⁵ The measurements were made by gas chromatography on a Perkin-Elmer Model 154 DG apparatus. A 4.1-m long silica gel column was used at 50° . Argon was used as the gas carrier.

Results

Changes in Potential. It was assumed initially that

(6) H. A. Schwarz, *J. Am. Chem. Soc.*, **77**, 4960 (1955).

(7) A. O. Allen, *Radiation Res. Suppl.*, **4**, 54 (1964).

(8) E. J. Hart, *Radiation Res.*, **2**, 33 (1955).

(9) J. H. Baxendale and D. H. Smithies, *Z. Physik. Chem. (Frankfurt)*, **7**, 242 (1956).

(10) E. Hayon, *Trans. Faraday Soc.*, **61**, 273 (1965).

(11) G. V. Buxton and F. S. Dainton, *Proc. Roy. Soc. (London)*, **A287**, 427 (1965).

(12) D. S. Ovcin, O. I. Mičić, and I. G. Draganić, *Radiation Res.*, **24**, 324 (1965).

(13) C. I. Zalkind and V. I. Veselovski, "Dejstvie ioniziruiuschchih izluchenii na neorganicheskie i organicheskie sistemi," Academy of Sciences of the USSR, Moscow, 1958.

(14) B. B. Radak and I. G. Draganić, *Bull. Boris Kidrić Inst. Nucl. Sci. (Belgrade)*, **13**, 77 (1962).

(15) L. V. Petković, M. M. Kosanić, and I. G. Draganić, *ibid.*, **15**, 9 (1964).

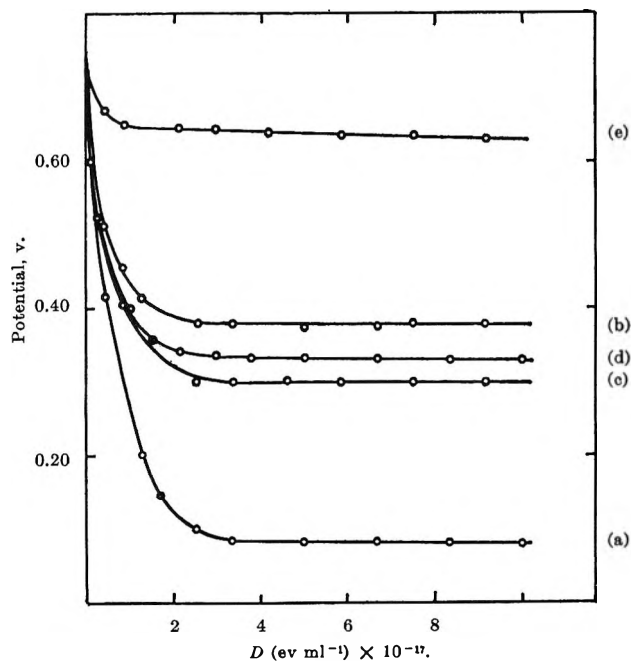


Figure 1. Potential-dose curves for $5 \times 10^{-2} M$ H_2SO_4 solutions for different cupric sulfate concentrations. Platinum electrode: (a) 0, (b) $1 \times 10^{-2} M$, (c) $1 \times 10^{-3} M$. Gold electrode: (d) $1 \times 10^{-2} M$, (e) 0. In (d) and (e) $3.5 \times 10^{-3} M$ $H_2C_2O_4$ was also present in the irradiated solution.

if measurable concentrations of the Cu^+ intermediates were formed during irradiation, changes in the oxidation-reduction potential of Cu^+-Cu^{2+} ions had to be observed on an inert electrode such as the platinum. It should be mentioned that in this case also the molecular radiolytic products of water, hydrogen and hydrogen peroxide, might establish the potential. However, under our experimental conditions a potential change may be due only to the presence of molecular hydrogen¹² and, probably, to the Cu^+ intermediate. As can be seen in Figure 1, curve a, the potential at first falls sharply and then it remains constant (80 mv against the hydrogen electrode in the same solution). This corresponds to the potential of molecular hydrogen which under the given conditions is established owing to the H_2 formed during the irradiation. The presence of copper sulfate in the same solution (Figure 1, curves b and c) considerably increases the measured value of the potential, indicating that in this case, besides molecular hydrogen, there must also be other species, *i.e.*, Cu^+ ions.

To confirm that cuprous ions really contribute to the buildup of the potential, we also give some data obtained in an earlier work.³ These results were obtained by using the gold electrode in sulfuric acid solution, with and without cupric sulfate. In these experiments oxalic acid ($3.5 \times 10^{-3} M$) was added to

the solution so that there would be no oxidation products. It can be seen that in the absence of copper sulfate (curve e), irradiation causes a negligible change. Addition of cupric sulfate to the solution sharply reduces the potential during irradiation (curve d) which can be attributed only to the establishment of potential of Cu^+ and Cu^{2+} ions.

Limiting Currents. After establishing the stationary potential in the solutions studied, we determined the dependence of the polarization current on the potential. It was found, for all the solutions used, that for potentials more positive than 0.4 v the polarization current did not depend on the potential; *i.e.*, the limiting current of hydrogen and cuprous ions is established already at this potential. These measurements suggested us to choose 0.5 v as the working potential. All the subsequent measurements of the limiting current were made at this potential.

Limiting Current of the Cu^+ Intermediate. Figure 2 shows data for the change in limiting current during

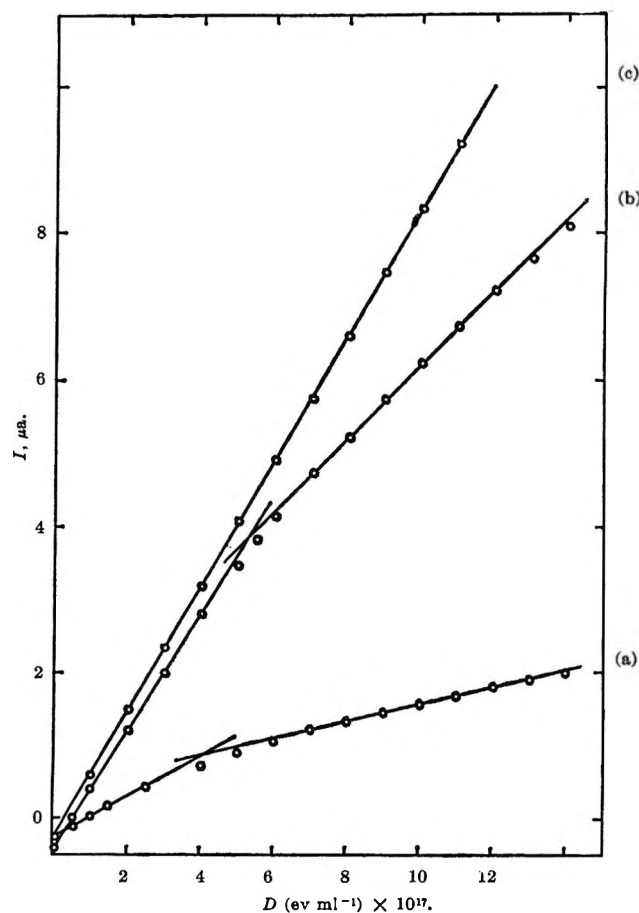


Figure 2. Limiting current-dose curves, measured on Pt rotating electrode, in $5 \times 10^{-2} M$ H_2SO_4 solution containing (a) $1 \times 10^{-3} M$ $CuSO_4$, (b) $5 \times 10^{-3} M$ $CuSO_4 + 1 \times 10^{-3} M$ C_2H_6OH , (c) $1 \times 10^{-3} M$ C_2H_6OH .

irradiation of sulfuric acid solutions ($5 \times 10^{-2} M$) containing $10^{-2} M$ CuSO_4 (curve a) or $5 \times 10^{-3} M$ $\text{CuSO}_4 + 10^{-3} M$ $\text{C}_2\text{H}_5\text{OH}$ (curve b). For comparison (curve c), the dependence of the limiting current on the absorbed dose in the absence of copper sulfate is shown. It can be seen that, in the presence of cupric sulfate, the initial part of the experimental curves have more pronounced slopes. This refers both to the formation of molecular hydrogen and to the formation of cuprous ions. After a dose of about 4×10^{17} ev ml^{-1} , the slope decreased with increasing dose. Stationary concentration of the Cu^+ intermediate is established, and the rise in limiting current refers only to molecular hydrogen for which the concentration increases with increasing dose. This was not the case for the gold electrode,³ on which molecular hydrogen does not react. In the latter case, after a certain time of irradiation, the limiting current was independent of the dose.

It is obvious that in order to calculate the concentration of cuprous ions, the limiting current measured on the platinum electrode must be corrected because of the presence of molecular hydrogen. The experiments were performed without irradiation in order to see also the possible influence of the presence of cupric sulfate on the hydrogen oxidation. The limiting current of hydrogen was measured in CuSO_4 ($10^{-3} M$) and H_2SO_4 ($5 \times 10^{-2} M$) solution. The rotating platinum electrode was kept at a constant potential of 0.5 v during saturation of the solution with hydrogen gas. This potential was chosen so as to avoid separation of metallic copper. The results show that the limiting current in this case was slightly smaller than in the solution of pure sulfuric acid, but it decreased visibly with time (about 10% in the course of 10 min). This decrease is probably due to the cupric ion absorption on the surface of the electrode and to interference by some other electrochemical processes.

It is fairly difficult to standardize the experimental conditions in routine work, and the dispersion of the limiting currents measured could amount up to 20%. In order to minimize this source of error, the hydrogen limiting current was subtracted from the initial slope of the current-dose curve in all experiments. The slope of an experimental curve, corrected in this way for the hydrogen contribution, was used to calculate the Cu^+ ion concentration. We used the calibration curve for hydrogen ($I = KC$) in sulfuric acid ($5 \times 10^{-2} M$) without irradiation and converted it to the corresponding current of cuprous ions. In the calculation we assumed that the diffusion coefficient of cuprous and cupric ions is the same. This assumption seems reasonable since their masses are the same. It is also

well known that the metallic-ion diffusion coefficients differ very little. In this way we calculated the value $K = 4.7 \times 10^{-17} \mu\text{a ml molecule}^{-1}$ for Cu^+ intermediates. Stationary concentration of Cu^+ intermediates was derived from the intercept of two straight lines as shown in Figure 2.

Influence of the pH on the Limiting Current of Cu^+ Intermediates under Various Conditions. Table I summarizes the results for the limiting current of cuprous ions; they were measured by a rotating platinum electrode in $5 \times 10^{-2} M$ sulfuric acid solutions and different cupric sulfate concentrations with and without ethanol. The pH of the solution varied from 1.5 to 4.5. The experimental curves had the same shape as in Figure 2. The slopes were calculated from the linear part. Depending on the experimental conditions, the values varied from 0.134 to 0.320 $\mu\text{a min}^{-1}$. The slopes are given as the mean value of at least five similar experiments.

Table I: Radiation Chemical Yields of the Cu^+ Intermediate under Different Conditions

pH	Solution, ^a M		Slope, $\mu\text{a min}^{-1}$ $\times 10$	$G(\text{Cu}^+)$	Stationary concn of Cu^+ ions, $M \times 10^6$
	CuSO_4	+ $\text{C}_2\text{H}_5\text{OH}$			
1.5	1×10^{-3}		1.72	3.56	4.2
1.5	1×10^{-2}		1.74	3.61	4.0
2.5	1×10^{-3}		1.52	3.14	3.4
3.5	1×10^{-3}		1.34	2.76	2.0
4.5	1×10^{-3}		1.43	2.96	0.9
1.5	5×10^{-3}	1×10^{-3}	3.20	6.58	19
1.5	5×10^{-3}	1×10^{-2}	3.18	6.55	15
1.5	1×10^{-2}	1×10^{-2}	3.16	6.54	16
2.5	5×10^{-3}	1×10^{-2}	2.94	6.08	15
3.5	1×10^{-3}	1×10^{-3}	2.62	5.42	12
3.5	5×10^{-3}	1×10^{-2}	2.58	5.33	10
3.5	1×10^{-3}	1×10^{-2}	2.54	5.25	8
4.5	1×10^{-3}	1×10^{-2}	2.49	5.15	10
4.5	1×10^{-3}	1×10^{-3}	2.52	5.21	7
4.5	1×10^{-4}	1×10^{-2}	>1

^a The ionic strength of the solutions was always the same (0.15).

Molecular Hydrogen Yields under Various Conditions. Table II summarizes the radiation chemical yields of molecular hydrogen obtained by gas chromatographic measurements in the irradiated solutions. The yields are taken as the mean value of six individual irradiations.

Measurements of Hydrogen Peroxide. Hydrogen peroxide was determined spectrophotometrically by the titanium sulfate method. Since this method was not

Table II: Molecular Hydrogen Yields under Various Conditions

pH	Solution, <i>M</i>		<i>G</i> (H ₂)
	CuSO ₄	+ C ₂ H ₅ OH	
1.5	1 × 10 ⁻²		0.43
4.5	1 × 10 ⁻³		0.45
1.5	4 × 10 ⁻³	1 × 10 ⁻²	2.23
1.5	1 × 10 ⁻³	1 × 10 ⁻²	3.18
1.5	2 × 10 ⁻³	1 × 10 ⁻²	2.86
1.5	5 × 10 ⁻⁴	1 × 10 ⁻²	3.59
1.5	1 × 10 ⁻²	1 × 10 ⁻²	1.40
3.6	1 × 10 ⁻⁴	1 × 10 ⁻²	2.39
3.6	2 × 10 ⁻⁴	1 × 10 ⁻²	1.89
3.7	5 × 10 ⁻⁵	1 × 10 ⁻²	2.73
4.1 ^a	1 × 10 ⁻⁴	1 × 10 ⁻²	1.70
4.3 ^a	1 × 10 ⁻⁴	1 × 10 ⁻²	1.58
4.8	1 × 10 ⁻²	1 × 10 ⁻²	1.22

^a Sodium sulfate present (5 × 10⁻² *M*).

sensitive enough as to enable the determination of the initial yield, hydrogen peroxide was determined at absorbed doses for which stationary state of cuprous ions had already been established. We found that the stationary concentration of hydrogen peroxide amounts to about 10⁻⁵ *M* H₂O₂.

Discussion

Radiation Chemical Yields of Cu⁺ Intermediates. Measurements of the changes in potential and the limiting currents in cupric sulfate solution showed that the cuprous ions can be electrochemically monitored. As may be seen from the data in Figure 1, the establishment of a stationary potential on the platinum electrode during irradiation of an aqueous solution in which cupric sulfate is present (curves b and c) is due not only to the presence of the H₂ and H⁺ ions but also to the Cu⁺ and Cu²⁺ ions. The establishment of this potential on a gold electrode is due only to the presence of the Cu⁺ and Cu²⁺ ions (curve d). That Cu⁺ intermediates are really detected is also quite evident from Table III where experimentally obtained Cu⁺ and Cu²⁺ stationary potentials are compared with the calculated potentials. In this calculation we used a potential 0.16 v as the normal potential and the Cu⁺ stationary concentration from the last column of Table I. For comparison, potentials measured in sulfuric acid without cupric sulfate are also presented.

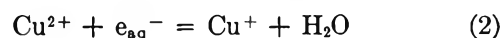
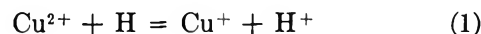
As may be seen from Table III, the calculated values for the platinum electrode are in good agreement with those obtained experimentally. They are slightly higher because the correction for the low potential decrease, due to presence of hydrogen in the irradiated solution, could not be taken into account.

Table I shows the values for *G*(Cu⁺) obtained under various conditions.

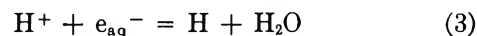
Initial Mechanism. Based on the general assumption that the radiolytic decomposition of water may be written



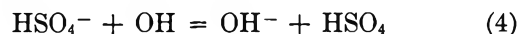
the reduction of bivalent copper is attributed to the reactions of cupric ions with reducing short-lived species



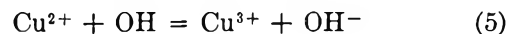
In acid medium the following very fast reaction should be also taken into account.



In aqueous solutions containing only sulfuric acid besides cupric sulfate, the fate of hydroxyl radicals is in slow reaction

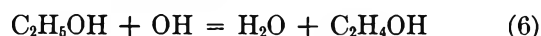


In his experiments with pulsed electron beam, Baxendale¹⁶ suggests that, in the absence of an efficient OH scavenger, the possible reaction could also be



Sufficient data to support reaction 5 are not available. If Cu³⁺ ions form under our working conditions and are reduced very rapidly in some chemical reaction, we might not be able to register them electrochemically. Nevertheless we feel that we could observe them under certain conditions. In pure cupric sulfate solutions the measured Cu⁺ limiting current would thus be reduced owing to either their participation in the limiting current (at 0.5 v they would reduce the total positive current measured) or to their possible reaction with Cu⁺ ions. However, the values for primary short-lived species, derived from the measured *G*(Cu⁺) and the proposed reaction scheme, are in reasonable agreement with values derived from other systems. Hence, it seems not very probable that reaction 5 is of any significance to the results of measurements in our working conditions.

In the presence of ethanol which is a very efficient scavenger for OH radicals, we have



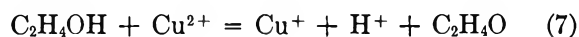
The C₂H₄OH radicals formed disappear in reaction with cupric ions

(16) J. H. Baxendale, E. M. Fielden, and J. P. Keene, *Proc. Roy. Soc. (London)*, **A286**, 320 (1965).

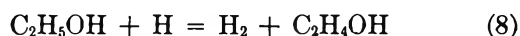
Table III: Experimentally Obtained Stationary Potentials and Calculated Oxidation-Reduction Potentials for $\text{Cu}^+ - \text{Cu}^{2+}$ Ions

Potential ^a		Solution	Electrode	Stationary concn, $M \times 10^6$
Experimentally determined	Calculated for $\text{Cu}^+ - \text{Cu}^{2+}$			
0.30	0.30	$1 \times 10^{-2} M \text{CuSO}_4 + 5 \times 10^{-2} M \text{H}_2\text{SO}_4$	Platinum	4.0
0.22	0.24	$1 \times 10^{-3} M \text{CuSO}_4 + 5 \times 10^{-2} M \text{H}_2\text{SO}_4$	Platinum	4.2
0.08	...	$5 \times 10^{-2} M \text{H}_2\text{SO}_4$	Platinum	...
0.25	0.25	$1 \times 10^{-2} M \text{CuSO}_4 + 5 \times 10^{-2} M \text{H}_2\text{SO}_4 + 3.5 \times 10^{-4} M \text{H}_2\text{C}_2\text{O}_4$	Gold	20
0.56	...	$5 \times 10^{-2} M \text{H}_2\text{SO}_4 + 3.5 \times 10^{-3} M \text{H}_2\text{C}_2\text{O}_4$	Gold	...

^a The values of the potential are given against the normal hydrogen electrode.



In the presence of ethanol we also have the reaction with H atoms



which is in competition with reaction 1. The reaction with solvated electrons may be neglected as being very slow in comparison with reactions 2 and 3.

For initial conditions, reactions 1 through 5 offer the possibility of calculating primary yields of water radiolysis by means of the experimental data for Cu^+ intermediates. For the usual kinetic treatment, where steady-state conditions for the free radicals are assumed, we have

$$G(\text{Cu}^+) = G_{\text{H}} + G_{\text{e}_{\text{aq}}^-} \quad (9)$$

$$G(\text{H}_2) = G_{\text{H}_2} \quad (10)$$

If, besides cupric sulfate, ethanol is also present in the sulfuric acid solution, the yield of Cu^+ intermediate is a measure of the total free-radical yield

$$G(\text{Cu}^+)_{\text{Et}} = G_{\text{H}} + G_{\text{e}_{\text{aq}}^-} + G_{\text{OH}} \quad (11)$$

In this case we also have

$$G(\text{H}_2) = G_{\text{H}_2} + \frac{G_{\text{H}}}{1 + \frac{k_1[\text{CuSO}_4]}{k_8[\text{C}_2\text{H}_5\text{OH}]}} + \frac{G_{\text{e}_{\text{aq}}^-}}{\left[1 + \frac{k_1[\text{CuSO}_4]}{k_8[\text{C}_2\text{H}_5\text{OH}]}\right] \left[1 + \frac{k_2[\text{CuSO}_4]}{k_3[\text{H}^+]}\right]} \quad (12)$$

pH Influence on Primary Radiolytic Products in Aqueous Solutions. The data on radiation yields for Cu^+ intermediates and eq 9 and 11 allow us to calculate the yields of the short-lived primary products. Thus, from eq 9 we have

$$G_{\text{H}} = G_{\text{e}_{\text{aq}}^-} = G(\text{Cu}^+)$$

while eq 11 gives

$$G_{\text{H}} + G_{\text{e}_{\text{aq}}^-} + G_{\text{OH}} = G(\text{Cu}^+)_{\text{Et}}$$

By subtracting (9) from (11) we can determine the yield of the oxidizing species at the given pH.

$$G_{\text{OH}} = G(\text{Cu}^+)_{\text{Et}} - G(\text{Cu}^+) \quad (13)$$

In eq 13, $G(\text{Cu}^+)$ is the yield of cuprous ions in a cupric sulfate solution, and $G(\text{Cu}^+)_{\text{Et}}$ is the corresponding yield in a cupric sulfate solution in the presence of ethanol.

Figure 3 summarizes the primary yields derived from our experimental data and eq 9, 11, and 13. The standard deviations were calculated in the usual way, all the measurements being taken into account. Figure 3a presents the yields calculated from the direct measurements of Cu^+ intermediates in cupric sulfate solu-

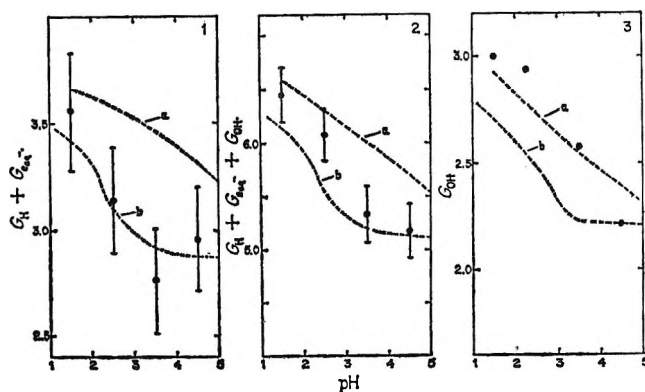


Figure 3. pH influence on primary radical yields. Points derived from experimental measurements with calculated standard deviations: (1) $G_{\text{H}} + G_{\text{e}_{\text{aq}}^-} = G(\text{Cu}^+)$, (2) $G_{\text{H}} + G_{\text{e}_{\text{aq}}^-} + G_{\text{H}} = G(\text{Cu}^+)_{\text{Et}}$, (3) $G_{\text{OH}} = G(\text{Cu}^+)_{\text{Et}} - G(\text{Cu}^+)$. Dashed lines show data from (a) Draganić, *et al.*,¹ (b) Hayon.¹⁰

tions. As can be seen, standard deviations are fairly high, up to 9%. The reason for this is mainly the rather narrow linear part of the current-dose curve which is a consequence of the relatively fast establishment of a Cu^+ stationary concentration (Figure 2, curve a). Figure 3b gives the total free-radical yields calculated from the data obtained in the cupric sulfate-ethanol system. As the linear part of the experimental curve is considerably larger (Figure 2, curve b), the accuracy is higher and the size of the standard deviation seems quite reasonable (5%). In Figure 3c the yields of the short-lived oxidizing species derived according to eq 13 are plotted. It should, however, only be taken as an illustration since the possible errors are very high. These values are derived from a difference where each factor was measured with a fairly high standard deviation. For comparison, we also plotted Hayon's recent data¹⁰ for ethanol-oxygen and the data obtained from the oxalate-oxygen system.¹ As can be seen, the general trend in our values is in good agreement with those cited above. However, the decrease in yield for short-lived reducing species with increasing pH as obtained here is larger than that obtained from the oxalate-oxygen system. In our case it is especially pronounced at about pH 3. For the total free-radical yields, our values fall somewhere in between. If we adopt Hayon's definition,¹⁰ that a dilute solution is the one where $k_{\text{RS}}[\text{S}] \leq 10^7 \text{ sec}^{-1}$, then we will have to take into account the following with regard to the data presented in Figure 3: Hayon's curve (dashed) is normalized to $k_{\text{RS}}C_s \leq 10^7 \text{ sec}^{-1}$; up to pH 3.5, $k_{\text{RS}}C_s$ in our experiments does not exceed $1 \times 10^7 \text{ sec}^{-1}$ (at pH higher than this it amounts, in some cases only, up to $3.8 \times 10^7 \text{ sec}^{-1}$); in the oxalic acid-oxygen system $k_{\text{OH}, \text{H}_2\text{C}_2\text{O}_4}[\text{H}_2\text{C}_2\text{O}_4] \leq 1 \times 10^6 \text{ sec}^{-1}$.

The Relative Rate Constant for Some Reactions Studied. Experimental data for hydrogen (given in Table II, and eq 12 with certain transformations) allow us to calculate the relative rate constant for the H atom reactions with cupric sulfate and ethanol at pH 1.5. Assuming that $[\text{H}^+] \gg [\text{CuSO}_4]$ and also introducing eq 9 and 10, we obtain an expression suitable for graphical representation

$$\frac{G(\text{Cu}^+)}{G(\text{H}_2)_{\text{Et}} - G(\text{H}_2)} = 1 + \frac{k_1[\text{CuSO}_4]}{k_8[\text{C}_2\text{H}_5\text{OH}]} \quad (14)$$

where $G(\text{H}_2)_{\text{Et}}$ is the molecular hydrogen yield measured in the cupric sulfate solution in the presence of ethanol. $G(\text{H}_2)$ is the molecular hydrogen yield measured in the corresponding solution without ethanol. It is presented in Figure 4 together with our experimental results. By the least-squares method, the intercept

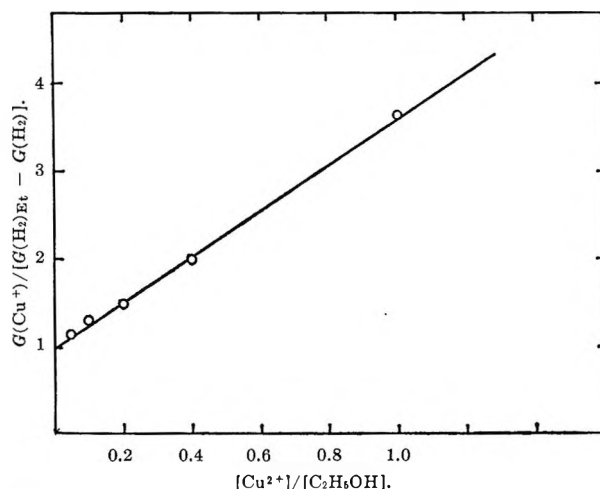


Figure 4. Competition between cupric sulfate and ethanol for H atoms.

is determined to be 0.99, and the slope of the curve to be $k_1/k_8 = 2.64 \pm 0.06$.

Values for k_8 are known and found to be in rather good agreement. If we adopt the value¹⁷ $1.6 \times 10^7 \text{ M}^{-1} \text{ sec}^{-1}$, we obtain for the reaction studied (1) that $k_{\text{H}, \text{CuSO}_4} = 4.2 \times 10^7 \text{ M}^{-1} \text{ sec}^{-1}$. This value is two or three orders of magnitude lower than those given earlier^{7,8} for acid medium. It is about one order of magnitude lower than recent data given for neutral medium.¹⁸ However, it is in fairly good agreement with the value $6.4 \times 10^7 \text{ M}^{-1} \text{ sec}^{-1}$ given for acid medium by Baxendale.¹⁷

From our experimental data we may also derive the rate constant ratio for solvated electron reactions with cupric sulfate and H^+ ions. In the case where $[\text{C}_2\text{H}_5\text{OH}] \gg [\text{CuSO}_4]$, eq 12 may be written as

$$\frac{1}{G(\text{H}_2)_{\text{Et}} - G(\text{H}_2) - G_{\text{H}}} = \frac{1}{G_{\text{e, aq}}} \left[1 + \frac{k_2[\text{CuSO}_4]}{k_3[\text{H}^+]} \right] \quad (15)$$

If we adopt here $G_{\text{H}} = 0.55$, which is obtained from measurements in neutral medium,^{19,20} and introduce this value into eq 15 together with the experimental data given in Table II, we obtain the characteristic competition curve (Figure 5). The slope of the curve is determined to be 0.73 and the intercept 0.44. Hence, we can calculate $k_2/k_3 = 1.64 \pm 0.04$. This rate constant ratio has not been measured earlier, but the constants k_2 and k_3 have been determined under other

(17) J. H. Baxendale, *Radiation Res. Suppl.*, **4**, 114 (1964).

(18) E. Hayon and M. Moreau, *J. Chim. Phys.*, **43**, 391 (1965); A. Appleby, G. Scholes, and M. Simić, *J. Am. Chem. Soc.*, **85**, 3891 (1963).

(19) A. O. Allen and G. Scholes, *Nature*, **187**, 218 (1960).

(20) I. Rabani and G. Stein, *J. Chem. Phys.*, **37**, 1865 (1962).

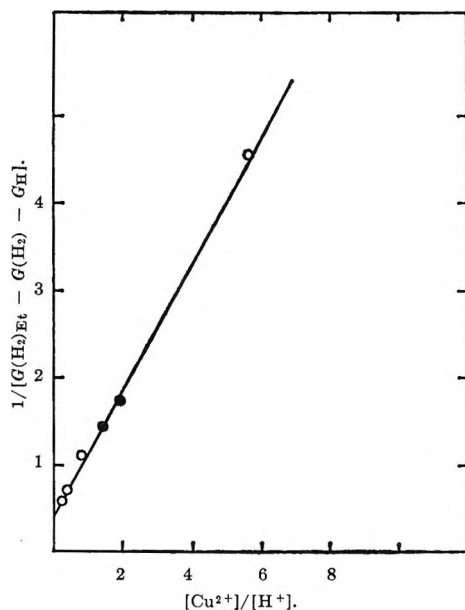


Figure 5. Competition between cupric sulfate and H^+ ions for solvated electrons: ●, sodium sulfate present ($5 \times 10^{-2} M$); ○, sodium sulfate absent.

conditions and are well known. If we take the value reported by Keene,²¹ $k_3 = (2.07 \pm 0.08) \times 10^{10} M^{-1} \text{sec}^{-1}$, then from our measurements we can derive the absolute value for the reactions (2), where k_{eaq^-} , $\text{CuSO}_4 = 3.4 \times 10^{10} M^{-1} \text{sec}^{-1}$. This value is in good agreement with the values obtained by absolute measurements in pulsed radiolysis by Hart,²² $3.3 \times 10^{10} M^{-1} \text{sec}^{-1}$, and Baxendale,²³ $2.9 \times 10^{10} M^{-1} \text{sec}^{-1}$.

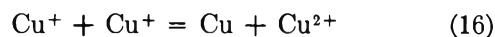
The intercept in Figure 5 provides for the calculation of the primary yield of solvated electrons in the pH region 3.6 to 4.8 studied, $G_{\text{eaq}^-} = 2.3 \pm 0.1$. This value is lower than that obtained by Rabani and Stein²⁰ and by Czapski and Allen.²⁴ It should be pointed out that this value is also lower than the primary yield of reducing short-lived species derived from our measurements of Cu^+ intermediate; the difference is the value adopted for G_{H} .

Remarks on the Scavenging Efficiency of Dissociated and Undissociated Cupric Ions. As can be seen in Figure 4, the experimental data are not plotted on the abscissa as a function of the concentration of dissociated ions but rather in terms of the cupric sulfate concentration. The experimental points fit well to a straight line, which would probably not be the case if only the dissociated cupric ions react efficiently as scavengers. The observations are probably more convincing in determining k_2/k_3 (Figure 5). No difference could be observed between the values measured with and without sodium sulfate ($5 \times 10^{-2} M$), i.e.,

whether or not a suppression of the dissociation exists. This clearly indicates that all the cupric sulfate present reacts as a scavenger, not only the dissociated part as suggested before.⁶

It can be seen that in measuring the constant ratio k_2/k_3 , we did not observe any influence of the ionic strength. This was to be expected since, at the ionic strength of 0.15, the undissociated cupric sulfate molecules replace Cu^{2+} ions.

Remarks on the Reactions in Cu^+ Steady State. It can be seen in Figures 1 and 2 that the stationary concentration of Cu^+ intermediates is not established already under initial conditions. This region did not have any special interest in our experiments; nevertheless, the data obtained allow certain observations. In the case where disproportion is the only cause for an equilibrium state, the mechanism in cupric sulfate solutions could be presented by reactions 1 through 4 and 16.

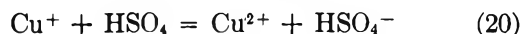
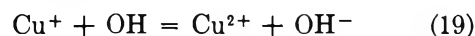
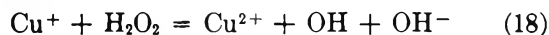


Hence, the following equation would be the consequence.

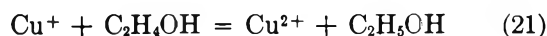
$$\frac{[\text{Cu}^+]}{[\text{Cu}^+_{\text{Et}}]} = \left[\frac{G(\text{Cu}^+)}{G(\text{Cu}^+)_{\text{Et}}} \right]^{1/2} \quad (17)$$

If experimental data from Table I are introduced in eq 17, it is found that this is not the case. This is the reason why the equilibrium state seems to be a result of the reactions of cuprous intermediates with some radiolytic products.

It seems evident that, besides reactions 1 through 4, one may also expect the following reactions in sulfuric acid solutions where only cupric sulfate is present.



In the presence of ethanol, the disappearance of Cu^+ intermediate may also result from the reaction



The existence of reaction 18 was indicated from our determination of the H_2O_2 equilibrium concentration.

(21) J. P. Keene, *Radiation Res.*, **22**, 1 (1964).

(22) S. Gordon, C. J. Hart, M. S. Matheson, J. Rabani, and K. Thomas, *J. Am. Chem. Soc.*, **85**, 1375 (1963).

(23) J. H. Baxendale, E. M. Fielden, and J. P. Keene, *Proc. Chem. Soc.*, 242 (1963).

(24) C. Czapski and A. O. Allen, *J. Phys. Chem.*, **66**, 262 (1962).

Electron Spin Resonance Studies of Fundamental Processes in Radiation and Photochemistry. II. Photochemical Reactions in γ -Irradiated Nitriles at 77°K

by P. B. Ayscough, R. G. Collins, and T. J. Kemp

*School of Chemistry and Cookridge Radiation Laboratories, The University, Leeds 2, England
(Received April 14, 1966)*

The γ radiolysis of acetonitrile at 77°K in the absence of light results in the formation of trapped $\dot{\text{C}}\text{H}_2\text{CN}$ radicals together with a highly photosensitive species which yields methyl radicals when irradiated with infrared or red light. Irradiation with white light results in the disappearance of methyl radicals and the formation of further $\dot{\text{C}}\text{H}_2\text{CN}$ radicals. These reactions are interpreted in terms of a mechanism involving both trapped electrons and positive "holes." The comparative behavior of propionitrile and malononitrile is also discussed briefly.

In part I of this series¹ we presented a general survey of reactions observed by means of electron spin resonance in γ -irradiated aqueous, alcoholic, ethereal, and olefinic glasses at low temperatures and attributed to mobile thermal electrons. Many of these reactions could be simulated by the photochemical generation of electrons or by remobilization of trapped electrons by thermal or photochemical methods. When acetonitrile was incorporated into a glassy matrix of 8 *N* sodium hydroxide at 77°K, methyl radicals were formed by the reaction of mobile electrons according to the dissociative capture process (1), but in a report by Dunbar, Hale, Harrah, Rondeau, and Zakanycz² there is no mention of the appearance of methyl radicals in γ -irradiated pure acetonitrile between 77°K and room temperature. The present investigation was undertaken to attempt to resolve this apparent contradiction and to examine the possibility of observing the reactions of electrons trapped in this polycrystalline matrix.

Experimental Section

Electron spin resonance spectra were recorded by means of a Varian V-4500 epr spectrometer with 100 kc/sec modulation and a low-power microwave bridge.

Acetonitrile was of spectroscopic grade and was not further distilled. Propionitrile and malononitrile were obtained from B.D.H. Ltd. and Eastman Kodak Ltd., respectively, and were freshly distilled before use. All samples were degassed by the freeze-pump-thaw procedure before being distilled into Spectrosil grade quartz sample tubes for irradiation and examination by esr. γ -Irradiations were carried out using a (nominal) 1700-curie ⁶⁰Co source and doses of 2 to 12 $\times 10^5$ rads were given in complete darkness. Samples were kept in darkness by means of a light-tight brass housing while esr spectra were recorded. A shutter was provided so that light could be admitted from a tungsten lamp through a 1-cm² aperture in front of which was a close-fitting attachment for holding spectral filters. Note: irradiated samples of propionitrile invariably shattered violently when melted.

Results

Figure 1a depicts the spectrum obtained from acetonitrile after a dose of 2 $\times 10^5$ rads at 77°K in darkness. The triplet composed of a narrow central line and asymmetric outer peaks is characteristic of a rotating methyl-

(1) P. B. Ayscough, R. G. Collins, and F. S. Dainton, *Nature*, **205**, 965 (1965).

(2) D. Dunbar, D. Hale, L. Harrah, R. Rondeau, and S. Zakanycz, *Develop. Appl. Spectry.*, **3**, 361 (1964).

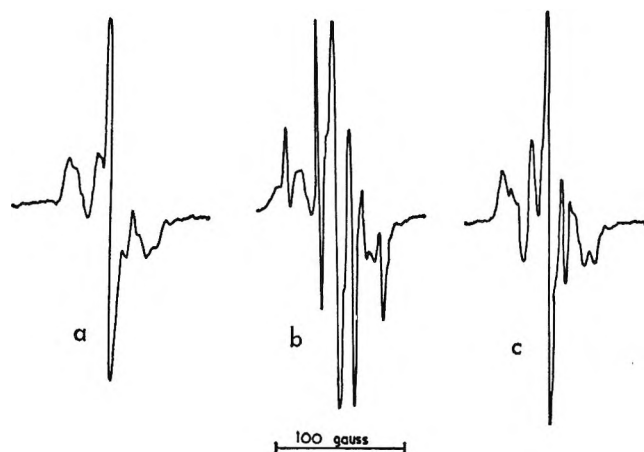


Figure 1. Electron spin resonance spectra of acetonitrile γ -irradiated at 77°K in darkness. Dose 2×10^5 rads: (a) observed at 77°K in darkness; (b) observed at 77°K after 10-sec illumination with red light in cavity; (c) observed at 77°K after 1-min illumination with visible light in cavity.

ene group and may be attributed without doubt to $\dot{\text{C}}\text{H}_2\text{CN}$ radicals.² The additional minor peaks indicate the presence of a small number of methyl radicals. Figure 1b shows the spectrum observed after a 10-sec exposure to red light (using a Chance OR-1 filter). The methyl radical quartet has increased enormously in size, but there is no change in the size of the $\dot{\text{C}}\text{H}_2\text{CN}$ signal. Further exposure to unfiltered light for about 1 min or to red light for about 40 min causes the disappearance of the methyl quartet and a 60% increase in the size of the $\dot{\text{C}}\text{H}_2\text{CN}$ peak (see Figure 1c). In other experiments it was shown that the most careful screening of light from the sample during γ irradiation did not entirely eliminate the trace of methyl radicals in the original spectrum. It was also shown that exposure of γ -irradiated samples to infrared light (>8000 Å) also brought about the increase in concentration of methyl radicals shown in Figure 1b though much more slowly.

Incorporation of electron scavengers in the samples before γ irradiation caused little or no change in the observed spectra. For example, 0.2 M nitrous oxide and 0.04, 0.1, 0.4, and 1 M sulfuric acid have no effect; in a 4 M solution of sulfuric acid (glassy rather than polycrystalline) the yield of $\dot{\text{C}}\text{H}_2\text{CN}$ radicals was more than doubled, and a longer period of photolysis was needed to give a rather less intense methyl radical signal subsequently.

The behavior of CD_3CN was identical apart from the replacement of the $\dot{\text{C}}\text{H}_2\text{CN}$ triplet by the pentet of $\dot{\text{C}}\text{D}_2\text{CN}$ and the $\dot{\text{C}}\text{H}_3$ quartet by the $\dot{\text{C}}\text{D}_3$ septet.

When propionitrile was subjected to the same treat-

ment, the initial spectrum consisted of approximately equal proportions of the normal twelve-line spectrum of C_2H_5 and a broader five-line spectrum (average peak separation 20 gauss) attributed to $\text{CH}_3\dot{\text{C}}\text{HCN}$. Illumination with red light increased the concentration of ethyl radicals, but further illumination with unfiltered light did not bring about any further change.

It was found that malononitrile required approximately six times the radiation dose to achieve the same radical concentration as acetonitrile, and an illumination time two orders of magnitude greater was needed to bring about the change shown in Figure 2b. We interpret Figure 2a as being composed mainly of $\dot{\text{C}}\text{H}_2\text{CN}$ with smaller amounts of $\dot{\text{C}}\text{H}_3$ and perhaps $\dot{\text{C}}\text{H}(\text{CN})\text{CH}_2\text{CN}$, the outer peaks of which appear outside the $\dot{\text{C}}\text{H}_3$ quartet. The final spectrum obtained after illumination with unfiltered light is a predominant doublet, probably attributable to $\dot{\text{C}}\text{H}(\text{CN})_2$. When irradiated in the presence of light, the spectrum is mainly $\dot{\text{C}}\text{H}(\text{CN})_2$ ($a_{\text{H}} = 22.0$ gauss, $a_{\text{N}} = 9.5$ gauss) and no change occurs on further illumination. Hydrogen atoms were present in all irradiated samples but were unaffected by illumination.

Discussion

Those observations relating to the final spectra observed in acetonitrile are in agreement with those of earlier reports,^{2,3} but the additional information derived from the other nitriles and from the photolysis experiments suggests some modification of the reaction mechanism. We must distinguish between processes

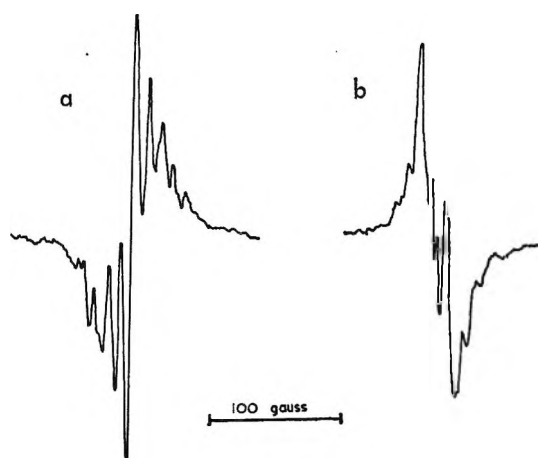
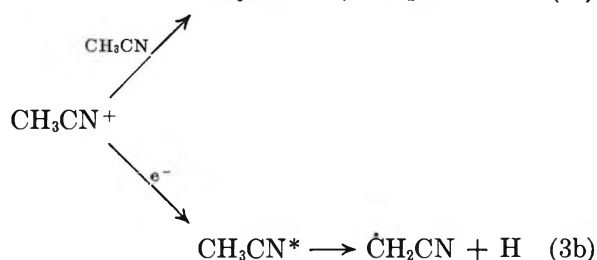


Figure 2. Electron spin resonance spectra of malononitrile γ -irradiated at 77°K. Dose 1.2×10^6 rads: (a) observed at 77°K in darkness; (b) observed at 77°K after 10-min illumination with visible light outside cavity.

(3) N. V. Eliseeva, B. V. Kotov, V. A. Sharpatzi, and A. N. Pravednikov, *Opt. Spectry*. (USSR), 18, 470 (1965).

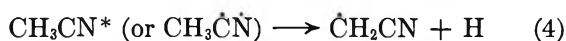
occurring in the dark at 77°K and those occurring under the influence of infrared and/or visible radiation.

In our work and in that of Dunbar, *et al.*, the main species trapped initially at 77°K is $\dot{\text{C}}\text{H}_2\text{CN}$ suggesting a primary ionization (2) followed by the ion-molecule reaction (3a) or the dissociative electron-captive reaction (3b).

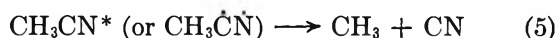


Dunbar, *et al.*, suggest that a poorly resolved triplet coincident with the central peak of $\dot{\text{C}}\text{H}_2\text{CN}$ indicates the presence of CN, but our own observations that these features follow exactly the changes in the $\dot{\text{C}}\text{H}_2\text{CN}$ concentration during photolysis experiments lead us to identify them as partially resolved hyperfine interaction with ^{14}N in $\dot{\text{C}}\text{H}_2\text{CN}$ itself. This conclusion is supported by (a) the absence of C_2N_2 or HCN in the products and (b) the exact equivalence of g factors for $\dot{\text{C}}\text{H}_2\text{CN}$ and the "CN" radical. In propionitrile the radicals $\text{CH}_3\dot{\text{C}}\text{HCN}$ and C_2H_5 are observed (products of reactions analogous to (2) and (3)) but again no CN is found.

The observation by Dunbar, *et al.*, of a purple color in "quick-frozen" samples of acetonitrile which disappeared on warming to 147°K accompanied by a 40% increase in $\dot{\text{C}}\text{H}_2\text{CN}$ concentration closely parallels our own observations of the effect of photolysis at 77°K, apart from the transient appearance of large numbers of methyl radicals during the photolysis. Dunbar, *et al.*, suggest that the increase in $\dot{\text{C}}\text{H}_2\text{CN}$ is caused by the thermal dissociation of an excited species CH_3CN^* , possibly a triplet-state molecule, which is trapped at 77°K and is responsible for the purple color (reaction 4). Our own experiments suggest that CH_3 is a pre-



cursor of $\dot{\text{C}}\text{H}_2\text{CN}$ certainly during the illumination and probably during thermal annealing of irradiated samples also. This might suggest the sequence of reactions 5 and 6. However, the failure to detect CN

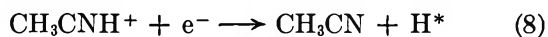


even when formed by the extremely low-energy process (5) induced by infrared radiation is powerful evidence against this interpretation. Furthermore, no HCN was found by Dunbar, *et al.*

It is important to stress that during the photolysis of γ -irradiated acetonitrile at 77°K there is a large increase in the absolute concentration of trapped radicals detected by their esr spectra. This can arise only by dissociation of a diamagnetic species or from reaction of a paramagnetic species which fails to give an observable esr spectrum. When combined with the requirement that this species should adsorb in the infrared and yield methyl radicals, directly or indirectly, with great efficiency and a very low quantum of energy, the suggestion that the species is a trapped electron is more acceptable than a triplet state of CH_3CN . The failure to observe the characteristic spectrum of trapped electrons as observed in polar matrices such as aqueous or alcoholic glasses might be attributed to line broadening caused by interaction with ^{14}N nuclei in cyanide ions close to the trap. Also, the failure of electron scavengers such as nitrous oxide to interfere with the photolysis may well be caused by the strong electrophilic character of acetonitrile itself and to the fact that the migration distance of the electron is less than the dimensions of the microcrystal of acetonitrile. Since this is polycrystalline, the scavenger molecules are likely to be in the interstices. Dissociative electron-capture processes such as (1) would then account for the photolytic generation of methyl and ethyl radicals without the simultaneous formation of CN radicals.

The subsequent disappearance of methyl radicals on prolonged irradiation with visible light is probably a consequence of photoionization of CN^- , a much less efficient process than that by which the radicals are formed. Van Dusen and Truby⁴ have proposed a similar mechanism to explain the effect of photolysis of γ -irradiated methyl bromide in cyclohexane at 77°K. They suggest that electrons formed by photoionization of bromide ions combine with a positive "hole" while the bromine atom recombines with a methyl radical initially formed in close proximity. In acetonitrile the positive "hole" is probably CH_3CNH^+ formed by reaction 3a, so reaction of the electron photoejected from CN^- may take the course represented by (8) and (9) where H^* is the "hot" hydrogen atom. The disappearance of methyl and the simultaneous formation of $\dot{\text{C}}\text{H}_2\text{CN}$ would then be explained by a mechanism

(4) W. Van Dusen, Jr., and F. K. Truby, *J. Am. Chem. Soc.*, **87**, 188 (1965).



very similar to that proposed for the photolysis of γ -irradiated methanol⁵ at low temperatures.

There is no evidence for the participation of any highly photosensitive intermediate in the radiolysis of malononitrile, and the presence of methyl radicals can be explained only by suggesting that they are derived from acetonitrile formed during the prolonged radiolysis. The change brought about by continued photolysis with visible light is similar to that observed in the final stages of the photolysis of acetonitrile, though very much slower. It seems likely that the same mechanism applies though the reasons for the differences in yields from the radiolysis and the subsequent photolysis are not yet clear.

It appears, therefore, that our observations can be interpreted more readily in terms of a mechanism

involving trapped electrons which can be remobilized by photolysis than one involving trapped excited singlet or triplet acetonitrile molecules, though the nature of the electron trap is not well defined. In general, the prerequisite for the formation of a "good" electron trap is a glassy matrix of high dielectric constant in which the electron can cause local polarization by some reorientation of the solvent dipoles. Acetonitrile has a high dielectric constant, but reorientation of its dipole around a thermalized electron is difficult because of its polycrystalline nature so that stabilization energy of the electron is likely to be low.

Acknowledgment. We are grateful to the Science Research Council for financial assistance and to Professor F. S. Dainton, F. R. S., for helpful discussions.

(5) F. S. Dainton, G. A. Salmon, and J. Tepy, *Proc. Roy. Soc. (London)*, **A286**, 27 (1965).

Hydrogen Iodide as a Radical Scavenger in the Radiolysis of Hydrocarbons¹

by D. Perner and Robert H. Schuler

Radiation Research Laboratories, Mellon Institute, Pittsburgh, Pennsylvania (Received January 4, 1966)

Hydrogen iodide has been used as a scavenger to measure the total radical yield in the radiolysis of saturated alkanes. Initially, the radicals react with the hydrogen iodide to produce iodine. As iodine builds up, competitive scavenging occurs between the two solutes present. It is found possible to treat the competition kinetics analytically and correct the iodine production curves for the reaction with iodine so as to obtain an accurate value for the initial yield. This yield is found to be equal to that of iodine disappearance in the corresponding iodine-alkane system. The ratio for the rate constants for the two scavenging reactions can be obtained from a detailed consideration of the growth and decay of iodine as the irradiation progresses. The value for the ratio k_{R+I_2}/k_{R+HI} is found to be 2.0 in hexane at room temperature.

In spite of the fact that hydrogen iodide was suggested some time ago² as a scavenger to measure the over-all radical yield in hydrocarbon radiolysis, no such studies were carried out until those of Hanrahan and co-workers.³⁻⁵ In conjunction with studies in which tritium iodide has been used to produce labeled hydrocarbon products from the radicals,⁶ we have also examined the use of hydrogen iodide in some detail and present the results here. Since a second competing scavenger, iodine, is always present in this system, quantitative treatment of the data involves certain inherent difficulties. Even in the presence of these difficulties, however, this system has a number of advantages which include, as discussed below, certain chemical simplifications of the reactions due to hydrogen atoms, the measurement of product formation rather than reactant disappearance, and the production of stable labeled hydrocarbons through the use of deuterium and tritium iodide. The present results give measurements of radical yields which are quite comparable to those obtained with other scavengers and in addition indicate a ratio between the rate constants for reaction of radicals with iodine and with hydrogen iodide which is quite close to unity.

Experimental Section

Sample Preparation. Samples of Phillips Research grade hexane, decane, and tridecane were thoroughly dried on a high-vacuum line over freshly distilled sodium and distilled into the irradiation cell. Hydrogen

iodide was prepared by dehydrating a solution of hydriodic acid (Baker 47% aqueous HI solution) with P_2O_5 . Free iodine and other impurities were removed by distillation at Dry Ice temperature. A measured gas volume of the hydrogen iodide was added to 3 ml of the hydrocarbon. The vapor volume above the liquid sample was ~ 3 ml. With experience and care it was found possible to prepare HI solutions with no observable iodine ($[I_2] < 10^{-5} M$).

Irradiation and Analysis. The irradiation cells were 1-cm Suprasil (nonradiation coloring) quartz cells suitable for insertion into the spectrophotometer. These were connected to the vacuum line through graded seals. Irradiations were carried out inside a cylindrical Co^{60} source at an absorbed dose rate in hexane of 9.3×10^{18} ev g^{-1} hr^{-1} . Standard Fricke dosimetry, with appropriate corrections for the electron density of the absorbing material, was used.

(1) Supported in part by the U. S. Atomic Energy Commission. Presented at the 151st National Meeting of the American Chemical Society, Pittsburgh, Pa., March 1966.

(2) R. H. Schuler, *J. Phys. Chem.*, **62**, 37 (1958).

(3) B. N. Hughes and R. J. Hanrahan, *ibid.*, **69**, 2707 (1965).

(4) I. Mani and R. J. Hanrahan, Abstracts, 150th National Meeting of the American Chemical Society, Atlantic City, N. J., Sept 1965; *J. Phys. Chem.*, **70**, 2233 (1966).

(5) Hydrogen iodide has, however, been used in alkyl iodide systems; cf., R. J. Hanrahan and J. R. Willard, *J. Am. Chem. Soc.*, **79**, 2434 (1957); D. L. Bunbury, R. R. Williams, and W. H. Hamill, *ibid.*, **78**, 6228 (1956); H. A. Gillis, R. R. Williams, and W. H. Hamill, *ibid.*, **83**, 17 (1961).

(6) D. Perner and R. H. Schuler, to be published.

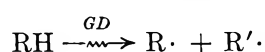
The iodine concentration was determined during the course of the intermittent irradiation by measurement of the absorbance at $525\text{ m}\mu$ with a Cary 14 spectrophotometer. Because many of the measurements were made at low absorbances, the scale expansion available for use with the Cary instrument for absorbances up to 0.2 was used to provide increased accuracy in this region. The extinction coefficients for iodine used in this work were $914\text{ M}^{-1}\text{ cm}^{-1}$ in hexane, $920\text{ M}^{-1}\text{ cm}^{-1}$ in decane, and $935\text{ M}^{-1}\text{ cm}^{-1}$ in tridecane.

For the runs at -78° with hexane the samples were precooled in a Dry Ice bath and then kept at this temperature in the source by a thin layer of Dry Ice. The samples were warmed to room temperature for absorbance measurements.

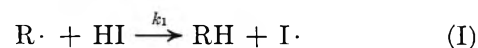
The Idealized Kinetics

In this system the radicals produced by the radiation are expected, at conventional intensities and scavenger concentrations, to react with the hydrogen iodide added to the system to form a hydrocarbon and iodine. In the absence of complications, the initial iodine production yields should be equal to the iodine disappearance yield in the iodine-hydrocarbon systems. Because of an increased importance of scavenging of radicals by iodine and decrease in the hydrogen iodide concentration, one qualitatively expects that, as the radiolysis progresses, the iodine will at first build up in concentration and then later on decrease. The detailed form of the iodine production curve will, of course, depend on the ratio of rate constants for the two scavenging reactions. Since this ratio is known to be of the order of magnitude of unity, an exact solution to the kinetic problem is desirable. Mathematical analysis of the problem is rather complex and one cannot, in fact, obtain an explicit solution for either the iodine or the hydrogen iodide concentration as a function of dose. As is shown here, a general, though somewhat indirect, solution of the problem does exist. Mani and Hanrahan⁴ have considered this same problem and carried out numerical calculations based on iterative considerations of the rates of the competing scavenging processes as the reaction progresses. The forms of the curves resulting from their calculations are virtually the same as those obtained by the present treatment.

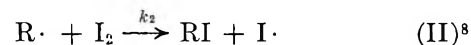
We consider here the idealized problem in which radicals produced at a constant rate GD



react competitively either with HI initially added to the system



or with molecular iodine produced as a result of the combination of the iodine atoms formed in (I).⁷



From the appropriate kinetic expressions, it can be shown that the stoichiometry is represented by the relationship

$$GDt = 2\{[\text{HI}]_0 - [\text{HI}] - [\text{I}_2]\} \quad (1)$$

where GDt is the total number of radicals produced, $[\text{HI}]_0$ is the initial hydrogen iodide concentration, and $[\text{HI}]$ and $[\text{I}_2]$ are the hydrogen iodide and iodine concentrations present at dose Dt . The number of radicals produced is thus measured by the number of equivalents of HI lost from solution minus the number of equivalents of iodine built up, with 1 mole of each reactant representing 2 equiv in the over-all reaction. Introducing this stoichiometric relationship into the appropriate rate expression, one obtains

$$-\frac{d[\text{HI}]}{dt} = GD \frac{k_1[\text{HI}]}{(k_1 - k_2)[\text{HI}] + k_2\left([\text{HI}]_0 - \frac{GDt}{2}\right)} \quad (2)$$

Equation 2 is the basic differential equation which must be integrated to give the dependence of the hydrogen iodide and iodine (*via* eq 1) concentrations upon dose.

The Limiting Cases. The two limiting cases, where either the rate of reaction I or II dominates the over-all kinetics, are trivial and can be treated by inspection. Where $k_1/k_2 \gg 1$ the radicals react exclusively with HI at a rate equal to GD and iodine builds up at a rate equal to $GD/2$. When the HI becomes exhausted, iodine will be present at a concentration of $[\text{HI}]_0/2$ and will then disappear at a rate equal to $GD/2$. This behavior, which gives the respective lower and upper limits to the HI and I_2 concentrations, is illustrated by the dashed curves of Figure 1. Where $k_1/k_2 \ll 1$ iodine will disappear as rapidly as it is formed and will be present only at a very low concentration during the course of the reaction. The HI concentration will decrease at a rate of $GD/2$ since each

(7) S. W. Benson [*J. Chem. Phys.*, **20**, 1605 (1952)]; "The Foundations of Chemical Kinetics," McGraw-Hill Book Co., Inc., New York, N. Y., 1960, p 45] has treated a somewhat similar general case where competition exists between the reactions $\text{B} + \text{A} \rightarrow \text{C}$ and $\text{B} + \text{C} \rightarrow \text{D}$. The case under consideration here is somewhat more restrictive in that one reactant (B) is produced at a constant rate so that the dependence of the sum of the other reactants (A + C) upon time is known (*cf.* eq 5a).

(8) The reaction $\text{R}\cdot + \text{HI} \rightarrow \text{RI} + \text{H}\cdot$ will not occur because of the high endothermicity of this reaction.

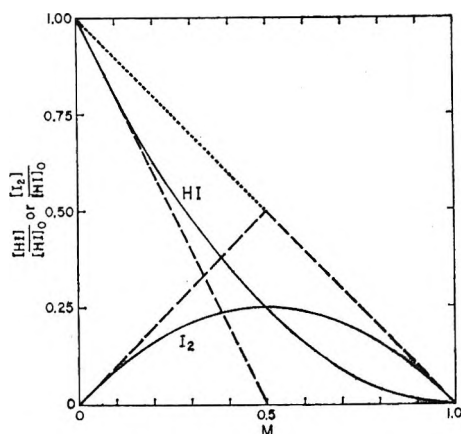


Figure 1. Idealized dependence of hydrogen iodide and iodine concentrations upon the reduced dose M for the cases where $k_1 = k_2$ (solid curves) and where $k_1 \gg k_2$ (dashed curves). When $k_1 \ll k_2$, the iodine concentration remains trivially small and the hydrogen iodide concentration follows the upper dotted and dashed curve (which also expresses the total scavenger concentration in all cases).

molecule of HI will react with two radicals. This represents the upper limit to the HI concentration.

The Special Case Where $k_1 = k_2$. For the case where $k_1 = k_2$ the coefficient of [HI] in the denominator of (2) becomes zero, and the expression may be readily integrated to give

$$[\text{HI}] = [\text{HI}]_0 - GDt + \frac{1}{4} \frac{(GDt)^2}{[\text{HI}]_0} \quad (3)$$

From eq 1

$$[\text{I}_2] = \frac{1}{2} GDt - \frac{1}{4} \frac{(GDt)^2}{[\text{HI}]_0} \quad (4)$$

At this point it is convenient to define dose in terms of M , the fraction of the dose required for complete exhaustion of the scavenger present, *i.e.*

$$M = \frac{GDt}{2[\text{HI}]_0} \quad (5)$$

Equations 3 and 4 may be rewritten in the form of reduced hydrogen iodide and iodine concentrations to give

$$\frac{[\text{HI}]}{[\text{HI}]_0} = (1 - M)^2 \quad (6)$$

and

$$\frac{[\text{I}_2]}{[\text{HI}]_0} = M(1 - M) \quad (7)$$

These equations are represented by the solid curves of Figure 1. The total scavenger present of course

decreases linearly with dose as is expected from (1) and is shown by summing (6) and (7).

$$\frac{[\text{HI}]}{[\text{HI}]_0} + \frac{[\text{I}_2]}{[\text{HI}]_0} = 1 - M$$

Expression of the variables in terms of the reduced quantities $[\text{HI}]/[\text{HI}]_0$, $[\text{I}_2]/[\text{HI}]_0$, and M therefore allows one to write general equations which describe the dependence at all values of scavenger concentrations. It is seen below that this also holds for the general case.

The General Case. For the general case where $k_1/k_2 \neq 1$, eq 2 cannot be integrated directly since neither [HI] nor t can be factored out of the right side of the equation. With appropriate substitutions the variables of differential eq 2 can, however, be separated and the equation integrated to give M and $[\text{I}_2]/[\text{HI}]_0$ as nonlinear functions of $[\text{HI}]/[\text{HI}]_0$ (*cf.* Appendix I). The resultant expressions are

$$M = 1 - \frac{[\text{HI}]}{[\text{HI}]_0} \frac{1}{2 \left(1 - \frac{k_2}{2k_1}\right)} \left\{ \left(\frac{[\text{HI}]}{[\text{HI}]_0} \right)^{(k_2/2k_1) - 1} - \left(\frac{k_2}{k_1} - 1 \right) \right\} \quad (8)$$

and

$$\frac{[\text{I}_2]}{[\text{HI}]_0} = \frac{[\text{HI}]}{[\text{HI}]_0} \frac{1}{2 \left(1 - \frac{k_2}{2k_1}\right)} \left\{ \left(\frac{[\text{HI}]}{[\text{HI}]_0} \right)^{(k_2/2k_1) - 1} - 1 \right\} \quad (9)$$

Thus, although it is not possible to solve eq 8 and 9 for [HI] and $[\text{I}_2]$ as explicit functions of dose (except of course where $k_2 = k_1$) it is possible, given the ratio k_2/k_1 , to calculate the dose M at which the concentration of hydrogen iodide will be reduced by a given fraction and to also calculate the iodine concentration corresponding to this dose. Curves showing the dependence of $[\text{I}_2]/[\text{HI}]_0$ upon M for a number of specific values of k_2/k_1 are given in Figure 2.

Determination of Radical Yield from I_2 Production Rate. The radical production rate GD can be determined from the initial rate of production of I_2 , which is equal to $GD/2$. However, since initial yields are difficult to measure accurately, it is desirable to find a method to relate subsequent points on the $[\text{I}_2]$ vs. dose graphs to the radical yield. A correction factor F may be defined by

$$F[\text{I}_2] = \frac{GDt}{2} \quad (10)$$

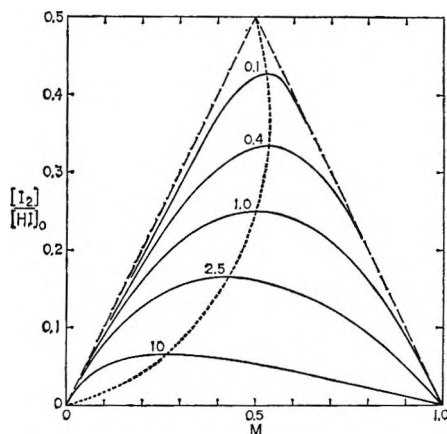


Figure 2. Dependence of iodine concentration upon reduced dose for various values of k_2/k_1 (solid curves). Dotted curve gives locus of the iodine maximum for all values of k_2/k_1 .

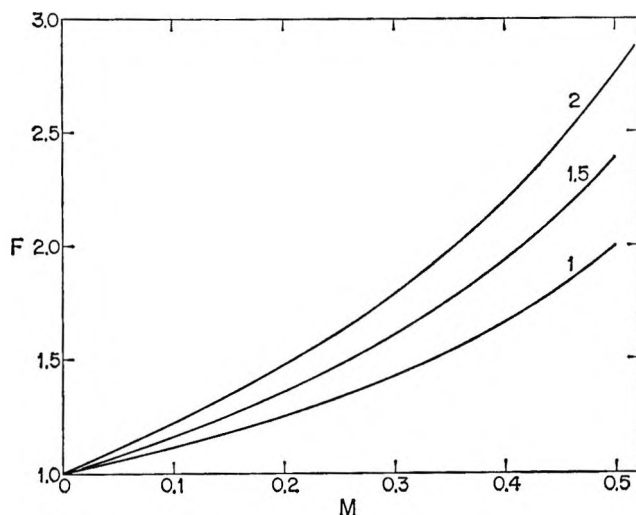


Figure 3. Values of the factor $F (= M([I_2]/[HI]_0)^{-1})$ used to correct the production of iodine for reaction II at ratios of k_2 to k_1 of 1, 1.5, and 2.

If reaction II did not occur, F would be unity throughout the experiment. Dividing (10) by $[HI]_0$ gives

$$F \frac{[I_2]}{[HI]_0} = \frac{G D t}{2 [HI]_0} = M$$

F may therefore be evaluated from the corresponding values of M and $[I_2]/[HI]_0$ determined from eq 8 and 9. For $k_2/k_1 = 1$ this factor is simply $1/(1 - M)$. Curves calculated by this method for the rate constant ratios of 1, 1.5, and 2 are given in Figure 3 as a function of M .

The Iodine Maximum. The complexity of eq 8 and 9 together with the fact that the desired dependence, *i.e.*, $[I_2] = f(Dt)$, can be calculated only indirectly, makes the general utility of this type of solution some-

what limited. The availability of these equations does, however, make certain other facets of the analytical solution of the problem tractable. In particular, one can show, as is done in Appendix II, that the reduced quantity $[I_2]/[HI]_0$ at the maximum iodine concentration is independent of the value of $[HI]_0$ and is a function (eq 11) only of the ratio k_2/k_1

$$\left(\frac{[I_2]}{[HI]_0}\right)_{\max I_2} = \frac{1}{2} \left(\frac{k_2}{2k_1}\right)^{\frac{1}{1 - (k_2/2k_1)}} - 1 \quad (11)$$

This dependence is given in Figure 4. The lack of dependence of $([I_2]/[HI]_0)_{\max I_2}$ upon initial hydrogen iodide concentration was demonstrated empirically in the recent study of Hughes and Hanrahan.³ Values for the other variables, $M_{\max I_2}$ and $([HI]/[HI]_0)_{\max I_2}$, which are similarly independent of $[HI]_0$ are given by eq 29 and 28 in Appendix II. From these relationships the locus of the iodine maximum may be calculated and is represented in Figure 2 by the dotted curve. Where the rate constants are comparable, the value of M at which the maximum occurs does not depend strongly on the ratio of the rate constants, being a maximum of ~ 0.535 at $k_2/k_1 \sim 0.2$ and only decreasing to 0.468 at $k_2/k_1 = 2$. The value of $[I_2]/[HI]_0$ at the maximum does, however, depend significantly on the ratio of the rate constants so that a reasonably accurate estimate should be possible from the experimental measurements if the competition at all approximates these idealized kinetics.

Results and Discussion

Typical results obtained in hexane solutions for the dependence of iodine concentration upon dose are given by the lower curves in Figure 5. These are very similar in form to the dependences reported by Hanrahan and co-workers for cyclopentane³ and cyclohexane⁴ solutions. In the absence of complications, the scavenger is expected to be used up at a dose Dt_c equal to $2[HI]_0/G$. The tails of the iodine concentration curves were extrapolated to the axis and the resultant doses are plotted in Figure 6 as a function of the initial hy-

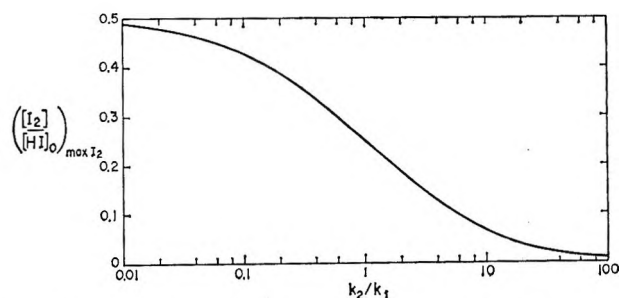


Figure 4. Dependence of $([I_2]/[HI]_0)_{\max I_2}$ upon k_2/k_1 .

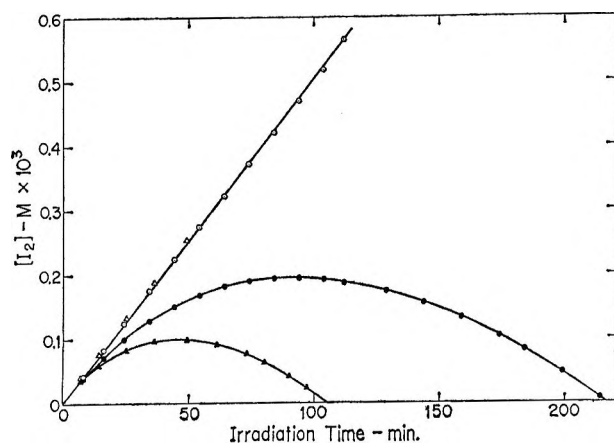


Figure 5. Dependence of $[I_2]$ upon dose for hexane solutions initially containing $1.06 \times 10^{-3} M$ HI (●) and $5.2 \times 10^{-4} M$ HI (▲). Open points are the values obtained by multiplying the observed concentrations by the appropriate factors from Figure 3.

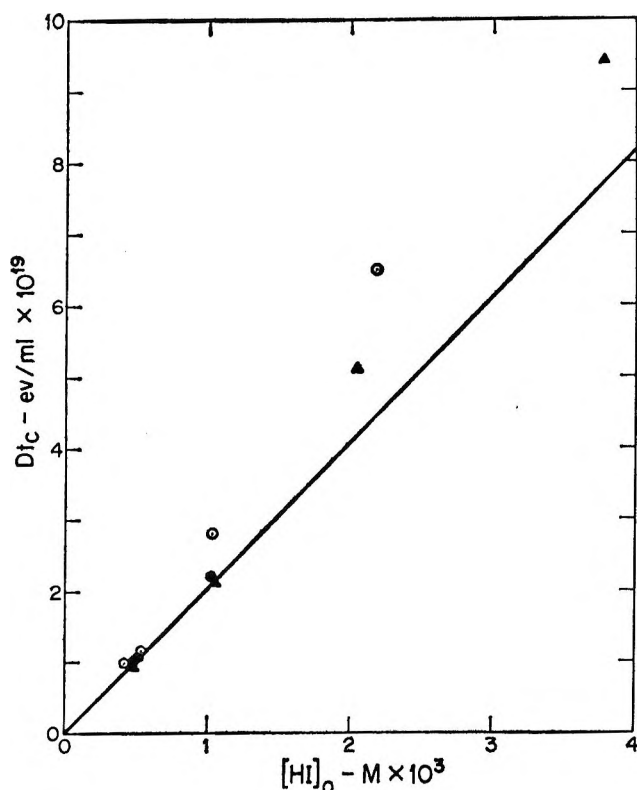
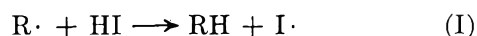
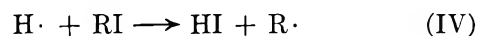


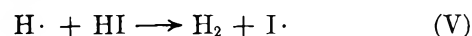
Figure 6. Dependence of dose required for complete exhaustion of scavenger (D_{tc}) upon the initial HI concentration. Hexane at room temperature (●), at -78° (○), decane at room temperature (▲). Solid curve corresponds to a yield of 5.9.

drogen iodide concentration. It is seen that the data exhibit in upward curvature; *i.e.*, the average yield determined in this way decreases with increasing hy-

drogen iodide concentration. The principal reason for this decrease is almost certainly due to reaction of hydrogen atoms with the iodine and alkyl iodides present after the irradiation has progressed.

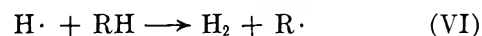


It is seen from the sum of reactions III and I that the reaction of hydrogen atoms with iodine effectively results in the formation of a hydrocarbon molecule without the consumption of any scavenger. The average radical yield will therefore be decreased by twice the contribution of reaction III to the over-all kinetics. Reaction IV similarly results in the effective conversion of a hydrogen atom to an iodine atom and the loss of two equivalents contribution to the yield. Hydrogen atoms which react with HI to form hydrogen gas will cause no complications in that they are included in the normal count of radicals.



In the early stages of the reaction, (V) dominates over (III) and (IV) so that the initial slope should accurately reflect the total radical yield (including that of the hydrogen atoms).⁹

In the experiments reported in Figure 5, it should be noted that the iodine concentration builds up to only $1-2 \times 10^{-4} M$. Since it is known from the lack of an effect on the hydrogen production at this iodine level¹⁰ and also from the high reactivity of hydrogen atoms produced in the photolysis of tritium iodide solutions¹¹ that at these scavenger concentrations the hydrogen atoms predominantly abstract from the solvent



complications from reactions III and IV should be at a minimum. In the over-all kinetics the conversion of hydrogen atoms to alkyl radicals *via* reaction VI

(9) When iodine itself is used as the radical scavenger, any hydrogen atoms which react with the iodine will during the initial stages of the reaction result in the disappearance of one equivalent of iodine and be counted in the radical yield in the normal way. As the HI builds up and subsequently reacts, the average apparent radical yield will decrease as in the present case. One expects, therefore, that iodine consumption will at first be linear with dose with an upward curvature appearing only at the late stage in the reaction when the ratio $[HI]/[I_2]$ becomes significant. Experimentally this is found to be the case [see R. H. Schuler, *J. Phys. Chem.*, 63, 925 (1959)]. The curvature should be small at low iodine concentrations ($<10^{-3} M$) where reaction VI converts hydrogen atoms to alkyl radicals and thus decreases the importance of (III).

(10) R. H. Schuler, *J. Phys. Chem.*, 61, 1472 (1957).

(11) D. Perner and R. H. Schuler, *ibid.*, 70, 317 (1966).

is important in that it permits the idealized kinetics described earlier to be obeyed rather accurately.

The values for the ratio $[I_2]/[HI]_0$ at the maximum iodine concentration is 0.185 and 0.188 for the two experiments at room temperature reported in Figure 5. The following discussion is based on an assumed value of k_2/k_1 of 2 for which $([I_2]/[HI]_0)_{\max} = 0.184$ (cf. Appendix III). The total radical production, obtained by multiplying the observed iodine concentration by the appropriate factors from Figure 3, is plotted as the upper curve in Figure 5. The slope of this line corresponds to $G(R) = 5.88$. In this treatment the correction factors are obtained from successive approximations of values of M based on the reaction rate estimated either from the initial slope or from the data of Figure 6. Fortunately, the slope is not strongly dependent on the value of M in the initial stages of the reaction so that this approximation converges rather rapidly. Previous measurements of iodine disappearance in hexane gave values of $G(R)$ of 5.60 with γ rays and 5.55 with electrons.¹² The slight difference between these values is for the most part within the experimental error of determining the initial slope of each of the curves although it may possibly reflect, to a small extent, the dependence of yield found at very much higher HI concentrations (see below).

The reduced iodine concentration, $[I_2]/[HI]_0$, is plotted in Figure 7 as a function of M where M is calculated from eq 5 taking G to be 5.9. The growth and decay curves calculated from eq 8 and 9 are given by the solid curves in Figure 7 for $k_2/k_1 = 2$ and 1.

It is seen that at room temperature the experimental data fit the curve for $k_2/k_1 = 2$ quite well with only a very slight skewing toward lower values of M . Since the average radical yield of 5.72 determined from the observed value of Dt_c agrees very well with the above-mentioned initial yield of 5.88, a high degree of agreement is expected between the idealized kinetics and the experimental data in this form of plot. From the ratio of these yields the maximum fractional contribution from reaction III may be estimated to be $\frac{1}{2}[(5.88/5.72) - 1] = 0.014$ (or a G of 0.08). This is in the range indicated by the tracer experiments for scavenger concentrations of the order of $10^{-4} M$.

Data were also obtained on solutions irradiated at -78° . Here $([I_2]/[HI]_0)_{\max}$ is very close to the value of 0.25 expected for $k_2/k_1 = 1$. Correcting the observed iodine concentrations as indicated above gives an initial slope corresponding to $G = 5.5$. These data therefore indicate that over this range there is only a small effect of temperature on the radical yield. The reduced concentrations are plotted in Figure 7 as a function of $Gdt/2[HI]_0$. While the values initially

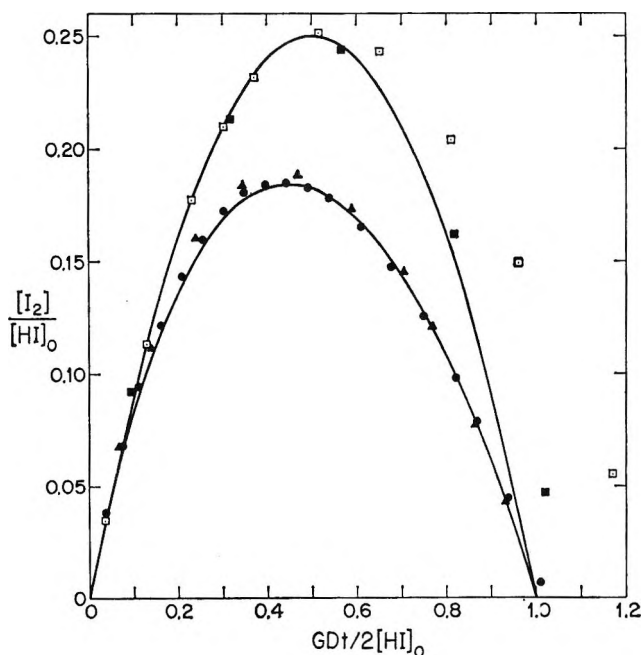


Figure 7. Dependence in hexane of reduced I_2 concentration on reduced dose. Closed circles and triangles correspond to the points in Figure 5 taken at room temperature. Values obtained at -78° for solutions 1.03 and $0.54 \times 10^{-3} M$ are given by open and closed squares, respectively. Curves are for the idealized case with $k_2/k_1 = 1$ (upper) and 2 (lower).

follow the calculated curve very accurately they straggle at higher values of M . This behavior is not unexpected since conversion of hydrogen atoms to other radicals *via* reaction VI becomes less important at the lower temperature. The average radical yield determined from measurements of Dt_c is 5.1 at the lower and 4.4 at the higher concentration reported in the figure. The distortion of the growth and decay curves by the increased importance of (III) and (IV) will however have only a slight influence on the value of $[I_2]/[HI]_0$ at the maximum. We take the data of Figure 7 to indicate, therefore, that k_2/k_1 is very close to 1 at the lower temperature.

It would appear from the above that the rate constant ratio changes by approximately a factor of 2 in going from room temperature to -78° . This change correspond to an activation energy for reactions of radicals with I_2 800 cal mole $^{-1}$ greater than for reaction with HI. Since the actual rates favor the reaction of radicals with iodine at room temperature, this activation energy difference must be compensated by a steric factor somewhat smaller for the reaction with HI. The observed relative rate constants can be expressed by the empirical relationship

(12) R. H. Schuler, *J. Phys. Chem.*, **63**, 925 (1959).

$$\frac{k_2}{k_1} = \frac{1}{0.13} e^{-800/RT}$$

Since the rate of reaction of radicals with iodine is known to be very close to that for a diffusion-controlled reaction,¹³ the above indicates that in that case the steric factor must be very close to unity and therefore that the activation energy for the reaction with hydrogen iodide is very close to zero. From the above-indicated value of 800 cal mole⁻¹, a diffusion-controlled rate constant of 10⁹ M⁻¹ sec⁻¹ and a steric factor of unity, an absolute rate of 3 × 10⁸ M⁻¹ sec⁻¹ is calculated. This agrees with the estimate¹³ made for the rate constant for the reaction of methyl radicals with iodine.

Experiments similar to the above were also carried out at room temperature with decane. In this case ([I₂]/[HI]₀)_{max} ~ 0.216, which corresponds to a value for k₂/k₁ of 1.5. Plots of the reduced values of the form given in Figure 7 show good agreement with the curve calculated for k₂/k₁ of 1.5. The measured initial radical yield is 6.1. Measurements of Dt_c were made at various HI concentrations and are given in Figure 6. At the lowest concentrations, average radical yields of 6.0 and 5.9 were obtained from these measurements. Determinations of the initial radical yield were also made for tridecane at a hydrogen iodide concentration of 4 × 10⁻⁴ M and gave a value of 6.3.

At higher hydrogen iodide concentrations, the initial iodine production rates can be readily measured without significant interference from reaction II. Yields measured in hexane are given in Figure 8. It is seen that in the region of 10⁻² M scavenger, the yields increase by about two units. A similar increase was also found in the cases of decane and tridecane. Measurements of the yield of formation of alkyl iodide product at high concentrations of iodine (~10⁻² M) in butane¹⁴ and in cyclohexane¹⁵ show a similar increase in yield.

These higher observed initial yields correspond to points below the linear relationship in Figure 6 so that the increase in apparent radical yield cannot be explained by any of the reactions written above. In particular, the interference with the abstraction reaction (VI) by the scavenging of hydrogen atoms with HI should not change the number of equivalents of iodine produced. It has also been noted that the total hydrogen yield from these solutions is greater than for the pure hydrocarbons¹⁰ and that there is an appreciable H₂ yield from HI-deuteriocyclohexane¹⁶ and D₂ yield from DI-hexane solutions.¹⁷ These various complications show that there are physical effects such as energy transfer or electron capture which result in dissociation of the solute and which can

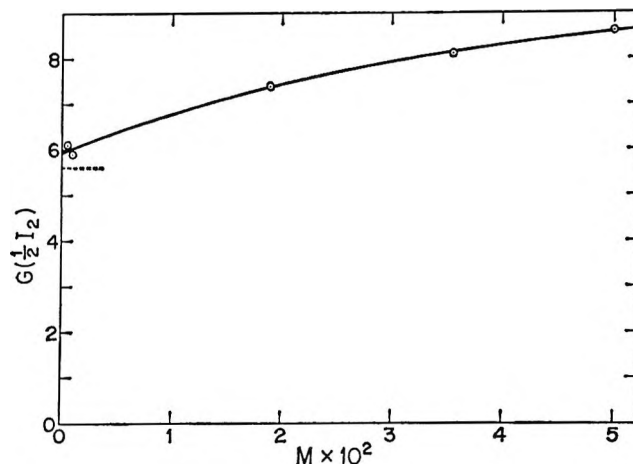


Figure 8. Dependence of initial yield for the formation of I₂ upon HI concentration (in hexane).

be operative at even moderate concentrations. As in all scavenging experiments, extreme caution must therefore be used in the interpretation of results at higher concentrations, *i.e.*, in this case at HI concentrations above 10⁻³ M. At lower concentrations the present results, as well as the studies with labeled hydrogen iodide, indicate that complications are small.

Appendix I

Integration of the General Equation. The variables of eq 2 can be separated if one rewrites this equation in the form

$$-\frac{d[\text{HI}]}{dt} = GD \frac{1}{\frac{k_1 - k_2}{k_1} + \frac{k_2}{k_1} \frac{[\text{HI}]_0 - \frac{GDt}{2}}{[\text{HI}]}} \quad (12)$$

and defines a new variable

$$y = \frac{[\text{HI}]_0 - \frac{GDt}{2}}{[\text{HI}]} \quad (13)$$

Differentiating (13) and solving for dt, one obtains

$$dt = -\frac{2}{GD} \{ [\text{HI}] dy + y d[\text{HI}] \} \quad (14)$$

Insertion of the new variable into (12) gives

(13) R. H. Schuler and R. R. Kuntz, *J. Phys. Chem.*, **67**, 1004 (1963).

(14) C. E. McCauley and R. H. Schuler, *J. Am. Chem. Soc.*, **79**, 4008 (1957).

(15) R. W. Fessenden and R. H. Schuler, *ibid.*, **79**, 273 (1957).

(16) J. R. Nash and W. H. Hamill, *J. Chem. Phys.*, **66**, 1097 (1962).

(17) D. Perner, to be published.

$$-\frac{d[\text{HI}]}{dt} = GD \frac{1}{\frac{k_1 - k_2}{k_1} + \frac{k_2}{k_1} y}$$

which can be solved for dt

$$dt = -\frac{1}{GD} \left\{ \frac{k_1 - k_2}{k_1} + \frac{k_2}{k_1} y \right\} d[\text{HI}] \quad (15)$$

Equating the right sides of (14) and (15)

$$2[\text{HI}]dy + 2y d[\text{HI}] = \left\{ \frac{k_1 - k_2}{k_1} + \frac{k_2}{k_1} y \right\} d[\text{HI}] \quad (16)$$

allows separation of the variables in the form

$$2[\text{HI}] \frac{dy}{d[\text{HI}]} = \frac{k_1 - k_2}{k_1} + \left(\frac{k_2}{k_1} - 2 \right) y \quad (17)$$

or

$$\frac{d[\text{HI}]}{[\text{HI}]} = \frac{2}{\frac{k_1 - k_2}{k_1} + \left(\frac{k_2}{k_1} - 2 \right) y} dy \quad (18)$$

Since $y = 1$ at $t = 0$, i.e., where $[\text{HI}] = [\text{HI}]_0$

$$\int_{[\text{HI}]_0}^{[\text{HI}]} \frac{d[\text{HI}]}{[\text{HI}]} = \int_1^y \frac{2}{\frac{k_1 - k_2}{k_1} + \left(\frac{k_2}{k_1} - 2 \right) y} dy \quad (19)$$

which upon integration gives

$$\ln \frac{[\text{HI}]}{[\text{HI}]_0} = \frac{2}{\left(\frac{k_2}{k_1} - 2 \right)} \ln \left\{ -1 \left[\frac{k_1 - k_2}{k_1} + \left(\frac{k_2}{k_1} - 2 \right) y \right] \right\} = \frac{1}{\frac{k_2}{2k_1} - 1} \ln \left\{ \frac{k_2 - k_1}{k_1} + 2 \left(1 - \frac{k_2}{2k_1} \right) \frac{[\text{HI}]_0 - \frac{GDt}{2}}{[\text{HI}]} \right\} \quad (20)$$

One can therefore write

$$\left(\frac{[\text{HI}]}{[\text{HI}]_0} \right)^{(k_2/2k_1) - 1} = \left(\frac{k_2}{k_1} - 1 \right) + 2 \left(1 - \frac{k_2}{2k_1} \right) \frac{[\text{HI}]_0 - \frac{GDt}{2}}{[\text{HI}]} \quad (21)$$

At this point it is again convenient to substitute in the value for the reduced dose defined by eq 5.

$$\left(\frac{[\text{HI}]}{[\text{HI}]_0} \right)^{(k_2/2k_1) - 1} = \left(\frac{k_2}{k_1} - 1 \right) + 2 \left(1 - \frac{k_2}{2k_1} \right) \frac{[\text{HI}]_0(1 - M)}{[\text{HI}]} \quad (22)$$

Solving (22) for M gives eq 8.

$$M = 1 - \frac{[\text{HI}]}{[\text{HI}]_0} \frac{1}{2 \left(1 - \frac{k_2}{2k_1} \right)} \times \left\{ \left(\frac{[\text{HI}]}{[\text{HI}]_0} \right)^{(k_2/2k_1) - 1} - \left(\frac{k_2}{k_1} - 1 \right) \right\} \quad (8)$$

Substituting (5) into (1)

$$\frac{[\text{I}_2]}{[\text{HI}]_0} = 1 - M - \frac{[\text{HI}]}{[\text{HI}]_0} \quad (23)$$

$$= \frac{[\text{HI}]}{[\text{HI}]_0} \left\{ \frac{1}{2 \left(1 - \frac{k_2}{2k_1} \right)} \times \left[\left(\frac{[\text{HI}]}{[\text{HI}]_0} \right)^{(k_2/2k_1) - 1} - \left(\frac{k_2}{k_1} - 1 \right) \right] - 1 \right\} \quad (24)$$

which simplifies to eq 9.

$$\frac{[\text{I}_2]}{[\text{HI}]_0} = \frac{[\text{HI}]}{[\text{HI}]_0} \frac{1}{2 \left(1 - \frac{k_2}{2k_1} \right)} \left\{ \left(\frac{[\text{HI}]}{[\text{HI}]_0} \right)^{(k_2/2k_1) - 1} - 1 \right\} \quad (9)$$

Appendix II

Evaluation of the Variables at the Iodine Maximum. The relative iodine and hydrogen iodide concentrations may be obtained by dividing both sides of eq 9 by $[\text{HI}]/[\text{HI}]_0$.

$$[\text{I}_2]/[\text{HI}] = \frac{\left([\text{HI}]/[\text{HI}]_0 \right)^{(k_2/2k_1) - 1} - 1}{2 \left(1 - k_2/2k_1 \right)} \quad (25)^{18}$$

At the maximum iodine concentration, the rates of reactions I and II are equal

$$k_2 [\text{I}_2]_{\text{max I}_2} = k_1 [\text{HI}]_{\text{max I}_2}$$

or

$$\left(\frac{[\text{I}_2]}{[\text{HI}]} \right)_{\text{max I}_2} = \frac{k_1}{k_2} \quad (26)$$

Introducing the value of $([\text{I}_2]/[\text{HI}])_{\text{max I}_2}$ obtained from (25) one can write

$$\frac{k_1}{k_2} = \frac{1}{2 \left(1 - \frac{k_2}{2k_1} \right)} \left\{ \left(\frac{[\text{HI}]}{[\text{HI}]_0} \right)_{\text{max I}_2}^{(k_2/2k_1) - 1} - 1 \right\} \quad (27)$$

(18) This expression is of the same form as that given by S. Benson [*J. Chem. Phys.*, **20**, 1605 (1952)] for the general competition of two reactants with a third substance. It can be obtained more directly by dividing the rate expression for $[\text{HI}]$ by that for $[\text{I}_2]$ to eliminate time as a variable and then separating variables by substitution of $y = [\text{I}_2]/[\text{HI}]$.

Multiplying by $2[1 - [k_2/2k_1]]$

$$2(k_1/k_2) - 1 = \left(\frac{[\text{HI}]}{[\text{HI}]_0} \right)_{\max I_2}^{(k_2/2k_1) - 1} - 1$$

which gives

$$\left(\frac{[\text{HI}]}{[\text{HI}]_0} \right)_{\max I_2} = \left(\frac{k_2}{2k_1} \right)^{1/[1 - (k_2/2k_1)]} \quad (28)$$

Introducing this value into (9) gives

$$\left(\frac{[\text{I}_2]}{[\text{HI}]_0} \right)_{\max I_2} = \left(\frac{k_2}{2k_1} \right)^{1/[1 - (k_2/2k_1)]} \times \frac{1}{2 \left(1 - \frac{k_2}{2k_1} \right)} \left\{ \left(\frac{k_2}{2k_1} \right)^{-1} - 1 \right\}$$

which readily simplifies to

$$\left(\frac{[\text{I}_2]}{[\text{HI}]_0} \right)_{\max I_2} = \frac{1}{2} \left(\frac{k_2}{2k_1} \right)^{1/[1 - (k_2/2k_1)] - 1} \quad (11)$$

The equation for $M_{\max I_2}$ can be obtained either by substituting (28) and (11) into (23) or by substituting (28) into (8). The former is somewhat less laborious and gives

$$\begin{aligned} M_{\max I_2} &= 1 - \left(\frac{k_2}{2k_1} \right)^{1/[1 - (k_2/2k_1)]} - \\ &\quad \frac{1}{2} \left(\frac{k_2}{2k_1} \right)^{1/[1 - (k_2/2k_1)] - 1} \\ &= 1 - \left(\frac{k_2}{2k_1} \right)^{1/[1 - (k_2/2k_1)]} \left(1 + \frac{1}{k_2/k_1} \right) \quad (29) \end{aligned}$$

The locus of the iodine maximum as a function of k_2/k_1 can therefore be obtained from (11) and (29) and is given by the dotted curve in Figure 2.

Appendix III

Evaluation of the Equations When $k_2 = 2k_1$. In general, numerical evaluation of the quantities given by the above equations, though somewhat involved, can be readily carried out. We would like to mention here, however, the special case when $2k_1 = k_2$ for which the equations as written become indeterminate. The

equations can be evaluated by substituting in the quantity $(k_2/2k_1) = 1 + \Delta$ and evaluating the expressions as $\Delta \rightarrow 0$. Thus for this case (11) becomes

$$\begin{aligned} \left(\frac{[\text{I}_2]}{[\text{HI}]_0} \right)_{\max I_2} &= \lim_{\Delta \rightarrow 0} \frac{1}{2} (1 + \Delta)^{1/[1 - (1 + \Delta)] - 1} = \\ &= \lim_{\Delta \rightarrow 0} \frac{1}{2} \left(\frac{1}{1 + \Delta} \right)^{1/\Delta} \left(\frac{1}{1 + \Delta} \right) \\ &= \frac{1}{2e} \end{aligned}$$

and (29) becomes

$$\begin{aligned} M_{\max I_2} &= \lim_{\Delta \rightarrow 0} \left\{ 1 - (1 + \Delta)^{1/[1 - (1 + \Delta)]} \times \right. \\ &\quad \left. \left(1 + \frac{1}{2(1 + \Delta)} \right) \right\} \\ &= \lim_{\Delta \rightarrow 0} \left\{ 1 - \left(\frac{1}{1 + \Delta} \right)^{1/\Delta} \frac{3 + 2\Delta}{2(1 + \Delta)} \right\} \\ &= 1 - \frac{3}{2e} \end{aligned}$$

Similarly, general eq 9 becomes

$$\begin{aligned} \frac{[\text{I}_2]}{[\text{HI}]_0} &= \lim_{\Delta \rightarrow 0} \frac{[\text{HI}]}{[\text{HI}]_0} \frac{1}{2(-\Delta)} \left\{ \left(\frac{[\text{HI}]}{[\text{HI}]_0} \right)^\Delta - 1 \right\} \\ &= \lim_{\Delta \rightarrow 0} \frac{[\text{HI}]}{[\text{HI}]_0} \frac{1}{2} \left\{ \frac{1 - \left(\frac{[\text{HI}]}{[\text{HI}]_0} \right)^\Delta}{\Delta} \right\} \end{aligned}$$

which can be evaluated by differentiating both numerator and denominator with respect to Δ . Thus one obtains

$$\frac{[\text{I}_2]}{[\text{HI}]_0} = -\frac{1}{2} \frac{[\text{HI}]}{[\text{HI}]_0} \ln \frac{[\text{HI}]}{[\text{HI}]_0}$$

which gives [from (1) and (5)]

$$M = 1 - \frac{[\text{HI}]}{[\text{HI}]_0} \left\{ 1 - \frac{1}{2} \ln \frac{[\text{HI}]}{[\text{HI}]_0} \right\}$$

(19) The value of $\lim_{\Delta \rightarrow 0} (1/(1 + \Delta))^{1/\Delta} = 1/e$ is readily obtained from the series $e^x = 1 + x + \dots$

Scavenger Kinetics in the Radiolysis of Cyclohexane Solutions. I.

Pure Cyclohexane

by Inder Mani and Robert J. Hanrahan

Department of Chemistry, University of Florida, Gainesville, Florida (Received January 11, 1966)

A series of experiments has been done to study competitive reactions of HI and I₂ with free radicals in γ -irradiated liquid cyclohexane. The experimental data consist of graphs of iodine concentration *vs.* dose in experiments in which I₂, HI, or both are added to pure degassed cyclohexane before radiolysis. Rate equations, based on previously proposed mechanisms, have been set up and their integration has been done by numerical calculations using the second-order Runge-Kutta method on an IBM 709 computer. The theoretical curves so obtained fit the experimental curves well. A value for the ratio $k_{\text{HI}}/k_{\text{I}_2}$ for competitive scavenging of alkyl radicals by HI and I₂ in cyclohexane has been obtained.

Introduction

It is inherent in the concept of a free radical yield in radiation chemistry that radical scavengers should react by a process of "indirect action." That is, radicals produced in the irradiated solvent are presumed to react with the solute, so that the G value for consumption of the scavenger should be independent of scavenger concentration. Iodine is one of the most reliable free radical scavengers used in studying the radiation chemistry of hydrocarbons,¹ but its use is not entirely without complications. Although initial G values for iodine disappearance can be measured rather readily, some ambiguity is introduced by the fact that graphs of iodine concentration *vs.* dose are not merely straight lines, indicative of a constant value for $G(-\text{I}_2)$, but rather are always concave upward, indicating an apparent G value for iodine disappearance which decreases as the dose increases.² A simple interpretation of this phenomenon is that hydrogen atoms, produced from radiolysis of the hydrocarbon solvent, react with iodine to form HI, which then enters into competition with I₂ for the radicals present. Some years ago, this interpretation appeared untenable because HI could not be identified as a radiolysis product.¹ The presence of HI in irradiated hydrocarbon-iodine solutions was later established by Meshitsuka and Burton,³ but to date no attempt to explain quan-

titatively the curvature of the iodine-dose curves on the basis of HI has been published.

A further advantage of an interpretation of HI-I₂ competition kinetics in hydrocarbon radiolysis is that it should be possible to apply such an analysis to systems in which HI rather than I₂ is added initially as a free radical scavenger. In such solutions, I₂ is produced during radiolysis, and again the competition between HI and I₂ occurs. Another test of such a kinetic scheme is provided by solutions in which both HI and I₂ are added initially, so that the competition occurs from the beginning.

This paper presents the results of a study of HI-I₂ competition kinetics in irradiated cyclohexane solutions. A somewhat similar kinetic situation was interpreted earlier by Hanrahan and Willard⁴; analytical integration was made possible by a simplifying assumption concerning the rate constant ratios. During the course of the present investigations, Schuler and Perner⁵ developed a method of treating several aspects

(1) R. W. Fessenden and R. H. Schuler, *J. Am. Chem. Soc.*, **79**, 273 (1957).

(2) B. M. Hughes and R. J. Hanrahan, *J. Phys. Chem.*, **69**, 2707 (1965).

(3) G. Meshitsuka and M. Burton, *Radiation Res.*, **10**, 499 (1959).

(4) R. J. Hanrahan and J. E. Willard, *J. Am. Chem. Soc.*, **79**, 2434 (1957).

(5) D. Perner and R. H. Schuler, *J. Phys. Chem.*, **70**, 2224 (1966).

of the HI-I₂ competition kinetics using an indirect analytical integration. In the work described here, numerical integration on an IBM 709 computer was employed. This was done largely to make possible direct extension of the method to the somewhat more complicated situations which occur in the radiolysis of cyclohexane-alkyl iodide solutions. Results on such systems will be described in future publications.

Experimental Section

Phillips "pure grade" cyclohexane was passed through silica gel before use. Examination of this material by infrared spectroscopy and flame ionization gas chromatography indicated that it contained about 1% of a mixture of branched-chain saturated hydrocarbons eluting before the parent on a silicone rubber column, but no detectable cyclohexene. Iodine and hydriodic acid were Baker Analyzed reagents. Hydrogen iodide was produced by dehydrating hydriodic acid. The hydriodic acid was frozen to liquid nitrogen temperature in a round-bottom flask and P₂O₅ was added on top of it. The frozen acid was then attached to the vacuum line and degassed. The hydriodic acid was allowed to melt and interact with P₂O₅, and the hydrogen iodide released was collected in another portion of the vacuum system. This collected hydrogen iodide was degassed and stored at liquid nitrogen temperature until used. The amount of hydrogen iodide added to the samples was determined by gas measurements.

Individual 4-ml samples were prepared volumetrically, dried with P₂O₅, degassed, transferred under vacuum to the irradiation vessels, and sealed off. The irradiation vessels were 13 × 100-mm test tubes with attached spectrophotometer cells. Irradiations were performed using a Co⁶⁰ γ irradiator which has been described previously.⁶ The dose rate in the Fricke dosimeter [$G(\text{Fe}^{3+}) = 15.6$] was found to be 0.554×10^{18} ev/ml min. For cyclohexane, the value of $\mu(\text{sample})/\mu(\text{dosimeter})$ was 0.780 as obtained on the basis of electron density ratios. Iodine was analyzed spectrophotometrically using a Beckman DU spectrophotometer. The position of λ_{max} and the extinction coefficient were used as given by Croft and Hanrahan.⁷

Results

Measurements of iodine concentration *vs.* dose were made during the radiolysis of several cyclohexane solutions which initially contained concentrations of iodine varying from 0.3×10^{-3} to 2.0×10^{-3} M. The results of some of these experiments are shown by the circles in Figure 1.⁸ (The lines are theoretical; see below.) It can be seen that all of the curves are

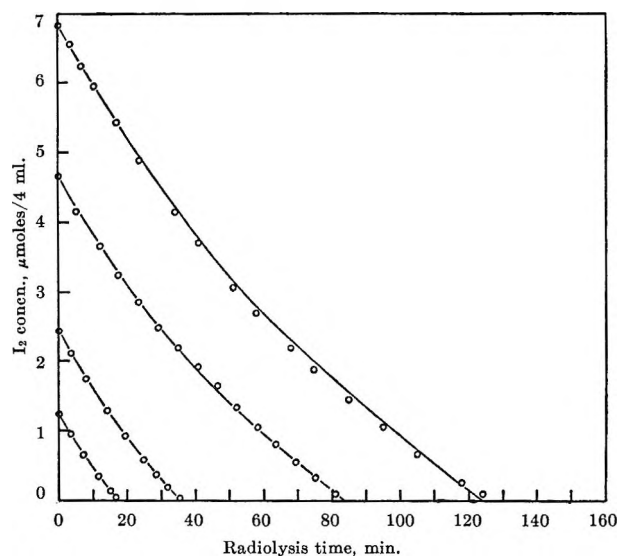


Figure 1. Iodine consumption in the radiolysis of pure cyclohexane with added I₂ as a function of radiation time. Circles are experimental; smooth curves are computed. Initial I₂ concentrations, reading left to right, are 0.31×10^{-3} , 0.61×10^{-3} , 1.16×10^{-3} , and 1.71×10^{-3} M.

concave upward, with the solutions having higher initial iodine concentration showing the most curvature. However, the initial rate of iodine uptake in such experiments has been reported to be independent of initial iodine concentration over the range 5×10^{-6} to 5×10^{-3} M.⁹ We have confirmed this observation for the range of concentration used in our experiments. We found an average initial rate of iodine uptake of 3.08 molecules/100 ev.¹⁰

When HI is added to a hydrocarbon prior to radiolysis, I₂ is produced initially rather than consumed. Alkyl radicals abstract H atoms from HI, releasing iodine atoms which later form I₂. The results of several

(6) R. J. Hanrahan, *Intern. J. Appl. Radiation Isotopes*, **13**, 254 (1962).

(7) T. S. Croft and R. J. Hanrahan, *J. Phys. Chem.*, **66**, 2188 (1962).

(8) Radiation chemical yields are normally given as *G* values, defined as the number of molecules of a substance produced or consumed per 100 ev deposited in the system. In the present case, since concentration and time must be used as iteration parameters on a digital computer, it is necessary to use more convenient units. We have chosen to state concentrations as micromoles per 4-ml sample, and to use time in minutes, which is proportional to radiation dose.

(9) R. H. Schuler, *J. Phys. Chem.*, **62**, 37 (1958).

(10) The value obtained for the initial *G* value of iodine uptake depends somewhat on the procedure used to interpret the concentration-dose graphs, since the graphs are nonlinear. It is especially disadvantageous to use directly the initial concentration-dose increments, since the first few points often show the most scatter. We have found most successful the procedure of calculating the net change of concentration (or optical density) from time zero to each successive radiolysis time *t*, graphing $\Delta(\text{concentration})/t$ *vs.* *t*, and extrapolating this graph to zero time, which gives the desired initial rate.

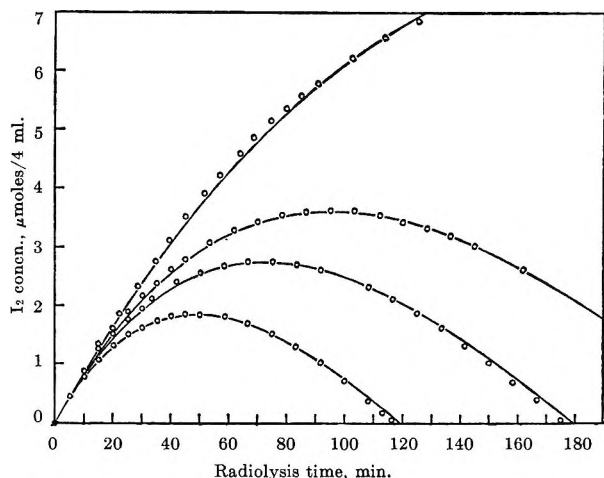


Figure 2. Iodine production in the radiolysis of pure cyclohexane with added HI as a function of radiation time. Circles are experimental; smooth curves are computed. Initial HI concentrations, reading downward, are 8.88×10^{-3} , 4.10×10^{-3} , 3.18×10^{-3} , and $2.11 \times 10^{-3} M$.

experiments of this type are shown in Figure 2. As the radiolysis proceeds, the I_2 produced enters into competition with HI for free radicals so that the net rate of iodine production decreases to zero (at the maximum of the curves) and then becomes negative; if the experiment is continued to a sufficiently high dose, all of the I_2 and HI are finally consumed. It can be seen from Figure 2 that the iodine maximum and final "end points" of the experiments increase with initial HI concentration. However, the initial G value of iodine production is independent of initial HI concentration. Experiments with initial HI concentrations from 2×10^{-4} to $9 \times 10^{-3} M$ gave initial values of $G(I_2)$ ranging from 2.8 to 3.0 with no apparent dependence on initial HI concentration. A value of 2.96, based on several of the most reliable experiments, was used in the calculations described below.

If it is true that production of HI is responsible for the curvature of I_2 vs. dose plots with added I_2 , then additives which prevent the back-reaction of HI should tend to linearize the curves. Additives which might be expected to react with HI and prevent its role as a radical scavenger include BaO and water; the latter has been used previously for this purpose by several workers.^{3,11} Results of the radiolysis of cyclohexane-iodine solutions with added BaO and with added H_2O are compared with experiments with only iodine added in Figure 3. It can be seen that experiments with BaO or H_2O give iodine disappearance graphs starting with about $1.5 \times 10^{-3} M I_2$ which are much less curved than in the case of a similar experiment with only I_2 added. (The experiments shown in

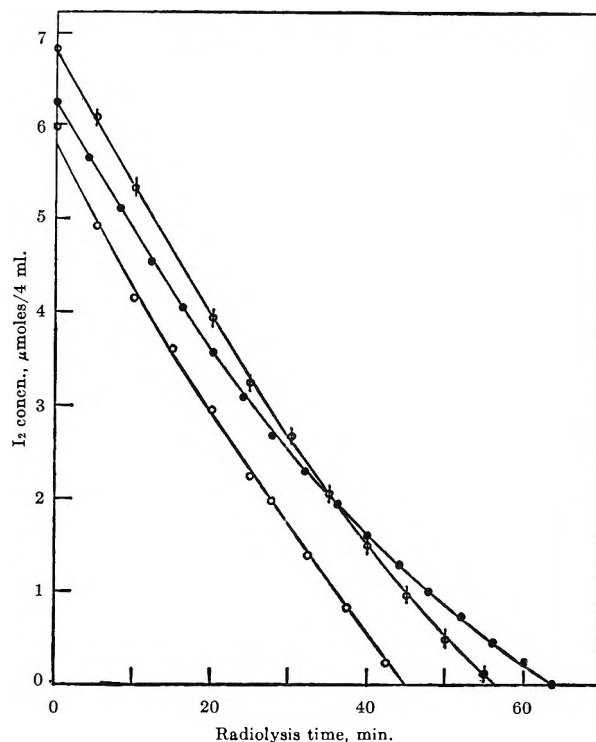


Figure 3. Effect of added base in the radiolysis of pure cyclohexane with added I_2 as a function of radiation time. Initial I_2 concentrations were about $1.5 \times 10^{-3} M$; ●, with no base; ○, with added BaO; ○, with added H_2O .

Figure 3 were done using about 20 μl of H_2O added to 4 ml of cyclohexane-iodine solution,¹¹ or about 1 g of BaO attached to the radiolysis cell through a fritted glass disk.)

Discussion

Kinetic Analysis. Although a great variety of conflicting viewpoints have been expressed on the mechanism of cyclohexane radiolysis, essentially all investigators have agreed that cyclohexyl radicals are involved.¹²⁻¹⁶ The role of hydrogen atoms is far more obscure; at least one research group¹⁴ prefers to talk of "precursors" which provide hydrogen atoms but which may or may not actually be hydrogen atoms. In an attempt to provide an internally consistent free-radical description which goes as far as possible toward in-

(11) L. J. Forrestal and W. H. Hamill, *J. Am. Chem. Soc.*, **83**, 1535 (1961).

(12) Numerous papers have been published dealing with cyclohexane radiolysis. References 13-16 present several representative viewpoints, and give further references to the literature.

(13) R. H. Schuler, *J. Phys. Chem.*, **61**, 1472 (1957).

(14) P. J. Dyne and W. M. Jenkinson, *Can. J. Chem.*, **39**, 2163 (1961); **38**, 539 (1960).

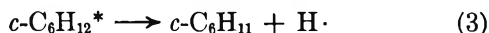
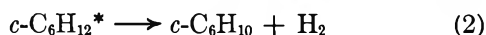
(15) P. J. Dyne, *J. Phys. Chem.*, **66**, 767 (1962).

(16) S. K. Ho and G. R. Freeman, *ibid.*, **68**, 2189 (1964).

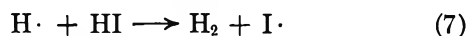
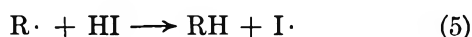
interpreting the present experimental results, we have adopted a simplified mechanism which assumes the presence of hydrogen atoms with an *effective* yield dependent on the total concentration of scavengers present. (At lower scavenger concentrations, it is assumed that the hydrogen atoms are replaced by a complementary yield of cyclohexyl radicals; see below.)

At sufficiently high concentrations, both HI and I₂ may become involved in electron capture or energy transfer processes.^{13,17} However, the highest concentration of scavenger which we have used is about 10⁻² M, and most of our experiments were done at millimolar scavenger concentrations. There is justification¹³ for assuming that HI and I₂ behave predominantly as free radical scavengers at near millimolar concentration levels. Hence, for the present purposes we assume that the net result of primary processes is the production of hydrogen atoms and alkyl radicals, which then take part in competitive reactions under steady-state conditions.

Reactions in Spurs¹⁸



Thermal Radical Reactions



The above reaction scheme can be treated by conventional kinetics. It is assumed that H atoms and alkyl radicals are produced according to zero-order kinetics by the radiation, and that I₂ and HI then compete for the radicals and H atoms according to eq 4 to 7. The rate constants for reactions 4 and 6 and for reactions 5 and 7 might be expected to be quite similar. The ratios k_6/k_4 and k_7/k_6 should be even more similar; we have assumed these ratios to be equal, which greatly simplifies our calculations.

The steady-state assumption is applied to the alkyl radical and H-atom concentrations. We shall let A be the rate of production of thermal alkyl radicals and D be the rate of production of thermal H atoms which escape from the spurs. Then we set the thermal alkyl production rate equal to the rate of removal by reactions 4 and 5

$$\begin{aligned} A &= k_4[\text{R}\cdot][\text{I}_2] + k_5[\text{R}\cdot][\text{HI}] \\ &= [\text{R}\cdot](k_4[\text{I}_2] + k_5[\text{HI}]) \end{aligned} \quad (9)$$

and

$$[\text{R}\cdot] = A/(k_4[\text{I}_2] + k_5[\text{HI}]) \quad (10)$$

Similarly, we set the thermal H-atom production rate equal to the rate of removal by reactions 6 and 7

$$\begin{aligned} D &= k_6[\text{H}\cdot][\text{I}_2] + k_7[\text{H}\cdot][\text{HI}] \\ &= [\text{H}\cdot](k_6[\text{I}_2] + k_7[\text{HI}]) \end{aligned} \quad (11)$$

and

$$[\text{H}\cdot] = D/(k_6[\text{I}_2] + k_7[\text{HI}]) \quad (12)$$

The rate of iodine production may be expressed as

$$\begin{aligned} d[\text{I}_2]/dt &= -(k_4/2)([\text{I}_2][\text{R}\cdot]) + \\ &\quad (k_6/2)([\text{HI}][\text{R}\cdot]) - \\ &\quad (k_6/2)([\text{I}_2][\text{H}\cdot]) + (k_7/2)([\text{HI}][\text{H}\cdot]) \end{aligned} \quad (13)$$

The factor of 1/2 is introduced because only 1/2 mole of iodine is consumed when a mole of radicals reacts with I₂ (reactions 4 and 8). After substituting expressions for [R·] and [H·] and rearranging, this becomes

$$\begin{aligned} d[\text{I}_2]/dt &= -(A/2)(k_4[\text{I}_2] - \\ &\quad k_5[\text{HI}])/(k_4[\text{I}_2] + k_5[\text{HI}]) - \\ &\quad (D/2)(k_6[\text{I}_2] - k_7[\text{HI}])/(k_6[\text{I}_2] + k_7[\text{HI}]) \end{aligned} \quad (14)$$

After putting $k_6/k_4 = k_7/k_6 = k_{\text{HI}}/k_{\text{I}_2}$ and simplifying further, this can be expressed as

$$\begin{aligned} d[\text{I}_2]/dt &= (A + D)/2 - \\ &\quad (A + D)[\text{I}_2]/([\text{I}_2] + [\text{HI}]k_{\text{HI}}/k_{\text{I}_2}) \end{aligned} \quad (15)$$

Similarly, the rate of HI production can be expressed as

$$\begin{aligned} d[\text{HI}]/dt &= -k_5[\text{HI}][\text{R}\cdot] + \\ &\quad k_6[\text{I}_2][\text{H}\cdot] - k_7[\text{HI}][\text{H}\cdot] \end{aligned} \quad (16)$$

After substitution for [R·] and [H·] and simplification this becomes

$$\begin{aligned} d[\text{HI}]/dt &= -(A + D) + \\ &\quad (A + 2D)[\text{I}_2]/([\text{I}_2] + [\text{HI}]k_{\text{HI}}/k_{\text{I}_2}) \end{aligned} \quad (17)$$

In order to obtain equations giving the I₂ concentration as a function of time (and incidentally, also giving HI concentration as a function of time), it is necessary to solve eq 15 and 17, a pair of simultaneous, first-

(17) J. R. Nash and W. H. Hamill, *J. Phys. Chem.*, **66**, 1097 (1962).

(18) Asterisks represent electronically excited species.

order, nonlinear differential equations. A similar set of equations has recently been solved by Schuler and Perner,⁵ who used an indirect analytical procedure. Their analysis applies to a kinetic scheme which is similar to ours except that no allowance is made for direct participation of hydrogen atoms. (It is assumed by them that hydrogen atoms attack the substrate and are converted to alkyl radicals; the question of the role of hydrogen atoms is discussed below.) Because we wished to treat not only the present case but also the similar, somewhat more complicated kinetic scheme applicable to the radiolysis of hydrocarbon-alkyl iodide solutions, we chose to attack the problem using numerical integration. Slight modification of a published program¹⁹ for the second-order Runge-Kutta method of solving simultaneous differential equations proved applicable.

Assignment of Parameters. Before eq 15 and 17 can be solved by the computer, it is necessary to provide values for the quantities A and D (alkyl radical yield and hydrogen atom yield), and for the ratio of rate constants k_{HI}/k_{I_2} . Some information is obtained from limiting forms of eq 15. When the concentration of HI greatly exceeds that of I_2 , the equation reduces to the form

$$\left(\frac{d[I_2]}{dt}\right)_{\max} = (A + D)/2 \quad (18)$$

and when the concentration of I_2 greatly exceeds that of HI, one obtains

$$\left(\frac{d[I_2]}{dt}\right)_{\min} = -(A + D)/2 \quad (19)$$

The subscripts max and min are used because the first case refers to the initial, maximum value of the rate of production of I_2 with added HI, whereas the second refers to the initial rate of consumption of I_2 with added I_2 , which is a minimum in the algebraic sense.

From eq 18 and 19 it is clear that the initial rate of iodine production with added HI and the initial rate of iodine consumption with added I_2 should be identical. The values which we obtained, 2.96 and 3.08, respectively, can be considered the same within experimental error. An average of the two values was used in establishing a value of the quantity $(A + D)$, the total yield of alkyl radicals and hydrogen atoms.

The value of the hydrogen atom yield D cannot be established directly from our experimental results. Some evidence on its value is given by the experiments of Meshitsuka and Burton³ in which the initial value of the yield of HI in cyclohexane with added I_2 was found to be 2.1 molecules/100 ev. This can be taken

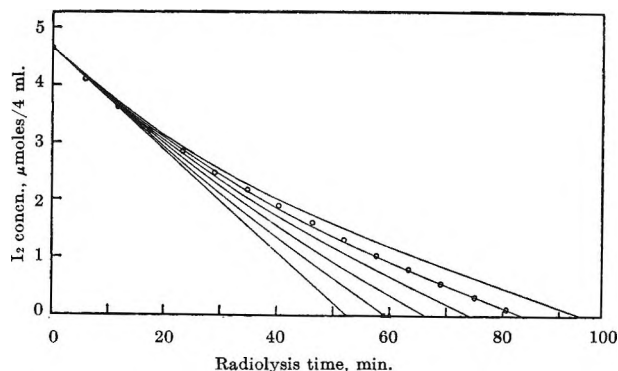
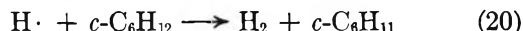


Figure 4. Role of H-atom yield as an adjustable parameter: I_2 consumption in the radiolysis of pure cyclohexane with added I_2 ($1.16 \times 10^{-3} M$) as a function of radiation time. H-atom production rates, reading left to right, are 0.0, 0.01, 0.02, 0.03, 0.04, and 0.05 $\mu\text{moles}/4 \text{ ml min}$. Corresponding G values are 0.0, 0.35, 0.7, 1.05, 1.4, and 1.74, respectively. Circles are experimental; smooth curves are computed.

as an upper limit for the hydrogen atom yield, applicable in solutions with scavenger concentrations of about $2 \times 10^{-2} M$ or greater. At sufficiently low scavenger concentrations (of the order of 10^{-4}), the scavengable hydrogen atom yield is effectively zero, because the hydrogen atoms react with the hydrocarbon substrate to form H_2 and are replaced by a corresponding yield of alkyl radicals



At higher concentrations, iodine and other good scavengers can compete with this reaction. Using iodine, the reduction in the corresponding hydrogen yield occurs mainly in the concentration range from 10^{-3} to $10^{-2} M$.¹³ It has been reported that a concentration of $3 \times 10^{-3} M$ iodine decreases the hydrogen by 50% of the ultimately observed reduction.¹³ Hence, for our purposes, the effective G value of scavengable hydrogen atoms should vary from zero at $10^{-4} M I_2$ or HI to a maximum of about 2 at $ca. 2 \times 10^{-2} M$ scavenger.

Since sufficiently detailed data were not available, the hydrogen atom yields in the present study were obtained by using the D factor in eq 15 and 17 as an adjustable parameter for curve fitting. The alkyl radical yield A was obtained by difference, since the sum $(A + D)$ is calculable. The calculated effect of varying the hydrogen yield on a typical experiment on the radiation-induced uptake of I_2 is shown in Figure 4. It can be seen that increasing $G(H \cdot)$

(19) J. M. McCormick and M. G. Salvadori, "Numerical Methods in Fortran," Prentice-Hall, Inc., Englewood Cliffs, N. J., 1964, pp 253-255.

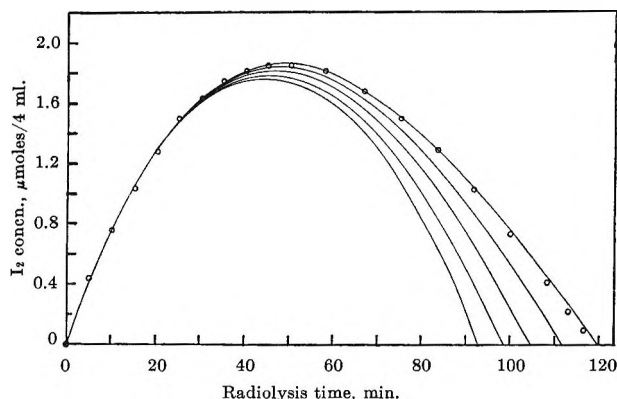


Figure 5. Role of H-atom yield as an adjustable parameter: I_2 production in the radiolysis of pure cyclohexane with added HI ($2.11 \times 10^{-3} M$) as a function of radiation time. H-atom production rates, reading left to right, are 0.0, 0.01, 0.02, 0.03, and $0.04 \mu\text{moles}/4 \text{ ml min.}$ Corresponding G values are 0.0, 0.35, 0.70, 1.05, and 1.4, respectively. Circles are experimental; smooth curves are computed.

increases the end point of the experiment, the dose for complete removal of I_2 . In Figure 5 it can be seen that increasing $G(\text{H}\cdot)$ causes a similar increase in end point for experiments with added HI. (In Figures 4 and 5 the ratio $k_{\text{HI}}/k_{\text{I}_2}$ was taken as 0.71, which is the value giving the best fit of experimental data.)

Although there is experimental evidence suggesting that $k_{\text{HI}}/k_{\text{I}_2}$ in nonpolar solvents is of the order of unity,⁴ there were insufficient data to assign an accurate value for our experiments. Accordingly, the ratio $k_{\text{HI}}/k_{\text{I}_2}$ was also treated as an adjustable parameter in the calculations. Figure 6 shows that changing this ratio modifies the curvature of a graph of I_2 concentration *vs.* radiolysis time, but does not affect the end point unless the ratio is essentially zero. In that case, the products at the end point would include HI as well as alkyl iodides. As long as $k_{\text{HI}}/k_{\text{I}_2}$ is finite, then all of the iodine in the chemical intermediate HI as well as that present as I_2 must ultimately appear as alkyl iodides. It can be seen that the end point of the experiment is the same for all finite values of $k_{\text{HI}}/k_{\text{I}_2}$, but the curvature increases as $k_{\text{HI}}/k_{\text{I}_2}$ decreases. (This is perhaps opposite to what a casual consideration of the kinetics might lead one to expect.) It will be seen that the initial slope is the same in all cases (except $k_{\text{HI}}/k_{\text{I}_2} = \infty$) and approaches that for which $k_{\text{HI}}/k_{\text{I}_2} = 0$.

The computed effect of varying $k_{\text{HI}}/k_{\text{I}_2}$ for an experiment with added HI is shown in Figure 7. Again, variation of $k_{\text{HI}}/k_{\text{I}_2}$ does not affect the end point. As $k_{\text{HI}}/k_{\text{I}_2}$ increases, the maximum iodine concentration achieved in the experiment becomes greater, and the radiolysis time corresponding to the maximum

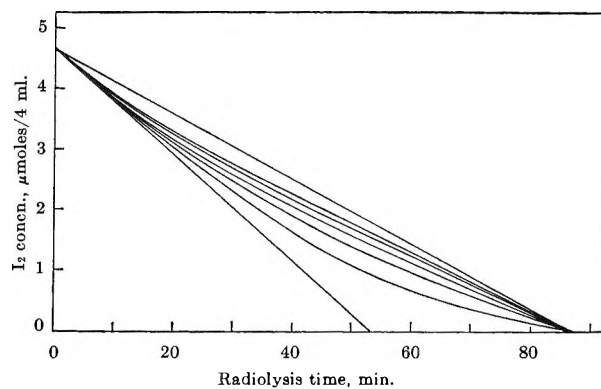


Figure 6. Role of $k_{\text{HI}}/k_{\text{I}_2}$ as an adjustable parameter: I_2 consumption in the radiolysis of pure cyclohexane with added I_2 ($1.16 \times 10^{-3} M$) as a function of radiation time. Ratios of $k_{\text{HI}}/k_{\text{I}_2}$, reading left to right, are 0.0, 0.3, 0.6, 0.9, 1.5, 2.0, and ∞ .

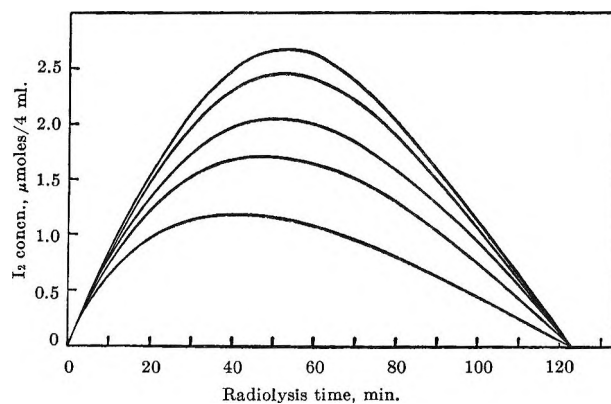


Figure 7. Role of $k_{\text{HI}}/k_{\text{I}_2}$ as an adjustable parameter: I_2 production in the radiolysis of pure cyclohexane with added HI ($2.11 \times 10^{-3} M$) as a function of radiation time. Ratios of $k_{\text{HI}}/k_{\text{I}_2}$, reading downward, are 2.0, 1.5, 0.9, 0.6, and 0.3.

increases. (Again, a superficial examination of the kinetics could easily give the opposite prediction.)

Comparison with Experiment. Since varying the H-atom yield affects the end point but the ratio $k_{\text{HI}}/k_{\text{I}_2}$ does not, it is quite easy to adjust both of these quantities to give the best fit of the experimental data. The results of such efforts are shown by the smooth curves in Figures 1 and 2; the circles represent experimental data. Since the radiolysis temperature ($25 \pm 2^\circ$) was constant for all experiments and the solvent was essentially pure cyclohexane, the ratio $k_{\text{HI}}/k_{\text{I}_2}$ should be the same in all cases. In fact, it was found that $k_{\text{HI}}/k_{\text{I}_2} = 0.71$ gave a good fit in all cases. (Schuler and Perner find a ratio of 0.83 in *n*-decane.⁵)

Because of the competition between solvent cyclohexane and added scavenger for H atoms, the D factor is expected to be dependent on initial scavenger con-

centration. Since the scavenger concentration during each experiment decreases as the experiment progresses, it is possible to account for scavenging of hydrogen atoms only semiquantitatively. However, the alkyl iodides produced during radiolysis are also good hydrogen atom scavengers¹¹ so the change in total scavenger concentration is never more than a factor of 2.²⁰ The effective hydrogen atom yields used in the calculations for Figure 1 for the various values of initial iodine concentration are as follows: $0.31 \times 10^{-3} M$, $G(\text{H}\cdot) = 0.70$; $0.61 \times 10^{-3} M$, $G(\text{H}\cdot) = 0.80$; $1.16 \times 10^{-3} M$, $G(\text{H}\cdot) = 1.40$; $1.71 \times 10^{-3} M$, $G(\text{H}\cdot) = 1.43$. For the experiments in Figure 2, the H-atom yields which correspond to various initial hydrogen iodide concentrations are as follows: $2.11 \times 10^{-3} M$, $G(\text{H}\cdot) = 1.40$; $3.18 \times 10^{-3} M$, $G(\text{H}\cdot) = 1.46$; $4.10 \times 10^{-3} M$, $G(\text{H}\cdot) = 1.57$; $8.88 \times 10^{-3} M$, $G(\text{H}\cdot) = 1.74$. It will be noted that a greater concentration of HI than of I_2 is required to achieve a given value of $G(\text{H}\cdot)$, implying that I_2 is a somewhat better hydrogen atom scavenger than HI.

Consideration of Figures 4-7 allows comparison of the present kinetic analysis with that of Perner and Schuler.⁵ Starting with essentially the same mechanism as used by us, they present a simplified kinetic scheme for experiments with added HI. Their equations can be integrated analytically, although indirectly. Their analysis allows variation of the parameter $k_{\text{HI}}/k_{\text{I}_2}$ (actually used in the form of the reciprocal by them) but does not provide for direct allowance for the reaction of H atoms with I_2 producing additional HI. However, this effect is clearly evident in their results as shown by deviations in experimental data compared with predictions of their kinetic scheme, and is so interpreted by them. Their analysis would give a curve identical with that for $D = 0$ in Figure 5. Since the error in ignoring the H-atom effect is rather large for concentrations as great as $2 \times 10^{-3} M$ (corresponding to Figure 5), they worked mainly at much lower HI concentrations. For experiments with added I_2 , the approximation that $G(\text{H}\cdot) = 0$ gives merely a straight line (Figures 4 and 6), so Perner and Schuler did not treat this case. However, they did note the curvature of experimental I_2 vs. dose graphs, and interpret this effect as we do. Their analysis of the effect of varying $k_{\text{HI}}/k_{\text{I}_2}$ is qualitatively similar to ours; the resulting graphs differ slightly because of our allowance for the hydrogen atom yield (Figure 7).

Two types of scavenging experiments, with I_2 or HI added initially, have been discussed above. Another possibility is to conduct experiments in which both HI and I_2 have been added initially. As a further test of the kinetic scheme, we performed a series of

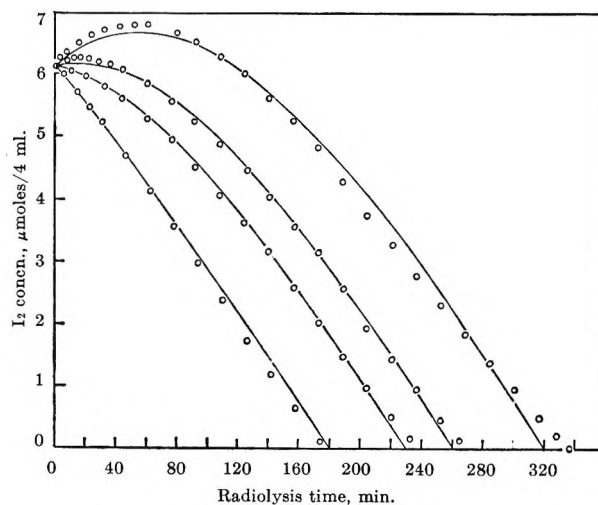


Figure 8. Iodine production in the radiolysis of pure cyclohexane, with both HI and I_2 added, as a function of radiation time. Circles are experimental; smooth curves are computed using $G(\text{H}\cdot) = 1.5$ and $k_{\text{HI}}/k_{\text{I}_2} = 0.71$. HI concentrations, reading left to right, are 1.08×10^{-3} , 1.91×10^{-3} , 2.43×10^{-3} , and $3.43 \times 10^{-3} M$. I_2 concentration is $1.53 \times 10^{-3} M$ in all cases.

experiments all starting with an initial iodine concentration of $1.53 \times 10^{-3} M$, but using various amounts of added HI. The resulting experimental points and corresponding theoretical curves are shown in Figure 8. As in the previous cases, the value taken for $k_{\text{HI}}/k_{\text{I}_2}$ was 0.71. On the basis of the work described above, the range of values of $G(\text{H}\cdot)$ expected for combined HI and I_2 concentrations in the experiments shown in Figure 8 was 1.40 to 1.60. For convenience, $G(\text{H}\cdot) = 1.50$ was used for all of the calculations illustrated. (Preparation of a series of solutions with the same initial iodine concentration was facilitated by the use of a vacuum line buret.²¹)

In view of the various assumptions made, the agreement between the predicted curves and experimental points in Figures 1, 2, and 8 seems quite satisfactory. Further, the values of the parameters (rate constant ratio and hydrogen atom yields) which give the best fit of the data appear to be reasonable.^{22,23} For the

(20) Perner and Schuler⁵ have pointed out similarities in over-all stoichiometry which suggest that the "effective H atom yield," approximation is less drastic than it may appear.

(21) R. J. Hanrahan, *J. Chem. Educ.*, **41**, 623 (1964).

(22) Our rate constant ratios should be fairly accurate because they depend on the maxima rather than the tails of the graphs. It has recently become possible to compare our hydrogen atom yields with data obtained by Schuler and Perner²³ on photolysis of TI in *n*-hexane. Using a nominal maximum G value for hydrogen atoms of 2.0 and their rate constant ratio for reaction of T atoms with TI vs. hexane, a graph can be constructed showing a prediction of effective H-atom yield vs. scavenger concentration, covering the range of about 10^{-4} to $10^{-1} M$ scavenger. Our effective hydrogen atom

most part, the deviations which occur are most pronounced toward the end of the experiments. This is just the condition where the ambiguity concerning scavenging of H atoms by alkyl iodides is most significant. An additional source of error likely to become important at large doses is the reaction of HI and I₂ with cyclohexene, which is known to be a product of the radiolysis. However, such reactions would remove scavengers from solution and shorten the end point of the experiments; this effect would be opposite to the trend of the data. Reaction of hydrogen atoms with cyclohexene can probably be ignored because HI, I₂, and cyclohexyl iodide are all better H-atom scavengers,^{11,23,24} and at least one of them is always present in greater concentration than cyclohexene. Results of the radiolysis of pure cyclohexane¹³⁻¹⁶ provide evidence that the reaction of cyclohexyl radicals with cyclohexene is not significant.

It might be possible to include in the kinetic analysis quantitative corrections for reactions involving cyclo-

hexene and alkyl iodide products. However, the kinetic scheme is already moderately complicated and these further refinements would probably obscure its value as an aid in obtaining an insight into the behavior of a kinetic system of this type.

Acknowledgment. This work was supported by Atomic Energy Commission Contract No. AT-(40-1)-3106 and by the University of Florida Nuclear Science Program. Services of the IBM 709 computer were provided by the University of Florida Computing Center. Some of the data presented here were obtained by Mr. William C. Blasky of this laboratory.

yields parallel this graph quite systematically, but are about a factor of 2 higher in the low concentration region. (R. H. Schuler, private communication.) There may be some uncertainties involved in comparing the two systems. However, due to the approximations involved in our use of an "effective" hydrogen atom yield, our values would not be expected to be more accurate than about $\pm 50\%$.

(23) D. Perner and R. H. Schuler, *J. Phys. Chem.*, **70**, 317 (1966).

(24) T. J. Hardwick, *ibid.*, **66**, 291, 2246 (1962).

The Electrical Conductivities of Boron Trifluoride in Pure and Mixed Halogen Fluorides¹

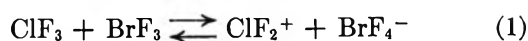
by Madeline S. Toy and William A. Cannon

*Douglas Missile and Space Systems Division, Astropower Laboratory, Newport Beach, California
(Received January 5, 1966)*

The electrical conductivities of solutions of boron trifluoride in chlorine and bromine trifluorides have been studied as a function of temperature and concentration. Dilute solutions of boron trifluoride in bromine trifluoride have conductive properties similar to strong electrolytes in water, with an approximate Onsager slope of 80.2 and equivalent conductance at infinite dilution of $131 \text{ cm}^2 \text{ ohm}^{-1} \text{ equiv}^{-1}$ at 25° , while the equivalent conductances of dilute solutions of boron trifluoride in chlorine trifluoride decrease with dilution. Their differences and mechanisms are discussed. The preparation and identification of difluorobrominium tetrafluoroborate is described.

Introduction

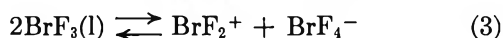
The physical and chemical properties of halogen fluorides have been studied extensively.² Particular interest has been shown in the self-ionization of many of the halogen fluorides. Haszeldine³ has observed that chlorine trifluoride dissolves in both bromine trifluoride and iodine pentafluoride and is not evolved upon heating the resulting solution to $60\text{--}70^\circ$, although chlorine trifluoride boils at 12° . Whitney and co-workers⁴ have treated alkali metal fluorides in chlorine trifluoride and bromine pentafluoride at 100° to form the respective alkali metal tetrafluorochlorates and hexafluorobromates; the compounds KClF_4 , RbClF_4 , CsClF_4 , KBrF_6 , RbBrF_6 , and CsBrF_6 have been prepared. Rogers and Katz⁵ have studied the exchange of radioactive F^{18} between chlorine and bromine trifluorides and suggested that chlorine trifluoride acts as a base in bromine trifluoride solution, the exchange reaction proceeding through the equilibrium



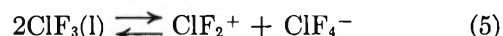
The electrical conductivity of mixed halogen fluorides has been reported by Quarterman, Hyman, and Katz⁶ for solutions of bromine trifluoride and bromine pentafluoride.

Boron trifluoride itself is a nonconductor of electricity. The solutions of boron trifluoride and halogen fluorides are examples of electrolytic conduction

caused by "potential electrolytes" in the sense of the definition given by Kortum and Bockris.⁷ The nonpolar BF_3 molecules react with the self-ionizing BrF_3 molecules to form electrolytes as described by eq 2 and 3.



In the case of BF_3 in a mixed solvent system ($\text{BrF}_3\text{--ClF}_3$), the set of eq 1 to 5 is postulated.



Selig and Shamir⁸ have prepared difluorochlorinium tetrafluoroborate according to eq 4, and we have pre-

(1) Presented in part at the Western Regional Meeting of the American Chemical Society, Los Angeles, Calif., Nov 20, 1965.

(2) A. G. Sharpe, *Quart. Rev.* (London), **4**, 115 (1950); V. Gutmann, *Angew. Chem.*, **62**, 312 (1950); H. C. Clark, *Chem. Rev.*, **58**, 869 (1958).

(3) R. N. Haszeldine, *J. Chem. Soc.*, 3037 (1950).

(4) E. D. Whitney, R. O. MacLaren, C. E. Fogle, and T. J. Hurley, *J. Am. Chem. Soc.*, **86**, 2583 (1964).

(5) M. T. Rogers and J. J. Katz, *ibid.*, **74**, 1375 (1952).

(6) L. A. Quarterman, H. H. Hyman, and J. J. Katz, *J. Phys. Chem.*, **61**, 912 (1957).

(7) G. Kortum and O. Bockris, "Textbook of Electrochemistry," Vol. I, Elsevier Publishing Co., New York, N. Y., 1951, pp 99, 100.

(8) H. Selig and J. Shamir, *Inorg. Chem.*, **3**, 294 (1964).

pared difluorobrominium tetrafluoroborate according to eq 2 (see Experimental Section). For the isolation of a pure and stable product, a lengthy evacuation is required to eliminate trace amounts of BrF_3 (bp 125–127°) or compounds as $x\text{BrF}_3 \cdot y\text{BF}_3$ trapped in the pure $\text{BrF}_3 \cdot \text{BF}_3$ solid.

Experimental Section

Materials. Boron trifluoride, bromine trifluoride, and chlorine trifluoride were obtained from the Matheson Co. Chlorine trifluoride and boron trifluoride were purified by passing the vapor through a sodium fluoride scrubber to remove possible hydrogen fluoride impurity. Bromine trifluoride was purified by removing the first fraction under reduced pressure at room temperature. The melting point and specific conductivity of the bromine trifluoride agreed with the literature values.^{2,6,9} The purity of boron trifluoride and chlorine trifluoride was checked by vapor spectroscopic spectra and specific conductivities of the liquids. These samples were indistinguishable from the samples which had been exhaustively fractionated. However, the specific conductivity of chlorine trifluoride employed, $8.8 \times 10^{-9} \text{ ohm}^{-1} \text{ cm}^{-1}$, was slightly higher than the best literature value, $3.9 \times 10^{-9} \text{ ohm}^{-1} \text{ cm}^{-1}$.²

Apparatus. The conductivity cells were made of borosilicate glass with smooth platinum electrodes. Cell constants ranged from 0.03 to 0.5 cm^{-1} . An internal thermocouple well located near the electrodes was used for temperature measurement.

Cell-resistance measurements were made with a General Radio Type 1650-A impedance bridge. It was equipped with an internal, 1000-cycle signal source and tuned null detector. Measurements were also made with an external signal source ranging from 200 to 10,000-cycles to permit correction for polarization. For more sensitive balance a Hewlett-Packard 400 L vacuum tube voltmeter was used as an external null detector.

A stainless steel vacuum line constructed of 304 stainless steel tubing and 316 stainless steel needle valves was employed for manipulation of boron trifluoride and halogen fluorides. Mercury manometers cannot be used; therefore pressure was measured with a stainless steel Bourdon gauge covering the range from 30-in. vacuum to 30 psi pressure. Careful exclusion of moisture is essential in handling these compounds as the presence of any water vapor will cause noticeable attack on glass and stainless steel and will likewise affect conductivity measurements. The metal parts of the vacuum system were first degreased with trichloroethylene, rinsed with Freon, then vacuum dried. After assembly, the vacuum system was passivated by filling

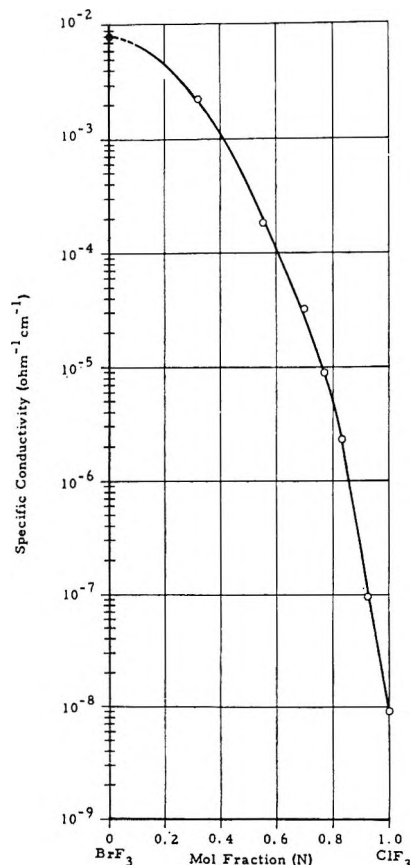


Figure 1. Specific conductivities of solutions of BrF_3 and ClF_3 at 0°.

with gaseous fluorine to 1 atm for 18 hr. Finally, the system was evacuated. Under these conditions, it is found that bromine trifluoride does not appreciably attack the stainless steel or glass during the time required to carry out the experiments, *viz.* 1 to 2 hr. The specific conductivity of chlorine trifluoride is so low that its conductivity is altered by trace impurities from attack on glass. This could readily account for the difference in the observed specific conductivity reported here and the lowest value reported in the literature.²

Preparation of Difluorobrominium Tetrafluoroborate. The adduct was prepared by bubbling gaseous boron trifluoride through liquid bromine trifluoride at room temperature. Rapid initial gas absorption was accompanied by exothermic reaction. The solid product did not precipitate, but upon vacuum evaporation to dryness at room temperature, a white residue, mp (in sealed tube) 180° dec, was obtained. The same solid

(9) M. S. Toy and W. A. Cannon, "Symposium on Advanced Propellant Chemistry," *Advances in Chemistry Series*, No. 56, American Chemical Society, Washington, D. C., in press.

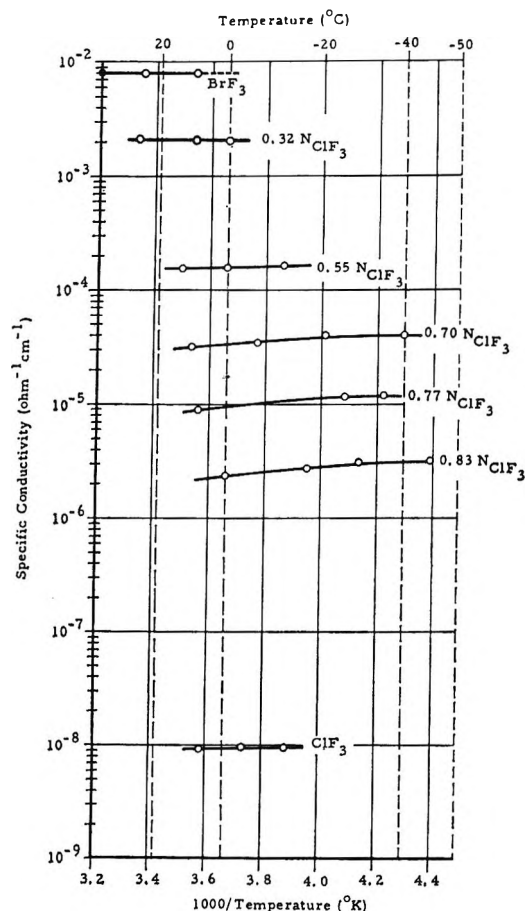


Figure 2. Specific conductivities of solutions of BrF_3 and ClF_3 as a function of temperature.

was obtained by condensing gaseous boron trifluoride in excess on top of frozen bromine trifluoride at liquid nitrogen temperature, warming to room temperature, and vacuum evaporating to dryness.

When gaseous boron trifluoride was introduced into a closed evacuated system above liquid bromine trifluoride at room temperature, a pressure drop was observed as boron trifluoride dissolved. This process was repeated until no additional gas dissolved at 1 atm. Then the yellow liquid was vacuum evaporated at room temperature to dryness. The yield of the same white product was poor in all these preparations. The solid sample should always be evacuated at room temperature for several hours, preferably overnight, before vacuum sealing the sample for analytical purposes.

Anal. Calcd for BrF_2BF_4 : F, 55.69; Br, 39.04; B, 5.33. Found: F, 55.37; Br, 38.71; B, 5.91.

The infrared spectrum of thin solid film of the product shows a strong broad band in the region $1020\text{--}1100\text{ cm}^{-1}$ indicative of tetrafluoroborate ion.¹⁰ A 0.3 M solution of BrF_2BF_4 in BrF_3 possesses a specific con-

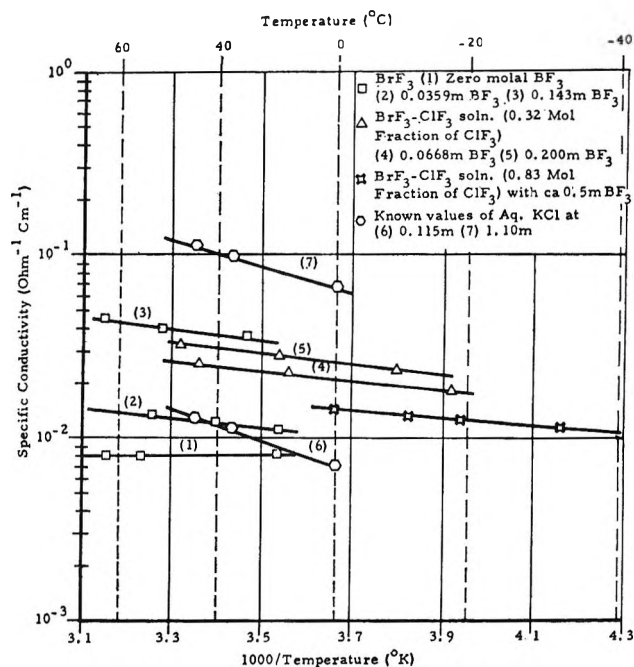


Figure 3. Effect of temperature and concentration on specific conductivity of BF_3 in solutions of BrF_3 and ClF_3 .

ductivity of $3.31 \times 10^{-2}\text{ ohm}^{-1}\text{ cm}^{-1}$ at 25° , while the specific conductivity of BrF_3 at 25° is $8.0 \times 10^{-3}\text{ ohm}^{-1}\text{ cm}^{-1}$. The formula $(\text{BrF}_2)^+(\text{BF}_4)^-$ is postulated as consistent with conductivity and infrared data.

Results and Discussion

Figure 1 shows the conductivities of solutions whose composition lies between pure bromine trifluoride and pure chlorine trifluoride. The conductivity decreases smoothly from the maximum in pure bromine trifluoride to a minimum in pure chlorine trifluoride. The conductivity of pure liquid bromine trifluoride and chlorine trifluoride are almost temperature independent (Figure 2), while the solutions of the two solvents show very slight negative temperature coefficients of conductivity. Figure 3 shows the temperature coefficient of conductivity for BF_3 in pure BrF_3 and solutions of BrF_3 and ClF_3 as similar and both being smaller than aqueous KCl solutions. Figure 4 shows the increase of conductivity of halogen fluorides with increase of concentration of boron trifluoride. By subtracting the specific conductivity of solvent from the specific conductivity of the solution, the equivalent conductance *vs.* the square root of concentration of difluorobrominium tetrafluoroborate can be estimated

(10) R. W. Sprague, A. B. Garrett, and H. H. Sisler, *J. Am. Chem. Soc.*, **82**, 1059 (1960); F. Seel and O. Detmar, *Z. Anorg. Allgem. Chem.*, **301**, 8 (1959).

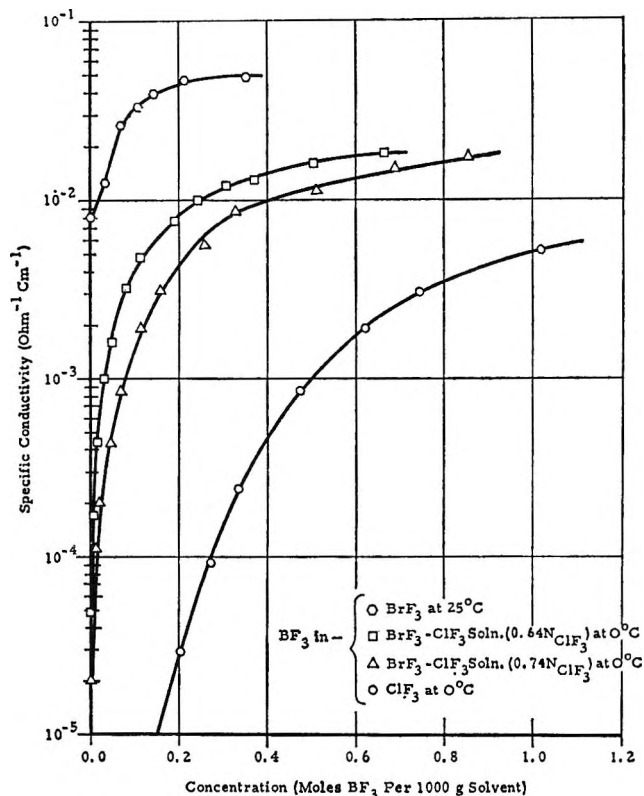


Figure 4. Specific conductivity as a function of concentration of BF_3 in solutions of BrF_3 and ClF_3 .

and extrapolated to infinite dilution. The approximate equivalent conductance of infinite dilution of BrF_2BF_4 in BrF_3 is $131 \text{ cm}^2 \text{ ohm}^{-1} \text{ equiv}^{-1}$ with an Onsager slope of 80.2 at 25° . The aqueous potassium chloride curve¹¹ is included in Figure 5 for comparative purposes. In dilute concentrations of BF_3 in BrF_3 , the solutions resemble strong electrolytes in water, but BF_3 in ClF_3 solutions behave very differently. This behavior is in accordance with the presumed high dielectric constant of liquid BrF_3 ⁶ and the low dielectric constant of liquid ClF_3 .¹² Thus the phenomenon of decreasing equivalent conductance with decreasing concentration of boron trifluoride in liquid ClF_3 can be

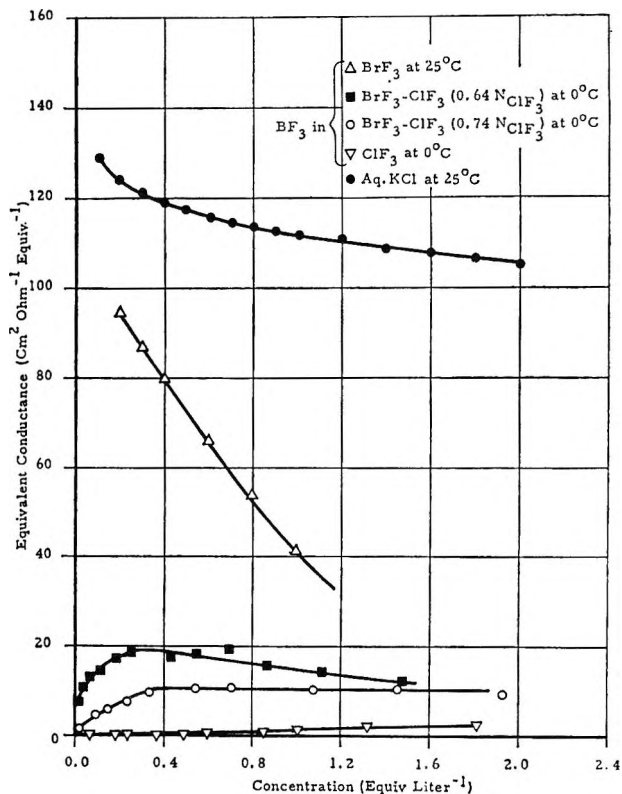


Figure 5. Equivalent conductance of BF_3 in solutions of BrF_3 and ClF_3 as a function of concentration.

explained by the stable association of ions to form ion pairs as compared with simply solvated ions for high dielectric constant solvents.

Acknowledgment. The authors wish to thank the U. S. Army Advanced Research Project Agency for support of this work under Contract No. DA-31-124-ARO-(D)-115.

(11) J. F. Chambers, J. M. Stokes, and R. H. Stokes, *J. Phys. Chem.*, **60**, 985 (1956); R. A. Robinson and R. H. Stokes, "Electrolyte Solutions," 2nd ed, Butterworth and Co. Ltd., London, 1959, pp 154, 466.

(12) M. T. Rogers, H. B. Thompson, and J. L. Speirs, *J. Am. Chem. Soc.*, **76**, 4841 (1954).

Spectroscopic Evidence for the Enol Imine-Keto Enamine Tautomerism of N-(*o*- and *p*-Hydroxybenzylidene) Anils in Solution

by John W. Ledbetter, Jr.

Department of Chemistry, University of Kentucky, Lexington, Kentucky (Received January 6, 1966)

In alcoholic and acidic solvents N-(*o*- and *p*-hydroxybenzylidene) anils exhibit an additional long wavelength band in the neighborhood of 400 m μ . Evidence strongly indicates that this band is due to the absorption spectrum of the quinoid tautomer of the anil. First, isosbestic points in the cyclohexane-ethanol system demonstrate two absorbing species. Spectra of various molecular structures show that the N-(*o*- or *p*-hydroxybenzylidene) anil structure is required. It is also essential for the proposed tautomerism that hydrogen bonding occur between the solute (the imine nitrogen) and a solvent acidic hydrogen. Increasing the dielectric constant and the acidity of the solvent increases the tautomerism. It is believed that the intermolecular hydrogen bonding provides both a route for the mechanism through hydrogen transfer and the necessary stability for the quinoid tautomer.

Introduction

Recently, an interest has been stimulated in the general spectroscopy of Schiff bases, mainly due to interest in the phototropism of solid N-(*o*-hydroxybenzylidene) anils. Authors¹⁻⁴ have explained this phenomenon as due to a reversible tautomerism with the quinoid structure of the anil. A requirement for the process has been shown to be an intramolecular hydrogen bond bridge between the *o*-hydroxy and the imine nitrogen. The tautomerism then occurs *via* an intramolecular hydrogen transfer. Visually, the tautomerism results in a color change of the solid from yellow to red.

There has been little evidence forthcoming, however, on the proposed tautomerism occurring in solution. It was reported earlier⁵ that the phototropism did not occur in solution. The quinoid isomer of the benzylamine anil of 1-hydroxy-2-acetylnaphthalene in CDCl₃ has been shown to exist at room temperature using nmr data.⁶ This same anil of *o*-hydroxybenzaldehyde did not exhibit a quinoid isomer under the same conditions. Recently, transient spectra observed in the flash photolysis of ethanol solutions of N-(*o*-hydroxybenzylidene)aniline have been attributed to a short-lived quinoid isomer.⁷ Azo-hydrazone tautomerism of 1-phenylazo-2-hydroxynaphthalene and the 1,4 derivative is more common and has been reported by a number of authors.⁸⁻¹¹ Flashing of solutions of 2-

hydroxy-5-methylazobenzene has produced a short-lived species which is postulated to be the hydrazone tautomer.

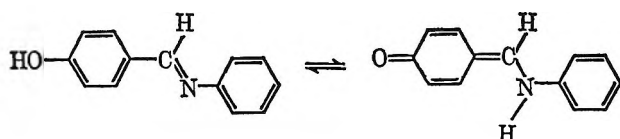
On observation by the author of a yellow color in ethanol solutions of 10⁻⁴ M N-(*o*-hydroxybenzylidene)-*o*-aminophenol, the color not being present in cyclohexane, the phenomenon was investigated further. Cyclohexane-ethanol solutions of the above compound exhibit isosbestic points characteristic of two absorbing species. A thorough spectral study based on molecular structure and solvent strongly indicates that an enol imine-keto enamine tautomerism of the following type

- (1) G. M. J. Schmidt, *Acta Cryst.*, **10**, 793 (1957).
- (2) M. D. Cohen, Y. Hirshberg, and G. M. J. Schmidt, "Hydrogen Bonding," D. Hadzi, Ed., Pergamon Press, London, 1959, p 293.
- (3) M. D. Cohen and G. M. J. Schmidt, Symposium on Reversible Photochemical Processes, Durham, N. C., 1962, p 119.
- (4) M. D. Cohen and G. M. J. Schmidt, *J. Phys. Chem.*, **66**, 2442 (1962).
- (5) V. DeGaouck and R. J. W. LeFevre, *J. Chem. Soc.*, 1457 (1939).
- (6) G. O. Dudek and R. H. Holm, *J. Am. Chem. Soc.*, **83**, 3914 (1961).
- (7) D. G. Anderson and G. Wettermark, *ibid.*, **87**, 1433 (1965).
- (8) R. Kuhn and F. Bar, *Ann.*, **516**, 143 (1935).
- (9) E. Sawicki, *J. Org. Chem.*, **22**, 743 (1957).
- (10) A. Burawoy and A. R. Thompson, *J. Chem. Soc.*, 1443 (1953).
- (11) E. Fischer and Y. F. Frei, *ibid.*, 3159 (1959).

exists in alcoholic and acid solvents capable of hydrogen bonding with the solute.



This phenomenon was also observed in the case of *N*-(*p*-hydroxybenzylidene)aniline. The following tautomerism for this compound is proposed.



The tautomerism was found to increase with the dielectric constant and acidity of the solvent. The dependence of the tautomerism on intermolecular hydrogen bonding with the solvent leads to two conclusions. The hydrogen bonding provides both a route for the mechanism by hydrogen transfer and the necessary stability for the quinoid isomer.

Experimental Section

The following compounds were prepared by the appropriate condensation of aldehyde and amine in ethanol or methanol and recrystallized from the same solvent: *N*-(*o*-hydroxybenzylidene) derivatives of *o*-aminophenol (I), *p*-aminophenol (II), aniline (III), and *m*-aminophenol (IV); *N*-(*p*-hydroxybenzylidene) derivatives of *p*-aminophenol (V) and aniline (VI); *N*-benzylidene derivatives of *p*-aminophenol (VII) and *o*-aminophenol (VIII); and *N*-(*m*-hydroxybenzylidene)-aniline (IX). The melting points agreed with those in the literature and the elemental analyses were in accord.

Most of the solvents used for the spectral study were of spectral quality. Exceptions were *t*-butyl alcohol, 2,2,2-trifluoroethyl alcohol, acetic acid, formic acid, and sulfuric acid which were of reagent quality. The ethyl alcohol was absolute and the water was distilled.

The spectra were recorded at room temperature with a Cary Model 15 recording spectrophotometer using 1.00-cm quartz cells. The wavelengths between 500 and 280 $m\mu$ were calibrated according to a holmium oxide filter. Accuracy of the recorded spectra is to the nearest millimicron. Most solution spectra were recorded at $5.0 \times 10^{-5} M$.

Results and Discussion

It was initially observed that ethanol solutions of I exhibited an additional electronic absorption band at energies less than that required for the $\pi^* \leftarrow \pi$ transi-

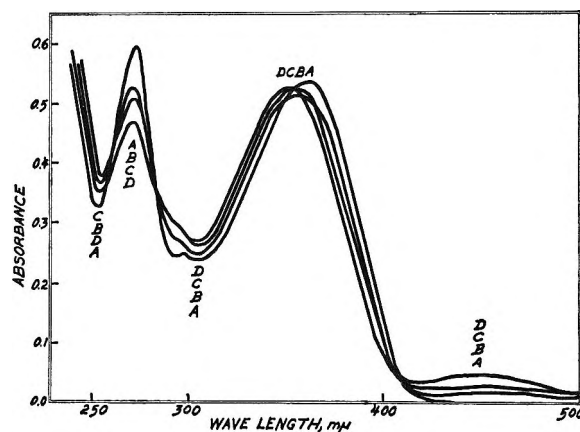


Figure 1. Absorption spectra of *N*-(*o*-hydroxybenzylidene)-*o*-aminophenol in cyclohexane-ethanol: (A) cyclohexane, (B) 97:3 cyclohexane-ethanol, (C) 90:10 and (D) 50:50 by volume. $M = 5.0 \times 10^{-5}$.

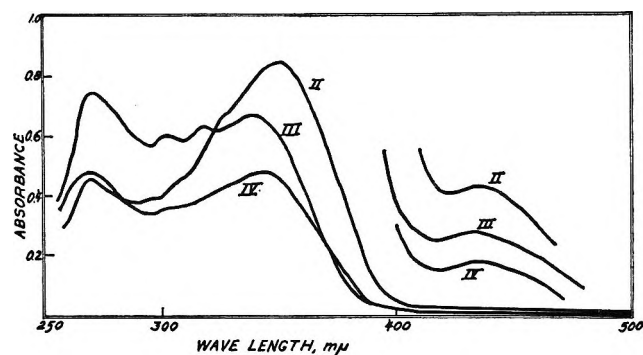


Figure 2. Absorption spectra of *N*-(*o*-hydroxybenzylidene)-*p*-aminophenol (II), *N*-(*o*-hydroxybenzylidene)aniline (III), and *N*-(*o*-hydroxybenzylidene)-*m*-aminophenol (IV) in methanol. $M = 5.0 \times 10^{-5}$.

tion. The $\pi^* \leftarrow \pi$ transition for similar compounds has been assigned by a number of authors.¹²⁻¹⁴ The possibility of the additional long wavelength band being due to the $\pi^* \leftarrow n$ transition was ruled out owing to the large intensity and its absence in a number of solvents (see Table II). In the cyclohexane-ethanol solvent system of I (Figure 1), isosbestic points at 406, 352, and 280 $m\mu$ definitely point out the existence of two molecular absorbing species in equilibrium.

If the absorbance of the two long wavelength bands of I is determined as a function of the concentration in methanol (Beer's law), the 349- $m\mu$ band gives a linear

(12) H. H. Jaffé, S. J. Yeh, and R. W. Gardner, *J. Mol. Spectry.*, **2**, 120 (1958).

(13) W. F. Smith, *Tetrahedron*, **19**, 445 (1963).

(14) V. I. Minkin, et al., *Opt. Spectry.*, **18**, [4] 328 (1965).

Table I: Dependence of Spectra in Methanol on Molecular Structure

No.	Structure	Spectra, $m\mu$ (ϵ)			
I		444 (1600)	349 (9800)	269 (8600)	228 s (13,700)
II		435 (400)	349 (17,000)	269 (9100)	230 (17,300)
III		432 (280)	338 (13,400)	270 (14,000)	225 (22,700)
IV		435 (240)	341 (9600)	268 (9600)	230 s (14,400)
V		420 (280)	333 (16,700)	284 (14,300)	230 s (11,500)
VI		415 (150)	313 (16,500)	295 s (15,300)	226 (14,400)
VII			336 (14,000)	264 (13,600)	
VIII			345 (9500)	265 (14,600)	238 s (10,000)
IX			316 (10,300)	266 (14,100)	222 (20,800)

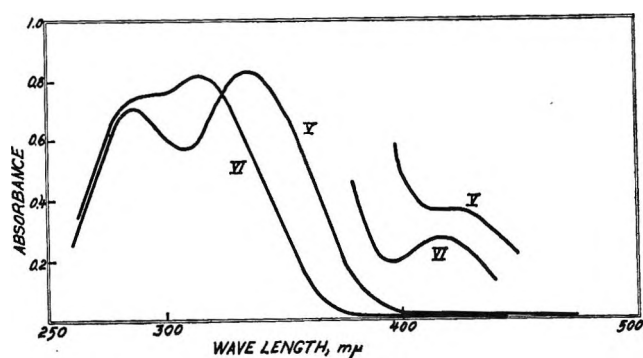


Figure 3. Absorption spectra of N-(*p*-hydroxybenzylidene)-*p*-aminophenol (V) and N-(*p*-hydroxybenzylidene)aniline (VI) in methanol. $M = 5.0 \times 10^{-5}$.

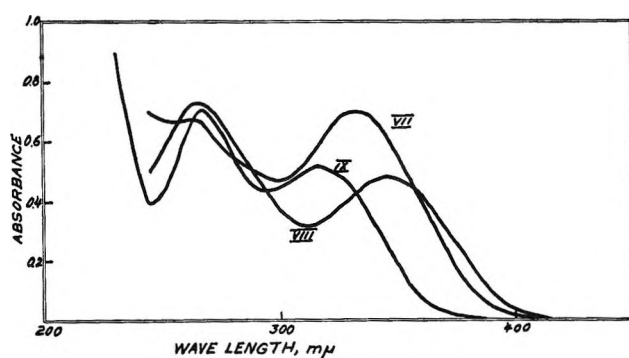


Figure 4. Absorption spectra of N-benzylidene-*p*-aminophenol (VII), N-benzylidene-*o*-aminophenol (VIII), and N-(*m*-hydroxybenzylidene)aniline (IX) in methanol. $M = 5.0 \times 10^{-5}$.

plot while the 444- $m\mu$ band plot is practically linear. It is, in fact, linear over the range 2.0×10^{-5} to at least $10.0 \times 10^{-5} M$. For the plots to be linear, an equilibrium must exist between the absorbing species. The equilibrium, subsequently, depends on the solvent.

To determine any structural requirements for the formation of such an equilibrium, several hydroxy-sub-

stituted benzylidene anils were prepared. The spectra of the anils were recorded in methanol and are shown in Figures 2, 3, and 4, while Table I lists the critical spectral data. The small inset curves of Figures 2 and 3 demonstrate the formation of the longer wavelength band at higher concentrations. The most obvious point, and the most significant, of the spectra is that an N-(*o*- or *p*-hydroxybenzylidene) anil structure is neces-

Table II: Solvent Effects on the $\pi^* \leftarrow \pi$ Band System^a

Solvent	N-(<i>o</i> -Hydroxybenzylidene)- <i>o</i> -aminophenol $m\mu$ (ϵ)		N-(<i>p</i> -Hydroxybenzylidene)- <i>p</i> -aminophenol $m\mu$ (ϵ)	
	Cyclohexane	358 (10,800)		333 (14,300)
Carbon tetrachloride	358 (13,400)		333 (14,100)	
1,4-Dioxane	352 (8900)		334 (15,600)	
Ethyl acetate	349 (13,600)		330 (15,700)	
Acetonitrile	348 (11,400)		329 (16,000)	
Chloroform	354 (10,800)	440 s (100)	331 (11,600)	
Alcohols				
<i>t</i> -Butyl	350 (9600)	432 (500)	332 (17,300)	435 s (24)
Isopropyl	348 (12,000)	446 (1000)	334 (17,700)	428 s (48)
Ethyl	350 (12,000)	448 (1400)	334 (17,500)	423 s (140)
Methyl	349 (9800)	444 (1600)	333 (16,700)	420 (280)
20% Ethyl (water) ^b	333 (5800)	438 (3200)		408 (1500)
2,2,2-Trifluoroethyl	342 (10,800)	437 (7800)		
Acids ^c				
Acetic	332 (6700)	402 (4000)	381	
Formic	(Overlapped)	392 (11,200)	380 (28,000)	
Sulfuric	352 (8000)	390 (7800)	365 (9900)	

^a Solvents in each group are in order of increasing dielectric constant. ^b Extinction coefficients are very approximate because of rapid hydrolysis. ^c Acetic, 99.8%; formic, 90.0%; sulfuric, 95.5–96.5%. Extinction coefficients are approximate because of small amounts of water present.

sary for the additional band to occur. Since the isobestic study demonstrated two absorbing molecular species in equilibrium, the *o*- and *p*-hydroxy substituents suggest that a quinoid structure is possible in solution. The equilibria would then involve enol-keto tautomerisms as shown previously. According to previous workers,¹⁵ the *trans* isomer of N-(benzylidene)-aniline is the more stable configuration at room temperature. Also, it has been shown¹⁶ that intramolecular hydrogen bonding exists in N-(*o*-hydroxybenzylidene) anils. Hence, the tautomerism is thought to occur from the *trans* configuration of the benzenoid structure. It is reasonable to believe that the long wavelength band for the quinoid isomer would appear at longer wavelengths, since, for 1-phenylazo-2-hydroxynaphthalene and the 1,4 derivative, it appears at about 470 $m\mu$.¹¹ This is about 80 $m\mu$ longer than the azo isomer. The average shift in Table I is 93 $m\mu$.

The compounds which exhibit the proposed tautomerism may be divided into three groups based on molecular structure and the intensity of the additional long wavelength band in methanol. This band intensity is taken as an approximate measure of the extent of tautomerism to the quinoid isomer. Compound I comprises the first group with the most intense band, four times greater than any of the others. Compounds II, III, and IV comprise the second group. The intensities of this group are found to decrease in

the order of decreasing imine basicity. The extent of tautomerism would be expected to decrease with the imine basicity if the tautomerism were by hydrogen transfer. The third group consists of the *p*-hydroxy derivatives, V and VI, whose band intensities are comparatively even less. The same relation of the intensity of the quinoid band with imine basicity is evident. It is reasonable that the increase in the tautomerism in going from the *p*-hydroxy to the *o*-hydroxy derivatives is due to intramolecular hydrogen bonding possibilities of the latter in the quinoid structure.

Two important aspects in this tautomerism are the mechanism and the stability of the two forms. While it is difficult to define mechanisms, a solvent study of the phenomenon has pointed out that hydrogen bonding of the solute with the solvent is essential for the process. Table II tabulates the results of the spectra of compounds I and V in various solvents. The purpose of including V is to demonstrate clearly this property of the *p*-hydroxy derivatives and to eliminate intramolecular hydrogen bonding. The solvents can be divided into four groups. First, there are those solvents which do not allow the tautomerism. These are followed by chloroform, the alcohols, and last, the acids, in which occurs the most intense response. The spectra of V in

(15) E. Fischer and Y. Frei, *J. Chem. Phys.*, **27**, 808 (1957).

(16) S. B. Hendricks, O. R. Wulf, G. B. Hilbert, and U. Lidell, *J. Am. Chem. Soc.*, **58**, 1955 (1936).

the acids show only one band in the region of interest. It is reasonable to believe that it is a composite of both bands since the hypsochromic shift for I from ethyl or methyl alcohol to the acids is reflected in the spectra of V. The hydrogen bond conceived to be responsible is between the solvent acidic hydrogen and the imine nitrogen. It is believed that the hydrogen bonding provides a basis for hydrogen transfer to the imine nitrogen. Also, it was found that the formation of the additional long wavelength band with solvent was a reversible process. The strength of the intramolecular hydrogen bond between the *o*-hydroxy group of *N*-(*o*-hydroxybenzylidene)aniline and the imine nitrogen¹⁸ is evidently not sufficient to initiate tautomerism in the first group of solvents. The possibility of an intramolecular hydrogen transfer with this compound in other solvents is being studied further.

Two other facts are immediately evident besides the hydrogen bonding. They are that the tautomerism increases with the acidity and the dielectric constant of the solvent. The aforementioned azo-hydrazone tautomerism also increases with solvent polarity.¹¹ The largest factor, however, seems to be the acidity. It is then proposed that the stability of the quinoid isomer is found through intermolecular hydrogen bonding with the solvent. The stability furthermore increases with the dielectric constant of the solvent. The enamine nitrogen of the quinoid isomer is expected to be more basic than the imine nitrogen. In addition, an increase in tautomerism with the pK_{NH^+} of the corresponding aminophenol is observed. Increasing both the nitrogen basicity and the solvent acidity would increase a tautomerism of this type where solute-solvent hydrogen bonding is the critical feature.

Nonequivalence of Protons and Related Phenomena in Some Organonitrogen and Organophosphorus Compounds¹

by T. H. Siddall, III

*Savannah River Laboratory, E. I. du Pont de Nemours and Co., Aiken, South Carolina
(Received January 10, 1966)*

Proton nonequivalence was rationalized in a variety of molecules in terms of the symmetry properties of the nonequivalent protons, groups, or radicals. The compounds that were studied included amides, an amine, a carbamylphosphinate (VIII), carbamylmethylenephosphonates (IX-XIII), and diphosphonates (XIV-XVIII).

Introduction

Nonequivalence of magnetic nuclei, or even of whole groups or radicals that contain such nuclei, has been widely observed. We have now observed such nonequivalence for protons in a still further variety of compounds. The purpose of this paper is to report these observations and to show how they can always be explained in terms of the symmetry properties of the protons, groups, or radicals.

Experimental Section

The proton magnetic resonance (pmr) spectra were measured on a Varian Associates A-60 spectrometer fitted with the Varian variable temperature probe and dewar insert. Except where noted, measurements

(1) The information contained in this article was developed during the course of work under Contract AT(07-2)-1 with the U. S. Atomic Energy Commission.

were made on solutions that were made by diluting 250 mg of compound to 1 ml with CDCl_3 .

The chemical compounds were all prepared by conventional synthetic techniques.^{2,3} All compounds were purified by vacuum distillation and/or crystallization until no extraneous signals could be observed in the pmr spectra.

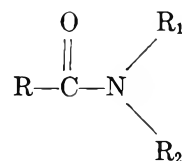
Results and Discussion

Conditions for Nonequivalence. In view of the variety of compounds for which proton nonequivalence is reported here and in order to help in organizing the discussion, it seems desirable to state the conditions that are necessary for nonequivalence to be observable, even though many investigators may be aware of these conditions. The most precisely defined condition for protons (or groups or radicals) to be nonequivalent is (1) that there must not be any molecular motions that correspond to a symmetry operation for the protons which are completed in a time that is short compared to the nmr signal width. The symmetry operations are the familiar symmetry operations of stereochemistry.^{4,5} Even in the presence of one or more symmetry elements corresponding to the above operations, protons may still be nonequivalent *provided* that the molecular motion(s) that corresponds to the symmetry operation is slow on the nmr time scale.

Two other conditions, which cannot be stated so precisely as the symmetry condition are: (2) there must be a field gradient between the protons, and (3) there must not be any rapid internal molecular motions that produce an approximation of symmetry that is good enough to prevent the observation of nonequivalence. Condition 3 has been the subject of considerable discussion.⁶ The analysis⁷ of rotation around an ethane-like bond is an example of the achievement of approximate, but incomplete, symmetry. Another

could arise when there are two asymmetry centers in a molecule, one not inverting and the other inverting rapidly. The rapid inversion of only one of the two centers does not correspond to inversion as a symmetry operation. As a consequence, nonequivalence might still be observable in spite of rapid inversion of one of the two asymmetric centers.

Amides. Slow rotation around the carbonyl to nitrogen bond (called the amide bond in the following discussion) removes the possibility of any molecular motions that correspond to a symmetry operation for



the radicals that are attached to nitrogen. As a consequence these radicals are nonequivalent as entire radicals.⁸ In general, the geminal protons or groups within a radical are equivalent, since there is a molecular symmetry plane. This is true even when the bonding to nitrogen is pyramidal, since rapid inversion of the nitrogen atom corresponds to the symmetry operation of reflection. However, if the molecule possesses an asymmetry center, no symmetry plane exists and geminal nonequivalence could be observable.

The observations for the amides in Table I show that this prediction is fulfilled (see Figure 1 as an example). In compounds I, II, and III, the asymmetry center is in the carbonyl substituent (R group) of the molecule. Similar effects were achieved when the asymmetry center was

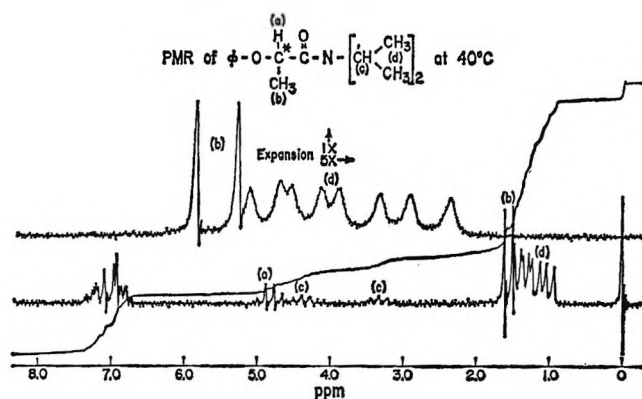
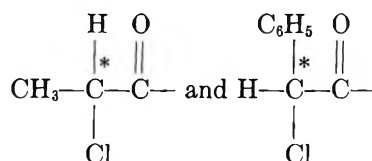


Figure 1.

At lower temperatures the four methyl groups in the nitrogen substituents with $\text{R}_1 = \text{R}_2$ each has its own

(2) (a) W. J. Hickinbottom, "Reactions of Organic Compounds," Longmans, Green and Co., New York, N. Y., 1957; (b) R. B. Wagner and H. D. Zook, "Synthetic Organic Chemistry," John Wiley and Sons, Inc., New York, N. Y., 1953.

(3) G. M. Kosolapoff, "Organophosphorus Compounds," John Wiley and Sons, Inc., New York, N. Y., 1950.

(4) F. A. Cotton, "Chemical Applications of Group Theory," John Wiley and Sons, Inc., New York, N. Y., 1963.

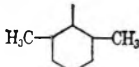
(5) G. W. Wheland, "Advanced Organic Chemistry," John Wiley and Sons, Inc., New York, N. Y., 1960.

(6) G. M. Whitesides, D. Holtz, and J. D. Roberts, *J. Am. Chem. Soc.*, **86**, 2628 (1964).

(7) H. S. Gutowsky, *J. Chem. Phys.*, **37**, 2196 (1962).

(8) H. S. Gutowsky and C. H. Holm, *ibid.*, **25**, 1228 (1956).

Table I: Pmr Data^a for Amides

Compd	R	R ₁	R ₂	Data
I	$\begin{array}{c} \text{H} \\ \\ \text{C}_6\text{H}_5\text{OC}- \\ \\ \text{CH}_3 \end{array}$	Ethyl	Ethyl	-CH ₂ - of ethyl just barely nonequivalent. About the same at -40° as +40°
II	$\begin{array}{c} \text{H} \\ \\ \text{C}_6\text{H}_5\text{OC}- \\ \\ \text{CH}_3 \end{array}$	2-Propyl	2-Propyl	Four β-methyl sets (2-propyl) 1.42, 1.33, 1.17, 0.98; two methine sets 4.39, 3.33 at +40°. At 75° in C ₂ Cl ₄ H ₂ all β collapsed into a hump; methine lost in noise. β two sets at 100°, 1.27, 1.15. β two sets 1.25, 1.18 at 145°. Methine still collapsed at 100°, but sharp at 130°, 3.85
III	$\begin{array}{c} \text{H} \\ \\ \text{C}_6\text{H}_5\text{OC}- \\ \\ \text{CH}_3 \end{array}$	Isobutyl	Isobutyl	Four γ-methyl sets (0.94, 0.89, 0.82, 0.78); N-CH ₂ - nonequivalent at -40°. At +40° only one N-CH ₂ - set, 3.20; γ, two sets 0.87, 0.82 (1:3 intensity). At 75° in C ₂ Cl ₄ H ₂ one N-CH ₂ - set, 3.14; one γ set, 0.83
IV	$\begin{array}{c} \text{H} \\ \\ \text{C}_6\text{H}_5\text{OC}- \\ \\ \text{CH}_3 \end{array}$	Methyl	C ₆ H ₅ CH ₂	No definite nonequivalence even at -40°
V	CH ₃	$\begin{array}{c} \\ \text{C}_6\text{H}_5-\text{CHCH}_3 \end{array}$	2-Propyl	One amide isomer from -40° (CDCl ₃) to 145° (C ₂ Cl ₄ H ₂), but two sets of methyl (2-propyl) signals over entire range. Chemical shift between sets lies between 0.032 and 0.040 for whole range. Low-field set at 1.22 at -40°, at 1.34 at 145°
VI	CH ₃	$\begin{array}{c} \\ \text{C}_6\text{H}_5-\text{CHCH}_3 \end{array}$		Only one amide isomer down to -40°. <i>o</i> -Methyl at 2.14, 1.67 at +40°
VI-U	Uranyl nitrate adduct of VI			Only one amide isomer at +40°. <i>o</i> -Methyl at 2.49, 1.88

^a Unless specified otherwise, all data are for solutions of 250 mg of compound made up to 1.0 ml in CDCl₃. All chemical shifts are in ppm from tetramethylsilane; all coupling constants in cps (same for other tables and figures).

doublet for the isobutyl (III) and 2-propyl (II) derivatives. The radicals are nonequivalent as also are the geminal methyl groups within the radicals. As the temperature is raised, rotation around the amide bond becomes rapid and the radicals become equivalent (~75° for II and slightly less than 40° for III); but even then, the geminal methyl groups remain nonequivalent in II up to 145°, since the only possible molecular motions that correspond to symmetry operations for them involve inversion of the asymmetric carbon atom, which does not occur. With more freedom of motion in the longer isobutyl chain, geminal methyl nonequivalence in III disappears between 40

and 75° but still is observable at a higher temperature than is radical nonequivalence.

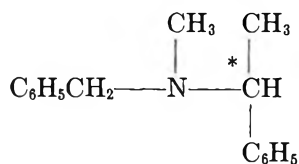
The geminal protons in I and III are nonequivalent in these compounds but to a much smaller extent than the geminal methyl groups in II and III. Evidently either condition 2 or 3 or both are not well satisfied. In compound IV there was possibly some broadening of the methylene signals, but no definite indication of the outer components for the quartets that would arise from an AB pattern.

Compounds V and VI demonstrate the effect of having the asymmetry center in one of the radicals attached to nitrogen (R₁). In both cases the signals

from only one of the two possible amide isomers was observed. (From work in this laboratory with many similar compounds, this effect probably results from a great preponderance of one isomer over the other rather than from rapid rotation around the amide bond.) In both cases nonequivalence was observed. The chemical shift is small, but remarkably near to constant from -40 to 145° for V. Methyl nonequivalence would be anticipated for V, but for VI, even with an asymmetry center, there is a molecular motion that corresponds to a symmetry operation for the methyl groups on the benzene ring, *i.e.*, rotation around the benzene to nitrogen bond. However, this rotation probably has a half-time of many hours, even well above 100° .⁹ Consequently, these methyl groups are nonequivalent. The protons in the 3 and 5 positions in this benzene ring should also be nonequivalent, but no analysis could be made because of interference from signals from the other benzene ring.

Slow rotation around the benzene to nitrogen bond can itself provide the required asymmetry center, since with unsymmetrical substitution in the benzene ring there is no molecular symmetry plane. We have reported our examination of this special situation in other publications.^{10,11} This situation is of considerable interest since the molecular motions that make geminal groups equivalent correspond to the symmetry operation of molecular inversion at the nitrogen atom.

Compound VII. The behavior of compound VII as the temperature is increased illustrates condition 3 stated at the beginning of this discussion. It also



VII

shows that the effects of an asymmetric center can be demonstrated in amines. The geminal protons of the methylene group in the benzyl radical are nonequivalent. However, the chemical shift between these protons decreases in a gradual and regular manner over the whole temperature span (-40 to 180°) that was studied. There is no molecular motion (that corresponds to a symmetry operation) that becomes rapid. The only available motion would be inversion at the asymmetric carbon atom. Instead, a combination of internal motions apparently approaches approximate correspondence to a symmetry operation (condition 3) as the temperature rises. Inversion of the nitrogen may be the most important motion in this combination. Inversion of the nitrogen atom produces diastereomers

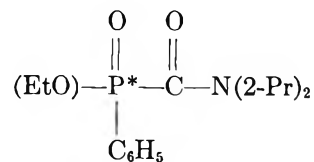
which presumably have different energies and different abundances. However, increasing temperature tends to populate the less abundant isomer and helps to produce approximate symmetry.

The AB pattern contains the information for following this process down to small chemical shifts, even beyond the direct resolution of the instrument. Even when the inner components of the AB quartet have almost merged, the high-field outer component is detectable. (The low-field outer component is lost in the signals from $\text{C}_6\text{H}_5\text{CH}-\text{C}-$.) But the relative intensity, outer-to-inner component, is $R = (Q - J)/(Q + J)$,¹² where Q is the distance between the first and third (or second and fourth) components of the quartet and J is the geminal coupling constant; and the chemical shift $\Delta\nu$ (in cps) is calculated by the formula $\Delta\nu = (Q^2 - J^2)^{1/2}$ or

$$\Delta\nu = J \left[\frac{(R + 1)^2}{(1 - R)^2} - 1 \right]^{1/2} = \frac{2J}{1 - R} (R)^{1/2} \quad (1)$$

Chemical shifts between the benzyl methylene protons ($\Delta\nu$) are plotted as a function of temperature in Figure 2. The points designated Φ were calculated from eq 1; the points designated Δ , from signal separation. The geminal coupling constant, J_{AB} , was 13.8 ± 0.2 cps over the range 60 – 180° . Resolution of this compound (undiluted) becomes very poor below 60° because of increasing viscosity. However, $\Delta\nu$ continues to increase in CDCl_3 solution at least down to -40° (at -40° in CDCl_3 $\Delta\nu = 24$ cps, $J_{AB} = 16$ cps). As would be expected, the Δ points fall below the Φ points as $\Delta\nu$ becomes small, since as the central signals begin to merge, the apparent signal separation is less than the real separation.

Compound VIII. In the carbamylphosphinate



VIII

the asymmetry center is the phosphorus atom. At temperatures below 90° four equal sets of methyl signals (1.45, 1.33, 1.25, and 0.92 ppm in CDCl_3 at

(9) R. Adams, *Record Chem. Progr.* (Kresge-Hooker Sci. Lib.), **10**, 91 (1949).

(10) T. H. Siddall, III, and C. A. Prohaska, *Nature*, **208**, 582 (1965).

(11) T. H. Siddall, III, and C. A. Prohaska, submitted for publication.

(12) K. B. Wiberg and B. J. Nist, "Interpretation of NMR Spectra," W. A. Benjamin Inc., New York, N. Y., 1962.

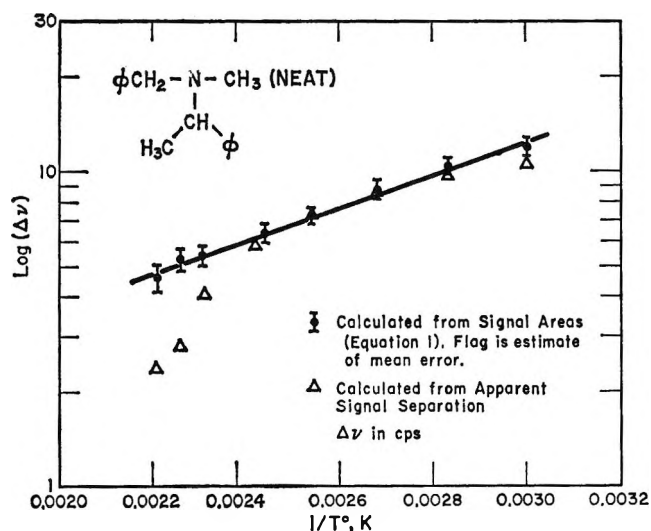


Figure 2. $\Delta\nu$ for methylene protons of the benzyl group.

40°) and two sets of methine signals (5.04 and 3.37 ppm) are observed for the 2-propyl radicals (see Figure 3). The signals of both sets of methine signals are further split at 40° by about 2 cps (perhaps by coupling to phosphorus). The methylene protons of the ethyl group are nonequivalent with a chemical shift of about 0.1 ppm. Nonequivalence of geminal protons in a radical attached to a phosphoryl group does not appear to have been reported before, although it has in a thiophosphoryl analog [(EtO)₂P(=S)CH₃].¹³

At about 90°, with undiluted compound VIII, the methyl signals of the 2-propyl radical begin to coalesce and the methine signals become broad humps and lose all detail. At 170° the methyl signals have coalesced into two sets of sharp signals ($\Delta\nu$ 0.088 ppm), while the methine signals have become one set with broadened components that is partly overlapped by the methylene signals from the ethyl radical.

The behavior of the signals from the 2-propyl radical is easily explained, as with the amides, on the basis of the onset of rapid rotation around the amide bond above about 90°. Below that temperature the 2-propyl radicals are nonequivalent as entire radicals, since rotation around this bond is required for correspondence to any symmetry operation. The methyl groups within a radical are nonequivalent because the asymmetric phosphorus atom removes all molecular symmetry planes.

The signals from the ethyl radical never lose their sharpness, even during coalescence of the 2-propyl signals. However, there is a continuous change for the methylene signals as the temperature is raised. The main feature of this change is apparently a decrease in the chemical shift between the methylene

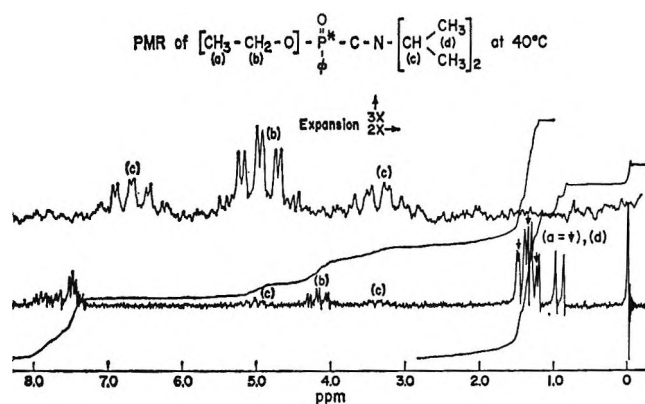
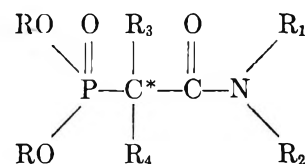


Figure 3.

protons. At 170° these protons are nearly, if not completely, equivalent. This gradual decrease in chemical shift is very similar to that observed for the methylene protons in VII and may be connected with increasing rate of rotation around the amide bond. If so, the connection is not direct or simple, since at 120° (well above the coalescence of the 2-propyl signals) the methylene protons are still nonequivalent.

Carbamylmethylenephosphonates and Related Compounds. These compounds can be regarded as amides with a phosphoryl-containing substituent. Only five comparatively simple examples of this class are in-



cluded in Table II. We have synthesized and examined the spectra of many others and from this can state certain generalities. One such generality is that as a rule R radicals are nonequivalent as radicals, and geminal methyl groups within an R radical are nonequivalent whenever the bridge carbon atom (i) is an asymmetry center. The α geminal protons (ii) in R₁ and R₂



often exhibit a very complex and not readily analyzable signal pattern, which we take as indicative of geminal proton nonequivalence. (For geminal methyl groups

(13) H. Finegold, *J. Am. Chem. Soc.*, **82**, 2641 (1960).

Table II: Pmr Data for Carbamylmethylenephosphonates

Compd	R	R ₃	R ₄	R ₁	Data
IX	CH ₃	H	C ₆ H ₅ CH ₂	CH ₃	R at 3.84, 3.80; R ₁ at 2.85, 2.75 (2.85 further split 1.6 cps, by coupling to bridge H?)
X	CH ₃	H		CH ₃	R at 3.83, 3.79, 3.51, 3.44; R ₁ at 2.99, 2.67, both very broad; bridge CH ₃ at 1.49, 1.32
XI	2-Propyl	H	C ₆ H ₅ CH ₂	Isobutyl	R methyl at 1.39, 1.38, 1.35, 1.36; R ₁ γ methyl at 0.85, 0.80, 0.65, 0.53
XII	2-Propyl	H		Ethyl	R methyl at 1.46, 1.43, 1.38 (ratio 1:2:1); R ₁ methyl at 0.91, 0.35
XIII	2-Propyl	CH ₃	C ₆ H ₅ CH ₂	CH ₃	R methyl at 1.35, 1.32; R ₁ at 3.18, 3.16 (3:1); bridge CH ₃ 1.40; C ₆ H ₅ CH ₂ nonequivalent; center of pattern at 3.33; Δν between first and fifth peak 0.96 ppm; J _{AB} = 13.6 cps, J _{H,P} = J _{Hb,P} = 9.2 cps

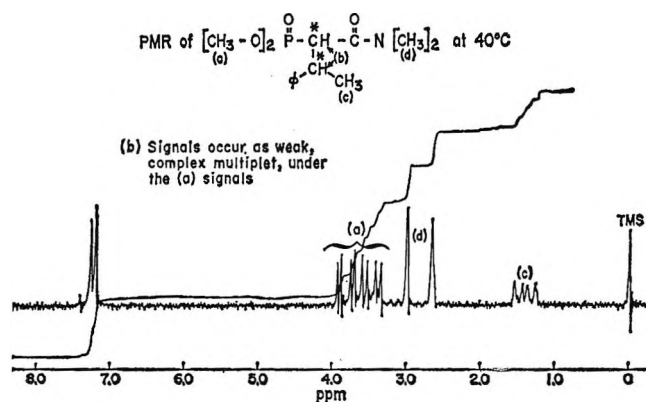


Figure 4.

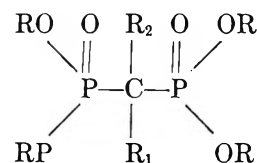
in R₁ and R₂ that are conspicuously nonequivalent, see compound XI as an example.)

Compound X (see Figure 4) shows the effect of two asymmetry centers. This is clearest for the R signals which occur as four sets. Evidently, asymmetry causes the R groups to be nonequivalent in both diastereoisomers.

Compound XIII is interesting in that the C₆H₅-CH₂- protons attached to the bridge are nonequivalent. The rather large degree of nonequivalence suggests that there may be rather strong rotamer preference around the C₆H₅CH₂-C- bond. This same phenomenon for XI (R₃ = H) would help to account for the rather large effects on groups as far away as the

γ-methyl groups. However, when R₃ = H, the overlap from the signals from this proton has prevented our analyzing the signals from the aryl-CH₂- protons. The stiffness of the amide bond is probably also a factor in producing large effects at a distance. The chance of internal motion producing approximate symmetry would be reduced by these restrictions. The shift to high field of two of these γ signals suggest that the γ-methyl groups of one isobutyl radical are on the average in a plane that is substantially perpendicular to the plane of the benzene ring. The effect is even more pronounced in compounds with a naphthyl group in the place of this benzene ring. This is seen in XII where one methyl signal center is at 0.35 ppm. Rotamer preference may be increased with the larger naphthyl group and the fused ring system certainly provides a larger magnetic field than does the simple benzene ring.

Diphosphonates. So long as R₂ = R₁, the R radicals are equivalent as whole radicals in these diphosphonates, since there is a symmetry plane. Even so,



geminal protons (or groups) within an R radical may be nonequivalent, since they possess no symmetry element. (This situation has been studied for the

Table III: Pmr Data for Diphosphonates

Compd	R	R ₁	R ₂	Signals		Additional data
				α Proton	β-Methyl	
XIV ^a	2-Propyl	H	H	4.79	1.35	
XIV-U	Uranyl nitrate chelate ^b			5.19	1.37, 1.58	
XV	2-Propyl	C ₆ H ₅ CH ₂	H	4.77	1.32, 1.28, 1.26; intensity 2:1:1	C ₆ H ₅ CH ₂ CH overlaps
XV-U	Uranyl nitrate chelate			5.14	1.57, 1.50, 1.33, 1.22	C ₆ H ₅ CH ₂ CH overlaps
XV-T	Thorium nitrate chelate			4.9	1.47, 1.44, 1.23, 1.08	
XVI	2-Propyl	C ₆ H ₅ CH ₂	C ₆ H ₅ CH ₂	4.75	1.19	C ₆ H ₅ CH ₂ - at 3.35, J _{HP} = 16.2
XVII	2-Propyl			4.77	1.10, 1.20	at 3.92, J _{HP} = 18, center peak broad
XVIII	Ethyl	C ₆ H ₅ CH ₂	H	4.04	1.26	C ₆ H ₅ CH ₂ CH overlaps
XVIII-U	Uranyl nitrate chelate			Complex	1.37, 1.32	C ₆ H ₅ CH ₂ CH overlaps

^a 10% by volume. ^b All chelates 250 mg/ml in CDCl₃.

simple esters, (RO)₂POR₁.^{14,15} With the simple esters, only groups are nonequivalent, and not whole radicals.) However, as soon as R₁ ≠ R₂ the two R's attached to a phosphorus become nonequivalent, since there is now no molecular symmetry plane that is also a symmetry plane for the R's.

These various considerations as well as condition 2 are illustrated by the series given in Table III. (The first two entries are from a previous study.¹⁶) Evidently there is not enough field gradient in XIV itself to produce any nonequivalence, but the uranyl group in the uranyl nitrate chelate (XIV-U) provides a strong anisotropic magnetic field. The chelate ring¹⁶ that is formed by bonding of the uranium atom to the phosphoryl oxygens reduces the flexibility of the molecule, even though the bonding is mobile and exchange is rapid. The β-methyl groups within a 2-propyl radical become nonequivalent in the uranyl nitrate chelate, but since there is a symmetry plane for the 2-propyl radicals, as a whole, the radicals are equivalent. With compound XV the appropriate symmetry plane is lacking, and potentially both the entire radicals and the β-methyl groups are nonequivalent. However, only three β-methyl signal sets are observed, but

with an intensity ratio of 2:1:1. Two of the four β-methyl groups (for each phosphorus) happen to be equivalent. In the uranyl nitrate adduct (XV-U) there are four equal sets of β-methyl signals. Again through condition 2, and almost certainly (3) as well, greater multiplicity is realized. The formation of the chelate ring is now probably very important in making the maximum multiplicity observable. It is unlikely that the bridge grouping (C₆H₅CH₂CH-) can be rotated through the chelate ring. This would tend to fix the C₆H₅CH₂- group on one side of the chelate molecule, thereby diminishing motions that approximate symmetry operations. This effect is illustrated in the thorium nitrate chelate where presumably there is little or no additional contribution to condition 2 over XV, but about the same change in condition 3 as there is for XV-U.

With XVI, the molecular symmetry plane is restored. Since there is only one signal set for the β-methyl groups,

(14) T. H. Siddall, III, and C. A. Prohaska, *J. Am. Chem. Soc.*, **84**, 2502 (1962).

(15) T. H. Siddall, III, and C. A. Prohaska, *ibid.*, **84**, 3467 (1962).

(16) T. H. Siddall, III, and C. A. Prohaska, *Inorg. Chem.*, **4**, 783 (1965).

it is evident that an approximate symmetry is also achieved within a 2-propyl radical. However, with XVII, the approximate symmetry within a radical is lost and two β -signal sets are observed. The fused naphthyl rings enforce a high rigidity on this molecule. This factor, plus the larger magnetic field from these rings, must account for the loss of approximate symmetry as compared to XVI. Unfortunately, we have not been able to isolate the naphthyl analog of XV; this compound would allow interesting comparisons. Compound XVIII and its uranyl nitrate adduct add no new conclusions but do confirm those found with the 2-propyl analog. The uranyl nitrate chelate XVIII-U gives two sets of methylene signals, presumably one set for each radical on a phosphorus atom. The methine signals of the 2-propyl radicals are already so complex (14 lines) that it is hard to say whether or not there is still further multiplicity. Also, it is possible that the methylene protons of XVIII and XVIII-U should be nonequivalent within an ethyl radical). This would lead to a theoretical total of 64 lines [4 (for J_{HH}) \times 2 (for J_{HP}) \times 2 (for nonequivalent radicals) \times 4 (for nonequivalence within a radical)]. There does not appear to be that much multiplicity for XVIII-U.

The $\text{C}_6\text{H}_5\text{CH}_2$ - protons should be equivalent (a symmetry plane) for all the compounds in Table III. However, for XVIII, the expected triplet is so broad

in its center component that this component is no higher than the wing components. Possibly the rotation around the $\text{C}_6\text{H}_5\text{CH}_2\text{-CH}$ bond may be slow (the symmetry operation that corresponds to reflection in a molecular symmetry plane). However, at -40° , this component is much the same as at $+40^\circ$.

Conclusions

The power of elementary symmetry considerations to rationalize nonequivalence in a variety of circumstances is perhaps adequately demonstrated by the examples cited above. The chief problem that remains is the weakness of this formalization in predicting nonequivalence. It is evident that increased predictive ability can arise only as conditions 2 and 3 can be made more explicit. Gutowsky's "asymmetry effect"⁷ is a beginning in that direction. It seems that chelates with uranyl salts may be especially useful as model compounds for studies of conditions 2 and 3. The geometry of the chelate ring system is often well known, and the anisotropic field of the uranyl group is subject to measurement. Further studies along these lines are in progress in this laboratory.

Acknowledgment. The author wishes to thank M. A. Davis for the preparation of several of the diphosphonates used in these studies.

Catalysis over Supported Metals. V. The Effect of Crystallite Size on the Catalytic Activity of Nickel

by J. L. Carter, J. A. Cusumano, and J. H. Sinfelt

Esso Research and Engineering Co., Linden, New Jersey (Received January 11, 1966)

The effect of nickel crystallite size on the catalytic activity of nickel supported on silica-alumina was investigated, using ethane hydrogenolysis as the test reaction. The crystallite size of the nickel was varied by sintering in hydrogen at varying temperatures. Data on nickel surface areas and crystallite sizes were obtained from hydrogen chemisorption isotherms and from measurements of the effect of chemisorbed hydrogen on the magnetization of the nickel. It was found that the catalytic activity of the nickel decreased with increasing crystallite size to a larger extent than could be accounted for by the corresponding decrease in nickel surface area. The specific catalytic activity of the nickel (activity per unit of nickel surface area) thus decreased as the crystallite size increased. The results indicate that the intrinsic properties of small metal crystallites change in the course of increasing the crystallite size by sintering.

It is well known in heterogeneous catalysis that the catalytic activity of a supported metal depends on the degree of dispersion of the metal on the support. It is commonly considered that catalytic activity increases with increasing dispersion, *i.e.*, with increasing surface area or decreasing crystallite size. However, while the importance of crystallite size in catalysis has been recognized, the detailed nature of the crystallite size effect is not clear; *i.e.*, there is relatively little information available to determine if the effect of crystallite size is limited to the effect on surface area, or whether there is an effect over and above this.¹ For unsupported platinum blacks, the recent results of McKee on propane cracking indicate that the effect is more than one of surface area, since the sintering or growth of the platinum crystallites on heating resulted in a decrease in catalytic activity far greater than the corresponding decrease in surface area.² For supported nickel catalysts, Selwood, *et al.*,³ have suggested that the effect of crystallite size is more than an effect on surface area. However, very little information of a quantitative nature is available for supported metal systems, where kinetic data and metal surface area measurements have been obtained on samples in which the crystallite size has been varied systematically by controlled sintering procedures.

In view of its importance to the understanding of the catalytic properties of supported metals, the nature of crystallite size effects is an important area for further investigation. To this end we have studied the effect of nickel crystallite size on the rate of hydrogenolysis of ethane over nickel supported on silica-alumina. The crystallite size was varied by sintering at various temperatures in a stream of hydrogen. The nickel surface areas of the sintered samples were determined by hydrogen chemisorption measurements and also by observing the effect of adsorbed hydrogen on the ferromagnetism of the nickel. Values of average nickel crystallite sizes were determined from these same measurements. It was thus possible to evaluate the specific catalytic activity of the nickel as a function of the nickel crystallite size.

Experimental Section

Apparatus and Procedure. The hydrogen chemisorption measurements were made in a conventional glass vacuum system with an 80-l./sec oil diffusion

(1) G. C. Bond, "Catalysis by Metals," Academic Press Inc., New York, N. Y., 1962, p 31.

(2) D. W. McKee, *J. Phys. Chem.*, **67**, 841 (1963).

(3) P. W. Selwood, S. Adler, and T. R. Phillips, *J. Am. Chem. Soc.*, **77**, 1462 (1955).

pump. The apparatus has been described previously.⁴ Using a trap cooled in liquid nitrogen, ultimate dynamic vacua of about 10^{-7} torr were obtained. The sample cells were made of Pyrex glass and had two stopcocks to permit hydrogen to flow through the bed of material.

In the adsorption measurements a sample, weighing about 2 g, was put in a vacuum apparatus. After evacuation at 100° for a short time, hydrogen was passed through the bed of sample at a flow rate of 500 cm^3/min . The temperature of the sample was then increased, in the flowing hydrogen, to 450° . This temperature was maintained for 3 hr, after which the sample was evacuated for 1 hr at the same temperature. In one case a reduction temperature of 370° was employed. After evacuation at the reduction temperature, the sample was cooled to -78° by surrounding the adsorption cell with a Dry Ice-alcohol mixture. A hydrogen adsorption isotherm was then measured at this temperature. In the measurement of an isotherm, three or more points up to a pressure of about 30 cm were usually obtained.

In the preparation of the sintered catalyst samples, the catalyst was charged to a quartz tube and heated for 1 hr in flowing hydrogen, using a flow rate of 1 l./min. The sintered samples were then cooled and purged with nitrogen prior to exposure to the atmosphere. This procedure undoubtedly results in the formation of an oxide layer at the surface of the nickel, but this introduces no problem since the samples are re-reduced in place prior to the chemisorption, magnetic, or catalytic measurements.

The magnetic measurements were made using the Faraday method in apparatus similar to that described by other workers.^{5,6} In this apparatus the sample was suspended from a Cahn electrobalance in a quartz bucket located midway between the pole faces of a Varian 4-in. magnet. The sample could be reduced in flowing hydrogen or evacuated to 10^{-6} torr *in situ*. The electrobalance measures the force, f , exerted by the magnetic field, H , on the sample. The magnetic susceptibility χ is determined from the relation

$$f = m\chi H \frac{dH}{ds} \quad (1)$$

where m is the mass of sample, dH/ds is the field gradient, and s represents the vertical distance from a horizontal reference line between the pole faces. Magnetic fields up to 6500 oersteds were attainable with the apparatus. Specially designed pole caps obtained from the manufacturer gave a constant value of the quantity HdH/ds over the region within which the sample was suspended. Ferrous ammonium sulfate was used to calibrate the apparatus, which was in turn

checked with a sample of bulk nickel. The values obtained for the magnetization of the bulk nickel were in excellent agreement with published data.⁷

The ethane hydrogenolysis data were obtained in a flow reactor system at atmospheric pressure, using a vertically mounted stainless steel reactor tube 1.0 cm in diameter and 8.0 cm in length. Details of the reactor assembly, flow rate measurements, and the gas chromatographic analysis of the reaction products have been reported previously.⁸ The ethane and hydrogen were mixed with helium and passed downflow through a bed containing 0.20 g of catalyst diluted uniformly with 0.50 g of ground Vycor glass. By appropriate adjustment of the helium flow rate, it was possible to vary the partial pressures of ethane and hydrogen individually. The total gas flow was maintained at 1 l./min throughout. In a typical run the reactant gases were passed over the catalyst for 3 min prior to sampling products for analysis. The ethane was then cut out and the hydrogen flow continued for 10 min prior to another reaction period. Prior to any reaction rate measurements, the catalysts were reduced for 3 hr in flowing hydrogen at 450° in the reactor, except for one sample which was reduced at 370° .

Materials. The nickel catalyst used in the present study contained 10 wt % nickel and was prepared by impregnating silica-alumina with a solution of $\text{Ni}(\text{NO}_3)_2 \cdot 6\text{H}_2\text{O}$ dissolved in deionized water. The material was then dried overnight at 105° , after which it was pressed into wafers which were subsequently crushed and screened to a size between 45 and 60 mesh. The silica-alumina was Type DA-1 cracking catalyst (nominally 13% Al_2O_3 , 87% SiO_2) with a surface area of 450 m^2/g , and was obtained from Davison Chemical Co. Samples of the nickel catalyst were heated at different temperatures (370 , 450 , 500 , 580 , 700°) in hydrogen to vary the nickel crystallite size, as described in a previous paragraph.

The ethane used in this work was obtained from the Matheson Co. A chromatographic analysis showed no detectable impurities. It is estimated that an impurity, *e.g.*, methane, would have been detected by the chromatographic analysis if it were present at a concentration above 0.01 wt %. High purity hydro-

(4) D. J. C. Yates, W. F. Taylor, and J. H. Sinfelt, *J. Am. Chem. Soc.*, **86**, 2996 (1964).

(5) P. E. Jacobson and P. W. Selwood, *ibid.*, **76**, 2641 (1954).

(6) P. W. Selwood, "Magnetochemistry," 2nd ed, Interscience Publishers, Inc., New York, N. Y., 1956, pp 11-13.

(7) "American Institute of Physics Handbook," 2nd ed, McGraw-Hill Book Co., Inc., New York, N. Y., 1963, Section 5, p 170.

(8) J. H. Sinfelt, *J. Phys. Chem.*, **68**, 344 (1964).

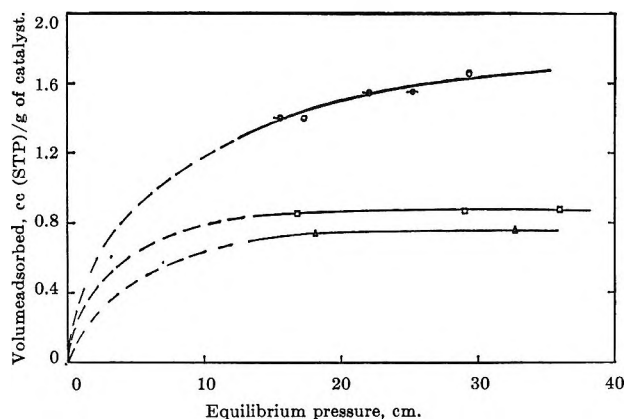


Figure 1. Hydrogen adsorption isotherms at -78° for nickel on silica-alumina catalyst sintered in hydrogen at various temperatures: \ominus , 370° ; \circ , 450° ; \square , 500° ; \triangle , 580° .

gen was obtained from the Linde Co., Linden, N. J. It was further purified in a "Deoxo" unit containing palladium catalyst to remove trace amounts of oxygen. The water formed was then removed by a trap cooled in Dry Ice or by a molecular sieve dryer, the latter having been employed for the hydrogen used in the kinetic measurements.

Results

The results of hydrogen chemisorption measurements at -78° on samples of the nickel on silica-alumina catalyst sintered in hydrogen at various temperatures are shown in Figure 1. The hydrogen adsorption decreases with increasing sintering temperature. A decrease is not observed for the interval from 370 to 450° , suggesting that loss of nickel surface area is not significant below about 450° . From the adsorption data the number of hydrogen atoms adsorbed per nickel atom can be determined. Taking the adsorption at 25 cm pressure as the monolayer point, and assuming that one hydrogen atom is adsorbed on each nickel atom in the surface, one then has a value for the fraction of total nickel atoms which are present in the surface of the nickel crystallites. Values for the various sintered samples are included in Figure 3.

In the measurements of the magnetic properties of the sintered catalyst samples, the specific magnetization was determined as a function of magnetic field strength and temperature down to liquid nitrogen temperature. Typical data for the sample sintered and reduced in hydrogen at 450° are shown in Figure 2. The specific magnetization, σ , is defined by the relation, $\sigma = \chi H$, where H is the magnetic field strength in oersteds and χ is the magnetic susceptibility per unit mass. The units of χ are reciprocal density, cm^3/g . The data shown in Figure 2 were obtained at a

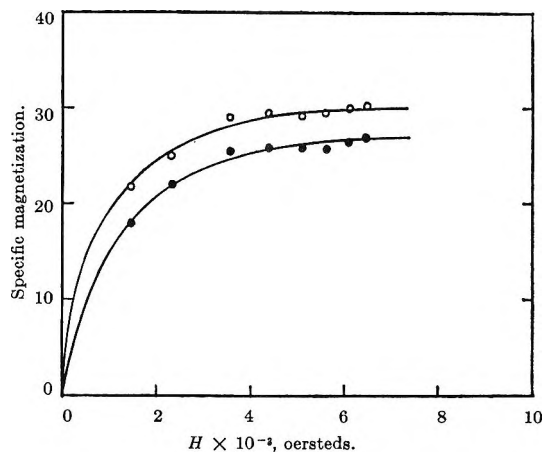


Figure 2. Typical magnetization-field strength curves at 77°K for nickel on silica-alumina catalyst sintered in hydrogen at 450° : \circ , after reduction at 450° and evacuation; \bullet , after subsequent adsorption of hydrogen at room temperature and 1 atm.

temperature of 77°K . Data are presented for the freshly reduced sample after evacuation at the reduction temperature and after subsequent adsorption of hydrogen on the nickel. The hydrogen was actually adsorbed at room temperature and 1 atm, and the sample then cooled to 77°K to measure the effect of the adsorbed hydrogen on the magnetization of the nickel. The presence of adsorbed hydrogen clearly lowers the specific magnetization of the nickel. By inspection of the curves in Figure 2, it is seen that the specific magnetization approaches a limiting value at the higher fields. The limiting value was found to increase with sintering temperature. In treating the magnetization data, the practice was adopted of plotting the reciprocal of the specific magnetization *vs.* the reciprocal of the field strength. When this is done, a satisfactory linear relation is obtained, and by extrapolation to zero reciprocal field ($1/H = 0$) an apparent saturation value is obtained for the specific magnetization. Apparent saturation magnetizations at 77°K determined in this manner for various sintered catalyst samples are given in Table I. The extrapolation gives magnetization values only slightly higher than those actually measured at the highest field employed (6500 oersteds). We have termed the extrapolated value the apparent saturation magnetization, since the variation of specific magnetization with field strength is small at fields above 3000 oersteds. While these samples appear to be magnetically saturated, the specific magnetization values are significantly lower than that of bulk nickel, which is 57 at 77°K .⁷ This behavior is typical of supported nickel catalysts in which the nickel exists in a highly dispersed state

and is related to a phenomenon that has been termed "collective paramagnetism."^{9,10} As the crystallite size of the nickel is increased by sintering at progressively higher temperatures, the apparent saturation magnetization approaches the value for bulk nickel.

Table I: Summary of Magnetization Data on Sintered Ni Catalysts

Sintering temp, °C	Apparent satn magnetization at 77°K ^a	% decrease in magnetization after H ₂ adsorption ^b
370	34.4	12
450	35.7	7
500	42.1	..
580	49.2	5
800	51.0	2

^a Obtained from extrapolation of plot of $1/\sigma$ vs. $1/H$ to $1/H = 0$. ^b H₂ adsorbed at 1 atm and room temperature prior to measurement of specific magnetization at 77°K.

The apparent saturation magnetization as defined here is a strong function of temperature and for highly dispersed nickel is much lower than the corresponding quantity for bulk nickel. However, this does not mean that the true saturation magnetization, *i.e.*, the value at 0°K and infinite field, is different from that of bulk nickel. The difference between the magnetic properties of finely divided and bulk nickel tends to disappear at very low temperatures. It is recognized that the term "apparent saturation magnetization" as used in the present work may have no particular fundamental significance. However, it is a convenient way to refer to the limiting value of the magnetization approached at sufficiently high fields at temperatures well above 0°K. Furthermore, it is useful in the discussion of matters such as the extent of reduction of the metal and the effect of sintering on crystallite size.

In considering the technique of varying nickel crystallite size by heating in hydrogen at various temperatures, it is important to consider the possibility that the samples heated in hydrogen at the lower temperatures, *e.g.*, at 370°, were not completely reduced, and that part of the increase in magnetization with increasing sintering temperature may have been due to better reduction of the nickel. To obtain data on this question, a sample reduced at 370° in the usual way was evacuated at 370° and then heated to 800° *in vacuo* prior to determination of the magnetization at 77°K. It was observed that the apparent saturation magnetization increased from a value of 34 to 51 after this treatment. Because the sample was

heated in the absence of hydrogen, the increase in magnetization was not due to further reduction of the nickel, but rather to increasing the size of the smaller crystallites in the sample to the point where they became ferromagnetic. Since the value approached that of bulk nickel, it is concluded that the nickel is essentially completely reduced after treatment with hydrogen at 370°.

The decrease in magnetization on hydrogen chemisorption is attributed to the transfer of electrons from the hydrogen into the unfilled d band of the nickel.³ Each chemisorbed hydrogen atom effectively erases the contribution of a nickel atom to the magnetization. Data on the percentage decrease in magnetization after chemisorption of hydrogen are given in Table I. It should be noted that the adsorbed hydrogen has less of an effect on the magnetization in the case of the more highly sintered samples. This is reasonable since these samples have lower nickel surface areas and hence chemisorb less hydrogen. The effect of chemisorbed hydrogen on the magnetization offers an approximate method of estimating the fraction of the atoms in the nickel crystallites which are present in the surface. This quantity is simply equal to the fractional decrease in magnetization after adsorption of hydrogen. Values of the fraction of the total nickel atoms present in the accessible surface of the nickel crystallites are shown in Figure 3 as a function of sintering temperature. The plot contains values derived from the effect of adsorbed hydrogen on magnetization along with values of this quantity determined from the hydrogen adsorption isotherms in Figure 1. The values derived from the adsorption isotherms and from the magnetic measurements show reasonably good agreement, with the individual points all falling about a single curve. The points derived from the effect of chemisorbed hydrogen on magnetization show a continuous decrease in the surface nickel atoms as the sintering temperature is increased above 370°. By comparison, the adsorption isotherms in Figure 1 indicated that loss of nickel surface area was not significant until the temperature was increased above 450°. In the case of the values derived from magnetic data, the points for the lower sintering temperatures are only approximate, since the smaller crystallites in the mildly sintered samples are not magnetized and hence escape detection. This means that the values of the fraction of nickel atoms in the surface, as determined from the magnetic data, are probably underestimated for the mildly sintered samples.

(9) P. W. Selwood, "Adsorption and Collective Paramagnetism," Academic Press Inc., New York, N. Y., 1962, p 37.

(10) See ref 9, p 44.

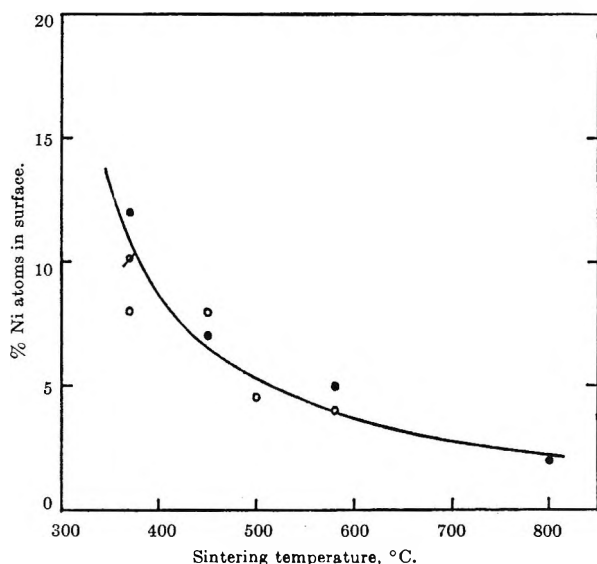


Figure 3. Per cent nickel atoms in the surface of the nickel crystallites as a function of sintering temperature: ●, from decrease in magnetization as a result of adsorbing hydrogen; ○, from hydrogen adsorption isotherms at -78° ; ◊, from hydrogen adsorption isotherm at room temperature.

From the curve in Figure 3, values for the surface area of the nickel can be determined, assuming that an area of 6.5 \AA^2 is associated with each surface nickel atom.¹¹ Nickel surface areas are shown as a function of sintering temperature in Table II. Relative crystallite sizes, which are inversely proportional to the surface areas, are also given. Absolute values of the crystallite size can also be estimated from the

Table II: Effect of Sintering Temperature on Nickel Surface Area and Crystallite Size

Sintering temp, °C	Ni surface area, m^2/g of catalyst ^a	Relative crystallite size, l/l_0 ^b	Absolute crystallite size, \AA ^c
370	7.5	1.0	<40
450	4.4	1.7	...
500	3.4	2.2	57
580	2.6	2.9	71
700	1.9	4.0	88

^a Calculated assuming 6.5 \AA^2 per surface nickel atom.¹¹

^b Crystallite size l relative to the crystallite size l_0 of the sample reduced at 370° . ^c Determined by X-ray diffraction line broadening.

surface areas. If it is assumed that the crystallites are cubes and that one of the six faces is in contact with the support, the other five faces will be exposed surface. If l is a side of the cube and S represents the

surface-to-volume ratio determined from the density and the specific surface area of the nickel, the relation, $l = 5/S$, can be employed to calculate the average crystallite size. When this is done, one obtains values ranging from 77 to 305 \AA for the crystallite sizes corresponding to the different sintering temperatures in Table II. However, X-ray diffraction line-broadening data give crystallite sizes several-fold lower, ranging from less than 40 to 88 \AA . These data are included in Table II. The crystallite sizes shown in Table II are mean dimensions perpendicular to the 111 plane of the nickel. The procedure employed in calculating the crystallite sizes from the line-broadening data was similar to that described previously by Selwood and co-workers.³ In agreement with the previous findings of these investigators on supported nickel catalysts, crystallite sizes determined from gas adsorption data are considerably larger than those determined from X-ray line-broadening measurements. In the course of the reduction of the nickel in the catalysts, it may be that a substantial part of the nickel becomes inaccessible to adsorbing gases. For whatever reason, absolute crystallite sizes determined from gas adsorption data appear too high for the nickel catalysts. However, the adsorption data can be expected to give a good approximation of relative crystallite sizes.

The calculation of crystallite size directly from magnetization values has been considered by several investigators, as discussed by Selwood.¹⁰ The preferred method involves an adaptation of a low-field approximation of the Langevin theory for the magnetization of an assembly of particles. This requires data at very low fields where the magnetization is small compared to the saturation magnetization. In general, the magnetization measurements in the present work were not made at fields low enough to apply the method satisfactorily. However, a very rough estimate for the sample reduced at 370° indicates a crystallite size of the order of 30 \AA , when the low-field approximation method described by Selwood¹⁰ is applied. The only point to be made here is that the value is consistent with that determined by X-ray line broadening, in which case the crystallite size is indicated to be less than 40 \AA because the crystallites are too small to be detected by the X-ray method.

Turning to results on the catalytic activity of the sintered catalyst samples, Figure 4 shows Arrhenius plots for the hydrogenolysis of ethane to methane as a function of sintering temperature. The rates of ethane hydrogenolysis were determined at constant ethane and

(11) D. F. Klemperer and F. S. Stone, *Proc. Roy. Soc. (London)*, **A243**, 375 (1958).

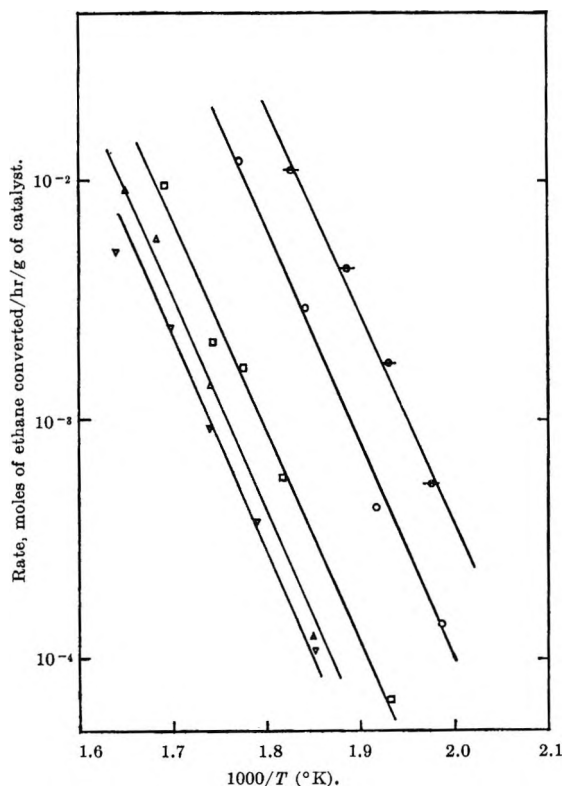


Figure 4. Catalytic activity of nickel on silica-alumina catalyst sintered in hydrogen at various temperatures. The data are for ethane hydrogenolysis at ethane and hydrogen partial pressures of 0.030 and 0.20 atm, respectively: \ominus , sintered at 370°; \square , sintered at 450°; \triangle , sintered at 580°; ∇ , sintered at 700°.

hydrogen partial pressures of 0.030 and 0.20 atm, respectively, in the presence of helium diluent. The apparent activation energies determined from the Arrhenius plots are not significantly different for the various sintered catalyst samples, except possibly for the sample sintered at 700°. The apparent activation energy is 40 kcal/mole. The data clearly show that sintering the nickel decreases the catalytic activity markedly. From the rate data in Figure 4 and the nickel surface areas in Table II, the specific catalytic activity of the nickel can be calculated. In Figure 5 the specific activity is shown as a function of the nickel crystallite size. The specific activity clearly decreases with increasing crystallite size, thus demonstrating an influence of crystallite size over and above that resulting from the effect on the metal surface area.

Discussion

The results of the present investigation indicate that the effect of nickel crystallite size on the rate of ethane hydrogenolysis over supported nickel is not solely a matter of nickel surface area. The catalytic activity

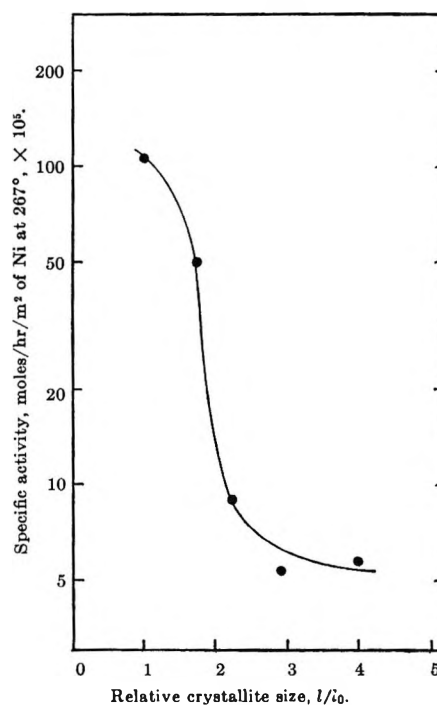


Figure 5. Effect of nickel crystallite size on specific catalytic activity for ethane hydrogenolysis at 267°. The crystallite size, l , is plotted as the ratio, l/l_0 , where l_0 is the crystallite size of the sample reduced at 370°.

per unit surface area of the nickel decreases with increasing size of the nickel crystallites. While the idea is not new that an intensive property of a supported metal, such as the specific catalytic activity, may vary with crystallite size, there seems to have been little attempt to obtain the necessary data on metal surface area, crystallite size, and catalytic activity for a given system to really establish such an effect. One of the few investigations of this type is that reported by Selwood, Adler, and Phillips³ for benzene hydrogenation over Ni-SiO₂ catalysts. These investigators reported that the benzene hydrogenation activity of Ni-SiO₂ catalysts decreased more rapidly with sintering temperature than did the nickel surface area calculated from crystallite size distributions determined from thermomagnetic curves. The findings of the present investigation support these earlier results and are also directionally in agreement with results on unsupported platinum blacks recently reported by McKee.² This latter work indicated that the specific activity of the platinum black for propane cracking decreased sharply as the platinum was sintered at progressively higher temperatures.

While the results of the present investigation show that the specific activity of nickel on silica-alumina for ethane hydrogenolysis decreases with increasing

crystallite size, the results of a previous investigation on nickel supported on silica⁴ did not show an effect comparable in magnitude to that observed in the present study. In the previous work, the crystallite size of the nickel was varied by heating samples of silica impregnated with nickel nitrate in air at various temperatures prior to reducing the nickel. It was found that the specific activity decreased only slightly for a threefold decrease in nickel surface area, *i.e.*, for a threefold increase in crystallite size. The nickel surface areas were generally higher and the corresponding crystallite sizes lower in the previous work than in the present investigation, although there was some overlapping at the limits of the size ranges investigated. It is conceivable that a decrease in specific catalytic activity with increasing crystallite size is not substantial below a certain level of crystallite size, but becomes important at sufficiently large crystallite sizes comparable to those investigated in the current work. It is also possible that the effect of crystallite size may vary with the particular support.

The results of the present investigation on the effect of crystallite size on the catalytic activity of nickel for ethane hydrogenolysis may have a bearing on the interpretation of previous observations of the effect of varying the support.¹² In the work cited, it was observed that the specific catalytic activity of nickel varied markedly when the nickel was supported on different oxide carriers. Since the average nickel crystal-

lite size varied by a factor of 2 for the different carriers, it is possible that the effect of the carrier is in part associated with an influence on the crystallite size or size distribution of the nickel.

In considering an explanation for the effect of crystallite size on specific catalytic activity, we note that the electronic properties of very small crystallites should be different from those of large crystallites owing to the differences in the fraction of the total atoms which are present in the surface. The electronic properties of surface atoms are different from those of atoms in the bulk because of the incomplete coordination at the surface. Based on the assumption that the catalytic activity of a metal is related to its electronic properties, we might then expect the activity to vary with crystallite size. Finally, it seems reasonable that the sintering of a fresh catalyst, where the metal is initially in a highly dispersed state, may eliminate defects in the metal crystallites which are responsible for catalytic activity. The concentration of such defects may well decrease more rapidly than the surface area during sintering, thus causing a decrease in the specific catalytic activity. However, a clearer understanding of the factors responsible for crystallite size effects will require more information on the properties of very small metal crystallites.

(12) W. F. Taylor, D. J. C. Yates, and J. H. Sinfelt, *J. Phys. Chem.*, **68**, 2962 (1964).

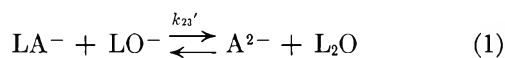
Rapid Reactions in Methanol-Water Solvents¹

by Ronald P. Jensen,² Edward M. Eyring,³ and William M. Walsh

Department of Chemistry, University of Utah, Salt Lake City, Utah 84112 (Received January 24, 1966)

Acid dissociation constants in water-methanol solvents ranging in methanol concentration up to 80 vol. % have been measured potentiometrically for the following dicarboxylic acids: maleic acid, citraconic acid, di-*n*-butylmalonic acid, and ethylisopropylmalonic acid. Temperature-jump relaxation method measurements of the rate constant, k , for the reaction $\text{HA}^- + \text{LO}^- \rightarrow \text{A}^{2-} + \text{LOH}$, where HA^- denotes the sample acid monoanion and L denotes either H or CH_3 , have also been carried out with these acids in the same solvents. Plots of $\log k$ vs. the reciprocal dielectric constant are linear up to 50 vol. % methanol. Over this linear portion we have applied Hiromi's electrostatic equation. This is a modification of earlier theoretical work by Laidler and Landskroener based on Kirkwood's calculation of the dependence of the activity coefficient on dielectric constant. This interpretation of our data points to a nonlinear symmetrical transition-state structure for the abstraction of a proton from the intramolecularly hydrogen-bonded monoanion.

Several kinetic studies of the rapid reaction



in water and in deuterium oxide, where L represents a hydrogen atom when water is the solvent or a deuterium atom when D_2O is the solvent and LA^- is the monoanion of a dicarboxylic acid having a ratio of dissociation constants $K_{a1}/K_{a2} \geq 10^4$, have been carried out in this laboratory.⁴⁻⁷ The results are consistent with the postulate⁸ that an intramolecular hydrogen bond exists in the monoanion of such acids. The measured deuterium oxide solvent kinetic isotope effect $k_{23}^{\text{H}}/k_{23}^{\text{D}} \simeq 2$ for the forward reaction and Brønsted acid catalysis plots indicate a rate-determining proton transfer with L^+ bonded equally strongly to A^{2-} and LO^- in the activated complex. In the experiments described below, we have made temperature-jump measurements of the rate constants of equilibrium 1 for several simple acids in methanol-water solvents at 25° ranging in composition from 0 to 0.65 mole fraction of methanol. We have also determined acid dissociation constants in the mixed solvents for maleic, citraconic (*i.e.*, methylmaleic), ethylisopropylmalonic, and di-*n*-butylmalonic acids and for *o*-cresol sulfonephthalein (*i.e.*, cresol red). These data permit us to identify the transition state of reaction 1 as being a nonlinear symmetric configuration, thus demonstrating the utility of extending temperature-jump kinetic studies into mixed solvent media.

Experimental Section

Di-*n*-butylmalonic and ethylisopropylmalonic acids were obtained from basic hydrolysis of readily available substituted malonic esters. Both acids were recrystallized from water-acetone and melted sharply at literature values. Maleic acid was obtained from the anhydride by hydrolysis in neutral aqueous solution and recrystallized from ether. Both the citraconic acid (J. T. Baker) and the cresol red (Eastman) were used as obtained. A check on purity was provided by the end points of the titrations, and in all cases errors were less than 1%.

Solvents were prepared volumetrically from freshly boiled absolute methanol (Malinckrodt) and doubly dis-

(1) Abstracted from a Ph.D. Thesis submitted by R. P. Jensen to the Graduate School, University of Utah, Feb 1966. Acknowledgment is made to the donors of the Petroleum Research Fund, administered by the American Chemical Society, for support of this research and to the University of Utah Research Fund for an equipment grant.

(2) American Chemical Society Petroleum Research Fund Fellow, 1963-1966.

(3) To whom communications should be addressed.

(4) J. L. Haslam, *et al.*, *J. Am. Chem. Soc.*, **87**, 1 (1965).

(5) J. L. Haslam, *et al.*, *ibid.*, **87**, 4247 (1965).

(6) M. H. Miles, *et al.*, *J. Phys. Chem.*, **69**, 487 (1965).

(7) M. H. Miles, E. M. Eyring, W. W. Epstein, and M. T. Anderson, in preparation.

(8) For a bibliography, see L. Ebersson and I. Wadso, *Acta Chem. Scand.*, **17**, 1552 (1963).

tiled, freshly boiled water. Solvents were stored in polyethylene bottles protected from atmospheric CO_2 and moisture, and delivered from these containers by siphon. Experiments conducted using freshly prepared solvent as well as solvent that had been stored up to 60 days showed no significant differences. Solvent compositions are designated herein as volume per cent defined by the relation⁹ $\text{vol. } \% \text{ CH}_3\text{OH} = [V_{\text{CH}_3\text{OH}} / (V_{\text{CH}_3\text{OH}} + V_{\text{H}_2\text{O}})] \times 100$. Carbonate-free KOH was prepared by a method based on that of Armstrong¹⁰ and was standardized against potassium hydrogen phthalate with potentiometric determination of the end point.

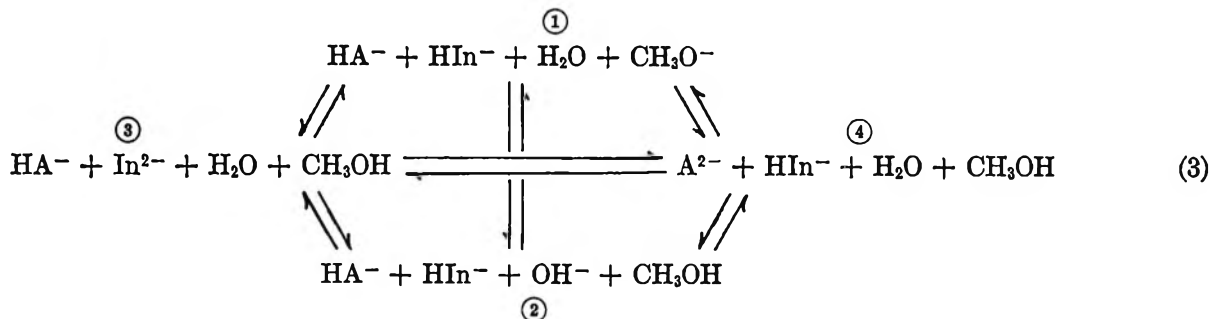
Our temperature-jump and potentiometric titration techniques were essentially the same as previously described.^{4,6} The validity of glass electrode determinations of hydrogen ion activity in methanol-water

These constants are related to the thermodynamic acid dissociation constants K_a^T by the relation¹⁵

$$pK_{a_1}^M = pK_{a_1}^T + \log \gamma_{\pm} = \text{pH} + \log \frac{[\text{HA}^-]}{[\text{H}_2\text{A}]} \quad (2)$$

with an analogous relation for the second dissociation constant. Large values ($\gg 10^4$) for the ratio $K_{a_1}^M / K_{a_2}^M$ have been attributed to intramolecular hydrogen bonding in the monoanion of an acid.¹⁶ It is interesting to note that the increase in the ratio $K_{a_1}^M / K_{a_2}^M$ as the per cent methanol in the solvent increases is much more pronounced for those acids for which intramolecular hydrogen bonds in the monoanion have been postulated. (See Table II.)

Kinetic Data. The complete reaction scheme for our sample system in basic methanol-water media is given by relationship 3 which is shown below



media has been established.¹¹ Our electrodes were required to perform stably in aqueous media over the pH range of 3–11 before being accepted for work in mixed media. A glass electrode was equilibrated for at least 24 hr in a given mixed solvent prior to actual use. When not in use, electrodes were stored in solvent having the same composition as that in which they were equilibrated. Each glass electrode was standardized in buffered solvents of the same methanol-water composition as those in which it was used. We employed the buffers proposed by Bates, *et al.*,¹² and Deligny and Rehbach.¹³ In conducting temperature-jump experiments on methanol-water solutions, the decreasing heat capacity with increasing methanol content¹⁴ required lower voltages for the higher methanol content solvents to induce equivalent temperature jumps. The high methanol-water content solutions are especially susceptible to cavitation; hence temperature jumps as small as 5° were frequently employed. In all cases the initial temperature was adjusted to yield a final temperature of 25° .

Results and Discussion

Equilibrium Data. In Table I we have assembled mixed acid dissociation constants K_a^M for the acids used.

where HA^- is the monoanion of a dicarboxylic acid and HIn^- is the monoanion of cresol red. Such a scheme would lead to a spectrum of relaxation times; however, over the time range being examined (10^{-5} to 10^{-2} sec) only one relaxation was, in fact, observed. Equilibria $\textcircled{1} \leftrightarrow \textcircled{2}$, $\textcircled{1} \leftrightarrow \textcircled{3}$, and $\textcircled{2} \leftrightarrow \textcircled{3}$ involve proton exchange between nonintramolecularly hydrogen bonded species and hence should have rate constants characteristic of diffusion-controlled processes.¹⁷ Such reactions would have relaxation times of the order of 1 μsec or less and hence would not be observed. We are

(9) C. Carr and J. A. Riddick, *Ind. Eng. Chem.*, **43**, 692 (1951).

(10) D. M. G. Armstrong, *Chem. Ind.* (London), 1405 (1955).

(11) A. L. Bacarella, *et al.*, *J. Phys. Chem.*, **62**, 856 (1958).

(12) R. G. Bates, M. Paabo, and R. A. Robinson, *ibid.*, **67**, 1833 (1963).

(13) C. L. Deligny and M. Rehbach, *Rec. Trav. Chim.*, **79**, 727 (1960).

(14) "International Critical Tables," Vol. 5, 1st ed, 1929, p 116.

(15) A. Albert and E. P. Serjeant, "Ionization Constants of Acids and Bases," Methuen and Co., Ltd., London, 1962.

(16) D. H. McDaniel and H. C. Brown, *Science*, **118**, 370 (1953).

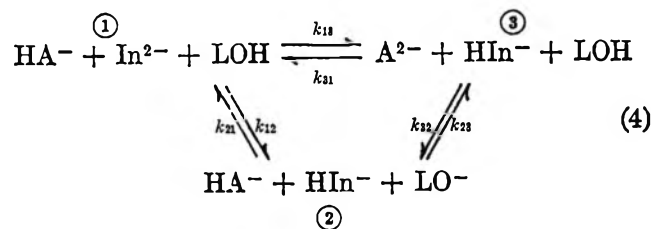
(17) M. Eigen and L. DeMaeyer, "Technique of Organic Chemistry," Vol. VIII, Part II, S. L. Friess, E. S. Lewis, and A. Weissberger, Ed., Interscience Publishers, Inc., New York, N. Y., 1963, Chapter 18.

Table I: Mixed Acid Dissociation Constants^a in Methanol-Water Solvents at 25°

Acid	Vol. % CH ₃ OH	K_{a1}^M	K_{a2}^M
Di- <i>n</i> -butylmalonic	0	Insol.	$4.36 \times 10^{-8}{}^b$
	25	Insol.	$(5.35 \pm 0.71) \times 10^{-9}$
	40	$(1.79 \pm 0.11) \times 10^{-3}$	$(1.00 \pm 0.08) \times 10^{-9}$
	70	$(4.27 \pm 0.13) \times 10^{-4}$	$(1.52 \pm 0.03) \times 10^{-10}$
	80	$(2.06 \pm 0.04) \times 10^{-4}$	$(6.90 \pm 0.26) \times 10^{-11}$
Ethylisopropylmalonic	0	$9.34 \times 10^{-3}{}^b$	$7.94 \times 10^{-9}{}^b$
	25	$(3.10 \pm 0.18) \times 10^{-3}$	$(1.38 \pm 0.10) \times 10^{-9}$
	40	$(4.37 \pm 0.40) \times 10^{-3}$	$(2.19 \pm 0.24) \times 10^{-10}$
	70	$(6.44 \pm 0.11) \times 10^{-4}$	$(3.21 \pm 0.17) \times 10^{-11}$
	80	$(4.21 \pm 0.49) \times 10^{-4}$	$(1.52 \pm 0.07) \times 10^{-11}$
Maleic	0	$1.20 \times 10^{-2}{}^c$	$5.95 \times 10^{-7}{}^c$
	25	$(4.73 \pm 0.76) \times 10^{-3}$	$(1.65 \pm 0.05) \times 10^{-7}$
	40	$(4.64 \pm 0.22) \times 10^{-3}$	$(4.66 \pm 0.12) \times 10^{-8}$
	70	$(2.95 \pm 0.26) \times 10^{-3}$	$(6.34 \pm 0.08) \times 10^{-9}$
	80	$(2.88 \pm 0.19) \times 10^{-3}$	$(3.00 \pm 0.08) \times 10^{-9}$
Citraconic	0	$5.14 \times 10^{-3}{}^d$	$7.15 \times 10^{-7}{}^d$
	25	$(1.19 \pm 0.05) \times 10^{-3}$	$(2.49 \pm 0.19) \times 10^{-7}$
	40	$(2.36 \pm 0.48) \times 10^{-3}$	$(5.99 \pm 0.56) \times 10^{-8}$
	70	$(5.56 \pm 0.11) \times 10^{-4}$	$(1.13 \pm 0.04) \times 10^{-8}$
	80	$(3.06 \pm 0.12) \times 10^{-4}$	$(6.31 \pm 0.53) \times 10^{-9}$
Cresol red	0	$(6.16 \pm 0.40) \times 10^{-9}$	
	25	$(3.07 \pm 0.11) \times 10^{-9}$	
	40	$(7.00 \pm 0.33) \times 10^{-10}$	
	70	$(2.91 \pm 0.12) \times 10^{-10}$	
	80	$(1.46 \pm 0.02) \times 10^{-10}$	

^a Averages of 10–20 values tabulated with mean deviations. ^b See ref 6. ^c W. H. German, *et al.*, *Phil. Mag.*, **22**, 790 (1936). ^d H. W. Ashton and J. R. Partington, *Trans. Faraday Soc.*, **30**, 598 (1934).

then concerned only with reactions involving abstraction of a proton from the hydrogen-bonded monoanion. Since investigations in water and D₂O⁴⁻⁷ indicated that in such a reaction the rate-determining step is cleavage of the intramolecular hydrogen bond, we propose the following as the most probable representation of the observed relaxation



where L is taken hereafter to represent H or CH₃. In equating the two bases OH⁻ and CH₃O⁻, we are assuming the difference in their basicities is not important; for OH⁻ in water pK_b = -1.74 and for CH₃O⁻ in water pK_b = -0.86.¹⁸ Application of known mathe-

Table II: Ratios of Mixed Acid Dissociation Constants for Water and 80 Vol. % Methanol

Acid	$(K_{a1}^M/K_{a2}^M)_{\text{H}_2\text{O}}$	$(K_{a1}^M/K_{a2}^M)_{80}$
Fumaric	32	41
Maleic	204,000	1,820,000
Succinic	23	30
Diethylmalonic	850,000	3,160,000

tical techniques¹⁹ leads to the following expression for the rate of proton abstraction by lyate ion

$$k_{23} = \frac{\left(\frac{1}{\tau}\right)^2 - A\left(\frac{1}{\tau}\right) + B}{C\left(\frac{1}{\tau}\right) - D} \quad (5)$$

¹⁸ J. Koskikallio, *Suomen Kemistilehti*, **30B**, 111 (1957).

¹⁹ G. W. Castellan, *Ber. Bunsenges. Physik. Chem.*, **67**, 898 (1963).

where

$$A = k_{13}([\text{HA}^-] + [\text{In}^{2-}]) + k_{31}([\text{A}^{2-}] + [\text{HIn}^-]) + k_{12} + k_{21}([\text{LO}^-] + [\text{HIn}^-]) \quad (6)$$

$$B = k_{21}[\text{HIn}^-]\{k_{13}([\text{HA}^-] + [\text{In}^{2-}]) + k_{31}([\text{A}^{2-}] + [\text{HIn}^-])\} + (k_{12} + k_{21}[\text{LO}^-])(k_{13}[\text{In}^{2-}] + k_{31}[\text{HIn}^-]) \quad (7)$$

$$C = [\text{HA}^-] + [\text{LO}^-] + \frac{K_a}{K_{a2}M} \quad (8)$$

$$D = -C\{k_{13}([\text{HA}^-] + [\text{In}^{2-}]) + k_{31}([\text{A}^{2-}] + [\text{HIn}^-]) + k_{12} + k_{21}[\text{LO}^-]\} + (C - [\text{HA}^-])(k_{13}[\text{In}^{2-}] + k_{31}[\text{HIn}^-] - k_{21}[\text{HIn}^-]) \quad (9)$$

In applying eq 5 to our rate data, we utilized values for $K_a = a_{\text{LOH}_2^+} \cdot a_{\text{LO}^-}$ reported by Koskikallio.¹⁸ The value of k_{21} for the diffusion-controlled loss of a proton by the indicator monoanion has already been reported.²⁰ Values for the rate of removal of the proton by the indicator anion, k_{13} , were taken to be approximately one order of magnitude smaller than k_{23} . Such a choice is based on measured values of k_{13} in systems where it can be observed (near pH 7.0) and also on a parametric analysis of the rate equations discussed elsewhere.⁴ In Table III we have assembled rate data taken in water-methanol solvents for the di-*n*-butylmalonic acid. Similar data for the other acids led to the average values listed in Table IV. A plot of the results shown in Table IV against the reciprocal of the dielectric constant²¹ yields the curves shown in Figure 1. The initial linear portion of these curves fit the predictions of electrostatic theory^{22,23} and the negative slope would be expected for the reaction of two ions of like charge.²⁴ The dependence of the rate constant on the dielectric constant of the medium was treated recently by Laidler and Landskroener.²⁵ Starting with Kirkwood's²⁶ expression for the activity coefficient of an ion as a function of dielectric constant and applying absolute rate theory, they obtained an expression for the rate constant as a function of dielectric constant. Kirkwood's model of an ion in solution is shown in Figure 2. This model pictures an ion as a sphere of radius b contained in a continuous medium of dielectric constant D . Within the sphere are embedded an arbitrary number of point charges e_1, \dots, e_R . The distances from the center of the sphere to these point charges are designated r_1, \dots, r_R . The separation of two charges is characterized by R_{k1} and θ_{k1} . In evaluating Kirkwood's expression, Laidler and Landskroener assumed the condition $r_k \ll b$.

Table III: Relaxation Spectra^a of Di-*n*-butylmalonic Acid in 0.05 *M* Ionic Strength^b Methanol-Water Solvents for the Reaction $\text{HA}^- + \text{LO}^- \xrightarrow{k_{23}} \text{A}^{2-} + \text{LOH}$

C^c $10^{-4} M$	Vol. % CH ₃ OH	pH* ^d	$\tau,^e$ msec	$k_{23},^f$ $10^7 M^{-1}$ sec ⁻¹
1.0	25	8.41	0.393	7.81
5.0	25	8.48	0.098	7.91
2.5	25	8.48	0.235	6.05
7.5	25	8.46	0.083	6.19
5.0	25	8.48	0.115	6.62
1.0	25	8.48	0.441	6.91
1.0	25	8.41	0.430	7.10
1.0	40	8.90	0.550	2.77
5.0	40	8.81	0.147	2.66
0.75	40	8.69	0.685	2.64
0.75	40	8.69	0.675	2.68
2.5	40	8.81	0.248	2.93
2.5	40	8.81	0.303	2.38
5.0	40	8.81	0.188	2.05
7.5	40	8.69	0.615	2.95
2.5	40	8.50	0.225	2.96
2.5	40	8.50	0.235	2.82
7.5	40	8.74	0.093	2.80
2.5	40	8.76	0.270	2.63
5.0	70	9.33	0.195	1.15
2.5	70	9.36	0.380	0.977
2.5	70	9.31	0.325	1.14
2.5	70	9.31	0.368	1.01
2.5	70	9.31	0.362	1.02
5.0	70	9.33	0.203	1.11
2.5	70	9.36	0.392	0.947
1.0	70	9.46	0.611	0.976
1.0	70	9.46	0.595	1.00
5.0	80	9.19	0.190	0.967
5.0	80	9.20	0.212	0.866
5.0	80	9.50	0.221	0.844
5.0	80	9.50	0.190	0.983
10.0	80	9.62	0.131	0.817
5.0	80	9.55	0.213	0.843
2.5	80	9.65	0.320	0.858
2.5	80	9.65	0.292	0.941
1.0	80	9.54	0.477	0.853

^a All for 25° with $1.0 \times 10^{-5} M$ cresol red indicator. ^b Adjusted with KCl. ^c Total sample acid concentration. ^d pH in methanol-water solvents with standard state the infinitely dilute solvent of the composition indicated. ^e Experimental relaxation time determined by temperature jump. ^f Rate constant calculated with eq 5.

(20) M. Eigen, *et al.*, *Progr. Reaction Kinetics*, **2**, 315 (1964).

(21) Values for the dielectric constants of methanol-water mixtures were obtained from P. S. Albright and L. J. Gosting, *J. Am. Chem. Soc.*, **68**, 1061 (1946).

(22) H. Eyring and K. Laidler, *Ann. N. Y. Acad. Sci.*, **39**, 303 (1940).

(23) E. S. Amis, *J. Chem. Educ.*, **28**, 635 (1951); **25**, 237 (1952); **30**, 351 (1953).

(24) A. A. Frost and R. G. Pearson, "Kinetics and Mechanism," 2nd ed, John Wiley and Sons, Inc., New York, N. Y., 1961, p 147.

Table IV: Rate Constants^a for the Reaction $\text{HA}^- + \text{LO}^- \rightarrow \text{A}^{2-} + \text{LOH}$ in Methanol-Water Mixtures at 25° and Ionic Strength $\mu = 0.05 M$

Acid	Rate constants, $M^{-1} \text{sec}^{-1}$				
	0	25	40	70	80
Di- <i>n</i> -butyl-malonic	1.4×10^8 ^b	$(6.25 \pm 0.65) \times 10^7$	$(2.49 \pm 0.34) \times 10^7$	$(1.00 \pm 0.08) \times 10^7$	$(8.95 \pm 0.75) \times 10^6$
Ethylisopropyl-malonic	5.50×10^7 ^b	$(2.65 \pm 0.24) \times 10^7$	$(1.04 \pm 0.05) \times 10^7$	$(4.49 \pm 0.12) \times 10^6$	$(3.11 \pm 0.26) \times 10^6$
Citraconic	3.5×10^9 ^c	$(1.18 \pm 0.13) \times 10^9$	$(3.42 \pm 0.33) \times 10^8$	$(1.50 \pm 0.20) \times 10^8$	$(1.15 \pm 0.17) \times 10^8$
Maleic	1.0×10^9 ^d	$(3.13 \pm 0.48) \times 10^8$	$(1.06 \pm 0.11) \times 10^8$	$(4.11 \pm 0.27) \times 10^7$	$(3.27 \pm 0.33) \times 10^7$

^a Averages of at least ten values tabulated with mean deviations. ^b M. H. Miles, Ph.D. Dissertation, University of Utah, 1966. ^c Obtained by extrapolation of $\text{CH}_3\text{OH-H}_2\text{O}$ data. ^d See ref 20, p 312.

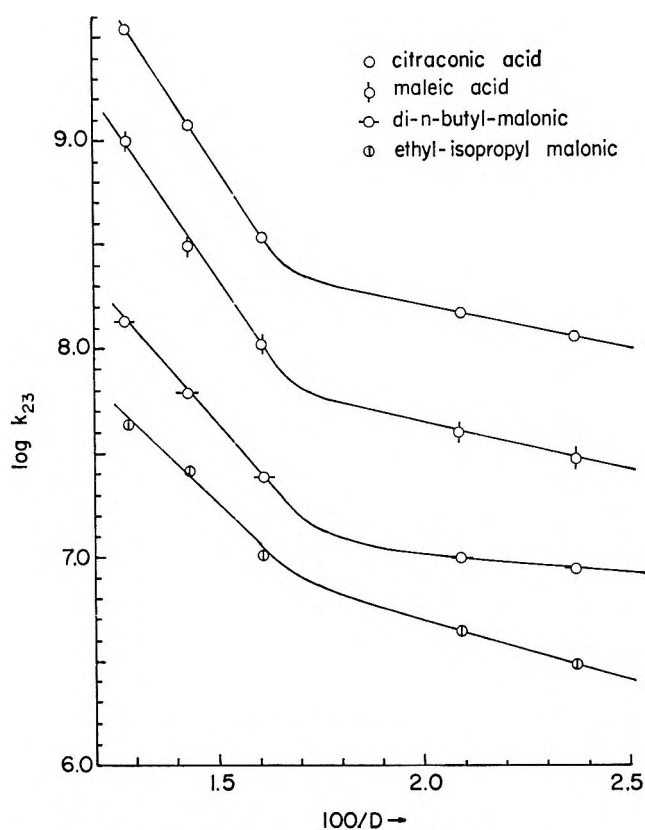


Figure 1. $\log k_{23}$ ($M^{-1} \text{sec}^{-1}$) vs. $100/D$ for the reaction $\text{HA}^- + \text{LO}^- \xrightarrow{k_{23}} \text{A}^{2-} + \text{LOH}$ in methanol-water solvents.

However, as pointed out by Hiromi,²⁷ such a condition very often does not exist; *i.e.*, very often the charges in an ion are located close to the surface. Hiromi has therefore carried out the evaluation of Kirkwood's expression with no restrictions and we have employed his equation

$$\ln k = \ln k_0 + \frac{e^2}{2k'T} \left(\frac{1}{D} - \frac{1}{D_0} \right) \left(\frac{L_A}{b_A} + \frac{L_B}{b_B} - \frac{L_{\ddagger}}{b_{\ddagger}} \right) \quad (10)$$

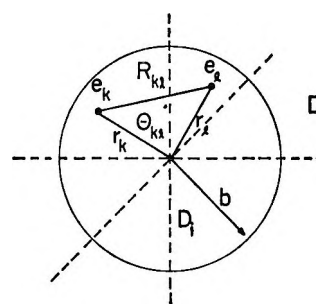


Figure 2. Kirkwood's model of an ion in a solution of dielectric constant D .

where

$$L_i = \sum_{k=1}^M z_k^2 f_{kk} + \sum_{k=1}^M \sum_{l \neq k}^M z_k z_l g_{kl} \quad (11)$$

$$f_{kk} = \frac{2}{1 - x_{kk}} - \frac{1}{x_{kk}} \ln(1 - x_{kk}) \quad (12)$$

$$g_{kl} = \frac{2}{(1 - 2\alpha_{kl}x_{kl} + x_{kl}^2)^{1/2}} + \frac{1}{x_{kl}} \ln \left[\frac{1 - \alpha_{kl}}{(1 - 2\alpha_{kl}x_{kl} + x_{kl}^2)^{1/2} + x_{kl} - \alpha_{kl}} \right] \quad (13)$$

$$x_{kl} = \frac{r_k r_l}{b^2}; \quad x_{kk} = \left(\frac{r_k}{b} \right)^2; \quad \alpha_{kl} = \cos \theta_{kl} \quad (14)$$

In eq 10 the subscripts A, B, and \ddagger refer to participants in the reaction $\text{A} + \text{B} \rightarrow \text{activated complex} (\ddagger) \rightarrow \text{products}$. The symbols k_0 and D_0 are the rate constant and dielectric constant of the same reaction carried out in some reference state. Taking the derivative of eq 10 with respect to $1/D$, Hiromi obtained the following expression for the slope of the $\log k$ vs. $1/D$ plots

(25) K. Laidler and P. A. Landskroener, *Trans. Faraday Soc.*, **52**, 200 (1956).

(26) J. G. Kirkwood, *J. Chem. Phys.*, **2**, 351 (1934).

(27) K. Hiromi, *Bull. Chem. Soc. Japan*, **33**, 1251 (1960).

$$\text{slope} = \frac{e^2}{4.606k'T} \left(\frac{L_A}{b_A} + \frac{L_B}{b_B} - \frac{L_{\pm}}{b_{\pm}} \right) \quad (15)$$

Evaluation of the right-hand side of eq 15 requires a knowledge of the structure of both reactants and the transition state. While the dimensions of the reactants can be obtained, those of the activated state are not known. Hence, we shall take the empirical slope and generate from eq 15 values for the parameter b_{\pm} , the effective radius of the activated complex taken as a spherical ion. The lyate ion is assigned a radius of 1.4×10^{-8} cm which is the radius of the hydroxyl ion.²⁸ The structure of the acid monoanion for the substituted malonic acids is shown in Figure 3. The planar configuration shown is chosen as most probable since it provides for a minimum of interaction with the alkyl substituents. The charge in the monoanion is shown displaced toward the proton because of the influence of the intramolecular hydrogen bond. A similar configuration is suggested for maleic and citraconic acid but rotation of the carboxyl group out of a coplanar configuration makes a drawing impractical. The dimensions used for maleic and citraconic acids are given in Table V. Figure 4 shows the symmetrical transition state formed from the reactants when the monoanion is assumed to contain an intramolecular hydrogen bond. Again this is the specific case of a disubstituted malonic acid. The location of the charges within the activated complex is assigned to represent conditions approximately halfway to the formation of the dianion. Results from the application of eq 15 are shown in Table VI.

The alternative configuration for the activated state would not involve the intramolecular hydrogen bond.

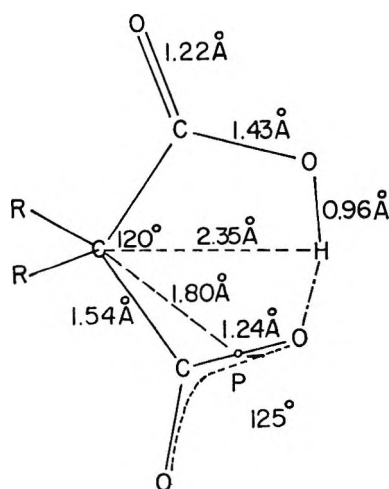


Figure 3. Diagram of monoanion for a disubstituted malonic acid.

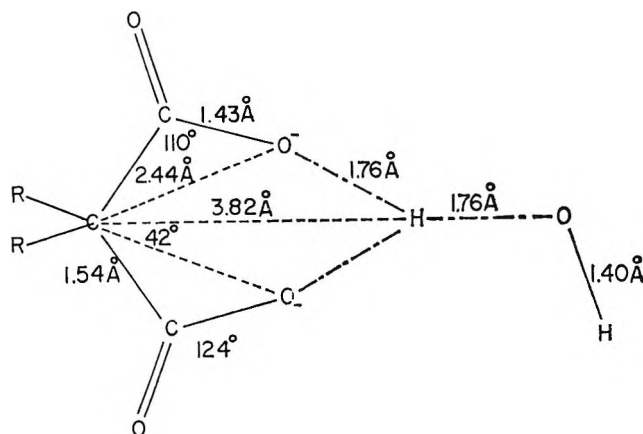


Figure 4. Diagram of symmetrical configuration of transition state involving the monoanion of a disubstituted malonic acid and hydroxide ion.

Table V: Transition State Radii, b_{\pm} , Computed from Eq 15 Using a Symmetrical Configuration for the Activated Complex^a

Acid	Slope	L_{\pm}	b_{\pm} , Å
Di- <i>n</i> -butylmalonic	-231	11.9	3.00
Ethylisopropylmalonic	-130	9.98	3.19
Maleic ^b	-290	17.2	2.95
Citraconic ^b	-304	17.5	2.94

^a See Figure 4. ^b For the monoanion of both maleic and citraconic acids the center of the molecule was taken as the midpoint of the carbon-carbon double bond. The distance to the charge was taken as 2.1×10^{-8} cm in both the monoanion and the transition state; θ_{12} in the activated complex was taken as 45° . These values were found by using Dreiding models.

Table VI: Transition State Radii, b_{\pm} , Computed from Eq 15 Using a Linear Configuration for the Activated Complex^a

Acid	Slope	L_{\pm}	b_{\pm} , Å	r_{\pm} , Å ^b
Di- <i>n</i> -butylmalonic	-231	12.3	2.27	2.40
Ethylisopropylmalonic	-130	10.8	2.34	2.40
Maleic ^c	-290	14.9	2.55	2.80
Citraconic ^c	-304	15.4	2.54	2.80

^a See Figure 5 for diagram of the substituted malonic acid linear transition state. ^b This is the distance from the center of the molecule to the charge being transferred from the lyate to the carboxyl group. ^c Dimensions used in maleic and citraconic cases were obtained by allowing maximum separation between oxygen atoms in the carboxyl and carboxylate groups. Taking the molecule center at the midpoint of the C-C double bond this configuration led to the values $\theta_{12} = 85^\circ$, $r_1 = 2.0$ Å, $r_2 = 2.80$ Å.

(28) J. Buchanan and S. D. Hamann, *Trans. Faraday Soc.*, **49**, 1425 (1953).

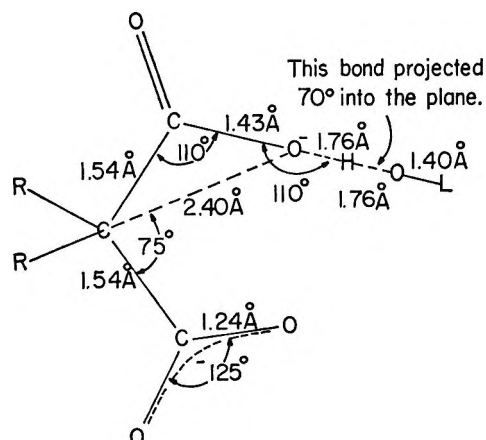


Figure 5. Diagram of linear configuration for the transition state involving a disubstituted malonic acid monoanion reacting with lyate ion.

Such a configuration is shown in Figure 5 for the substituted malonic acids. We have shown the proton of the carboxyl group rotated 90° out of the plane so as to represent minimum interaction with the carboxylate group. Further rotation does not result in any difference in the computed values of b_{\ddagger} . The result of application of Hiromi's equation to this configuration is

shown in Table VI. The fifth column of this table also lists the values for the separation of the charge at the reacting site from the center of the molecule. Inasmuch as the radius of the activated complex is computed to be less than the distance to the charge, such a linear arrangement in the activated state is improbable.

The deviations from linearity (Figure 1) found at high methanol content (70–80 vol. %) can be ascribed in large measure to the effects of selective solvation. As noted by Woodhead, *et al.*,²⁹ the primary hydration of ionic species in systems of relatively high methanol content involves only water molecules. This hydration sphere then creates an effective dielectric constant of higher value than the bulk dielectric constant in the immediate vicinity of the ion. Thus, as we have found experimentally, the rate constant should take on a higher value than that predicted by a linear extrapolation of the initial slope. The same break in plots of experimental $\log k$ vs. $1/D$ have been observed previously with reactions whose rates can be measured by classical techniques.³⁰

(29) M. Woodhead, *et al.*, *J. Res. Natl. Bur. Std.*, **69A**, 263 (1965).

(30) V. K. La Mer and M. E. Kamner, *J. Am. Chem. Soc.*, **57**, 2669 (1935).

Normal Stress Effect in Dilute Polymer Solutions. II. Polystyrene in Chlorinated Diphenyl

by Kunihiro Osaki, Katsuhisa Tanaka, Michio Kurata, and Mikio Tamura

Department of Industrial Chemistry and Institute for Chemical Research,
Kyoto University, Kyoto, Japan (Received January 25, 1966)

Normal stresses of a series of 0.3–2.0 wt % polystyrene solutions in chlorinated diphenyl (good solvent) were measured with a parallel plate rheogoniometer. The shear stresses and the complex moduli were also measured with a coaxial cylinder rheometer. The normal stress ($-\partial P/\partial \ln r$) and shear stress ($\sigma_{12} - \kappa\eta_s$) were linear in κ^2 and κ , respectively, in the lowest range of shear rate κ observed. The ratios $(-\partial P/\partial \ln r)/\kappa^2$ and $(\sigma_{12} - \kappa\eta_s)/\kappa$ decreased with increasing rate of shear more rapidly than did those of polystyrene solutions in dioctyl phthalate (poor solvent). It was also found that both the normal stress and shear stress were proportional to the number of polymer molecules per unit volume, n . For a wide variety of molecular weights and concentrations, the reduced (or intrinsic) normal and shear stresses, $(-\partial P/\partial \ln r)/n$ and $(\sigma_{12} - \kappa\eta_s)/n$, were found to be universal functions of the reduced rate of shear $(\eta_0 - \eta_s)\kappa/n$. The effect of heterogeneity in molecular weight was also investigated through a comparison of the data obtained for ordinary fractionated samples and an anionically polymerized sample.

Introduction

Measurement of normal stress effect of dilute solutions of fractionated polystyrenes in dioctyl phthalate (a poor solvent) was reported in part I of this series.¹ The incremental normal stress attributable to the polymer was found to be exerted primarily in the flow direction and to be proportional to the square of the rate of shear κ over a wide range of κ . As for the effect of molecular weight and concentration, the data obtained with various combinations of the variables were superimposed to give a composite curve in the plot of $(-\partial P/\partial \ln r)M/c$ vs. $\kappa(\eta_0 - \eta_s)M/c$. Here $(-\partial P/\partial \ln r)$ is the normal stress as measured with a parallel plate rheogoniometer, η_0 is the zero shear viscosity of the solution, η_s is the viscosity of the solvent, M is the molecular weight, and c is the concentration in grams per cubic centimeter. All of the findings mentioned above were compatible with the predictions of the spring-beads model theory for the normal stress effect,^{2,3} which corresponds to the Rouse⁴ or Zimm⁵ theory for the dynamic mechanical properties. Not only qualitative but also quantitative agreement was found between the observed and the theoretical values of the steady-

state compliance after an appropriate correction was made for the effect of molecular weight distribution ($M_w/M_n = 1.8$). However, we could not assess the degree of the hydrodynamic draining effect, because the steady-state compliance was rather insensitive to the hydrodynamic interaction for the material used.

In this paper, we report the results of normal stress measurements carried out in a polymer-good solvent system, polystyrene solutions in chlorinated diphenyl. The effect of molecular weight distribution is also studied.

Experimental Section

Materials. The fractionated polystyrene used in this study was prepared by thermal polymerization at 95° without solvent or catalyst. Fractionation was performed at 30° from a 0.5% benzene solution using

- (1) M. Tamura, M. Kurata, K. Osaki, and K. Tanaka, *J. Phys. Chem.*, **70**, 516 (1966).
- (2) Y. Ikeda, *Kobunshi*, **5**, 635 (1957).
- (3) M. C. Williams, *J. Chem. Phys.*, **42**, 2988 (1965).
- (4) P. E. Rouse, Jr., *ibid.*, **21**, 1272 (1953).
- (5) B. H. Zimm, *ibid.*, **24**, 266 (1956).

methanol as precipitant. The viscosity-average molecular weight of each fraction was evaluated by

$$[\eta] = 1.13 \times 10^6 M_v^{0.73} \quad (\text{benzene, } 25^\circ)^6 \quad (1)$$

and tabulated in Table I. Among these samples, F1, F3, and F4 are the same samples as used in the previous study.¹

Table I

Nomen- clature	M_v
F1	5.0×10^6
F3	1.2×10^6
F4	0.66×10^6
F5	0.54×10^6
F6	0.27×10^6
S111	2.39×10^6 ^a

^a M_w evaluated by Dr. H. W. McCormick, Dow Chemical Co.

Another polystyrene, S111*, prepared by anionic polymerization was also used in this study. (This sample was kindly given us by Dr. J. E. Frederick, University of Wisconsin.) The weight-average molecular weight M_w of this sample was 2.39×10^6 and M_w/M_n was 1.08 as reported by Dr. H. W. McCormick, Dow Chemical Co.

Aroclor 1248 (mixture of chlorinated diphenyl and polyphenyl, Monsanto Chemicals Ltd.) was used as the solvent. This was a good solvent for polystyrene, and the viscosity was as high as 2.70 poises at 25°.

Polymer solutions were prepared by storing weighed amounts of polymer and solvent at 50° with occasional stirring with a spatula. Several weeks was necessary for obtaining homogeneous solutions. Evaporation of the solvent was negligible.

Apparatus and Method. Measurement of the normal stress was performed with a parallel plate rheogoniometer. A precise description of the apparatus has been published previously.⁷ In this apparatus, the pressure exerted on the upper (stationary) plate by the test fluid is related to the components of the normal stress by⁸

$$-\partial P / \partial \ln r = \sigma_{11} - \sigma_{33} + \partial(\sigma_{22} - \sigma_{33}) / \partial \ln \kappa \quad (2)$$

$$\kappa = r\Omega/l$$

where σ_{11} , σ_{22} , and σ_{33} are the normal stress components in the flow direction, in the shear plane, and in the plane perpendicular to both the flow direction and the shear plane, respectively, r is the distance from the cen-

ter, l is the gap between the two plates, and Ω is the angular velocity of the lower (rotating) disk.

The shear stress σ_{12} was measured with a coaxial cylinder rheometer. The single-bob method of Krieger and Maron⁹ was applied to determine the shear stress as a function of the rate of shear. The complex modulus was measured with the same coaxial cylinder rheometer. A detailed description of the apparatus was also published earlier.¹⁰

Separate determination of the components of the normal stress was based on the phenomenological theory of Coleman and Noll.¹¹ As was shown by Coleman and Markovitz,¹² this theory leads to the following relationships for the so-called second-order fluid

$$\lim_{\omega \rightarrow 0} G' / \omega^2 = \frac{1}{2} \lim_{\kappa \rightarrow 0} (\sigma_{11} - \sigma_{22}) / \kappa^2 \quad (3)$$

$$\frac{1}{2} \lim_{\kappa \rightarrow 0} \left(\frac{\partial P}{\partial \ln r} / \kappa^2 \right) - \lim_{\omega \rightarrow 0} G' / \omega^2 = \frac{3}{2} \lim_{\kappa \rightarrow 0} (\sigma_{22} - \sigma_{33}) / \kappa^2 \quad (4)$$

The two components, $(\sigma_{11} - \sigma_{22})$ and $(\sigma_{22} - \sigma_{33})$, of the normal stress can be determined separately from each other by using these relationships. A detailed account of the method may be found in our previous publication.¹³

Results and Discussion

Figure 1 shows comparison of the results of steady-shear measurement with those of dynamic measurement. The small and large black circles represent the incremental shear stress $(\sigma_{12} - \kappa\eta_s)$ and the normal stress $-\frac{1}{2}(\partial P / \partial \ln r)$ plotted against the rate of shear κ , respectively. The factor $\frac{1}{2}$ is introduced in front of $-(\partial P / \partial \ln r)$ for the sake of convenience (see eq 4). Small and large white circles represent the incremental loss modulus $(G'' - \omega\eta_s)$ and the storage modulus G' plotted against the angular frequency ω , respectively. The incremental shear stress $(\sigma_{12} - \kappa\eta_s)$ and loss modulus $(G'' - \omega\eta_s)$ are proportional to κ and ω , respectively, only in the lowest region of the variables (κ or $\omega < 10$).

(6) W. R. Krigbaum and P. J. Flory, *J. Polymer Sci.*, **11**, 37 (1953).

(7) M. Tamura, M. Kurata, and T. Kotaka, *Bull. Chem. Soc. Japan*, **32**, 471 (1959); T. Kotaka, M. Kurata, and M. Tamura, *J. Appl. Phys.*, **30**, 1705 (1959).

(8) H. Markovitz, *Trans. Soc. Rheology*, **1**, 37 (1957).

(9) I. M. Krieger and S. H. Maron, *J. Appl. Phys.*, **23**, 147 (1952).

(10) T. Kotaka and K. Osaki, *Bull. Inst. Chem. Res. Kyoto Univ.*, **39**, 331 (1961); K. Osaki, M. Tamura, M. Kurata, and T. Kotaka, to be published.

(11) B. D. Coleman and W. Noll, *Arch. Rational Mech. Anal.*, **6**, 355 (1960); *Ann. N. Y. Acad. Sci.*, **89**, 672 (1961).

(12) B. D. Coleman and H. Markovitz, *J. Appl. Phys.*, **35**, 1 (1964).

(13) K. Osaki, M. Tamura, T. Kotaka, and M. Kurata, *J. Phys. Chem.*, **69**, 3642 (1965).

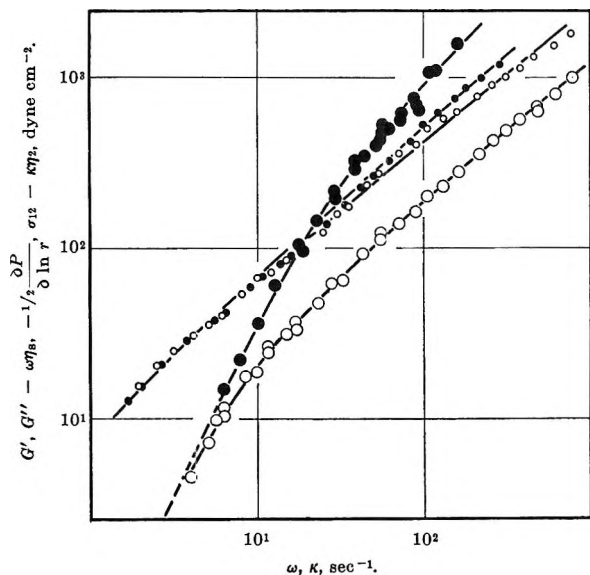


Figure 1. Comparison between stresses in steady shear and dynamic moduli of a 1 wt % solution of polystyrene (F3) in Aroclor 1248 at 25°: small black circles, incremental shear stress ($\sigma_{12} - \kappa\eta_s$) plotted against the rate of shear κ ; large black circles, normal stress measured as $-1/2(\partial P/\partial \ln r)$ and plotted against κ ; small open circles, loss modulus ($G'' - \omega\eta_s$) plotted against the angular frequency ω ; large white circles, storage modulus G' plotted against ω .

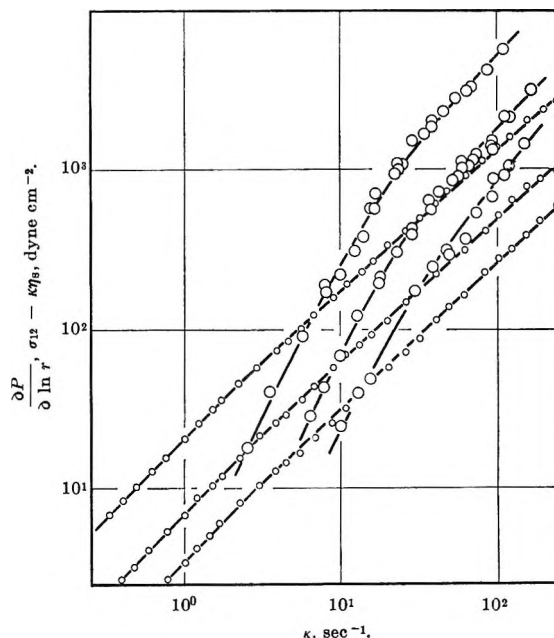


Figure 2. Effect of concentration on normal and shear stresses in solutions of polystyrene (F3) in Aroclor 1248 at 25°. Concentrations are 1, 0.5, and 0.3% in weight from left to right, respectively. Small circles represent ($\sigma_{12} - \kappa\eta_s$) and large circles ($-\partial P/\partial \ln r$).

The normal stress ($-\partial P/\partial \ln r$) and storage modulus G' are not proportional to κ^2 and ω^2 , respectively, over almost the whole range of variables, except at the lowest values, say $\kappa, \omega < 5 \text{ sec}^{-1}$. In other words, the system behaves as a second-order fluid only in a very narrow range of long time scale (small κ or ω). This is in sharp contrast to the previous observation for polystyrene in dioctyl phthalate (poor solvent), to which the second-order fluid approximation was applicable over a fairly wide range of κ or ω .

Now, in the range of κ or ω lower than 5 sec^{-1} , it may be natural to expect from the figure that $-1/2(\partial P/\partial \ln r)$ and G' come to coincidence with each other. This, in turn, implies that the $(\sigma_{22} - \sigma_{33})$ component of normal stress, if it exists, should be quite small compared with the $(\sigma_{11} - \sigma_{22})$ component at least in this range of small κ . Accordingly, we may assume $(-\partial P/\partial \ln r)$ to be equal to the $(\sigma_{11} - \sigma_{22})$ component of the normal stress. Although this conclusion seems inescapable so far as our data are concerned, this is not based on the direct evaluation of the normal stress components. Therefore, we do not insist that σ_{22} is equal to σ_{33} . Final solution of this problem is still open to future study.

For a higher rate of shear, at which the solution does not behave as a second-order fluid, we cannot determine two components of the normal stress separately from each other by the parallel-plate data alone.

Figure 2 shows the log-log plots of the incremental shear stress ($\sigma_{12} - \kappa\eta_s$) and the normal stress ($-\partial P/\partial \ln r$) against rate of shear κ , which were obtained for a series of solutions of polystyrene (F3) in Aroclor 1248 with various concentrations. The large circles represent $(-\partial P/\partial \ln r)$ and the small circles, $(\sigma_{12} - \kappa\eta_s)$. Figures 3 and 4 show the effect of molecular weight on the normal stress ($-\partial P/\partial \ln r$) and the incremental shear stress ($\sigma_{12} - \kappa\eta_s$). Figure 3 gives the results obtained for 0.5% solutions of fractionated polystyrenes (F1, F3, and F4) and Figure 4 gives the results for 2% solutions of fractionated polystyrenes (F5 and F6) and the living polystyrene (S111).

Viscosities of relatively high molecular weight polystyrenes depend markedly on the rate of shear in the measured range of the rate of shear (Figure 3). This effect is observed even in the lowest concentration tested, 0.3% (Figure 2). On the other hand, viscosities of relatively low molecular weight polystyrenes are practically independent of the rate of shear (Figure 4).

The log-log plot of $(-\partial P/\partial \ln r)$ against κ has a slope lower than the second-order fluid slope, 2, at any value of κ . This deviation of the observed slope from 2 exists to some extent even in the case of low molecular weight samples whose viscosities are practically independent of κ .

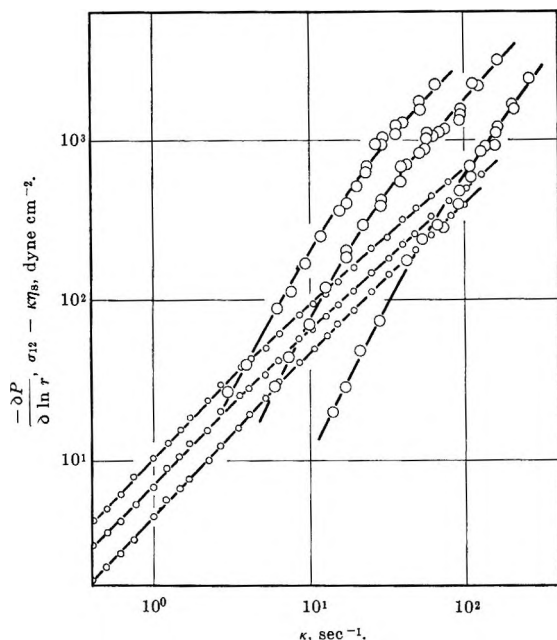


Figure 3. Effect of molecular weight on normal and shear stresses in 0.5 wt % solutions of polystyrene F1, F3, and F4 (from left to right) in Aroclor 1248 at 25°. Molecular weight of polystyrene is 5.0×10^6 for F1, 1.2×10^6 for F3, and 0.66×10^6 for F4. Small circles represent $(\sigma_{12} - \kappa\eta_s)$ and large circles represent $(-\partial P/\partial \ln r)$.

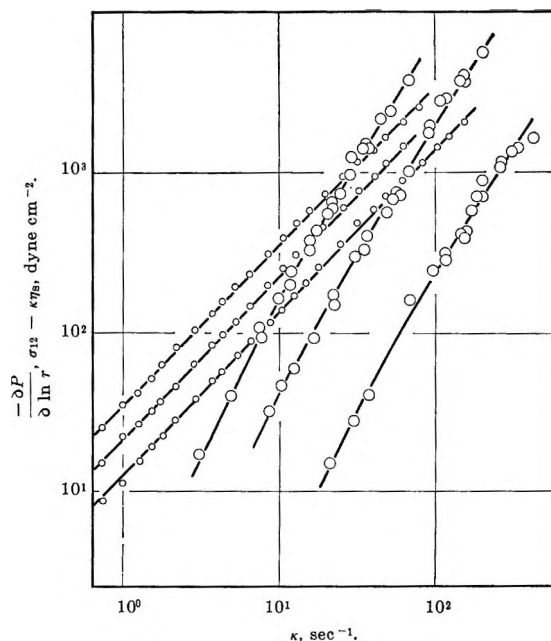


Figure 4. Effect of molecular weight on normal and shear stresses in 2.0 wt % solutions of polystyrene F5, F6, and S111 (from left to right) in Aroclor 1248 at 25°. Molecular weight of polystyrene is 5.4×10^6 for F5, 2.7×10^6 for F6, and 2.39×10^6 for S111. Small circles represent $(\sigma_{12} - \kappa\eta_s)$ and large circles represent $(-\partial P/\partial \ln r)$.

Finally, it is to be noted that in Figure 4, the normal stress of the solution of the living polystyrene (S111) is considerably lower in magnitude than that of the fractionated polystyrene (F6) which has an approximately equal molecular weight. This difference may be due to the difference in molecular weight distribution and will be discussed later.

Now, it has been found by Harrison and collaborators¹⁴ that dynamic mechanical data obtained for dilute polystyrene solutions with various molecular weight polystyrenes and concentrations can be superimposed on a composite curve by using reduced variables. These are: $G'M/c$ for the storage modulus, $(G'' - \omega\eta_s)M/c$ for the loss modulus, and $\omega(\eta_0 - \eta_s)M/c$ for the angular frequency, where c is the polymer concentration in grams per cubic centimeter and hence c/M is the number of moles in a unit volume. We may expect in analogy that the reduced plots of $(-\partial P/\partial \ln r)M/c$ and $(\sigma_{12} - \kappa\eta_s)M/c$ against $\kappa(\eta_0 - \eta_s)M/c$ also give composite curves in the case of steady-shear data (see eq 3 and 4 and Figure 1). This expectation was tested in Figure 5, where the data given in Figures 2 to 4 all were replotted using the reduced scales. The data of $(\sigma_{12} - \kappa\eta_s)$ and $(-\partial P/\partial \ln r)$ obtained for various combinations of molecular weights and concentrations except for S111 were superimposable on two composite

curves, one for the shear stress and the other for the normal stress. Excellent superposition was obtained when the procedure was applied to the data obtained for different concentrations of the single sample F3. They are represented in Figure 5 by various types of circles. A closer inspection of the figure reveals that the reduced normal stress for F3 is slightly larger than those for other fractions. The same tendency was also observed in dioctyl phthalate.¹ (The parameter γ defined in eq 5 was about 25% higher for the solution of F3 than for the solution of F1 or F4 in dioctyl phthalate. See ref 1.) Therefore, the difference may be attributable to possible difference in molecular weight distribution among these samples.

In conclusion, we may say that the stresses in steady-shear flow of dilute polymer solutions are essentially proportional to the number of polymer molecules in a unit volume. In Figure 5, we show by the dashed lines the reduced curves obtained in dioctyl phthalate for the sake of comparison.¹ At high reduced rates of shear, $(-\partial P/\partial \ln r)M/c$ and $(\sigma_{12} - \kappa\eta_s)M/c$ in Aroclor (good solvent) are both smaller than those in dioctyl phthalate (poor solvent). At lower reduced rates of shear, no solvent effect is observed on the reduced

(14) G. Harrison, J. Lamb, and A. J. Matheson, *J. Phys. Chem.*, **68**, 1072 (1964).

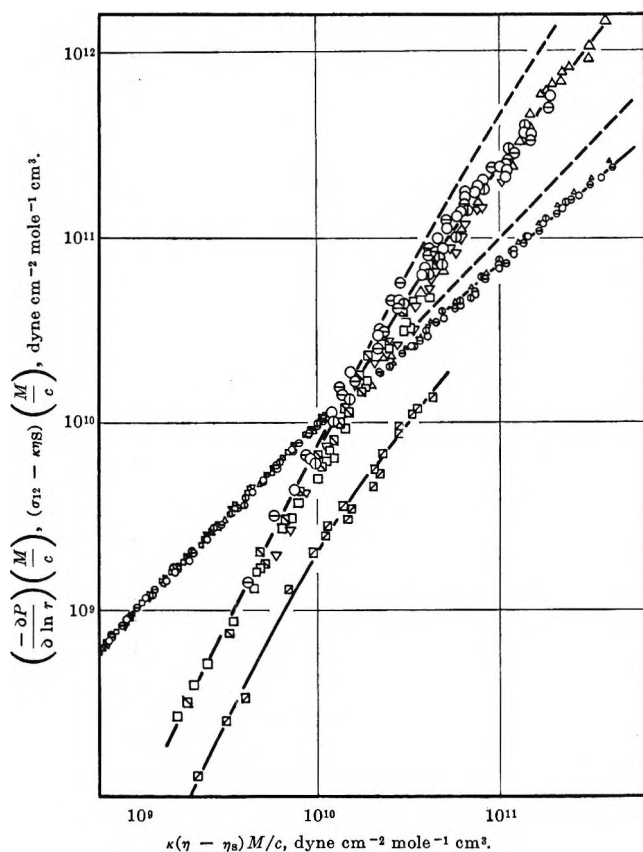


Figure 5. Reduced plot of the normal and shear stresses obtained for polystyrene in Aroclor 1248 with various combinations of M and c : Δ , F1 with $c = 7.25 \times 10^{-3}$ g/cc (or 0.5 wt %); \odot , \circ , F3 with $c = 1.45 \times 10^{-2}$ (or 1.0 wt %); $c = 7.25 \times 10^{-3}$ (or 0.5 wt %) and $c = 4.35 \times 10^{-2}$ (or 0.3 wt %) respectively; ∇ , F4 with $c = 7.25 \times 10^{-2}$ (or 0.5 wt %); \square , F5 with $c = 2.90 \times 10^{-2}$; \boxtimes , F6 with $c = 2.90 \times 10^{-2}$; \boxdot , S111 with $c = 2.90 \times 10^{-2}$.

normal stress as well as on the reduced shear stress. This leads to the parameter γ which is independent of the nature of the solvent.

$$\gamma = \frac{1}{2} \frac{cRT}{M} \lim_{\kappa \rightarrow 0} \frac{(-\partial P / \partial \ln r)}{(\sigma_{12} - \kappa \eta_s)^2} \quad (5)$$

According to Frederick and co-workers, the dynamic mechanical properties of dilute polymer solutions change from Zimm-like to Rouse-like behavior with increasing solvent power.¹⁵ If this is the case, the parameter γ which is affected by the degree of hydrodynamic interaction should be a function of the solvent power. Our results apparently conflict with this conjecture. However, as was mentioned in the previous paper, the parameter γ is also affected by the molecular weight distribution, and it becomes rather insensitive to the degree of hydrodynamic interaction if the heterogeneity is such that $M_w/M_n = 1.8$ –2.0. Since the heterogeneity

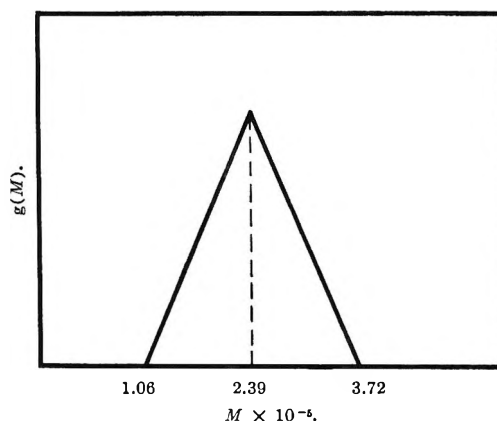


Figure 6. Triangular distribution of molecular weight.

of our samples is possibly in this region, we cannot derive any definite conclusion on the solvent effect on γ from the above observation.

The normal and shear stresses of S111 solution give 0.35 for γ . A theoretical value of γ for the heterogeneous polymer with $M_w/M_n = 1.08$ is also calculated according to the theory of Lovell, *et al.*,¹⁶ for the cases of zero and infinite hydrodynamic interaction. Two types of molecular weight distribution are assumed. One is the Schulz distribution and the other is the triangular distribution illustrated in Figure 6, where the weight distribution function of molecular weight $g(M)$ is shown. The calculated values of γ are given in Table II. The triangular distribution gives a little larger value of γ than does the Schulz distribution.

Table II

Hydrodynamic interaction	Calcd value of γ	
	Triangular distn	Schulz distn
0	0.526	0.500
∞	0.308	0.270

The observed value 0.35 does not agree with the value for the limit of zero nor infinite hydrodynamic interaction when the Schulz distribution is used. On the other hand, if the triangular distribution is adopted, the theoretical value of γ for the limit of infinite hydrodynamic interaction comes quite close to the ob-

(15) J. E. Frederick, N. W. Tschoegl, and J. D. Ferry, *J. Phys. Chem.*, **68**, 1974 (1964).

(16) S. E. Lovell and J. D. Ferry, *ibid.*, **65**, 2274 (1961).

served value. Remembering that the triangular distribution, rather than the Schulz distribution is more appropriate for this type of polymer, we may conclude that the polymer S111 displays Zimm-like, instead of Rouse-like, behavior in Aroclor.

Acknowledgment. Discussions with Professor T. Kotaka of this university have been indispensable during the course of this study. We are also indebted to Professors J. D. Ferry and J. E. Frederick for their kind supply of the solvent and the living polystyrene.

Electrolysis with Constant Potential. Diffusion Currents of Metal Species Dissolved in Spherical Mercury Electrodes

by William G. Stevens¹ and Irving Shain

Department of Chemistry, University of Wisconsin, Madison, Wisconsin (Received January 25, 1966)

The hanging mercury drop electrode was used in a potentiostatic method for the determination of the diffusion coefficient of metal species in mercury. The amalgam was prepared in a constant-potential preelectrolysis step, during which the quantity of electricity involved in the electrodeposition was measured to determine the amalgam concentration. Then, current-time curves were obtained for the diffusion-controlled dissolution of the amalgam. Diffusion coefficients calculated from the time-dependent current decay were compared with those calculated from the "spherical correction" term in a critical evaluation of the method. As a demonstration system, the diffusion coefficient of cadmium in mercury was measured. The value was 1.61×10^{-5} cm²/sec, relative standard deviation 3.0%.

The use of stationary spherical mercury electrodes in potentiostatic experiments has been suggested previously^{2,3} for the unambiguous determination of the diffusion coefficients of electroactive species. By evaluating the diffusion coefficients from both the slope and the intercept of potentiostatic current-time curves, it was shown that the uncertainties involving other experimental parameters, particularly the electrode area, could be minimized.

This method has been applied previously only for the determination of reducible ions in the solution. It is obvious, however, that the same approach could be used to determine diffusion coefficients of metal atoms in a hanging mercury drop electrode, by analyzing the current-time curves obtained from potentiostatic experiments involving the oxidation (dissolution) of the amal-

gams. Developing the method appeared to be of considerable importance as a result of the possibility of studying intermetallic compound reactions in the mercury.⁴ For any such studies, accurate values of the diffusion coefficients are required.

The use of the hanging mercury drop electrode in stripping analysis had indicated that it would be possible to prepare amalgams of known concentration by electrodeposition in a carefully controlled preelectrolysis step.⁵ This work was carried out to determine exactly

(1) National Science Foundation Predoctoral Fellow, 1961-1965.

(2) I. Shain and K. J. Martin, *J. Phys. Chem.*, **65**, 254 (1961).

(3) I. Shain and D. S. Polcyn, *ibid.*, **65**, 1649 (1961).

(4) W. Kemula, Z. Galus, and Z. Kublik, *Bull. Acad. Polon. Sci. Ser. Sci. Chim., Geol. Geograph.*, **6**, 661 (1958); W. Kemula and Z. Galus, *ibid.*, **7**, 553, 607, 729 (1959).

how precisely such hanging amalgam drops could be prepared, to present the detailed theory for the diffusion-controlled dissolution of the amalgam, and to make a careful comparison between the theory and experimental results for the potentiostatic dissolution of a cadmium amalgam.

Theory

For the oxidation of a metal dissolved in a stationary spherical mercury electrode



under diffusion-controlled conditions at a potential far anodic of the formal E° for the system, the boundary value problem is

$$\partial C_{\text{R}}/\partial t = D_{\text{R}}[\partial^2 C_{\text{R}}/\partial r^2 + (2/r)(\partial C_{\text{R}}/\partial r)] \quad (1)$$

$$t = 0, 0 \leq r \leq r_0; C_{\text{R}} = C_{\text{R}}^* \quad (2)$$

$$t > 0, r \longrightarrow 0; C_{\text{R}} \text{ remains bounded} \quad (3)$$

$$t > 0, r = r_0; C_{\text{R}} = 0 \quad (4)$$

Here, C_{R} is the concentration of the metal in the amalgam, C_{R}^* is its initial uniform concentration in the spherical mercury electrode, D_{R} is its diffusion coefficient, t is the time, r is the distance from the center of the electrode, and r_0 is the electrode radius.

The solution to this boundary value problem can be obtained by a straightforward application of the Laplace transform, or from the solution of the analogous problem in heat transfer.⁶

$$i = nFAD_{\text{R}}C_{\text{R}}^* \left[-1/\sqrt{\pi D_{\text{R}}t} + 1/r_0 - (2/\sqrt{\pi D_{\text{R}}t}) \sum_{n=1}^{\infty} e^{-(n^2 r_0^2 / D_{\text{R}}t)} \right] \quad (5)$$

In the usual method of analyzing such current-time curves, plots are made of i vs. $1/\sqrt{t}$. The third term on the right side of eq 5 is small for times less than about 30 sec, and the plot is a straight line over this time interval. One value of the diffusion coefficient can be obtained from the slope of this i vs. $1/\sqrt{t}$ plot and a second can be obtained from the intercept of the plot extrapolated to long times. Since the spherical diffusion process is divergent, the "spherical correction" term acts to reduce the current below the values expected for a plane electrode. As a result, the i vs. $1/\sqrt{t}$ plot (which is based on the first two terms of eq 5, valid only for short times) extrapolates to a positive value.

The exact role of the third term in eq 5 can be defined by evaluating it for long times. Since n always appears as n^2 (which is shown in relationship 6 given above)

$$\sum_{n=1}^{\infty} e^{-(n^2 r_0^2 / D_{\text{R}}t)} = \sum_{n=-1}^{-\infty} e^{-(n^2 r_0^2 / D_{\text{R}}t)} \quad (6)$$

and since when $n = 0$, the exponential is unity, eq 5 can be written

$$i = nFAD_{\text{R}}C_{\text{R}}^* \left[1/r_0 - (1/\sqrt{\pi D_{\text{R}}t}) \sum_{-\infty}^{\infty} e^{-(n^2 r_0^2 / D_{\text{R}}t)} \right] \quad (7)$$

as $t \rightarrow \infty$, $(r_0^2 / D_{\text{R}}t) \rightarrow 0$, and the summation can be replaced by an integral to obtain

$$\lim_{t \rightarrow \infty} i = nFAD_{\text{R}}C_{\text{R}}^* \left[1/r_0 - (1/\sqrt{\pi D_{\text{R}}t}) \int_{-\infty}^{\infty} e^{-(n^2 r_0^2 / D_{\text{R}}t)} dn \right] \quad (8)$$

or, since the integral is symmetrical around zero

$$\lim_{t \rightarrow \infty} i = nFAD_{\text{R}}C_{\text{R}}^* \left[1/r_0 - (2/\sqrt{\pi D_{\text{R}}t}) \int_0^{\infty} e^{-(n^2 r_0^2 / D_{\text{R}}t)} dn \right] \quad (9)$$

The definite integral in eq 9 can be evaluated from standard tables of integrals⁷

$$\int_0^{\infty} e^{-a^2 x^2} dx = \sqrt{\pi}/2a \quad (10)$$

Thus, eq 9 reduces to

$$\lim_{t \rightarrow \infty} i = nFAD_{\text{R}}C_{\text{R}}^* [1/r_0 - 1/r_0] \quad (11)$$

and the current goes to zero as the electroactive material in the finite volume of the electrode is depleted.

Preelectrolysis Procedure

Three methods of preparing a known amalgam concentration in a hanging mercury drop electrode were investigated. In each case the procedure involved electrolysis at a constant potential cathodic of the formal E° for the system.

The first method was the normal preelectrolysis step of a stripping analysis, based on the consideration that if the cathodic current can be maintained constant and reproducible by controlled stirring, accurately known amalgams can be made by controlling the electrolysis time and the electrode volume. For analytical applications, sufficiently reproducible stirring can be

(5) I. Shain and J. Lewinson, *Anal. Chem.*, **33**, 187 (1961).

(6) H. S. Carslaw and J. C. Jaeger, "Conduction of Heat in Solids," 2nd ed, Oxford University Press, London, 1959, p 310; see also N. G. Chovnyk and V. V. Vashchenko, *Zh. Fiz. Khim.*, **37**, 538 (1963).

(7) B. O. Pierce and R. M. Foster, "A Short Table of Integrals," 4th ed, Ginn and Co., Boston, Mass., 1957, p 68.

obtained by a small Teflon-covered stirring bar placed in the solution and driven from below the cell by another magnet mounted on a synchronous motor. This procedure works well for trace analysis, where the concentration of the reducible ion is very low and relatively long preelectrolysis times can be used. However, in this work, it was necessary to use relatively high concentrations of reducible species ($\sim 10^{-3} M$) so that the solution concentration would be known and precisely reproducible. Under these conditions, the instantaneous currents ranged $\pm 10\%$ from the average value, corresponding to erratic fluctuations in the stirring. These could not be averaged out reproducibly in the short preelectrolysis times used and this method could not be applied here.

In an attempt to minimize the erratic fluctuations in the stirring, experiments were carried out in which the hanging mercury drop was rotated, as first suggested by Barendrecht.⁸ The electrodes were constructed from carefully selected straight sections of 6-mm soft glass tubing and mounted in an eight-jaw chuck which was belt driven by a synchronous motor. The eight-jaw chuck permitted precise centering of the electrode. Drops of mercury from a dropping-mercury electrode capillary were hung on these electrodes and could be rotated up to about 30 rpm. The instantaneous current fluctuations were markedly reduced and the average preelectrolysis current could be reproduced to at least $\pm 3\%$. The major difficulty was that with the size of mercury drop used here, the electrode could not be rotated fast enough to eliminate entirely diffusion from the bulk of the solution as a means of mass transport. Nevertheless, by monitoring the current during the preelectrolysis step, the effect of the deviations in the constant current could be evaluated, and this method of producing known amalgams was used in some of the experiments.

The third method of preparing known hanging amalgam drops did not require controlling either the current or the time of preelectrolysis, but rather involved direct control of the quantity of electricity flowing during the preelectrolysis. In this procedure, a step-functional controlled potential was applied to the cell. First, the preelectrolysis potential was applied. During this interval, an electrodeposition of the amalgam was carried out, and simultaneously a signal proportional to the current flowing was fed to an analog integrator. When the output of the integrator reached a preset value (normally in about 15 sec) signifying the accumulation of the desired amount of metal in the mercury, the electrolysis cell was automatically removed from the circuit for a 1-min quiescent period, during which the potential assumed its equilibrium

(zero-current) value. This interval is required to permit diffusion of the metal atoms in the mercury so that concentration gradients within the mercury drop are minimized.⁵ After this quiescent period, the potential was manually switched to the stripping potential and the anodic current-time curve was recorded. Using this procedure, the composition of the amalgam drops could be reproduced to at least 1%. The main advantage of this procedure, of course, is that since the preelectrolysis step is controlled directly by the quantity of amalgam accumulated, the mechanism of mass transport in the solution is no longer an important variable and does not have to be controlled.

Experimental Section

All experiments were carried out on an instrument based on the operational amplifiers manufactured by G. A. Philbrick Researches, Inc. (Boston). The circuit was essentially the same as that presented previously,⁹ except that the controller amplifier did not include a booster amplifier because fairly low electrolysis currents were used. Using the previous notation, PS-1 and PS-2 were battery-operated, low-voltage power supplies. M-1 was a Leeds and Northrup Speedomax G Series 6000 recorder with a chart speed of 27.9 ± 0.2 in./min, a full-scale sensitivity of 10 mv, and a nominal full-scale response time of 0.4 sec. M-2 was a single operational amplifier (Philbrick K2-XA) connected as a "contactor with hysteresis"¹⁰ used to switch the electrolysis cell out of or into the circuit by operating mercury-wetted relays. The circuit was normally set to operate when the output of the integrator reached a preset level of the order of 40 v. The relay coil circuits included diodes (with manual polarity reversal) so that the contactor could be used with either positive- or negative-going outputs from the integrator, and thus could be used for either anodic or cathodic experiments.

The cell was similar to that described previously,¹¹ except that the Teflon lid was provided with neoprene O-rings fitted into each hole for the electrodes, scoop, nitrogen inlet, etc., to ensure that no air could enter. To reduce the number of holes required in the lid, the counterelectrode (2 in. of 18-gauge platinum wire) was mounted on the mercury drop transfer scoop. The working electrodes were made from 6-mm glass tubing and to minimize shielding effects,^{2,11} the tips of the elec-

(8) E. Barendrecht, *Nature*, **181**, 764 (1958).

(9) See Figure 9 in W. L. Underkofler and I. Shain, *Anal. Chem.*, **35**, 1778 (1963).

(10) See Figure 3.3 in "Applications Manual for Philbrick Octal Plug-in Computing Amplifiers," G. A. Philbrick Researches, Inc., Boston, 1956, p 19.

(11) G. S. Alberts and I. Shain, *Anal. Chem.*, **35**, 1859 (1963).

trodes were ground to a point so that very little glass remained around the platinum-glass seal. Convection shields were used on the working electrode as described previously.¹¹ The reference electrode was Ag-AgCl, placed directly in the cell. Thus, a salt bridge was not used, and convection in the solution resulting from flow of the electrolyte through the Luggin capillary was eliminated.

All experiments were carried out at $25.0 \pm 0.1^\circ$. The cell and thermostat were mounted on a 60-lb slab of concrete, supported by four semiinflated plastic balls (8-in. diameter) to minimize vibration. High-purity nitrogen was passed through each solution for at least 15 min to remove oxygen. All chemicals were reagent grade, and were used without further purification. The electrode area was determined after each experiment by collecting the individual hanging mercury drop and weighing it on a microbalance.

Results

To demonstrate and evaluate the application of this method of determining the diffusion coefficients of metal species dissolved in mercury, the reduction-oxidation sequence for the Cd(II)-Cd(amal) system was studied. The preelectrolysis potential was -0.725 v and the stripping potential was -0.525 v, both with respect to the Ag-AgCl electrode. Anodic current-time curves were analyzed by plotting the parameter $i\sqrt{t}$ as a function of \sqrt{t} as suggested by Lingane,¹² to provide a more sensitive evaluation of the spherical correction term, and to give a more realistic weighting of the data on the time scale, as compared with the previously used i vs. $1/\sqrt{t}$ plots. In addition, the effects of the depletion of the mercury drop (the third term in brackets in eq 5) could be more easily noted. A typical plot of $i\sqrt{t}$ vs. \sqrt{t} is shown in Figure 1, where the experimental results for the oxidation of a cadmium amalgam are compared with theory, *i.e.*, eq 5 multiplied by \sqrt{t} . Shielding effects at the top of the mercury drop were found to be very small, and the electrode area could be taken as $4\pi r_0^2$, contrary to the case in which the electroactive material is in the solution and diffuses toward the drop.¹¹

In utilizing plots as shown in Figure 1 for the calculation of the diffusion coefficient, the intercept at $t = 0$ provides a value of $\sqrt{D_R}$ associated with the time-dependent decay of the current, while the slope of the straight line portion (up to 30 sec) provides a value of D_R associated with the "spherical correction" term. Generally, deviations between the two values of D_R obtained can be used to evaluate other sources of error, particularly in determining the electrode area. The results obtained in one series of experiments are sum-

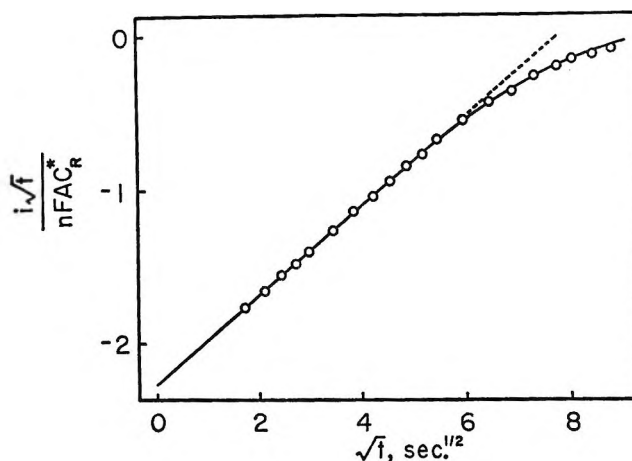


Figure 1. Comparison of experimental results with theory for the dissolution of a cadmium amalgam; solution: 8.4×10^{-5} M Cd(II); 0.1 M potassium chloride; amalgam concentration after 180-sec preelectrolysis at a rotating electrode, 1.20×10^{-3} M; electrode radius, $r_0 = 0.0536$ cm; solid line, theoretical (eq 5 multiplied by \sqrt{t}); dashed line, theoretical (first two terms only); points, experimental. Ordinate in units of $\text{cm}/\sqrt{\text{sec}}, \times 10^{-3}$.

marized in Table I. These data were obtained over a period of several days; the different values of r_0 correspond to collecting 1, 2, or 3 drops of mercury from the capillary to form the hanging drop electrode. The close agreement between the mean values obtained from the slope and intercept indicate that the extraneous determinate errors have been minimized. How-

Table I: Diffusion Coefficient of Cadmium in Mercury, Calculated from Experimental Plots of $i\sqrt{t}$ vs. \sqrt{t}

r_0 , cm	$D_{\text{Cd}/\text{Hg}} (\times 10^6), \text{cm}^2/\text{sec}^2$			
	Intercept	Slope	Ratio	
0.0520	1.61	1.57	1.52	
0.0656	1.61	1.57	1.52	
0.0751	1.60	1.59	1.61	
0.0524	1.55	1.62	1.71	
0.0660	1.54	1.68	1.84	
0.0525	1.55	1.59	1.64	
0.0661	1.59	1.71	1.84	
0.0756	1.63	1.69	1.76	
0.0526	1.69	1.63	1.57	
0.0658	1.61	1.62	1.63	
0.0755	1.63	1.69	1.76	
	Mean	1.60	1.63	1.67
	Std dev	0.04	0.05	0.12

^a $D_{\text{Cd}/\text{Hg}} = 1.61 \times 10^{-5}$ cm^2/sec , relative standard deviation 3.0%, calculated from "intercept" and "slope" data only.

(12) P. J. Lingane, *Anal. Chem.*, **36**, 1732 (1964).

ever, relatively poor precision of the individual measurements over the series indicates that other factors such as convection (possibly induced by drop movement when the potential is changed²) are still important.

It is also possible to calculate the diffusion coefficient from the ratio of the slope to the intercept

$$D_{\text{R}} = \left[\frac{(\text{slope})(r_0)}{(\text{intercept})(\sqrt{\pi})} \right]^2 \quad (12)$$

This method was thought to be of interest since it is not necessary to know explicitly the bulk concentration, number of electrons, or electrode area (although the radius must be known, which is equivalent). These results are also included in Table I, but this method of treating the data does not appear to be as precise as the others, possibly because it is more sensitive to small errors in determining the electrode radius.

The results summarized in Table I are a realistic evaluation of the method, using relatively conventional instrumentation. Although literature values^{6,13-15} of

$D_{\text{Cd/Hg}}$ ranging from 1.45 to 2.45×10^{-5} cm²/sec have been reported, this method would seem to yield a less ambiguous result than the other methods. Any significant improvement in the precision probably would require extensive changes in the experimental approach, including better elimination of vibration and probably a digital read-out system. However, the technique is rapid and convenient, and the precision is adequate for most studies on amalgam systems, where it should find wide application.

Acknowledgment. This work was supported in part by the U. S. Atomic Energy Commission under Contract No. AT(11-1)-1083. Some of the preliminary experiments were carried out by John Lewinson.

(13) N. H. Furman and W. C. Cooper, *J. Am. Chem. Soc.*, **72**, 5667 (1950).

(14) M. S. Zakharov and A. G. Stromberg, *Zh. Fiz. Khim.*, **38**, 130 (1964).

(15) A. G. Stromberg and E. A. Zakharova, *Elektrokhimiya*, **1**, 1036 (1965).

The Photochemistry of Phosphorus Compounds. IV. Photolysis of Sodium Hydrogen Phosphate in Aqueous Solution

by M. Halmann and I. Platzner

Isotope Department, The Weizmann Institute of Science, Rehovoth, Israel (Received January 28, 1966)

Aqueous solutions of Na_2HPO_4 and methanol on irradiation at 1849 Å decompose, releasing hydrogen gas. In the presence of nitrous oxide, nitrogen is also formed. Added acetone or H_2PO_4^- ions decrease the nitrogen yield. The relative rates of the above reactions indicate that photolysis of aqueous HPO_4^{2-} produces the hydrated electron (e_{aq}^-). These results confirm previous conclusions from the absorption spectrum of phosphate anions, that the strong band below 2000 Å is due to a charge-transfer-to-solvent type of transition. The second-order rate constant (in $M^{-1} \text{sec}^{-1}$) for the following reaction was determined at 25° and ionic strength $\mu = 1.5$ [based on $e_{\text{aq}}^- + \text{N}_2\text{O} \rightarrow \text{N}_2 + \text{OH} + \text{HO}^-$ ($k = (5.6 \pm 2) \times 10^9$)], $e_{\text{aq}}^- + \text{H}_2\text{PO}_4^- \rightarrow \text{H} + \text{HPO}_4^{2-}$ [$k = (4.9 \pm 2) \times 10^7$].

I. Introduction

The photochemistry of aqueous solutions of various anions, such as halides, hydroxide, and sulfate, has recently been studied.¹ Irradiation at 1849 Å of such solutions also containing methanol and nitrous oxide yielded molecular hydrogen and nitrogen. The mechanism proposed involved the formation of a hydrated electron, ejected from an excited state of the ion. The absorption spectrum of the phosphate ion² is similar to that of the above anions³ in having a steep absorption edge below 2000 Å. Environmental effects on the spectrum indicated that absorption of light in this region for these anions is due to a charge-transfer-to-solvent type transition, presumably involving formation of the hydrated electron.¹ The purpose of the present work is also to obtain photochemical evidence about the nature of the excited phosphate anion. Evidence will be sought for other intermediate species, such as hydrated electrons, e_{aq}^- , and hydrogen atoms, as well as on the reactivity of these species with phosphate anions.

II. Results

(a) *Photolysis in the Presence of Methanol.* The quantum yields of the formation of molecular hydrogen in the photolysis of evacuated aqueous sodium hydrogen phosphate, containing only added methanol as an

efficient scavenger for hydrogen atoms,⁴ are shown in Table I and Figure 1. The hydrogen yield increases with methanol concentration. Concentrations above 1.2 M methanol could not be used because of insufficient solubility of sodium hydrogen phosphate at higher proportions of methanol in the solvent. Table I also includes the corrections for direct photolysis of methanol and water.

(b) *Photolysis in the Presence of Methanol and Nitrous Oxide.* Quantum yields of molecular nitrogen and hydrogen upon irradiation at 1849 Å of solutions of

(1) (a) J. Jortner, M. Ottolenghi, and G. Stein, *J. Phys. Chem.*, **66**, 2037 (1962); **68**, 247 (1964); (b) F. S. Dainton and S. R. Logan, *Proc. Roy. Soc. (London)*, **A287**, 281 (1965); (c) F. S. Dainton and P. Fowles, *ibid.*, **A287**, 312 (1965); (d) J. Barrett, M. F. Fox, and A. L. Mansell, *Nature*, **200**, 257 (1963); *J. Phys. Chem.*, **69**, 2996 (1965); (e) M. Shirom and G. Stein, *Nature*, **204**, 778 (1964).

(2) (a) M. Halmann and I. Platzner, *Proc. Chem. Soc.*, 261 (1964); (b) M. Halmann and I. Platzner, *J. Chem. Soc.*, 1440 (1965); (c) M. Halmann and I. Platzner, *ibid.*, 5380 (1965).

(3) (a) H. Ley and B. Arends, *Z. Physik. Chem.*, **B6**, 240 (1929); **B15**, 311 (1932); (b) M. Smith and M. C. R. Symons, *Trans. Faraday Soc.*, **54**, 338, 346 (1958); (c) T. R. Griffiths and M. C. R. Symons, *ibid.*, **56**, 1125 (1960); (d) M. J. Blandamer, T. R. Griffiths, L. Shields, and M. C. R. Symons, *ibid.*, **60**, 1524 (1964); (e) G. Stein and A. Treinin, *ibid.*, **55**, 1086, 1091 (1959); (f) J. Jortner, B. Raz, and G. Stein, *ibid.*, **56**, 1273 (1960); (g) J. Jortner, B. Raz, and G. Stein, *J. Chem. Phys.*, **34**, 1455 (1961); (h) S. J. Strickler and M. Kasha, *ibid.*, **34**, 1077 (1961); (i) J. L. Weeks, G. M. A. C. Meaburn, and S. Gordon, *Radiation Res.*, **19**, 559 (1963).

(4) J. Barrett and J. H. Baxendale, *Trans. Faraday Soc.*, **56**, 37 (1960).

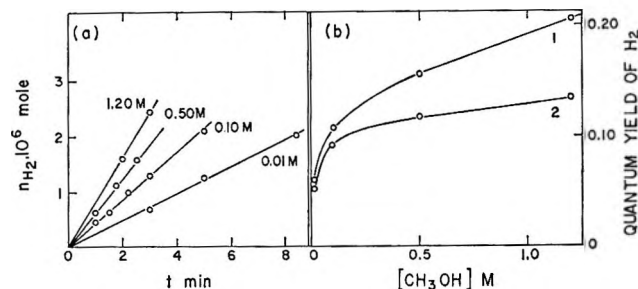


Figure 1. Yield of hydrogen as a function of time and of methanol concentration in the photolysis of aqueous sodium hydrogen phosphate (0.100 M): (a) yield vs. time at various methanol concentrations; (b) quantum yield (1, total; 2, corrected for photolysis of water and methanol) as a function of methanol concentration.

Table I: Quantum Yield of Hydrogen, ϕ_{H_2} , as a Function of Methanol Concentration in the Photolysis of Aqueous Sodium Hydrogen Phosphate (0.100 M)

CH_3OH, M	0.01	0.10	0.50	1.20
ϕ_{H_2} (obsd)	0.060	0.107	0.155	0.205
$\epsilon(HPO_4^{2-}), M^{-1} cm^{-1}$	455 ± 5	440 ± 10	420 ± 10	400 ± 10
Fraction of light absorbed by HPO_4^{2-}	0.969	0.955	0.902	0.821
$\phi_{H_2}(\text{cor})^a$	0.051	0.092	0.117	0.134

^a $\phi_{H_2}(\text{cor})$ represents the net quantum yield of hydrogen from the photolysis of HPO_4^{2-} .

sodium hydrogen phosphate are presented in Table II. These solutions also contain sodium dihydrogen phosphate, as well as added methanol for scavenging of hydrogen atoms, and nitrous oxide, for efficient scavenging of hydrated electrons.⁵ As shown in Figure 2, the yield of molecular nitrogen at first increases with the nitrous oxide concentration, reaching a limiting value, presumably by almost complete scavenging of hydrated electrons, at $[N_2O] = (7-11) \times 10^{-3} M$, with a quantum yield of 0.506 ± 0.006 . On the other hand, the molecular hydrogen yield drops with increasing nitrous oxide concentration to a limiting value of about 0.02. An identical minimum concentration of nitrous oxide was reported^{1a-c} for the photolysis of aqueous solutions of chloride, bromide, sulfate, or hydroxide ions.

(c) *Photolysis in the Presence of Methanol, Nitrous Oxide, and Acetone.* Acetone is known to be an efficient scavenger for hydrated electrons.^{6e} In the photolysis of aqueous sodium hydrogen phosphate, containing constant concentrations of methanol, $H_2PO_4^-$, and nitrous oxide, acetone indeed was found to decrease the quantum yield for formation of molecular nitrogen (see Table III).

Table II: Relative Quantum Yields of Nitrogen, ϕ_{N_2} , and Hydrogen, ϕ_{H_2} , as a Function of Nitrous Oxide Concentration in the Photolysis of Aqueous Sodium Hydrogen Phosphate Containing Methanol (0.25 M) and $H_2PO_4^-$

$HPO_4^{2-}, 10^2 M$	$H_2PO_4^-, 10^3 M$	$N_2O, 10^3 M$	ϕ_{H_2}	ϕ_{N_2}	ϕ_{N_2}/ϕ_{H_2}	Φ^a
444	56	11	0.040	0.465	11.6	0.505
444	56	8	0.045	0.360	8.00	0.405
444	56	5	0.056	0.262	4.70	0.318
444	56	2	0.120	0.125	1.04	0.245
444	56	0.85	0.162	0.050	0.31	0.212
490	10	11	0.024	0.481	20.1	0.505
490	10	8	0.031	0.385	12.4	0.416
490	10	5	0.040	0.275	6.87	0.315
490	10	2	0.074	0.165	2.24	0.239
500	4	19.4	0.017	0.490	28.8	0.507
500	4	16.2	0.025	0.487	19.5	0.512
500	4	11	0.020	0.487	24.4	0.507
500	4	8	0.024	0.487	20.5	0.511
500	4	6.8	0.025	0.438	17.5	0.463
500	4	5	0.030	0.325	10.8	0.355
500	4	4.5	0.035	0.310	8.86	0.345
500	4	3	0.049	0.230	4.70	0.279
500	4	2	0.051	0.148	2.88	0.199
500	4	1.4	0.070	0.117	1.68	0.187
500	4	0.85	0.066	0.066	1.00	0.132

^a $\Phi = \phi_{H_2} + \phi_{N_2}$.

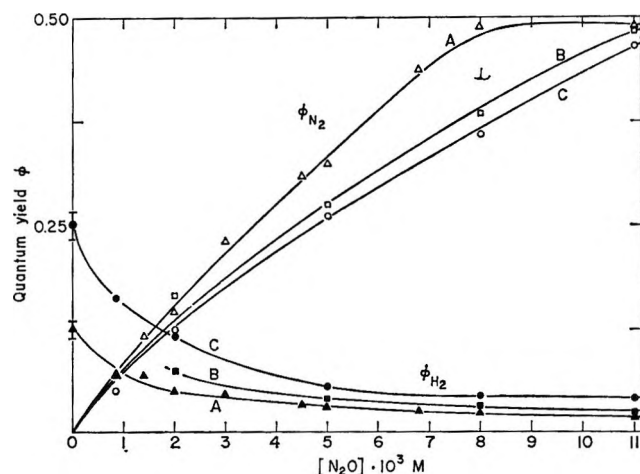


Figure 2. Quantum yields of hydrogen ϕ_{H_2} (upper curves) and of nitrogen ϕ_{N_2} (lower curves) as a function of nitrous oxide concentration in the photolysis of aqueous sodium hydrogen phosphate (0.44–0.50 M) containing methanol (0.25 M) and $H_2PO_4^-$ (A, 0.004; B, 0.010; C, 0.056 M).

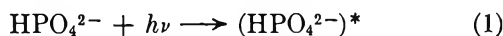
(5) (a) F. S. Dainton and S. A. Sills, *Nature*, **186**, 879 (1960); (b) G. Czapski and J. Jortner, *ibid.*, **188**, 50 (1961); (c) J. H. Baxendale, *et al.*, *Nature*, **201**, 468 (1964); (d) J. P. Keene, *Radiation Res.*, **22**, 1 (1964); (e) M. Anbar and P. Neta, *Intern. J. Appl. Radiation Isotopes*, **16**, 227 (1965).

Table III: Quantum Yield of Nitrogen, ϕ_{N_2} , as a Function of Acetone Concentration in the Photolysis of Aqueous Sodium Hydrogen Phosphate (0.500 M) Containing $H_2PO_4^-$ (0.004 M), Methanol (0.25 M), and Nitrous Oxide (0.002 M)

Acetone, M	0	0	0	0.002	0.002	0.004	0.004
ϕ_{N_2}	0.150	0.145	0.148	0.087	0.080	0.065	0.063

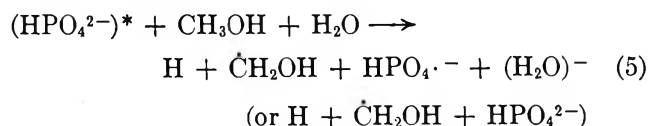
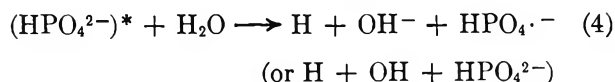
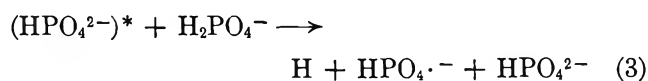
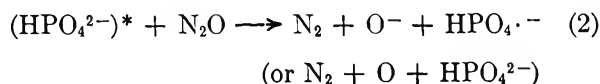
III. Discussion

In order to account for the observed quantum yields of nitrogen and hydrogen from the photolysis of aqueous solutions of disodium hydrogen phosphate containing nitrous oxide and methanol, several mechanisms may be examined. Since all irradiations were carried out under conditions such that 96-99% of the light was absorbed by the phosphate dianion, the initial process must be a transition of this ion to some electronically excited state, which we shall denote by $(HPO_4^{2-})^*$



The excited state may revert to the ground state, without photochemical consequences, or it may react with some component of the solution, or it may dissociate to release some reactive fragment, such as a hydrogen atom or an electron.

A. Direct interaction of the excited state with the components of the solution may involve both charge and energy transfer, as shown below for reactions 2 to 5, or it may involve merely energy transfer (shown below in brackets for several of these reactions). Both variants of this mechanism are indistinguishable with respect to stable products. Possible reactions are



followed by scavenging of hydrogen atoms with methanol to form molecular hydrogen. The radical and ion fragments $HPO_4^{\cdot-}$, O^- , O , and OH are scavenged by the methanol in the solution, without giving gaseous products. The radical $\dot{C}H_2OH$ disproportionates to

formaldehyde and methanol, or combines to yield ethylene glycol.^{1d} The relative quantum yield of nitrogen and hydrogen required on the basis of the above scheme is (assuming homogeneous kinetics)

$$\phi_{N_2}/\phi_{H_2} = k_2[N_2O]/(k_3[H_2PO_4^-] + k_4[H_2O] + k_5[CH_3OH])$$

Therefore, the relative yield ϕ_{N_2}/ϕ_{H_2} should be proportional to the nitrous oxide concentration. As shown in Figure 3, such a proportionality was not obtained.

B. Direct dissociation of the excited state to release hydrogen atoms, which subsequently react with nitrous oxide or with methanol, would require the following expression for the relative quantum yields of nitrogen and hydrogen

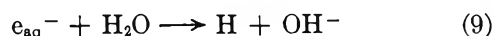
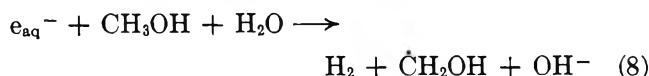
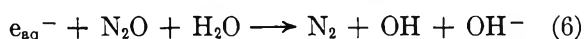
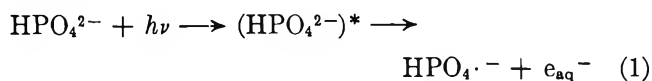
$$\phi_{N_2}/\phi_{H_2} = k_{(H+N_2O)}[N_2O]/k_{(H+CH_3OH)}[CH_3OH]$$

The reactivity of hydrogen atoms with methanol and with nitrous oxide has been measured before by different groups.⁶ Taking^{6b} $k_{(H+CH_3OH)} = 1.6 \times 10^6 M^{-1} sec^{-1}$ and $k_{(H+N_2O)} = 1.2 \times 10^4 M^{-1} sec^{-1}$, we can predict for a solution containing nitrous oxide (0.02 M) and methanol (0.25 M) a ratio of quantum yields

$$\phi_{N_2}/\phi_{H_2} = 1.2 \times 10^4 \times 0.02 / 1.6 \times 10^6 \times 0.25 = 6 \times 10^{-4}$$

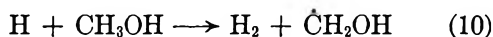
The observed relative quantum yield under such conditions was about 30 (see Table II), and this mechanism can therefore be excluded.

C. After release of an electron from the excited state to the solvent, this electron may presumably react as the hydrated electron, e_{aq}^- , the reactivity of which toward many compounds has been studied by flash radiolysis or photolysis.^{5,7} The following reactions of hydrated electrons are expected to occur in the system under study



(6) (a) F. S. Dainton and S. A. Sills, *Proc. Chem. Soc.*, 223 (1962); (b) F. S. Dainton and P. Fowles, *Proc. Roy. Soc. (London)*, **A287**, 295 (1965).

(7) (a) E. J. Hart, J. K. Thomas, and S. Gordon, *Radiation Res. Suppl.*, **4**, 74 (1964); (b) E. J. Hart, *Science*, **146**, 19 (1964).



The reaction with water, k_9 , can be neglected because of its very small rate constant, $(4.5 \pm 0.4) \times 10^2 \text{ M}^{-1} \text{ sec}^{-1}$.^{5e} For discussion of the competitive scavenging of the hydrated electron, it is useful to investigate separately three regions: (a) at high nitrous oxide concentrations, $[\text{N}_2\text{O}] \geq 10^{-2} \text{ M}$, (b) at moderate concentrations where $0 < [\text{N}_2\text{O}] < 10^{-2} \text{ M}$, and (c) in the absence of nitrous oxide.

(a) *Above about 0.01 M Nitrous Oxide.* The limiting total quantum yield ($\phi_{\text{N}_2} + \phi_{\text{H}_2}$) equals 0.506 ± 0.006 . According to Dainton and Fowles,^{1c} under such conditions the scavenging of electrons and hydrogen atoms proceeds by homogeneous kinetics. Therefore, at high nitrous oxide concentrations

$$(\phi_{\text{H}_2} - Q)/\phi_{\text{N}_2} = (\Sigma kC + k_7[\text{H}_2\text{PO}_4^-])/(k_6[\text{N}_2\text{O}])$$

where Q represents the yield of hydrogen by direct photolysis of methanol and water, and ΣkC represents the sum of hydrogen-producing reactions of the hydrated electron, except for reaction 7.

Thus, a plot of $(\phi_{\text{H}_2} - Q)[\text{N}_2\text{O}]/\phi_{\text{N}_2}$ vs. $[\text{H}_2\text{PO}_4^-]$ should be linear, with a slope k_7/k_6 . From a least-square plot of the results in Table IV, we get for the rela-

Table IV: Quantum Yields of Hydrogen, ϕ_{H_2} , and Quantum Yields of Nitrogen in the Photolysis of Aqueous Sodium Hydrogen Phosphate (0.44 to 0.50 M) Containing Nitrous Oxide and Methanol (0.25 M) as a Function of Dihydrogen Phosphate Concentration

$[\text{H}_2\text{PO}_4^-]$ M	$[\text{N}_2\text{O}]$ M	$\phi_{\text{H}_2}/\phi_{\text{N}_2}$	$10^4(\phi_{\text{H}_2} - Q) \times$ $[\text{N}_2\text{O}]/\phi_{\text{N}_2}$
0.004	0.019	0.0376	3.50
0.004	0.011	0.0419	2.70
0.004	0.008	0.0482	2.64
0.010	0.011	0.0495	3.66
0.037	0.011	0.0690	5.84
0.056	0.011	0.0862	7.55

tive rate constants at ionic strength $\mu = 1.45 \pm 0.05$.

$$k_7/k_6 = (8.8 \pm 0.7) \times 10^{-3}$$

Choosing for reaction of the hydrated electron with nitrous oxide the value^{5c,d} $k_6 = (5.6 \pm 2) \times 10^9 \text{ M}^{-1} \text{ sec}^{-1}$, we get

$$k_7 = (4.9 \pm 2) \times 10^7 \text{ M}^{-1} \text{ sec}^{-1}$$

The present result for k_7 , the rate constant for reaction of the hydrated electron with the phosphate mono-anion at ionic strength 1.45, can be extrapolated to ionic strength zero by using the extended Debye-

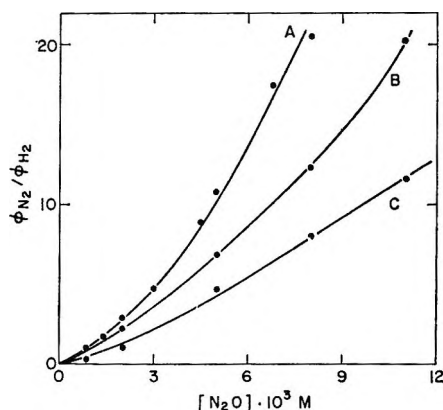


Figure 3. Relative quantum yields of nitrogen and hydrogen $\phi_{\text{N}_2}/\phi_{\text{H}_2}$ as a function of nitrous oxide concentration in the photolysis of aqueous sodium hydrogen phosphate (0.44 to 0.50 M) containing methanol (0.25 M) and H_2PO_4^- (A, 0.004; B, 0.010; C, 0.056 M).

Hückel theory of ionic solutions and the Brønsted-Bjerrum relationship between rate constants and ionic strengths⁸

$$\log(k_7/k_7^0) = 1.02(Z_{\text{e}_2\text{q}^-})(Z_{\text{H}_2\text{PO}_4^-})\{\mu^{1/2}/[1 + a(\mu^{1/2})]\}$$

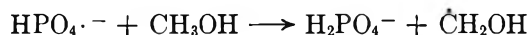
where k_7^0 is the rate constant at zero ionic strength; a is taken as unity. Thus, we get $k_7/k_7^0 = 3.5$; therefore $k_7^0 = 1.4 \times 10^7 \text{ M}^{-1} \text{ sec}^{-1}$. Previously, reported values for k_7^0 by different methods are $(5.5 \pm 0.9) \times 10^6$, 1.2×10^7 , and $1.7 \times 10^7 \text{ M}^{-1} \text{ sec}^{-1}$.⁹

(b) *At Nitrous Oxide Concentrations below 0.01 M.* As shown in Figure 2, the quantum yield of nitrogen rises, while the quantum yield of hydrogen drops, with increasing nitrous oxide concentration. The total yield of gaseous products, $\Phi = \phi_{\text{N}_2} + \phi_{\text{H}_2}$, also depends on the nitrous oxide concentration. Analogous non-linear changes in quantum yields as a function of scavenger concentration had been obtained also in the photolysis of other anions in aqueous solution.^{1c}

(c) *In the Absence of Nitrous Oxide.* As seen in Figure 1, the quantum yield of hydrogen from the direct photolysis of HPO_4^{2-} depends on the methanol concentration. At the highest methanol concentrations used (1.2 M), the quantum yield of hydrogen reaches values of 0.14. Figure 1b shows that low concentrations of methanol considerably affect the hydrogen yield. Possibly, the methanol in this region, in addition to reacting with the hydrated electron according to reaction 8, also scavenges the $\text{HPO}_4^{\cdot-}$ radical ion, according to the following reaction

(8) G. Czapski and H. A. Schwartz, *J. Phys. Chem.*, **66**, 471 (1962).

(9) J. Rabani in "Solvated Electron," *Advances in Chemistry Series*, No. 50, American Chemical Society, Washington, D. C., 1965, p 245.



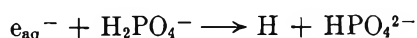
thus preventing the back-reaction of the radical ion with the hydrated electron.

The much lower quantum yield for scavenging of the hydrated electron by dihydrogen phosphate ion than by nitrous oxide seems to suggest a different mechanism for scavenging by the two reagents. A similar observation had been made in a study of the photolysis of aqueous sulfate, where the quantum yields of scavenging hydrated electrons by nitrous oxide^{1c} and methanol^{1d} are 0.71 and 0.37, respectively. In the photochemistry of aqueous ferrocyanide it was shown that the dihydrogen phosphate ion is also a much less effective scavenger for the hydrated electrons than nitrous oxide.^{1e} The increase in the quantum yield of hydrogen with the dihydrogen phosphate ion concentration (Figure 2) is in agreement with reaction 7.

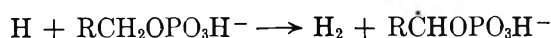
IV. Conclusions

The relative quantum yields of hydrogen and nitrogen at high scavenger concentrations after photolysis of aqueous sodium hydrogen phosphate are in agreement with those expected for reactions of the hydrated electron with the various scavengers in solution. It therefore seems proven that hydrated electrons are the initial reactive species following the absorption of light in the hydrogen phosphate dianion. This result supports the spectroscopic evidence that the absorption band of phosphate anions in the 1850-A region is due to a charge-transfer-to-solvent type of transition.

Dissociative capture of the electron by a dihydrogen phosphate ion



followed by hydrogen abstraction



seems to be of interest as a model of the effects of hydrated electrons on various organic or inorganic phosphorus derivatives.^{1c,2c} Some of the photolytic or radiolytic "damage" on organic phosphates of biological importance may be by reactions of this type.

V. Experimental Section

Light Source. A spiral-shaped, flat-headed, low-pressure mercury lamp (Thermal Syndicate) was operated at 3000 v and 30 ma from a transformer connected to a stabilized 220-v supply. No filters were used. About 12% of the ultraviolet emission of this lamp appears at the 1849-A line.

Irradiation. Solutions were irradiated in a cylindrical flat-bottomed quartz cell (12-cm length, 23-mm i.d.), the lower part of which could be immersed in a removable thermostat ($25.0 \pm 0.5^\circ$). The cell contained a glass-covered magnetic stirring bar (15-mm length, 2-mm o.d.); it was connected to the vacuum line through a glass stopcock. Irradiation was carried out by placing the lamp below the cell.

Actinometry. The output of the lamp at 1849 A was obtained by measuring the amount of hydrogen evolved by the irradiation of 5 M aqueous methanol. Accepting the reported^{6b} quantum yield of about 0.5, a light flux of 4×10^{-6} einstein min^{-1} was found to be incident upon the reaction cell at this wavelength.

It should be pointed out that the quantitative interpretation in this work is based only on the *ratio* of quantum yields, which is independent of the value chosen for the quantum yield of the actinometer.

Procedure. Freshly prepared phosphate solution (10 ml) was pipetted into the cell and connected to the vacuum line for degassing by repeated freezing (-80°) and pumping out (three times). Finally, the solution was stirred while the cell was closed and then connected for a few seconds to the vacuum line. The final pressure, measured with a Philips gauge above a liquid air trap, was less than 10^{-4} mm. For equilibration of solutions with nitrous oxide, the cell was connected to a flask (about 250 ml) containing a known pressure of nitrous oxide and was stirred for 2 hr.^{1a} The cell was then disconnected from the line and irradiated for periods from 2 to 5 min.

Gas Analysis. The gaseous products were analyzed by gas chromatography, using a molecular sieve (Linde Air Products Co. 5A 35-50 mesh) column (2.0-m length, 3-mm i.d.) which was activated by maintaining for 24 hr at 350° in a slow stream of argon. The column was operated with argon carrier gas (16 ml min^{-1} flow rate) and a thermal conductivity cell (Gow-Mac Instrument Co., Model TRIIB) at 100° . The gas samples were transferred with a Toepler pump through one trap at -80° (to retain water and methanol) and one trap cooled by liquid air (to retain nitrous oxide) into the inlet tube of the gas chromatograph. Hydrogen, oxygen, and nitrogen were completely separated by the column used, with peak maxima appearing after 1.6, 2.4, and 5.6 min, respectively. No measurable amounts of oxygen could be detected in the gas after irradiation; its quantum yield must be less than 0.002.

Materials and Solutions. Sodium hydrogen phosphate ($\text{Na}_2\text{HPO}_4 \cdot 12\text{H}_2\text{O}$), potassium dihydrogen phosphate (KH_2PO_4) (both Analar), methanol (spectroscopic grade) (all by British Drug Houses), and acetone

(Fluka AG, Puriss) were used without further purification. Water was redistilled from alkaline permanganate and then from phosphoric acid, atmospheric carbon dioxide being excluded. Nitrous oxide (Matheson Co., Inc.) was purified by repeated freezing with liquid air and evacuation. Only fresh solutions were used, contained in glass-stoppered flasks, covered with plastic foil (to protect from carbon dioxide).

In solutions of the concentrations used, 96–99% of the absorption of light at 1849 Å was due to the HPO_4^{2-} ion. The methanol, water, acetone, H_2PO_4^- ion, and nitrous oxide absorbed about 0.8, 0.8, 0.6, 0.1–1.5, and 0.1–0.2% of the light, respectively. Formation of nitrogen by the direct photochemical decomposition of nitrous oxide (by absorption of the 2537-Å line of the lamp) could be shown to contribute

only 0.4% of the total quantum yield of nitrogen. The values of molar absorptivity at 1849 Å of phosphate mono- and dianion,^{2b} methanol,^{3h} acetone,¹⁰ and nitrous oxide^{6c} taken were 60, 420, 6.2, about 300, and 60 $M^{-1} \text{ cm}^{-1}$, respectively. Water has an absorption coefficient of 1.45 cm^{-1} at this wavelength.¹¹ The correction Q for hydrogen yield resulting from the direct photolysis of methanol and water is estimated to be 0.008.^{6b}

Acknowledgment. This investigation was supported in part by Research Grant GM-05842 from the U. S. Public Health Service.

(10) E. Kosower, *J. Am. Chem. Soc.*, **80**, 3261 (1958).

(11) M. Halmann and I. Platzner, *J. Phys. Chem.*, **70**, 580 (1966).

The Apparent Molal Volumes of the Alkali Metal Chlorides in Aqueous Solution and Evidence for Salt-Induced Structure Transitions

by Fred Vaslow

Chemistry Division, Oak Ridge National Laboratory,¹ Oak Ridge, Tennessee 37831 (Received January 31, 1966)

High-precision, closely spaced measurements have been made of the apparent molal volumes (densities) of aqueous solutions of the alkali metal chlorides at 25° from 0.02 to 3.5 m . Above 0.1 m it is found that the results for LiCl are represented within experimental error as a linear function of $c^{1/2}$ in two sections of different slope with a narrow transition region at about 1 N . For heavier salts the transition region becomes wider and the center moves to lower concentrations, the linear portions essentially disappearing for the RbCl curve. Comparing the volume curves with the behavior of the heat contents and viscosities of the solutions, it is concluded that the curve transitions actually do indicate some kind of physical transition of the solutions. It is tentatively suggested that the effect is due to a cooperative action of several ions on the solvent structure in the neighborhood of the ions.

Introduction

In connection with studies on thermal effects in ion-exchange resins, a number of graphs of literature values of the relative apparent molal heat contents of alkali metal halides and other salts were prepared. In many of the curves, where for convenience the independent variable had been taken as the log of the ratio moles of

water to moles of salt, it appeared as if in the neighborhood of 1 m there were substantial, possibly abrupt changes in the slope or form of the curves. At lower concentrations the curves more or less paralleled the con-

(1) Research sponsored by the U. S. Atomic Energy Commission under contract with the Union Carbide Corp.

centration axis but in the neighborhood of 1 *m* they turned upward or downward depending on the salt. The interionic interaction energy is presumably slowly varying in this concentration region, and the concentration is well below the region where one might expect hydration shell effects, and the concentration dependence was wrong for an ion-pairing effect. Consequently, there did not seem to be any reasonable or simple explanation for a change in character of the curves, and since no quantitative or objective description of the "effect" could be given, it seemed sensible to consider these "effects" as artifacts.

About the time of these observations several new concepts of liquid structure were introduced: the "significant structure theory" of Eyring,² the "statistical geometry" of Bernal,³ and the pentagonal tetrahedron suggested by Pauling⁴ as a basis for the structure of water. While different in purpose, a concept common to each of these theories was the idea of a "crystallite" or "pseudo nucleus" which contained a number of liquid molecules in some type of cluster large compared to what might be expected in the first hydration shell of an ion.

In particular, the type of cluster suggested by Pauling was a regular dodecahedron containing 20 water molecules. In the liquid there would probably be a small number of nonordered molecules associated with each of the dodecahedra so that perhaps a total of 25 molecules could be associated with each group which was about the ratio of water molecules to ions where the changes in the heat curve occurred. It has been pointed out⁵ that under certain conditions such groups need not be disrupted by the fields of neighboring ions and conceivably the effect might represent an interaction of the ions with an individual cluster of the Pauling or other type.

With this rather speculative possibility in mind, the apparent molal heat content data as well as literature data on other properties such as volumes and viscosities were closely examined to see whether serious consideration of an effect was in fact warranted. Of particular interest were the apparent molal volume curves for NaCl⁶ and NaBr^{6,7} which showed that both above and below a short region around 1 *N* the curves were very accurately linear functions of $c^{1/2}$ (c is the molar concentration).⁸ In a short region around 1 *N*, the proportionality constant for the square-root law changed from one definite value to another slightly different value.⁹

If there were an ideal physical situation where the true functional relationship between some property of the solution and the concentration were known and this relationship changed over a limited region to another

and different relationship, then some sort of complex, nonlinear process would have to occur. For example, a component or a particular type of site could be exhausted or a cooperative change of structure could occur, not involving a first-order phase change, however. The essential point is not that there is a sharp angle or even an abrupt change in the curves but that the curves go asymptotically from one accurately defined functional form to another different form in a limited region.

In a real experimental situation these considerations are still valid but the problem is to decide with any degree of assurance whether a given experimentally found relationship is physically significant and not simply a matter of inaccurate data or a fortuitous tangency over a limited range of the curve. In the case of the $c^{1/2}$ relationship for the apparent molal volume, this function has been found applicable to a great many solutions^{10,11} over wide concentration ranges. For some of the most accurately measured systems,^{6,7,12} on either side of the transition region and on a highly expanded scale, the data show no obvious nonrandom deviation from the square-root relationship over extended concentration ranges. The concentration regions where the slope changes occur appear to be the same regions originally observed for the changes of the heat content curves, and the centers of these transition regions can be accurately and unambiguously defined. It is tempting, therefore, to consider that this behavior might be of physical significance and should be tested using whatever criteria that may be applicable or available.

(2) H. Eyring, T. Ree, and N. Herai, *Proc. Natl. Acad. Sci. U. S.*, **44**, 683 (1958).

(3) J. D. Bernal, *Nature*, **185**, 68 (1960).

(4) L. Pauling, "The Nature of the Chemical Bond," 3rd ed, Cornell University Press, Ithaca, N. Y., 1960, p 472.

(5) F. Vaslow, *J. Phys. Chem.*, **67**, 2773 (1963).

(6) W. Geffken and D. Price, *Z. Physik. Chem.*, **B26**, 81 (1934), Figure 1.

(7) W. Geffken, A. Kruis, and L. Solana, *ibid.*, **B35**, 317 (1937), Figure 3.

(8) D. O. Masson, *Phil. Mag.*, [7] **8**, 218 (1929).

(9) It must be emphasized that only relatively high concentrations are being considered in this paper. At low concentrations the Debye-Hückel universal limiting laws for each property are approached and neither the high concentration square-root relationship nor a linear and a $c^{1/3}$ relationship used later in the paper are valid. While at low concentrations, the data presented here are completely consistent with the theoretical limiting law, the agreement has been considered in the sense of a sensitive test for the data rather than a new confirmation of the theory.

(10) H. S. Harned and B. B. Owen, "The Physical Chemistry of Electrolyte Solutions," 2nd ed, Reinhold Publishing Corp., New York, N. Y., 1950, p 253.

(11) W. Y. Wen and S. Saito, *J. Phys. Chem.*, **68**, 2639 (1964).

(12) A. Kruis, *Z. Physik. Chem.*, **134**, 1 (1936).

In the work presented here very accurate and closely spaced measurements of the apparent molal volumes (densities) of the alkali metal chlorides have been made in order to define the functional relationships as clearly as possible. Statistical criteria are applied in order to test the validity of a mathematical description of the curves in terms of two segments and a transition region, and finally comparisons are made of the volume curves with those of other properties.

It is at least tentatively concluded on the basis of the evidence presented that an effect or "transition" does occur. The transition occurs at different concentrations for different salts and hence is not indicative of any single type of solvent group. The degree of sharpness is found to be strongly dependent on the nature of the salt. A brief discussion is given of some possible interpretations of the effect although it is recognized that much more work in this area is necessary.

Experimental Section

The apparatus used was a differential hydrostatic balance very similar to that described by Redlich and Bigeleisen.¹³ Fused quartz bobs of 450-ml volume and mean density 1.2 were used with 0.002-in. tungsten wire suspensions. The small size of the support wires made corrections for changes in displacement or surface tension unnecessary; however, as with Pt wires a clean surface on the solution was essential. For rapid mixing of stock solution additions, identical motor-driven stirrers running in U tubes at the sides of the main containers were used. The system sensitivity was about two parts in 10^7 in relative density. The salts used were specially purified LiCl and KCl showing less than 0.03 and 0.01% by weight, respectively, of other alkalis and alkali earths by flame photometer analyses. All of the NaCl and the KCl used in run III were Harshaw single-crystal optical grade materials containing less than 10 ppm of other alkali metals and Ca. The RbCl and CsCl were from Penn Rare Chemical Co. and assayed about 99.9% by weight with the CsCl containing about 0.1% carbonate. The equivalent weights used were 42.40, 58.45, 74.55, 120.94, and 168.37 for LiCl, NaCl, KCl, RbCl, and CsCl, respectively. Water triply distilled from quartz was taken to have a density of 0.997071 g/ml at 25.000°. The temperature was controlled with a commercial regulator having drifts of a few thousandths of a degree per day which had no apparent effect on the runs.

At the start of a run the weights of the individual suspensions and bobs were obtained as well as the system zero with both bobs in pure water. After determining the zero point of the balance, accurately weighed portions of stock solution were added to one of the cham-

bers which contained about 850 ml of water known to about 0.1%. After each three or four additions of stock solution and the subsequent density measurements, a weight buret was used to withdraw and accurately weigh a sample of the solution for analysis. From the analyzed number of equivalents of salt added and removed and the measured concentrations, the exact amount of water in the system (to 0.01%) was calculated and used to interpolate concentrations between the analytical values.

All of the analyses for LiCl, RbCl, and CsCl were by differential potentiometric titration of Cl^- with AgNO_3 solution with a procedure similar to that used by Kunze and Fuoss.¹⁴ Standardization of the AgNO_3 was against stock solutions of NaCl or KCl. The stock solutions as well as some of the more concentrated experimental solutions of KCl and NaCl were analyzed by direct weighing of dried (at 400° for KCl and 500° for NaCl) residues of the solutions with a minimum salt weight of 2 g. All weights were reduced to *in vacuo* values. Depending somewhat on the size of the sample, standard deviations of the sets of titration analyses ranged from 0.005 to 0.015% with the gravimetric analyses generally differing by less than 0.01%. The deviations in absolute standardization of the AgNO_3 solutions from run to run were slightly larger than the average deviations within a run. Consequently, in a few runs small adjustments were made of the apparent AgNO_3 concentration in order to bring the data from different runs into better over-all coincidence. In the first run of this work NaCl-I the technique had not been fully developed and a slightly larger adjustment has been made. The adjustments to the AgNO_3 solutions normally about 0.13 mequiv/g of solution were multiplicative factors equal to 1.0005 for NaCl-I and a maximum of 1.0002 for any others. The effect of the adjustment is to change the concentration by a constant factor for each point of the particular run, lowering or raising the entire curve by a corresponding approximately constant amount. At least two independent runs were made for each salt with four runs for NaCl and three for KCl.

Errors were considered on the basis of the equation given by Redlich and Bigeleisen¹³

$$\delta\phi = -\frac{1000\delta d}{d^0c} + \frac{1000(d - d^0)\delta c}{c} \quad (1)$$

$\delta\phi$, δd , and δc are the uncertainties in volume, density, and concentration, respectively, d^0 is the density of pure water, and d is the solution density.

(13) O. Redlich and J. Bigeleisen, *J. Am. Chem. Soc.*, **64**, 758 (1942).

(14) R. W. Kunze and R. M. Fuoss, *J. Phys. Chem.*, **66**, 30 (1962).

Taking the chloride analyses as being accurate to $\pm 0.01\%$, i.e., $\delta c/c = 0.0001$, there is an uncertainty in volume of about 0.002, 0.003, 0.005, 0.010, and 0.015 for LiCl, NaCl, KCl, RbCl, and CsCl, respectively, with only a small dependence on concentration. The estimated error in the density measurements is based on an uncertainty of 0.1 mg on the balance which corresponds to about 0.002 ml at 0.1 *m*. Since this error decreases as $1/m$, above 0.1 *m* for all salts and for RbCl and CsCl at any concentration the errors are mainly due to concentration uncertainties. As shown in Table II of the Discussion, the error estimates shown here are consistent with statistical analyses of the data for LiCl, NaCl, and KCl solutions but apparently too large for RbCl and CsCl. Since the numbers of points for RbCl and CsCl are lower, the statistical significance is less; however, the results might also indicate that the estimated error of analysis is conservative.

Results

The experimental results are shown graphically in Figure 1 where the theoretical limiting law, $\phi = \bar{V}_2^0 + 1.86\sqrt{c}$,¹⁵ has been subtracted from the data. This subtraction allows a somewhat larger scale to be used than would be otherwise possible.

The values of \bar{V}_2^0 were obtained by fitting the equation, $\phi = \bar{V}_2^0 + 1.86\sqrt{c} + Bc$,¹⁶ to the data up to 0.1 *N* using a computer least-squares program to determine the parameters \bar{V}_2^0 and *B*. Points below 0.1 *N* were weighted according to the formula $W = 10N$. The values of \bar{V}_2^0 obtained are 16.991 ± 0.01 , 16.628 ± 0.006 , 26.886 ± 0.01 , 31.94 ± 0.03 , and 39.15 ± 0.05 ml for LiCl, NaCl, KCl, RbCl, and CsCl, respectively. The errors given are based primarily on an estimated uncertainty in the absolute concentration which determines a larger error than that corresponding to statistical variations. No corrections have been made for impurities in the salts.

Also shown in Figure 1 are points from previous work for KCl and NaCl. With the exception of the points for KCl at low concentration, the agreement seems generally very good. The differences for KCl are larger than the expected errors, however, and run KCl-III was done as a check on the first two runs using an independent sample of high-purity KCl and a slightly different procedure. The new results were within experimental error of the first two runs.

The approach of the curves to the limiting law should be a sensitive test of the quality of the data at low concentrations and the present data are completely consistent with this law. At the same time, the agreement at higher concentrations suggests that the ana-

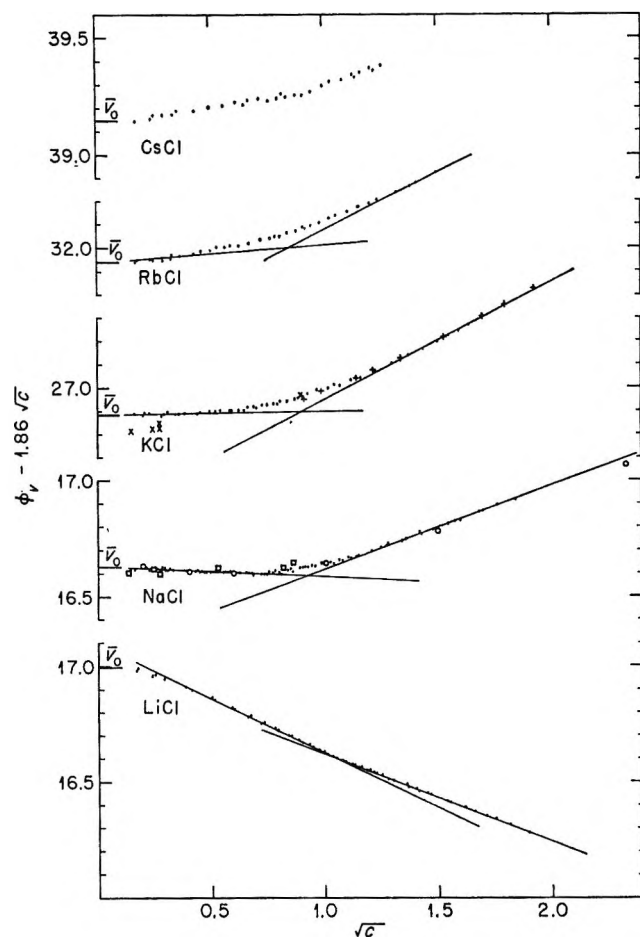


Figure 1. Apparent molal volumes of alkali metal chlorides with limiting law subtracted from experimental points: \square , Kruis,¹² magnetic float; \circ , Wirth;¹⁵ \times , Geffken and Price,⁶ magnetic float; $+$, Kruis,¹² dilatometer.

lytical procedures are accurate and consequently it is difficult to account for the discrepancy.

An accurate summary¹⁷ of the data is contained in Table I, where the points have been read from very large-scale plots of all of the original data using spline-drawn smooth curves. For a more detailed examination of the original data, Table II gives one complete run for LiCl showing molality, apparent volume, and the change in density from that of pure water.

Discussion

The principal purpose of these experiments has been to examine as critically as possible the validity of the description of the volume curves in terms of two dif-

(15) H. E. Wirth, *J. Am. Chem. Soc.*, **62**, 1129 (1940), Figure 1.

(16) O. Redlich and D. M. Meyer, *Chem. Rev.*, **64**, 221 (1964).

(17) The complete original data are available in Oak Ridge National Laboratory Report TM-1438.

Table I: The Apparent Molal Volumes of the Alkali Metal Chlorides in Aqueous Solution at 25.00° (ml/mole)

<i>m</i>	LiCl	NaCl	KCl	RbCl	CsCl
0	16.991	16.628	26.886	31.94	39.15
0.05	17.386	17.032	27.310	32.355	39.578
0.1	17.525	17.210	27.480	32.549	39.760
0.2	17.715	17.437	27.723	32.810	40.018
0.3	17.856	17.579	27.912	33.000	40.220
0.4	17.972	17.775	28.075	33.175	40.385
0.5	18.074	17.909	28.221	33.323	40.525
0.6	18.167	18.038	28.357	33.465	40.655
0.7	18.252	18.158	28.482	33.595	40.778
0.8	18.331	18.271	28.601	33.713	40.887
0.9	18.406	18.380	28.711	33.826	40.996
1.0	18.476	18.433	28.820	33.935	41.105
1.2	18.606	18.670	29.015	34.135	41.306
1.4	18.731	18.854	29.195	34.321	41.475
1.6	18.846	19.024	29.374	34.492	41.642
1.8	18.953	19.186	29.532	34.646	
2.0	19.055	19.336	29.688	34.000	
2.5	19.288	19.674	30.038		
3.0	19.495	19.990			
3.5	19.677	20.267			
	(3.8375 <i>m</i>)	(3.6602 <i>m</i>)	(2.9343 <i>m</i>)	(2.4487 <i>m</i>)	(1.6977 <i>m</i>)
	19.788	20.353	30.322	35.115	41.722

Table II: Apparent Molal Volumes and Change in Densities of LiCl Solutions

<i>m</i>	1000Δ <i>D</i>	φ _v , ml/mole
0.028513	0.7146	17.297
0.056754	1.4156	17.403
0.084772	2.1064	17.488
0.16984	4.1843	17.665
0.26432	6.4643	17.806
0.35556	8.6415	17.920
0.44371	10.7247	18.016
0.52891	12.7204	18.099
0.62177	14.8758	18.185
0.71126	16.9359	18.260
0.79758	18.9074	18.329
0.88090	20.7956	18.392
0.96825	22.7623	18.453
1.0524	24.6428	18.511
1.1335	26.4432	18.564
1.2118	28.1671	18.614
1.2938	29.9608	18.667
1.3727	31.6772	18.714
1.4488	33.3213	18.760
1.5222	34.8964	18.803
1.6908	38.4863	18.895
1.9129	43.1389	19.014
2.0467	45.9043	19.082
2.1974	49.0027	19.150
2.5119	55.3356	19.292
2.9179	63.3078	19.462
3.2687	70.0109	19.601

ferent function segments and a transition region connecting the segments. If this description is valid and is consistent with other physical properties, then it is presumed that the transition represents a physically significant and interesting property of the solution.

Examining the curves of Figure 1 it is seen that above about 0.1 *N* ($c^{1/2} = 0.4$) the description for LiCl solutions is a very good one. For the heavier salts the width of the transition region increases until for RbCl most of the curve is transition and the description is not applicable. Comparing these curves with those for some other salt solutions where reasonable data are available and the above behavior seems clear, the NaBr curve⁶ appears to have a slightly sharper transition at a slightly higher concentration than NaCl. In the tetraalkylammonium bromides measured by Wen and Saito,¹¹ a sequence similar to that of the alkali chlorides is present in that the sharpness of the slope change (not the minimum in the curve) increases on going from the tetramethyl to the tetrapropyl salt. The tetrabutyl salt shows a slight dip just before the minimum and may indicate that the transition has been hidden by the minimum. It is of interest that the sequence of increasing sharpness of the transition parallels the sequence of increasing solvent ordering for both the alkali metal salts and the tetraalkylammonium salts.¹⁸⁻²¹

Returning to the alkali chlorides, it is desirable, insofar as possible, to test mathematically the validity of the segmental concept of the curves. For this purpose an explicit description of the curves in terms of two slopes and a transition is derived and fitted to the data and this is compared with polynomials in $c^{1/2}$ (*i.e.*, $\phi = A + Bc^{1/2} + Cc + Dc^{3/2} \dots$) or from three to six parameters fitted to the data by a computer least-squares procedure. The Gauss criterion²² is used to establish a statistically justifiable number of parameters and accuracy of fit (*i.e.*, standard deviation) of the equations.

The explicit description of the curves requires two slopes, a zero intercept, an intersection point, and a parameter describing the relative sharpness of the transition. The transition itself can be described through the use of a function which rises from 0 to 1 in the appropriate region. The simplest function having this property and being a type common in chemical equilibrium expressions is of the form

$$f(c^{1/2}) = \frac{(c^{1/2})^n}{K^n + (c^{1/2})^n} \quad (2)$$

K is very nearly the intersection point of the two slopes and n a parameter governing the width of the region. The parameter n has arbitrarily been limited to even integers. The slopes of the volume curves are then given by the expression

$$\frac{d\phi}{dc^{1/2}} = S_1 + \frac{S_2(c^{1/2})^n}{K^n + (c^{1/2})^n} \quad (3)$$

where S_1 is the initial slope and S_2 is the slope increment. The volume is given by

$$\phi = \phi^0 + S_1c^{1/2} + S_2 \int_0^{c^{1/2}} \frac{(c^{1/2})^n dc^{1/2}}{K^n + (c^{1/2})^n} \quad (4)$$

where ϕ^0 is a constant of integration not equal to \bar{V}_2^0 .

Although the integral can be explicitly written, the expression is complicated for $n > 2$ and it is simpler to evaluate the integral at each concentration by a computer calculation. For values of $c^{1/2}$ sufficiently far from the transition, the function is either 0 or 1 and ϕ can be directly calculated using ϕ^0 , S_1 , S_2 , and K in a simple linear form. Above the lowest concentrations, the maximum deviation of two straight lines from the experimental points is about 0.04 ml for NaCl and 0.004 ml for LiCl.

Initial parameters for eq 4 were obtained directly from the curves and these parameters refined by comparing the computed and experimental values of ϕ . Since no explicit minimizing of the mean-square deviation was done, some increase in this quantity over that

obtained from the power series expressions can be expected. The values of the standard deviations and Gauss criteria for the polynomials and eq 4 are shown in Table III. Only points above 0.1 N were used and eq 4 was not applied to the RbCl and CsCl data.

Table III: Gauss Criterion and Standard Deviations

Salt		No. of parameters				
		3	4	5	6	Eq 4
LiCl	$\Omega \times 10^6$	14.4	13.4	4.2	4.3	4.4
	$\sigma \times 10^3$	3.7	3.5	1.9	1.9	2.0
NaCl	Ω	44.2	15.5	10.2	7.7	8.4
	σ	6.5	3.8	3.1	2.7	2.8
KCl	Ω	23.8	24.1	21.5	21.0	22.8
	σ	4.7	4.7	4.4	4.2	4.5
RbCl	Ω	4.7	4.5	4.2	4.1	
CsCl	σ	9.6	7.1	6.9	6.6	

The differences of points computed with eq 4 from the experimental values are shown in Figure 2 on a scale expanded on the original drawing approximately fifteen times that of Figure 1, along with the parameters used. The computed curves are almost indistinguishable from the points of Figure 1 on the scale of this figure.

Returning to Table III, it is seen that five parameters are justified for the LiCl curve and five or six for NaCl. The differences of the standard deviations of eq 4 from those of the five- or six-parameter power series are statistically insignificant and it can be concluded that eq 4 also represents the data within experimental error. While eq 4 cannot be justified for KCl, consistency with the LiCl and NaCl curves might justify its use.

It has not been possible to show that eq 4 has any more than a marginal statistical preference over five-parameter polynomials and the question is: does the comparison support the segment concept? In this

(18) R. W. Gurney, "Ionic Processes in Solution," Dover Publications Inc., New York, N. Y., 1962, p 258.

(19) H. Yamatera, B. Fitzpatrick, and G. Gordon, *J. Mol. Spectry.*, 14, 268 (1964).

(20) S. Lindenbaum and G. E. Boyd, *J. Phys. Chem.*, 68, 911 (1964).

(21) S. Lindenbaum, *ibid.*, 70, 814 (1966).

(22) A. G. Worthing and J. Geffner, "Treatment of Experimental Data," John Wiley and Sons, Inc., New York, N. Y., 1943, p 260. The Gauss criterion Ω is defined as

$$\Omega = \frac{\sum(y_0 - y)^2}{n - m}$$

where $y_0 - y$ is the difference of calculated and experimental values, n is the number of points, and m is the number of variable parameters. The function is minimized for the statistically justifiable number of parameters.

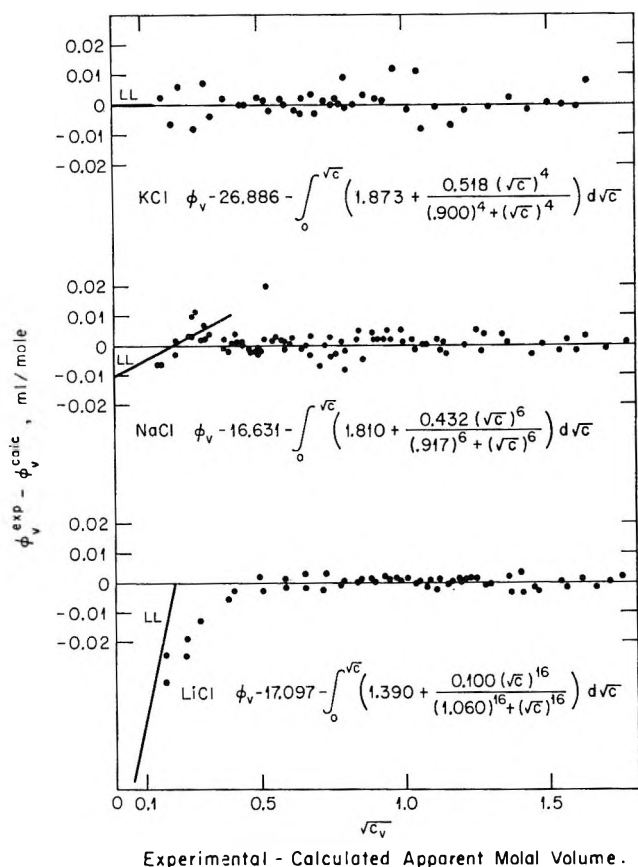


Figure 2. Deviations of apparent molal volumes from eq 4.

respect the justification of five or six parameters in itself requires data of a very high accuracy and polynomials of this complexity can accurately represent very involved curves. The conclusion that can be made under the circumstances is that eq 4 does represent the data within experimental accuracy and no simpler polynomial has been found which can equal this accuracy.

If the transition observed in the volume curves does correspond to a real physical transition of the solution, then it should be observable in properties other than the volume. The presumed transition is small and diffuse, however, and detection is difficult unless it is possible to establish with some confidence that the property does obey a simple physical law. The criteria for the law are, for lack of a definitive theory, exactness and extent of fit, requiring again accurate, closely spaced data for the test.

For two properties of LiCl and NaCl solutions, the relative apparent molal heat content²³⁻²⁵ and the relative viscosity,²⁶⁻³⁰ reasonable data are available at moderate-to-high concentrations. Also, in some concentration regions it is empirically found that the

relative viscosity is linear in c and the heat content linear in $c^{1/3}$. Although these rules do not have a rigorous theoretical foundation, the linear relationship may be related to the Einstein viscosity law and the $c^{1/3}$ relationship corresponds to the energy behavior of a regular ionic lattice and hence they are not wholly arbitrary functions. In order to show clearly the nature of the agreement of these functions with experiment, relative to the deviations, differences of experimental and calculated points are determined and plotted on a substantially enlarged scale. Parameters of the appropriate equation are obtained by a visual fit to the data and then used to calculate values of the property for each point.

Figure 3 shows the LiCl heat curve, Figure 4 shows the NaCl heat curve, and Figure 5 shows both viscosity curves. The parameters are given in the figures and the arrows show the values of K obtained from the volume measurements. It is seen that in each of these curves as well as in the curve showing the slope of the apparent molal heat capacity given by Young and Machin³¹ there is a strong deviation of the data from the simple function as the transition region is approached. Anticipating the Conclusions section, the reason that NaCl heat contents do not follow the $c^{1/3}$ law below 1 N as does LiCl may be in a relative instability of the solvent structure in the neighborhood of the Na^+ ion.

The volume and other properties can be plotted as functions of other variables, *i.e.*, m or $m^{1/3}$, rather than those used and in each case the graphs are curved with no apparent straight portion. The transition region can still be observed and hence is not an artifact of the equation or method of plotting. However, the appearance of the transition is that of a small change in curvature in the total curve. It is much less obvious and the observation is much more critically dependent on having accurate and closely spaced data.

The existence of elementary relationships which do not show the transition property cannot be excluded

- (23) E. Lange and F. Dürr, *Z. Physik. Chem.*, **121**, 361 (1926).
 (24) S. G. Lipsett, F. M. G. Johnson, and O. Maass, *J. Am. Chem. Soc.*, **50**, 2701 (1928).
 (25) J. Wust and E. Lange, *Z. Physik. Chem.*, **116**, 161 (1925).
 (26) V. D. Laurence and J. H. Wolfenden, *J. Chem. Soc.*, 1144 (1934).
 (27) L. Nickels and A. J. Allmand, *J. Phys. Chem.*, **41**, 861 (1937).
 (28) G. Jones and S. M. Christian, *J. Am. Chem. Soc.*, **59**, 484 (1937).
 (29) C. E. Ruby and F. Kawai, *ibid.*, **48**, 1119 (1926).
 (30) A. Chambers, Thesis data in R. H. Stokes and R. Mills, "Viscosity of Electrolytes and Related Properties," Pergamon Press, Ltd., Oxford, 1965, p 118.
 (31) T. F. Young and J. S. Machin, *J. Am. Chem. Soc.*, **58**, 224 (1936).

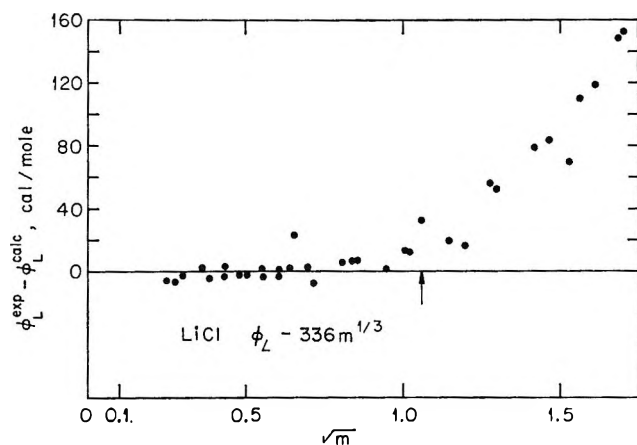


Figure 3. Deviations of the relative apparent molal heat content of LiCl from $m^{1/3}$ law; data from Lange and Dürr.²³

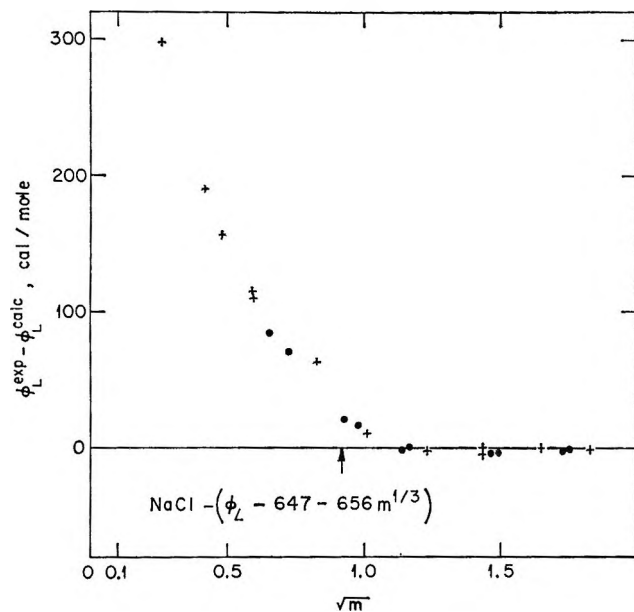


Figure 4. Deviations of the relative apparent molal heat content of NaCl from $m^{1/3}$ law: +, Lipsett, Johnson, and Maass;²⁴ ●, Wust and Lange.²⁵

nor can it be proven that the relationships used are physically significant. The significance would appear to be in that, for each of these properties where it has been possible to find an elementary functional relationship, the data deviate sharply on approaching the transition region. In no case has it been possible to find such a relationship valid across the transition region.

Conclusions

Accepting at least tentatively that a transition does take place over a limited concentration range, some consideration can be given to possible causes of the

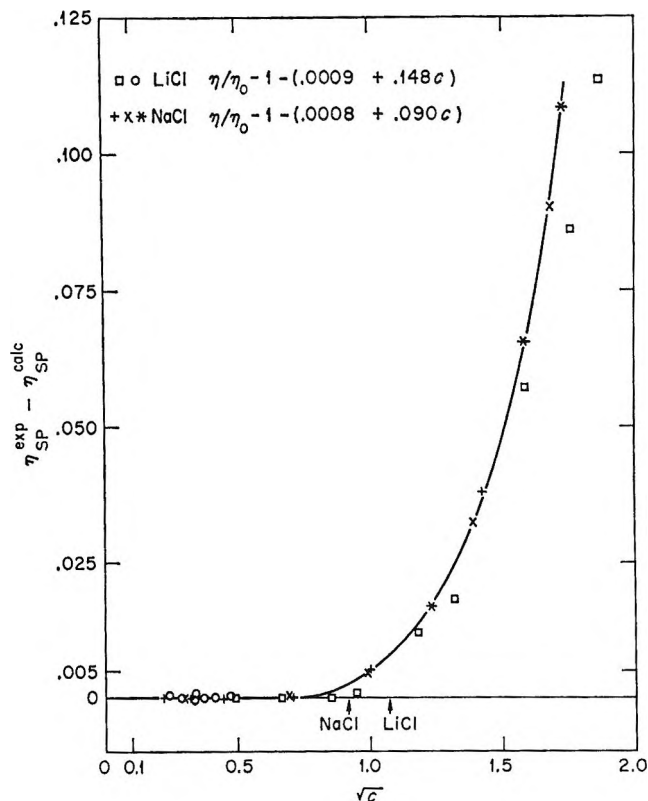


Figure 5. Deviations of the specific viscosities of LiCl and NaCl from a linear function of c : O, Laurence and Wolfenden;²⁶ □, Nickels and Allmand;²⁷ +, Jones and Christian;²⁸ ×, Ruby and Kawai;²⁹ *, Chambers.³⁰

effect. The evidence is limited and the discussion highly speculative; however, a few remarks can be made.

The original incentive for this work was provided by the idea that the transitions in the curves might indicate the existence of a specific type of structure group in water. If the concentration at the intersection of the lines is taken as determining the size of the group, then apparently there is no obvious fixed group since the intersection point varies from 0.81 (K^2) in KCl to 1.14 in LiCl and about 0.5 in tetrapropylammonium bromide. The results are not inconsistent with theories proposing varying cluster sizes such as those of Némethy and Scheraga³² or Luck.³³

An explanation of the results involving a filling up of one type of site for the ions and the initiation of a different type at the transition would also appear to be ruled out. In order to obtain a sharp segregation into the different sites such as evidenced by the sharp

(32) G. Némethy and H. A. Scheraga, *J. Chem. Phys.*, **36**, 3382 (1962).

(33) W. Luck, *Ber. Bunsenges., Physik. Chem.*, **69**, 626 (1965).

change of slope in the LiCl solutions, a large difference in the partial molal free energy per site would be necessary and this is not seen in the activity coefficient curve of LiCl. A similar argument would apply against any simple hydration shell picture based on the idea that the transition occurred when all of the water molecules were already in hydration shells and new ions had to penetrate these shells.

In order to obtain a narrow transition region without a large partial molal free energy change, a cooperative effect among the ions appears necessary and this would seem borne out by the relatively high powers of the concentration found for eq 4. Whatever the nature of the solvent structure around an individual ion, as groups of ions approach one another, this structure is cooperatively changed. Those ions which initially had the most stable or ordered solvent structures in their neighborhood would require the largest number of cooperating ions to transform the structure. Ions with unstable neighboring solvent structures would

show the most diffuse effect starting at the lowest concentrations.

It has been previously suggested by Samoilov³⁴ and by the author⁵ that in a dilute solution the organization of solvent molecules in the neighborhood of an ion is largely determined by the normal water structure. Samoilov continues that in concentrated solutions the organization is determined by the combined ionic fields. The effects studied here might therefore be interpreted as a transition between the dilute and concentrated solution types of solvent organization.

Acknowledgment. The author is indebted to Mr. R. B. Quincy and Mr. D. E. Lavalley for preparation of some of the purified salts used and to Dr. T. F. Young for critical reviews and discussions of the manuscript.

(34) O. Ya. Samoilov, "The Structure of Aqueous Solutions and the Hydration of Ions," English Translation, Consultants Bureau, New York, N. Y., 1965, p 134.

Thermodynamic Properties in the Exchange of Silver with Sodium Ions in Cross-Linked Polystyrene Sulfonate Cation Exchangers¹

by F. Vaslow and G. E. Boyd

Oak Ridge National Laboratory, Oak Ridge, Tennessee 37831 (Received February 9, 1966)

Standard free energy and enthalpy changes, ΔG° and ΔH° , respectively, for the exchange reaction of silver ion in dilute aqueous solutions with sodium ion in a series of cross-linked polystyrenesulfonic acid type cation exchangers were estimated from equilibrium selectivity coefficient and heat of exchange measurements at 25°. The standard entropy changes, ΔS° , derived from ΔG° and ΔH° , showed that the selective uptake of Ag^+ ion was accompanied by an entropy increase. The ΔH° values were either small or zero except with the most highly cross-linked exchanger; the magnitude of the decrease in ΔG° therefore was governed by the magnitude of $T\Delta S^\circ$. The unusual behavior of silver ion, in contrast with other singly charged cations where ΔG° is governed by the enthalpy decrease, was explained in terms of "site-binding" of Ag^+ by the sulfonate groups of the exchanger. The strongly selective uptake of trace quantities of silver was attributed to a charge-transfer interaction of Ag^+ ion with the benzene groups in the exchanger.

Silver ions in dilute aqueous solution are known to differ significantly from the alkali metal cations in their ion-exchange reactions with strong-acid type cation exchangers. Thus, the selective uptake of Ag^+ in its exchange reactions with Na^+ ion is appreciably larger than expected either on the basis of the ionic (crystal) radii or on the basis of the effective radii of the two hydrated ions which are nearly the same.^{2a} The similarity of these two cations in aqueous solution is reflected also by their hydration entropies, which have been estimated as -15.8 and -14.5 eu for gaseous Ag^+ and Na^+ , respectively.^{2b} The free energies of hydration for the same ions are -106 and -91.5 kcal mole⁻¹, respectively, so that if ion-exchange selectivity is obtained because of more complete cation hydration³ in the dilute external solution than in the resin phase, sodium should have been the preferred ion. However, several types of measurements suggest that ion-water interactions by themselves do not determine the ion-exchange behavior of Ag^+ ion. (a) The small osmotic coefficients of very lightly cross-linked silver polystyrene sulfonate⁴ relative to the coefficients for salts with other cations show that Ag^+ ion interacts strongly with the sulfonate group. (b) The relatively large penetration (Donnan invasion) of the silver forms of cross-linked

cation exchangers by anions from an external aqueous solution⁵ requires that Ag^+ ion be extensively associated. (c) The electric conductivities⁶ and self-diffusion coefficients⁷ for singly charged ions in cross-linked sulfonic acid exchangers have shown that the mobility of silver is much less than that of sodium ion, whereas in aqueous solutions the situation is reversed, thus indicating strong binding of argentous ion in the exchanger.

A distinctive feature in the behavior of silver ion compared with other singly charged cations is its strongly preferred uptake, especially by highly cross-linked sulfonic acid exchangers, when it is present in trace concentrations in aqueous solutions. The results of several ob-

(1) Research sponsored by the U. S. Atomic Energy Commission under contract with the Union Carbide Corp.

(2) (a) E. R. Nightingale, Jr., *J. Phys. Chem.*, **63**, 1381 (1959); (b) W. M. Latimer, *J. Chem. Phys.*, **23**, 90 (1955).

(3) D. C. Whitney and R. M. Diamond, *Inorg. Chem.*, **2**, 1284 (1963).

(4) B. A. Soldano and Q. V. Larson, *J. Am. Chem. Soc.*, **77**, 1331 (1955).

(5) J. F. Duncan, *Proc. Roy. Soc. (London)*, **A214**, 344 (1952).

(6) E. Heymann and I. J. O'Donnell, *J. Colloid Sci.*, **4**, 405 (1949).

(7) G. E. Boyd and B. A. Soldano, *J. Am. Chem. Soc.*, **75**, 6091 (1953).

servers⁸⁻¹¹ are in agreement on this effect, for which as yet no explanation has been given.

The calorimetric and equilibrium selectivity coefficient measurements reported in this paper were undertaken to determine if information on the heat and entropy of the exchange of silver ion would aid in the elucidation of the nature of its binding by cation exchangers. The preferential uptake of the alkali metal cations has been found to be accompanied by the evolution of heat and by a decrease in entropy.^{12,13} This result has been interpreted¹³ as indicating that the binding of these cations was nonspecific (*i.e.*, ion atmosphere binding) and that ion-pair formation (*i.e.*, site binding) in the sense that the cation and the anionic exchanger group possessed a definite structure involving one or more water molecules probably did not occur. During the course of our work, Redinha and Kitchener¹⁴ published a calorimetric study on the silver-sodium and silver-hydrogen ion-exchange reaction in several cross-linked polystyrenesulfonic acid exchangers. However, their work on the former system was much less extensive than ours, and the interpretation given below differs in several respects.

Experimental Section

The calorimeter was the same as in our measurements¹⁵ of the heats of exchange of the halide ions in variously cross-linked strong-base anion exchangers, except for the temperature-sensing element which was changed from a 36-junction copper-constantan thermocouple to a pair of 2000-ohm thermistors connected to the opposite sides of a bridge circuit. A highly stable sensitivity of about 15 μ deg was realized with the thermistors, which compares favorably with that observed with the multijunction thermocouple. The over-all reliability of the calorimeter system was checked by measurements of the heat of solution of NaCl(c) and of the heats of dilution of HCl solutions of accurately known concentrations. Excellent agreement with literature values was obtained.

Strong-acid cation exchangers of the Dowex-50 type (polystyrenesulfonic acid) nominally cross linked with 1, 4, 8, 16, and 24% divinylbenzene (DVB) and with exchange capacities of 5.18, 5.24, 5.06, 4.73, and 4.64 mequiv/g of dry HR, respectively, were employed. Selectivity coefficients, $D_{Na^+}^{Ag^+}$, for the uptake of Ag^+ by the sodium form of the exchangers were measured at 25° with aqueous $NaNO_3$ - $AgNO_3$ mixtures at a constant ionic strength of 0.1 M. The distribution of silver ion between the exchanger and the equilibrium aqueous electrolyte mixture was measured with 270-day ¹¹⁰Ag and 15-hr ²⁴Na tracers. The variation of $D_{Na^+}^{Ag^+}$, with the equivalent fraction of the preferred Ag^+ ion in the exchanger, x_{Ag^+} , is shown in Figure 1.

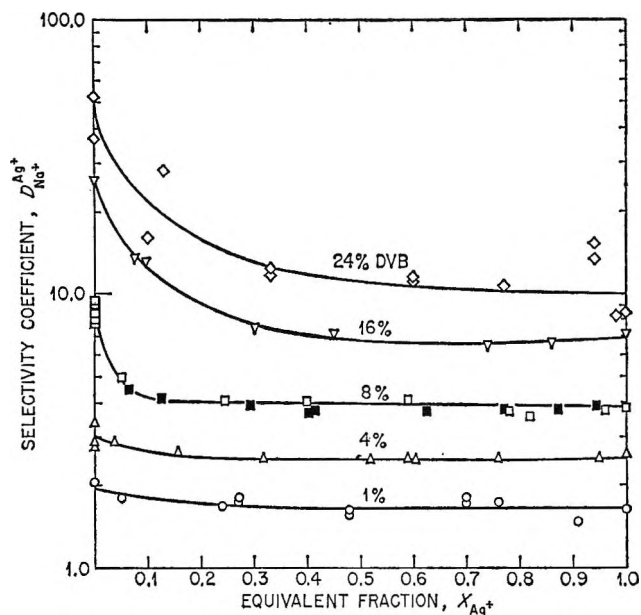


Figure 1. Selectivity coefficients for the silver-sodium ion exchange at 25° with variously cross-linked Dowex-50. (Data for filled symbols taken from ref. 9.)

Results and Discussion

Certain general features of the dependence of the selectivity coefficients (Figure 1) and of the differential heats of exchange (Figure 2) on the cross linking and ionic composition of the cation exchangers may be noted. The selectivity coefficients showed a regular increase with cross linking and were nearly independent of the equivalent fraction of silver, x_{Ag^+} , in the exchanger except for a marked increase in the uptake of Ag^+ by the most highly cross-linked exchangers below $x_{Ag^+} = 0.1$ to 0.2. There were no selectivity coefficient cross-overs or inversions in contrast, for example, with the K^+ - Na^+ and Cs^+ - Na^+ ion-exchange systems¹⁶ and many others. The measurements on the 8% DVB exchanger were in

(8) (a) E. Högfeldt, E. Ekedahl, and L. G. Sillén, *Acta Chem. Scand.*, **4**, 1471 (1950); (b) E. Högfeldt, *ibid.*, **6**, 610 (1952); (c) E. Högfeldt, *ibid.*, **7**, 561 (1954).

(9) G. E. Boyd, B. A. Soldano, and O. D. Bonner, *J. Phys. Chem.*, **58**, 456 (1954).

(10) G. E. Wilson, A. W. Davidson, and W. J. Argersinger, Jr., *J. Am. Chem. Soc.*, **76**, 3824 (1954).

(11) (a) O. D. Bonner and V. Rhett, *J. Phys. Chem.*, **57**, 254 (1953); (b) O. D. Bonner and W. H. Payne, *ibid.*, **58**, 183 (1954); (c) O. D. Bonner, *ibid.*, **58**, 318 (1954).

(12) E. H. Cruickshank and P. Meares, *Trans. Faraday Soc.*, **53**, 1289 (1957).

(13) G. E. Boyd, F. Vaslow, and S. Lindenbaum, *J. Phys. Chem.*, **68**, 590 (1964).

(14) J. S. Redinha and J. A. Kitchener, *Trans. Faraday Soc.*, **59**, 575 (1963).

(15) F. Vaslow and G. E. Boyd, *J. Phys. Chem.*, in press.

(16) G. E. Myers and G. E. Boyd, *ibid.*, **60**, 521 (1956).

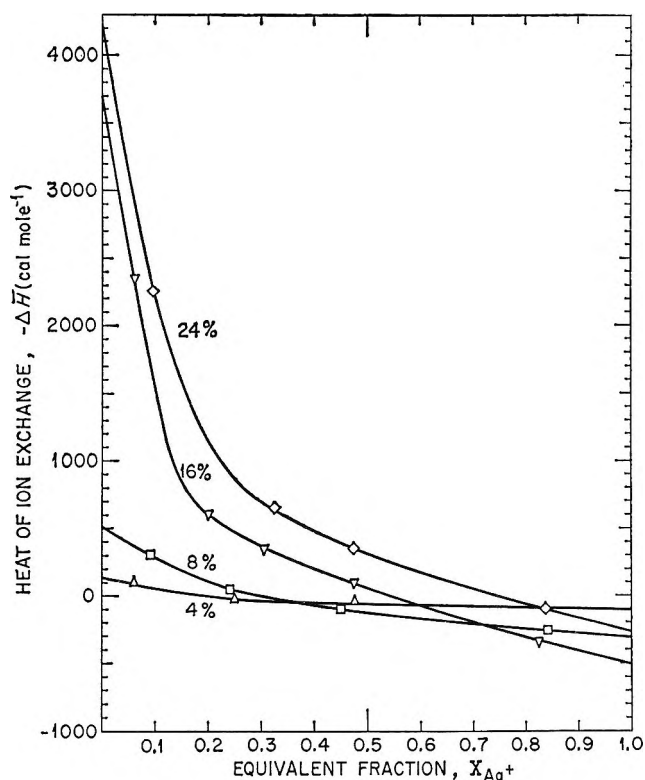


Figure 2. Differential heats of exchange at 25° of silver with sodium ions in variously cross-linked Dowex-50.

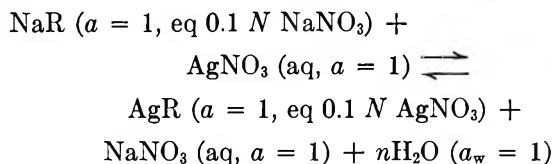
excellent agreement with previous determinations⁹ in the composition range $0.06 < x_{\text{Ag}^+} < 0.95$. The more extensive measurements made in this research for $x_{\text{Ag}^+} < 0.06$, however, revealed a nearly twofold increase in the selectivity coefficient as the amount of silver in the exchanger approached zero. The $D_{\text{Na}^+}^{\text{Ag}^+}$ values for the nominal 16% DVB also are in good agreement with other measurements^{11c} on the same preparation. The relatively large selectivity coefficients exhibited by the nominal 1% DVB cross-linked preparation are consistent with the view that Ag^+ ion is one of the most strongly bound of all the singly charged cations formed by the group I elements.

The dependence of the heats of exchange (Figure 2) on cross linking and exchanger composition contrasts with the behavior of the equilibrium selectivity coefficients already noted. For high cross linking and small silver ion loadings, the reaction was strongly exothermic. However, over most of the composition range except for the nominal 24% DVB preparation it was weakly endothermic. In the nominal 1% DVB cross-linked preparation the exchange reaction was athermal within the experimental error.

Integral heats of exchange, defined by

$$\Delta H = \int_0^1 (\partial \Delta H / \partial x_{\text{Ag}^+}) dx_{\text{Ag}^+}$$

were estimated by graphical integrations (Figure 2). Standard heats of cation exchange, ΔH° , for the hypothetical reaction



were derived by correcting the integral heats by the difference in the relative apparent molal heat contents, ϕ_L , of the two 0.1 N aqueous solutions

$$\Delta H^\circ = \Delta H - \Delta \phi_L$$

A value of $\Delta \phi_L = \phi_L(\text{NaNO}_3) - \phi_L(\text{AgNO}_3) = 56 \text{ cal mole}^{-1}$ at 25° was estimated with data taken from a recent compilation.¹⁷

Standard free energies, ΔG° , were computed from the data in Figure 1 with the formula

$$-\Delta G^\circ = 2.303RT \int_0^1 \log D_0 dx_{\text{Ag}^+}$$

where D_0 is the experimentally measured equilibrium selectivity coefficient corrected for aqueous electrolyte solution activity coefficients. The required values for this correction, $\gamma_{\pm}^2(\text{NaNO}_3)/\gamma_{\pm}^2(\text{AgNO}_3)$, which did not exceed 3%, were derived for an ionic strength of $\mu = 0.1$ following Robinson and Stokes.¹⁸

Standard-state thermodynamic quantities for the exchange of Ag^+ with Na^+ ion in variously cross-linked polystyrene sulfonates are given in Table I. The data in the table show that the selective uptake of silver ion was governed by the entropy increase in its ion-exchange reaction. The standard heat was small and was either positive (*i.e.*, heat absorbed) or negative or zero, whereas ΔS° became progressively more positive with increasing exchanger cross linking. The heat and free energy measurements of Redinha and Kitchener¹⁴ on nominal 4.5 and 8% DVB cross-linked polystyrene sulfonates gave standard entropy increases of 1.8 and 2.6 eu, respectively. A value of 3.5 eu may be derived from their results with a 16% DVB exchanger. All of these values agree reasonably well with corresponding entries in Table I. Interestingly, the measurements by these authors also show that ΔS° for the silver-hydrogen ion exchange is much less positive than for the exchange with sodium ion and that the selective uptake of silver ion was determined by the enthalpy decrease.

(17) V. B. Parker, "Thermal Properties of Aqueous Uni-univalent Electrolytes," National Standard Reference Data Series, National Bureau of Standards, NSRDS-NBS 2, Washington, D. C., 1965.

(18) R. A. Robinson and R. H. Stokes, "Electrolyte Solutions," Butterworth and Co. Ltd., London, 1955, p 440.

Table I: Standard Free Energies, Heats, and Entropies of Exchange at 298.2° of Silver with Sodium Ion in Various Cross-Linked Polystyrene Sulfonates

Nominal cross linking, % DVB	$-\Delta G^\circ$, kcal mole ⁻¹	$-\Delta H^\circ$, kcal mole ⁻¹	ΔS° , cal deg ⁻¹ mole ⁻¹
1	0.30	0.00	1.0
4	0.56	-0.04	2.0
8	0.83	-0.11	3.1
16	1.23	0.12	3.7
24	1.47	0.34	3.8

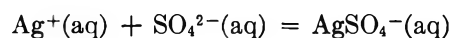
Our results with the nominal 8% DVB exchanger (Table I) have been combined with the ΔG° , ΔH° , and ΔS° values reported earlier¹³ on the same exchanger to give additional thermodynamic quantities for the exchange of Ag^+ with H^+ , Li^+ , K^+ , and Cs^+ ions (Table II). These results show that the selective uptake of silver ion in exchange reactions with strongly hydrated cations (*i.e.*, Li^+ , H^+) is governed by the enthalpy decrease, while with weakly hydrated cations (*i.e.*, Cs^+) the entropy increase is the determinant. The small, slightly negative ΔS° in the exchange of Ag^+ for Li^+ ion suggests that the partial dehydration of silver ion on entering the exchanger was compensated by the more complete hydration of lithium ion when the latter is displaced into the dilute aqueous electrolyte phase. In the exchange of Ag^+ with Cs^+ ion probably only a small, negative entropy change is associated with the displacement of the latter ion into the aqueous phase, so that most of the entropy increase (Table II) can be assigned to the dehydration of Ag^+ as it enters the exchanger and interacts with the sulfonate exchange groups. The net absorption of heat accompanying the silver-cesium ion exchange possibly mirrors the energy to dehydrate Ag^+ ion, while the net heat evolution in the exchange with Li^+ is a consequence of the relatively large energy release when the latter ion becomes fully hydrated.

Table II: Thermodynamic Quantities in the Exchange of Silver Ion with Other Singly Charged Cations in a Nominal 8% DVB Cross-Linked Polystyrene Sulfonate

Exchange system	$-\Delta G^\circ$, kcal mole ⁻¹	$-\Delta H^\circ$, kcal mole ⁻¹	ΔS° , eu
$\text{Ag}^+ - \text{Li}^+$	1.19	1.35	-0.5
$\text{Ag}^+ - \text{H}^+$	1.06	1.07	0.1
$\text{Ag}^+ - \text{Na}^+$	0.83	-0.11	3.1
$\text{Ag}^+ - \text{K}^+$	0.58	-0.66	4.1
$\text{Ag}^+ - \text{Cs}^+$	0.51	-0.88	4.6

The foregoing discussion emphasizes the role of ion-solvent interaction in ion-exchange selectivity, and this must be regarded as an oversimplification; other entropy and enthalpy changes such as those in the copolymer network of the exchanger, etc., undoubtedly contribute to the net observed ΔS° and ΔH° . These other changes, however, are believed to be small compared with the ion-solvent contributions, and this may justify our interpretation.

The interaction of silver ion with the sulfonate groups of the exchanger has appeared to be stabilized by the entropy increase caused by the release of water of hydration. It is possible, although not likely, that the sulfonate group may substitute for water in the primary coordination sphere of the highly stable $\text{Ag}(\text{H}_2\text{O})_2^+$ ion.¹⁹ However, in its interaction with silver ion, the sulfonate ion may very well lose its water of hydration. Recent information on thermodynamic quantities for ion-pair formation by silver with sulfate ion in aqueous solutions is relevant. Hopkins and Wulff,²⁰ in a calorimetric study of the equilibrium



have found $\Delta H^\circ = 1.5 \pm 0.3$ kcal mole⁻¹. This result, when combined with the value for the association constant, $\text{p}K = 1.3$ determined by Righellato and Davies,²¹ gives $\Delta S^\circ = 11$ eu. Additional ion pairs formed by silver for which thermodynamic information is available are $\text{AgIO}_3(\text{aq})$ ²² and AgCl ;²³ their standard enthalpy and entropies of association are 5.14 ± 4.54 kcal mole⁻¹ and 20.3 ± 14.7 eu and -2.7 kcal mole⁻¹ and 6 eu, respectively. The association of silver ion in aqueous solutions therefore appears to be accompanied by an entropy increase and usually by the absorption of heat.

The large selectivity for silver ion present in tracer concentrations observed in this and in other work with highly cross-linked exchangers does not appear to have been caused by an entropy increase but, rather, by a marked lowering of the enthalpy. This behavior can be explained if silver ion forms a charge-transfer complex with the benzene rings of the ion exchanger. There is spectroscopic evidence for silver ion complex formation

(19) The possibility that the silver species in the exchanger was Ag_2^{2+} rather than Ag^+ ion is considered unlikely in view of the report by D. N. Waters and L. A. Woodward, *J. Chem. Soc.*, 3250 (1954), that no Raman effect assignable to the double argentous ion was observed even in concentrated (8.4 M) aqueous solutions of AgNO_3 .

(20) H. P. Hopkins, Jr., and C. A. Wulff, *J. Phys. Chem.*, **69**, 9 (1965).

(21) E. C. Righellato and C. W. Davies, *Trans. Faraday Soc.*, **26**, 592 (1930).

(22) J. J. Reinier and D. S. Martin, Jr., *J. Am. Chem. Soc.*, **78**, 1833 (1956).

(23) J. H. Jonte and D. S. Martin, Jr., *ibid.*, **74**, 2052 (1952).

with polystyrene in alcoholic solutions.²⁴ The charge-transfer energy for each of two benzene-silver bonds formed in the silver perchlorate-benzene complex has been estimated as *ca.* 16 kcal mole⁻¹ of silver ion.²⁵ While this complex ordinarily does not form in the presence of water, when the benzene rings and Ag⁺ ions are con-

strained to favorable configurations as might occur in highly cross-linked exchangers, the formation of such charge transfer complexes is conceivable.

(24) D. F. Evans, *J. Chem. Phys.*, **24**, 1244 (1956).

(25) H. G. Smith and R. E. Rundle, *J. Am. Chem. Soc.*, **80**, 5075 (1958).

Measurements of the Intradiffusion Coefficients¹ at 25° of the Ternary

Systems (Labeled L- α -Alanine)-(DL- α -Alanine)-Water and

(Labeled β -Alanine)-(β -Alanine)-Water

by J. G. Albright²

Diffusion Research Unit, Research School of Physical Sciences, Australian National University, Canberra, Australia, and the Institute for Enzyme Research, University of Wisconsin, Madison, Wisconsin 53706
(Received January 31, 1966)

Intradiffusion coefficients have been measured at 25° for the systems (labeled L- α -alanine)-(DL- α -alanine)-water and (labeled β -alanine)-(β -alanine)-water over concentration ranges of 0.0-1.5 and 0.0-5.0 moles/l., respectively. The four diffusion coefficients for these ternary systems are calculated at a series of concentrations from the intradiffusion coefficients obtained in this study and some previously reported data for the mutual-diffusion coefficients. The results show that at higher concentrations in the system with β -alanine the cross-term diffusion coefficients may be an appreciable fraction of the main-term diffusion coefficients. Thermodynamic transport coefficients related to solute-solute interaction and to solvent-solute interaction have been calculated and discussed.

Introduction

In recent years interest has developed in the study of isothermal diffusion in three-component systems. It is hoped that such studies will help yield a better understanding of the complex transport phenomena which occur in biological systems as well as improve the understanding of diffusion in industrial processes.

A system composed of a solvent containing two solutes which are chemically equivalent but isotopically different constitutes a three-component system of particular interest. In this case the four diffusion coefficients, which are necessary to describe a three-com-

ponent system, may be calculated in a simple manner from the values of the intradiffusion coefficients and mutual-diffusion coefficients for the system.³ Data

(1) The term intradiffusion was introduced and explicitly defined in ref 3. Intradiffusion coefficients are equal to tracer-diffusion coefficients for the systems described here where the unlabeled solute is chemically equivalent to the labeled solute.

(2) The experimental work reported in this article was performed by the author while visiting the laboratory of Dr. R. Mills at the ANU during the tenure of the NIH Postdoctoral Fellowship No. 4-F2-GM-19,747-02. Subsequent treatment of the data was performed at the author's present address, Institute for Enzyme Research, and supported in part by Public Health Service Research Grant AM-05177 from the Institute of Arthritis and Metabolic Diseases.

obtained for this type of system should be an interesting supplement to the data obtained for the more complicated case of three chemically different components. There are, however, few data on intradiffusion coefficients available in the literature, especially for aqueous solutions of organic solutes. Thus the systems (labeled L- α -alanine)-(DL- α -alanine)-water and (labeled β -alanine)-(β -alanine)-water, where the labeled components contained C¹⁴, were investigated in this study.⁴

Experimental Section

Materials. Fluka "puriss" reagent grade DL- α -alanine, L- α -alanine, and β -alanine were used in preparing the nonradioactive solutes. These materials were purified by recrystallization in which ethanol was added to warm (60°) concentrated aqueous solutions of each of the materials to form the crystals. The mother liquor was removed from these solutions, when they had been cooled to room temperature, by centrifugal drainage. Conductance measurements made over extended periods of time on concentrated solutions of each of these materials showed that ionic impurities were negligible. There was only a small increase of conductance with time which indicated that growth of biological organisms would not be an important factor in the diffusion experiments. The materials were dried under vacuum at room temperature for 2 days and then stored open to an atmosphere dried by P₂O₅ in a desiccator.

Small quantities of L- α -alanine and β -alanine labeled with carbon-14 were obtained from the New England Nuclear Corp. Each sample had an activity of 0.5 mcurie. By adding these samples to 1.0-g nonradioactive portions of the same chemical materials and purifying by the procedures described above, but on a smaller scale, 0.5-g samples of the two materials were obtained. For the first six experiments on the system (labeled L- α -alanine)-(DL- α -alanine)-water, the radioactive sample had been recrystallized once. It was then discovered that when the sample was recrystallized a second time, the measured values of intradiffusion coefficients appeared to be slightly higher. Thus, for the remaining four experiments, doubly recrystallized radioactive samples were used. For all of the experiments on the system (labeled β -alanine)-(β -alanine)-water, the radioactive material was recrystallized twice.

The KCl used for the calibration of the diaphragm cell was recrystallized once from water followed by centrifugal drainage. Naphthalene for the scintillation solution was recrystallized once from methanol. The rest of the materials used in preparing the solutions for counting were of reagent grade quality. The water

which was used to prepare the solutions had been distilled and then deionized.

Apparatus. Two diaphragm cells with magnetic stirring of the type developed by Stokes⁵ were used. The cells had Pyrex glass sinters of porosity No. 4 (5-10 μ). The total volume of either cell was about 100 cc and the ratio of the volumes of the two chambers in each cell was within 3% of unity. A special bottom plug as described in ref 3 was used in all experiments. The stirring rods were rotated at 60 rpm. The cells were mounted in a thermostat which was maintained at 25° to within $\pm 0.01^\circ$ with the diaphragms always within a 1° angle of being horizontal. As a precaution against the growth of microorganisms, the diaphragms were cleaned with nitric acid after each diffusion experiment.

Concentrations of the solutions of KCl from calibration experiments were determined by precise conductance measurements with a Jones bridge. The oil thermostat for the conductivity cells was maintained at $25 \pm 0.01^\circ$.

A new unit for liquid scintillation counting was designed and built for these experiments. This unit, which is immersed in a thermostat and held at a set temperature to within $\pm 0.02^\circ$, contains two photomultiplier tubes (EMI Type 9536S) and can count radioactive events in two counting bottles at one time. Four specially designed counting bottles are kinematically mounted in a bottle-holding assembly which in turn has four kinematic mounting positions relative to the photomultiplier tubes. Each counting bottle may be set before either photomultiplier tube.

In the counting operation a pair of counting bottles, one bottle for each of the two solutions from a diffusion experiment, is used in conjunction with each photomultiplier tube. Radioactive events in each member of the pair are counted for alternate equal intervals (usually 100 sec) of time by shifting the bottle-holder assembly between two mounting positions. This procedure reduces error in the measurement of the relative counting rates of the two solutions arising from drift in the electronic apparatus.

Error arising from the difference in optical efficiency of the members of each bottle pair is canceled by reversing the solutions in the pair of bottles after a first set of counting intervals and obtaining a second set of counts over a period of time equal to that for the first set of counts. After the background counting

(3) J. G. Albright and R. Mills, *J. Phys. Chem.*, **69**, 3120 (1965).

(4) Here DL- α -alanine designates an equal mixture of the D and L forms of α -alanine.

(5) R. H. Stokes, *J. Am. Chem. Soc.*, **72**, 763 (1950).

rate, which is separately measured, is subtracted, a ratio of counting rates for the two solutions is calculated from the ratio of the number of counts accumulated from each solution.

Identical sets of electronic apparatus were used in conjunction with the two photomultiplier tubes. These consisted of a Fluke high-voltage power supply, Model 412 A, a Franklin linear amplifier and pre-amplifier, Model 358, an RIDL scaler, Model 49-44, and an RIDL timer, Model 54-8.

Counting Methods. Scintillation solutions were prepared by dissolving 20-50 g of naphthalene, 4 g of PPO (2,5-diphenyloxazole), and 0.4 g of POPOP [2,2'-*p*-phenylenebis(5-phenyloxazole)] in 1 l. of dioxane. These solutions were added to the aqueous solutions from the experiments in an accurately measured ratio of about 2:1. Difficulty with solubility was experienced with the more concentrated solutions for both of the experimental systems. It was necessary to dilute the aqueous solutions with water and to lower the concentration of naphthalene in the scintillator solutions in order to achieve solubility. After preparation of the solutions it was important to scrutinize them carefully to be sure that there was no separation of phases. Greater solubility was obtained for the more concentrated solutions of β -alanine by the addition of dilute sulfuric acid.⁶ In this case, a chemical reaction seemed to occur in the solutions as evidenced by a high and decreasing background counting rate and by some color change, but after a sufficient time the color and background rate returned to normal and stable counting rates were obtainable. In these cases the solutions were allowed to stand for several days before counting.

To reduce error arising from coincidence effects, the more radioactive of the two solutions from a diffusion experiment was first diluted with nonradioactive but chemically identical stock solution so that the resulting two solutions had approximately the same level of radioactivity. The dilution ratio, based on an expected value of the diffusion coefficient, was accurately determined by gravimetric measurements. Gravimetric procedures were used in all stages of the preparation of these two solutions, as well as a portion of stock solution for counting background events, so that the resulting complex solutions still had identical chemical composition.

Before use, the exteriors of the counting bottles were always carefully cleaned with a cloth of a type that is commercially sold for cleaning eye glasses. The interiors were cleaned by rinsing in turn with dioxane, water, and acetone and then dried *in vacuo*.

For most experiments the pulse height discriminator

on the Franklin amplifier was set so that approximately 1000-1500 counts/sec were obtained. Lower counting rates were used in several instances to make the background counting rate a smaller fraction of the total counting rates for the solutions.

Two sets of bottle pairs were used in the measurement of the ratio of the concentrations of the tracer component in the two solutions from a diffusion experiment. In these measurements over a million counts were obtained for each solution in each bottle. The ratio measured with each of the two pairs of bottles was used to calculate a diffusion coefficient. An average of these two results gave the measured diffusion coefficient for the experiment. The difference of the two results indicated the experimental error of the counting measurements. For most experiments this error was $\pm 0.1\%$ or less.

Calibration. By following the method described by Stokes,⁷ the diaphragm-cell constants were determined by calibration experiments where KCl in a 0.5 *M* aqueous solution was allowed to diffuse into pure water. These constants were about 0.17 and 0.18 cm^{-2} for the two cells that were used in this experimental work. Calibration experiments were performed at regular intervals in order to obtain the cell constants as a function of the accumulated stirring time of the cells. There was only a minor variation of the cell constants with time, and the measured constants were fitted to a straight line with a rms (root-mean-square) deviation of less than $\pm 0.1\%$.

Supplementary Data

Mutual-Diffusion Coefficients. Gutter and Kegeles⁸ have measured the mutual-diffusion coefficients for the system (DL- α -alanine)-water by the Gouy interferometric method. They expressed their experimental results by the following polynomial in molarity.

$$D_v \times 10^5 = 0.9146 - 0.14277c + 0.01943c^2 \quad (1)$$

Here the subscript *v* designates the volume-fixed frame of reference.

Donoian and Kegeles⁹ have measured the mutual-diffusion coefficient for the system (β -alanine)-water by the Gouy interferometric method. For use in the analysis of the data to be presented here, their data

(6) This acid was originally used because it was a safe strong acid that did not excessively quench the scintillation process or form insoluble complexes with components of the solution. However, because of the slow chemical reaction a more suitable choice could undoubtedly be found for future experiments on similar systems.

(7) R. H. Stokes, *J. Am. Chem. Soc.*, **73**, 3527 (1951).

(8) F. J. Gutter and G. Kegeles, *ibid.*, **75**, 3893 (1953).

(9) H. C. Donoian and G. Kegeles, *ibid.*, **83**, 255 (1961).

were expressed by the following polynomial in molarity.

$$D_v \times 10^5 = 0.939 - 0.1549c + 0.05535c^2 - 0.0118c^3 + 0.000827c^4 \quad 0 \leq c \leq 5.4 \quad (2)$$

This expression fitted their experimental results with an rms deviation of $\pm 0.2\%$.

Osmotic Coefficients. Osmotic coefficients, ϕ , for the aqueous solutions of DL- α -alanine and β -alanine at 25° are used in the calculations of the coefficients, R_{ik} , in the treatment of experimental data which is to follow. Smith and Smith^{10,11} have measured the osmotic coefficients for these systems by the isopiestic method where the solutions were equilibrated with aqueous solutions of sucrose. The expressions for the osmotic coefficients of sucrose which they used in their calculations are significantly different from the more recent and more accurate expressions, for the appropriate concentration ranges, which are given by Robinson and Stokes.¹² Therefore, with the aid of a computer,¹³ the results given in ref 10 and 11 have been recalculated in terms of the newer values for sucrose. Accordingly, for each system, the osmotic coefficients ϕ_{S1} , ϕ_{A1} , ϕ_{S2} , and ϕ_{A2} given below are, respectively, the original value for the sucrose solution, the original value for the alanine solution, the newer value for the sucrose solution, and the recalculated value for the alanine solution. Polynomial expressions in molality for these osmotic coefficients for the system (DL- α -alanine)-water are

$$\begin{aligned} \phi_{S1} &= 1 + 0.095m + 0.0013m^2 \\ \phi_{A1} &= 1 + 0.010m - 0.001m^2 \quad (0 \leq m \leq 1.5) \\ \phi_{S2} &= 1 + 0.0740m + 0.0100m^2 \quad (0 \leq m \leq 2.0) \\ \phi_{A2} &= 1 - 0.008708m + 0.006428m^2 \\ &\quad (0 \leq m \leq 1.5) \quad (3) \end{aligned}$$

and for the system (β -alanine)-water are

$$\begin{aligned} \phi_{S1} &= 1 + 0.084m + 0.0104m^2 - 0.00237m^3 + 0.000115m^4 \\ \phi_{A1} &= 1 - 0.018985m + 0.019307m^2 - 0.002431m^3 + 0.000109m^4 \quad (0 \leq m \leq 5.0) \\ \phi_{S2} &= 1 + 0.07028m + 0.01847m^2 - 0.004045m^3 + 0.000228m^4 \quad (0 \leq m \leq 5.7) \\ \phi_{A2} &= 1 - 0.030156m + 0.02512m^2 - 0.0034911m^3 + 0.000172m^4 \quad (0 \leq m \leq 5.0) \quad (4) \end{aligned}$$

In obtaining the recalculated expressions, the equation $m_S\phi_{S1} = m_A\phi_{A1}$, where m_S and m_A denote the molalities of the sucrose and alanine solutions, respectively, was used to calculate values of m_A at 50 evenly

spaced values of m_S over an appropriate concentration range. This gave the molalities at which the sucrose solutions and alanine solutions were found to have equal vapor pressure. The revised expression, ϕ_{S2} , for sucrose was then substituted in the above equation, and values for ϕ_{A2} were calculated for each value of m_S and the corresponding value of m_A . These values of ϕ_{A2} were used to determine the coefficients in polynomials 3 and 4 by the method of least squares with the constant term set to unity.

Because the osmotic coefficients are expressed in terms of molality and the diffusion coefficients are expressed in terms of molarity, it was necessary in the treatment of the experimental data to calculate the molalities at a series of molarities. The values of density used in these calculations were those obtained by Gucker and Allen.¹⁴ By letting $(d_\alpha)_{25}$ and $(d_\beta)_{25}$ designate the density in g/ml at 25° for the systems (DL- α -alanine)-water and (β -alanine)-water, respectively, their results are

$$\begin{aligned} (d_\alpha)_{25} &= 0.997074 + 0.028663c - 5.73 \times 10^{-4}c^2 \\ (d_\beta)_{25} &= 0.997074 + 0.030543c - 7.147 \times 10^{-4}c^2 \end{aligned}$$

A molecular weight of 89.09 g/mole was assumed for both solutes.

Results

The intradiffusion coefficients,¹⁵ $(D^\dagger)_v$, measured in this work for the system (labeled L- α -alanine)-(DL- α -alanine)-water are shown on the left side of Table I. The values obtained with doubly recrystallized labeled L- α -alanine were found to be consistently higher than the rest of the data by 0.4%. In treating the data, it seemed reasonable to obtain an analytical expression for $(D^\dagger)_v$ vs. concentration by first using the data for once-recrystallized labeled L- α -alanine to determine the coefficients in a cubic equation by the method of least squares and then increasing the constant term by 0.4%. This procedure yielded a value for $(D^\dagger)_v$ at infinite dilution of 0.928×10^{-5} where the rms deviation of the fit

(10) P. K. Smith and E. R. B. Smith, *J. Biol. Chem.*, **121**, 607 (1937).

(11) E. R. B. Smith and P. K. Smith, *ibid.*, **132**, 47 (1940).

(12) R. A. Robinson and R. H. Stokes, *J. Phys. Chem.*, **65**, 1954 (1961).

(13) These computations were performed at the University of Wisconsin Computing Center.

(14) F. T. Gucker, Jr., and T. W. Allen, *J. Am. Chem. Soc.*, **64**, 191 (1942).

(15) As in the case of the mutual-diffusion coefficients, the subscript v denotes the volume-fixed frame of reference. Of course, for intradiffusion this frame of reference coincides with other commonly used frames of reference such as the solvent-fixed frame and the number-fixed frame because of the chemical identity of the solutes and the special initial conditions for intradiffusion.

Table I: Intradiffusion Coefficients of Aqueous Solutions of Alanine Solutes Measured at 25°

(Labeled L- α -alanine)- (DL- α -alanine)-water		(Labeled β -alanine)- (β -alanine)-water	
c_s, M	$(D^\dagger)_v \times 10^5,$ cm ² /sec	c_s, M	$(D^\dagger)_v \times 10^5,$ cm ² /sec
0.05 ^a	9.17	0.1	0.928
0.10	9.02	1.0	0.783
0.25	8.69	2.0	0.623
0.50	8.19	2.99	0.475
0.75	7.68	4.0	0.350
0.75 ^a	7.71	5.0	0.262
0.75 ^{a,b}	7.76		
1.00	7.20		
1.50	6.39		
1.50 ^a	6.42		

^a Experiments with doubly recrystallized labeled L- α -alanine.

^b Experiment with L- α -alanine as unlabeled solute.

in the first step was $\pm 0.1\%$. However, the intradiffusion coefficient and the mutual-diffusion coefficient should be equal at infinite dilution for the system; in the subsequent calculation of the coefficients, R_{ik} , expressions for $(D^\dagger)_v$ and D_v which approach the same value as c goes to 0 will be necessary for meaningful results at this limit. Since the Gouy method, which was used in ref 8, is probably the more accurate method of measuring absolute values of diffusion coefficients, the constant value in the expression for $(D^\dagger)_v$ was set equal to the constant term in eq 1, and the resulting analytical expression for $(D^\dagger)_v$ became

$$(D^\dagger)_v \times 10^5 = 0.9146 - 0.227c + 0.0239c^2 \quad 0 \leq c \leq 1.5 \quad (5)$$

In the treatment of these data, the D and L forms of α -alanine are assumed to be chemically equivalent. This assumption is justified by the results of the experiments reported in ref 8. There it was found that the mutual-diffusion coefficients at equal concentrations of aqueous solutions of L- α -alanine, D- α -alanine, and DL- α -alanine were equal within experimental error. The intradiffusion coefficient which was obtained in this work when L- α -alanine was used as the unlabeled solute in a 0.75 M solution is slightly higher than that obtained with DL- α -alanine. However, the difference is small and may be only experimental error.

The intradiffusion coefficients measured in this work for the system (labeled β -alanine)-(β -alanine)-water are presented on the right side of Table I. An analytical expression was obtained for these intradiffusion coefficients by using the data in Table I to determine the coefficients in a third-degree polynomial.¹⁶ The con-

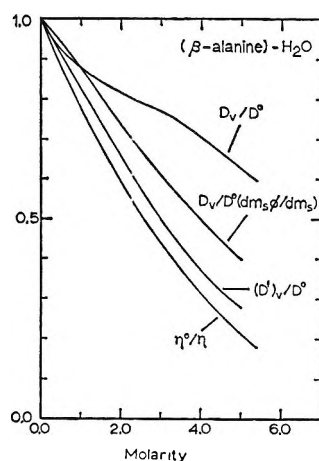
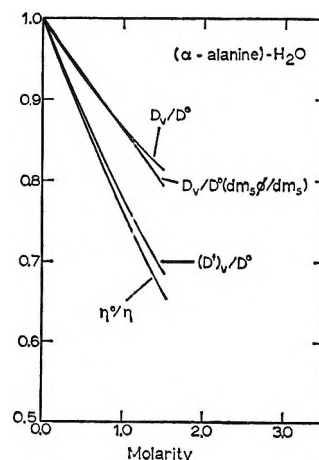


Figure 1. Concentration dependence of the normalized diffusion coefficients and the relative viscosity for aqueous solutions with α -alanine solutes and with β -alanine solutes.

stant term, the value of $(D^\dagger)_v$ at $c = 0$, of the polynomial was 0.944×10^{-5} . However, it was again appropriate to set the constant term of the polynomial for the intradiffusion coefficient equal to the value of the mutual-diffusion coefficient at $c = 0$. By using the constant term in eq 2, the expression for the intradiffusion coefficient, $(D^\dagger)_v$, became

$$(D^\dagger)_v \times 10^5 = 0.939 - 0.1563c - 0.00617c^2 + 0.00203c^3 \quad 0 \leq c \leq 5.0 \quad (6)$$

Discussion

Figure 1 shows the concentration dependence of the intradiffusion coefficients, the mutual-diffusion coef-

(16) This order of polynomial is rather high relative to the number of data points. This order was used, however, because a marked improvement of fit from that of the next lower degree was obtained. The second-degree polynomial fitted the data with an rms deviation of $\pm 0.6\%$, whereas the third-degree polynomial fitted the data with an rms deviation of $\pm 0.03\%$.

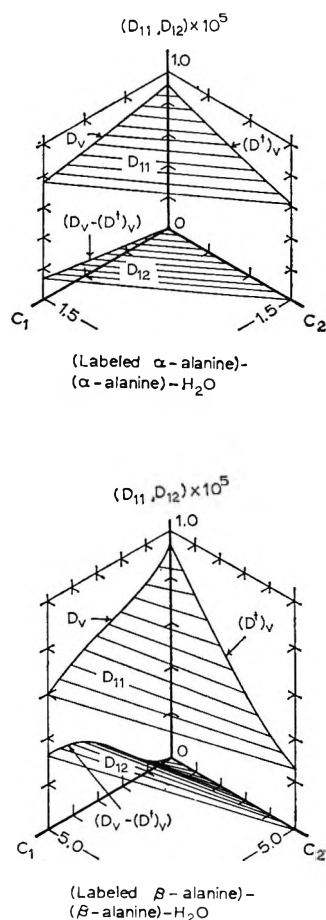


Figure 2. Dependence of the main-term diffusion coefficient, D_{11} , and the cross-term diffusion coefficient, D_{12} , on the concentrations, c_1 and c_2 , of the two chemically identical solutes in the indicated aqueous solutions.

ficients, and the reciprocal of the relative viscosity¹⁷ for the systems reported here. The diffusion coefficients were normalized by dividing by the limiting value of the diffusion coefficients at zero concentration, D_0 . The quantity $D_v/[D_0 d(m\phi)/dm]$ for each system, where m is the molality and ϕ is the osmotic coefficient, is included to give a comparison of terms involved in the calculation of the coefficients, R_{12} , discussed below. Figure 1 shows that the intradiffusion coefficients are more closely related to viscosity than are the mutual-diffusion coefficients. Such a result has been found for other nonelectrolyte systems.¹⁸

The experimental systems considered here may be described as three-component systems with the labeled and unlabeled forms of the solute representing the two solute components and the solvent as the third component.³ The flow equations for diffusion in one dimension for these systems may be written

$$-(J_i)_v = \sum_{k=1}^2 (D_{ik})_v \frac{\partial c_k}{\partial x} \quad (i = 1, 2) \quad (7)$$

Here the subscripts 1 and 2 arbitrarily are chosen to denote for the flows, J_i , and the molarities, c_k , the labeled and unlabeled forms of the solute, respectively; however, the equations to follow would be equally valid if the solute components were numbered in the reverse order. The subscript v again denotes the volume-fixed frame of reference. In ref 3 the four diffusion coefficients are related to the mutual and intradiffusion coefficients by the equations

$$(D_{ik})_v = \frac{c_i}{c_s} (D_v - (D^1)_v) + \delta_{ik} (D^1)_v \quad (i = 1, 2; k = 1, 2) \quad (8)$$

where δ_{ik} is unity when $i = k$ and zero when $i \neq k$ and where $c_s = c_1 + c_2$.

In Figure 2 the values of D_{11} and D_{12} are plotted as functions of c_1 and c_2 for the systems reported here. The graphs will also show D_{22} and D_{21} in place of D_{11} and D_{12} , respectively, if the labeling of the axes for c_1 and c_2 are reversed. When c_1 is present only in trace amounts and is essentially zero, D_{11} is equal to the intradiffusion coefficient, $(D^1)_v$, and D_{12} is zero. When c_2 is essentially zero, D_{11} will be equal to the mutual-diffusion coefficient and D_{12} will be equal to $D_v - (D^1)_v$. For a constant value of the sum of the concentrations, c_s , the values of D_{11} and D_{12} will lie on two parallel straight lines that connect the limiting values for D_{11} and D_{12} at $c_1 = 0$ and at $c_2 = 0$. The value of D_{12} is seen to increase rapidly for both systems with an increase in c_1 when c_2 remains small, and in the case of β -alanine D_{12} becomes 60% of the value of D_{11} at the higher concentrations of c_1 . Although these results are for the special case of chemically equivalent solutes, they give an indication of the result that would be obtained if one solute were replaced by a similar but chemically different solute. The relatively large values of D_{12} obtained for the system with β -alanine show the importance of including the cross-term diffusion coefficients in developing theories for transport processes.

In recent years interest has developed in describing diffusion processes in terms of the thermodynamics of irreversible processes. By applying the equations presented by Onsager,¹⁹ the process of isothermal diffusion

(17) The values of relative viscosity were obtained from L. S. Mason, P. M. Kampmeyer, and A. L. Robinson, *J. Am. Chem. Soc.*, **74**, 1287 (1952).

(18) This may be seen, for example, in the experimental results for the system benzene-cyclohexane: R. Mills, *J. Phys. Chem.*, **69**, 3116 (1965).

(19) L. Onsager, *Ann. N. Y. Acad. Sci.*, **46**, 241 (1945).

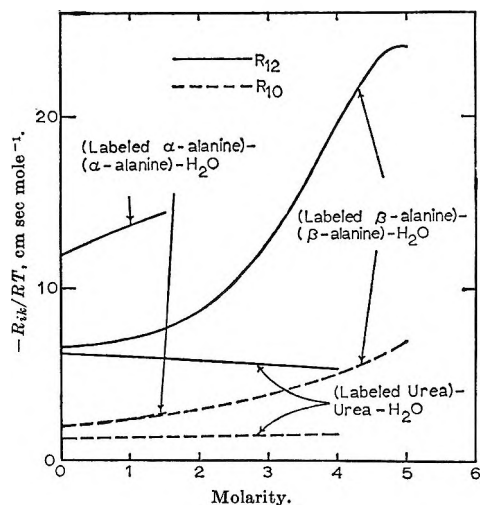


Figure 3. Values of the coefficients, R_{10} and R_{12} , which are related, respectively, to the interaction of the solvent and either solute and to the interaction of the chemically identical solutes.

in one dimension for a three-component system may be described by the equations

$$-\partial\mu_i/\partial x = \sum_{k=0}^2 R_{ik} J_k \quad (i = 0, 1, 2) \quad (9)$$

Here μ_i is the chemical potential of component i , the coefficients, R_{ik} , are thermodynamic transport coefficients, and the rest of the quantities have the same significance as in eq 7. The subscripts 0, 1, and 2 are used to denote, respectively, the solvent, the labeled solute, and the unlabeled solute in the system. Onsager gives the condition that

$$\sum_{k=0}^2 R_{ik} c_k = 0 \quad (i = 0, 1, 2) \quad (10)$$

and in this representation the Onsager reciprocal relations

$$R_{ik} = R_{ki} \quad (11)$$

apply. These coefficients, R_{ik} , are independent of the frame of reference for the flows.

For systems in which the two solutes are chemically the same and only isotopically different, the coefficients, R_{ik} , may be calculated from the following equations.³

$$R_{ik} = RT \left[\frac{\bar{V}_0 c_0 (d \ln a_s / dc_s)}{1000 D_v} - \frac{1}{(D^\dagger)_{v,c_s}} + \frac{\delta_{ik}}{c_i (D^\dagger)_{v,c_i}} \right] \quad (i = 1, 2; k = 1, 2) \quad (12)$$

Here \bar{V}_0 is the partial molal volume of the solvent in milliliters per mole and a_s is the activity for the binary system of concentration, c_s , where the two forms of the solute are not separately identified. Since most of the

data for the activity coefficients of nonelectrolytes in aqueous systems have been obtained by the isopiestic method, it is of interest to express eq 12 in terms of osmotic coefficients which are directly obtained by this method. In converting eq 12, the expression

$$\frac{\bar{V}_0 c_0}{1000} = \frac{m_s}{c_s} \frac{dc_s}{dm_s} \quad (13)$$

is used which may be obtained, for example, from equation A-7 in ref 20. Here m_s is the molality at molarity c_s . With the definition of the osmotic coefficients, ϕ

$$\ln a_0 = -\frac{m_s \phi M_0}{1000} \quad (14)$$

where M_0 and a_0 are, respectively, the molecular weight and the activity of the solvent, and with the condition from the Gibbs-Duhem equation that

$$\frac{1000}{M_0} d \ln a_0 = -m_s d \ln a_s \quad (15)$$

where m_s is the total molality of the solute, eq 12 may be written

$$R_{ik} = \frac{1000RT}{c_s} \left[\frac{d(m_s \phi) / dm_s}{D_v} - \frac{1}{(D^\dagger)_{v,c_s}} + \frac{c_s \delta_{ik}}{c_i (D^\dagger)_{v,c_i}} \right] \quad (i = 1, 2; k = 1, 2) \quad (16)$$

In eq 16 the constant 1000 (an approximation of the more exact constant 1000.027) is included to convert liters to cubic centimeters and thus to simplify the units of R_{ik} . By noting that $c_0 = (1000c_s)/(M_0 m_s)$ and by applying eq 10, the rest of the coefficients, R_{ik} , become²¹

$$R_{10} = R_{20} = R_{01} = R_{02} = -\frac{1000}{m_s M_0} R_{00} = -\frac{RT m_s M_0}{c_s} \frac{d(m_s \phi) / dm_s}{D_v} \quad (17)$$

In Table II values of R_{10} and R_{12} are presented²²⁻²³ which have been calculated from eq 16 and 18.

Because R_{12} involves relatively small differences between large quantities, its experimental accuracy should not be considered better than $\pm 5\%$; the quantities involved in the calculations of R_{12} are shown as normalized reciprocals in Figure 1. In principle, the ex-

(20) P. J. Dunlop and L. J. Gosting, *J. Phys. Chem.*, **63**, 86 (1959).

(21) Here it should be noted that a minus sign is missing from the last term of eq 28 in ref 3. However, all the tabulated values of R_{10} for urea in that reference have the correct sign.

(22) Ellerton, *et al.*,²³ had previously calculated values for the case of R_{10} by using the original thermodynamic activity data obtained by Smith and Smith.

(23) H. D. Ellerton, G. Reinfelds, D. E. Mulcahy, and P. J. Dunlop, *J. Phys. Chem.*, **68**, 403 (1964).

Table II: Thermodynamic Transport Coefficients

α -Alanine			β -Alanine		
c , M	$-R_{10}/RT$ cm sec mole $^{-1}$	$-R_{12}/RT$, cm sec mole $^{-1}$	c , M	$-R_{10}/RT$, cm sec mole $^{-1}$	$-R_{12}/RT$, cm sec mole $^{-1}$
0.03	1.987	12.0	0.1	1.957	6.6
0.3	2.100	12.5	0.5	2.103	6.8
0.6	2.236	13.0	1.0	2.332	7.1
0.9	2.387	13.6	2.0	2.969	8.6
1.2	2.554	14.0	3.0	3.867	12.7
1.5	2.739	14.4	4.0	5.074	19.5
			5.0	7.058	24.0

perimental error would be infinite at zero concentration if one attempted to measure directly each quantity in eq 16 at this concentration. However, because of the procedure of analysis in which all the quantities were calculated from low-degree polynomials which in turn were obtained by a least-squares fit of the experimental data over the entire concentration range for the systems, the values of R_{12} should retain good significance at zero concentration.

The values for R_{10} and R_{12} presented in Table II are plotted in Figure 3 along with the results that have previously been reported for the system (labeled urea)-urea-water.

The coefficients ($-R_{ik}$), with $i \neq k$, have been interpreted²⁴⁻³² to be a measure of the friction between molecules of type i and k . With this interpretation the larger values of R_{12} relative to R_{10} for the systems shown in Figure 3 are expected because of the relatively smaller size of the solvent molecules.

For the system with β -alanine, the values of R_{10} and R_{12} increase by approximately the same percentage of their values at zero concentration as the concentration increases from 0 to 5 M . However, R_{12} shows a greater deviation from linearity than does R_{10} over this concentration range.

It is curious that the magnitude of R_{12} should be

greater for the solutions with α -alanine than for the solutions with β -alanine since the latter material has the larger dipole moment.

Acknowledgments. The author wishes to thank Dr. R. Mills for his advice and support of this research and Dr. L. J. Gosting for his many helpful criticisms in the preparation of the manuscript. Special thanks go to R. J. Boland for his collaboration in the design and construction of the counting apparatus used for this experimental work and to Mrs. Sharon R. Albright for her help in preparing the manuscript.

(24) The sign of R_{ik} for the equations presented in this article is determined by the original formulations of Onsager (ref 19) and is consistent with the equations presented in ref 3. However, the rate of entropy production for isothermal diffusion of n solutes may be given according to the equation

$$2T\sigma = \sum_{i=0}^n \sum_{k=0}^n (-R_{ik})c_i c_k (v_i - v_k)^2$$

where T is absolute temperature, σ is the rate of entropy production, and $(v_i - v_k)$ is the difference in the velocities of components i and k . This form of the entropy production equation indicates that the quantity $(-R_{ik})$ with the $i \neq k$ should be used with the concept of friction. It should be noted here that Dunlop^{23,25} has adopted the opposite sign for the coefficients, R_{ik} , and thus has obtained equations which have the appropriate signs of the coefficients, R_{ik} , for the concept of friction. Also the coefficients φ_{ik} and r_{ik} introduced by Lamm^{26,27} and Klemm,²⁸ respectively, where $\varphi_{ik} = -R_{ik}c_i c_k$ and $r_{ik} = -R_{ik}C$, wherein C designates the total number of moles of all components per cubic centimeter of solution, were originally chosen by these authors to have the proper sign for the friction concept.

(25) P. J. Dunlop, *J. Phys. Chem.*, **68**, 26 (1964).

(26) O. Lamm, *Arkiv Kemi Mineral. Geol.*, **18B**, No. 2 (1944).

(27) O. Lamm, *J. Phys. Chem.*, **61**, 948 (1957).

(28) A. Klemm, *Z. Naturforsch.*, **8a**, 397 (1953).

(29) Lamm²⁹ was the first to emphasize the use of the concept of friction for describing diffusion in multicomponent systems. Laity³⁰ presented equations showing how the R_{ik} coefficients of Onsager could be described as friction coefficients. An intercomparison of the Lamm and Onsager approaches is presented by Ljunggren.³¹ A verification of the concept of friction has been provided by Dullien³² who has applied this concept with reasonable success in relating viscosity to intradiffusion coefficients.

(30) R. W. Laity, *J. Phys. Chem.*, **63**, 80 (1959).

(31) S. Ljunggren, *Trans. Roy. Inst. Technol., Stockholm*, No. 172 (1961).

(32) F. A. L. Dullien, *Trans. Faraday Soc.*, **59**, 856 (1963).

Photochemistry of the Fluoro Ketones. Pentafluoroethyl Ethyl Ketone¹

by R. L. Thommarson and G. O. Pritchard

Department of Chemistry, University of California, Santa Barbara, California 93106
(Received January 31, 1966)

The photochemistry of the title ketone was investigated at 3130 Å and its behavior is compared to that of other fluoroalkyl ketones. Quantum yield data as functions of temperature and pressure are determined, and it is concluded that the primary decomposition mode is $C_2F_5COC_2H_5 + h\nu \rightarrow C_2F_5 + COC_2H_5$. The disproportionation/combination ratio for C_2F_5 and C_2H_5 radicals is 0.56, and the cross-combination ratio is about 2, both almost independent of the temperature. The activation energies for H-atom abstraction from the ketone are 5.6 and 6.8 kcal mole⁻¹ for C_2F_5 and C_2H_5 radicals, respectively.

Introduction

In our previous investigation² on the photolysis of $C_3F_7COC_2H_5$, we obtained some surprisingly strong temperature dependencies for the disproportionation/combination and cross-combination ratios for C_3F_7 and C_2H_5 radicals. This investigation represents a determination of these ratios for C_2F_5 and C_2H_5 radicals; also quantum yield data as functions of the temperature and pressure for the photodecomposition of the ketone are presented.

Experimental Section

The apparatus was identical with that used in the $C_3F_7COC_2H_5$ experiments.² The $C_2F_5COC_2H_5$ was obtained from Columbia Organic; it appeared to be pure from vpc and mass spectrometric analysis. The extinction coefficient at 3130 Å is 7.3 l. mole⁻¹ cm⁻¹.

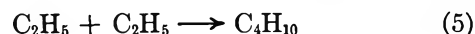
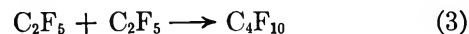
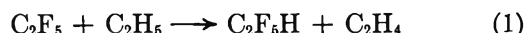
Photolysis temperatures varied from room temperature to over 300°, and times varied from 2 min to 4 hr. Runs of short duration and higher intensities were employed when radical-radical interactions were being investigated. Longer times were employed when quantum yield determinations were being made and solution filters were used.² Under these conditions the incident intensity was either 2.2 or 2.8×10^{13} quanta/cc sec, depending on the filter combination. The absorbing intensity without the filters was ~20–30 times greater. The pressure of the ketone used was maintained at 4.5 ± 0.3 cm, except when the pressure dependence of Φ_{CO} was being determined.

Product analysis was effected by low-temperature fractionation and vpc. CO was separated at -210°

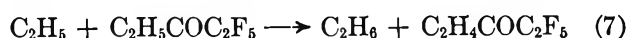
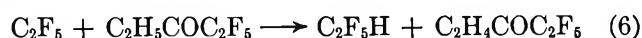
and occasionally checked on the mass spectrometer. C_2H_6 and C_2H_4 were collected at -175° and analyzed on a 1-m 3% squalane-on-silica gel column. C_2F_5H , C_4H_{10} , C_4F_{10} , and $C_2F_5C_2H_5$, together with some $C_2F_5COC_2H_5$, were collected at -110° and analyzed on a 0.5-m 3% squalane-on-alumina column followed by a 2-m 15% silicone oil-on-Chromosorb W column. The ketone was retained by the alumina column, and the other components were identified by mass spectrometric analysis and vpc retention times. $C_2F_5C_2H_5$ was prepared from the reduction of pentafluoro-1-butene, obtained from Peninsular ChemResearch.

Results and Discussion

Radical-Radical Interactions. The following reactions are of interest.



C_2F_5H and C_2H_6 are also formed in the abstraction reactions



(1) This work was supported by a grant from the National Science Foundation.

(2) G. O. Pritchard and R. L. Thommarson, *J. Phys. Chem.*, **69**, 1001 (1965).

At higher temperatures, the radical formed in reactions 6 and 7 may decompose into $C_2H_4^*$ (from rearrangement of CH_3CH), CO, and C_2F_5 , or, as a referee has suggested, into CH_3CHCO and C_2F_5 . We did not distinguish between these two possibilities. As we previously assumed,² the C_2H_4 formed in reaction 1 was found by subtracting 0.14 of the C_4H_{10} yield from the total ethylene formed. The Arrhenius plot of k_1/k_2 for a number of representative runs is shown in Figure 1. The results are very scattered, due to difficulties that we encountered in obtaining accurate ethylene analyses. The total ethylene formed varied between ~ 35 and 57% (at high temperatures) of the -175° fraction, and any error in the butane analysis is reflected in the k_1/k_2 values. The line drawn represents the average value of $k_1/k_2 = 0.56$, independent of temperature, for the 14 runs recorded. A line of positive slope could also very well represent most of the points, yielding a value of $E_1 - E_2 \simeq -1.5$ kcal mole⁻¹, in good agreement with the comparable value that we obtained for C_3F_7 and C_2H_5 radicals.² In view of the uncertainties involved, it would appear simpler to conclude that these relatively large activation energy differences are not established, although it is reasonably certain that $E_{\text{disproportionation}} < E_{\text{combination}}$ for alkyl radical interactions,³ the difference being of the order of 300 kcal mole⁻¹.

The cross-combination ratio $k_2/k_3^{1/2}k_5^{1/2} = R_{C_2F_5C_2H_5}/R_{C_4F_{10}}^{1/2}R_{C_4H_{10}}^{1/2}$, where R represents mean rate of formation, is also plotted in the Arrhenius form in Figure 1 (all the values are close to the theoretical value of 2). A least-squares line through the points given yields $k_2/k_3^{1/2}k_5^{1/2} = 4.7e^{(-750 \pm 400)/RT}$. This is a similar but lesser temperature effect than we obtained in the $C_3F_7 + C_2H_5$ system.² If we include the disproportionation reactions in the cross-combination ratio, a correction factor of $1.56/(1.14)^{1/2}$ is needed, assuming that the disproportionation/combination ratios for $C_2F_5 + C_2H_5$ and $2C_2H_5$ radicals are independent of temperature; the temperature dependence of the cross combination will remain unaffected.

The present data suggest very small, < 1 kcal mole⁻¹, if any, temperature dependencies for C_2F_5 and C_2H_5 interactions as opposed to the larger energy barrier differences, ~ 2 kcal mole⁻¹, found for C_3F_7 and C_2H_5 interactions.² The reason for this is not clear, as interactions between perfluoroalkyl radicals show no temperature dependence.⁴ The $C_3F_7 + C_2H_5$ data may not, as yet, be discounted for it should be noted that a strong temperature dependence has also been reported for the $C_3F_7 + CH_3$ cross-combination ratio.⁵

A few experiments were carried out at lower pressures, ~ 4 mm, to investigate the possibility of HF

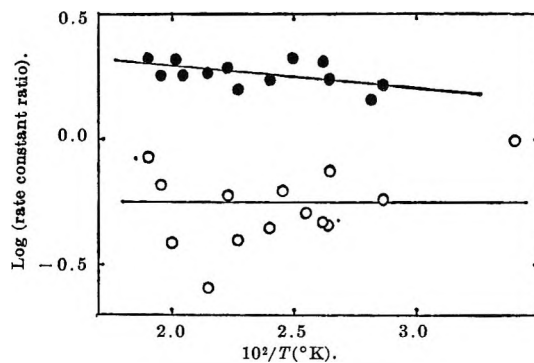


Figure 1. Arrhenius plots of C_2F_5 and C_2H_5 radical interactions: ●, $k_2/k_3^{1/2}k_5^{1/2}$; ○, k_1/k_2 .

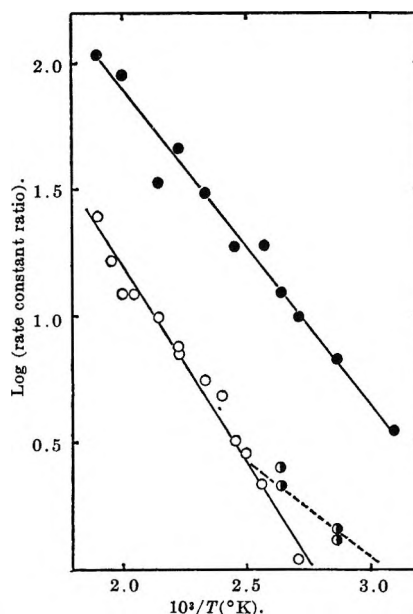


Figure 2. Arrhenius plots for H-atom abstractions: ●, $k_6/k_3^{1/2}$ mole^{-1/2} cc^{1/2} sec^{-1/2}; ○, $k_7/k_5^{1/2}$ mole^{-1/2} cc^{1/2} sec^{-1/2}; ◐, high-intensity, low-temperature runs.

elimination from the vibrationally excited $C_2F_5C_2H_5^*$ species formed in reaction 2. No evidence was found for such a reaction owing to the large number of available degrees of freedom in the excited molecule.²

H-Atom Abstraction Data. The conventional Arrhenius plots for $k_6/k_3^{1/2}$ and $k_7/k_5^{1/2}$, both in units of mole^{-1/2} cc^{1/2} sec^{-1/2}, are shown in Figure 2. A least-squares treatment of the data leads to the expressions

$$k_6/k_3^{1/2} = 2.2 \times 10^4 e^{-5600/RT} \text{ mole}^{-1/2} \text{ cc}^{1/2} \text{ sec}^{-1/2}$$

(3) P. S. Dixon, A. P. Stefani, and M. Szwarc, *J. Am. Chem. Soc.*, **85**, 2551, 3344 (1963); R. Klein, M. D. Scheer, and R. Kelley, *J. Phys. Chem.*, **68**, 598 (1964).

(4) G. O. Pritchard, J. R. Dacey, W. C. Kent, and C. R. Simonds, *Can. J. Chem.*, **44**, 171 (1966).

(5) G. O. Pritchard, Y. P. Hsia, and G. H. Miller, *J. Am. Chem. Soc.*, **85**, 1568 (1963).

and

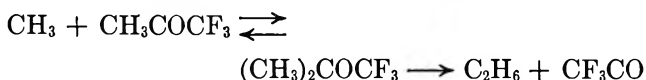
$$k_7/k_5^{1/2} = 1.4 \times 10^4 e^{-6800/RT} \text{ mole}^{-1/2} \text{ cc}^{1/2} \text{ sec}^{-1/2}$$

with limits of ± 200 cal on the activation energy differences in each case. The preexponential ratios are normal, and the activation energy differences are those that would be expected for abstraction of a secondary H atom by the respective radicals.^{2,4}

Quantum Yields. Some quantum yield data are given in Figure 3. C_4F_{10} and $C_2F_5C_2H_5$ have not been included because of the very low values that we obtained for them; $\Phi_{C_4F_{10}}$ was about 0.002 and $\Phi_{C_2F_5C_2H_5}$ about 0.01 over the temperature range. The $\Phi_{C_2H_6} > 1$ at 570°K may be a valid observation, as in the photolysis of CF_3COCH_3 Sieger and Calvert⁶ found that CH_4 was formed by a chain process at this temperature, owing to a reaction such as



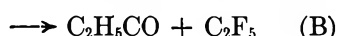
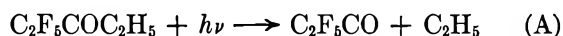
An analogous process could occur with C_2F_5 and $C_2F_5COC_2H_5$. The quantum yield data for the radical containing products in the two systems are very similar, except for the comparison between $\Phi_{C_2H_6}$ and $\Phi_{C_4H_{10}}$. The high values for $\Phi_{C_2H_6}$ (0.7 at 570°K in CF_3COCH_3 photolysis) were thought to be due to the reaction⁶



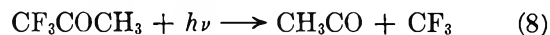
A comparable mode of formation of butane is not evident in our system. The decomposition of the CF_3CO radical thus formed leads to $\Phi_{CO} > 1$ at temperatures greater than 470°K. In the $C_2F_5COC_2H_5$ system, Φ_{CO} only approaches unity, within experimental error, at 570°K.

The temperature dependence of the Φ_{CO} is typical of that for simple aliphatic ketones, other than $(CF_2H)_2CO$,⁷ where after the initial electronic excitation Φ_{CO} will depend upon the extent to which radiative and radiationless transitions occur, and the lifetimes and possible reactions of C_2H_5CO and/or C_2F_5CO radicals.

Primary Process. We may consider the two possible primary processes



Calvert and Sieger⁶ favored a type-A decomposition, but in a recent reinvestigation of CF_3COCH_3 photolysis⁸ the identification of biacetyl in the reaction products certainly indicates the importance of a type-B process



Assuming that decomposition occurs mainly through the conversion of the original electronic excitation into vibrational energy, which becomes distributed throughout the molecule,⁹ the dissociative fate of the molecule will depend upon the nature of the energy distribution and the relative C-C bond strengths. The generation of CF_3 radicals in the systems $CH_3 + CF_3COCF_3$ ¹⁰

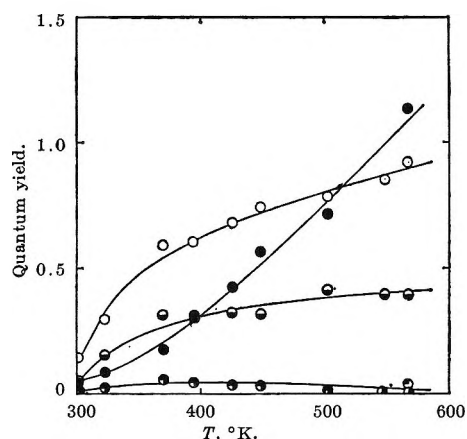


Figure 3. Quantum yields for $C_2F_5COC_2H_5$ photolysis ($p = 4.5 \pm 0.3$ cm) vs. temperature: O, CO; ●, C_2H_6 ; ⊖, C_2F_5H ; ⊙, C_4H_{10} ; ⊕, C_2H_4 ; ⊗, C_4H_{10} or C_2H_4 .

and $CH_3 + CF_3N_2CF_3$ ¹¹ has been known for some time^{10a,11a} and has recently been subjected to careful reinvestigation.^{10b,c,11b} From these observations it may be rationalized^{11b} that the CF_3-N and CF_3-C bonds are at most equal to or more likely weaker than the corresponding CH_3-N and CH_3-C bonds.¹²

(6) R. A. Sieger and J. G. Calvert, *J. Am. Chem. Soc.*, **76**, 5197 (1954).

(7) G. O. Pritchard and J. T. Bryant, *J. Phys. Chem.*, **70**, 1441 (1966).

(8) E. A. Dawidowicz and C. R. Patrick, *J. Chem. Soc.*, 4250 (1964).

(9) P. Seybold and M. Gouterman, *Chem. Rev.*, **65**, 413 (1965).

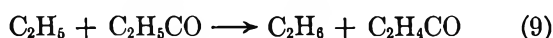
(10) (a) G. O. Pritchard and E. W. R. Steacie, *Can. J. Chem.*, **35**, 1216 (1957); (b) W. G. Alcock and E. Whittle, *Trans. Faraday Soc.*, **61**, 244 (1965); (c) R. D. Giles and E. Whittle, *ibid.*, **61**, 1425 (1965).

(11) (a) G. O. Pritchard and J. R. Dacey, unpublished data, 1961; (b) L. Batt and J. M. Pearson, *Chem. Commun.*, 575 (1965).

(12) The effect of fluorination upon C-C bond strengths is uncertain. A recent tabulation (E. Tschuikow-Roux, *J. Phys. Chem.*, **69**, 1075 (1965)) puts $D(CF_3-CF_3)$ in the range 65 to 95 kcal mole⁻¹, compared to $D(CH_3-CH_3) \cong 84$ kcal mole⁻¹. Recent evidence (I. P. Fisher, J. B. Homer, and F. P. Lossing, *J. Am. Chem. Soc.*, **87**, 957 (1965); J. P. Simons, *Nature*, **205**, 1308 (1965)) puts $D(CF_2=CF_2)$ at 70-80 kcal mole⁻¹, and one would expect the single bond in C_2F_6 to be weaker than the double bond in C_2F_4 , which indicates a low value for $D(CF_3-CF_3)$. Cottrell (T. L. Cottrell, "The Strengths of Chemical Bonds," Butterworth and Co. Ltd., London, 1958) quotes the average C-C internuclear separation in the ground state as 1.31 and 1.52 Å for C_2F_4 and C_2F_6 , respectively. Chlorination of ethane leads to a weakening of the C-C bond; $D(CCl_3-CCl_3)$ has recently been quoted as 68.4 kcal mole⁻¹ (G. J. Martens and G. H. Huybrechts, *J. Chem. Phys.*, **43**, 1845 (1965)).

The rupture of a particular C-C bond requires the instantaneous localization of sufficient energy in the bond. The increased vibrational energy capacity of perfluoroalkyl groups over alkyl groups can be imagined to cause an excess of vibrational energy adjacent to the perfluoroalkyl group-carbon bond, facilitating the localization of sufficient energy for decomposition in that bond. This would add to the probability of the type-B ketone photodecomposition and the CF_3 generation reactions^{10,11} that have been observed.

It should be noted that our ethane yields exceeded the ethylene yields (see Figure 3) even at room temperature, when reaction 7 is very slow. Moreover, the Arrhenius plot for $k_7/k_5^{1/2}$ showed distinct upward curvature (dotted line, Figure 2) below about 100° at high intensities. This presents strong evidence for the finite existence of the $\text{C}_2\text{H}_5\text{CO}$ radical and the occurrence of the reaction¹³



Experiments conducted at low relative intensities (when quantum yield determinations were being made) did not exhibit such curvature. The radical-radical disproportionation (reaction 9) would be expected to be more important at high intensities.¹⁴

Φ_{CO} vs. Pressure. This is shown in Figure 4 for the temperatures 27, 45, and 90° . The decrease in Φ_{CO} with increasing pressure at a given temperature may be correlated with increased collisional quenching rates of excited ketone molecules $\text{C}_2\text{F}_5\text{COC}_2\text{H}_5^*$ and also, at low temperatures, $\text{C}_2\text{H}_5\text{CO}^*$, which is formed containing excess vibrational energy. The reaction probability of this radical is also increased at higher pressures.¹⁵

Before a more complete interpretation can be made, the radiative processes need to be examined. Ausloos and Murad¹⁶ have observed both fluorescence and phosphorescence in CF_3COCH_3 vapor following photochemical excitation at 3130 Å. The participation of both singlet and triplet molecules is also evident in the photochemical excitation of $\text{C}_2\text{H}_5\text{COC}_2\text{H}_5$ at 3130 Å.¹⁷ The photochemistry of the three perfluoro ketones, CF_3COCF_3 , $\text{C}_2\text{F}_5\text{COC}_2\text{F}_5$, and $\text{C}_3\text{F}_7\text{COC}_3\text{F}_7$, have been investigated in some detail by Steacie and his co-workers; their photochemical behavior at 3130 Å is very similar.¹⁸ Fluorescence yields were originally obtained for CF_3COCF_3 , and, although phosphorescence was not observed,¹⁹ the formation of triplet state molecules was suggested.²⁰ More recently, phosphorescence yields have been obtained at 3130 Å for CF_3COCF_3 .²¹ It would seem that both singlet and triplet processes will be involved in the photochemistry

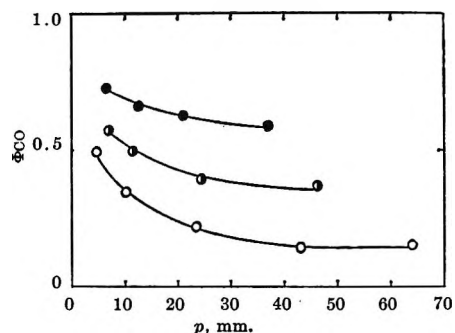
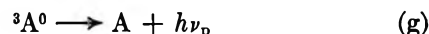
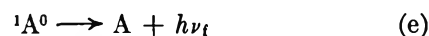
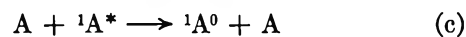


Figure 4. Φ_{CO} vs. ketone pressure (mm):
●, 90° ; ◐, 45° ; ○, 27° .

of $\text{C}_2\text{F}_5\text{COC}_2\text{H}_5$ at 3130 Å. We may write a sequence of primary events²¹



where ${}^1\text{A}^*$ is a ketone molecule in a high vibrational level of the upper singlet state (A is a ground-state molecule and A^* a vibrationally excited ground-state molecule), ${}^1\text{A}^0$ is a molecule in a low-lying, non-dissociating level of that singlet-state, and ${}^3\text{A}^0$ is a molecule in a low-lying vibrational level of an upper triplet state from which dissociation can occur with a small activation energy.²²

(13) $\text{C}_2\text{F}_6 + \text{C}_2\text{H}_5\text{CO} \rightarrow \text{C}_2\text{F}_5\text{H} + \text{C}_2\text{H}_4\text{CO}$ will also occur, but curvature would be less evident in the $k_6/k_3^{1/2}$ plot as $E_6 < E_7$. The possibility of curvature is evident in the $k_6/k_3^{1/2}$ plot; see ref 10c for an observation of this nature in the $\text{CF}_3 + \text{CH}_3\text{CO}$ reaction.

(14) P. Ausloos and E. W. R. Steacie, *Can. J. Chem.*, **33**, 47 (1955).

(15) The participation of the $\text{C}_2\text{H}_5\text{CO}$ radical in $\text{C}_2\text{H}_5\text{COC}_2\text{H}_5$ photolysis appears to be significantly less than in $\text{C}_2\text{H}_5\text{COC}_2\text{F}_5$ photolysis: see K. O. Kutschke, M. H. J. Wijnen, and E. W. R. Steacie, *J. Am. Chem. Soc.*, **74**, 714 (1952).

(16) P. Ausloos and E. Murad, *J. Phys. Chem.*, **65**, 1519 (1961).

(17) D. S. Weir, *J. Am. Chem. Soc.*, **83**, 2629 (1961).

(18) G. Giacometti, H. Okabe, S. J. Price, and E. W. R. Steacie, *Can. J. Chem.*, **38**, 104 (1960).

(19) H. Okabe and E. W. R. Steacie, *ibid.*, **36**, 137 (1958).

(20) G. Giacometti, H. Okabe, and E. W. R. Steacie, *Proc. Roy. Soc. (London)*, **A250**, 287 (1959).

(21) P. G. Bowers and G. B. Porter, *J. Phys. Chem.*, **68**, 2982 (1964).

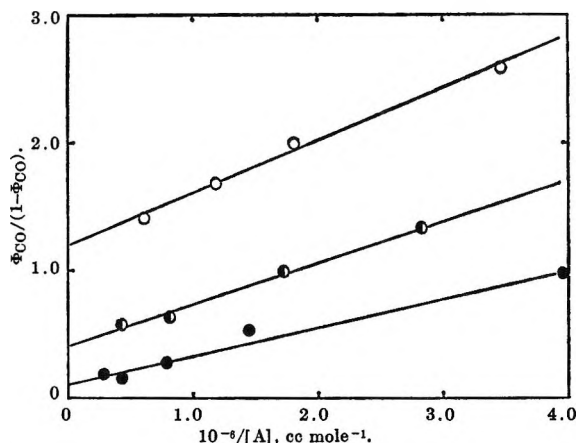


Figure 5. $\Phi_{CO}/(1 - \Phi_{CO})$ vs. reciprocal of ketone concentration: O, 90°; ◐, 45°; ●, 27°.

Assuming that $k_c[A] \gg k_b$, the following equation is obtained from the above mechanism:²³ $\Phi_{CO}/(1 - \Phi_{CO}) = k_b/k_c[A](1 - \alpha) + \alpha/(1 - \alpha)$, where $\alpha = k_d k_b / (k_d + k_e + k_f)(k_g + k_h + k_i)$, the quantum yield at infinite concentration.^{18,20} Plots of $\Phi_{CO}/(1 - \Phi_{CO})$ vs. the reciprocal of ketone concentration are given in Figure 5. Good straight lines are obtained similar to those obtained for $C_2F_5COC_2F_5$ at 3130 Å.¹⁸ The values of α which may be obtained from the intercepts (0.11 at 27°, 0.26 at 45°, and 0.54 at 90°) can be plotted in the form^{18,20} of $\log [(1/\alpha) - 1]$ vs. $1/T$

(°K) leading to an apparent negative activation energy of 7.5 ± 1.5 kcal mole⁻¹, which is the energy barrier mainly associated with decomposition from the triplet state,¹⁸ reaction h. The values of α are very similar to those given for the three perfluoroketones, CF_3COCF_3 , $C_2F_5COC_2F_5$, and $C_3F_7COC_3F_7$, over the same temperature range at 3130 Å, leading to apparent negative activation energies of 9.2, 8.9, and 7.8 kcal mole⁻¹, respectively.¹⁸

Acknowledgment. We are indebted to Dr. Bernard Kirtman for helpful discussions.

(22) This is not necessarily the correct mechanism, but it has been chosen so that we may compare directly our data with the perfluoro ketones. CF_3COCH_3 is presumably a better comparative model, but Φ_{CO} vs. pressure data at different temperatures are not available in the literature. (The data⁸ on Φ_{CO} vs. pressure at 117° show the expected quenching effect.) It is not clear that the intersystem crossover should be represented solely by reaction d, or necessarily by $^1A^* \rightarrow ^3A^*$ as Ausloos and Murad suggest for CF_3COCH_3 .¹⁶ Presumably the singlet-triplet "leak" may occur more readily at some other level in the vibrational cascade. Ausloos and Murad observed¹⁶ an increase in the phosphorescence with increasing pressure, compatible with the step $^3A^* + A \rightarrow ^3A^0 + A$, but at still higher pressures (at 3130 Å) the phosphorescence decreased. They further observed no pressure effect on the fluorescence yield, which was difficult to visualize.¹³

(23) The assumption that primary quantum yield = Φ_{CO} neglects the fraction of C_2H_5CO radicals that do not dissociate; this will be more important at lower temperatures. This will not, however, affect the nature of the pressure dependencies as depicted in Figure 4, which are identical with those observed for $C_2F_5COC_2F_5$, where there is no evidence of a nondissociative fate for the C_2F_5CO radical.¹

The Zero-Charge Potential of Indium Amalgams in Perchloric Acid

by James N. Butler

Tyco Laboratories, Inc., Waltham, Massachusetts 02154 (Received February 2, 1966)

The potential of zero charge for amalgam electrodes containing up to 64 mole % indium has been measured in perchloric acid solutions of concentration from 0.01 to 1.0 *M* at 25°. The results indicate that the specific adsorption of perchlorate ion is smaller on the amalgams than on mercury and goes through a minimum at approximately 5 mole % indium. The temperature coefficient of the zero-charge potential for mercury and indium amalgams in 0.1 *M* HClO₄ was measured in a cell without liquid junctions. Using thermodynamic data together with some nonthermodynamic values, temperature coefficients of the Galvani potential difference between metal and electrode were calculated. These values were compared with those calculated from data in the literature; the comparison confirms the observation that specific adsorption of perchlorate ion on the amalgams is probably smaller than on mercury. The increase of double-layer capacity with indium concentration is thus probably due to changes in the structure of the dipolar layers at the interface, and not to specific adsorption of ions.

Introduction

Accurate measurements of the potential of zero charge are a vital prerequisite for theoretical analysis of electrical double-layer capacities. The zero-charge potential of a liquid metal electrode can be measured most precisely by observing the potential at which no charging current flows when the area of the electrode is changed. However, this method is restricted, not only by the condition that the electrode be a liquid metal, but also by the requirement that the electrode be ideally polarized. No charge-transfer reactions can have an appreciable rate in the potential range under consideration, or else the zero potential obtained is not a thermodynamic property of the interface, but instead depends on the nature of the charge-transfer reaction.

These requirements greatly restrict the number of systems on which accurate measurements of zero-charge potential can be made. For mercury in aqueous solutions, a wide range of data has been obtained,¹⁻⁸ but little work has been done using other electrode materials. There is good reason for this: virtually all liquid alloys of mercury and gallium with other metals undergo dissolution reactions, making the measurement of zero-charge potentials much less accurate than on mercury.^{9,10}

Indium amalgams, however, provide a good approximation to the ideal polarized electrode over a wide range of potentials, including the zero-charge potential. This system has the further advantage of wide composition range; liquid alloys containing up to 70% indium in mercury can be prepared at room temperature. In a previous publication¹¹ we presented some preliminary measurements of the zero-charge potential of indium amalgams in 0.1 *M* HClO₄ at 25°, but no measurements giving the variation of zero-charge

- (1) D. C. Grahame, R. P. Larsen, and M. A. Poth, *J. Am. Chem. Soc.*, **71**, 2978 (1949).
- (2) D. C. Grahame, E. M. Coffin, J. I. Cummings, and M. A. Poth, *ibid.*, **74**, 1207 (1952).
- (3) R. Parsons, *Proc. Intern. Congr. Surface Activity*, **2nd**, **3**, 38 (1957).
- (4) D. C. Grahame and R. Parsons, *J. Am. Chem. Soc.*, **83**, 1291 (1961).
- (5) R. Parsons and F. G. R. Zobel, *J. Electroanal. Chem.*, **9**, 333 (1965).
- (6) R. Payne, Thesis, Imperial College, London, 1962; G. J. Hills and R. Payne, *Trans. Faraday Soc.*, **61**, 316, 326 (1965).
- (7) R. Payne, *J. Electroanal. Chem.*, **7**, 343 (1964); *J. Chem. Phys.*, **42**, 3371 (1965); *J. Phys. Chem.*, **69**, 4113 (1965).
- (8) R. Payne, *ibid.*, **70**, 204 (1966).
- (9) A. N. Frumkin and F. J. Cirves, *ibid.*, **34**, 74 (1930).
- (10) J. N. Butler, *J. Electroanal. Chem.*, **9**, 149 (1965).
- (11) J. N. Butler and A. C. Makrides, *Trans. Faraday Soc.*, **60**, 1664 (1964).

potential with electrolyte composition or temperature were reported.

From the variation of the zero-charge potential with the composition of the solution, qualitative information about the specific adsorption of anions can be obtained,^{3,8,12,13} and such measurements are the logical antecedent to measurements of capacity¹⁴ and interfacial tension¹⁵ from which quantitative information about adsorption can be obtained. The variation of the zero-charge potential with temperature, although it is often difficult to interpret theoretically, is again an essential prerequisite to any studies of the temperature dependence of adsorption phenomena by means of capacity measurements.

One of the questions which arose in our previous studies of the electrical double layer on indium amalgams¹⁴ was whether the increase in capacity with increasing indium concentration was due to specific adsorption or to changes in the dipolar structure of the interface. The study presented here was undertaken primarily to answer this question.

By analogy with mercury,^{16,17} indium amalgams might be expected to show relatively little specific adsorption of fluoride ions. However, preliminary experiments with sodium fluoride solutions showed that the indium amalgams underwent reversible dissolution at potentials where the surface charge was still negative. This happened because the high stability of fluoride ion complexes¹⁸ with In^{+3} in aqueous solutions can shift the reversible potential of the In/In^{+3} electrode as much as 200 mv more negative than perchlorate solutions. The streaming electrode method is thus unsatisfactory for determining the zero-charge potentials of indium amalgams in fluoride solutions. Perchlorate ion forms only very weak complexes with indium¹⁸ and shows only moderate specific adsorption on mercury,^{8,17} so perchlorate solutions were the next choice after fluoride solutions.

In this paper we report measurements of the zero-charge potentials of indium amalgams in solutions of HClO_4 as a function of temperature and composition, and interpret these in terms of the specific adsorption of perchlorate ions in the electrical double layer.

Experimental Section

The electrolyte was prepared from triple-distilled water, using reagent grade perchloric acid (J. T. Baker), and was purified by preelectrolysis with platinum electrodes for 16 hr. The solution was saturated with purified hydrogen throughout preelectrolysis and measurement. The cell was constructed entirely of glass and Teflon, cleaned with chromic-sulfuric acid, and rinsed in triple-distilled water. A platinized-

platinum hydrogen reference electrode in the same solution, separated from the main compartment by a glass frit, was used for all of the measurements.

Indium amalgams were prepared from triple-distilled mercury (Doe and Ingalls) and 99.999% pure indium (American Smelting and Refining Co.) by mixing weighed quantities of the two materials under an argon atmosphere. The indium dissolved in the mercury to give a homogeneous liquid within a few minutes.

Most of the values for zero-charge potentials reported here were measured by the streaming electrode method: method V described by Grahame.¹ The amalgam flowed from a reservoir through a capillary into the solution, and its potential was measured with respect to a reversible hydrogen electrode in the same solution. Since measurements of electrode impedance¹⁴ show that no reversible electron-transfer reactions take place under these conditions, the streaming electrode potential should be the potential of zero charge. However, an irreversible electrode reaction could shift the streaming electrode potential and yet have no effect on the ac impedance of a dropping electrode, but such a reaction should be detectable as a dependence of streaming electrode potential on the rate of flow of amalgam. We observed no such dependence.

As an additional test, direct measurements of surface charge were made using a dropping electrode. As we have shown previously,¹⁹ a plot of $I t^{1/3}$, where I is the instantaneous current flowing at time t from the birth of the drop, under potentiostatic conditions, can be extrapolated to zero time to give a quantity A proportional to the surface charge density q

$$A = \frac{2}{3}(36\pi)^{1/3}q(m/\rho)^{2/3}$$

where m is the mass flow rate of amalgam through the capillary and ρ is the density of the amalgam.

Potentiostatic current-time curves were measured for dropping electrodes at several potentials either side of the streaming electrode potential, extrapolated to

(12) O. A. Esin and B. F. Markov, *Acta Physicochim. URSS*, **10**, 353 (1939).

(13) P. Delahay, "Double Layer and Electrode Kinetics," Interscience Publishers, Inc., New York, N. Y., 1965, Chapter 4.

(14) J. N. Butler, M. L. Meehan, and A. C. Makrides, *J. Electroanal. Chem.*, **9**, 237 (1965).

(15) J. N. Butler, *J. Phys. Chem.*, **69**, 3817 (1965).

(16) D. C. Grahame, *J. Am. Chem. Soc.*, **76**, 4819 (1954).

(17) D. C. Grahame, M. A. Poth, and J. I. Cummings, *ibid.*, **74**, 4422 (1952).

(18) N. Sundén, *Svensk Kem. Tidskr.*, **66**, 50 (1954).

(19) J. N. Butler and M. L. Meehan, *J. Phys. Chem.*, **69**, 4051 (1965).

zero time as described,¹⁹ and the intercepts plotted as a function of potential. The point at which the interpolation curve crossed the axis was taken to be the potential of zero charge. Although this method gives somewhat less precise (± 2 mv) values of zero-charge potential than does the streaming electrode, any interference from reversible or irreversible charge-transfer reactions is immediately apparent as a non-zero slope for the curve $It^{1/2}$ vs. t or $t^{1/2}$; this method thus serves as an additional check on the accuracy of the streaming electrode potentials.

Results

Zero-charge potentials of mercury and indium amalgams in perchloric acid solutions at 25° are given in Table I. We have also listed values for the activity of indium in the amalgam²⁰ and of HClO₄ in the electrolyte.²¹

In Table I, we have given a value of -0.160 v vs. a reversible hydrogen electrode for the zero-charge potential of mercury in 0.1 M HClO₄. This agrees with Payne's precise value²² of -0.162 , and with Grahame's values² for 0.1 M KClO₄ and NaClO₄, both of which correspond to -0.162 . This value is more positive than our previously published^{11,14} values of -0.165 and -0.170 , and the value of -0.183 (0.493 vs. sce) obtained by Hansen, *et al.*,²³ from the maximum of the electrocapillary curve for mercury in 0.1 M HClO₄.

Figure 1 shows the dependence of the zero-charge potential (vs. a fixed reference electrode) on the concentration of indium in the amalgam and perchloric acid in the electrolyte. The differences for tenfold change in perchloric acid concentration are smaller (20 to 30 mv) than the differences observed for mercury (30 to 50 mv). The values obtained previously^{11,14} for indium amalgams in 0.1 M HClO₄ agree within experimental error with the present measurements. The probable error of the present data is approximately 2 mv, a considerable improvement over errors of up to 10 mv in the older data.

Zero-charge potentials in 0.1 M HClO₄ at various temperatures are listed in Table II. Very few data exist with which our results on the temperature coefficient (Table III) can be compared. Randles and Whiteley²⁴ measured the temperature coefficient of the zero-charge potential for mercury in three cells without liquid junctions. The temperature coefficients given by Grahame²⁵ for mercury in KCl and NaF were measured in cells with the reference electrode held at constant temperature. Only for KCl are sufficient data available so that these results may be compared with ours.

The values given by Lee and Tai²⁶ for the tempera-

Table I: Zero-Charge Potentials of Indium Amalgams in HClO₄ at 25°

Mole % In	a_{In}	E_z^a
1.00 M HClO ₄ ($a_{\pm} = 0.823$)		
0	0	-0.273
5.00	0.0707	-0.375
10.00	0.196	-0.407
20.00	0.717	-0.462
39.83	3.83	-0.561
63.02	13.46	-0.637
0.100 M HClO ₄ ($a_{\pm} = 0.0803$)		
0	0	-0.160
0	0	-0.160*
0.015	0.00015	-0.167*
0.138	0.0014	-0.202*
1.23	0.0134	-0.255*
5.00	0.0707	-0.297*
5.97	0.0900	-0.301
10.00	0.196	-0.334*
10.02	0.197	-0.327
20.34	0.743	-0.388
39.89	3.84	-0.483
63.02	13.46	-0.553
0.0100 M HClO ₄ ($a_{\pm} = 0.00903$)		
0	0	-0.086
5.97	0.0900	-0.241
10.02	0.197	-0.267
20.34	0.743	-0.321
39.89	3.84	-0.400
63.02	13.46	-0.468

^a The zero-charge potential E_z is given in volts vs. a reversible hydrogen electrode in the same solution. To convert to the saturated calomel electrode scale (Figure 1), add -0.250 to the 1.0 M values, -0.310 to the 0.1 M values, and -0.365 to the 0.01 M values. Measurements were by the streaming electrode method except those marked with an asterisk (*), which were measured by the direct surface charge method.

ture coefficient of the zero-charge potential of mercury in KCl, which were quoted in a recent review,²⁷ appear to be incorrect.²⁴ These values were not in fact measured by Lee and Tai but were calculated from some

(20) J. N. Butler, *J. Phys. Chem.*, **68**, 1828 (1964).

(21) R. A. Robinson and R. H. Stokes, "Electrolyte Solutions," 2nd ed, Butterworth and Co. Ltd., London, 1959, pp 491-501.

(22) R. Payne, private communication.

(23) R. S. Hansen, D. J. Kelsh, and D. H. Grantham, *J. Phys. Chem.*, **67**, 2316 (1963).

(24) J. E. B. Randles and K. S. Whiteley, *Trans. Faraday Soc.*, **52**, 1509 (1956).

(25) D. C. Grahame, *J. Am. Chem. Soc.*, **79**, 2093 (1957).

(26) F. H. Lee and Y. K. Tai, *J. Chinese Chem. Soc.*, **8**, 60 (1941).

(27) B. E. Conway, "Modern Aspects of Electrochemistry," Vol. 1, Butterworth and Co. Ltd., London, 1954, pp 54-61.

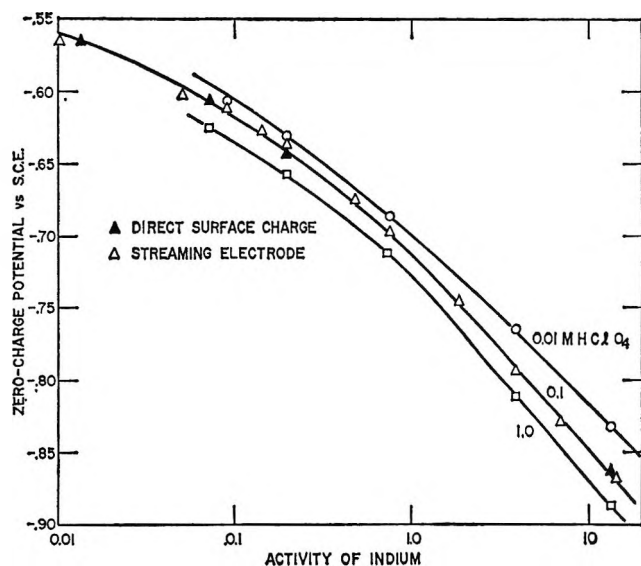


Figure 1. Zero-charge potentials of indium amalgams in HClO_4 solutions of various concentrations, with respect to the saturated calomel electrode (see Table I)

Table II: Zero-Charge Potentials in 0.1 M HClO_4 at Various Temperatures

Electrode material	Temp. °C	E_z^a
Hg	9.8	-0.1596
	19.4	-0.1600
	25.0	-0.1598
	26.5	-0.1586
	36.7	-0.1590
	50.0	-0.1597
	55.0	-0.1605
	59.0	-0.1614
20% In	25.0	-0.388
	59.0	-0.394
40% In	25.0	-0.483
	44.5	-0.485
	56.5	-0.488
	59.0	-0.488

^a E_z is in volts vs. a reversible hydrogen electrode in the same solution. All values were measured by the streaming electrode method.

values quoted in a textbook²⁸ for the "absolute emf of the calomel electrode." Unfortunately, no reference is given to the original measurements.

Composition Dependence

For an ideally polarized electrode, the shift of zero-charge potential with electrolyte composition is given by the equation^{3,13}

$$\left(\frac{\partial E_z}{\partial \ln a_{\pm}}\right)_q = \frac{RT}{F} \left[1 + 2 \left(\frac{\partial q_-}{\partial q}\right)_a \right] \quad (1)$$

where E_z is the potential with respect to an external, fixed reference electrode, a_{\pm} is the mean activity of the 1:1 electrolyte, q is the surface charge on the electrode, q_- is the charge in solution contributed by anions, R is the gas constant, T is the absolute temperature, and F is the Faraday constant.

If there is no specific adsorption of ions at the electrode, the charge in solution is entirely in the diffuse double layer, and the Gouy-Chapman theory may be used to calculate the dependence of q_- on q . At the potential of zero charge, this theory gives simply

$$\left(\frac{\partial q_-}{\partial q}\right)_{\substack{a_{\pm} = \text{const} \\ q = 0}} = -1/2 \quad (2)$$

which says that E_z is independent of a_{\pm} .

In the presence of specific adsorption, the coefficient $(\partial q_- / \partial q)$ is different from $-1/2$, a more negative value indicating stronger specific adsorption, and may often be independent of electrolyte concentration and surface charge. Studies of the variation of zero-charge potential and surface charge of mercury in KI, KBr, KCl, and HCl have shown^{3,12,13} that the potential at constant charge is closely approximated by a linear function of electrolyte activity, and that the slope of these lines is essentially independent of the surface charge. In the case of nitrate and perchlorate,^{7,8} which are more weakly adsorbed, this dependence is more complicated, but qualitatively similar. This means that a measurement of the dependence of zero-charge potential on electrolyte composition can give considerable qualitative information about the extent of specific adsorption of ions, without the extensive measurements required for a detailed study of capacity and interfacial tension. It cannot, of course, give the detailed form of the adsorption isotherms.

We calculated the coefficients $(\partial q_- / \partial q)$ from our data in the following manner. From the graphs of Figure 1, values of the zero-charge potential were interpolated at round values of indium concentration, and a plot of these interpolated values was made as a function of $\log a_{\pm}$. This plot was linear within experimental error over a 100-fold variation in concentration.

In Figure 2 are plotted the values of $(\partial q_- / \partial q)$ calculated using eq 1. The vertical bars indicate the approximate error in the values of the coefficient calculated from the measured slopes, and the line is a smooth function which approximates the calculated values.

(28) J. Reilly and W. N. Rae, "Physico-Chemical Methods," 2nd ed, D. Van Nostrand Co., Inc., New York, N. Y., 1933, p 731.

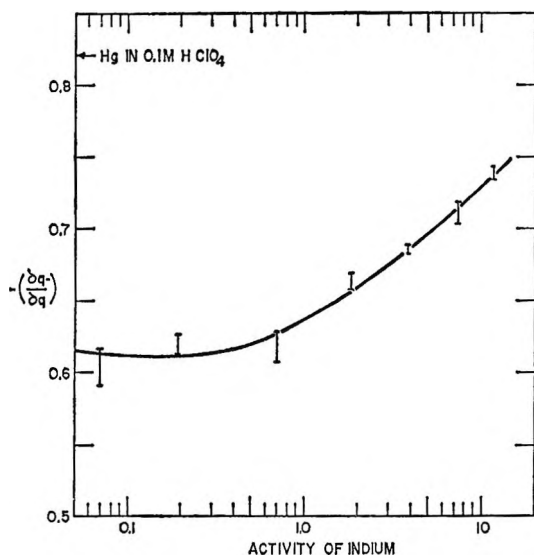


Figure 2. The coefficient $-(\partial q_0 / \partial q)$ calculated from the data in Figure 1, using eq 1. A larger value of this coefficient is a qualitative indication of increased specific adsorption of perchlorate ions.

A value for the coefficient $-(\partial q_0 / \partial q)$ greater than $1/2$ indicates that specific adsorption of the anion occurs, and from Figure 2 it is apparent that some specific adsorption of perchlorate ions occurs on indium amalgams, but less than on mercury. The adsorption appears to pass through a minimum at approximately 5 mole % indium ($a_{In} = 0.07$), and on the most concentrated amalgams is nearly as large as on mercury.

In our previous studies¹⁴ of the double-layer capacity of indium amalgams in 0.1 M HClO₄, we observed that at constant surface charge the capacity increases with increasing amalgam concentration. The results of the present study have shown that the adsorption of perchlorate ions is smaller on indium amalgams of all concentrations than on mercury. Specific adsorption of ClO₄⁻ ions is therefore unlikely to be responsible for the large increase in double-layer capacity with indium concentration. The other possible effect, a change in the dipolar structure of the amalgam-aqueous interface with composition, is more likely to be responsible for the increased capacity.

The lower specific adsorption of perchlorate ion and higher double-layer capacity on indium amalgams parallels the results for gallium. Frumkin, *et al.*,²⁹ observed that the adsorption of perchlorate, as well as other anions, is less on gallium than on mercury. This, together with the higher double-layer capacity, was attributed to a stronger bond between water and gallium than between water and mercury. A similar explanation could be invoked for the indium amalgams,

although data on adsorption of water vapor are not available to support this hypothesis.

In addition to changes in the electronic dipolar layer in the metal and the water dipole orientation in the electrolyte, the increased capacity of indium amalgams with respect to mercury could also be attributed to the indium-mercury dipoles in the interface. Our studies of interfacial tension¹⁵ showed that the surface deficiency of indium went through a maximum at approximately 20 mole % indium ($a_{In} = 0.7$), and that the surface deficiency itself was potential dependent. This implies that shifts in composition of the metallic side of the interface could contribute significantly to the capacity measured by an ac impedance bridge, and that this contribution would be most important in the region from 5 to 20% indium. This effect may be responsible, at least in part, for the maximum in capacity at the zero-charge potential observed between 1 and 20% indium.¹⁴

The minimum in the specific adsorption of perchlorate ions at approximately 5 to 10% indium (Figure 2) could result from the opposition of two tendencies. The decrease in specific adsorption at low indium concentrations may result from changes in the orientation of water dipoles in the same way that specific adsorption is lower on gallium than on mercury.²⁹ At higher indium concentrations, however, a larger fraction of the metal surface consists of indium atoms, and chemical bonding of the perchlorate ions to indium atoms may become important. To test this hypothesis effectively, measurements should be made of the complete adsorption isotherms for a number of anions having different effects on the structure of water and different affinities for indium and mercury.

Temperature Dependence

The temperature coefficient of the zero-charge potential in a cell without liquid junctions can be expressed as a combination of entropy terms, most of which are independently measurable. Three terms, however, occur in inseparable combination: the absolute entropy of the hydrogen ion (or any other single ion), the entropy of electrons in the metal, and the entropy associated with the specifically adsorbed ions and the dipolar layers at the metal-electrolyte boundary. Since the entropy of the hydrogen ion is approximately known, and is in any case independent of the nature of the metal or electrolyte being studied, and the entropy of electrons in the metal is small, the way in which the temperature coefficient of the zero-

(29) A. N. Frumkin, N. Polianovskaya, N. Grigorev, and I. Bagot-skaya, *Electrochim. Acta*, 10, 793 (1965).

Table III: Temperature Coefficient of Zero-Charge Potential Measured in Cells without Liquid Junctions

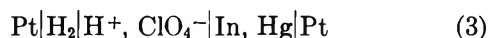
Ideal polarized electrode	Electrolyte	Ref electrode	Exptl dE_z/dT , mv/deg	Calcd ^a $d(\Delta\phi_z)/dT$, mv/deg	Ref
Hg	0.1 M HClO ₄	Pt H ₂ H ⁺	-0.05 ± 0.01	0.68	This work
20.0% In	0.1 M HClO ₄		-0.18 ± 0.05	0.55	This work
40.0% In	0.1 M HClO ₄		-0.15 ± 0.03	0.58	This work
Hg	1.0 M KCl	Hg Hg ₂ Cl ₂ Cl ⁻	+0.07	0.72	2, recalcd
Hg	0.1 M KCl		-0.184	0.63	2, recalcd
Hg	0.1 M KCl		-0.153	0.67	24
Hg	0.1 M KCl		-0.153	0.66	24, recalcd
Hg	0.1 M KOH	Hg HgO OH ⁻	+0.548	0.57	24
Hg	0.1 M KOH		+0.548	0.55	24, recalcd
Hg	0.1 M K ₂ SO ₄	Hg Hg ₂ SO ₄ SO ₄ ²⁻	+0.292	0.56	24
Hg	0.1 M K ₂ SO ₄		+0.292	0.51	24, recalcd

^a See Discussion.

charge potential varies can give some information about the structure of the double layer at the metal-electrolyte interface.

Unfortunately, measurements of the temperature coefficient of zero-charge potential sufficiently accurate to make even qualitative observations are extremely difficult to obtain. We have already mentioned the studies on mercury by Randles and Whiteley,²⁴ and this discussion of our measurements on indium amalgams follows theirs rather closely.

For our cell



where the amalgam-electrolyte interface is assumed to be at the zero-charge potential and ideally polarized, we may make the usual analysis of electrochemical equilibrium^{13,24} to obtain the cell potential E_z in terms of the chemical potentials of the components

$$E_z - \Delta\phi_z = \frac{1}{F} \left(\frac{1}{2} \mu_{\text{H}_2}^\circ - \mu_{\text{H}^+}^\circ - \mu_e^{\text{am}} \right) \quad (4)$$

where $\Delta\phi_z$ is the Galvani potential difference between the amalgam and electrolyte, $\mu_{\text{H}_2}^\circ$ and $\mu_{\text{H}^+}^\circ$ are the standard chemical potentials of H₂(g) and H⁺(aq), respectively, and μ_e^{am} is the chemical potential of electrons in the amalgam.

Taking the temperature derivative of eq 4, we obtain

$$\frac{dE_z}{dT} - \frac{d}{dT}(\Delta\phi_z) = \frac{1}{F} \left(-\frac{1}{2} S_{\text{H}_2}^\circ + S_{\text{H}^+}^\circ + S_e^{\text{am}} - R \ln a_{\text{H}^+} - RT \frac{\partial \ln \gamma_{\text{H}^+}}{\partial T} \right) \quad (5)$$

The absolute entropy of hydrogen gas³⁰ is $S_{\text{H}_2}^\circ = 32.211$ cal/mole deg. The activity coefficient²¹ of 0.1 M HClO₄ is 0.803, which gives $R \ln a_{\text{H}^+} = -5.01$

cal/mole deg. The partial molar enthalpy of dilution³¹ for 0.1 M HCl is 202 cal/mole, which gives a reasonable estimate of +0.34 cal/mole deg for the last term of eq 5. The other terms are not so well known, but can be estimated. The entropy of the conduction electrons in metals is small,²⁴ less than 0.1 cal/mole deg, and was assumed to be 0 for these calculations. The absolute entropy of the hydrogen ion, as estimated from measurements of the entropy of transfer in reversible cells,^{24,27} is approximately $S_{\text{H}^+}^\circ = -5.5$ cal/mole deg. Making these approximations, eq 5 yields the result

$$\frac{d}{dT}(\Delta\phi_z) = \frac{dE_z}{dT} + 0.73 \text{ mv/deg} \quad (6)$$

Our experimental results for dE_z/dT gave the values for $[d(\Delta\phi_z)/dT]$ shown in Table III, and are compared there with those obtained by other workers for the interface between mercury and various electrolytes. Since Randles and Whiteley²⁴ did not give the details of the values they used for the activity coefficients and partial molar enthalpies, we repeated their calculations. We have also calculated $[d(\Delta\phi_z)/dT]$ from Grahame's data.²

In our calculations of these data, the absolute entropies of Hg, Hg₂Cl₂, HgO, and HgSO₄ were taken from Latimer,³⁰ activity coefficients were taken from Robinson and Stokes,²¹ partial molar enthalpies of dilution were taken from Harned and Owen,³¹ the entropy of electrons in the metallic phase was assumed to be zero, and the absolute entropies of the various ions

(30) W. M. Latimer, "Oxidation Potentials," 2nd ed, Prentice-Hall, Inc., Englewood Cliffs, N. J., 1952, pp 30, 176.

(31) H. S. Harned and B. B. Owen, "Physical Chemistry of Electrolyte Solutions," 3rd ed, Reinhold Publishers, Inc., New York, N. Y., 1958, pp 709-710.

were calculated from Latimer's values,³⁰ assuming that the absolute entropy of H^+ was -5.5 cal/mole deg. As can be seen from Table III, in no case did the results agree exactly with the values obtained by Randles and Whiteley, but the difference was significant only in the case of Hg in K_2SO_4 .

Although the probable error in these values is large, certain trends do exist which may be related to the specific adsorption of anions, and to the structure of the dipole layer at the interface. Because the specific adsorption of an anion at the interface is not only exothermic, but also probably involves a loss in entropy, the extent of specific adsorption is probably smaller at higher temperatures, and hence the temperature coefficient of the potential drop across the interface will be larger in the presence of specific adsorption than if no specific adsorption occurs. Looking at the values for KCl measured by Grahame,² we see that the coefficient $[d(\Delta\phi_z)/dT]$ is larger for $1.0 M$ KCl than for $0.1 M$ KCl, which confirms this notion since the specific adsorption of chloride ion is much more extensive in the concentrated solution.^{17,32} Similarly, comparing the values obtained by Randles and Whiteley for KCl, KOH, and K_2SO_4 , we see that the temperature coefficient in KCl, where specific adsorption is moderate, is larger than in KOH or K_2SO_4 , where specific adsorption is probably small.^{6,7,17}

Turning now to our results for indium amalgams in perchloric acid we find that the temperature coefficient $[d\Delta\phi_z/dT]$ on mercury is comparable to the values obtained for KCl, indicating moderate specific adsorption. The indium amalgams show smaller values for the temperature coefficient, which is consistent with our observation that $-(\partial q_-/\partial q)$ is smaller on the amalgams than on mercury. Unfortunately, this result does not allow us to separate unambiguously specific adsorption from dipolar effects. Because of the larger entropy of the amalgam interface, due to its more complex dipolar structure, we expect that the coefficient $[d\Delta\phi_z/dT]$ would probably be smaller on the amalgams, even if there was no change in the degree of specific adsorption.

Acknowledgments. This work was supported by the U. S. Office of Naval Research, Materials Sciences Division. The author wishes to thank Mrs. Mary L. Meehan for her assistance with the experimental work, Dr. Richard Payne for data in advance of publication, and Dr. A. C. Makrides for his helpful criticism and discussion.

(32) J. R. Sams, C. W. Lees, and D. C. Grahame, *J. Phys. Chem.* **63**, 2032 (1959).

Chemical Relaxation Spectra: Calculation of Relaxation Times for Complex Mechanisms¹

by Gordon G. Hammes and Paul R. Schimmel²

Department of Chemistry, Cornell University, Ithaca, New York (Received February 2, 1966)

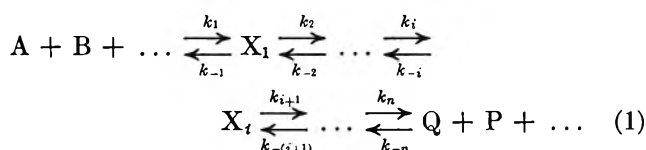
A theoretical treatment of chemical relaxation spectra is given; the only restrictive assumption employed is that for a given mechanistic scheme no more than two steps which equilibrate at comparable rates are coupled together *via* rapid reactions. A determinantal method for explicitly computing relaxation times is developed. For the general mechanism where the *i*th reaction is only coupled to the *i* - 1 and *i* + 1 reaction and where the products of the *i*th reaction are the reactants for the *i* + 1st reaction, the relaxation times characterizing the mechanism may be written by examination (without performing the usually complex mathematical operations) regardless of the number of steps in the mechanism or the molecularity (or order) of each reaction. Under certain conditions, the relaxation times for more complex mechanisms also may be written by examination.

Introduction

Chemical relaxation techniques are now being applied to a wide variety of reactions.³ Several theoretical treatments of chemical relaxation have been developed.³ Except for the most simple mechanisms, the mathematical analysis required for calculating the relaxation spectrum is somewhat complex and laborious. A similar difficulty exists in the mathematical analysis of other complex reaction kinetic phenomena and methods for simplifying the mathematical labor are highly desirable. Special mention should be made of the schematic method of King and Altman⁴ which has greatly reduced the computational labor in treating steady-state enzymatic mechanisms.

We present here an analysis of the relaxation spectrum of a mechanism which permits individual relaxation times to be readily calculated. The general theoretical treatment is based on the formulation of Kirkwood and Crawford⁵ and more recently, Castellan.⁶ Under certain conditions the relaxation spectrum can be written by inspection with the use of a schematic method.

The mechanism we will consider in detail is



where the number of intermediates, reactants, and products is arbitrary. Actually, as we will discuss later, the critical feature of this mechanism is that the *i*th step is only coupled to the (*i* - 1) and (*i* + 1) steps (*i* ≠ 1, *n*) and the products of the *i*th reaction are the reactants of the *i* + 1st reaction; each step can be of arbitrary molecularity or order. An exact computation of the *n* relaxation times when *n* is greater than 2 is virtually impossible; however, approximate calculations can be made which will be adequate to describe most of the situations encountered in actual practice. The simplifying assumption which is made is that no more than two steps which equilibrate at comparable rates are coupled together *via* rapid reactions. The method which is developed eliminates the necessity of solving a large number of simultaneous linear differential equations and under certain conditions may be ex-

(1) This work was supported by a grant from the National Institutes of Health (GM13292).

(2) National Institutes of Health Predoctoral Fellow.

(3) See, for example, the reviews by M. Eigen and L. de Maeyer in "Techniques of Organic Chemistry," Vol. VIII, Part II, S. L. Friess, E. S. Lewis, and A. Weissberger, Ed., Interscience Publishers, Inc., New York, N. Y., 1963, p 895, and M. Eigen and G. G. Hammes, *Advan. Enzymol.*, **25**, 1 (1963).

(4) E. L. King and C. Altman, *J. Phys. Chem.*, **60**, 1375 (1956).

(5) J. G. Kirkwood and B. Crawford, *ibid.*, **56**, 1048 (1952).

(6) G. W. Castellan, *Ber. Bunsenges. Physik. Chem.*, **67**, 898 (1963).

tended to include even more general mechanisms than described by eq 1.

General Theory

A direct approach for obtaining the n relaxation times for the mechanism of eq 1 is to linearize the n differential equations characterizing the mechanism;³ the resultant n differential equations are of the form

$$-\frac{d\Delta c_i}{dt} = \sum_{k=1}^n a_{ik}\Delta c_k \quad (i = 1 \dots n) \quad (2)$$

or

$$-\frac{d\Delta \mathbf{c}}{dt} = \mathbf{a}\Delta \mathbf{c} \quad (3)$$

where Δc_i is the deviation of the i th species from its equilibrium value, c_i , $\Delta \mathbf{c}$ is the column matrix of the Δc_i 's, and \mathbf{a} is a square matrix of the a_{ik} 's which are known functions of rate constants and equilibrium concentrations. The reciprocal relaxation times, $1/\tau$, are the n eigenvalues of the secular equation

$$\left| \mathbf{a} - \frac{1}{\tau} \mathbf{I} \right| = 0 \quad (4)$$

where \mathbf{I} is the unit matrix and $\left| \mathbf{a} - 1/\tau \mathbf{I} \right|$ is the determinant of the matrix $\mathbf{a} - 1/\tau \mathbf{I}$. The solutions to the n differential equations are of the form

$$\Delta c_i = \sum_{j=1}^n A_{ij} e^{-t/\tau_j} \quad (5)$$

In general, when n is large an exact analytical solution to eq 4 is not possible. However, approximate solutions are easily obtained for many special cases. For this purpose, the form of the matrix \mathbf{a} is inconvenient. Alternatively, we may introduce a change of variables which will yield a coefficient matrix of a more tractable form. Adopting the transformation employed by Kirkwood and Crawford⁵ and Castellan,⁶ we write

$$n_i = n_i^0 + \sum_{\alpha=1}^n \nu_{i\alpha} \xi_{\alpha} \quad (i = 1 \dots n) \quad (6)$$

$$\Delta n_i = \sum_{\alpha=1}^n \nu_{i\alpha} \Delta \xi_{\alpha} \quad (i = 1 \dots n)$$

where $\nu_{i\alpha}$ and ξ_{α} are the stoichiometric coefficients of the i th species in the α th reaction and degree of advancement of the α th reaction, respectively; n_i^0 is the reference value of the mole number of the i th species, and $\Delta \xi_{\alpha}$ is the deviation of the degree of advancement, ξ_{α} , from its equilibrium value, $\bar{\xi}_{\alpha}$. Castellan⁶ has shown that the relaxation times for any chemical reaction

mechanisms are the eigenvalues of the matrix \mathbf{b} which is defined by

$$-\frac{d\Delta \xi}{dt} = \mathbf{b}\Delta \xi \quad (7)$$

where $\Delta \xi$ is the column vector of the $\Delta \xi_{\alpha}$'s. The matrix \mathbf{b} may be written as a product of two matrices, \mathbf{r} and \mathbf{g} , which may be computed by use of rules given by Castellan.⁶ The matrix \mathbf{r} is a diagonal matrix whose typical diagonal element, r_i , is

$$r_i = k_i \prod_{\alpha} \bar{c}_{\alpha}^{-\nu_{i\alpha}} \quad (8)$$

where the product is taken over only the reactants of the i th reaction. (Obviously, r_i can also be written in terms of the reverse rate constants and concentrations of products if desired.) The typical element, g_{ij} , of \mathbf{g} is

$$g_{ij} = \sum_{\beta=1}^n \frac{\nu_{\beta i} \nu_{\beta j}}{\bar{c}_{\beta}} = g_{ji} \quad (9)$$

The element g_{ij} arises from the "coupling" between the i th and j th reaction. Thus the i th reaction gives rise to the i th row and column of \mathbf{g} and premultiplication of \mathbf{g} by a diagonal matrix \mathbf{r} yields \mathbf{b} whose elements in the i th row and column arise from the i th reaction and its coupling to other equilibria. Direct computation yields the matrix \mathbf{b} which is triple diagonal with all elements equal to zero except

$$b_{ii} = k_i + k_{-i}$$

$$b_{ij} = -k_i; \quad j = i - 1, \quad i \neq 1$$

$$b_{ij} = -k_{-i}; \quad j = i + 1, \quad i \neq n$$

If the first step in the mechanism is unimolecular, $b_{11} = k_1 + k_{-1}$; for two reactants $b_{11} = k_1(\bar{A} + \bar{B}) + k_{-1}$; for three reactants $b_{11} = k_1(\bar{AB} + \bar{AC} + \bar{BC}) + k_{-1}$ where the bars designate equilibrium concentrations. Extension to higher order reactions and to b_{nn} is obvious.

The relaxation times are given as solutions of the secular equation

$$\left| \mathbf{b} - \frac{1}{\tau} \mathbf{I} \right| = 0 \quad (10)$$

The analysis given above shows that the j th equilibrium is represented by the j th row and column of \mathbf{b} . This fact will be of importance when it is desirable to reduce the order of the matrix for various special cases considered below.

Case I: Calculation of Relaxation Times for Equilibria Coupled to Only Relatively Fast Reactions. If the

j th reaction is assumed to be slowly equilibrated compared to the remaining equilibria then

$$k_j + k_{-j} \ll k_i + k_{-i} \quad i \neq j \tag{11}$$

$$1/\tau \ll k_i + k_{-i} \quad i \neq j$$

where τ is the relaxation time associated with j th equilibria. The secular equation can then be written as

$$\left| \mathbf{b} - \frac{1}{\tau} \mathbf{I} \right| = \begin{vmatrix} k_1 + k_{-1} & -k_{-1} & 0 & \dots & \dots & \dots \\ -k_2 & k_2 + k_{-2} & -k_{-2} & \dots & \dots & \dots \\ \dots & \dots & \dots & \dots & \dots & \dots \\ \dots & 0 & -k_j & k_j + k_{-j} - 1/\tau & -k_{-j} & 0 \\ \dots & \dots & \dots & \dots & \dots & \dots \\ \dots & \dots & \dots & \dots & 0 & -k_n \quad k_n + k_{-n} \end{vmatrix} = 0 \tag{12}$$

Application of the theorem "If each element in one column is expressed as the sum of two terms, then the determinant is equal to the sum of two determinants, in each of which one of the two terms is deleted in each element of that column,"⁷ to the j th column of b enables eq 10 to be written as

$$\left| \mathbf{b} - \frac{1}{\tau} \mathbf{I} \right| = |\mathbf{b}| - \frac{1}{\tau} |\mathbf{b}_{jj}| = 0$$

or

$$\frac{1}{\tau} = \frac{|\mathbf{b}|}{|\mathbf{b}_{jj}|} \tag{13}$$

where $|\mathbf{b}_{jj}|$ is the cofactor of b_{jj} and is formally obtained by deleting the j th row and column of $|\mathbf{b}|$. The matrix \mathbf{b}_{jj} is a block diagonal form; the eigenvalues of a block diagonal form are the eigenvalues of the individual blocks. Thus, after the longest relaxation time is computed, corresponding say to the j th equilibrium, two sub-matrices are constructed, one consisting of all of the matrix elements above and to the left of b_{jj} , the other consisting of all elements below and to the right of b_{jj} . The longest relaxation time of each sub-matrix is then computed by the same procedure used for the original matrix, \mathbf{b} . This matrix "factorization" procedure is continued until the shortest relaxation time of each sub-matrix is obtained; this is the diagonal element associated with the fastest reaction in each sub-matrix. (For a 1×1 matrix, $|\mathbf{b}_{jj}|$ is defined as unity.) This procedure may be used to obtain explicit expressions for each of the n relaxation times as long as steps which equilibrate at comparable rates are not coupled together *via* rapid reactions.

Case II: Calculation of Coupled Relaxation Times. If two of the equilibria, the k th and m th, equilibrate at a comparable rate and are coupled *via* rapid reac-

tions to the remaining equilibria, then use of the assumption

$$1/\tau_k \text{ and } 1/\tau_m \ll k_i + k_{-i} \quad (i \neq k, m)$$

in eq 10 and reiterated use of the theorem employed previously, determines the two relaxation times as solutions of the quadratic (eq 14)

$$|\mathbf{b}_{kk,mm}| \left(\frac{1}{\tau} \right)^2 - (|\mathbf{b}_{kk}| + |\mathbf{b}_{mm}|) \frac{1}{\tau} + |\mathbf{b}| = 0 \tag{14}$$

where $|\mathbf{b}_{kk,mm}|$ is formally obtained by deleting the k th and m th row and column of $|\mathbf{b}|$. (For a 2×2 matrix $|\mathbf{b}_{kk,mm}|$ is defined as being equal to unity.) Therefore, the relaxation spectrum can be explicitly evaluated if no more than two steps, which are coupled *via* rapid reactions, equilibrate at comparable rates. In a similar fashion, solutions can be constructed for cases where more than two equilibria equilibrate at comparable rates and are coupled *via* rapid reactions. However, cubic or higher order equations must be solved so that such a procedure is of little practical utility.

Evaluation of the Determinants. The determinant $|\mathbf{b}|$ is triple diagonal in form with each diagonal element being a linear combination of the two adjacent off-diagonal elements, that is

$$b_{jj} = -(b_{j,j-1} + b_{j,j+1}) \quad (j \neq 1, n)$$

Because of this relationship, the determinant can be easily evaluated. We perform the following operations: add column two to column one; multiply column one by k_{-1}/k_1 and add to column two; multiply column one by k_1/k_{-1} . These operations do not change the value of the determinant.⁷ We now add column three to column one; multiply column three by $(1 + k_{-1}/k_1)$ and add to column two; multiply column three by $1/(1 + k_{-1}/k_1)$; multiply column two by k_{-2}/k_2 and add to column three; and finally multiply column two by k_2/k_{-2} . Repetition of this procedure $n - 1$ times yields eq 15

(7) F. B. Hildebrand, "Methods of Applied Mathematics," Prentice-Hall, Inc., Englewood Cliffs, N. J., 1952, Chapter I.

$$|\mathbf{b}| = \begin{vmatrix} k_1 & 0 & 0 & \dots & 0 \\ 0 & k_2 & 0 & \dots & 0 \\ \cdot & 0 & \cdot & \cdot & \cdot \\ \cdot & \cdot & \cdot & k_t & \cdot \\ \cdot & \cdot & \cdot & \cdot & \cdot \\ k_{-n} & k_{-n}(1 + k_{-1}/k_1) & \cdot & \cdot & k_n + k_{-n} \sum_{i=0}^{n-1} K_i^{n-1} \end{vmatrix} \quad (15)$$

where

$$K_i^{n-1} = \prod_{r=i+1}^{n-1} k_{-r}/k_r; \quad K_{n-1}^{n-1} = 1$$

and k_1 and k_{-n} are understood to be functions of equilibrium concentrations as previously discussed. This determinant can be easily evaluated to give

$$|\mathbf{b}| = \prod_{i=1}^n k_i + \prod_{i=1}^{n-1} k_i k_{-n} \sum_{j=0}^{n-1} K_j^{n-1} = \sum_{p=0}^n \left(\prod_{i=1}^p k_i \prod_{j=p+1}^n k_{-j} \right) \equiv P_1^n \quad (16)$$

It will be useful to define the symbol

$$P_m^s \equiv \sum_{p=m-1}^s \prod_{i=m}^p k_i \prod_{j=p+1}^s k_{-j} \quad (17)$$

where products running from a higher to a lower integer equal unity and m is an integer greater than zero. Each term can easily be written by examination. For

example, for $m = 1$ the first term in the sum is $\prod_{j=1}^s k_{-j}$;

the second term is $k_1 \prod_{i=2}^s k_{-i}$, etc.

The matrix \mathbf{b}_{jj} is obtained by deleting the j th row and column of \mathbf{b} . Since this matrix is in block diagonal form, the determinant is the product of the determinants of the two blocks (eq 18)

$$|\mathbf{b}_{jj}| = \begin{vmatrix} k_1 + k_{-1} & -k_{-1} & \cdot & 0 & 0 \\ -k_2 & k_2 + k_{-2} & 0 & \cdot & \cdot \\ 0 & \cdot & \cdot & \cdot & \cdot \\ 0 & 0 & \cdot & -k_{j-1} & k_{j-1} + k_{-(j-1)} \end{vmatrix} \times \begin{vmatrix} k_{j+1} + k_{-(j+1)} & -k_{-(j+1)} & \cdot & 0 & 0 \\ -k_{j+2} & \cdot & \cdot & \cdot & \cdot \\ \cdot & \cdot & \cdot & k_{n-1} + k_{-(n-1)} & -k_{-(n-1)} \\ 0 & \cdot & \cdot & -k_n & k_n + k_{-n} \end{vmatrix} \quad (18)$$

By use of the procedure previously described for evaluating $|\mathbf{b}|$, we find that

$$|\mathbf{b}_{jj}| = P_1^{j-1} P_{j+1}^n \quad (19)$$

From a similar analysis it may be shown that the determinant $|\mathbf{b}_{jj,kk}|$ is the product of three determinants

$$|\mathbf{b}_{jj,kk}| = P_1^{j-1} P_{j+1}^{k-1} P_{k+1}^n \quad (20)$$

If reactions of higher molecularity than one are involved, the rate constants are modified as previously discussed.

Summary of Results and Illustrations of the Method

For the reaction mechanism being considered, the relaxation time of the k th equilibrium which is coupled *via* rapid reactions to the i th thru $k - 1$ and $k + 1$ thru m th equilibria is

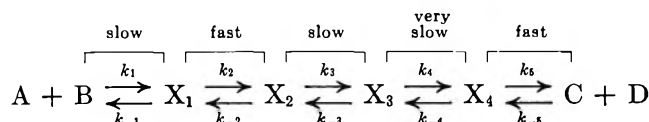
$$\frac{1}{\tau} = \frac{P_i^m}{P_i^{k-1} P_{k+1}^m} \quad (21)$$

where P_m^s is defined by eq 17 and is easily evaluated by examination.

If the j th and m th reactions equilibrate at comparable rates and are coupled to each other and the i th thru $j - 1$ st and $m + 1$ st thru r th equilibria *via* rapid reactions, the two relaxation times are solutions of the equation

$$(P_1^{j-1} P_{j+1}^{m-1} P_{m+1}^r)(1/\tau)^2 - (P_i^{j-1} P_{j+1}^r + P_i^{m-1} P_{m+1}^r)(1/\tau) + P_i^r = 0 \quad (22)$$

As a particular illustration of the methods described, consider the mechanism



The "very slow" step is coupled to all of the other reactions; hence the relaxation time is

$$\frac{1}{\tau_4} = \frac{P_1^5}{P_1^3 P_5^5}$$

$$P_1^5 = k_{-1}k_{-2}k_{-3}k_{-4}k_{-5}' + k_1'k_{-2}k_{-3}k_{-4}k_{-5}' + k_1'k_2k_{-3}k_{-4}k_{-5}' + k_1'k_2k_3k_{-4}k_{-5}' + k_1'k_2k_3k_4k_{-5}' + k_1'k_2k_3k_4k_5$$

$$P_1^3 = k_{-1}k_{-2}k_{-3} + k_1'k_{-2}k_{-3} + k_1'k_2k_{-3} + k_1'k_2k_3$$

$$P_5^5 = k_5 + k_{-5}'$$

$$k_1' = k_1(\bar{A} + \bar{B}); k_{-5}' = k_{-5}(\bar{C} + \bar{D})$$

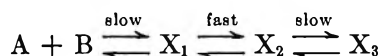
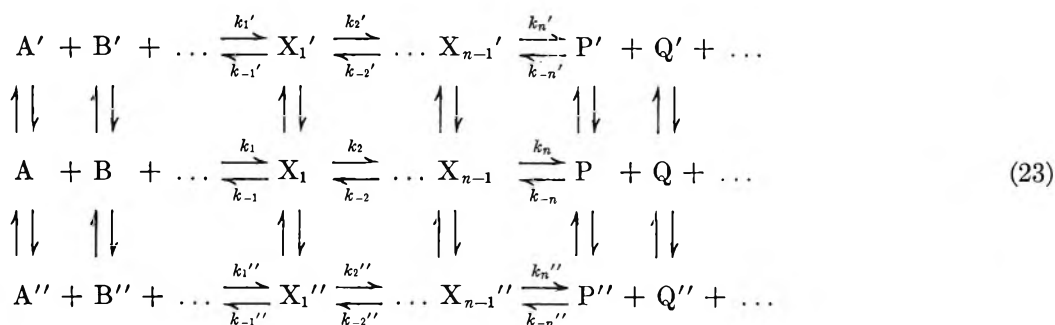
which gives

$$\frac{1}{\tau_4} = \frac{k_4}{1 + \frac{k_{-1}k_{-2}k_{-3} + k_1(\bar{A} + \bar{B})[k_{-2}k_{-3} + k_2k_{-3}]}{k_1(\bar{A} + \bar{B})k_2k_3}} + \frac{k_{-4}}{1 + \frac{k_5}{k_{-5}(\bar{C} + \bar{D})}}$$

The step $X_4 \rightleftharpoons C + D$ is not coupled to any other reactions, so

$$\frac{1}{\tau_5} = \frac{P_5^5}{P_5^4} = k_5 + k_{-5}(\bar{C} + \bar{D})$$

(note $P_5^4 = 1$). The sequence (below eq 23)



is not coupled to the remaining reactions. The relaxation time of the fast step is

$$\frac{1}{\tau_2} = P_2^2 = k_2 + k_{-2}$$

while the relaxation times for the two slow steps are solutions of the quadratic

$$\left(\frac{1}{\tau_{1,3}}\right)^2 P_2^2 - (P_2^3 + P_1^2) \left(\frac{1}{\tau_{1,3}}\right) + P_1^3 = 0$$

where

$$P_2^2 = k_2 + k_{-2}$$

$$P_2^3 = k_{-2}k_{-3} + k_2k_{-3} + k_2k_3$$

$$P_1^3 = k_{-1}k_{-2}k_{-3} + k_1'k_{-2}k_{-3} + k_1'k_2k_{-3} + k_1'k_2k_3$$

$$P_1^2 = k_1k_2 + k_1k_{-2} + k_{-1}k_{-2}$$

Thus we have explicitly evaluated the relaxation spectrum of our illustrative mechanism.

Discussion

The validity of the schematic method rests on the fact that the i th reaction in eq 1 is coupled to the $i - 1$ and $i + 1$ reactions only ($i \neq 1, n$) and the products of the i th reaction are the reactants of the $i + 1$ st reaction; if this were not the case, $|b|$ would no longer be in the proper triple diagonal form and could not be easily computed. The method is applicable to any reaction mechanism where the individual reactions bear this relationship to each other regardless of the molecularity or order of the individual reactions. For higher order reactions the associated matrix elements are obtained exactly as previously discussed for b_{11} .

Under certain limiting conditions the method may be employed to compute relaxation times for more complex forms of the general mechanism given by eq 1. For example, if the vertical pathways equilibrate rapidly compared to the horizontal steps in mechanism 23

the relaxation times for the horizontal steps are easily evaluated by the schematic method. Equation 23 corresponds to eq 1 if we regard X_j in eq 1 as the total concentration of the j th species, *i.e.*, $X_j + X_j' + X_j''$. The rate at which the $j - 1$ species is converted to the j th species is

$$k_j X_{j-1} + k_j' X_{j-1}' + k_j'' X_{j-1}'' = k_j^* [X_{j-1} + X_{j-1}' + X_{j-1}'']$$

where

$$k_j^* = \frac{[k_j + k_j'K_{j-1}' + k_j/K_{j-1}'']}{1 + K_{j-1}' + 1/K_{j-1}''}$$

and

$$K_i' = \bar{X}_i' / \bar{X}_i; K_i'' = \bar{X}_i'' / \bar{X}_i''$$

If a reaction is of higher order than one, the situation is somewhat more complex, but the same procedure given above may be used to calculate k_i^* . For example, in the case of a bimolecular reaction, the rate at which A and B are transformed into X_1 is given by the equation

$$k_1(A)(B) + k_1'(A')(B') + k_1''(A'')(B'') = k_1^*(A + A' + A'')(B + B' + B'')$$

where

$$k_1^* = \frac{k_1 + k_1'K_A'K_B' + k_1''/(K_A''K_B'')}{(1 + K_A' + 1/K_A'')(1 + K_B' + 1/K_B'')}$$

Proceeding exactly as before (*cf.* eq 8 and 9), it can be shown that the $n \times n$ matrix \mathbf{b} describing the relaxation of the horizontal steps is identical with that for eq 1 except k_i is replaced by k_i^* .

Any number of rapidly equilibrating vertical steps can be added to the general mechanism. Since each series of vertical steps is separated by the slowly equilibrating horizontal reactions, the relaxation spectrum of each vertical group may be obtained by the methods described in this paper.

A procedure such as that used above is applicable only if the vertical steps equilibrate rapidly relative to the horizontal steps (or *vice versa*). For the case of a single reactant and product, eq 23 is characterized by $3n + 2$ relaxation times, although $5n + 2$ equilibria exist. If the vertical and horizontal steps equi-

brate at comparable rates, the fact that some of the reactions are thermodynamically dependent must be taken into account. For this general case, the order of the secular equation, eq 10, can be reduced in a straightforward manner by the procedure given by Castellan.⁶ The determinantal method and matrix factorization procedure may then be applied to the reduced equation.

The results obtained here are useful in that the relaxation spectrum of the general mechanism in eq 1 and certain more complicated mechanisms may be obtained without explicitly doing the associated complex mathematics. The determinantal method and matrix factorization procedure which are outlined here are a reformulation and extension of previously described results and may be applied to an arbitrary reaction mechanism; only the actual evaluation of the determinants will differ. In general, the cofactors $|\mathbf{b}_{jj}|$ etc., will not be in block diagonal form so that factorization into lower order determinants may not be possible. Thus, for example, after the longest relaxation time is found, the entire determinant $|\mathbf{b}_{jj}|$ must be considered (rather than two separate determinants) in finding the next longest relaxation time.

The Effect of Solvent Structure on the Mobility of Symmetrical Ions in Aqueous Solution

by Robert L. Kay and D. Fennell Evans

Mellon Institute, Pittsburgh, Pennsylvania 15213 (Received February 2, 1966)

Conductance measurements are reported for Me_4NBr , Et_4NBr , Pr_4NBr , Bu_4NBr , Me_4NI , Pr_4NI , and Bu_4NI in aqueous solutions at 45° . Solvent structural influences on the limiting conductance of these large ions as well as on the alkali and halide ions in aqueous solution are investigated by considering the effect of temperature and pressure on the Walden product and by comparing their behavior in aqueous solution with that in nonaqueous solution. The mobility of the larger tetraalkylammonium ions is shown to be influenced to a considerable extent by the enforcement of water structure about their hydrocarbon chains. The same explanation applied to diffusion data for nonelectrolytes and dipolar ions accounts for the dependence of their Walden products on temperature and solvent. The possibility that solvent structural influences also cause the greater-than-normal decrease of the equivalent conductance with concentration for the tetraalkylammonium iodides is considered.

Introduction

A recent investigation of the conductance of the tetraalkylammonium halides in aqueous solution at 10 and 25° ¹ indicated that the limiting conductance of these large cations is influenced to a considerable extent by the formation of what have been called clathratelike structures of water about their hydrocarbon chains. It has been shown² that such an assumption will explain the differences in the limiting Walden product for these ions in H_2O and D_2O . Also, the concentration dependence obtained could best be explained by the assumption that they were slightly associated in aqueous solution and that the amount of association increased with increasing anion size. The purpose of this extension of the conductance measurements to 45° was to study both the limiting Walden product and the apparent association of these large tetraalkylammonium ions under conditions in which the amount of solvent structure has been reduced substantially.

In the Discussion section, the hydrodynamic properties of both large and small symmetrical ions are investigated by comparing their behavior in aqueous and nonaqueous solutions and particularly by noting their temperature and pressure dependence. The investigation is also extended to nonelectrolytes and

dipolar ions. It was found that solvent structural effects were essential to any consistent explanation of transport properties of ions in aqueous solution at infinite dilution.

Experimental Section

The conductance bridge, conductance cells, salt-cup dispensing device, and general techniques were the same as previously described^{1,3,4} with the exception of the constant-temperature bath. This was an insulated stainless steel tank containing 12 gallons of oil and fitted on top with a chamber which had a hinged Plexiglas cover. This chamber was heated to a temperature of 47° with two 100-w light bulbs so as to prevent condensation of the solvent in the salt-cup dispensing device.⁴

The change in the cell constant from 25 to 45° , as calculated from the cell geometry and coefficients of expansion given by Robinson and Stokes,⁵ was found to be less than 0.01%.

- (1) D. F. Evans and R. L. Kay, *J. Phys. Chem.*, **70**, 366 (1966).
- (2) R. L. Kay and D. F. Evans, *ibid.*, **70**, 4216 (1965).
- (3) D. F. Evans, C. Zawoyski, and R. L. Kay, *ibid.*, **69**, 3878, 4208 (1965).
- (4) J. L. Hawes and R. L. Kay, *ibid.*, **69**, 2420 (1965).

Temperature was controlled to $45 \pm 0.007^\circ$ as determined by a calibrated platinum resistance thermometer.

The purification procedures for the conductivity water and the salts have been adequately described elsewhere.^{1,3}

Results

The density increments for the tetraalkylammonium bromide solutions, used to calculate the volume concentrations, were obtained from density measurements on 0.06 *M* solutions and were assumed to follow the relationship $d = d_0 + \theta \bar{m}$, where $d_0 = 0.99024$ at 45° and where \bar{m} is the concentration in moles per kilogram of solution. The θ values were found to be: Me₄NBr, 0.039; Et₄NBr, 0.036; Pr₄NBr, 0.027; Bu₄NBr, 0.022. The corresponding values for the iodides were estimated by adding the iodide-bromide difference of 0.030 obtained from density measurements at both 10 and 25° .¹ The viscosity *B* coefficients were measured⁶ and found to be: Me₄NBr, 0.11; Et₄NBr, 0.30; Pr₄NBr, 0.64; Bu₄NBr, 0.99. The corresponding values for the iodides were assumed to be 0.03 lower in keeping with the results found at 10 and 25° .

The measured equivalent conductances, the corresponding concentration in moles per liter, and the solvent conductances are given in Table I. The data were analyzed by the Fuoss-Onsager conductance theory⁷ in the form

$$\Lambda = \Lambda_0 - SC^{1/2} + EC \log C + (J - B\Lambda_0)C \quad (1)$$

and also, in the case of Pr₄NI and Bu₄NI, where association was detected, by

$$\Lambda = \Lambda_0 - S(C\gamma)^{1/2} + EC\gamma \log C\gamma + (J - B\Lambda_0)C\gamma - K_A C\gamma \Delta f^2 \quad (2)$$

The $\Delta\Lambda$ values in Table I are the difference between the measured Λ and that calculated by eq 1 or by eq 2 in the case of Pr₄NI and Bu₄NI. The conductance parameters in Table II were determined by a least-squares computation using computer programs.^{3,8} A dielectric constant $\epsilon = 71.51^9$ and a viscosity $\eta = 0.5963$ cp¹⁰ were used for water at 45° . In Table II, the standard deviations in each parameter, the standard deviations of the individual points σ_Λ , and the values of *J* are given for convenience of computation.

The limiting conductances for the tetraalkylammonium ions at 45° are given in Table III. They were calculated using $\lambda_0(\text{Br}^-) = 110.69$ and $\lambda_0(\text{I}^-) = 108.76$, which were obtained from the corresponding values at 25° as quoted by Evans and Kay¹ and the temperature-dependent equation of Harned and Owen.¹¹

Table I

10°C	Λ	$\Delta\Lambda$	10°C	Λ	$\Delta\Lambda$
Me ₄ NBr, $10^7\kappa_0 = 1.5$			Me ₄ NI, $10^7\kappa_0 = 1.5$		
9.021	171.64	0.05	5.946	170.50	0.03
18.025	169.90	-0.01	13.269	168.81	-0.01
27.756	168.53	-0.02	22.087	167.35	-0.02
38.001	167.33	-0.02	29.232	166.40	0.00
46.982	166.44	-0.01	37.168	165.46	0.00
59.365	165.34	0.00	43.543	164.78	0.00
68.416	164.62	0.00	53.256	163.84	0.00
78.396	163.89	0.02	61.667	163.10	0.01
Et ₄ NBr, $10^7\kappa_0 = 1.3$			Pr ₄ NI, $10^7\kappa_0 = 1.4$		
7.677	155.06	0.08	5.071	141.56	0.02
18.812	152.87	-0.04	10.888	140.01	-0.04
26.150	151.86	-0.03	16.667	138.91	0.00
37.251	150.56	-0.03	23.767	137.75	0.00
43.986	149.88	-0.02	29.931	136.89	0.02
54.455	148.92	-0.01	37.755	135.87	-0.01
65.171	148.05	0.02	44.892	135.06	0.00
78.792	147.03	0.03	52.972	134.20	-0.01
Pr ₄ NBr, $10^7\kappa_0 = 1.6$			Bu ₄ NI, $10^7\kappa_0 = 1.6$		
7.070	143.02	0.03	4.181	136.31	0.01
12.828	141.74	-0.02	10.183	134.60	-0.02
21.612	140.32	-0.02	16.331	133.32	-0.01
29.771	139.25	-0.01	23.413	132.10	0.01
36.440	138.50	0.02	31.353	130.88	-0.02
Bu ₄ NBr, $10^7\kappa_0 = 1.7$			Bu ₄ NI, $10^7\kappa_0 = 1.6$		
9.997	137.09	0.00	39.379	129.85	0.01
15.456	136.04	-0.01	46.903	128.94	0.01
21.553	135.09	-0.01	57.472	127.77	-0.01
27.473	134.33	0.03			
33.865	133.52	0.00			
41.102	132.72	0.00			
47.565	132.06	0.01			

The agreement in the cation conductances from the bromide and iodide salts is entirely satisfactory and indicates that the techniques employed here permit conductance measurements to be carried out at elevated temperatures with almost the same precision as those at 25° .

(5) R. A. Robinson and R. H. Stokes, "Electrolyte Solutions," 2nd ed, Butterworths and Co. Ltd., London, 1959, p 97.

(6) R. L. Kay, T. Vituccio, C. Zawoycki, and D. F. Evans, *J. Phys. Chem.*, **70**, 2336 (1966).

(7) R. M. Fuoss and F. Accascina, "Electrolytic Conductance," Interscience Publishers, Inc., New York, N. Y., 1959.

(8) R. L. Kay, *J. Am. Chem. Soc.*, **82**, 2099 (1960).

(9) C. G. Malmberg and A. A. Maryott, *J. Res. Natl. Bur. Std.*, **56**, 1 (1956).

(10) See ref 5, p 457.

(11) H. S. Harned and B. B. Owen, "The Physical Chemistry of Electrolytic Solutions," 3rd ed, Reinhold Publishing Corp., New York, N. Y., 1958, p 233.

Table II: Conductance Parameters for Aqueous Solutions at 45°

Salt	Λ_0	\bar{a}	K_A	σ_A	J
Me ₄ NBr	175.67 ± 0.02	2.04 ± 0.04		0.03	167.4
Et ₄ NBr	158.64 ± 0.03	1.98 ± 0.08		0.04	152.5
Pr ₄ NBr	146.45 ± 0.03	1.8 ± 0.1		0.03	128.0
Bu ₄ NBr	141.19 ± 0.02	2.02 ± 0.07		0.02	144.9
Me ₄ NI	173.79 ± 0.01	1.59 ± 0.03		0.02	124.7
Pr ₄ NI	144.48 ± 0.02	0.40 ± 0.05		0.03	-72.9
	144.56 ± 0.03 ^a	5 ± 2 ^a	3 ± 1 ^a	0.02	368.0
Bu ₄ NI	138.94 ± 0.03	0.10 ± 0.02		0.05	-75.4
	139.07 ± 0.02 ^a	6 ± 1 ^a	5.0 ± 0.8 ^a	0.02	453.4

^a Equation 2.**Table III:** Limiting Cation Conductances in Aqueous Solution at 45°

	Br ⁻	I ⁻	Λ_v
Me ₄ N ⁺	64.98	65.03	65.01
Et ₄ N ⁺	47.95		47.95
Pr ₄ N ⁺	35.76	35.80	35.78
Bu ₄ N ⁺	30.50	30.31	30.40

Discussion

(1) *Walden Product. Alkali Halides.* Before discussing the Walden product for the tetraalkylammonium ions, it is necessary to review the known results for smaller, univalent, symmetrical ions. These have been collected in Table IV along with data for the quaternary ammonium ions in all solvents for which precise transference numbers or for which data on a

Table IV: Limiting Ion Conductances^a

Ion	H ₂ O (45°) ^b	H ₂ O (25°) ^b	H ₂ O (10°) ^b	D ₂ O ^e	CH ₃ OH ^o	C ₂ H ₅ OH ⁱ	CH ₃ NO ₂ ^m	CH ₃ CN ⁿ
Li ⁺	58.02	38.66	26.37		39.55	17.07		
Na ⁺	73.83	50.20	34.93	41.62	45.17	20.30		
K ⁺	103.61	73.55	53.08	61.40	52.44	23.55		
Cs ⁺	107.56	77.29	56.50	64.44	60.83 ^h	26.46 ^j		
Me ₄ N ⁺	65.01	44.42	30.93	36.61 ^f	68.73	30.01 ^k	54.50	94.15
Et ₄ N ⁺	47.95	32.22	21.90	26.44 ^f	60.5	29.53 ^k	47.60	84.64
Pr ₄ N ⁺	35.78	23.22	15.33	18.84 ^f	46.08		39.14	70.28
Bu ₄ N ⁺	30.40	19.31	12.56	15.62 ^f	38.94	19.18 ^l	34.07	61.36
<i>n</i> -Am ₄ N ⁺		17.38 ^c			34.8			
<i>i</i> -Am ₃ BuN ⁺		20.67 ^d			36.6			58.13
F ⁻		55.32 ^e		44.79				
Cl ⁻	108.96	76.39	54.33	62.83	52.36	21.87	62.70	98.7
Br ⁻	110.69	78.22	56.15	64.67	56.45	24.02 ^k	62.94	100.74
I ⁻	108.76	76.98	55.39	63.79 ^f	62.78	26.13 ^k		102.69

^a Solvent viscosities, in centipoises, used to obtain Walden products are: H₂O (25°), 0.8903; H₂O (10°), 1.306; D₂O, 1.096; CH₃OH, 0.5445; C₂H₅OH, 1.084; CH₃NO₂, 0.627; CH₃CN, 0.341. ^b This work and ref 1 and 8. ^c H. M. Daggett, E. J. Bair, and C. A. Kraus, *J. Am. Chem. Soc.*, **73**, 799 (1951); ^d J. F. Skinner and R. M. Fuoss, *J. Phys. Chem.*, **68**, 1882 (1964). ^e C. G. Swain and D. F. Evans, *J. Am. Chem. Soc.*, **88**, 383 (1966). ^f R. L. Kay and D. F. Evans, *J. Phys. Chem.*, **69**, 4216 (1965). ^g The split into ionic conductances is discussed in detail in ref 3. ^h R. L. Kay and J. L. Hawes, *J. Phys. Chem.*, **69**, 2787 (1965). ⁱ The ionic conductances for the alkali and halide ions are based on the transference data of J. R. Graham and A. R. Gordon, *J. Am. Chem. Soc.*, **79**, 2350 (1957), and the conductance data of J. R. Graham, G. S. Kell, and A. R. Gordon, *ibid.*, **79**, 2352 (1957), as recalculated by R. L. Kay; see ref 8. ^j See ref 4. ^k T. H. Mead, O. L. Hughes, and H. Hartley, *J. Chem. Soc.*, 1207 (1933), and M. Barak and H. Hartley, *Z. Physik. Chem.*, **A165**, 273 (1933). ^l H. Sadek and R. M. Fuoss, *J. Am. Chem. Soc.*, **76**, 5902 (1954). ^m R. L. Kay, S. C. Blum, and H. I. Schiff, *J. Phys. Chem.*, **67**, 1223 (1963). ⁿ Ion conductances obtained from the salt conductances reported in ref 3 and the assumption that both ions of triisooamylbutylammonium tetraphenylboride have equal conductances of 58.13 as reported by M. A. Coplan and R. M. Fuoss, *J. Phys. Chem.*, **68**, 1181 (1964).

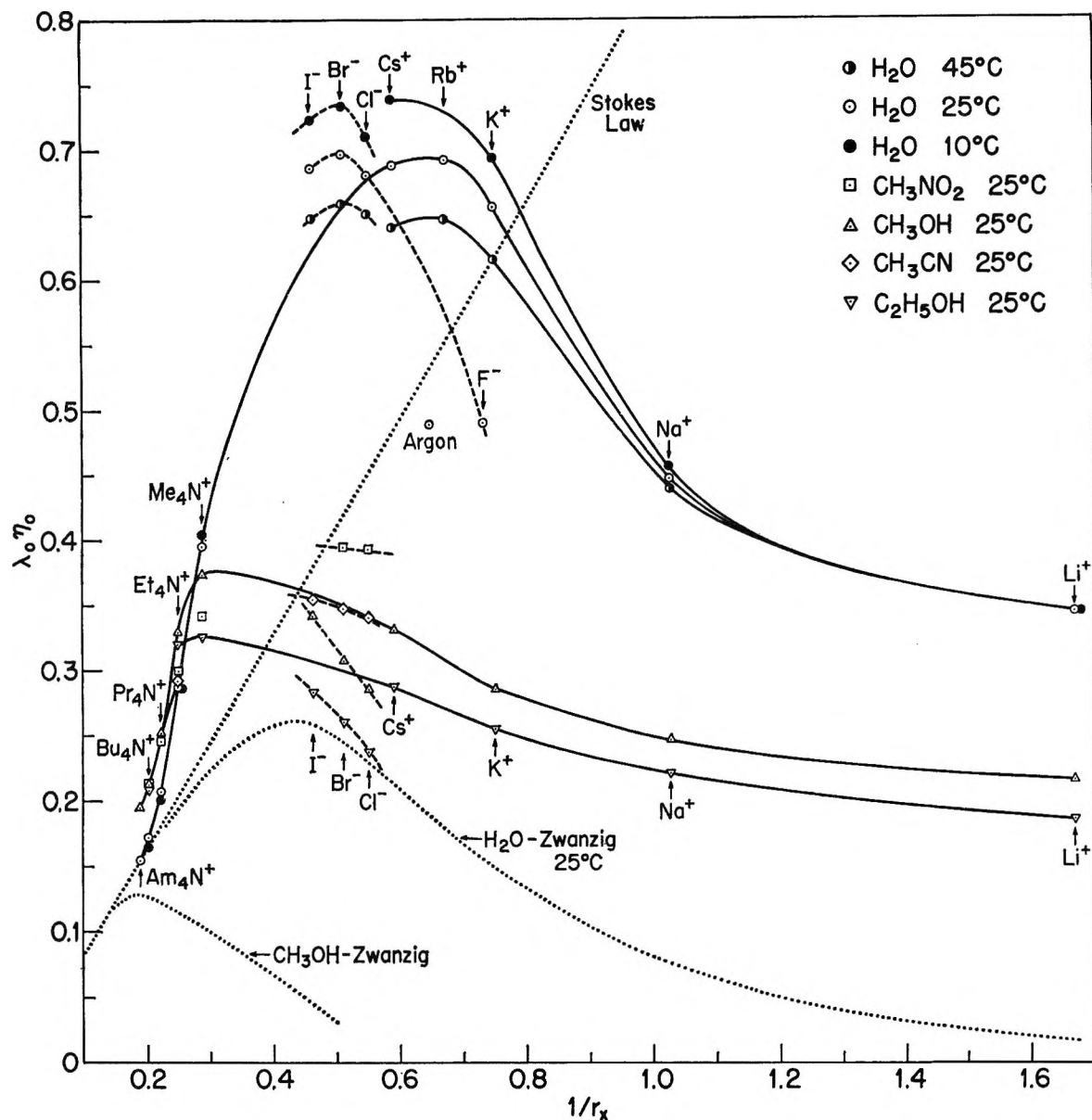


Figure 1. The limiting Walden product for the alkali halide and tetraalkylammonium ions as a function of crystallographic size, temperature, and solvent. Theoretical predictions are shown by the dotted curves.

reference electrolyte are available.¹² Where necessary, all conductances were recalculated to bring them into conformity with the Fuoss-Onsager equation (1) or (2). The data for D₂O and the nonaqueous solvents refer to 25°. The Walden products are plotted in Figure 1 as a function of the reciprocal estimated crystallographic ionic radii.¹³

It is obvious from the data for the alkali and halide ions in Figure 1 that Stokes' law¹⁴ given in terms of the Walden product by

$$\lambda_0 \eta / |Z| = F^2 / 6\pi N r_s \quad (3)$$

does not nearly describe the hydrodynamic behavior of the ions in any solvent, a fact that has been recognized for some time. One likely correction to Stokes'

(12) Owing to its unique transport mechanism, data for the H⁺ ion are not included. Although transference data are available for liquid ammonia solutions at -37° (J. L. Dye, R. Sankuer, and G. E. Smith, *J. Am. Chem. Soc.*, **82**, 4797 (1960)), ionic conductances are not known with a precision comparable to the data included in Table IV and, consequently, have not been included. Rough calculations indicate that the Walden product is about 0.50 for the halide ions and about 0.40 or less for the alkali ions, values considerably less than those for aqueous solution.

(13) See ref. 5, pp 125, 461.

(14) See ref 11, p 284.

law has been proposed by Fuoss¹⁵ and quantitatively evaluated by Zwanzig.¹⁶ This calculation takes into account the retardation due to the relaxation of solvent dipoles around the moving ion. It has been pointed out by Frank¹⁷ that the correction satisfactorily predicts the maximum in the λ_{07} curve but is too low in magnitude by a factor of almost 3, as can be seen in Figure 1. He has also shown that any reasonable modification of the equations involved is not nearly sufficient to account for the large discrepancy. A similar low result is obtained for methanol solution as is shown in Figure 1.

At this point, most discussions of the Walden product have taken one of the following two approaches. If the λ_{07} product results in a Stokes radius, as calculated from eq 1, greater than or equal to the crystallographic ionic radius, the ion in question is considered to be solvated or unsolvated, respectively. On the other hand, Stokes radii less than the crystallographic radii (λ_{07} above the Stokes' law line in Figure 1) cannot be attributed to solvation effects, and an appeal is made to the unrealistic model on which Stokes' law is based. A suitable calibration curve is then devised to correct for this deficiency.^{13,18} Our results for the tetraalkylammonium ions, which are discussed in detail below, show that the assumptions on which these calibration curves are based are invalid. Furthermore, it is impossible to obtain absolute values for the hydrodynamic ionic radii by merely appealing to solvation as a means of overcoming the inherent limitation of the model on which Stokes' law is based. Our approach here is to consider only ratios of Walden products in an effort to reduce errors due to inadequacies of the model and limitations of the concepts involved¹⁹ and thereby make our conclusions more meaningful.

In Figure 1, one aspect stands out very clearly: the Walden products for the alkali and halide ions in aqueous solution are substantially higher and show considerably more variation with crystallographic size than the corresponding values for nonaqueous solutions, all of which group closely together.²⁰ This apparent excess of mobility in aqueous solution could be attributed to far greater solvation in the nonaqueous solvents, and such an explanation would be sufficient if it were not for the temperature dependence of the Walden product. Unfortunately, although precise conductance data are available for methanol solution at 25 and 10°,³ transference measurements have been reported only for 25° (see Table IV), and a split into ionic conductances is not possible at 10°. However, as can be seen in Table V, the change in the Λ_{07} product from 10 to 25° for various salts is from 4 to 30 times greater in water than it is in methanol, but, for both sol-

vents, the change is in such a direction as to require greater solvation at higher temperatures, a prospect that is most unlikely. The Zwanzig equation predicts that the Walden product should increase 0.5% for a change in temperature from 10 to 25°, whereas the opposite behavior is observed for the alkali halides in aqueous solution.

Table V: Temperature Dependence of the Walden Product in H₂O and CH₃OH

	$(\Lambda_{07})_{10^\circ}/(\Lambda_{07})_{25^\circ}$	
	H ₂ O	CH ₃ OH
Me ₄ NBr	1.042	1.009
Et ₄ NBr	1.037	1.007
Pr ₄ NBr	1.034	1.006
Bu ₄ NBr	1.034	1.001
Me ₄ NI	1.044	1.011
Bu ₄ NI	1.035	1.002

It is generally accepted now²¹ that the larger alkali and halide ions possess an excess mobility in aqueous solution owing to their ability to break hydrogen bonds in their immediate vicinity and thereby reduce the local viscosity. An increase in temperature reduces the amount of hydrogen bonding in water and thereby reduces the effectiveness of these ions as structure breakers.

The subject of water structure and its effect on ionic properties has been discussed most recently by Frank²² and reviewed by Kavanau,²³ but Gurney²⁴ was the first to collect most of the evidence and clarify the con-

(15) R. M. Fuoss, *Proc. Natl. Acad. Sci. U. S.*, **45**, 807 (1959).

(16) R. Zwanzig, *J. Chem. Phys.*, **38**, 1603 (1963).

(17) H. S. Frank, "Chemical Physics of Ionic Solution," B. E. Conway and R. G. Barradas, Ed., Electrochemistry Society, John Wiley and Sons, Inc., New York, N. Y., 1966.

(18) E. R. Nightingale, Jr., *J. Phys. Chem.*, **63**, 1381 (1959).

(19) D. G. Miller, *ibid.*, **64**, 1598 (1960).

(20) It could be argued that the excess mobility of many ions in aqueous solution is due to the very high dielectric constant possessed by water. However, the same ions in other solvents of high dielectric constant do not show this large excess mobility. For example, the Walden products for formamide solutions at 25°, $\epsilon = 109.5$, range from 0.28 to 0.45 for the alkali ions and 0.57 to 0.55 for the halide ions. In Figure 1, it can be seen that these values are still lower than those for aqueous solutions. Transference data are from J. M. Notley and M. Spiro, *J. Phys. Chem.*, **70**, 1502 (1966).

(21) R. H. Stokes and R. Mills, "Viscosity of Electrolytes and Related Properties," Pergamon Press Inc., New York, N. Y., 1965, p 54.

(22) H. S. Frank, *Federation Proc.*, **24**, S-1 (1965).

(23) J. L. Kavanau, "Water and Solvent-Water Interactions," Holden-Day, Inc., San Francisco, Calif., 1964.

(24) R. W. Gurney, "Ionic Processes in Solution," McGraw-Hill Book Co., Inc., New York, N. Y., 1953.

cepts involved as far as transport properties are concerned. Here, we will use the Frank and Wen²⁵ model for ions in aqueous solution since it is sufficient in detail to explain the abnormal transport properties of the alkali, the halide, and the quaternary ammonium ions, as well as their temperature and pressure dependence. It has been used already to explain the difference in the Walden product obtained for H₂O and D₂O solutions.² In this model, the competitive influences of neighboring solvent dipoles and ionic charge on any given water molecule result in three separate regions around an ion. If the ionic charge predominates by a considerable amount, electrostriction occurs in which water molecules are immobilized to a considerable extent around the ion to form a solvation sheath. At much larger distances, where the effects of the ionic charge are insignificant, a given water molecule will be oriented solely by its neighboring water molecules, and consequently this region will have the properties of pure water. In the intermediate region, the ionic charge will not be strong enough to orient the water molecules completely, but it will interfere with the formation of the normal three-dimensional structures present in water. This region will be one with less solvent structure than bulk water, and this structure-breaking effect will become greater the smaller the charge-to-surface ratio of the ions. The region of immobilized water resulting from the structure-making effects of electrostriction will increase with increasing charge-to-surface ratio of the ions. Another effect has been postulated for the quaternary ammonium ions that possess large hydrophobic side chains. A water molecule at the surface of these large ions is influenced very little by either the ionic charge or the inert hydrocarbon chain on its one side. Consequently, the water molecules on this hydrophobic surface can be oriented to a greater extent by their nearest neighbors and can, in effect, be oriented into cages about the hydrocarbon side chains that are similar in structure, possibly, to the polyhedral clathrate hydrates of these ions.²⁶ These clathrate like structures can be considered a type of hydration, since they increase the size of the moving entity as is also the case with electrostrictive hydration. Ions experiencing this effect should have lower mobilities in aqueous solution than in nonaqueous solution since only water appears able to form any appreciable amount of three-dimensional structure.

On the basis of this model, at least part of the excess conductance of the alkali and halide ions in aqueous solution as shown in Figure 1 can be readily explained. With the possible exception of Li⁺, Na⁺, and F⁻, these ions are structure breakers in that they break down the hydrogen bonding in the water in their vi-

city and thereby decrease the local viscosity and increase the mobility of the ions. Perhaps the best experimental evidence comes from a comparison of the limiting diffusion coefficients of argon²⁷ and K⁺ and Cl⁻ ions in aqueous solution. As has been pointed out by Müller and Stokes,²⁸ although these are isoelectronic, the K⁺ and Cl⁻ ions are 34 and 39% faster, respectively, than the argon atom (see Figure 1). This difference can be attributed to the structure-breaking influence of the ions and possibility to the structure-making influence of the inert argon atom.²⁹ The diffusion coefficient of argon at 25° converts to a Walden product of approximately 0.49 and possibly indicates the maximum amount of the excess mobility in aqueous solution (34–39%) that can be attributed to the structure-breaking effect of the ions. As has been pointed out above, the decrease in Walden product with increased temperature for structure-breaking ions is due to the fact that there is less structure to break at higher temperatures. The fact, however, that the Walden products for these structure-breaking ions are still well above 0.49 at 100°⁵ indicates that this structural effect persists at even more elevated temperatures.³⁰

The smaller ions with large charge to surface ratios, such as the Li⁺, F⁻, and even Na⁺ ions, are less effective as structure breakers, and their conductance is controlled almost entirely by electrostrictive hydration that varies relatively little with increased temperature. The Walden products for multivalent ions are not shown in Figure 1, but, for the monatomic cations, they are all less than 0.3 in aqueous solution and are almost independent of ionic size and temperature, indicating that, because of their high charge density, their conductance is controlled almost exclusively by the amount of electrostrictive hydration.

It is interesting to apply these ideas to the effect of

(25) H. S. Frank and W. Y. Wen, *Discussions Faraday Soc.*, **24**, 133 (1957).

(26) P. T. Beurskens and G. A. Jeffrey, *J. Chem. Phys.*, **40**, 906 (1964).

(27) R. E. Smith, E. T. Friess, and M. F. Moralis, *J. Phys. Chem.*, **59**, 382 (1955).

(28) G. T. A. Müller and R. H. Stokes, *Trans. Faraday Soc.*, **53**, 642 (1957).

(29) H. S. Frank and M. W. Evans, *J. Chem. Phys.*, **13**, 507 (1945); A. Ben-Naim, *ibid.*, **42**, 1512 (1965).

(30) For example, Bu₄NBr in aqueous solution has been shown to have an excess partial molar heat capacity at 25° of almost 120 cal/deg mole due presumably to clathratelike structures of water enforced about its hydrocarbon side chains. This excess heat capacity is still detectable at temperatures as high as 130° (T. Ackermann, private communication, 1965). In this respect, it is interesting to note that Λ_{07} for K₂SO₄ decreases with increasing temperature between 100 and 400° at pressures high enough to keep the density of water equal to 1.0 (A. S. Quist, E. U. Franck, H. R. Jolley, and W. L. Marshall, *J. Phys. Chem.*, **67**, 2453 (1963)).

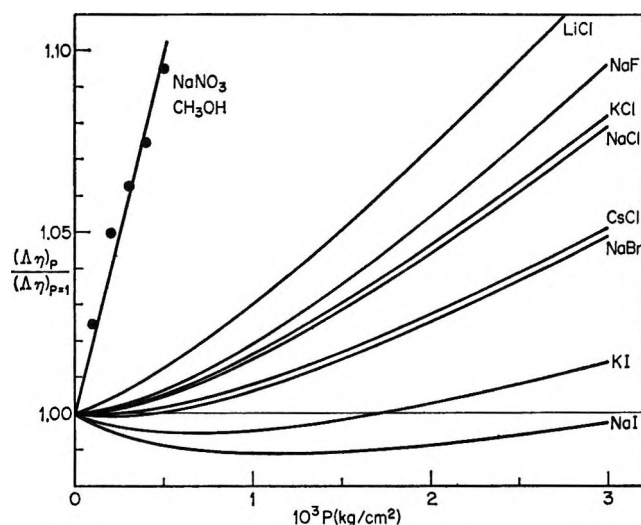


Figure 2. The relative change of the Walden product with pressure in 0.01 *N* aqueous and methanol solutions at 25°.

increased pressure on the Walden product in aqueous solution. One effect of increased pressure is to break down the bulky three-dimensional water structure and thereby produce a less structured solvent. This is verified by the fact that water is the only known liquid with a negative pressure coefficient of viscosity.^{31,32} As the pressure increases, all ions should become less effective structure breakers owing to this decreased amount of structure, and, consequently, the ions should lose some of their excess mobility. A possible second effect dealing with electrostrictively hydrated ions can also be predicted. Electrostriction results in a decrease in volume, as is shown by the increase in the dissociation constant of weak electrolytes as the pressure increases.^{33,34} Thus, small ions should become more hydrated as the pressure increases and therefore should have a lower conductance.

Both of these effects are evident in Figure 2 where the ratio of the Walden product at 30° and pressure *P* to that at atmospheric pressure and the same temperature are plotted as a function of pressure.³⁵ The Walden product for a 0.012 *N* solution of NaNO₃ in methanol increases very rapidly with increased pressure, whereas for all the salts in aqueous solution³⁶ the relative change in the Walden product as the pressure increases is considerably lower. Furthermore, the change with pressure is the lowest for the salts containing the best structure-breaking ions, such as the iodide and cesium ions. It can be seen that the Walden product actually decreases with increased pressure for KI and NaI. These observations are consistent with the idea that pressure breaks down the clusters of water structure and reduces the excess

conductance of structure-breaking ions. The main inconsistency with this argument is the fact that the sodium salts are all lower than the corresponding potassium salts, although potassium ion is a known better structure breaker. This could be a manifestation of the second effect; namely, increased hydration due to the high pressure could affect the sodium ion more than the potassium ion.³⁷ If it were not for the extensive hydration of the F⁻ and Li⁺ ions, NaF and LiCl would show a much greater increase in $\Delta\eta$ with pressure.

Further evidence that the interpretation of the pressure data given here is basically correct can be found in the effect of temperature on the pressure dependence of the Walden product. No effect, within the experimental error, is found in the pressure dependence of the Walden product for methanol solutions³⁵ on changing the temperature from 30 to 75°. In Figure 3, the results for aqueous solutions³⁵ are plotted where $R_{75^\circ}/R_{30^\circ}$ is given by

$$R_{75^\circ}/R_{30^\circ} = \left[\frac{(\Delta\eta)_P}{(\Delta\eta)_{P=1}} \right]_{75^\circ} / \left[\frac{(\Delta\eta)_P}{(\Delta\eta)_{P=1}} \right]_{30^\circ} \quad (4)$$

At 75° and $P = 1$ atm, there is less structure in water than at 30° and $P = 1$ atm. Consequently, there

(31) P. W. Bridgman, "The Physics of High Pressure," G. Bell and Son, Ltd., London, 1949, Chapter XII.

(32) K. E. Bett and J. B. Cappi, *Nature*, **207**, 620 (1965); J. B. Cappi, Ph.D. Thesis, University of London, 1964. We are indebted to Dr. Bett for a copy of these data prior to their publication.

(33) S. D. Hamann, P. J. Pearce, and W. Strauss, *J. Phys. Chem.*, **68**, 375 (1964).

(34) F. H. Fisher and D. F. Davis, *ibid.*, **69**, 2595 (1965).

(35) The conductance data for methanol solutions are those of S. B. Brummer and G. J. Hills, *Trans. Faraday Soc.*, **57**, 1823 (1961). The scatter in the points is due mainly to the lack of precision in the viscosity data.³¹ The conductance data for the various salts in aqueous solution at 30 and 75° were taken from W. A. Zisman, *Phys. Rev.*, **39**, 151 (1932), which, in the case of KCl, were found to be in fair agreement with the more recent data of F. Hensel and E. U. Franck, *Z. Naturforsch.*, **19**, 127 (1964). The viscosity data of Bett and Cappi³² for water at 30 and 75° were used. These data are in poor agreement with those of Bridgman but appear to be preferable since they are more consistent with the viscosity data at lower temperatures and agree better with those of W. Weber, *Z. Angew. Phys.*, **15**, 342 (1963), at lower pressures.

(36) The concentration here is 0.01 *M*. The relative Walden product has been found to be insensitive to concentration changes in the range 0–0.02 *M*.³⁴

(37) R. A. Horne, *Nature*, **200**, 418 (1963), has taken the opposite point of view that pressure "breaks up the structure of ionic hydration" so that LiCl lies higher than the other salts in Figure 2 since it undergoes the greatest decrease in the amount of hydration as the pressure increases. This interpretation, however, is not in agreement with the known fact that electrostrictive hydration results in a decrease in volume and therefore should be the preferred state as the pressure increases, as is noted above from the change of dissociation constants of salts with pressure. Also, his conclusion that all solvent structure has been destroyed at pressures above 2000 to 3000 kg/cm² is not well founded. It should be noted that Zisman's data have already been corrected for the solvent compressibility, and consequently the dotted line in Figure 2 of Horne's paper should not contain this factor.

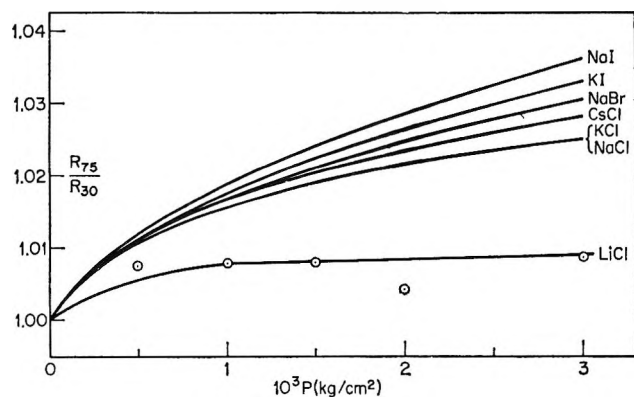


Figure 3. The Walden product at 75° relative to 30° as a function of pressure for aqueous solutions of the alkali halides.

should be less decrease of the Walden product at 75° upon increase in the pressure than at 30° for structure-breaking ions, and that is the result obtained from the data shown in Figure 3. The use of this double ratio is extending the data to the limit of their precision, but the results clearly illustrate that, in contrast to the other ions, the structure-making Li^+ ion shows little change with temperature.

Tetraalkylammonium Ions. The limiting Walden products for these ions are plotted in Figure 1 for comparison with the alkali and halide ions but are presented in more detail in Figure 4 as a function of the estimated crystallographic radii.¹³ It can be seen that, with the exception of Me_6N^+ and Et_4N^+ in hydroxylic solvents, the Walden products for these large ions in nonaqueous solvents are almost identical and fall on the solid line. In aqueous solution, however, the Me_6N^+ ion lies well above this line, suggesting it to be a structure breaker in aqueous solution as was found to be the case from a comparison of mobility data for H_2O and D_2O solutions.² At the other end of the scale, the Walden products for the Am_4N^+ , Bu_4N^+ , and Pr_4N^+ ions are well below this nonaqueous line, suggesting that in aqueous solution these ions are larger than in nonaqueous solvents. This is in keeping with the idea that clathrate-like structures form about the hydrocarbon portions of these ions as the length of the side chain increases. Such enforcement of water structure about the hydrophobic side chains of these ions would tend to increase the local viscosity as well as increase the size of the moving entity and thereby decrease the mobility.

The effect of temperature on the Walden product for these large cations is seen more readily in Figure 5, where the data of Lange³⁸ at 0° are included with our own at 10, 25, and 45°. Only the Et_4N^+ ion shows no temperature dependence, owing presumably to a can-

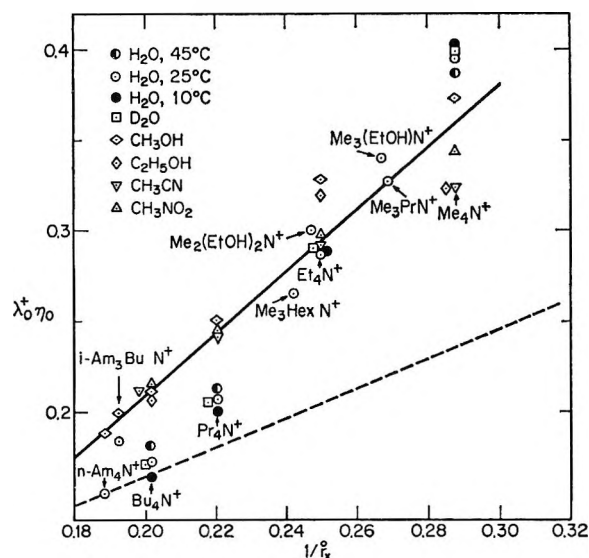


Figure 4. The limiting Walden product for various quaternary ammonium ions as a function of estimated crystallographic radii, temperature, and solvent.

cellation of the effects of structure breaking and structure making as judged by this criterion. The temperature dependence of viscosity B coefficients⁶ indicates this ion to be a slight structure maker whereas its mobility in D_2O relative to H_2O ² indicates a slight structure-breaking tendency. These seemingly conflicting results illustrate that the Et_4N^+ ion is a borderline case and that the different transport properties reflect slightly different aspects of ion-solvent interaction. The Me_6N^+ ion has a negative temperature coefficient, typical of structure-breaking ions, as was found with the larger alkali and halide ions. As the temperature increases, there is less structure available to be broken, and the Me_6N^+ ion is less effective in reducing the local viscosity. The Pr_4N^+ and Bu_4N^+ ions both have positive temperature coefficients as would be expected of ions forming clathratelike structures around their hydrocarbon side chains. As the temperature increases, these cages of water melt and produce a smaller and therefore faster-moving entity. Thus, the temperature dependence, the H_2O - D_2O comparison,² and the above comparison of Walden products in aqueous and nonaqueous solutions are consistent with the Frank-Wen²⁵ model for aqueous ionic solutions. It is also consistent with viscosity B coefficients and their temperature dependence.⁶

Further evidence for the existence of water structure enforcement about the hydrocarbon chains of the large tetraalkylammonium ions can be seen in Figure 4. The unsymmetrical $\text{Me}_3(\text{hexyl})\text{N}^+$ ³⁹ and Me_3 -

(38) J. Lange, *Z. Physik. Chem.*, **A168**, 147 (1934).

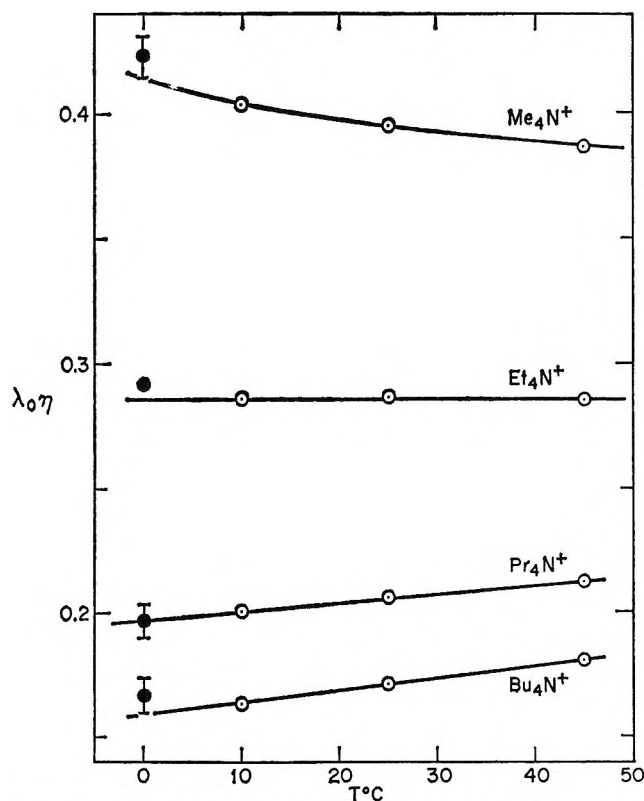


Figure 5. The change of the limiting Walden product for the tetraalkylammonium ions with temperature.

PrN⁺ ⁴⁰ ions follow the same pattern outlined above for the symmetrical tetraalkylammonium ions, but if a hydroxyl group is substituted for a terminal methyl group, the mobility of the resulting ion is somewhat greater than its alkyl analog. Thus, the Me₃(EtOH)N⁺ ^{40,41} and the Me₂(EtOH)₂N⁺ ⁴¹ ions have greater mobilities than the Me₃PrN⁺ and the Et₄N⁺ ions, respectively. Although the mobility difference is small, it is considerably greater than the possible error in the measurements. Contrary to the opinion of Spivey and Snell,⁴⁰ we believe that the introduction of a dipole moment into the side chains of these ions interferes with the formation of cages of structured water about the side chains and therefore produces a smaller moving entity than is the case with the alkyl analog. This is in keeping with the concept that it is the inert nature of the hydrocarbon chain that permits neighboring water molecules to orient themselves into a caged structure. Preliminary experiments⁴² with the (EtOH)₄N⁺ ion indicate that it has a considerably higher mobility than its alkyl analog, the Pr₄N⁺ ion. Similar conclusions were reached from partial molal volume and activity coefficient measurements on this ion at relatively high concentrations in aqueous solution.⁴³

It should be noted that, although the $\lambda_{0\eta}$ product for the *i*-Am₃BuN⁺ ion in methanol lies on the nonaqueous line, the corresponding value for aqueous solution is not nearly so low as the symmetrical R₄N⁺ ions. This would indicate that enforcement of water structure about four isoamyl groups placed tetrahedrally about a charged nitrogen atom may be less favorable than around four *n*-amyl groups. Temperature data would be of considerable help in answering this question.

The temperature dependence of the Walden product for the R₄N⁺ ions casts considerable doubt on the significance of hydration numbers calculated from Stokes' law as modified by Robinson and Stokes.¹³ These hydration numbers are based on the assumptions that all of the quaternary ammonium ions are unhydrated, that only the *n*-Am₄N⁺ ion fits Stokes' law in that its Stokes' radius and estimated crystallographic radius are identical, and that the smaller quaternary ammonium ions deviate from Stokes' law behavior because they are not of sufficient size so that the solvent can be considered a continuum.⁴⁴ On this basis, they developed a correction factor for this size deficiency and applied it to the Stokes radii of the other ions to obtain the hydrated radii and thereby hydration numbers. However, the temperature dependence of the Walden product for the larger R₄N⁺ ions indicates definitely that these ions are hydrated, a fact that completely invalidates the assumption on which these calibration curves and hydration numbers are based.

Nonelectrolytes and Dipolar Ions. Diffusion data for a number of nonelectrolytes and amino acids have been reported^{45,46} for aqueous solutions at 1 and 25° and for methanol solutions at 25°. We can use these data as a further test of the applicability of the concepts discussed above by again considering ratios of Walden products. Stokes' law, as applied to diffusion coefficients, states in eq 5 that

(39) M. J. McDowell and C. A. Kraus, *J. Am. Chem. Soc.*, **73**, 2170 (1951).

(40) H. O. Spivey and F. N. Snell, *J. Phys. Chem.*, **68**, 2126 (1964).

(41) J. Varimbi and R. M. Fuoss, *ibid.*, **64**, 1335 (1960). A value of $\lambda_0(\text{Me}_3(\text{EtOH})\text{N}^+) = 38.16$ was obtained by weighting these data and those of Spivey and Snell⁴⁰ by the standard deviation of the measurements.

(42) D. F. Evans, G. P. Cunningham, and R. L. Kay, to be published.

(43) W. Y. Wen and S. Saito, *J. Phys. Chem.*, **69**, 3569 (1965).

(44) E. R. Nightingale¹⁸ made the added assumption that the Me₄N⁺ ion was hydrated, and thereby he was able to develop a correction factor to be added to the Stokes' radius that converged to a finite value as the Stokes' radius approached zero. Otherwise, his hydration numbers are based on the same assumptions as Stokes and Robinson's.

(45) L. G. Longworth, *J. Am. Chem. Soc.*, **75**, 5705 (1953).

(46) L. G. Longworth, *J. Phys. Chem.*, **67**, 689 (1963).

$$D_{0\eta}/T = k/6\pi\tau_s \quad (5)$$

that is, it is the quantity $D_{0\eta}/T$ that should be independent of solvent and of temperature. The ratios of the Walden product for a number of nonelectrolytes in water and methanol, as given in Table VI, indicate that they diffuse too fast in water or too slowly in methanol; that is, they are either good structure breakers in aqueous solution or they are affected to greater extent by solvation in methanol than in water. Without temperature dependence of diffusion, it is difficult to distinguish between these two effects, and no such data are available for the substances listed in Table VI. However, as can be seen in the series, formamide, acetamide, and propionamide, the diffusion coefficient decreases in aqueous solution relative to methanol solution as the hydrocarbon portion of the molecules increases in length, a direction to be expected if the hydrocarbon chains were enforcing water structure. The absence of a charge in these polar nonelectrolytes could permit even a methyl group to add considerably to water structure enforcement in contrast to what is found for the charged Me_4N^+ ion. Likewise, urea and its mono- and dimethyl derivatives behave in a manner similar to the amides as methyl groups are added. Urea, itself, has a Walden product 42% greater in water than in methanol. This could be a good indication of structure-breaking properties for urea in aqueous solution.⁴⁷

Table VI: $(D_{0\eta})_{\text{H}_2\text{O}}/(D_{0\eta})_{\text{CH}_3\text{OH}}$ at 25°

Formamide	1.27	Ethylene glycol	1.15
Acetamide	1.18	Glycerol	1.18
Propionamide	1.08	Erythritol	1.14
		Dextrose	1.18
Urea	1.42	Sucrose	1.16
Methylurea	1.20		
1,3-Dimethylurea	1.06	Water	1.71 ^a

^a The recent data of Wang (see ref 48) would increase this ratio to 1.93.

Wang⁴⁸ has recently shown that the Walden product for the self-diffusion of water in water is independent of temperature. The almost 50% decrease in the Walden product for water in methanol indicates that the moving entity in methanol is definitely a solvated species.

The ratios given in Table VI for compounds with multiple hydroxyl groups are greater than unity indicating either structure breaking in water or greater solvation effects in methanol. The latter conclusion is preferable since it is in agreement with the tempera-

ture dependence of the Walden products for aqueous solution⁴⁵ given in Table VII. The ratio of the Walden product at 25° compared to that at 1° for the mono-, di-, and trisaccharides is greater than unity, typical of structure-making compounds. Since we have shown that exposed hydroxyl groups appear to inhibit the formation of clathrate structures in aqueous solution, we conclude that the sugars are solvated in both water and methanol but more so in methanol. Solvation is temperature dependent in the case of the sugars but not for the Li^+ ion because in sugars the solvation involves dipole-dipole interaction in contrast to the stronger charge-dipole interaction of ions with solvent.

Table VII: Temperature Dependence of the Walden Product in Aqueous Solution

	$(D_{0\eta}/T)_{25^\circ}$ $(D_{0\eta}/T)_{1^\circ}$
Glucose	1.019
Sucrose	1.025
Raffinose	1.026
Glycine	0.974
Diglycine	0.992
Triglycine	0.995
α -Aminopropionic acid (alanine)	1.001
β -Aminopropionic acid (β -alanine)	0.984
β -Hydroxy- α -aminopropionic acid (serine)	0.997
α -Aminobutyric acid	1.012
α -Aminoisovaleric acid (valine)	1.029
α -Aminocaproic acid (norleucine)	1.035
α -Aminoisocaproic acid (leucine)	1.034
Glycylleucine	1.032
Leucylglycine	1.029

The negative temperature coefficient of the "Walden product" for glycine (Table VII) indicates it is a fair structure breaker in aqueous solution, but as the charge separation increases in di- and triglycine, this property diminishes. As the hydrocarbon portion increases in length in the higher homologs of glycine, the structure-making features become more pronounced as seen by the increasing ratio in the series glycine, alanine, α -aminobutyric acid, valine acid, and leucine. Dis-

(47) This conclusion is in agreement with the temperature dependence of viscosity B coefficients for urea in aqueous solution calculated from the data of H. M. Chadwell and B. Asnes, *J. Am. Chem. Soc.*, 52, 3507 (1930). Their data show that B increases from approximately 0.025 to 0.045 between 5 and 25°. A positive $\partial B/\partial T$ has been shown⁶ to be typical of structure-breaking solutes in aqueous solution. See M. Abu-Hamdiyyah, *J. Phys. Chem.*, 69, 2720 (1965), for an alternate point of view.

(48) J. H. Wang, *ibid.*, 69, 4412 (1965).

placement of a charged amino group or a polar hydroxyl group into the hydrocarbon portion of the amino acid reduces the structure-making properties of the hydrocarbon portion as seen by the lower ratio for serine and β -alanine compared to that for alanine. These observations are verified by the entropies of dilution of Robinson for some of these compounds.⁴⁹ The two dipeptides at the bottom of Table VII reflect the structure-making properties of leucine.

We feel that the analysis of ionic mobilities based on the model of structure-breaking and structure-making properties of ions in aqueous solution is preferable to that based solely on electrostrictive hydration and arbitrary corrections to Stokes' law. The material we have discussed here adds considerably to the validity of this approach. No system has been found whose transport properties in aqueous solution are in conflict with this model. Furthermore, similar conclusions have been reached from a wide variety of measurements including nmr,⁵⁰ dielectric dispersion,⁵¹ viscosity,⁶ heats of dilution,⁵² and solubility.⁵³

It should be noted at this point that much of the success of this analysis of ionic mobilities has resulted from three rather unique properties of conductance data. First, they can be obtained rapidly with high precision. Second, owing to the existence of good theories for the measurable range, the data can be unambiguously extrapolated to infinite dilution where ion-solvent interactions are a maximum and ion-ion interactions disappear. Third, salt conductances can be split unambiguously at every temperature into ionic values. Also, the investigation of salts with common ions permits an internal check to be made on the accuracy of the measurements.

(2) *Concentration Dependence.* The ion-size parameters given in Table II follow the same pattern that was

found for these salts in aqueous solutions¹ at 10 and 25°. They are much lower than the value 3.7 found for the same ions in nonaqueous solvents,³ are about the same for the bromides, but decrease with increasing cation size for the iodides. As was the case at the lower temperatures, a better fit of the data was obtained for Pr₄NI and Bu₄NI if they were assumed to be slightly associated salts and eq 2 was used for their analyses. The actual values of K_A quoted here could be considerably in error owing to the problem of separating the last two terms of eq 2 when K_A is small, but they do agree with those obtained at 10 and 25° and for D₂O solutions within experimental error. This result could be interpreted as indicating that the ionic association involved is insensitive to solvent structural changes. However, this could be another example of the "compensation law"⁵⁴ in which changes in enthalpy and entropy compensate one another,⁵² resulting in little change in the free energy and therefore in the association constant. It is obvious that conductance data alone are not sufficient to answer this question.

Acknowledgment. This work was supported by Contract No. 14-01-0001-359 with the Office of Saline Water, U. S. Department of the Interior.

(49) A. L. Robinson, *J. Chem. Phys.*, **14**, 588 (1946).

(50) H. G. Hertz and M. D. Ziedler, *Ber. Bunsenges. Physik. Chem.*, **67**, 774 (1963); **68**, 821 (1964).

(51) G. H. Haggis, J. B. Hasted, and T. J. Buchanan, *J. Chem. Phys.*, **20**, 1452 (1952).

(52) Y. C. Wu and H. L. Friedman, *J. Phys. Chem.*, **70**, 166 (1966); S. Lindenbaum, *ibid.*, **70**, 814 (1966).

(53) J. E. Desnoyers, G. E. Pelletier, and C. Jolicœur, *Can. J. Chem.*, **43**, 3232 (1965).

(54) D. J. G. Ives and P. D. Marsden, *J. Chem. Soc.*, 649 (1965).

Viscosity B Coefficients for the Tetraalkylammonium Halides

by Robert L. Kay, T. Vituccio, C. Zawoyski, and D. F. Evans¹

Mellon Institute, Pittsburgh, Pennsylvania 15213 (Received February 2, 1966)

Viscosity measurements at concentrations up to 0.2 M for the tetramethyl-, tetraethyl-, tetrapropyl-, and tetrabutylammonium bromides and iodides are reported in H_2O , D_2O , CH_3OH , and CH_3CN at various temperatures between 0 and 65°. The viscosity B coefficients calculated from the Jones-Dole equation exhibit the same behavior as would be predicted from the dependence of the Walden product on solvent and on temperature. In aqueous solutions, the Pr_4N^+ and Bu_4N^+ ions appear to be excellent structure makers and the Me_4N^+ ion appears to be a structure breaker, while for the Et_4N^+ ion the two effects appear to cancel.

Introduction

In the preceding paper,² the Walden product for spherical ions in aqueous solution was shown to be influenced by solvent structural effects. Gurney³ has shown that there is a relationship between the temperature coefficients of the Walden product and viscosity B coefficients obtained from the Jones-Dole⁴ equation for the alkali halides in aqueous solution. Here we report viscosity B coefficients for the tetraalkylammonium bromides and iodides and show that a similar relationship exists for these large symmetrical ions depending on the specific structure-making or structure-breaking ability of the ions involved. Temperature dependence of the B coefficients have been measured in H_2O , D_2O , methanol, and acetonitrile solutions to illustrate clearly the dependence of transport properties on the amount and type of structure in the solvent. These B coefficients have been used already to correct the concentration dependence of conductance for the viscosity effect of these large cations.⁵

Experimental Section

The purification of all materials used as well as procedures in preparing solutions have been discussed in detail already.⁵ All viscosity measurements were carried out in a constant-temperature bath controlled to within 0.02° of the stated temperature with the absolute temperature determined by a calibrated platinum resistance thermometer. All solutions were prepared on a weight basis and vacuum and density corrected. For this purpose, the density increments

for all of the solutions at 65° were assumed to be identical with those at 45°.

Two Ubbelohde-type suspended-level viscometers with flow times for water at 25° of 500 sec were employed in all of the measurements. One of the viscometers⁶ was found to give the same calibration for a number of nonaqueous liquids of low surface tension, whereas the other was constructed here and gave accurate results for aqueous solvents. Neither viscometer was found to require a kinetic energy correction based on the results of repeated runs on a number of concentrated sugar solutions. Runs were repeated until three determinations within 0.2 sec were obtained.

Results

The relative change in viscosity, ψ , due to the addition of salt to the solvent, was obtained from the measured flow times, t and t_0 , for solutions and solvent, respectively, by means of

$$\psi \equiv \frac{\eta - \eta_0}{\eta_0} = \frac{\rho(t - \Delta t) - \rho_0 t_0}{\rho_0 t_0} \quad (1)$$

(1) Chemistry Department, Western Reserve University, Cleveland, Ohio 44106.

(2) R. L. Kay and D. F. Evans, *J. Phys. Chem.*, **70**, 2325 (1966).

(3) R. W. Gurney, "Ionic Processes in Solution," McGraw-Hill Book Co., Inc., New York, N. Y., 1953, p 170.

(4) G. Jones and M. Dole, *J. Am. Chem. Soc.*, **51**, 2950 (1929).

(5) R. L. Kay and D. F. Evans (a) *J. Phys. Chem.*, **69**, 3878, 4208 (1965); **70**, 366 (1966); (b) *ibid.*, **69**, 4216 (1965).

(6) Cannon Instrument Co., State College, Pa.

Table I: Viscosity Data for the Tetraalkylammonium Halides between 0 and 65°

10°C	$\psi/C^{1/2}$	10°C	$\psi/C^{1/2}$	10°C	$\psi/C^{1/2}$	10°C	$\psi/C^{1/2}$
H ₂ O, 0°				D ₂ O, 10°			
Bu ₄ NBr	Bu ₄ NI	Bu ₄ NBr	Bu ₄ NI	Bu ₄ NBr	Pr ₄ NBr	Me ₄ NBr	Me ₄ NI
0.80	0.16	3.95	0.333	1.33	0.188	0.90	0.149
1.97	0.244			2.75	0.268	1.58	0.192
3.96	0.343			5.12	0.359	4.15	0.310
4.36	0.360						
H ₂ O, 10°				D ₂ O, 25°			
Pr ₄ NBr	Bu ₄ NBr	Bu ₄ NBr	Pr ₄ NBr	Bu ₄ NBr	Pr ₄ NBr	Me ₄ NBr	Me ₄ NI
0.99	0.100	0.42	0.108	1.33	0.155	0.89	0.091
4.91	0.213	1.09	0.160	2.75	0.228	3.96	0.169
9.73	0.307	1.81	0.202	5.12	0.294		
14.44	0.384	2.98	0.258				
19.01	0.463	3.98	0.300				
Et ₄ NBr	Me ₄ NBr						
0.99	0.037	5.19	0.343				
11.94	0.139	15.89	0.029				
Pr ₄ NI	Bu ₄ NI						
1.08	0.095	0.50	0.109				
5.07	0.201	0.99	0.144				
9.70	0.285	1.39	0.172				
14.46	0.363	2.86	0.246				
18.94	0.423	3.93	0.289				
H ₂ O, 25°				CH ₃ OH, 10°			
Pr ₄ NBr	Pr ₄ NI	Bu ₄ NBr	Bu ₄ NI	Bu ₄ NBr	Bu ₄ NI	Me ₄ NBr	Me ₄ NI
0.99	0.085	0.50	0.064	0.65	0.096	1.79	0.131
4.90	0.182	1.08	0.081	2.58	0.163	7.03	0.237
9.70	0.256	5.06	0.170	4.93	0.213		
14.39	0.315	9.67	0.242	15.56	0.371	6.68	0.105
18.95	0.373	14.42	0.297	CH ₃ OH, 25°			
Bu ₄ NBr	Me ₄ NBr	Bu ₄ NBr	Me ₄ NBr	Bu ₄ NBr	Me ₄ NBr	Me ₄ NBr	Me ₄ NI
1.81	0.178	18.88	0.351	0.31	0.079	3.12	0.078
2.98	0.220	0.50	0.120	0.64	0.094	6.57	0.105
3.97	0.250	0.99	0.117	2.54	0.158	19.32	0.169
5.18	0.291	1.39	0.142	4.84	0.205		
Me ₄ NBr	Bu ₄ NI			15.31	0.354	Et ₄ NBr	
15.84	0.040	3.92	0.244	Bu ₄ NI	11.62	0.145	
				1.76	0.127	12.42	0.185
				6.91	0.226	Pr ₄ NBr	
						6.05	0.181
						12.50	0.253
H ₂ O, 45°				CH ₃ OH, 45°			
Bu ₄ NBr	Pr ₄ NBr	Bu ₄ NBr	Et ₄ NBr	Bu ₄ NBr	Et ₄ NBr	Pr ₄ NBr	Pr ₄ NBr
1.25	0.145	2.44	0.108	5.27	0.220	6.49	0.149
2.22	0.167	4.18	0.139	10.46	0.299	11.35	0.189
4.81	0.226	9.94	0.212			12.13	0.192
8.90	0.304	18.73	0.302				
Et ₄ NBr	Me ₄ NBr						
8.07	0.092	17.73	0.051				
15.78	0.131	28.75	0.063				
H ₂ O, 65°				CH ₃ CN, 10°			
Bu ₄ NBr	Me ₄ NBr	Bu ₄ NBr	Bu ₄ NI	Bu ₄ NBr	Bu ₄ NI	Pr ₄ NBr	Pr ₄ NBr
3.76	0.173	0.79	0.089	0.79	0.089	4.95	0.195
7.24	0.229	2.84	0.153	2.84	0.153		
10.21	0.268	4.90	0.195	4.90	0.195		
14.97	0.333						
Pr ₄ NBr	Et ₄ NBr	CH ₃ CN, 25°				Bu ₄ NBr	Bu ₄ NI
5.85	0.138	4.02	0.059	0.78	0.087	4.85	0.183
14.62	0.214	10.57	0.096	2.78	0.143		
				4.80	0.180		

This can be written as

$$\psi = \psi_M - \rho \Delta t / \rho_0 t_0 \quad (2)$$

where Δt is a flow time correction found necessary for some of the salts studied in aqueous solution and was detected by the fact that ψ_M did not extrapolate to zero as $C \rightarrow 0$. The magnitude of Δt was determined by measuring the viscosity of solutions so dilute ($C < 10^{-6} M$) that the flow time should have been that of the pure solvent. The maximum difference in time encountered amounted to 2 sec. The Δt determined in this way were found to give ψ that extrapolated to zero as $C \rightarrow 0$ in every case where the correction was required. This correction was required for only three sets of data, Bu₄NI, Pr₄NBr, and Pr₄NI, in aqueous solutions. The fact that Δt was detectable in such extremely dilute solutions suggests that it is a surface tension effect resulting from a minute trace of surface-active impurity in the salts in question. We have detected this same behavior in the data for Bu₄NBr reported by other workers.⁷ The values of $\psi/C^{1/2}$ in Table I for all systems studied have been corrected where necessary.

The solution densities used in eq 1 were obtained by direct measurement generally on the most concentrated solution studied. It was found that the relationship $d = d_0 + \theta \bar{m}$, where \bar{m} is the concentration in moles per kilogram of solution, held over a wide concentration and temperature range. Consequently, many of the required values of θ could be estimated from values obtained by direct measurement.

The viscosity *B* coefficients in Table II were obtained empirically from the Jones-Dole⁴ equation

$$\psi/C^{1/2} = A + BC^{1/2} \quad (3)$$

The validity of the relationship was established for each of the solvent systems investigated and for the temperature range studied by measuring at least one salt containing the larger ions at a number of points covering a wide concentration range. Once this was established, only one or two points were required to obtain *B* coefficients for other salts. Included in Table II are the data of Laurence and Wolfenden⁸ for Et₄NBr and the data of Hückel and Schaaf⁹ for Et₄NI and Me₄NI in aqueous solutions.

The intercepts *A* on a plot of eq 3 were small in every case and contributed very little to the concentration

(7) R. M. Fuoss and C. A. Kraus, *J. Am. Chem. Soc.*, **79**, 3304 (1957).

(8) V. O. Laurence and J. H. Wolfenden, *J. Chem. Soc.*, 1144 (1934).

(9) E. Hückel and H. Schaaf, *Z. Physik. Chem.*, **21**, 326 (1959). The values of *B* for 10° were extrapolated from data at somewhat higher temperatures.

Table II: Viscosity B Values at Various Temperatures

t , °C	Me ₄ NBr	Et ₄ NBr	Pr ₄ NBr	Bu ₄ NBr	Me ₄ NI	Et ₄ NI	Pr ₄ NI	Bu ₄ NI
				H ₂ O				
65	0.11	0.27	0.54	0.83				
45	0.10	0.30	0.64	0.99				
25	0.083	0.34 ^a	0.82	1.24	0.049 ^b	0.31 ^b	0.77	1.19
10	0.058	0.38	0.98	1.46	0.028 ^b	0.33 ^b	0.93	1.41
0				1.68				1.61
				D ₂ O				
25	0.076		0.79	1.26	0.034		0.74	1.21
10	0.049		0.94	1.56	0.00		0.88	1.48
				CH ₃ OH				
45		0.50	0.67	0.86				
25	0.35	0.48	0.66	0.85				0.80
10	0.35			0.89				0.82
				CH ₃ CN				
25				0.74				0.75
10				0.80				0.80

^a See ref 8. ^b See ref 9.

dependence of viscosity with the possible exception of the aqueous tetramethylammonium salts. At most A amounted to 0.01 in aqueous and 0.02 in nonaqueous solutions. This term in the viscosity equation is interpreted as the contribution from interionic forces that tend to interfere with the flow of one layer of solution past another. Theoretical values calculated from the Falkenhagen equation¹⁰ agreed within 25% with the measured values.

Plots of eq 3 were found to be linear up to concentrations of 0.1 M in aqueous solution and to somewhat higher concentrations in methanol. In aqueous solution, positive deviations were observed at higher concentration of the larger salts and introduced some uncertainty in the determination of B . The internal consistency of our results is shown in Table III by the constant difference in B for bromides and iodides in H₂O and D₂O solution. Our value of 0.05 compares well with the generally accepted value of 0.03 for aqueous solutions.¹¹ Furthermore, the difference between our Me₄NBr and Hückel and Schaaf's values for Me₄NI is 0.03 over the whole temperature range as can be seen in Figure 1, although the agreement between Et₄NBr and Et₄NI is not as good at temperatures above 25°. Our values for Et₄NBr at higher and lower temperatures are consistent with that of Laurence and Wolfenden at 25°, as is also shown in Figure 1. Kaminsky¹² has demonstrated the additivity of ionic B coefficients for aqueous solutions at various temperatures.

Table III: Values of ($B_{Br^-} - B_{I^-}$)

	t , °C	Bu ₄ N ⁺	Pr ₄ N ⁺	Me ₄ N ⁺
H ₂ O	10	0.05	0.05	
	25	0.05	0.05	
D ₂ O	10	0.08	0.06	0.05
	25	0.05	0.05	0.04

A plot of our B values for the bromides in water and methanol solutions at the various temperatures studied is given in Figure 2. Although Wen's¹³ values for Bu₄NBr in water are somewhat lower, the temperature dependence is in good agreement with our own. The value of 1.34 quoted by Fuoss and Kraus⁷ reduces to 1.27 if the high points at the two lowest concentrations reported are corrected for Δt as mentioned above. This value is in good agreement with our value of 1.24 quoted in Table II. Nightingale's¹⁴ B value for Me₄NBr is in good agreement with our data only at

(10) H. Harned and B. B. Owen, "The Physical Chemistry of Electrolytic Solutions," 3rd ed, Reinhold Publishing Corp., New York, N. Y., 1958, p 240.

(11) R. H. Stokes and R. Mills, "Viscosity of Electrolytes and Related Properties," Pergamon Press Inc., New York, N. Y., 1965, p 34.

(12) M. Kaminsky, *Discussions Faraday Soc.*, **24**, 171 (1957).

(13) W. Y. Wen, Ph.D. Thesis, University of Pittsburgh, 1957.

(14) E. R. Nightingale, Jr., *J. Phys. Chem.*, **66**, 894 (1962).

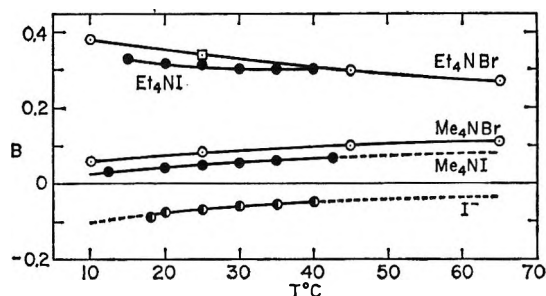


Figure 1. The temperature dependence of viscosity B coefficients for aqueous solution: Et_4NBr : \circ , our data; \square , see Laurence and Wolfenden, ref 8; Et_4NI and Me_4NI , see Hückel and Schaaf, ref 9; Me_4NBr , our data; I^- , see Kaminsky, ref 12.

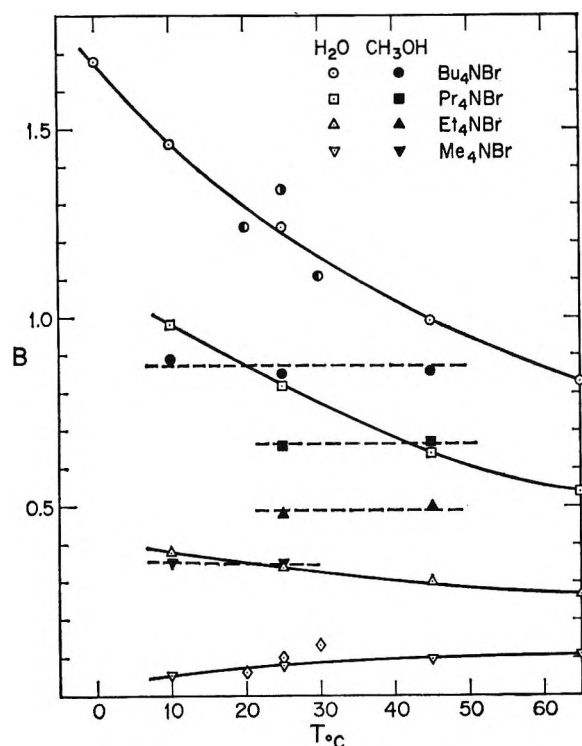


Figure 2. Viscosity B coefficients for the tetraalkylammonium bromides in water and methanol solutions as a function of temperature: \bullet , Fuoss and Kraus, ref 7; \circ , Wen, ref 13; \diamond , Nightingale, ref 14.

20° since his temperature dependence differs significantly from ours and from that reported by Hückel and Schaaf⁹ for Me_4NI (see Figure 1).

A satisfactory discussion of the temperature dependence of B coefficients requires the ionic rather than salt values. Unfortunately, there is no exact method of performing this operation since the equivalents of transference numbers do not exist for viscosity data. Kaminsky¹² assumed that $B_{\text{K}^+} = B_{\text{Cl}^-}$ at all temperatures and calculated ionic B values for a number of

the smaller ions from 12.5 to 45° . He justified this split on the basis of the almost identical cation and anion transference numbers for KCl at all temperatures and by the fact that he obtained ionic values in good agreement with those reported by Cox and Wolfenden¹⁵ that were based on the mobility difference for the Li^+ and IO_3^- ions. We have followed Kaminsky's procedure and have used his data for the iodide ion shown in Figure 1 and the difference ($B_{\text{Me}_4\text{NBr}} - B_{\text{Me}_4\text{NI}}$), also shown in Figure 1, to calculate B_{Br^-} and consequently all of the ionic B coefficients for the tetraalkylammonium ions given in Table IV. A similar split cannot be used to obtain ionic B values for methanol and acetonitrile solutions because of the lack of suitable data for KCl and KBr in these solvents. Viscosities of dilute methanol solutions of KCl and KBr as determined by Jones and Fornwalt¹⁶ produced two values of B , depending on the concentration range considered, whereas our data for the quaternary salts gave very linear plots of eq 3 and a single value of B over the same concentration range. Ionic B values for methanol solutions will require a reinvestigation of at least KCl in methanol solutions.

Table IV: Ionic B Values at Various Temperatures in H_2O

t , $^\circ\text{C}$	Bu_4N^+	Pr_4N^+	Et_4N^+	Me_4N^+	Br^-
0	1.75				-0.08
10	1.52	1.04	0.44	0.13	-0.07
25	1.28	0.86	0.38	0.12	-0.04
45	1.01	0.66	0.32	0.12	-0.02
65	0.84	0.55	0.28	0.12	-0.01

Our data for Me_4NBr and Bu_4NBr in CH_3OH at 25° are in acceptable agreement with the values 0.42 and 0.84, respectively, quoted by Tuan and Fuoss,¹⁷ but our values for Bu_4NBr and Bu_4NI in CH_3CN are consistently lower than their values of 0.93 and 0.87, respectively.

Discussion

Viscosity B coefficients from the Jones-Dole equation can be interpreted, at least qualitatively, by the Einstein equation¹⁸

(15) W. M. Cox and J. H. Wolfenden, *Proc. Roy. Soc. (London)*, **A145**, 475 (1934).

(16) G. Jones and H. J. Fornwalt, *J. Am. Chem. Soc.*, **57**, 2041 (1935).

(17) D. F.-T. Tuan and R. M. Fuoss, *J. Phys. Chem.*, **67**, 1343 (1963).

(18) A. Einstein, *Ann. Physik*, **19**, 289 (1906); **34**, 591 (1911).

$$B = 2.5v/c \quad (4)$$

where v is the total volume occupied by the ions per milliliter of solution. This equation predicts that the presence of ions should increase the solution viscosity in proportion to their size, and the increase should be independent of temperature inasmuch as electrostrictive solvation is independent of temperature. B coefficients for the relatively small alkali and halide ions in aqueous solution have been shown to deviate considerably from this behavior. The B values decrease with increasing ion size, often to negative values,^{3,11} and in such cases B increases with increased temperature.^{12,15,19} This is in the opposite direction for hydration effects, and, consequently, this behavior has been attributed to the ability of these ions to disrupt water structure in their vicinity.^{3,20} These ions have become known as structure breakers, and the same explanation has been used to account for the Walden product and its temperature dependence.² As a matter of fact, it has been shown^{3,20} that, owing to this dependence on water structure, B and the λ_{07} product for structure-breaking ions are related reciprocally in that, if B is low, λ_{07} is high, and, if B increases with temperature, λ_{07} decreases with increasing temperature.

No previous systematic study as is reported here has been carried out for B coefficients of the tetraalkylammonium ions. Frank and Evans have used Bingham's²¹ Δ values (the viscosity increase for a 1 *m* solution) to illustrate the relatively large increase in viscosity obtained in aqueous solutions of these ions and have attributed this excess viscosity to "iceberg" formation. However, in light of the Einstein equation, the measured viscosity could be attributed to the increased size of the tetraalkylammonium ions. Better criteria for structure influences can be obtained from the temperature dependence of the B coefficients. Hückel and Schaaf⁹ have investigated the temperature dependence of only the smaller of these ions. Wen's data¹³ for Bu_4NBr at 20 and 30° in aqueous solution illustrates the large negative temperature dependence of B coefficients for the larger quaternary ammonium ions. It is evidence such as this, when combined with data for nonaqueous solvents, that permits conclusions to be reached concerning the effects of ions on solvent structure.

The same type of relationship between B and λ_{07} is found here for the large quaternary ammonium ions in aqueous solution as was found for the alkali halides. In Figure 2 it can be seen that, at low temperatures, B for Bu_4NBr and Pr_4NBr in aqueous solution are larger than the corresponding values in methanol solutions and B decreases with increased temperature

for aqueous solutions, whereas the values are about constant for methanol solutions. These effects must be due to the large R_4N^+ ions since the contribution to the B values from the bromide ion is very small, as can be seen in the ionic values in Table IV. Corresponding behavior has been observed in the Walden product for these ions.² Thus, the viscosity data confirm the conclusions reached from the conductance data that water enforcement about the hydrocarbon side chains of the Pr_4N^+ and Bu_4N^+ ions forms a larger moving entity and, at the same time, increases the bulk viscosity by increasing the degree of hydrogen bonding in their vicinity. This interpretation is in agreement with all known data for these ions as was pointed out in the preceding paper.

The B values for Me_4NBr show a much different behavior. They are much smaller in aqueous than in methanol solution at all temperatures, and they show a slight increase with increasing temperature. This temperature dependence, however, is most likely due entirely to the Br^- ion, as can be seen from the data in Table IV. These results indicate that, if the B coefficient for the Me_4N^+ ion has any temperature dependence, it is small. This result is in agreement with that found by Hückel and Schaaf⁹ from more precise data on Me_4NI . The true temperature dependence here is difficult to determine because of the arbitrary nature of the split used to obtain ionic values. The Walden product for this ion was found² to be higher in aqueous than in methanol solutions and to decrease with increasing temperature. At least in its behavior in aqueous as opposed to nonaqueous solvents, these viscosity data confirm the structure-breaking properties of the Me_4N^+ ion.

The Et_4N^+ ion shows a mixed behavior since B for Et_4NBr is slightly lower in aqueous than in methanol solution but still shows a small decrease with increased temperature in aqueous solution. Both effects are too large to be accounted for by the bromide ion alone. Hückel and Schaaf⁹ have come to the same conclusion for the Et_4N^+ ion from their studies of aqueous Et_4NI . The Walden product² for this ion is lower in water than in methanol and shows little temperature dependence. Both the viscosity and conductance data can best be interpreted by assuming this ion is of an intermediate size for which structure-making and structure-breaking effects cancel.

Further evidence for the conclusions reached here is contained in the B values for D_2O solutions. They are

(19) J. D. Bernal and R. H. Fowler, *J. Chem. Phys.*, **1**, 515 (1933).

(20) H. S. Frank and M. W. Evans, *ibid.*, **13**, 507 (1945).

(21) E. C. Bingham, *J. Phys. Chem.*, **45**, 885 (1941).

almost identical with those for H₂O solutions. We had hoped to verify the increase in structure-making properties of the large hydrophobic cations, Bu₄N⁺ and Pr₄N⁺, in D₂O over that in H₂O as was demonstrated from conductance measurements.^{5b} Although the trends are in the expected direction, the effect is too small to be established by viscosity measurements with the precision reported here.

It is interesting to calculate *B* coefficients from eq 4 using data reported by Robinson and Stokes²² for the ionic radii. The results are given in Table V and indicate a surprisingly good agreement with the observed data for these salts in methanol solutions. However, considering the assumptions involved in the model used and the general lack of data for nonaqueous

solvents, this agreement must be considered fortuitous at the present time.

Table V: Viscosity *B* Values Calculated from Eq 4

Me ₄ NBr	Et ₄ NBr	Pr ₄ NBr	Bu ₄ NBr	Br ⁻
0.31	0.45	0.63	0.81	0.05

Acknowledgment. This work was supported by Contract No. 14-01-0001-359 with the Office of Saline Water, U. S. Department of the Interior.

(22) R. A. Robinson and R. H. Stokes, "Electrolyte Solutions," Butterworth Inc., New York, N. Y., 1959.

Thermal Diffusion in an Oxidation-Reduction Thermocell—the Bismuth-Bismuth Iodide System¹

by Jordan D. Kellner

*Atomics International, A Division of North American Aviation, Inc., Canoga Park, California
(Received January 4, 1966)*

The Soret effect was studied in a metal-fused salt system by measuring the final thermoelectric potential (in the Soret steady state) of a Bi-BiI₃ thermocell, containing inert electrodes, over the composition range 1-90 mole % bismuth. The value at 500° was large at low metal concentrations (-4600 μv/deg at 1 mole % metal) and diminished exponentially to that of the initial thermoelectric power at about 30% dissolved bismuth metal. From 30 to 90% bismuth, the initial and final thermoelectric powers were identical. No Soret effect is observed at compositions where electronic conduction predominates. At these compositions the results suggest that the transport properties of the cations (Bi⁺, Bi³⁺) are indistinguishable because the electron exchange between cations is much faster than ionic migration.

Introduction

The Soret effect occurs when a temperature gradient is imposed on a two-component liquid system. A partial demixing results which continues until a steady state is reached where the diffusion along the tempera-

ture gradient is just balanced by ordinary diffusion in the opposite direction along the concentration gradient.

(1) This work was supported by the Research Division of the U. S. Atomic Energy Commission.

When the system is fitted with two electrodes reversible to some species in the melt, the emf of the resulting thermocell can be used to monitor the approach to the steady state.

The Soret effect has been studied in fused salts² and in liquid metals.³ The fact that Bi and BiI₃ at temperatures above 458° are miscible in all proportions⁴ affords an opportunity to study the transport properties of a binary liquid system whose composition may be continuously varied from that of a fused salt to that of a molten metal. Various studies on this system^{4,5} have indicated that the salt-rich mixture (below 30% metal) consists of Bi⁺, Bi⁺³, and I⁻ ions, while the metal-rich mixture (>67% metal) consists of metallic bismuth, Bi⁺, and I⁻ ions. Recently, studies of the electrical conductivity⁶ and Seebeck coefficient⁷ in this system were interpreted on the basis of an electron "hopping" mechanism⁸ in which electron pairs were exchanged by Bi⁺ and Bi⁺³ cations in the melt. These exchanges are much more rapid than ionic migration,⁸ therefore, at those compositions where this mechanism predominates, the cations in the melt are indistinguishable as far as mass transport is concerned. The experiments reported herein were attempted to determine if a Soret effect could be detected at the compositions where electron exchange was the predominant mode of conduction.

Experimental Section

The Pyrex thermocell, shown in Figure 1, was similar to that of Huse, *et al.*⁹ A Pyrex sintered glass disk of medium porosity and 10-mm diameter separated the two compartments, each fitted with a 20-mil tungsten electrode and a thermocouple well. After the tungsten electrodes were sealed in the cell, they were cleaned electrochemically in an aqueous solution of KOH. The thermocouple wells contained two chromel-alumel thermocouples wired to buck each other, and the resulting signal was fed to a differential thermocouple controller which maintained the desired small temperature difference across the frit with an accuracy of $\pm 0.025^\circ$ over long periods of time. The cell was a closed system because of the appreciable vapor pressure of BiI₃ at 500° (about 340 mm). The compartments were connected above for pressure equilization. The cell was mounted in a Marshal furnace (2.5 in. i.d.) which, in turn, was mounted in a horizontal rocking frame to allow the cell to be agitated during the solution process. A transite collar fit around the disk portion of the cell and served as a heat barrier. Two inconel tubes on either side of the collar held it in place and reduced the temperature gradients in each compartment. The furnace was adjusted so that one com-

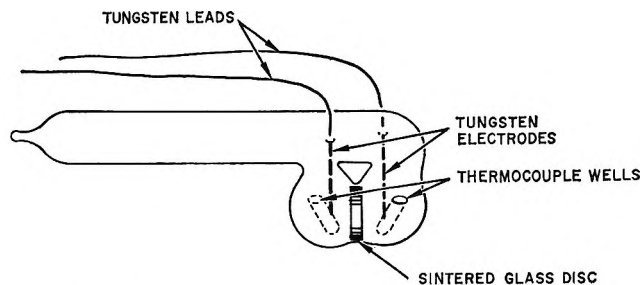


Figure 1. Soret cell.

partment was slightly cooler, and this section was fitted with a flexible tape heater energized by the magnetic amplifier of the controller.

The BiI₃ used in this work was obtained commercially and distilled twice *in vacuo*. The Bi was 99.99% pure, and oxide-free samples from the interior of solid ingots were used without further purification. The powders were weighed, mechanically mixed, and then introduced into the cell *via* a long fill tube. The cell was then evacuated and sealed at a pressure of 10^{-5} torr.

After the cell was agitated for 2 hr and equilibrated at $\Delta T = 0$ for about 1 day, the ΔT signal from the thermocouples and the cell emf were plotted simultaneously on a two-pen recorder that was calibrated frequently with a K-3 potentiometer. After a stable base emf was obtained, usually less than 100 μv , the ΔT was alternately raised to various values from 1 to 7° and returned to zero. The emf values from four or five values of the thermal gradient were plotted and the thermoelectric powers were obtained from the slope of the linear plot. In general, all emf values were stable to within a few microvolts over periods of several hours after the steady state had been reached. Those data that indicated a systematic drift were discarded.

The steady-state thermoelectric powers were measured at 500° for the compositions 0.01, 0.03, 0.05, 0.15, 0.20, 0.25, 0.30, 0.35, 0.50, 0.80, and 0.90 mole fraction Bi and at temperatures between 450 and 550° for the compositions 0.03, 0.15, 0.25, 0.30, and 0.35.

(2) (a) B. R. Sundheim and J. D. Kellner, *J. Phys. Chem.*, **69**, 1204 (1965); (b) S. Gustafsson and A. Lunden, *Z. Naturforsch.*, **17a**, 550 (1962).

(3) F. R. Winter and H. G. Drickamer, *J. Phys. Chem.*, **59**, 1229 (1955).

(4) S. J. Yosim, L. D. Ransom, R. A. Sallach, and L. E. Topol *ibid.*, **66**, 28 (1962).

(5) L. E. Topol and L. D. Ransom, *J. Chem. Phys.*, **38**, 1663 (1963).

(6) L. F. Grantham and S. J. Yosim, *ibid.*, **38**, 1671 (1963).

(7) D. O. Raleigh and L. E. Topol, *ibid.*, **41**, 3179 (1964).

(8) D. O. Raleigh, *ibid.*, **38**, 1677 (1963).

(9) E. S. Huse, D. J. Trevo, and H. G. Drickamer, *Rev. Sci. Instr.*, **21**, 60 (1950).

Results

In general, the steady-state thermoelectric potentials were reproducible to within 3% for the salt-rich compositions (*i.e.*, less than 25 mole % bismuth) and to within 1% for the remaining compositions, where the emf values were much more stable. The thermoelectric potential of pure bismuth was run as a check and the value obtained, 15 $\mu\text{V}/\text{deg}$ at 500°, compares well with previous results (16 $\mu\text{V}/\text{deg}$).¹⁰

The initial and steady-state thermoelectric potentials are shown in Table I, and are plotted against mole fraction bismuth in Figure 2 for 450, 500, and 550°. In this work, the sign of the hotter electrode is the sign of the thermoelectric potential. The differences found for the initial thermoelectric potential at the three temperatures were too small to be seen on this graph; therefore, only the data for 500° are shown. For those compositions undergoing a pronounced Soret effect in the thermocell (<20 mole % Bi), it was difficult to obtain reliable data for the initial potential because the cell emf changed so rapidly with time. Therefore, the data of Raleigh and Topol⁷ were used for these compositions. Initial potential results at other compositions were similar to those of Raleigh and Topol.⁷

Table I

X_{Bi}	$\epsilon_{\text{in}}, \mu\text{V}/\text{deg}$			$\epsilon_{\text{st}}, \mu\text{V}/\text{deg}$		
	450°	500°	550°	450°	500°	550°
0.01					-4600	
0.03		35 ⁷			-3100	-2200
0.05		19 ⁷			-2100	
0.10		12 ⁷			-580	
0.15		40 ⁷		-645	-460	-260
0.20		49			-230	
0.25		99		-72	49	115
0.30	90	97	93	90	97	93
0.35	82	79	71	82	79	71
0.50	56	42	33	56	42	33
0.80		25	25		25	25
0.90		18	17		18	17
1.00		15			15	

The value of the steady-state thermoelectric potential changed from -4600 $\mu\text{V}/\text{deg}$ at 1 mole % to 97 $\mu\text{V}/\text{deg}$ at 30 mole %. From 30 to 90 mole % the initial and steady-state values are identical, indicating no Soret effect at these compositions. Also, as the temperature is increased, the two curves become coincident at smaller metal concentrations.

Discussion

The bismuth-bismuth triiodide system is perhaps the best characterized electrically of any metal-metal

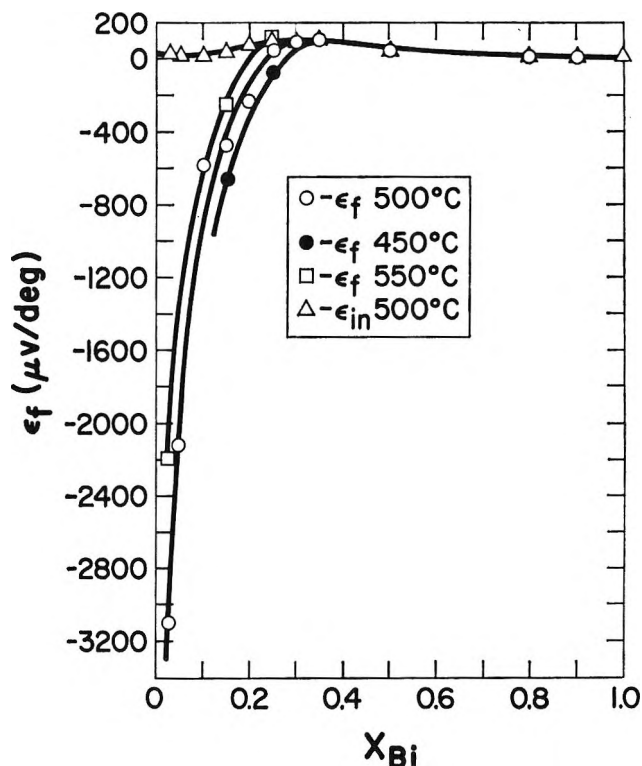


Figure 2. Initial and steady-state thermoelectric potential vs. mole fraction of bismuth.

halide melt at the present time. The experiments of Grantham and Yosim⁶ show an exponential increase in the specific conductivity with added bismuth over most of the composition range at 600° and above. At 500°, while the $\ln K$ vs. $1/T$ plot is not linear in the salt-rich region, the conductivity nevertheless increases faster than one would expect from a purely ionic mechanism. Raleigh⁸ has suggested an electron-hopping model, in which electrons are exchanged between the oxidized and reduced forms of the cations in the melt. Since at salt-rich compositions, bismuth metal is believed to be present as Bi^+ , a two-electron transfer between Bi^+ and Bi^{3+} was postulated. This mechanism is expected to be enhanced by decreasing cation-cation distance (*i.e.*, greater metal concentrations) and increasing temperature. Raleigh's treatment of the conductivity results is consistent with this model up to a concentration of about 50 mole % bismuth.

The electrode reactions are assumed to be



Thus a flow of current through the cell is accompanied

(10) C. C. Bradley, *Phil. Mag.*, 7, 1337 (1962).

by a flow of Bi^+ cations toward the oxidizing electrode and Bi^{3+} toward the reducing electrode.

The equation for the initial thermopotential may be derived in a number of ways; however, we choose to start with the equation derived by Schneebaum and Sundheim.¹¹ It was shown by these authors, using irreversible thermodynamics, that the initial thermoelectric potential (ϵ_{in}) of a thermocell containing two components can be expressed as

$$-T\epsilon_{\text{in}} = W_1Q_1^* + W_2Q_2^* + Q_3^* \quad (1)$$

where W_1 , W_2 , and Q_1^* and Q_2^* are the Washburn transference numbers and the heats of transfer for components one and two, respectively, Q_3^* is the Peltier heat in the steady state, and T is absolute temperature. We will assume that in the salt-rich region all of the added bismuth reacts with the BiI_3 and accordingly call BiI component 1 and BiI_3 component 2. The Washburn numbers W_1 and W_2 represent the number of moles of neutral species crossing a reference plane in the direction of positive current in the cell for each Faraday of charge passed, *i.e.*

$$W_1 = \bar{J}_1/\bar{J}_3; \quad W_2 = \bar{J}_2/\bar{J}_3 \quad (2)$$

where \bar{J}_1 and \bar{J}_2 are the fluxes of components 1 and 2, respectively, in units of moles/cm² sec, and \bar{J}_3 is the electrical flux in faradays/cm² sec. In order to apply eq 1 to the ionic species present in the melt, we determine the individual ionic fluxes in terms of the neutral fluxes \bar{J}_1 and \bar{J}_2 . For the flux of Bi^+ and Bi^{3+}

$$\bar{J}_{\text{Bi}^+} = \bar{J}_1 - 1/2\bar{J}_3 \quad (3)$$

$$\bar{J}_{\text{Bi}^{3+}} = \bar{J}_2 + 1/2\bar{J}_3 \quad (4)$$

where \bar{J}_{Bi^+} , and $\bar{J}_{\text{Bi}^{3+}}$ are the fluxes of Bi^+ and Bi^{3+} , respectively, in units of moles/cm² sec. The flux of Bi^+ is decreased by the amount produced at the electrode, one ion for every two electrons, hence the term $-1/2\bar{J}_3$. Similarly, the flux of Bi^{3+} is increased by this amount. The Washburn numbers may be converted to ionic transference numbers t_i by the use of eq 2, 3, and 4 and with the relationship

$$t_i/Z_i = \bar{J}_i/\bar{J}_3 \quad (5)$$

where Z_i is the charge of the i^{th} ion. Thus

$$W_1 = \frac{\bar{J}_{\text{Bi}^+}}{\bar{J}_3} + 1/2 = t_{\text{Bi}^+} + 1/2 \quad (6)$$

$$W_2 = \frac{\bar{J}_{\text{Bi}^{3+}}}{\bar{J}_3} - 1/2 = 1/3t_{\text{Bi}^{3+}} - 1/2$$

Also the heats of transport of BiI and BiI_3 are

$$Q_1^* = Q_{\text{Bi}^+}^* + Q_{\text{I}^-}^* \quad (7)$$

$$Q_2^* = Q_{\text{Bi}^{3+}}^* + 3Q_{\text{I}^-}^*$$

After eq 6 and 7 are substituted in eq 1, we have

$$-T\epsilon_{\text{in}} = (t_{\text{Bi}^+} + 1/2)(Q_{\text{Bi}^+}^* + Q_{\text{I}^-}^*) + (1/3t_{\text{Bi}^{3+}} - 1/2)(Q_{\text{Bi}^{3+}}^* + 3Q_{\text{I}^-}^*) + Q_3^*$$

Simplifying and noting that Q_3^* is the Peltier heat in the steady state, *i.e.*

$$Q_3^* = -T\epsilon_{\text{st}}$$

where ϵ_{st} is the steady-state thermoelectric potential, we obtain the expression

$$-T(\epsilon_{\text{in}} - \epsilon_{\text{st}}) = t_{\text{Bi}^+}Q_{\text{Bi}^+}^* + 1/3t_{\text{Bi}^{3+}}Q_{\text{Bi}^{3+}}^* + (t_{\text{Bi}^+} + t_{\text{Bi}^{3+}} - 1)Q_{\text{I}^-}^* + 1/2(Q_{\text{Bi}^+}^* - Q_{\text{Bi}^{3+}}^*) \quad (8)$$

As stated earlier, the conductivity data indicate that the electronic conductivity mechanism is operable over the entire composition range and accounts for nearly all of the current carried by melts containing over 30% bismuth. Since the electronic mechanism of conduction is believed to be⁸ electron-pair exchange between Bi^+ and Bi^{3+} cations, we can introduce a transport number for the electron pair, t_{2e} , and set the sum of the transport numbers equal to unity. Then

$$-T(\epsilon_{\text{in}} - \epsilon_{\text{st}}) = t_{\text{Bi}^+}Q_{\text{Bi}^+}^* + 1/3t_{\text{Bi}^{3+}}Q_{\text{Bi}^{3+}}^* - (t_{\text{I}^-} + t_{2e})Q_{\text{I}^-}^* + 1/2(Q_{\text{Bi}^+}^* - Q_{\text{Bi}^{3+}}^*) \quad (9)$$

For melts containing over 30% bismuth, it is assumed that there is no ionic conductivity. Therefore, we may set $t_{\text{Bi}^+} = t_{\text{Bi}^{3+}} = t_{\text{I}^-} = 0$ and $t_{2e} = 1$ at these compositions, and eq 9 becomes

$$-T(\epsilon_{\text{in}} - \epsilon_{\text{st}}) = 1/2(Q_{\text{Bi}^+}^* - Q_{\text{Bi}^{3+}}^*) - Q_{\text{I}^-}^* \quad (10)$$

Since at 30% metal and above, $\epsilon_{\text{in}} = \epsilon_{\text{st}}$

$$Q_{\text{I}^-}^* = 1/2(Q_{\text{Bi}^+}^* - Q_{\text{Bi}^{3+}}^*) \quad (11)$$

Even though the transport numbers for the cations are zero, cations are still effectively transported across the cell as a result of electron exchanges. Clearly, the flux of Bi^+ across the cell and Bi^{3+} in the opposite direction is equivalent to a net transport of two electrons, *i.e.*

$$Q_{\text{I}^-}^* = 1/2Q_{2e}^* \quad (12)$$

Therefore, at those compositions where $\epsilon_{\text{in}} = \epsilon_{\text{st}}$, the amount of heat transported by an iodide ion is the same as the heat transported by an electron. Because

(11) R. Schneebaum and B. R. Sundheim, *Discussions Faraday Soc.* 32, 197 (1961).

of electroneutrality requirements, at the steady state the iodide and electron fluxes are of opposite direction; therefore, an exchange of an electron and an iodide ion results in no transport of heat. Now, it can be shown¹² that the Soret coefficient, s , is given by

$$s = \frac{Q_1^* - Q_2^*}{RT^2} \quad (13)$$

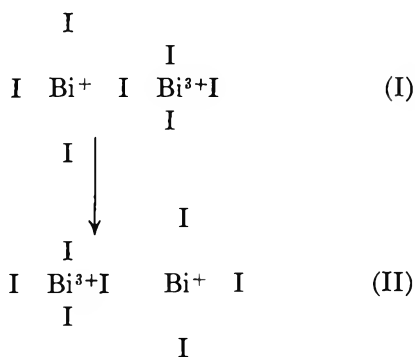
where R is the gas constant. From (13) and (7) we have

$$s = \frac{Q_{\text{Bi}^+}^* - Q_{\text{Bi}^{3+}}^* - 2Q_{\text{I}^-}^*}{RT^2} = \frac{Q_{2e}^* - 2Q_{\text{I}^-}^*}{RT^2} \quad (14)$$

Thus, the Soret effect is absent when $\epsilon_{\text{in}} = \epsilon_{\text{st}}$, since in that case eq 11 holds, and the term on the right of eq 14 is zero. It has been shown by Wirtz¹³ and Denbigh¹⁴ that the Soret coefficient is expressible in terms of the microscopic parameters q_A and q_B

$$s = \frac{q_A - q_B}{RT^2} \quad (15)$$

where q_A is the energy required to remove particle A from its site and q_B is the same quantity for B. Thus, by comparison of eq 14 with 15 we see that the same energy is required to remove the two iodide ions from their sites as the electron pair. This may be made clear by the following illustration in which adjacent cations are surrounded by iodide ions in a two-dimensional array.



In (I), the cation on the left is associated with the electron pair; *i.e.*, it has a charge of +1, and the adjacent cation has a charge of +3. The singly charged cation attracts its surrounding anions less strongly than the triply charged cation, and hence those anions are somewhat further away. Now in (II), the electron pair was transferred to the right, converting the singly charged cation to a triply charged one and *vice versa*. This exchange will take place only if the atmospheres are the same around each cation.⁸ On the other hand, iodide is also transferred when symmetrization occurs;

therefore both processes, the transfer of iodide and the two-electron jump, require one and the same energy. If the concentration of Bi⁺ cations is low, then the number of exchanging electrons is small and the ions can carry an appreciable part of the total current. In this case eq 12 no longer holds and thermal diffusion is observed. This effect occurred in the composition range up to about 30 mole % bismuth.

It is of interest to calculate the entropy of transport from the thermoelectric data and for this purpose we turn to the steady-state thermoelectric potentials. As was pointed out by Temkin and Khoroshin,¹⁵ the steady-state potential of a thermocell depends only on the transported entropy of the ion that is reversible to the electrodes. In the present case, since the electrodes are inert, they are reversible to electrons or, in other words, the flow of current may be represented by the flow of Bi⁺ ions toward the anode minus the flow of Bi³⁺ ions toward the cathode. An equation may be derived relating the final thermoelectric potential, ϵ_{st} , to the entropy of transport of this oxidation-reduction couple by setting up a heat balance at one of the electrodes (see, *e.g.*, Pitzer).¹⁶ We consider the entropy changes occurring at the hot electrode and equate the sum of these to the Peltier heat in the steady state, Q_3^* .

The entropy absorbed in the reaction at the hot electrode is $1/2(\bar{S}_{\text{Bi}^+} - \bar{S}_{\text{Bi}^{3+}}) - \bar{S}_{\text{el(ex)}}$, where \bar{S}_{Bi^+} and $\bar{S}_{\text{Bi}^{3+}}$ represent the partial molar entropies of the reduced and oxidized forms, respectively, and $\bar{S}_{\text{el(ex)}}$ is the entropy of an electron in the external circuit.

The entropy transported away from the hot electrode region by diffusion is $1/2(S^*_{\text{Bi}^+} - S^*_{\text{Bi}^{3+}}) - S^*_{\text{el(ex)}}$, where S^* 's are the entropies of transport. Summing these terms, we have

$$-F\nu\epsilon_{\text{st}} = 1/2(\bar{S}_{\text{Bi}^+} - \bar{S}_{\text{Bi}^{3+}}) - \bar{S}_{\text{el(ex)}} + 1/2(S^*_{\text{Bi}^+} - S^*_{\text{Bi}^{3+}}) - S^*_{\text{el(ex)}} \quad (16)$$

where ν is the number of equivalents of electricity (*i.e.*, unity) and F is the Faraday constant. Since the transported entropy \bar{S} is the sum of the entropy of transport S^* and the partial entropy, \bar{S} , eq 16 becomes

$$-F\epsilon_{\text{st}} = 1/2(\bar{S}_{\text{Bi}^+} - \bar{S}_{\text{Bi}^{3+}}) - \bar{S}_{\text{el(ex)}}$$

Now, if we recognize that in this system the tungsten

(12) H. J. V. Tyrrell, "Diffusion and Heat Flow in Liquids," Butterworth and Co. Ltd., London, 1961.

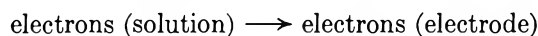
(13) K. Wirtz, *Z. Physik*, **44**, 221 (1943).

(14) K. G. Denbigh, *Trans. Faraday Soc.*, **48**, 1 (1952).

(15) M. I. Temkin and A. Z. Khoroshin, *Zh. Fiz. Khim.*, **26**, 500 (1952).

(16) K. S. Pitzer, *J. Phys. Chem.*, **65**, 147 (1961).

electrode is reversible only to electrons, since only they cross the electrode-solution interface, then the cell reaction may be written



Thus, the final thermoelectric power becomes

$$-F\epsilon_{\text{st}} = \frac{1}{2}\bar{S}_{2e} - \bar{S}_{eI(\text{ex})} \quad (17)$$

where \bar{S}_{2e} is the transported entropy of the electron pair in the solution. The value of $\bar{S}_{eI(\text{ex})}$ has been shown¹² to be small (about 0.05 eu) and is therefore neglected. The results for $\frac{1}{2}\bar{S}_{2e}$ at 500° are shown in Table II.

Table II

X_{Bi}	$\frac{1}{2}\bar{S}_{2e}$, eu	$\frac{1}{2}\bar{S}_{2e}$, eu	$\frac{1}{2}S^*_{2e}$, eu	$\frac{1}{2}Q^*_{2e}$, kcal
0.01	106	4.2	102	79
0.03	72	3.0	69	53
0.05	50	2.5	48	37
0.10	14	1.7	12	9.3
0.15	11	1.2	10	7.7
0.20	5.3	0.8	4.5	3.5
0.25	-1.2	0.5	-1.7	-1.3
0.30	-2.3	0.18	-2.5	-1.9
0.35	-2.8	0.0	-2.8	-2.2
0.50	-1.0	0.0	-1.0	-0.77
0.80	-0.58	0.0	-0.58	-0.45
0.90	-0.42	0.0	-0.42	-0.32

The transported entropy is rather unique in that it is an experimentally accessible single-ion quantity. However, the partial molar entropies are not, and some sort of estimate must be made in order that the entropy of transport may be calculated. Raleigh and Topol⁷ have used the expression

$$\bar{S}_{2e} = R \ln \frac{[\text{Bi}^{3+}]}{[\text{Bi}^{+}]} + \Delta S_{\text{Bi}} \quad (18)$$

in which the first term is a configurational entropy term and the second involves the change in entropy due to the change of ionic atmosphere of the cation when it changes its oxidation state. As was pointed out by Raleigh and Topol,⁷ the iodide ion is so much larger than the cations that the geometry of the system fixes to some extent the number of nearest neighbors surrounding either cation. Therefore, the term ΔS_{Bi} is probably fairly composition independent, and since the magnitude of this term is small compared to the transported entropy, we will neglect it in the qualitative discussion below. Then, substituting (18) into (17), we have

$$\frac{1}{2}S^*_{2e} = -F\epsilon_{\text{st}} - \frac{1}{2}R \ln \frac{[\text{Bi}^{3+}]}{[\text{Bi}^{+}]} \quad (19)$$

The values of $\frac{1}{2}S^*_{2e}$ obtained from eq 19 at 500° are shown in Figure 3 and are tabulated in Table II along with the heats of transport $\frac{1}{2}Q^*_{2e}$.

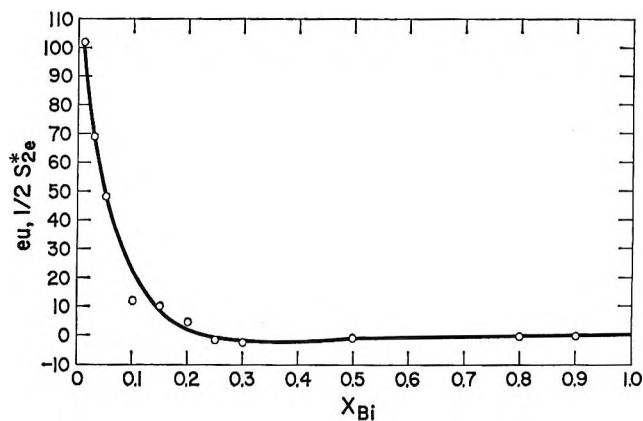


Figure 3. One-half of the entropy of transport of the electron pair in solution vs. mole fraction of bismuth.

The quantity $\frac{1}{2}(S^*_{\text{Bi}^{+}} - S^*_{\text{Bi}^{3+}})$ tends toward zero as metal is added between the compositions of nearly pure salt and 30% bismuth. This behavior is consistent with the electron-hopping theory, since as electron exchange becomes more common in the melt, more cations become indistinguishable as far as diffusion is concerned. Between 30 and 60% metal all the cations have an average charge between +2 and +1, and the system consists of a one-component melt with the formula BiI_x where x is between 2 and 1. At low metal concentrations where there is a smaller amount of electron exchange occurring, there is a larger difference in the effect the flux of each of the two cation forms has on its surroundings. Since it is this effect which determines the entropy of transport, the difference $\frac{1}{2}(S^*_{\text{Bi}^{+}} - S^*_{\text{Bi}^{3+}})$ is large.

Throughout the remainder of the compositions from 60 to 90% metal, no Soret effect is observed. The average cation charge at $\frac{1}{3}$ mole fraction metal is +2; *i.e.*, half the cations have a charge of +1 at any one instant even though the valence state of a particular cation is rapidly shifting. Above 50 mole %, the appearance of metallic bismuth is suggested by magnetic susceptibility data⁵ and beyond $\frac{2}{3}$ mole fraction metal, where the cations have an average charge between +1 and 0, the melt probably consists mostly of Bi^{+} cations, I^{-} ions, and metallic bismuth. If the conductivity mechanism shifts to a one-electron exchange between Bi and Bi^{+} , the cations would still be

indistinguishable, accounting for the lack of thermal diffusion. If the more easily ionized Bi is contributing electrons to some sort of conduction band, these ions would still be indistinguishable from the Bi⁺ cations in the melt. Therefore, the conductivity model would predict no thermal diffusion, and in fact none is observed. However, thermal diffusion experiments cannot distinguish between these mechanisms in the metal-rich region. In the region below $\frac{2}{3}$ mole fraction of bismuth, on the other hand, the fact that no Soret effect is observed clearly demonstrates that electron exchange is the conductivity mechanism. This is be-

cause it is the only mechanism by which Bi³⁺ and Bi⁺ can be rendered indistinguishable as far as mass transport is concerned.

The electron-jump mechanism would be facilitated by an increase in temperature.⁸ The data indicate less of a Soret effect at higher temperatures at compositions between 1 and 30 mole %. Due to a greater amount of exchange, the quantity $\frac{1}{2}(S_{\text{Bi}^+}^* - S_{\text{Bi}^{3+}}^*)$ thus decreases with increasing temperature.

Acknowledgment. The author is indebted to Dr. S. J. Yosim for helpful discussions and a critical reading of the manuscript.

Temperature Coefficient of the Unperturbed Dimension of Linear Polyethylene from Intrinsic Viscosity Measurements in Θ Solvents

by R. Chiang

Contribution No. 363 from the Chemstrand Research Center, Inc., Durham, North Carolina
(Received February 7, 1966)

Intrinsic viscosity measurements have been made on polyethylene fractions in various Θ solvents, biphenyl, diphenylmethane, diphenyl ether, octanol-1, decanol-1, and dodecanol-1 at 127.5, 142.2, 161.4, 180.1, 153.3, and 137.3°, respectively. The linear relationship between $[\eta]_{\Theta}$ and $M^{1/2}$ for polyethylene in diphenyl ether previously observed appears to be valid in all the Θ solvents investigated, the proportionality constant K ($[\eta]_{\Theta} = KM^{1/2}$ with $[\eta]_{\Theta}$ in dl g⁻¹) being equal to 3.23, 3.15, 2.95, 2.86, 3.02, and 3.07×10^{-3} at the respective Θ temperatures. The temperature coefficient, $d \ln \langle r^2 \rangle_0 / dT \times 10^3$ of the unperturbed dimension calculated from the intrinsic viscosities in biphenyl and diphenylmethane is -1.16 ± 0.5 , in agreement with the results obtained by Nakajima, *et al.*; the same quantity calculated from the intrinsic viscosities in the higher alcohols is $-1.19 \pm 0.2 \text{ deg}^{-1}$. One of the most striking features of the results reported here is the small difference between the alcohols on the one hand and the aromatic hydrocarbons on the other. The close similarity seems to indicate rather clearly that specific solvent effects for this nonpolar polymer must be quite small. The temperature coefficient values obtained here are essentially identical with those obtained by stress-temperature measurements (-1.16 ± 0.10) and by intrinsic viscosity measurements in athermal solvents (-1.2 ± 0.2). We are led to conclude that the results obtained with the three independent methods are consistent.

Introduction

The determination of the unperturbed dimension of polyethylene and its temperature coefficient has been a subject of interest in recent years.¹⁻³ Comparison of experimental results with theoretical calculations yields valuable information on the conformation and internal rotation of the polymer chain.³⁻⁶

As is known, the temperature coefficient has been successfully determined by the stress-temperature coefficient of a cross-linked network⁷ and by the temperature coefficient of the intrinsic viscosity $[\eta]$ of the polymer in athermal solvents.⁸

Recently, close agreement between the values of the unperturbed dimension obtained by intrinsic viscosity measurements in athermal solvents (with appropriate corrections for the excluded volume effect) and by direct measurements in a Θ solvent (diphenyl ether at 161.4°) has been achieved.⁹ One may be inclined to think that the temperature coefficient can be determined by

measuring the intrinsic viscosities directly in different Θ solvents at the respective Θ temperatures by making use of eq 1

$$\frac{d \ln \langle r^2 \rangle_0}{dT} = \frac{2}{3} \frac{d \ln [\eta]_{\Theta}}{dT} \quad (1)$$

where $\langle r^2 \rangle_0$ is the unperturbed mean-square end-to-end distance. However, careful examination reveals that

(1) See, for example, M. V. Volkenstein, "Configurational Statistics of Polymer Chains" (English transl), Interscience Publishers, Inc., New York, N. Y., 1963.

(2) P. J. Flory, C. A. J. Hoeve, and A. Ciferri, *J. Polymer Sci.*, **34**, 337 (1959).

(3) P. J. Flory, *Proc. Natl. Acad. Sci. U. S.*, **51**, 1060 (1964).

(4) C. A. J. Hoeve, *J. Chem. Phys.*, **35**, 1266 (1961).

(5) K. Kagai and T. Ishikawa, *ibid.*, **37**, 496 (1962).

(6) P. J. Flory and R. L. Jernigen, *ibid.*, **42**, 3509 (1965).

(7) A. Ciferri, C. A. J. Hoeve, and P. J. Flory, *J. Am. Chem. Soc.*, **83**, 1015 (1961).

(8) P. J. Flory, A. Ciferri, and R. Chiang, *ibid.*, **83**, 1023 (1961).

(9) R. Chiang, *J. Phys. Chem.*, **69**, 1645 (1965).

this direct procedure is not as simple as it may seem to be. In the first place, the temperature coefficient of $[\eta]_{\Theta}$ to be determined is very small, usually much smaller than that of $[\eta]$ itself near the Θ point; an error of 1–2° in the Θ point, which is not unlikely, will introduce an appreciable error in the final value of $d \ln \langle r^2 \rangle_0 / dT$. Even more bothersome is the fact that the solvent used plays an important role in determining the unperturbed dimension of the polymer chain (the so-called specific solvent effect^{10–12}). The specific solvent effect, though small, may easily be sufficient to invalidate the calculation. Thus Schulz and Baumann¹³ obtained the temperature coefficient for polystyrene in various solvents with no definite correlation, and Abe and Fujita,¹⁴ studying the effect of mixed solvents, reached the conclusion that the temperature coefficient can be positive, negative, or zero, depending on the values of the energy parameter κ_1 . Orofino and Ciferri¹⁵ were the first to obtain the temperature coefficient for polystyrene in agreement with the stress-temperature value by limiting their intrinsic viscosity measurements in 1-chloro derivatives of hydrocarbons with similar chemical structures.

In the case of polyethylene, Nakajima, Hamada, and Hayashi¹⁶ have determined the intrinsic viscosities in three different solvents, biphenyl, diphenylmethane, and diphenyl ether, and found that the temperature coefficient calculated from these three $[\eta]_{\Theta}$ values is in excellent agreement with the values obtained by stress-temperature measurements and by intrinsic viscosity measurements in athermal solvents. However, no reference was made to measurements in other solvents, nor to the possible influence of the specific solvent effect on the calculated value of the temperature coefficient of the unperturbed dimension. Thus any specific solvent effects would not have been revealed in their investigation. In the present study, we are primarily concerned with this effect and therefore determined the intrinsic viscosities of polyethylene in different series of Θ solvents for the purpose of (1) obtaining more data to check our previous intrinsic viscosity $[\eta]_{\Theta}$ obtained in diphenyl ether;⁹ (2) determining the specific solvent effect, if any; and (3) confirming, in a definitive manner, the value of the temperature coefficient obtained by other methods.^{7,8}

Polyethylene, the simplest member in the polymer family, is of particular interest because its unperturbed dimension has been treated most extensively. It is also the most nonpolar polymer whose dimension should be least affected by the solvent. The Θ solvents used here belonged to three different homologous series, each with great similarities in chemical structure, and hence in physical properties such as dipole moments,

cohesive energy densities, etc., which might affect the dimension of the polymer. The Θ solvents included (1) aromatic hydrocarbons (biphenyl and diphenylmethane), (2) diphenyl ether, and (3) higher alcohols (octanol-1, decanol-1, and dodecanol-1). The Flory Θ points for the respective solvents are taken from the paper by Nakajima, *et al.*¹⁷ The values in biphenyl and dodecanol-1 reported by these authors are in agreement with the corresponding values obtained by Stacy and Arnett¹⁸ and the value in diphenyl ether is in agreement with that reported by Chiang.⁹ All of the above Θ points were obtained by the liquid-liquid phase separation technique first developed by Shultz and Flory.¹⁹ Scholte and Koningsveld,²⁰ on the basis of the light scattering results, confirmed Nakajima's result of 127° as a correct Θ temperature for polyethylene in biphenyl.

Experimental Section

Polymer Samples. The samples used here were fractions separated from Marlex 50 and most of them were used in our previous studies.⁹ Characteristics of the fractions are given in Table I.

Solvents. All of the solvents were obtained from the Eastman Kodak Co. and used without further purification. Since polyethylene is sensitive to oxidation at elevated temperatures, it is imperative to protect the polymer during measurements by the addition of a stabilizer and rigorous exclusion of air. In the experiments reported here phenyl- β -naphthylamine used as a stabilizer was introduced at room temperature at a concentration of 0.2% into the solvent. In order to decompose any peroxides originally present, the solvent was first saturated with nitrogen, then heated to a

(10) K. J. Ivin, H. A. Ende, and G. Meyerhoff, *Polymer*, **3**, 129 (1962).

(11) V. Crescenzi and P. J. Flory, *J. Am. Chem. Soc.*, **86**, 141 (1964).

(12) T. A. Orofino and J. W. Mickey, Jr., *J. Chem. Phys.*, **38**, 2512 (1963).

(13) G. V. Schulz and H. Baumann, *Makromol. Chem.*, **60**, 120 (1963).

(14) M. Abe and H. Fujita, *J. Phys. Chem.*, **69**, 3263 (1965).

(15) T. A. Orofino and A. Ciferri, *ibid.*, **68**, 3136 (1964).

(16) A. Nakajima, F. Hamada, and S. Hayashi, paper presented at the joint U. S.–Japan Symposium on Polymer Physics, Kyoto, Japan, Oct 1965.

(17) A. Nakajima, H. Fujiwara, and F. Hamada, "Phase Relationships and Thermodynamic Interactions in Linear Polyethylene-Diluent Systems," *J. Polymer Sci.*, in press. The author is indebted to Prof. Nakajima and his co-workers for allowing him to use their results.

(18) C. J. Stacy and R. L. Arnett, *J. Phys. Chem.*, **69**, 3109 (1965).

(19) A. R. Shultz and P. J. Flory, *J. Am. Chem. Soc.*, **74**, 4760 (1952); P. J. Flory, "Principles of Polymer Chemistry," Cornell University, Ithaca, N. Y., 1953.

(20) Results cited by A. Opschoor, *Makromol. Chem.*, **85**, 249 (1965).

Table I: Polymer Fractions

Fraction no.	$[\eta]$ in decalin at 135°, dl g ⁻¹	$\bar{M}_w \times 10^{-3}$
VII-1	0.530	(15.4) ^a
VII-2	0.618	21.9
VIII-4	0.936	35.6
VIII-5	1.055	(41.2)
VIII-6	1.445	74.4
VIII-7	1.885	(94.7)
VIII-8	2.13	126
IX	3.80	299
X	9.85	1035

^a Numbers in the parentheses are calculated from the equation, $[\eta]^{135}_{\text{decalin}} = 6.2 \times 10^{-4} \bar{M}_w^{0.70}$.

temperature a few degrees above the temperature required for the viscosity measurement. Bubbling of nitrogen was not interrupted until the solvent had cooled down to room temperature. Under no conditions was the polymer or the solvent allowed to come in contact with air at elevated temperatures. Specific volumes used to calculate the concentrations in grams per deciliter were measured pycnometrically.

Viscometry. Viscosities were measured at the respective Θ temperature with a modified Cannon-Ubbelohde dilution viscometer, the construction of which has been described previously.⁸ A coarse sintered glass filter was fitted in the viscometer to remove any extraneous insoluble material before the solution was allowed to come into the capillary. Viscometers with appropriate capillary sizes were used; flow times, measured to the nearest 0.1 sec, were 169.10, 151.02, 131.72, 110.58, 181.48, and 161.30 sec for biphenyl, diphenylmethane, diphenyl ether, octanol-1, decanol-1, and dodecanol-1 at the corresponding Θ temperatures.

Solutions were prepared by introducing measured quantities of the polymer and the solvent into the viscometer. Concentrations of the solutions were so adjusted that the specific viscosities ranged from 0.08 to 0.40. To exclude traces of air, the viscometer was operated under a slight positive pressure of nitrogen. The procedure of degassing, dilution, and measurement has been described previously.⁸ Special attention was given to the preparation of uniform solutions, rigorous exclusion of air, and proper alignment of the viscometer. In the absence of air, polyethylene is very stable. One sample, for example, heated in dodecanol at 200° for 1 hr, 190° for 2 hr, and maintained at 150° overnight, showed no sign of change in viscosity. Failure

to exclude oxygen often yielded abnormally high viscosity. Possibly, the polymer radical combines with another radical (or molecule), forming a polymer with molecular weight higher than the original polymer. Loss of solvent by evaporation presents a problem at elevated temperatures since octanol, bp 194°, has an appreciable vapor pressure at 180° and biphenyl tends to sublime somewhat. However, the specific viscosity obtained on each solution by successive dilution and by the use of a fresh solution at the corresponding concentration did not exceed 1% and the solution upon standing overnight did not show change in flow time. Thus under the experimental conditions the amount of solvent lost was negligible.

Results and Discussion

Since the temperature coefficient of the intrinsic viscosity of polyethylene is very small, in the neighborhood of $-1.8 \times 10^{-3} \text{ deg}^{-1}$, intrinsic viscosities must be determined with a high degree of accuracy. To optimize the conditions of measurements, the temperature range over which the measurements are carried out should be as wide as possible and the temperature coefficient of the intrinsic viscosity near the Θ point should be small. Using samples of high $[\eta]$ helps somewhat, but the advantage is offset by the weighing error of the small size of the sample and by the difficulties of dissolving the high molecular weight material. Among all the solvents studied, higher alcohols seem to best meet the above requirements. It is important to note that the temperature coefficient of the intrinsic viscosity near the Θ point is relatively small; for example, the temperature coefficient, $d \ln [\eta]/dT$, is approximately 0.0021 deg^{-1} in dodecanol as compared to 0.0070 deg^{-1} in diphenyl ether. Thus, an error of 2° in Θ point results in an error of 0.4% in $[\eta]_{\Theta}$ when measured in alcohols, as compared to 1.4% in diphenyl ether. Everything else being equal, this three- to fourfold reduction in $d \ln [\eta]/dT$ of the polymer near the Θ point in alcohols will make the error in $d \ln \langle r^2 \rangle_0/dT$ tolerable even if we have an experimental error of 2° in locating the true Θ point.

Intrinsic Viscosities in Dodecanol-1 at Its Θ Temperature

Table II: Viscosity Data on Polyethylene Fractions in Dodecanol-1 at 137.3°

$[\eta]_{\Theta}$, dl g ⁻¹	k in eq 2
0.621	0.70
0.945	0.69
1.060	0.78
3.13	0.63–0.70

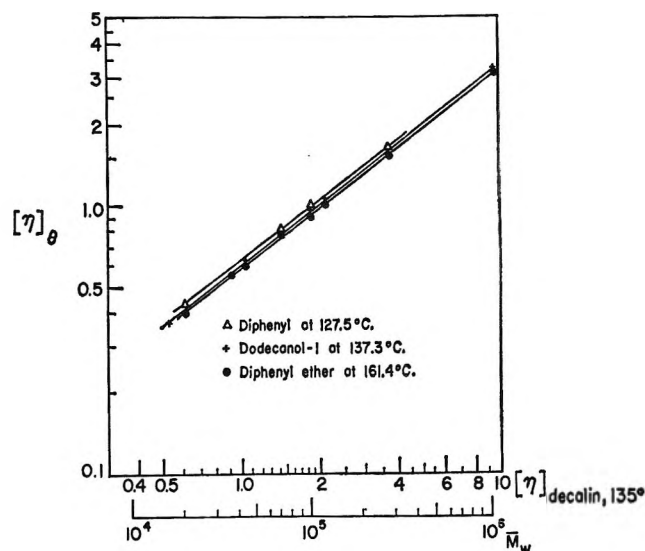


Figure 1. Logarithmic plot of $[\eta]_{\theta}$ against M for polyethylene in various Θ solvents. The lines are drawn with a theoretical slope of $1/2$, illustrating the linear relationship between $[\eta]_{\theta}$ and $M^{1/2}$.

ture. To illustrate the consistency of the results, the intrinsic viscosities obtained on different polyethylene fractions in dodecanol-1 at 137.3° are shown in Table II. The concentration dependence can be described by the equation

$$\frac{\eta_{sp}}{c} = [\eta] + k[\eta]^{2.5}c \quad (2)$$

The exponent 2.5 of $[\eta]$ in the second term of eq 2 was adjusted arbitrarily in order to retain the constancy of the value of k over a wide range of molecular weights.

The $[\eta]_{\theta}$ - $M^{1/2}$ Relationship. Intrinsic viscosities of various samples determined in diphenyl ether, dodecanol-1, and biphenyl are plotted against the molecular weight (calculated from the intrinsic viscosity measured in decalin at 135°) on a logarithmic scale (Figure 1). The lines are drawn with a theoretical slope of $1/2$. The linearity between $[\eta]_{\theta}$ and $M^{1/2}$ reported previously⁹ appears to be valid for all the solvents investigated, the proportionality constant K ($[\eta]_{\theta} = KM^{1/2} dl g^{-1}$) being equal to 3.23, 3.15, 2.95, 2.86, 3.02, and 3.07×10^{-3} in biphenyl, diphenylmethane, diphenyl ether, octanol-1, decanol-1, and dodecanol-1 at their respective Θ temperatures.

The Temperature Coefficient $d \ln [\eta]_{\theta}/dT$. In the determination of the effect of temperature on $[\eta]_{\theta}$, only one fraction, VIII-7, was used to avoid uncertainties due to sample variations. Results thus obtained are given in Table III.

When $[\eta]_{\theta}$ values are plotted against Θ , two lines can

be drawn, one passing through the points for biphenyl and diphenylmethane (line 1) and the other for the higher alcohols (line 2). The two nearly parallel lines obtained are separated by a "gap" of 0.03 to 0.04 in intrinsic viscosity units which exceeds the limit of the experimental error. This seems to suggest that the specific solvent effects commonly observed on polar polymers can also be detected even in the case of polyethylene. It further indicates that the specific solvent effects are minimized by grouping the intrinsic viscosities according to the chemical structures of the solvents.

The temperature coefficients $d \ln \langle r^2 \rangle_0/dT$ obtained in the hydrocarbons and in the alcohols are -1.16 and -1.19×10^{-3} , respectively. However, the agreement cannot be considered anything more than coincidental in view of the fact that the former value is less certain because of the narrow temperature range used. On the other hand, the temperature coefficient obtained from the $[\eta]_{\theta}$ of the polymer in the higher alcohols, for the reasons discussed above, is more accurate. If the assumption that the specific solvent effects are minimized (or nullified) in the alcohols is true, then we are reasonably sure of the value of -1.19×10^{-3} for $d \ln \langle r^2 \rangle_0/dT$, with a possible error of $\pm 0.2 \times 10^{-3}$.

The temperature coefficient calculated by using the intrinsic viscosity in diphenyl ether is open to question. Nakajima, *et al.*, concluded that the temperature coefficient can be calculated from the $[\eta]_{\theta}$ measured in biphenyl, diphenylmethane, and diphenyl ether as well (line 1). Our results, however, indicate that diphenyl ether, for no apparent theoretical reason, falls on line 2 along with the higher alcohols. The discrepancy appears to arise through the use of different Θ temperatures, namely 163.9° by Nakajima and 161.4° by Chiang. The least-squares analysis of Nakajima's data (Table II, ref 16) gives a value of 161.9° for the Θ temperature of polyethylene in diphenyl ether. Taking the value of 163.9° reported by Nakajima and applying the factor 0.0070 deg^{-1} for the change in $\ln [\eta]$ with respect to temperature, we observe that diphenyl ether will then fall on line 1 as reported by Nakajima (open square in Figure 2). Thus the results obtained by Nakajima and by us are internally consistent.

In any event, inasmuch as the temperature coefficient can be calculated from the intrinsic viscosities in aromatic hydrocarbons or in higher alcohols, the result in diphenyl ether is of little importance for the present purpose of confirming the value of the temperature coefficient of the dimension of polyethylene.

Table III: $[\eta]_{\theta}$ of Fraction VIII-7 in Various Solvents at the Respective θ Temperatures^a

Hydrocarbons			Higher alcohols			$\theta^{\circ}\text{C}$	$[\eta]_{\theta}$	
	$\theta^{\circ}\text{C}$	$[\eta]_{\theta}$		$\theta^{\circ}\text{C}$	$[\eta]_{\theta}$			
Biphenyl	127.5	0.996	Dodecanol-1	137.3	0.943	Diphenyl	161.4	0.910 ^b
Diphenyl- methane	142.2	0.971	Decanol-1	153.3	0.930	ether	(163.9)	(0.926) ^c
		0.968			0.925			
			Octanol-1	180.1	0.875			
					0.886			

$$-\frac{d \ln [\eta]_{\theta}}{dT} \times 10^3 = 1.74 \pm 0.7^d \quad 1.78 \pm 0.3$$

$$-\frac{d \ln \langle r^2 \rangle_0}{dT} \times 10^3 = 1.16 \pm 0.5 \quad 1.19 \pm 0.2$$

^a It should be emphasized that the value of $d \ln [\eta]_{\theta}/dT$ given here is derived from a single sample. However, our data also justify the use of the more general form $d \ln K/dT$ in place of $d \ln [\eta]_{\theta}/dT$. ^b As compared to 0.907 calculated from the intrinsic viscosity in decalin at 135° (ref 9). ^c See text. ^d The deviations are estimated on the basis that the experimental error in measuring $[\eta]_{\theta}$ is ± 0.01 intrinsic viscosity unit.

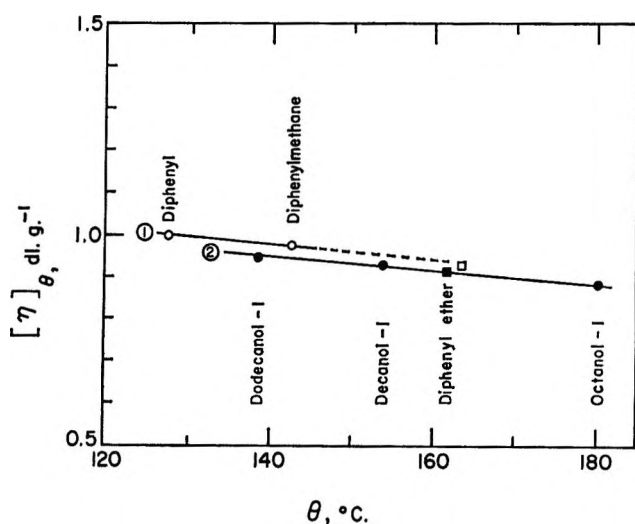


Figure 2. Variation of $[\eta]_{\theta}$ with θ for polyethylene in various θ solvents. The lines are drawn empirically according to the chemical structure of the solvent.

Conclusions

One of the most striking features of the results reported here is the small difference in $[\eta]_{\theta}$ (compared,

of course, at the same temperature) between alcohols on the one hand and the aromatic hydrocarbons on the other. The close similarity seems to indicate rather clearly that specific solvent effects for this nonpolar polymer must be quite small. They seem to be much smaller than those found by Schulz and Baumann for polystyrene and by Crescenzi and Flory for poly(dimethylsiloxane). The small solvent effect permits calculation of the temperature coefficient in this manner without introducing serious error.

In summary, the temperature coefficient $d \ln \langle r^2 \rangle_0/dT$ calculated from the intrinsic viscosities in biphenyl and diphenylmethane is $-1.16 \times 10^{-3} \text{ deg}^{-1}$ with a high degree of uncertainty and that from the intrinsic viscosities in higher alcohols is $-1.19 \times 10^{-3} \text{ deg}^{-1}$ with a possible error of only $\pm 0.2 \times 10^{-3}$. These results, in addition to those reported by Nakajima, *et al.*, furnish further experimental evidence in support of the values deduced from stress-temperature measurements as well as from intrinsic viscosity measurements in athermal solvents.

Acknowledgment. The author wishes to express his appreciation to Professor P. J. Flory of Stanford University for his valuable suggestions.

Ion-Molecule Reactions in Acetonitrile and Propionitrile^{1a}

by J. L. Franklin, Yasuo Wada, P. Natalis,^{1b} and P. M. Hierl

Department of Chemistry, Rice University, Houston, Texas (Received February 7, 1966)

The mass spectra of acetonitrile and propionitrile have been determined as a function of pressure and time. The principal secondary ion formed with each compound is the $M + 1$ ion. With CH_3CN the ion $\text{C}_2\text{H}_4\text{CN}^+$ is also formed with moderate abundance, and with $\text{C}_2\text{H}_5\text{CN}$, C_2H_5^+ , C_2H_6^+ , CH_3CN^+ , and CH_4CN^+ are formed in moderate abundance. Both compounds exhibit a large number of secondary ions formed in small amounts. The doubly solvated proton is observed with both compounds but in intensities too small for study. In order to establish the composition of the various ions, spectra were obtained of the perdeuterated compounds also. Rate studies were made by varying both pressure and time, and rate constants were obtained for most of the principal reactions.

Introduction

Ion-molecule reactions in acetonitrile and propionitrile have been subjected to two previous investigations.² Each of these was undertaken for rather special purposes and did not consider all of the reactions occurring. Both studies were carried out at pressures below about 2μ and thus at conditions where many secondary ions could not be observed, and neither employed variation of both time and pressure in the determination of reaction rates. In view of the limited conditions employed in the previous studies, this investigation was undertaken to obtain more complete knowledge of the collision reactions of the ions in acetonitrile and propionitrile.

Experimental Section

Mass spectra were obtained by means of a Bendix time-of-flight mass spectrometer Model 12-107 equipped with a special ion source and auxiliary pumping system Model 1077, capable of operating at source pressures up to 100μ . Pressures in the ionization region were measured by an M. K. S. Type 77 Baratron pressure meter connected directly to the ionization chamber through a 0.25-in. i.d. opening in the flange upon which the source was mounted. The ionization region was separated from this opening only by a backing electrode made of a highly porous mesh of fine wire. Pressures were kept constant during an experiment by using a 12-l. sample gas reservoir and a suitable gold foil leak system. The variation of the residence time of ions in the ionization region was accomplished by de-

laying the ion focus pulse over a continuously variable range from 0 to several μsec after shutting off the electron pulse.

The samples of acetonitrile and propionitrile were spectrograde products from Eastman Organic Chemicals. The samples of acetonitrile- d_3 and propionitrile- d_5 were obtained from Merck Sharp and Dohme of Canada Ltd. The mass spectra of CH_3CN and $\text{C}_2\text{H}_5\text{CN}$ showed no significant impurities and were in good agreement with those reported in the literature. From mass spectral analyses the deuterium content of acetonitrile- d_3 and propionitrile- d_5 was found to be 99.4 and 98.7%, respectively.

The ionization potentials of all compounds were determined using a Consolidated Electroynamics Corp. mass spectrometer, Type 21-701,³ against Xe as reference gas. The appearance potentials of major primary and secondary ions were determined, using the Bendix time-of-flight mass spectrometer mentioned above against the parent ions as voltage standards. The extrapolated difference method⁴ and the technique of Lossing, Tickner, and Bryce⁵ were used for deter-

(1) (a) This work was supported by a grant from the Robert A. Welch Foundation. (b) Chercheur qualifié de la Belgian Fonds National de la Recherche Scientifique. On leave of absence from the University of Liege, Belgium.

(2) (a) T. W. Martin and C. E. Melton, *J. Chem. Phys.*, **32**, 700 (1960); (b) T. F. Moran and W. H. Hamill, *ibid.*, **39**, 1413 (1963).

(3) P. Natalis and J. L. Francklin, *J. Phys. Chem.*, **69**, 2935 (1965).

(4) J. W. Warren, *Nature*, **165**, 811 (1950).

(5) F. P. Lossing, A. W. Tickner, and W. A. Bryce, *J. Chem. Phys.*, **19**, 1254 (1951).

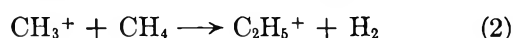
mination of ionization and appearance potentials. The reproducibility of the data so obtained was 0.05 to 0.3 v.

It has been observed that the resolution of adjacent peaks of unit mass difference becomes poorer with increase of either pressure or time delay. This makes it difficult to measure peak heights of ions of small intensity with good accuracy at the higher conditions of pressure or time delay.

Reaction rates were determined by two methods: (1) varying the source pressure and (2) varying the reaction time. In the pressure studies the reaction time was taken as the rise time plus pulse duration, which was maintained at 0.25 μ . This involves a slight error due to the fact that the ions spend a small additional interval in the source while being swept out by the ion-focus pulse. Since the potential employed to withdraw the ions from the source was about 300 v and the distance 1.14 mm, the additional time required for the ions to reach an energy too great for reaction to occur was small enough to be neglected.

In the time studies pressure was held constant at about 30 μ and the time varied, the total time being the sum of the rise time, electron-pulse duration, and ion-focus pulse delay, the latter being changed in increments of 0.25 μ sec. Although it is possible to delay the ion-focus pulse as much as 20 μ sec, delays of more than 1–1.5 μ sec give very doubtful results since most ions begin to reach the wall by diffusion and be destroyed there after 1–1.5 μ sec. In all of the studies the source temperature was assumed to be 300°K.

As a check upon the reliability of our measurements the rates of the reactions



were determined by measuring both the depletion of CH_4^+ and CH_3^+ and the formation of CH_5^+ and C_2H_5^+ as a function of time at several pressures. The results are given in Table I. These results are in reasonable agreement with the values of 9.9×10^{-10} and 7.9×10^{-10} for reactions 1 and 2, respectively, determined by Field, Franklin, and Munson.⁶ It is of especial interest that these results for reaction 1 agree reasonably well with values of 1.16×10^{-97} and 1.11×10^{-98} cc/molecule sec obtained by a similar pulse technique in which reaction occurs in an essentially field-free source.

Results and Discussion

Typical spectra for both the nitriles and the corresponding perdeuterionitriles are given in Table II. The spectra are in generally satisfactory agreement with those obtained in other laboratories employing

Table I

Pressure, μ	—10%k, cc/molecule sec—			
	— CH_4^+	+ CH_5^+	— CH_3^+	+ C_2H_5^+
10	1.23	1.23	...	0.72
14	1.32	1.39	0.70	0.72
15	1.20	...	0.65	...
20	0.87	...
30	0.64	...
48	1.25	1.39	0.66	0.57
Average	1.25	1.34	0.70	0.67

magnetic instruments.⁹ The table includes low-pressure spectra as well as typical results at source pressures of about 30 μ . The latter data are given to indicate especially the principal secondary ions that are formed. Unfortunately, we are not in a position from mass numbers alone to establish the composition of several ions that are present in the mass spectra of these compounds. For example, the ion at mass 26 may be either C_2H_2 or CN ; that at mass 27 may be C_2H_3 or HCN , etc. Because of this ambiguity, the low-pressure spectra were obtained on a high-resolution instrument, and these indicate the approximate composition of some of the ions of nominal mass numbers between 24 and 30. This could not be done for secondary ions because of pressure limitations of the instrument. Consequently, studies were also made of the perdeutero compounds. From the shifts in mass for ions of corresponding intensity, it was possible in most cases to make clear determinations of the composition of the probable secondary ions. Table III lists these secondary ions for both acetonitrile and propionitrile. Since the majority of these ions were present in very small intensity, it was not possible to obtain rate data or to identify the corresponding precursors for many of them.

Acetonitrile. As an aid in identifying the precursors of the principal secondary ions, the appearance potentials of these ions and of the principal primary ions in the mass spectrum of acetonitrile were determined. Only the ionization potentials of the two perdeutero compounds were determined, since the appearance potentials of deuterated ions would differ little from

(6) F. H. Field, J. L. Franklin, and M. S. B. Munson, *J. Am. Chem. Soc.*, **85**, 3575 (1963).

(7) V. L. Tal'roze and E. L. Frankevich, *Russ. J. Phys. Chem.*, **34**, 1275 (1960).

(8) C. W. Hand and H. Von Weyssenhoff, *Can. J. Chem.*, **42**, 195 (1964).

(9) "Catalog of Mass Spectral Data," American Petroleum Institute, Agricultural and Mechanical College of Texas, College Station, Texas.

Table II: Mass Spectra

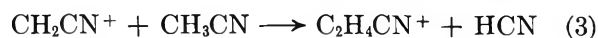
<i>m/e</i>	CH ₃ CN		CD ₃ CN		C ₂ H ₅ CN		C ₂ D ₅ CN	
	10 ⁻³ μ	30 μ	10 ⁻³ μ	30 μ	10 ⁻³ μ	30 μ	10 ⁻³ μ	30 μ
12	1.15	0.97	0.30	0.47	0.26	0.04	0.12	
13	0.87	0.66			0.31	0.20		
14	4.48	3.47	0.30	0.50	1.15	0.44	0.37	
15	0.85	1.91			3.73	2.82		
15.8		1.52				0.70		
16			3.50	3.28			0.75	0.39
18			1.14	1.74			4.40	2.7
19.3				0.4				Trace
24	0.45	0.11						
25	1.35	0.73						
26	1.92 ^a	2.25	0.93	0.66	7.78 ^c	5.39		
27	1.19 ^b	4.18			7.35 ^d	6.21		
28	2.07	2.24	1.16	1.97	38.22 ^e	24.36	6.70	3.44
29						2.73		
30			1.17	4.71		1.35	13.90	8.60
32							32.30	20.40
34								1.70
36								0.80
38	3.07	2.67	0.31	1.80	1.42	0.95	1.10	0.62
39	6.80	5.03			1.62	2.06		
40	23.48	21.97	4.48	5.08	2.05	1.71	1.30	0.71
41	51.50	27.81			0.26	1.05		
42	0.80	21.29	23.8	23.15	0.02	1.71	1.90	1.90
44			58.1	32.9			0.03	...
46				19.6				1.40
51					2.51	1.17		
52					3.63	2.87	0.50	
53		0.57			1.56	1.42		
54		2.22		0.29	21.10	17.55	1.50	0.96
55					5.62	4.31		
56				0.24	0.43	21.61	1.20	1.00
58				1.62			19.50	13.50
60							6.50	6.30
62								19.30

^a Approximately 60% CN⁺, 40% C₂H₂⁺. ^b Approximately 85% HCN⁺, 15% C₂H₃⁺. ^c Approximately 98% C₂H₂⁺, 2% CN⁺.
^d Approximately 93% C₂H₃⁺, 7% HCN⁺. ^e Approximately 80% C₂H₄⁺, 20% H₂CN⁺.

that of the corresponding protium ions. It will be evident from Table IV that the parent ion is the principal precursor of CH₄CN⁺ and that CH₂CN⁺ is the principal precursor of C₂H₄CN⁺ in acetonitrile. As will be shown subsequently, CH₃CN⁺ is not the only precursor of CH₄CN⁺, but, since CH₃CN⁺ has the lowest appearance potential of any primary ion in the spectrum it will be the one which determines the appearance potential of its product ion (CH₄CN⁺).

As a further means of establishing the principal ion-molecule reactions and also as a means of determining the reaction rates, spectra were obtained over a range of source pressures up to 100 μ for both CH₃CN and CD₃CN. The effect of time was studied while holding the source pressure fixed at 30 μ. Figure 1 shows the changes of the primary and secondary ions from acetonitrile against pressure and Figure 2 against time. Qualitatively the results are what one would expect. The CH₃CN⁺ decreases in a quite similar fashion with both pressure and time, and the corresponding CH₄CN⁺ ion increases in comparable amount with pressure but in considerably greater amount with time. The same observations hold for the perdeuterio compound.

The results are less satisfactory for the reaction



At the lower pressures (below about 30 μ) the decay of CH₂CN⁺ and the increase of C₂H₄CN⁺ are approximately equal. At higher pressures or longer times (at 30 μ) the decay of CH₂CN⁺ becomes considerably greater than the increase in C₂H₄CN⁺. It thus appears that CH₂CN⁺ is enhanced by some ion-molecule reac-

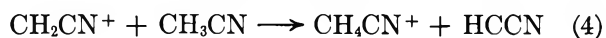
Table III: Secondary Ions

Acetonitrile (50 μ)			Propionitrile (40 μ)		
<i>m/e</i>	Composition	% of total ion current	<i>m/e</i>	Composition	% of total ion current
42	CH ₄ CN ⁺	30.8	29	C ₂ H ₅ ⁺	3.9
51	HC ₂ CN ⁺	<0.1	30	C ₂ H ₆ ⁺	3.0
52	C ₂ H ₂ CN ⁺	0.5	41	CH ₃ CN ⁺	1.1
53	C ₂ H ₃ CN ⁺	0.8	42	CH ₄ CN ⁺	2.0
54	C ₂ H ₄ CN ⁺	3.4	56	C ₂ H ₆ CN ⁺	25.5
64	C ₃ N ₂ ⁺	<0.1	65	C ₃ H ₃ CN ⁺	<0.1
65	HC(CN) ₂ ⁺	<0.1	66	C ₃ H ₄ CN ⁺	<0.1
66	H ₂ C(CN) ₂ ⁺	<0.1	67	CH ₃ (CN) ₂ ⁺	<0.1
67	CH ₃ (CN) ₂ ⁺	<0.1	68	C ₃ H ₆ CN ⁺	<0.1
79	C ₂ H ₃ (CN) ₂ ⁺	0.2	70	C ₃ H ₈ CN ⁺	0.2
81	C ₂ H ₅ (CN) ₂ ⁺	0.1	78	C ₄ H ₄ CN ⁺	<0.1
83	H(CH ₃ CN) ₂ ⁺	0.2	79	C ₄ H ₆ CN ⁺	<0.1
			80	C ₄ H ₈ CN ⁺	0.2
			81	C ₄ H ₇ CN ⁺	<0.1
			82	C ₄ H ₉ CN ⁺	<0.1
			83	C ₄ H ₉ CN ⁺	<0.1
			94	C ₅ H ₈ CN ⁺	<0.1
			111	H(C ₂ H ₅ CN) ₂ ⁺	0.2

tion during the early stages of reaction, but as the precursor becomes depleted the depletion of CH₂CN⁺ becomes apparent in a greatly increased rate of disappearance. We think that a portion of the CH₂CN⁺ must go to form CH₄CN⁺ which, as was mentioned above, is formed at a considerably greater rate than that at which CH₃CN⁺ disappears. These considerations apply to both the protium and deuterium compounds.

For a pseudo-first-order reaction a semilogarithmic plot of ion intensity against either pressure or time will give a straight line, the slope of which will yield the rate constant. Rate constants determined in this way are given in Table V.

The decay of the principal primary ions (*m/e* 40 and 41) with pressure and time agree reasonably well, the poorest agreement being *k_p*(H₂CCN⁺). This value was computed for pressures above 30 μ where the evident enhancement of H₂CCN⁺ by reaction of some other ion was no longer important. It presumably represents the reaction of H₂CCN⁺ to form both CH₄CN⁺ and C₂H₄CN⁺ according to reactions 3 and 4. The amount



of C₂H₄CN⁺ produced is about half of the CH₂CN⁺ disappearing so the rate constants for the two processes are approximately equal. Similar behavior is observed with CD₃CN. Since CH₃CN⁺ is formed by two different processes, a rate constant for its formation would be meaningless.

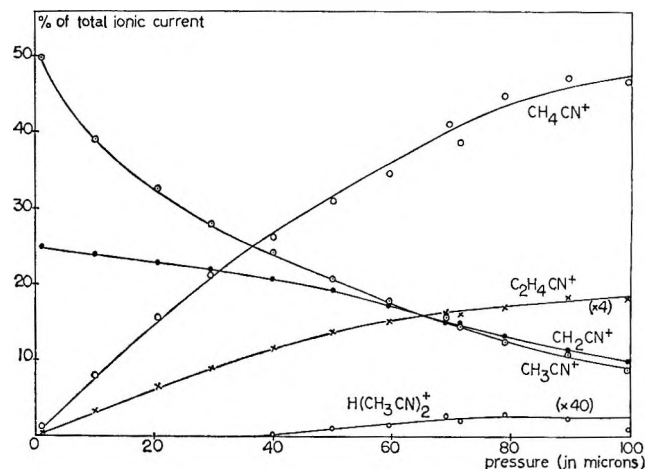


Figure 1. Effect of pressure on intensities of the principal ions of CH₃CN.

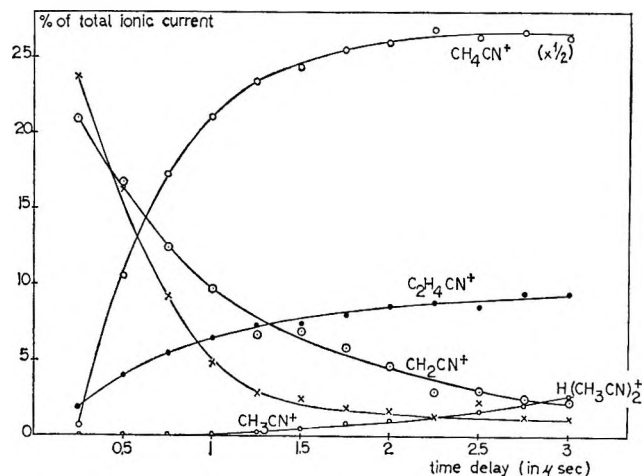


Figure 2. Effect of time on intensities of the principal ions of CH₃CN.

One ion of interest is that at mass 83 in the CH₃CN spectrum (see Table III) and the corresponding one at mass 90 in the spectrum of CD₃CN. This ion is obviously the doubly solvated proton (or deuteron). Similar multiply solvated protons have been reported for a number of other systems.^{10,11} The appearance potential of this ion is 13.35 ev and thus seems to correspond most closely to that of CH₂CN⁺. In spite of this we suspect that it comes from the CH₄CN⁺ ion which results from CH₃CN⁺ as well as CH₂CN⁺. In either case the reaction would appear to be third order. The fact that the appearance potential of H(CH₃CN)₂⁺ is between those of CH₃CN⁺ and CH₂CN⁺ is not surprising in view of its small intensity.

(10) P. F. Knewstubb and A. W. Tickner, *J. Chem. Phys.*, **36**, 674, 684 (1962).

(11) M. S. B. Munson, *J. Am. Chem. Soc.*, **87**, 2332 (1965).

Table IV: Appearance Potentials

m/e	Ion	AP, ev ^a	Reaction	ΔH_{ion}	AP, lit.
CH ₃ CN					
15.8	CH ₃ ⁺	12.29 ± 0.05	See Discussion	...	
40	CH ₂ CN ⁺	13.54 ± 0.08	CH ₃ CN → CH ₂ CN ⁺ + H + e	281	14.3 ^b
41	CH ₃ CN ⁺	12.23 ± 0.05	CH ₃ CN → CH ₃ CN ⁺ + e	303	12.39 ^b 12.52 ^c
42	CH ₄ CN ⁺	12.27 ± 0.15	CH ₃ CN ⁺ + CH ₃ CN → CH ₄ CN ⁺ + CH ₂ CN		
54	C ₂ H ₄ CN ⁺	13.59 ± 0.05	CH ₂ CN ⁺ + CH ₃ CN → C ₂ H ₄ CN ⁺ + HCN	≤ 271	
83	H(CH ₃ CN) ₂ ⁺	13.25 ± 0.08	See Discussion		
42	CD ₃ CN ⁺	12.29 ± 0.05	CD ₃ CN → CD ₃ CN ⁺ + e	304	
C ₂ H ₅ CN					
28	C ₂ H ₄ ⁺	12.40 ± 0.05	C ₂ H ₅ CN → C ₂ H ₄ ⁺ + HCN + e	271	
54	C ₂ H ₄ CN ⁺	12.55 ± 0.05	C ₂ H ₅ CN → C ₂ H ₄ CN ⁺ + H + e	254	
55	C ₂ H ₅ CN ⁺	11.70 ± 0.05	C ₂ H ₅ CN → C ₂ H ₅ CN ⁺ + e	286	11.85 ^c
56	C ₂ H ₆ CN ⁺	12.56 ± 0.05	See Discussion	≤ 206	
70	C ₃ H ₅ CN ⁺	12.00 ± 0.05	See Discussion		
80	C ₆ H ₄ CN ⁺	15.26 ± 0.25	?		
60	C ₂ D ₅ CN ⁺	11.75 ± 0.05	C ₂ D ₅ CN → C ₂ D ₅ CN ⁺ + e	287	

^a Indicated uncertainties are mean deviations from the mean, not absolute errors. ^b C. A. McDowell and J. W. Warren, *Trans. Faraday Soc.*, **48**, 1084 (1952). ^c J. D. Morrison and A. J. C. Nicholson, *J. Chem. Phys.*, **20**, 1021 (1952).

Table V: Rate Constant for the Disappearance of Various Ions in Acetonitrile (cc/molecule sec)

CH ₃ CN				CD ₃ CN			
m/e	Ion	10 ³ k _p	10 ³ k _t	m/e	Ion	10 ³ k _p	10 ³ k _t
14	CH ₂ ⁺	1.76	3.4	16	CD ₂ ⁺	1.76	
25	C ₂ H ⁺	3.64		26	{ C ₂ D ⁺ } { CN ⁺ }	4.8	8.6 ?
26	{ C ₂ H ₂ ⁺ } { CN ⁺ }	1.34	1.20	28	{ C ₂ D ₂ ⁺ } { DCN ⁺ }	1.56	3.10
27	{ HCN ⁺ } { C ₂ H ₃ ⁺ }	...	1.43	30	{ D ₂ CN ⁺ } { C ₂ D ₃ ⁺ }		1.05
38	C ₂ N	2.6	...				
39	HC ₂ N ⁺	3.0		40	DCCN ⁺	2.5	6.7 ?
40	H ₂ CCN ⁺	1.78	1.07	42	D ₂ CCN ⁺	1.15	1.08
41	H ₃ CCN ⁺	2.01	2.38	44	D ₃ CCN ⁺	2.45	1.98

It is of interest to consider some of the minor ions in the spectrum of the two acetonitriles. Some of these decrease in intensity with pressure or time and others increase somewhat. We have no means, however, of determining the products of these reactions, although in some instances we can determine the rates of disappearance of the ion. In Table V we give values for the rate of disappearance of several of these ions against both pressure and time. A difficulty that we necessarily encounter in dealing with the ions of masses 25–28 and 38–40 from CH₃CN and for masses 26–30 and 38–42 from CD₃CN is that in all probability each ion of lower mass extracts a hydrogen (or deuterium) and

thus becomes an ion of the next higher mass. This causes the ion of next higher mass to increase slightly or to decrease in intensity more slowly than it would if it were not being so enhanced. In most instances the ion of lower mass is sufficiently depleted at pressures above about 30 μ so the rate of decrease of the ion of higher mass can be observed and measured. In our studies the rate constants for variation with both pressure and time were determined at pressures above about 30 μ. Because of this competition between growth and decay, the rate constants for these processes are only approximate.

For those ions which comprise a single compound

(CH_3CN , CD_3CN , CH_2CN^+ , CD_2CN^+ , and C_2H_2^+) and are of sufficient intensity to permit good measurement, the precision of the measurement of k can be taken as $0.15\text{--}0.25 \times 10^{-9}$ cc/molecule sec. The results for the less intense ions are in general considerably less precise.

One rather important ion remains to be discussed. This is the ion whose peak centers around mass 15.8. This peak is a broad, irregularly shaped one, characteristic of an ion formed either with a wide energy spread or formed in a portion of the instrument other than the electron beam. Such a peak is thus similar to those observed in magnetic instruments as a result of either metastable transitions or collision-induced decompositions occurring in the ion gun or in the analyzer. In the present instance we are inclined to think that this ion occurs as a result of a collision-induced decomposition. The appearance potential as seen in Table IV is 12.29 eV, in close agreement with the ionization potential of CH_3CN . The peak shows a third-order pressure dependence and so presumably results not from the decomposition of a primary ion but of a secondary one. We suspect therefore, because of its large size (at 100μ it is, after mass 42, the largest peak in the spectrum), that it results from the collision of CH_4CN^+ with CH_3CN . Such a reaction would show a third-order pressure dependence and an appearance potential equal to the ionization potential of CH_3CN .

We assume that an ion of mass m_0 separates into daughter ion of mass m and a neutral during withdrawal from the source. We further assume that this decomposition occurs after the parent ion has fallen through a voltage V_1 of a total accelerating voltage V . This assumption is slightly erroneous since the total withdrawal voltage is applied in two stages, but this introduces little error in the calculations. The energy of the daughter ion at the time of its formation is $(m/m_0)eV_1$ and after complete acceleration is

$$KE_d = \frac{m}{m_0}eV_1 + e(V - V_1) = \frac{1}{2}mv^2 \quad (5)$$

The flight time for the daughter ion is

$$t = \frac{L}{v} = \frac{L}{\left[\frac{2e}{m} \left(\frac{m}{m_0} V_1 + V - V_1 \right) \right]^{1/2}} \quad (6)$$

where L is the length of the flight tube.

An ion of apparent mass m^* would have an energy

$$eV = \frac{1}{2}m^*v^2 \quad (7)$$

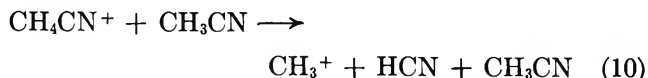
and would require an apparent time

$$t = \frac{L}{\left(\frac{2eV}{m^*} \right)^{1/2}} \quad (8)$$

Equating times from (6) and (8) and simplifying

$$m^* = \frac{m}{1 + \frac{V_1}{V} \left(\frac{m}{m_0} - 1 \right)} \quad (9)$$

It will be evident from this equation that decomposition occurring before acceleration will give the daughter ion and that decomposition occurring after complete acceleration will appear as the parent ion. Decompositions occurring during acceleration will yield an apparent ion mass between that of the daughter and the parent. One would expect such decompositions to occur during acceleration in the ion source, where the pressure is highest. The width of the peak corresponds to about 300 v, thus supporting the view that decomposition occurs in the source. Further, since the greater part of the time during acceleration is in the early stages, one would expect V/V_1 to be small (probably 0.1) with the result that the apparent mass should be only slightly greater than that of the daughter ion. With these considerations it would appear that the ion at mass 15.8 is probably due to the ion at mass 15 formed by collision during acceleration. We thus consider the probable reaction to be

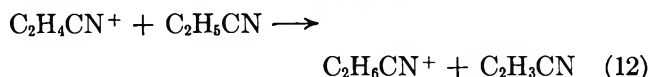
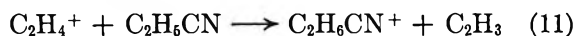


The peak at about m/e 18.6–19.3 from CD_3CN appears to be formed in the same way. No doubt similar considerations would apply to the small peak at mass 14.8, but the intensity of this peak was too small to permit satisfactory study. Similar peaks were observed in propionitrile but were too small to study quantitatively.

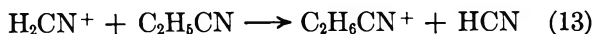
Propionitrile. High resolution was used to identify all the ions in the primary mass spectrum of $\text{C}_2\text{H}_5\text{CN}$. The spectrum showed that over 90% of the ionic current at m/e 27 is due to C_2H_3^+ . There is very little HCN^+ from $\text{C}_2\text{H}_5\text{CN}$, in contrast to CH_3CN . Similarly, the ion at m/e 26 is almost entirely C_2H_2^+ . The major ion in propionitrile is at m/e 28 which is due to the doublet $\text{C}_2\text{H}_4^+ - \text{H}_2\text{CN}^+$ in the ratio of intensities 4/1. Ions observed in the mass range 38–41 are of minor intensity, and mass shifts of these peaks in the mass spectrum of $\text{C}_2\text{D}_5\text{CN}$ indicate that the major part of these ions contains the CN group. The group 38–41 is therefore principally CCN^+ , CHCN^+ , ..., CH_3CN^+ rather than C_3H_2^+ , ..., C_3H_5^+ .

The spectrum of C_2H_5CN at high pressure is much more complicated than that of CH_3CN . A number of collision-induced secondary ions are observed between 10 and 100 μ of pressure. The assignment of formulas of all secondary ions was made by measurement of the mass number shifts in C_2D_6CN and the comparison of the relative intensities of the corresponding ions in C_2H_5CN and C_2D_6CN . As with CH_3CN , it turns out that each secondary ion has a unique formula and that all but one retain nitrogen. The secondary ions are listed in Table III. Figures 3 and 4 show the behavior of the principal ions with changes in pressure and time.

The appearance potentials of the principal primary and secondary ions in propionitrile are listed in Table IV. The two most intense ions in the primary spectrum ($C_2H_4^+$ and $C_2H_4CN^+$), unfortunately, have almost identical appearance potentials, and thus it is very difficult to identify the precursor of the principal secondary ions. By far the most intense secondary ion in the spectrum of propionitrile is $C_2H_6CN^+$ (or $C_2D_6CN^+$). The appearance potential of this ion is quite close to those of m/e 28 ($C_2H_4^+ + H_2CN^+$) and m/e 54 ($C_2H_4CN^+$), and its intensity is approximately equal at each pressure to the reduction in the intensities of m/e 28 plus $C_2H_4CN^+$ (Table VI). Thus it is probable that $C_2H_6CN^+$ is derived from both of these principal primaries by the reactions



Since about 20% of the peak at m/e in the undeuterated compound is H_2CN^+ , it is probable that this also transfers a proton (or deuteron) to the parent compound; thus



Comparisons, similar to that against pressure in Table

Table VI: Comparison of Intensity of $C_2H_6CN^+$ with Reduction of Intensities of Precursors

Pressure, μ	C_2H_5CN		C_2D_5CN	
	$I(56)$	$-\Delta I(28)$ $+ 54$	$I(62)$	$-\Delta I(32)$ $+ 58$
10	10	10	6.5	4
20	17	16	14.5	12
30	21.6	17.5	19	18
40	23.8	20.5	21.7	20.5
50	23.7	21	24.2	24
60	28	26.5	27.6	26.5
80	38 (?)	33	31	31
90	28.6	32	32	31

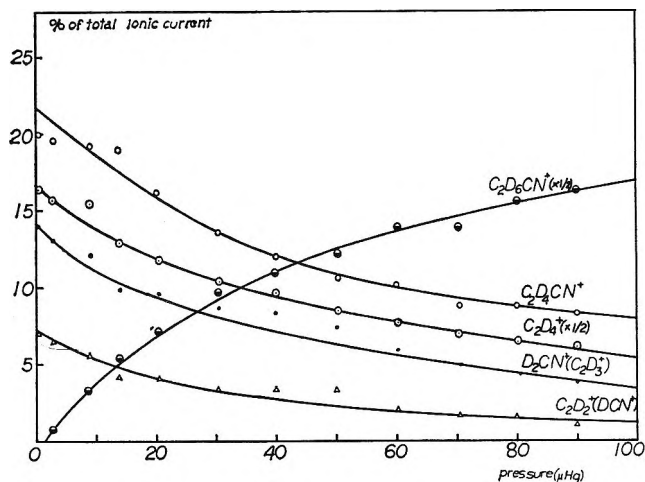


Figure 3. Effect of pressure on intensities of the principal ions of C_2D_5CN .

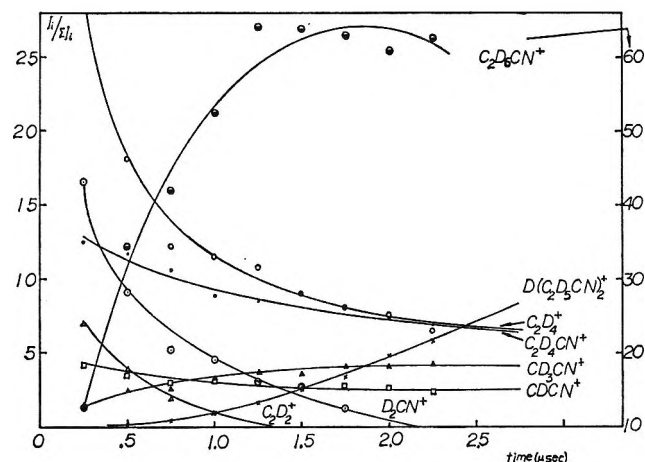


Figure 4. Effect of time on intensities of the principal ions of C_2D_5CN .

VI, when made against time, show the $C_2H_6CN^+$ and $C_2D_6CN^+$ ions to increase somewhat faster than the assumed precursors decay. Presumably some other ions also react to produce $C_2H_6CN^+$ and $C_2D_6CN^+$, but we have no way of knowing what they are.

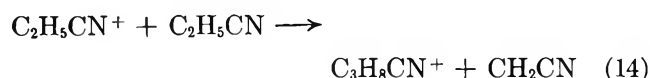
The parent ion is a relatively minor component of the mass spectrum of propionitrile. Further, the intensity of the parent ion shows very little change with either pressure or time. While it is possible that this constancy in intensity results from a balance of the rates of formation and loss of the parent ion, the shapes of the curves are not consistent with such a mechanism. Thus it seems that the ion is simply not very reactive. Apparently it does not contribute to the formation of $C_2H_6CN^+$ since the ionization potential is about 0.7 v less than the appearance potential of $C_2H_6CN^+$. This

Table VII: Rate Constants for the Decay of Various Primary Ions from Propionitrile (cc/molecule sec)

C_2H_5CN				C_2D_5CN			
m/e	Ion	10^3k_p	10^3k_t	m/e	Ion	10^3k_p	10^3k_t
14	CH_2^+	3.12		18	CD_3^+	2.4	2.3
15	CH_3^+	2.2	2.9	28	$C_2D_2^{+b}$	2.5	2.9
26	$C_2H_2^{+a}$	2.7	2.2	30	$C_2D_3^+$ (78%)	1.2	2.3
27	$C_2H_3^{+c}$	0.7	1.6	30	D_2CN^+ (22%)	8.2	...
28	H_2CN^+ (33%)	14.4		32	$C_2D_4^+$	1.5	2.0
28	$C_2H_4^+$ (67%)	0.5	1.76				
38	C_2N^+	2.1	2.0				
40	H_2CCN^+	0.9	1.0				
51	HC_2CN^+	3.7					
52	$H_2C_2CN^+$	1.9					
54	$C_2H_4CN^+$	1.2	0.6	58	C_2D_4CN	1.7	0.5

^a Trace of CN. ^b Trace DCN. ^c Trace HCN.

is surprising since HCN^+ and CH_3CN^+ undergo such reactions. The $M + 15$ ion ($C_3H_8CN^+$) exhibits an appearance potential very close to that of the parent ion so $C_3H_8CN^+$ is probably formed according to the reaction



However, this ion is observed in only very weak intensities and would not reduce the intensity of the parent ion significantly at the conditions of these studies.

From the above it appears that there is no important collision reaction involving the parent ion. This disagrees with the conclusions of Martin and Melton^{2a} that the H self-abstraction is important in all alkylcyanides.

An ion of very small intensity is observed at m/e 111 in C_2H_5CN . This is presumably $H^+(C_2H_5CN)_2$, the doubly solvated proton. Its intensity was much too low to study, however, except at high pressures and long time delay where it is very difficult to obtain definite identification of the precursor. From the shape of the curves at 30μ and time delays up to 2.5μ sec, it appears that $C_2H_6CN^+$ is the precursor to $H(C_2H_5CN)_2^+$ as would seem reasonable.

The determination of rate constants for collision reactions in propionitrile is complicated by the fact that the principal secondary ion arises from two or more primaries with the further difficulty that the most abundant primary (m/e 28) is about 75% $C_2H_4^+$ and 25% H_2CN^+ , both of which are presumably reactive. A semilog plot of the intensity of the ion of m/e 28 against pressure drops rapidly at the lower pressures, then about 30μ becomes a straight line of considerably reduced slope. This behavior is characteristic of a system of two apparently identical compounds react-

ing at different rates. It may be presumed that the most reactive component has disappeared at the higher pressures, in this case above about 30μ . The linear, high-pressure portion of the curve will yield the rate constant of the slow reaction, and extrapolation to zero pressure gives the (approximate) initial intensity of this slow component. A plot of the difference between the total m/e 28 curve and the extrapolated curve for the slow reaction yields the curve for the disappearance of the faster component from which the rate constant and initial intensity are readily obtained. This treatment is unfortunately not very precise but usually serves to give approximate values. In this way the rates of disappearance and relative abundances of $C_2H_4^+$ and H_2CN^+ and of $C_2D_3^+$ and D_2CN^+ shown along with other data in Table VII were computed. The results, while not so satisfactory as one might wish, are at least in approximate agreement.

For those ions, such as CH_3^+ and $C_2H_2^+$, which definitely comprise only a single molecular species agreement among the k_p and k_t for both the hydrogen and deuterium compounds are in reasonable agreement. They are also of a magnitude expected for reactions with highly polar molecules.² For the m/e 28 ions from C_2H_5CN (H_2CN^+ and $C_2H_4^+$) and for the m/e 30 ions from C_2D_5CN ($C_2D_3^+$ and D_2CN^+) for which the rates of reaction of the individual components had to be determined by difference as discussed above, the results are less satisfactory. This treatment appears to give values that are somewhat too low for the slow reaction and too fast for the fast reaction. We can offer no explanation for this other than the usual one that values obtained by difference are often not very precise. One other discrepancy is not readily explained. This is the large difference between k_p and k_t for $C_2H_4CN^+$ and $C_2D_4CN^+$ although the two k_p and k_t values agree reasonably well.

Rate constants for the disappearance of several minor ions have been determined in the manner discussed for acetonitrile (Table VII). The secondary ions $C_2H_5^+$ and $C_2H_6^+$ are formed in moderate abundance. From the shapes of the curves of intensity against pressure and time, it appears that these ions probably are formed from $C_2H_2^+$ and $C_2H_3^+$. The nonendoergic limitation makes it probable that C_2H_2 is the precursor of $C_2H_6^+$ and $C_2H_3^+$ of C_2H_5 .

The $(M + 1)^+$ Ion in Acetonitrile. Several investigators¹²⁻¹⁶ have reported anomalously large intensities of $(M + 1)^+$ ions at quite low (10^{-6} mm) pressures. Further, with some compounds a plot of $(M + 1)^+/M^+$ shows a definite maximum near the onset of ionization. We have observed similar behavior with plots of CH_4CN^+/CH_3CN^+ and CD_4CN^+/CD_3CN^+ against electron energy. Examination of the ionization efficiency curves for $(M + 1)^+$ and M^+ shows that the former did not go to zero intensity but leveled out 1 or 2 above onset,

while the curve for M^+ continued decreasing to zero intensity. We have tentatively concluded that this is an experimental artifact probably attributable to the Cermak¹⁷ effect.

Acknowledgments. The authors wish to express their gratitude to the Robert A. Welch Foundation for support of this research. P. N. is indebted to the Belgian "Fonds National de la Recherche Scientifique."

-
- (12) F. W. McLafferty, *Anal. Chem.*, **34**, 26 (1962).
(13) R. Wertzler and J. F. Kinder, Consolidated Electrodynamics Corp., Pasadena, Calif., Group Rept. 54, July 1948.
(14) R. Beugelmans, D. H. Williams, H. Budzikiewicz, and C. Djerassi, *J. Am. Chem. Soc.*, **86**, 1386 (1964).
(15) J. H. Beynon, "Mass Spectrometry and Its Applications to Organic Chemistry," Elsevier Publishing Co., Amsterdam, 1960.
(16) J. H. Beynon, G. R. Lester, R. A. Saunders, and A. E. Williams, *Trans. Faraday Soc.*, **57**, 1259 (1961).
(17) V. Cermak and Z. Herman, *Nucleonics*, **19**, 106 (1961).

The Radiation-Induced Isomerization of Stilbene in Benzene and Cyclohexane

by Robert R. Hentz, D. B. Peterson, S. B. Srivastava,
Helmut F. Barzynski, and Milton Burton

Department of Chemistry and the Radiation Laboratory,¹ University of Notre Dame, Notre Dame, Indiana 46556
(Received February 9, 1966)

The γ -radiation-induced isomerizations of *cis*- and *trans*-stilbene were studied in cyclohexane, benzene, and the mixed solvents. In cyclohexane at low stilbene concentrations ($<0.01 M$), the ratio $G_{c \rightarrow t}/G_{t \rightarrow c}$ approximates the corresponding quantum yield ratio (~ 0.85) obtained in photochemical studies. With an increase in stilbene concentration beyond $0.01 M$, $G_{c \rightarrow t}$ continues to increase as $G_{t \rightarrow c}$ approaches a limiting value of ~ 1.4 . In benzene solutions, the ratio $G_{c \rightarrow t}/G_{t \rightarrow c}$ approximates the quantum yield ratio up to $0.1 M$ stilbene, beyond which concentration $G_{t \rightarrow c}$ approaches a limiting value of ~ 2.9 as $G_{c \rightarrow t}$ continues to increase. Effects of various additives were examined. In the mixed solvent systems, the isomerization yield of $10^{-2} M$ *trans*-stilbene increases with benzene concentration in a manner related to suppression of $G(H_2)$ by benzene in cyclohexane-benzene mixtures. A proposed mechanism of isomerization suggests that the isomerization of *cis*-stilbene at low concentrations and of *trans*-stilbene at all concentrations occurs *via* triplet states of stilbene. At higher *cis*-stilbene concentrations, direct ionic chain isomerization occurs by charge transfer between "free" stilbene ions and stilbene molecules. At low stilbene concentrations ($<0.05 M$) in benzene, isomerization proceeds largely *via* transfer from benzene triplet states. At higher stilbene concentrations in benzene (as always in cyclohexane), the triplet state of stilbene is formed directly by neutralization of stilbene ions. According to the proposed mechanism, in cyclohexane, $G(\text{ion pairs}) \approx 2.6$ and the ionic chain length is 14 at $0.2 M$ *cis*-stilbene. In benzene, $G(\text{triplets}) = 5.4$ and the ionic chain length is 31 at $1.8 M$ *cis*-stilbene. The ratio $k(e^- + \text{stilbene})/k(e^- + \text{benzene}) = 70$. The decay time of triplet benzene produced by high-energy irradiation of the pure liquid is $<10^{-8}$ sec.

Introduction

Study of photoinduced *cis-trans* isomerization has helped to elucidate various features of the triplet state and of the processes in which it is involved or formed. Also, it has yielded ideas concerning the configuration of the potential-energy surface along the isomerization coordinate.² Photosensitization experiments² and studies involving intersystem crossing from the directly excited singlet state have provided information on kinetics and energetics of formation of triplet states in a number of cases.^{3,4} Although the most thoroughly studied *cis-trans* isomerization is that of stilbene, there are still a number of unresolved problems in that case.²⁻⁴ Nevertheless, the amount of already well-established information and certain other advantages make the stilbene isomerization process itself, when combined with other observations, a potentially useful

tool. This paper describes how it has been employed for exploration of other processes and for identification and estimation of yields of a variety of transient intermediates (ions, triplet states, and singlet states) presumably involved in the radiolysis of organic liquids.⁵

(1) The Radiation Laboratory of the University of Notre Dame is operated under contract with the U. S. Atomic Energy Commission. This is A.E.C. Document No. COO-38-445.

(2) G. S. Hammond, J. Saltiel, A. A. Lamola, N. J. Turro, J. S. Bradshaw, D. O. Cowan, R. C. Counsell, V. Vogt, and C. Dalton, *J. Am. Chem. Soc.*, **86**, 3197 (1964).

(3) S. Malkin and E. Fischer, *J. Phys. Chem.*, **68**, 1153 (1964).

(4) R. H. Dyck and D. S. McClure, *J. Chem. Phys.*, **36**, 2326 (1962).

(5) Cf. R. B. Cundall and P. A. Griffiths (a) *Discussions Faraday Soc.*, **36**, 111 (1963); (b) *J. Phys. Chem.*, **69**, 1866 (1965), who have reported the use of butene-2 isomerization for such a purpose; (c) J. Nosworthy, *Trans. Faraday Soc.*, **61**, 1138 (1965), who has examined the radiation-induced isomerization of dimethyl fumarate; and (d) H. P. Lehmann, G. Stein, and E. Fischer, *Chem. Commun.*,

Experimental Section

Materials. Baker Analar grade and Fisher (crystallizable) benzene were used. The benzene was purified by distillation with a Nester-Faust spinning-band column and by three successive crystallizations with rejection of about one-fourth of the benzene at each freezing. No impurities were detectable by vapor phase chromatography with a flame ionization detector. Fisher Spectrograde cyclohexane was purified by several partial freezings and passage through a silica gel column. After a final distillation, no unsaturated impurities were detectable by either ultraviolet spectrophotometry or vapor phase chromatography. Fisher Spectrograde carbon tetrachloride was used without further purification. Pyridine and piperidine were purified by distillation over sodium hydroxide. The 2,5-diphenyloxazole (PPO) was used as received from the Pilot Chemical Co. Very high grade azulene (obtained through the courtesy of Professor G. O. Schenck) also was used without further purification.

In some experiments, scintillation grade *trans*-stilbene (mp 124–125°) supplied by Matheson Coleman and Bell (MCB) was used without further purification; vapor phase chromatography indicated 0.25% *cis* impurity. *cis*-Stilbene (bp 144–145° (13 mm)) as supplied by MCB contained about 1% *trans* impurity that was reduced to about 0.35% by purification on a Wilkens Autoprep 700 using a 3/8-in. × 10-ft Apiezon L column at 200°. In later experiments, K and K stilbenes were used. Such *trans*-stilbene was recrystallized in cyclohexane three times. The only impurity detectable by vapor phase chromatography was <0.01% *cis*-stilbene. The *cis*-stilbene was purified by several vacuum distillations in which the middle fraction was collected each time. The only detectable impurity was <0.1% *trans*-stilbene.

Preparation and Irradiation of Samples. Solutions were deaerated by conventional freeze-pump-thaw techniques and sealed off under vacuum. They were irradiated in the Notre Dame 10-kcurie ⁶⁰Co facility at dose rates between 2×10^{19} and 2×10^{21} ev l.⁻¹ min⁻¹. Unless otherwise specified, samples were irradiated at a dose rate of about 1.5×10^{21} ev l.⁻¹ min⁻¹. Dose rates were determined by Fricke dosimetry using $G(\text{Fe}^{3+}) = 15.6$.

Product Analysis. The stilbenes were determined by vapor phase chromatography using an F and M Model 609 gas chromatograph equipped with a flame ionization detector. A 1/4-in. × 10-ft column packed with silicone grease on 60–80 mesh Chromosorb P gave excellent resolution of the two isomers of stilbene at 200°. A study of the effect of injection-port temperature on the analysis of stilbenes showed that, up to about 220°,

thermal isomerization during analysis is insignificant. At higher injection-port temperatures thermal isomerization was observed. All results reported were obtained at an injection-port temperature of 200°. Dibenzyl and *cis*-stilbene could not be resolved by the gas chromatographic method alone. In two experiments, the stilbene isomer produced was determined and isolated by gas chromatography; the collected stilbene then was dissolved in cyclohexane and determined spectrophotometrically by its absorption at 2900 Å. Excellent agreement was obtained between the spectrophotometric and vapor phase chromatographic analyses. No significant amount of dibenzyl could be detected.

Cyclohexene analysis was performed on a 1/4-in. × 10-ft column packed with β,β' -oxydipropionitrile on 60–80 mesh Chromosorb P operated at 50°. Bicyclohexyl was determined on a 1/4-in. × 10-ft column packed with polyester diethylene glycol on 60–80 mesh Chromosorb P operated at 150°.

Luminescence Measurements. The apparatus and procedure used in studies of the radiation-induced luminescence of PPO have been described.⁶ Solutions were deaerated by nitrogen bubbling.⁷

Results

Cyclohexane Solutions. Among other effects, γ irradiation of solutions of stilbene in cyclohexane causes isomerization. Figure 1 shows yields of isomerization of both isomers as a function of solute concentration; a number of points represent averages of several measurements. Occurrence of other processes involving the solute is evident in the data of Table I (which also includes data for solutions in which benzene is solvent) and, in Figure 2, in the variation, with stilbene concentration, of product yields characteristic of cyclohexane radiolysis. Production of bicyclohexyl might seem to imply production of atomic H as an intermediate. However, it is noteworthy that dibenzyl, which might be expected to appear as an ultimate product from the addition of thermal hydrogen atoms to stilbene (*via* disproportionation perhaps), is not produced in significant yield.

Isomerization yields in cyclohexane solutions (except in the prolonged irradiations reported in Table I) were measured at doses corresponding to less than 10% total conversion of the initial isomer of stilbene, except

583 (1965), who have studied the radiation-induced isomerization of stilbene at $<10^{-3} M$ in benzene.

(6) M. Burton, P. J. Berry, and S. Lipsky, *J. Chim. Phys.*, **52**, 657 (1955).

(7) M. Burton, M. A. Dillon, C. R. Mullin, and R. Rein, *J. Chem. Phys.*, **41**, 2236 (1964).

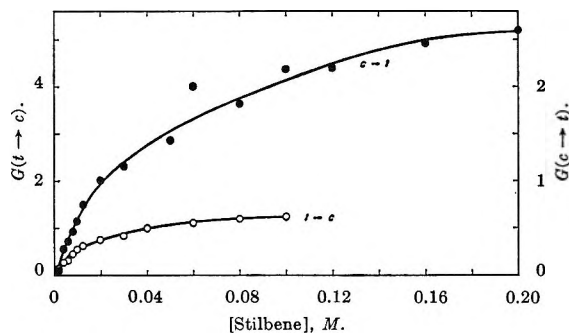
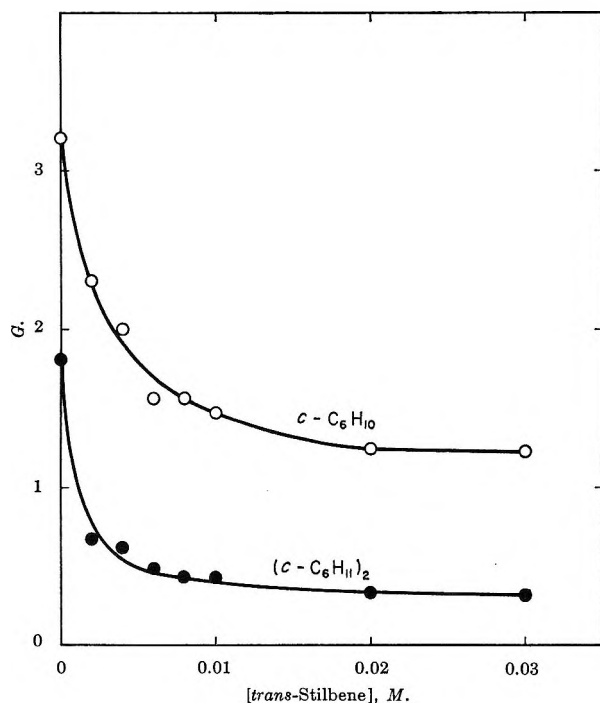


Figure 1. Isomerization of stilbene in cyclohexane.

Figure 2. Yields in cyclohexane solutions of *trans*-stilbene: O, cyclohexane; ●, bicyclohexyl.**Table I:** Effects of Extensive γ Irradiation on Isomerization and Other Changes of *cis*- and *trans*-Stilbenes in Cyclohexane and Benzene Solutions^a

[Stilbene], mole/l.	G_{iso}^b	G_{con}^c
2.3×10^{-3} (<i>cis</i> , C ₆ H ₁₂) ^d	0.05	0.41
0.65×10^{-3} (<i>trans</i> , C ₆ H ₁₂)	0.07	0.37
2.1×10^{-3} (<i>cis</i> , C ₆ H ₆)	0.41	0.25 ^e
2.8×10^{-3} (<i>trans</i> , C ₆ H ₆)	0.52	0.64

^a Dose = 1.2×10^{20} ev/g. ^b Isomerization yield. ^c The yield of consumption of initial isomer (includes the isomerization yield). ^d Symbols in parentheses denote isomer and solvent, respectively. ^e This number cannot be correct; it shows merely that within limits of measurement the four G values given for benzene solution are the same.

for the lowest initial concentrations where conversions may have been as high as 15%. Measurements at different doses for a number of concentrations indicated no significant effect of dose on isomerization yields at these conversions. $G(\text{isomerization})$ is independent of dose rate over the range 2×10^{19} to 2×10^{21} ev l.⁻¹ min⁻¹.

Table II shows the profound effect of carbon tetrachloride on the γ -induced isomerization yield in cyclohexane; by contrast, even 4 vol. % CCl₄ in cyclohexane showed no effect on the isomerization yield in

Table II: Effect of CCl₄ on γ -Induced Isomerization of *trans*-Stilbene in Cyclohexane

[CCl ₄], mole/l.	[<i>trans</i> -C ₁₄ H ₁₂], mole/l.		
	0.002	0.02	0.1
0	0.15	0.75	1.28
2.1×10^{-3}	0.08	0.56	...
2.1×10^{-2}	0.01	0.23	0.77
1.0×10^{-1}	0.0	0.13	0.59
2.1×10^{-1}	0.0	0.12	...
3.1×10^{-1}	0.0	0.07	...
4.2×10^{-1}	0.0	0.04	0.35
10.4 ^a	0.0	0.04	0.28

^a Pure CCl₄.

direct 2537-A excitation of 10^{-2} M stilbene. The γ -induced isomerization yield in cyclohexane is also suppressed by piperidine and pyridine; 0.1 M piperidine reduces $G_{t \rightarrow c}$ of 10^{-2} M *trans*-stilbene by 75% and 0.12 M pyridine by 70%. By contrast, Table III shows that addition of diphenyloxazole (PPO) increases the γ -induced isomerization yield significantly. On the other hand, according to Table IV, stilbene has but a small effect in the γ -induced luminescence of PPO.

Benzene Solutions. Figure 3 shows isomerization yields in benzene solutions as a function of stilbene concentration; a number of points represent averages of several measurements. Except for the experiments reported in Table I, most measurements were at doses corresponding to less than 1% conversion of stilbene. However, for the lowest concentrations, conversions may have reached 5–10%. Yields were independent of dose up to at least 2.5×10^{22} ev l.⁻¹ at 10^{-3} M stilbene and up to at least 3.2×10^{22} ev l.⁻¹ for stilbene concentrations greater than 10^{-2} M. Dose rate had no measurable effect on $G(\text{isomerization})$ over the range 2×10^{19} to 2×10^{21} ev l.⁻¹ min⁻¹. Table I shows that, within experimental error, the total concentration of stilbene isomers in benzene solutions re-

Table III: Effect of Various Solutes on the γ -Induced Isomerization of $4 \times 10^{-3} M$ *trans*-Stilbene in Benzene or Cyclohexane

Solution	[Solute], mole/l.	$G_{t \rightarrow c}$
Benzene	0	0.97
+ Azulene	2×10^{-3}	0.65
+ Azulene	4×10^{-3}	0.46
+ Azulene	8×10^{-3}	0.27
+ PPO ^a	4×10^{-3}	0.96
+ PPO ^a	2×10^{-2}	1.39
+ PPO ^a	1×10^{-1}	1.76
Cyclohexane	0	0.28
+ PPO	4×10^{-3}	0.54
+ PPO	2×10^{-2}	0.68
+ PPO	1×10^{-1}	1.11

^a Diphenyloxazole.

Table IV: Effect of *trans*-Stilbene on the Luminescence of Diphenyloxazole Solutions in Benzene or Cyclohexane

[<i>trans</i> -C ₁₆ H ₁₂], mole/l.	[PPO], mole/l.	I^a
Benzene		
4×10^{-3}	0	19
0	4×10^{-3}	101
4×10^{-3}	4×10^{-3}	80
0	4×10^{-2}	122
4×10^{-3}	4×10^{-2}	131
Cyclohexane		
4×10^{-3}	0	13
0	4×10^{-3}	40
4×10^{-3}	4×10^{-3}	37
0	4×10^{-2}	66
4×10^{-3}	4×10^{-2}	73

^a Relative luminescence intensity.

mained substantially unchanged during irradiation, in contrast to the effect in cyclohexane solutions.

The effect of various additives on the γ -induced isomerization of stilbene in benzene solution is shown in Figure 4 and Table III. Table IV shows the effect of stilbene on γ -induced PPO luminescence in benzene solution. It appears, just as in the cyclohexane solutions, that stilbene has only a small effect on the luminescence of PPO itself.

Solutions in Mixtures of Benzene and Cyclohexane. Table V, the middle column, shows how γ -induced isomerization of $10^{-2} M$ *trans*-stilbene increases with benzene concentration in mixtures of benzene and cyclohexane. The third column is discussed in another section.

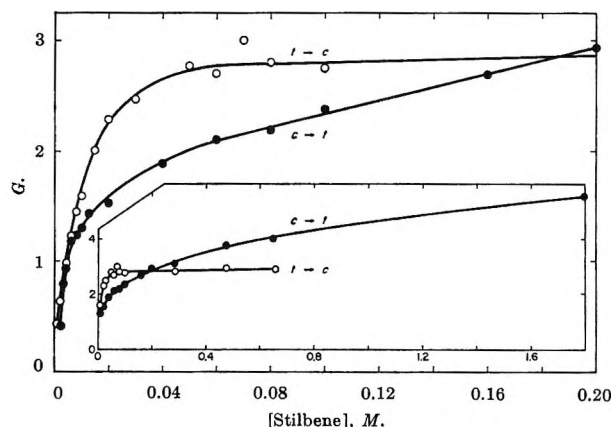


Figure 3. Isomerization of stilbene in benzene.

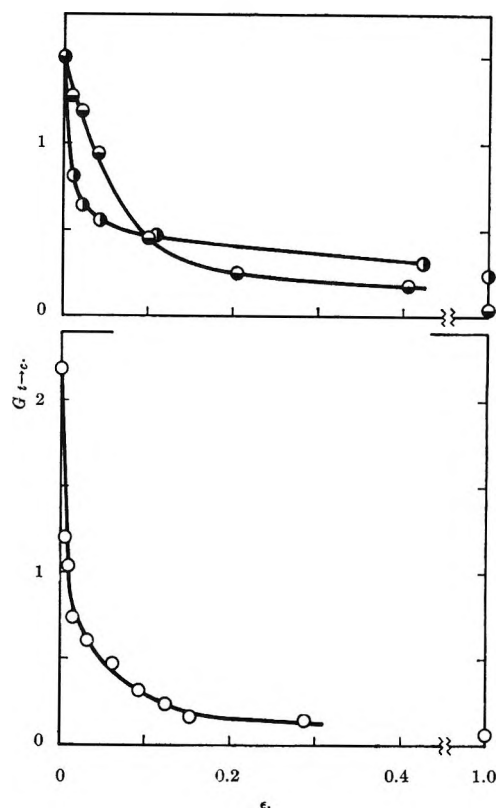


Figure 4. Effect of additives on the isomerization of *trans*-stilbene in benzene: \circ , carbon tetrachloride (for $\epsilon \leq 0.153$, $M \approx 6.7\epsilon$), [*trans*-stilbene] = $0.02 M$; \bullet , pyridine ($M \approx 12\epsilon$), [*trans*-stilbene] = $0.01 M$; \ominus , piperidine ($M \approx 10\epsilon$), [*trans*-stilbene] = $0.01 M$. (ϵ represents the electron fraction.)

Discussion

Cyclohexane Solutions. The over-all pattern of the data for the radiation-induced isomerization of stilbene in cyclohexane is consistent with the postulate that ionic species of the solvent play the major role in the sensitization process.

Table V: Isomerization of $10^{-2} M$ *trans*-Stilbene in Benzene-Cyclohexane Mixtures

Vol. % C ₆ H ₆	$G_{t \rightarrow c}$	$G_{t \rightarrow c}$ (calcd) ^a
0	0.53	0.53
10	0.94	1.04
20	1.25	1.27
30	1.34	1.40
40	1.50	1.49
50	1.50	1.55
100	1.69	1.69

^a Column 3 is explained in the Discussion in the section entitled, "Processes and Mechanistic Details; Mixed Solvents." The reference is to a calculation from eq VI.

For the benzophenone-sensitized isomerization of stilbene (presumably sensitized by the benzophenone triplet state), Hammond and collaborators² report for the quantum yield ratio $\phi_{c \rightarrow t}/\phi_{t \rightarrow c}$ values of about 0.8 and 0.9 at 0.001 and 0.05 *M* stilbene in benzene, respectively. For the direct photoisomerization in methylcyclohexane-isohexane solutions, Malkin and Fischer³ obtained a value for the same ratio of ~ 0.7 . From a comparison of these values with the values of $G_{c \rightarrow t}/G_{t \rightarrow c}$ in Table VI for cyclohexane solutions, certain general conclusions may be stated regarding the radiation-induced isomerization in cyclohexane. (1) Some sensitization process that proceeds *via* a state of stilbene other than its lowest singlet or triplet state must be involved. (2) This process favors formation of the more stable (by 6 kcal/mole⁸) *trans*-stilbene and may be governed by essentially thermodynamic considerations. (3) This process increases in importance with increase in stilbene concentration

Table VI: Comparison of Isomerization Yield Ratios in Benzene and in Cyclohexane

[Stilbene], mole/l.	$G_{c \rightarrow t}/G_{t \rightarrow c}$	
	C ₆ H ₆	C ₆ H ₁₂
4×10^{-3}	0.97	1.00
6×10^{-3}	0.96	1.16
8×10^{-3}	0.85	1.04
1×10^{-2}	0.78	1.02
1.23×10^{-2}	0.93	1.23
2×10^{-2}	0.67	1.31
3×10^{-2}	...	1.39
6×10^{-2}	0.78	1.82
8×10^{-2}	0.75	1.52
1×10^{-1}	0.87	1.76
2.9×10^{-1}	1.11	...
4.8×10^{-1}	1.27	...
6.6×10^{-1}	1.38	...

and becomes particularly significant at concentrations $\sim 0.01 M$.

Because the free-radical yield in radiolysis of cyclohexane appears to be relatively high,^{9,10} it is necessary to assess the possible role of free radicals formed therefrom in the sensitized isomerization. The data of Table I show an appreciable disappearance of stilbene in cyclohexane that may be attributable to reaction with free radicals or atoms. The behavior of yields of bicyclohexyl and cyclohexene as a function of stilbene concentration (*cf.* Figure 2) parallels that attributed by others to scavenging of cyclohexyl radicals.^{11,12}

Even though free-radical scavenging by stilbene may occur, this process cannot be properly connected with the isomerization process. First, it is not reasonable to invoke a "catalytic" function of strongly bonded cyclohexyl radicals and hydrogen atoms analogous to that of weakly bonded I,¹³ Br,¹⁴ or C₆H₅S.¹⁵ Second, with the 6 kcal/mole greater stability of *trans*-stilbene, free-radical sensitization should give a very large $G_{c \rightarrow t}/G_{t \rightarrow c}$. On the contrary, this ratio does not rise appreciably above unity until a concentration of stilbene is reached at which suppression of cyclohexene and bicyclohexyl yields is essentially complete. This second argument likewise negates the possibility of an isomerization process sensitized by hydrogen atom addition to stilbene and subsequent disproportionation with another free radical. Also, results of several independent studies¹⁶⁻¹⁸ indicate a yield of thermal hydrogen atoms ($G < 0.5$) in the radiolysis of cyclohexane insufficient to account for the isomerization yields in terms of such a disproportionation mechanism. The absence of detectable dibenzyl likewise argues against that mechanism. The conclusion is that free radicals

(8) R. B. Williams, *J. Am. Chem. Soc.*, **64**, 1395 (1942).

(9) E. N. Weber, P. L. Forsyth, and R. H. Schuler, *Radiation Res.*, **3**, 68 (1955), have assessed the meaning of results involving additives such as I₂ and DPPH.

(10) V. V. Voevodskii and Yu. N. Molin, *ibid.*, **17**, 366 (1962), consider the significance of esr results on glasses.

(11) J. A. Stone and P. J. Dyne, *Can. J. Chem.*, **42**, 669 (1964), employed CCl₄ as an additive.

(12) S. K. Ho and G. R. Freeman, *J. Phys. Chem.*, **68**, 2189 (1964), used O₂ and *p*-quinone as additives.

(13) R. M. Noyes, R. G. Dickinson, and V. Schomaker, *J. Am. Chem. Soc.*, **67**, 1319 (1945).

(14) H. Steinmetz and R. M. Noyes, *ibid.*, **74**, 4141 (1952).

(15) M. A. Golub, *ibid.*, **81**, 54 (1959); *J. Polymer Sci.*, **25**, 373 (1957).

(16) P. J. Dyne and W. M. Jenkinson, *Can. J. Chem.*, **38**, 539 (1960); P. J. Dyne and W. M. Jenkinson, *ibid.*, **39**, 2163 (1961); J. A. Stone and P. J. Dyne, *Radiation Res.*, **17**, 353 (1962).

(17) J. F. Merklin and S. Lipsky, *J. Phys. Chem.*, **68**, 3297 (1964).

(18) S. Z. Toma and W. H. Hamill, *J. Am. Chem. Soc.*, **86**, 4761 (1964).

do not contribute significantly to the isomerization, although a small contribution may account for values of $G_{c \rightarrow t}/G_{t \rightarrow c}$ slightly larger than 0.8–0.9 in the low concentration range.

The concentration dependence of $G_{t \rightarrow c}$ in Figure 1 is remarkably similar to that of $G(N_2)$ in radiolysis of N_2O - c - C_6H_{12} solutions¹⁹ and to that of $G(H_2)$ in the radiolysis of HI - c - C_6D_{12} solutions.²⁰ Indeed, if a yield, G_i , of isomerization precursors be estimated from

$$G_i = G_{t \rightarrow c}(1 + \phi_{c \rightarrow t}/\phi_{t \rightarrow c}) \quad (I)$$

by use of the photosensitization value of $\phi_{c \rightarrow t}/\phi_{t \rightarrow c} = 0.8$ – 0.9 , then an almost quantitative correspondence is obtained with $G(H_2)$ in HI - c - C_6D_{12} ; however, $G(N_2)$ in N_2O - c - C_6H_{12} is consistently somewhat larger (cf. Table VII). $G(N_2)$ and $G(H_2)$ in the systems cited were identified with electron-scavenging reactions of the respective solutes N_2O and HI . The correlation suggests that the radiation-induced *trans* \rightarrow *cis* isomerization in cyclohexane may be initiated by capture of an electron by stilbene. The possibility of such an electron capture receives some support from two recent observations. Dainton and Salmon²¹ report that the presence of 10^{-2} *M* *trans*-stilbene in a methyltetrahydrofuran (MTHF) glass irradiated at $77^\circ K$ reduces the intensity of the solvated electron absorption by 43% and gives several new bands, possibly of the stilbene anion. Shida and Hamill²² have identified the stilbene anion spectrophotometrically in MTHF glasses which were irradiated at $77^\circ K$.

Table VII: Comparison of Yields Obtained with Various Indicator Solutes in Irradiated Cyclohexane

[Solute], ^a mole/l.	G_i	$G(N_2)$	$G(H_2)$
4×10^{-3}	0.52	1.14	
5×10^{-3}	0.56		0.55
1×10^{-2}	0.98		0.83
2×10^{-2}	1.41	2.20	
3×10^{-2}	1.54		1.73
5×10^{-2}	1.94	3.00	
7×10^{-2}	2.13		2.18
1×10^{-1}	2.29	3.75	

^a Solutes were as follows: *trans*-stilbene for G_i , N_2O for $G(N_2)$, and HI in c - C_6D_{12} for $G(H_2)$.

The effect of CCl_4 on $G_{t \rightarrow c}$, shown in Table II, lends additional support to an electron-capture mechanism. The work of Hamill and collaborators²³ has established the effectiveness of CCl_4 as an electron scavenger in hydrocarbons both glassy at $77^\circ K$ and liquid at room temperature. Although the data of Table II are not

sufficiently complete or precise to permit a quantitative test of conformity to competition kinetics, competition between CCl_4 and stilbene for an isomerization precursor is apparent. A comparable suppression of hydrogen yields by CCl_4 in cyclohexane radiolysis has been attributed to electron scavenging by CCl_4 .¹¹ Very significant is our finding that 4% by volume of CCl_4 in cyclohexane has no effect on the isomerization yield of 10^{-2} *M* stilbene when the latter is excited by 2537-Å light; CCl_4 appears without effect on the excited stilbene species but has an effect under conditions when charged species are involved.

Notions of mechanism related to the foregoing presentation may be based on three *postulates*: (1) stilbene forms the anion by capture of an electron in competition with positive-ion neutralization in the spurs ("free electrons" inevitably form stilbene anions over the concentration range studied); (2) the energy of repulsion between phenyl groups (which is responsible for the 6 kcal/mole stability of *trans*- relative to *cis*-stilbene) is sufficiently large so that the stilbene anion (which has the less rigid, three-electron central bond) survives only in the *trans* form at room temperature;^{24,25} (3) neutralization of the stilbene anion by a cation, with high probability (approximating unity), yields a triplet state of stilbene, from which isomerization occurs, and decomposition of the solvent molecule is thus substantially averted.²⁶ The possibility of formation of solute triplets in radiolysis of cyclohexane has been established.²⁷

Within the framework postulated, it is possible to interpret a rather broad range of observations in a

(19) G. Scholes and M. Simic, *Nature*, **202**, 895 (1964).

(20) J. R. Nash and W. H. Hamill, *J. Phys. Chem.*, **66**, 1097 (1962).

(21) F. S. Dainton and G. A. Salmon, *Proc. Roy. Soc. (London)*, **A285**, 319 (1965).

(22) T. Shida and W. H. Hamill, private communication.

(23) Cf. M. R. Ronayne, J. P. Guarino, and W. H. Hamill, *J. Am. Chem. Soc.*, **84**, 4230 (1962); J. P. Guarino, M. R. Ronayne, and W. H. Hamill, *Radiation Res.*, **17**, 379 (1962); J. Roberts and W. H. Hamill, *J. Phys. Chem.*, **67**, 2446 (1963); W. Van Dusen, Jr., and W. H. Hamill, *J. Am. Chem. Soc.*, **84**, 3648 (1962).

(24) The reduction of *cis*-stilbene with alkali metals at temperatures as low as -60° apparently gives the *trans* anion; cf. R. Chang and C. S. Johnson, Jr., *J. Chem. Phys.*, **41**, 3272 (1964), and C. S. Johnson, Jr., and R. Chang, *ibid.*, **43**, 3183 (1965).

(25) G. J. Hoijtink and P. H. van der Meij, *Z. Physik. Chem. (Frankfurt)*, **20**, 1 (1959), report that the reduction of stilbene with alkali metals causes isomerization from *cis* to *trans*.

(26) Evidence for a process in which an excited aromatic molecule is the product of neutralization of its anion has been reported by E. A. Chandross and F. I. Sonntag, *J. Am. Chem. Soc.*, **86**, 3179 (1964).

(27) In pulse radiolysis of cyclohexane solutions of naphthalene, the triplet state of naphthalene has been observed; cf. F. S. Dainton, T. J. Kemp, G. A. Salmon, and J. P. Keene, *Nature*, **203**, 1050 (1964), and J. P. Keene, T. J. Kemp, and G. A. Salmon, *Proc. Roy. Soc. (London)*, **A287**, 49c (1965).

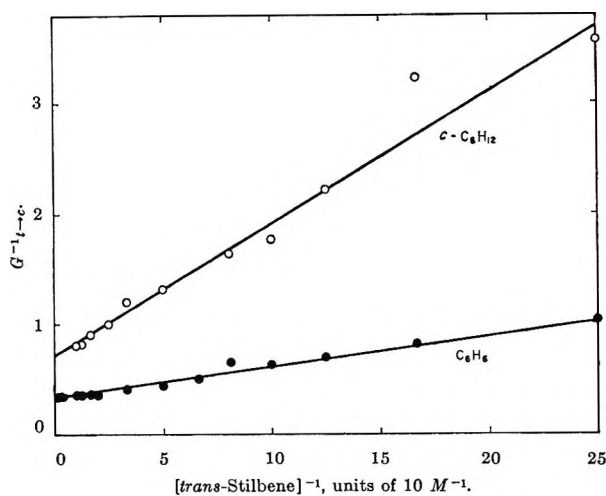


Figure 5. Stern-Volmer plots of *trans*-stilbene isomerization yields in cyclohexane and benzene.

plausible fashion. In this view, $G_{t \rightarrow c}$ is only indirectly related (*via* triplet formation) to production of ionized states. A reasonable estimate²³ of the lower limit for $G(\text{ion pairs})$ may be obtained (*via* eq I) as either the value of $G_i = 2.3$ obtained from $G_{t \rightarrow c} = 1.24$ at $0.1 M$ or, perhaps with somewhat greater accuracy, as $G_i = 2.6$ obtained from $G_{t \rightarrow c} = 1.41$ corresponding to the reciprocal of the intercept in Figure 5. To explain the curve for $G_{c \rightarrow t}$ in Figure 1, some additional speculation is necessary. Because the ratio $G_{c \rightarrow t}/G_{t \rightarrow c}$ (*cf.* Table VI) grows appreciably larger than unity as the stilbene concentration in cyclohexane increases beyond $\sim 0.01 M$, some specifically ionic process is indicated that (1) does not involve passage through an excited state of stilbene, (2) yields the *trans* isomer exclusively, and (3) has a probability that increases with increase in stilbene concentration. An electron-transfer reaction between stilbene molecules satisfies such requisites and is suggested as one possible explanation. In this way, an ionic chain isomerization of *cis* \rightarrow *trans* adds to the yield *via* the triplet-state isomerization which follows neutralization. Such an electron-transfer chain would necessarily involve the "separated" charged species ("free electrons") formed with an estimated $G \approx 0.1$.²⁸ The absence of a dose-rate effect suggests that chain termination results from electron transfer to a trace impurity present at constant concentration or that the chain itself is always confined to a limited region between a negative stilbene ion and its sibling positive hole.²⁹

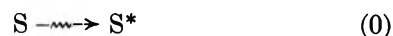
Comparison of the isomerization and luminescence data in Tables III and IV for addition of PPO to cyclohexane solutions of stilbene shows clearly that PPO luminescence is not at the expense of $G_{t \rightarrow c}$; thus, the

state of the system primarily excited by radiation and ultimately responsible for luminescence does not contribute significantly to isomerization of stilbene.³⁰ A very close correspondence between $G_{t \rightarrow c}$ as a function of total additive (PPO + stilbene) concentration in Table III and $G_{t \rightarrow c}$ as a function of stilbene concentration in Figure 1 suggests that PPO captures electrons with a specific rate about equal to that of stilbene and, on neutralization, forms a triplet state of sufficiently long lifetime to transfer essentially quantitatively to $4 \times 10^{-3} M$ *trans*-stilbene.

Cundall and Griffiths⁵ have reported inhibition of the isomerization of 2-butene in dodecane by piperidine. We also find that $0.1 M$ piperidine or $0.12 M$ pyridine reduces $G_{t \rightarrow c}$ of $10^{-2} M$ *trans*-stilbene in cyclohexane by 75 or 70%, respectively. In terms of the mechanism proposed, it would appear that protonated nitrogen compounds are formed by proton transfer from the solvent cation and that such positive ions neutralize the stilbene anion without formation of triplet stilbene (perhaps by proton transfer).

Processes and Mechanistic Details; Mixed Solvents. At this stage of our argument, there is advantage in consideration of the over-all processes which include the mechanistic details involved in the isomerization.

First, energy is deposited in the system *in toto* to produce nonlocalized conditions (*e.g.*, excitation and ionization in spurs or blobs³¹) which need not be described in detail to derive many of the very adequate kinetic equations which have been from time to time employed. In that sense the step (0) (where S is the system) is hidden



in the mechanisms usually suggested.

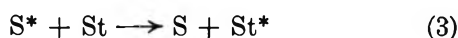
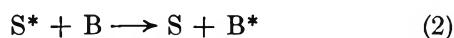
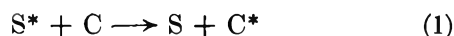
If we consider a two-solvent, one solute system (*e.g.*, cyclohexane, C, benzene, B, and stilbene, St—with *trans* and *cis* represented by *t*-St and *c*-St, respectively) we can write on a first level of sophistication for the immediately subsequent processes

(28) *Cf.* A. O. Allen and A. Hummel, *Discussions Faraday Soc.*, **36**, 95 (1963).

(29) In effect, the $G \approx 0.1$ for "free" ion pairs may correspond to a yield of ion pairs of sufficiently great separation (or sufficiently long recombination lifetime) to be separable by a strong electric field. In the absence of a field such ion pairs would undergo geminate recombination.

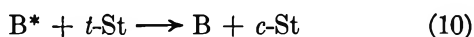
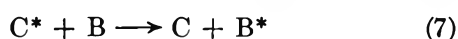
(30) A value of the luminescence parameter $Q' = 2.2 \times 10^{-3} M$ for PPO in cyclohexane is reported by M. Burton, M. A. Dillon, C. R. Mullin, and R. Rein, *J. Chem. Phys.*, **41**, 2236 (1964). This number means that excitation transfer to PPO would be 90% complete at $2 \times 10^{-2} M$ PPO in the absence of another excitation acceptor. Thus, if the same state of cyclohexane were involved in the isomerization, the isomerization yield would be trivial if luminescence were to be substantially unaffected.

(31) J. L. Magee, K. Funabashi, and A. Mozumder, *Proc. 6th Japan Conf. Radioisotopes, Tokyo, 1964*, **6**, 755 (1965).



where the probability of each of these energy localization steps (to produce unspecified excited or ionized species) seems to be related to the electron fraction of each component but is not precisely the same thing.³² Equations 1 and 2 are used, as an example, instead of the limited idea that the initial deposition of energy in cyclohexane-benzene mixtures is in specific molecules. However, kinetic equations derived therefrom, as in the works of Manion and Burton³³ and of Merklin and Lipsky¹⁷ (which assume direct initial excitation of each of the solvent species), would not be affected and the equations themselves could not reflect any of the subtleties which might be invoked in explanation of the probabilities of the processes by which the two solvents are excited.

If we continue with consideration of the *trans-cis* isomerization mechanism, according to the general devices of Merklin and Lipsky,¹⁷ we include also such equations as



At concentrations at which reaction 3 can be neglected, the 100-ev yield, G , of isomerization in the two-solvent mixture is related to the isomerization yields G_C and G_B in the single solvent mixtures by the relationship

$$G = G_B - \frac{\epsilon_C \{ [1 + \alpha' [B] (1 - \rho)] G_B - G_C \}}{1 + \alpha' [B]} \quad (II)$$

where α' is given by

$$\alpha' = k_7 / (k_4 + k_5 + k_6 [t\text{-St}]) \quad (III)$$

and

$$\rho \equiv \kappa_1 / \kappa_2 \quad (IV)$$

in which last equation κ_1 and κ_2 are the yields of reactions 1 and 2 per 100 ev localized in C and B, respectively.

A similar kinetic equation representing $G(H_2)$, the 100-ev yield of H_2 (other than that resulting *via* thermal

H), in a mixture of cyclohexane and benzene was obtained by Merklin and Lipsky.¹⁷ If we assume that κ_1 and κ_2 are approximately equal, eq II would reduce to

$$G = G_B - \epsilon_C (G_B - G_C) / (1 + \alpha' [B]) \quad (V)$$

which has a close resemblance to one of the ways of representation of the Merklin-Lipsky kinetics. According to their treatment, $k_7 / (k_4 + k_5)$ is $0.84 M^{-1}$. In the present work, the Stern-Volmer plot of Figure 5 for isomerization in cyclohexane would yield (in similar interpretation) $k_6 / (k_4 + k_5) = 59 M^{-1}$. Substitution of these values³⁴ into eq V, along with those of G_B , G_C , and $[t\text{-St}]$ from Table V gives

$$G = 1.69 - 1.16 \epsilon_C / (1 + 0.53 [B]) \quad (VI)$$

Values of G (*i.e.*, of $G_{t \rightarrow c}$) calculated from eq VI correspond well with the measured values shown in Table V, but one may well inquire whether such good correspondence is based on any reasonable notions of mechanism.

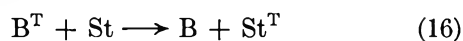
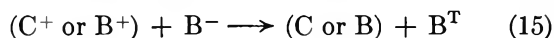
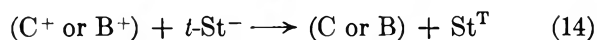
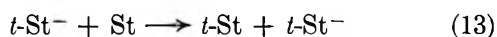
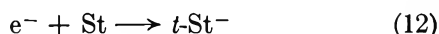
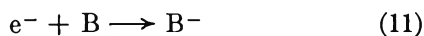
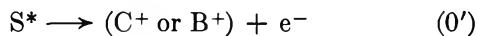
Consider, for example, the idea that the energy is localized, either in an initial stage (*i.e.*, without any reaction 0) or in an immediately subsequent stage, with approximately equal probability per electron in *individual* cyclohexane and benzene molecules. Such treatment no longer invokes the notion that either excited or ionized states or both overlap the surrounding molecules. Without such excitation overlap involving *more than one* molecule, it is difficult to understand how excited cyclohexane can survive long enough (*i.e.*, $\sim 10^{-13}$ sec without decomposition) to transfer excitation to surrounding molecules. Further, if both C ion pairs and C excited states are included under the general designation C^* , it is difficult to understand how their summed behavior can be represented by a single set of constants. Consequently, although it is possible to relate the observed kinetics to a "derivable" equation, such simulacrum of success is no support for a presumed mechanism.

However, there are some reactions which we invoke in our kinetic scheme which can be justified independently of the establishment of a detailed law. Irrespective of the origin of the species involved, we note the probability that the following detailed reactions are involved in the isomerization scheme in benzene, cyclohexane, and mixed solvent systems.

(32) Cf. K. Katsuura and M. Inokuti, *J. Chem. Phys.*, **41**, 989 (1964).

(33) J. P. Manion and M. Burton, *J. Phys. Chem.*, **56**, 560 (1952).

(34) These values also yield $k_6/k_7 = 70$, a number which would appear reasonable—dependent on the assumed mechanism. As an example, Scholes and Simic¹⁹ have reported for the ratio of trapping processes in $c\text{-C}_6\text{H}_{12}$ solutions, $k(e^- + \text{N}_2\text{O})/k(e^- + \text{C}_6\text{H}_6) \approx 100$.



In this scheme, St^T and B^T denote excited triplet states and St_i indicates the mixed isomer product. The scheme does not rule out contributions from other processes involving other species (*e.g.*, St^+). The point of this suggestion is that certain results can be explained readily in terms of reactions 11–17.

Reactions 11 and 12 suggest merely that the probability of formation of B and St negative ions depends on the concentrations of benzene and of stilbene; no consideration need be given to the possible formation (in a competing process) of a persistent negative cyclohexane ion.³⁵ Reactions 14 and 15 are strictly *ad hoc*. We know of no *theoretical* support for the suggestion that such a neutralization process with high probability yields a triplet state of the species which was negatively ionized.³⁶ The values of $G_{c \rightarrow t}/G_{t \rightarrow c}$ at low stilbene concentrations, shown in Table VI for both benzene and cyclohexane solvents, approximate the corresponding quantum yield ratio found in the photochemical processes^{2,3} and, thus, by implication suggest the formation and essential involvement of triplet stilbene in the high-energy induced isomerization.

The noteworthy feature of the isomerization chain (13) is the presumption that the negative stilbene ion, no matter how produced, is *trans* and remains *trans* after neutralization. Also involved in the notion of such a chain is that the stilbene negative ion readily transfers charge to *cis*-stilbene.³⁷ The number of stilbene molecules involved in the chain represented by reaction 13 (*i.e.*, the chain length) may be calculated, for the condition that all initially "separated" electrons are involved, on the assumption that $G_{t \rightarrow c}$ involves only triplet excited species and that $G_{c \rightarrow t}$ involves both triplet excited species and ion chains. The pertinent equation is

$$\Lambda = (G_{c \rightarrow t}/G_{t \rightarrow c} - \phi_{c \rightarrow t}/\phi_{t \rightarrow c})G_{t \rightarrow c}/G_e \quad (VII)$$

where Λ is the chain length, $G_e \approx 0.1^{28}$ is the 100-ev yield of "separated" electrons, and $\phi_{c \rightarrow t}/\phi_{t \rightarrow c}$ is taken as approximately 0.85. Thus, we may conclude from the data of Table VI and Figure 1 that, at 0.1 M *cis*-stil-

bene in cyclohexane, $\Lambda = 11$. Use of $G_{t \rightarrow c} = 1.41$ (corresponding to the reciprocal of the intercept in Figure 5) as the limiting value at high *trans*-stilbene concentration gives, for 0.2 M *cis*-stilbene in cyclohexane, $\Lambda = 14$.³⁸

Benzene Solutions. The isomerization results for benzene solutions fit rather well into the postulated framework. The data of Table I indicate little or no consumption of stilbene in benzene, a result to be expected on the basis of low free-radical yields in benzene^{9,10} and the scavenging ability of benzene itself. The ratio $G_{c \rightarrow t}/G_{t \rightarrow c}$ in benzene up to 0.1 M stilbene (*cf.* Table VI) agrees closely with the photosensitization ratio, $\phi_{c \rightarrow t}/\phi_{t \rightarrow c}$.² The specific rate of electron capture by benzene appears to be $\sim 1/70$ of that by stilbene³⁴; consequently, isomerization appears to proceed largely *via* the triplet state of benzene in the low concentration range. On the basis $k_6/k_7 = 70$, it follows that at 10^{-2} M stilbene, only 6% of the electrons would be captured by stilbene.³⁹ (Scholes and Simic¹⁹ report that at 0.05 M N_2O , $G(N_2)$ in benzene is only 0.3 times that in cyclohexane; also compare the electron-scavenging effectiveness of various solutes in cyclohexane and in benzene reported by Hamill and collaborators.^{20,23}) Electron capture by stilbene becomes appreciable only at stilbene concentrations exceeding that at which triplet-state transfer from benzene to stilbene is essentially complete. Thus, eq I and the reciprocal of the intercept in the Stern–Volmer plot of $G_{t \rightarrow c}$ in Figure 5 give an approximate yield of benzene triplets, $G_i = 2.9 \cdot (1 + \phi_{c \rightarrow t}/\phi_{t \rightarrow c}) = 5.4$. The ratio of slope to intercept in Figure 5 gives $k_t/k_d = 120 M^{-1}$, for the specific rate of triplet-state transfer from benzene to stilbene divided by the specific rate of decay of benzene triplet states. If a yield $G(\text{ion pairs})$ of ~ 3 is assumed,²³ it follows from $G_i = 5.4$ that the yield for production of benzene triplets *via excitation alone* must be ~ 2.4 .

The value $G_i = 5.4$ is somewhat larger than the triplet-state yield in benzene of $G = 4.2$ reported by Cundall and Griffiths, who studied the radiation-induced

(35) *Cf.* J. L. Magee and M. Burton, *J. Phys. Chem.*, **56**, 842 (1952).

(36) Indeed, according to theory presented by J. L. Magee, *Discussions Faraday Soc.*, **12**, 33 (1952), the probability is that the species which was positively ionized yields the excited species. See, however, ref 26 and 27.

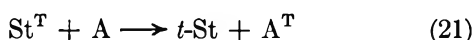
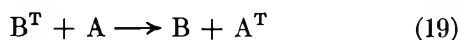
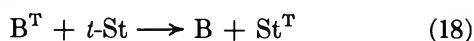
(37) According to esr studies (footnote 24) the transfer of charge between *trans*-stilbene anion and *trans*-stilbene occurs quite readily. On the assumption that the electron affinities are substantially the same for the *trans* and *cis* compounds, such transfer would be limited only by a presumably small activation energy.

(38) Because chain termination may involve trace impurities (note the absence of a dose-rate effect), $G_{c \rightarrow t}$ and the corresponding chain lengths may be sensitive to reagent purification procedures and, therefore, may not be readily reproducible by different experimenters.

(39) It must be remembered that, in addition, an appreciable yield of benzene triplet states may be formed by direct excitation.

isomerization of 2-butene in benzene solutions.⁴⁰ If a diffusion-controlled $k_t \approx 10^{10} M^{-1} \text{sec}^{-1}$ is assumed,⁴¹ a lifetime of $\sim 10^{-8}$ sec is obtained for the benzene triplet state in the pure (additive-free) liquid. This value is consistent with those obtained (for γ -ray and electron irradiation) by Cundall and Griffiths⁴⁰ and by Nosworthy⁵ and with conclusions from certain ultraviolet studies.^{40,42} On the other hand, both Lipsky⁴³ and Krongauz,⁴⁴ also on the basis of ultraviolet studies, assign a lower limit of 10^{-6} sec to the lifetime of triplet-state benzene. If the longer lifetime ($>10^{-6}$ sec) proves correct for ultraviolet-generated triplets, the shorter lifetime values obtained in irradiated systems may be attributable to an "effective lifetime" determined by the rate of triplet-triplet annihilation in spurs.⁴⁵ Certain features of luminescence-decay curves obtained in this laboratory provide some evidence for such a process.⁴⁶

Azulene. The azulene data of Table III support the notion that isomerization proceeds largely *via* the triplet state of benzene at low stilbene concentrations. On this basis, we can write



where A represents azulene and other symbols have their already indicated meaning. The usual steady-state analysis gives

$$G_0/G(1 + k_{21}[A]/k_{22}) = 1 + k_{19}[A]/(k_{18}[t\text{-St}] + k_{20}) \quad (\text{VIII})$$

in which G is the yield of *cis*-stilbene in the presence of azulene and G_0 is the yield in its absence. If benzene triplets were not involved (reactions 18–20 would be absent), a plot of G_0/G as a function of $[A]$ would be linear, as is not the case. However, as may be seen in Figure 6, good linearity is obtained in a plot of the left side of eq VIII against $[A]$ using the value of Hammond, *et al.*,² for $k_{21}/k_{22} = 78$. A slope of $151 M^{-1}$ so obtained gives (for $[t\text{-St}] = 4 \times 10^{-3} M$ and $k_{18}/k_{20} = k_t/k_d = 120 M^{-1}$) a value of $k_{19}/k_{20} = 224 M^{-1}$.

PPO. Comparison of the data in Tables III and IV for diphenyloxazole solutions suggests that the triplet state of benzene transfers to PPO and thence to *trans*-stilbene. The latter transfer (PPO to *trans*-stilbene) appears to be essentially complete at $4 \times 10^{-3} M$ *trans*-stilbene in cyclohexane; therefore, because in benzene $G_{t \rightarrow c} =$

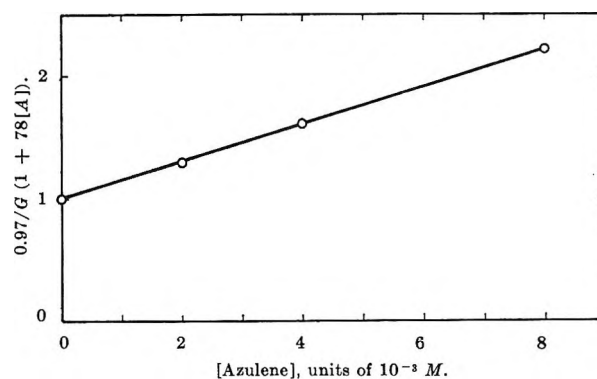


Figure 6. Kinetic plot (*cf.* eq VIII) of the effect of azulene on isomerization of $4 \times 10^{-3} M$ *trans*-stilbene in benzene.

1.76 at $0.1 M$ PPO and $4 \times 10^{-3} M$ *trans*-stilbene, as compared to $G_{t \rightarrow c} = 2.75$ at $0.1 M$ *trans*-stilbene in the absence of PPO, it is necessary to conclude that the specific rate for benzene triplet-state transfer to PPO is less than that for transfer to *trans*-stilbene. One could argue that a $G_{t \rightarrow c}$ of 1.76 in $0.1 M$ PPO is near a limiting value and represents, approximately, the total possible benzene triplet-state contribution. From such reasoning one might then conclude that $G_{t \rightarrow c} \approx 1$ represents the contribution of ${}^1B_{2u}$ states of benzene,⁴⁷ which (in the light of $Q' = 0.8 \times 10^{-3} M^{30}$) transfer 83% of their energy into $4 \times 10^{-3} M$ PPO and 99% into $0.1 M$ PPO. This argument is difficult to reconcile (1) with the absence of any enhancement by $4 \times 10^{-3} M$ PPO of $G_{t \rightarrow c}$ in the $4 \times 10^{-3} M$ *trans*-stilbene solution (*cf.* Table III), (2) with the good Stern-Volmer plot of Figure 5, from

(40) R. B. Cundall and P. A. Griffiths, *Trans. Faraday Soc.*, **61**, 1968 (1965).

(41) *Cf.* C. R. Mullin, M. A. Dillon, and M. Burton, *J. Chem. Phys.*, **40**, 3053 (1964). The value of $10^{10} M^{-1} \text{sec}^{-1}$ is reasonably low and the consequent value of $\sim 10^{-8}$ sec is an upper limit for the life of the triplet state.

(42) J. T. Dubois and F. Wilkinson, *ibid.*, **38**, 2541 (1963).

(43) S. Lipsky, *ibid.*, **38**, 2786 (1963).

(44) V. A. Krongauz, *Dokl. Akad. Nauk SSSR*, **155**, 638 (1964).

(45) Such a model has been proposed by G. S. Hammond to explain certain of his data for irradiated benzene-stilbene solutions (private communication).

(46) E. Grünhut, paper in preparation. Note also that conformity to Stern-Volmer kinetics (*cf.* Figure 5) is not necessarily evidence for a homogeneous, first-order decay of triplet benzene. Such kinetics also are observed in cyclohexane solutions in which the required decay process (in competition with isomerization) would appear to be geminate neutralization of ion pairs in spurs, with a distribution of "lifetimes." In particular, one must be wary about the interpretation of a straight line (in a Stern-Volmer equation) without adequate consideration of the fact that reciprocal plots tend to straighten out lines.

(47) S. Lipsky and M. Burton, *J. Chem. Phys.*, **31**, 1221 (1959); S. Lipsky, W. P. Helman, and J. F. Merklin, "Luminescence of Organic and Inorganic Materials," H. P. Kallman and G. M. Spruch, Ed., John Wiley and Sons, Inc., New York, N. Y., 1962, Chapter I, p. 83.

which the value $k_t/k_d = 120 M^{-1}$ is obtained (compare with $1/Q' = 1250 M^{-1}$), and (3) with the azulene data. Consequently, it is concluded that the ${}^1B_{2u}$ state of benzene does not contribute appreciably to the isomerization. Transfer from the ${}^1B_{2u}$ state to stilbene ought to be about as efficient as transfer to PPO; because approximately 90% of stilbene singlets undergo intersystem crossing to the triplet at room temperature,²⁻⁴ it is necessary to conclude that $G({}^1B_{2u})$ in benzene is small (*i.e.*, $\leq 0.5^{48}$) relative to $G(\text{triplets}) = 5.4$.

Chains in Benzene. Figure 3 and the data for benzene solutions in Table VI provide impressive support for the postulated ionic chain isomerization of *cis*-stilbene at higher concentrations ($>0.1 M$ in this case). From eq VII, we have for chain length as a function of stilbene concentration³⁸ the values found in Table VIII.

Table VIII

[<i>cis</i> -Stilbene], <i>M</i>	λ
0.29	7
0.48	12
0.66	15
1.8	31

It is evident that at corresponding stilbene concentrations, chain lengths are shorter in benzene than in cyclohexane.⁴⁹

The results shown in Figure 4 are of interest for comparison with the corresponding cyclohexane solutions; however, because many factors are involved in each case, a detailed analysis is not justified. Pyridine apparently transfers triplet energy to stilbene with less efficiency than does benzene. The lesser effect of piperidine on isomerization yields in benzene, as compared to the effect in cyclohexane, is in agreement with observations of Cundall and Griffiths⁵ and may be related to a lesser efficiency of proton transfer from benzene cations to piperidine.

Commentary

A mechanism has been presented for interpretation of the radiation-induced isomerizations of *cis*- and *trans*-stilbene in both benzene and cyclohexane solutions. This mechanism has emphasized the role of stilbene anions formed in electron-capture processes; completely parallel and equally satisfactory arguments might be presented in terms of stilbene cations formed by positive-charge-transfer processes. Indeed, both ionic types may contribute to the chains. Such alternative mechanisms are not ruled out. A tentative preference for the anionic mechanism is based on the fol-

lowing points: (1) the correlation noted between the behavior of the isomerization reaction and the effect of such electron scavengers as N_2O and HI on $G(N_2)$ and $G(H_2)$, respectively, in cyclohexane solutions; (2) the apparent competitive effect of CCl_4 in suppression of isomerization in cyclohexane solution; (3) an apparent rate of charge capture by stilbene that is ~ 70 times that of benzene, a number which appears to be reconcilable with an electron-capture process but not positive-charge transfer.

The essential features of the mechanism can be summarized as follows without reference to the details of the ionic processes involved. In cyclohexane, isomerization of *cis*-stilbene at low concentrations and of *trans*-stilbene at all concentrations occurs *via* triplet states of stilbene formed by neutralization of stilbene ions. At high *cis*-stilbene concentrations ($>10^{-2} M$) in cyclohexane, a direct ionic chain isomerization occurs by charge transfer between "free" stilbene ions and stilbene molecules. At low stilbene concentrations ($<0.05 M$) in benzene, isomerization proceeds largely *via* transfer from triplet states of benzene (*cf.*, also, ref 5). At higher stilbene concentrations, the triplet state of stilbene is formed directly by neutralization of stilbene ions, as in cyclohexane; the direct ionic chain isomerization of *cis*-stilbene becomes significant in benzene at concentrations greater than $0.1 M$.

Finally, the fact should be noted that 10 nsec is derived as an upper limit for the decay time of triplet benzene excited by high-energy radiation in the pure liquid. This figure may be compared with the longer decay time of 16 nsec now well established for the ${}^1B_{2u}$ state⁵⁰ under similar conditions.

An immediate explanation of such an anomalous relationship is that decay of triplets may be to a significant extent by triplet-triplet annihilation in the track.^{45, 46}

Acknowledgment. The authors are pleased to acknowledge the helpful suggestions and criticisms of Prof. A. A. Lamola and the experimental assistance of Dr. E. A. Rojo in the final stages of the work.

(48) This value is considerably less than that suggested by the work of D. B. Peterson, T. Arakawa, D. A. G. Walmsley, and M. Burton, *J. Phys. Chem.*, **69**, 2880 (1965).

(49) We are inclined to attribute this difference in chain length to a fundamental matter of the distance to which sibling positive hole and electron may separate as determined by the electronic properties of the medium; *e.g.*, cyclohexane cannot capture an electron but benzene can and the separation distance consequently would be less in the latter case. Recent experiments by K. Shima in this laboratory indicate that the chain length in cyclohexane may be increased by further purification. An effect of ultrapurification on the benzene system has not yet been observed.

(50) M. A. Dillon and M. Burton, "Pulse Radiolysis," Proceedings of the International Symposium, Manchester, 1965, M. Ebert, J. P. Keene, A. J. Swallow, and J. H. Baxendale, Ed., Academic Press, New York, N. Y., 1965, p 259 ff.

Electrode Processes without *a Priori* Separation of Double-Layer Charging

by Paul Delahay

Department of Chemistry, New York University, New York, New York 10003 (Received February 9, 1966)

A priori separation of faradaic and double-layer charging currents, as commonly accepted, is not justified theoretically for nonsteady-state conditions (transients or periodic variations). The idea of charge separation or recombination at an interface, without external current, is introduced and applied to the analysis of charging processes. There can be progressive transition in double-layer charging from the ideal polarized electrode (no charge separation or recombination) to the ideal reversible electrode (only charge separation or recombination). Unawareness of this idea vitiates some results obtained by relaxation or perturbation methods in electrode kinetics. Three general equations are derived which, after solution for any particular conditions, describe nonsteady-state electrode behavior and allow *a posteriori* determination of kinetic and double-layer parameters. Application is made to an electrode of varying area at constant overvoltage.

It is customary to derive faradaic currents for nonsteady conditions (transients or periodic variations) by ignoring double-layer charging. Experimental currents are subsequently corrected for double-layer charging by assuming behavior as an ideal polarized electrode. Thus, faradaic and double-layer charging processes are separated *a priori*. This procedure was refined recently, and methods were developed to separate the faradaic and charging processes from their differences in time or frequency dependence. (a) Sluyters and co-workers¹ devised a method for the analysis of electrode impedance measurements by assuming that the charging process is frequency independent, whereas the faradaic impedance is generally not. (b) Butler and Meehan² and independently the writer and co-workers³ attempted separation of faradaic and charging currents at a dropping liquid metal (mercury, amalgam, etc.) electrode from the difference in the time dependence of these two currents. (c) A similar analysis based on dependence on the rate of flow of mercury (amalgam) was devised³ for the streaming mercury electrode. These analyses still presuppose the *a priori* feasibility of separating faradaic and charging currents. It turns out, as will be shown below, that such a postulate is not justified theoretically and that it can lead to serious errors of interpretation in certain cases.

We shall begin with the analysis of two simple cases and shall then derive three general equations

which, after solution for any particular conditions, describe electrode behavior and allow *a posteriori* separation of kinetic and double-layer parameters. These three general equations should provide the key to the analysis of transitory and periodic electrode processes. Finally, we shall examine the application to an electrode of varying area at constant overvoltage. Analysis of the faradaic impedance has also been completed,⁴ and other methods (potentiostatic, galvanostatic, etc.) are being analyzed.

Charging Processes at a Metal Ion–Pure Metal Electrode

Ionic Transfer vs. Charge Separation or Recombination. We examine charging processes at an electrode of pure metal M in a solution of salt MX. The electrode reaction is $M^{+z} + ze = M$ with $z > 0$. The electrode area A is varied, and the electrode potential is maintained, *e.g.*, by a potentiostat, at the equilibrium value corresponding to the bulk activity of MX. Such idealized conditions can actually be closely approximated, *e.g.*, for an expanding mercury drop in

(1) M. Sluyters-Rehbach and J. H. Sluyters, *Rec. Trav. Chim.*, **82**, 525 (1963). See the same journal for previous and more recent papers in this series.

(2) J. N. Butler and M. L. Meehan, *J. Phys. Chem.*, **69**, 4051 (1965).

(3) G. Tessari, J. Murphy, R. de Levie, and P. Delahay, Louisiana State University, unpublished work.

(4) P. Delahay and G. G. Susbielles, *J. Phys. Chem.*, in press.

a Hg(I) solution.^{2,3} We shall assume here and in subsequent developments that solutions (and amalgams) are sufficiently dilute so that absolute and relative surface excesses are equal for all practical purposes.⁵ This condition is generally satisfied in practice.

There are two processes by which ions M^{+z} needed to maintain the equilibrium surface excess Γ_+ of M^{+z} in solution are supplied to or removed from the double layer, as the electrode area varies: (a) transfer of M^{+z} to or from the bulk of the solution; (b) charge recombination or separation at the interface by the reaction $M^{+z} + ze = M$. The charges on the electrode and in the double layer always remain equal and of opposite sign. Hence, the transfer of an ionic charge $(zF\Gamma_+)\delta A$ from or to the bulk of the solution, which results from a variation δA , requires addition to or removal from the electrode of an electronic charge $-(zF\Gamma_+)\delta A$. Current flows in the external potentiostat-cell circuit in this operation.

In contrast, charge recombination or separation at the metal-electrolyte interface by the process $M^{+z} + ze = M$ does *not* require an external current.⁶ For instance, dissolution of $\Gamma_+\delta A$ moles of M^{+z} produces an ionic charge $(zF\Gamma_+)\delta A$ in the double layer and leaves an equal electronic charge of opposite sign on the electrode. The charging current being measured thus depends on the relative contributions of two processes, and *recognition of the possibility of charge separation or recombination without an external current is the key idea of this paper.*

Charging Currents. We calculate the charging currents for the above processes on the assumption that only one charging process is to be considered. We also assume that the double layer is at equilibrium with respect to the ionic concentrations just outside the diffuse double layer. In the absence of supporting electrolyte, the charging current (not the current density) for *supposedly* pure ionic transfer is

$$I = zF(\Gamma_- - \Gamma_+)(dA/dt) \quad (1)$$

where Γ_- is the surface excess of X^- and $z > 0$. A positive current indicates transfer of a positive charge from the potentiostat to the electrode of varying area through the wire connected to the electrode. Since the charge density on the electrode is

$$q = -zF(\Gamma_+ - \Gamma_-) \quad (2)$$

one has

$$I = q(dA/dt) \quad (3)$$

Thus, the charging current is proportional to the charge density on the electrode, just as for an ideal polarized

electrode. This conclusion also holds for a solution with supporting electrolyte.

The charging current for *supposedly* pure charge separation or recombination is, in the absence of supporting electrolyte

$$I = zF\Gamma_-(dA/dt) \quad (4)$$

where $z > 0$. In view of eq 2 one has

$$I = (q + zF\Gamma_+)(dA/dt) \quad (5)$$

The charging current is proportional to $q + zF\Gamma_+$, and this result also holds in presence of a supporting electrolyte.

The quantity $q + zF\Gamma_+$ is precisely the one which is obtained by thermodynamic analysis of an ideal reversible electrode.^{7,8} Thus, charge separation or recombination is the sole process supplying or removing ions M^{+z} for an ideal reversible electrode. This is understandable since such an electrode must have, by definition, an exchange current density i_0 approaching infinity for any dynamic conditions of measurement. Hence, any driving force, no matter how small, will cause charge separation or recombination. The driving force, in the above example, is the vanishingly small overvoltage resulting from the vanishingly small gradient in the concentration of ions M^{+z} at the electrode. This gradient is caused by a vanishingly small contribution of ionic transfer to the charging process. Conversely, only ionic transfer of M^{+z} is operative when $i_0 \rightarrow 0$, and behavior as an ideal polarized electrode prevails.

These two behaviors are only limiting cases of the more general situation in which both ionic transfer and charge separation or recombination contribute to double-layer charging. The validity of considering only the limiting cases depends entirely on the relative contributions of the above two processes, *i.e.*, on experimental conditions. The current practice of using the charging current for an ideal polarized electrode should be nearly correct for sufficiently low i_0 values. Conversely, the charging current for an ideal reversible electrode should be used for sufficiently high i_0 values, but this has not been done. A general treatment is

(5) This matter was called to the author's attention by Dr. R. de Levie of Georgetown University, Washington, D. C.

(6) We neglect the displacement currents corresponding to movement of charges from the interface to the double layers in the metal and solution. These displacement currents are negligible in comparison with the current for ionic transfer in the bulk of the solution. The necessity of considering displacement currents was called to the author's attention by Dr. J. R. Macdonald of Texas Instruments, Dallas, Texas.

(7) D. C. Grahame and R. B. Whitney, *J. Am. Chem. Soc.*, **64**, 1548 (1942).

(8) D. M. Mohilner, *J. Phys. Chem.*, **66**, 724 (1962).

needed because there is no criterion to determine which charging current must be used and, in many instances, neither of these limiting values can be used because of the simultaneous contribution by ionic transfer and charge separation or recombination. Furthermore, the relative extent of these two contributions is time or frequency dependent, and the treatments of nonsteady-state processes have to be reexamined because they presuppose that the differential capacity of the double layer is constant. The resulting error can be quite serious in certain cases.

Three General Equations for Nonsteady-State Electrode Processes

We now show that faradaic and charging processes obey a set of three general equations for nonsteady-state conditions. These equations will be written first for metal ion-amalgam electrodes and afterwards for other types of electrode processes. The electrode area in this section is supposed to be constant. (The electrode of varying area is treated as an application at the end of the paper.) It is assumed that the double layer is always at equilibrium with respect to the activities just outside the diffuse double layer.

Metal Ion-Amalgam Electrodes. We consider the reaction $M^{+z} + ze = M(\text{Hg})$ and neglect the thicknesses of the double layers in the solution and metal (no displacement current of the type discussed in footnote 6). The amalgam-electrolyte interface thus is regarded, as far as mass transfer is concerned, as a plane on which are accumulated the ionic surface excesses, Γ_M of the neutral metal⁹ M, and the electronic charge density q . This simplification is justified since the thicknesses of the solution and metal double layers are negligible in comparison with diffusion layer thicknesses for M^{+z} and M for usual electrode kinetic measurements. This remark holds even for very short measuring times (10^{-7} sec or even shorter times) or high frequencies.

We first write the balance condition for production or consumption of M^{+z} at the interface. Thus

$$i_f = zFv_+ + zF(d\Gamma_+/dt) \quad (6)$$

Here i_f represents the faradaic current density as expressed in terms of the exchange current density, overvoltage, etc. A positive i_f corresponds to net oxidation, in agreement with our above convention of taking a positive charging current as one supplying a positive charge to the electrode through the wire connected to it. The flux v_+ of M^{+z} in solution is positive in the direction from the electrode toward the solution.

It must be stressed that not all the current i_f flows in the wire connecting the electrode to the external power

supply because part of i_f is used up in charge separation or recombination. Thus i_f , as given by the usual equations of electrode kinetics, is *not a measurable quantity in nonsteady-state conditions*. Both contributions of ionic transfer and charge separation or recombination are included in eq 6 but cannot be separated. It is only by solving the mass-transfer problem that one can calculate i_f in terms of the activities of reactants and products at the interface.

The second equation relates the continuity of fluxes at the interface with the variations of Γ_+ and Γ_M . Thus

$$v_M = v_+ + d\Gamma_+/dt + d\Gamma_M/dt \quad (7)$$

where the flux v_M of M is taken as positive from the bulk of the amalgam toward the interface.¹⁰

The third equation gives the current density being measured, i , in terms of the flux v_+ (which is derived by solution of the mass-transfer problem for the boundary conditions of eq 6 and 7). Thus

$$i = zFv_+ - \sum_{i \neq M^{+z}} z_i F(d\Gamma_i/dt) \quad (8a)$$

$$= zFv_+ + d(q + zF\Gamma_+)/dt \quad (8b)$$

where the ionic valences z_i are taken with their sign and q is the charge density on the electrode. No mass-transfer complications are supposed to prevail for all ions except M^{+z} in the writing of eq 8. The summation includes all ions except M^{+z} since the latter has already been counted in eq 6. The summation must be preceded by a minus sign with our convention, as one can readily ascertain by noting that bringing an anion in the double layer requires the supply of a positive current by the external source. Equation 8a is converted to 8b by noting that q is equal to $-\sum z_i F\Gamma_i$ for all ions including M^{+z} . The term zFv_+ in eq 8a and 8b corresponds to the total flux of the ions M^{+z} which are consumed or produced at the interface and accumulated in or removed from the double layer.

Solution of the General Equations. Equations 6 and 7 are the boundary conditions for which the mass-transfer problem must be solved. The resulting expression for v_+ is then introduced in eq 8 and i is obtained. To apply this procedure one must eliminate Γ_+ and Γ_M as unknown functions of time and express them as functions of the potential E of the electrode. The simplest case corresponds to the low overvoltage approximation by which one introduces the $(d\Gamma/dE)$'s

(9) Γ_M is completely equivalent in a formal way to the sum of the surface excess of ions M^{+z} in the metal and the same surface excess of electrons.

(10) One can, of course, write eq 6 as $i_f = zFv_M - zF(d\Gamma_M/dt)$ and use v_M instead of v_+ . This procedure is completely equivalent to the one followed here.

at the equilibrium potential. Thus all the $(d\Gamma/dt)$'s in eq 6 to 8 are replaced by

$$d\Gamma/dt = [(\partial\Gamma/\partial E)_{a, \eta=0} + (\partial\Gamma/\partial E)_{aM, \eta=0}](dE/dt) \quad (9)$$

where the subscript $\eta = 0$ indicates zero overvoltage. The $[(\partial\Gamma/\partial E)_{\eta=0}]$ terms in the resulting modified eq 6 to 8 are then constant coefficients. The expression for i_t is also simplified in that case since the usual linearized low-overvoltage i vs. η characteristic can then be used (although this is not necessary). It should be noted that we express Γ in eq 9 as a function of the single variable E although there are two varying concentrations (of M^{+z} and M). However, these two concentrations are not independent because the corresponding fluxes are related¹¹ by eq 7. This procedure cannot be applied when η is constant (potentiostatic conditions). One then uses *one* of the concentrations (or M^{+z} or M) as variable.

The boundary conditions (6) and (7) become much more cumbersome when the overvoltage variations are so large that the $(\partial\Gamma/\partial E)$'s at $\eta = 0$ cannot be used. It is then necessary to express the $(\partial\Gamma/\partial E)$'s as functions of E . Such functions are, in general, not known *a priori*, and one is left with the possibility of expanding Γ as a series of E . A quadratic expansion may suffice if the overvoltage interval is not too wide, but, anyhow, boundary value problems become rapidly more involved. This is only a practical difficulty but definitely not a fundamental one. This difficulty militates against the use of nonsteady-state methods involving large overvoltage (although other features may more than compensate the complexity of mathematical analysis).

A Posteriori Determination of Kinetic and Double Layer Parameters. We consider the low-overvoltage approximation first. The parameters to be determined at the equilibrium potential are i_0 , dq/dE , $d\Gamma_+/dE$, and $d\Gamma_M/dE$. It is assumed that the diffusion coefficients or any other parameters for mass transfer are determined in separate experiments for pure control by mass transfer or by some other method.

The two extrapolations of i against a function of time to $t = 0$ and $t \rightarrow \infty$ (or to infinite and zero frequency, respectively) give four relations, namely two slopes and two intercepts. At $t = 0$, the contribution of charge separation or recombination to charging is negligible for any finite i_0 , *i.e.*, v_+ for $t = 0$ should contain a term which cancels with the term in $d\Gamma_+/dt$ in eq 8b. It should then be feasible to obtain i_0 and dq/dE at the equilibrium potential. (Note that when $i_0 \rightarrow \infty$ the ideal reversible electrode behavior prevails even for

$t = 0$.) Conversely, charge separation or recombination should be the only contribution to charging, as far as M^{+z} is concerned, for $t \rightarrow \infty$, and charging as an ideal reversible electrode should prevail. The corresponding differential capacity of the double layer for $t \rightarrow \infty$ is not $d(q + zF\Gamma_+)/dE$ for an amalgam electrode but a somewhat more involved expression because both concentrations of M^{+z} and M vary simultaneously. The capacity $d(q + zF\Gamma_+)/dE$ corresponds to variation of a single concentration, the other concentration remaining constant (see thermodynamics of the ideal reversible electrode^{7,8}). Details of the separation of the double-layer parameters must be worked out in each particular condition of mass transfer and cannot be predicted. Corollary thermodynamic study of the electrode from electrocapillary curves appears advisable and possibly essential. In addition to the above two extrapolations, curve fitting over the whole time or frequency range seems advisable. Computer treatment of data may be necessary and almost essential if the low overvoltage approximation is not justified.

An objection may be raised to zero-time or infinite-frequency extrapolation. Thus, the thicknesses of the diffusion layers for M^{+z} and M approach zero for $t = 0$, whereas our model supposes that these layers are very thick in comparison with the double layers in the amalgam and solution. This contradiction is only apparent because the experimental results, which are extrapolated to time zero, correspond to conditions for which the model is entirely justified.

Comparison with the Usual Equations. We compare eq 6 to 8 with the equations usually applied, namely

$$i_t = zFv_+ \quad (10a)$$

$$v_M = v_+ \quad (10b)$$

$$i = zFv_+ + dq/dt \quad (10c)$$

These equations are erroneous for the following reasons: (a) they neglect the double-layer contribution in the expressions for i_t and v_M ; (b) they imply charging as an ideal polarized electrode. Equations 6 to 8 reduce to eq 10 when both $d\Gamma_+/dt$ and $d\Gamma_M/dt$ are negligible in comparison with other terms in eq 6 to 8. This condition is quite frequently *not* fulfilled, even in the absence of specific adsorption of M^{+z} , as one can readily ascertain by calculating $d\Gamma_+/dE$ from diffuse double-layer data and theory.¹² Specific ad-

(11) This was pointed out by Mr. G. G. Susbielles of this laboratory.

(12) In the absence of specific adsorption, one calculates from diffuse double-layer theory $zF(d\Gamma_+/dE) \approx 190 \mu\text{f cm}^{-2}$ for the following conditions: $10^{-3} M$ solution of M^{+z} , $z = 2$, 25° , a potential of -0.5

sorption should generally render eq 10 even less satisfactory.

Other Types of Electrode Processes. Equations 6 to 8 can be transposed to other processes. Metal ion-pure metal electrodes can be disposed of immediately since eq 6 and 8 remain, whereas eq 7 is deleted. The limiting cases for $t = 0$ and $t \rightarrow \infty$ correspond to a double-layer differential capacity equal to dq/dE and to $d(q + zF\Gamma_+)/dE$, respectively.

Transposition to the reaction $O^{+z} + ne = R^{+(z-n)}$ involving two species soluble in the electrolyte phase is also immediate. Equations 6 and 7 are directly applicable with the following transformations: z to n ; v_+ to v_O and v_M to v_R , the positive fluxes being toward the electrode for v_O and toward the bulk of the solution for v_R . The measured current density is also given by eq 8 with the above change of notations.

Application to a Metal Ion-Pure Metal Electrode of Varying Area at Constant Overvoltage

Forms of the General Equations. We consider this case because it has been studied experimentally^{2,3} and because it shows, in a simple manner and for a concrete example, the theoretical impossibility of a *a priori* separation of faradaic and charging currents. We assume the following conditions. (a) The electrode area A varies and the overvoltage η is applied at time $t = 0$ at which A begins to vary. Thus, the electrode is at the equilibrium potential before A varies. (b) The potentiostat-cell circuit is supposed to have a zero time constant. (c) The low overvoltage approximation is valid.

The general eq 6 to 8, which were derived for a constant electrode area and any overvoltage, must now be written for the conditions stated above. Thus

$$i_t = zFv_+ + zF(\Gamma_+)_{\eta=0}(1/A)(dA/dt) \quad (11)$$

$$v_M = v_+ + [(\Gamma_+)_{\eta=0} + (\Gamma_M)_{\eta=0}](1/A)(dA/dt) \quad (12)$$

$$i = zFv_+ + (q + zF\Gamma_+)_{\eta=0}(1/A)(dA/dt) \quad (13)$$

where eq 12 is not needed here (no amalgam). Note that i for the conditions assumed here also includes an infinite component at $t = 0$ which results from charging of the double layer from $\eta = 0$ to a finite η in an infinitely short time by means of a supposedly ideal potentiostat. We shall neglect this component of i .

The Problem. We shall use the usual low overvoltage approximation for i_t , that is

$$i_t = i_0[1 - (c/c_s)_{x=0} + (zF/RT)\eta] \quad (14)$$

where i_0 is the exchange current density, c is the concentration of M^{+z} , c_s is the bulk value of c , x is the distance from the electrode, and R and T are as usual.

A better approximation will not be used since our main purpose is not a detailed description of the i - η - t relationship but rather the analysis of the charging process. We also assume $(1/A)(dA/dt)$ to be constant because the mathematics are considerably simplified. [One has $(1/A)(dA/dt) = t^{-1}$ for an ideal expanding dropping mercury electrode.] Finally, we neglect the movement of the metal-electrolyte boundary resulting from the condition that $(1/A)(dA/dt)$ be constant. Thus, we do not correct Fick's equation in a manner similar to that developed by Ilkovic for the dropping mercury electrode. A treatment for the actual conditions at a dropping mercury electrode is being developed but is not expected to reveal any new feature about the principles involved.

Equation 11 is now

$$i_0[1 - (c/c_s)_{x=0} + (zF/RT)\eta] = -zFD(\partial c/\partial x)_{x=0} + zF(\Gamma_+)_{\eta=0}(1/A)(dA/dt) \quad (15)$$

where D is the diffusion coefficient of M^{+z} . The minus sign in front of the flux term results from the convention on the direction of v_+ (see eq 6). Furthermore, one has $c = c_s$ for $x \geq 0$ at $t = 0$ and $c \rightarrow c_s$ for $x \rightarrow \infty$ for $t \geq 0$.

The solution of Fick's equation was obtained by Laplace transform and the following current density i was obtained according to eq 13

$$i = [i_0(zF/RT)\eta - zF(\Gamma_+)_{\eta=0}(1/A)(dA/dt)] \exp(\lambda^2) \operatorname{erfc}(\lambda) + (q + zF\Gamma_+)_{\eta=0}(1/A)(dA/dt) \quad (16)$$

where

$$\lambda = i_0 t^{1/2} / zFD^{1/2}c_s \quad (17)$$

Note that the current i also includes the infinite component at $t = 0$ discussed in connection with eq 13.

If $i_0 \rightarrow \infty$ (so-called reversible process) eq 16 becomes after expansion of $\operatorname{erfc}(\lambda)$ for a large argument

$$i = zFc_s(D/\pi t)^{1/2}(zF/RT)\eta + (q + zF\Gamma_+)_{\eta=0}(1/A)(dA/dt) \quad (18)$$

where the term in $t^{-1/2}$ is the usual expression for the diffusion current density in this particular case.

Discussion

Equation 16 will be discussed by comparing it with the expression of i derived by *a priori* separation of

v vs. the point of zero charge. The values of the potential ϕ_2 in the plane of the closest approach were taken for 0.1 M KCl according to Grahame and Parsons.¹³ This example corresponds approximately to Zn⁺² discharge on Zn amalgam in a 0.1 M univalent supporting electrolyte on the assumption that no complex is formed ($z = 2$).

(13) D. C. Grahame and R. Parsons, *J. Am. Chem. Soc.*, **83**, 1291 (1961).

faradaic and charging processes. One obtains by using the charging current density for an ideal polarized electrode

$$i_1 = i_0(zF/RT)\eta \exp(\lambda^2) \operatorname{erfc}(\lambda) + q_{\eta=0}(1/A)(dA/dt) \quad (19)$$

(See also the remark about eq 13 and the infinite charging current at $t = 0$.) The faradaic component in eq 19 corresponds to the usual potentiostatic conditions at low overvoltage.¹⁴ Conversely, we obtain by assuming charging as an ideal reversible electrode and neglecting the infinite current at $t = 0$

$$i_2 = i_0(zF/RT)\eta \exp(\lambda^2) \operatorname{erfc}(\lambda) + (q + zF\Gamma_+)_{\eta=0}(1/A)(dA/dt) \quad (20)$$

The difference between eq 16, 19, and 20 can be quite pronounced as shown in Figure 1. This diagram was prepared for $F\Gamma_+ = 5 \mu\text{coulombs cm}^{-2}$ and $c_s = 10^{-6}$ mole cm^{-3} . These data correspond to significant but not particularly strong adsorption. We note from Figure 1 that

$$\begin{aligned} i &\rightarrow i_1 \text{ for } t \rightarrow 0 \\ i &\rightarrow i_2 \text{ for } t \rightarrow \infty \end{aligned}$$

There is a progressive transition in charging behavior from the ideal polarized electrode (eq 19) to the reversible electrode (eq 20). This is readily seen by considering the limiting forms of eq 16 for $\lambda \rightarrow 0$ and $\lambda \rightarrow \infty$. The physical interpretation is as follows: at $t = 0$ there is no time for charge separation or recombination to occur; at $t \rightarrow \infty$ the external faradaic current approaches zero and all M^{+z} ions are produced or consumed by charge separation or recombination. We also note that reversible electrode behavior in charging prevails at any t when $i_0 \rightarrow \infty$ (see eq 18).

As practical limits one can set

$$\begin{aligned} \exp(\lambda^2) \operatorname{erfc}(\lambda) > 0.95 \text{ for } \lambda < 0.05 \\ \text{(charging as ideal polarized electrode)} \end{aligned}$$

$$\begin{aligned} \exp(\lambda^2) \operatorname{erfc}(\lambda) < 0.05 \text{ for } \lambda > 10 \\ \text{(charging as ideal reversible electrode)} \end{aligned}$$

If one sets, for instance, $z = 1$, $D = 10^{-5} \text{ cm}^2 \text{ sec}^{-1}$, and $c_s = 10^{-6} \text{ mole cm}^{-3}$, one finds $\lambda < 0.05$ for $i_0 t^{1/2} < 1.5 \times 10^{-5} \text{ amp cm}^{-2} \text{ sec}^{1/2}$ and $\lambda > 10$ for $i_0 t^{1/2} > 3 \times 10^{-3} \text{ amp cm}^{-2} \text{ sec}^{1/2}$. If measurements are at the scale of 1 sec, a moderately slow process behaves in double-layer charging as an ideal polarized electrode, and a moderately fast process behaves in double-layer charging as an ideal reversible electrode. If the time scale decreases, the corresponding limits of i_0 increase accordingly.

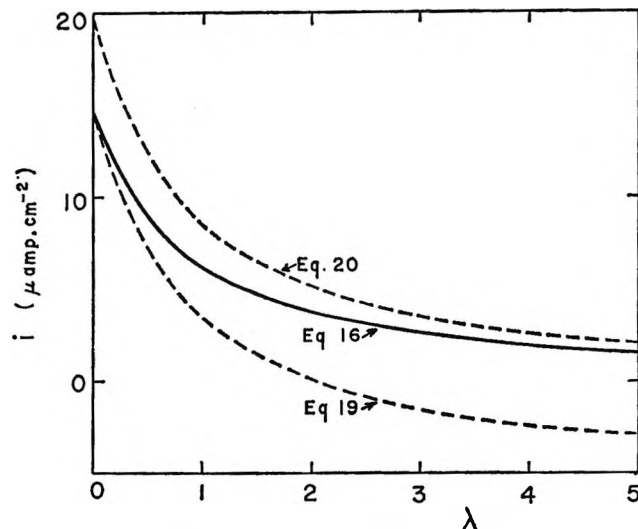


Figure 1. Measured current as a function of the parameter λ (proportional to $t^{1/2}$) for the following data: $z = 1$, $D = 10^{-5} \text{ cm}^2 \text{ sec}^{-1}$, $c_s = 10^{-6} \text{ mole cm}^{-3}$, $(1/A)(dA/dt) = 1 \text{ sec}^{-1}$, $i_0 = 10^{-4} \text{ amp cm}^{-2}$, $\eta = 5 \text{ mv}$, $T = 25^\circ$, $F\Gamma_+ = 5 \times 10^{-6} \mu\text{coulomb cm}^{-2}$. The Γ_+ 's are arbitrarily set to zero for all ions except M^{+z} (the corresponding term is independent of time).

Charging at the Equilibrium Potential. If one sets $\eta = 0$ in eq 16, one sees that the charging current still depends on $\exp(\lambda^2) \operatorname{erfc}(\lambda)$, *i.e.*, on i_0 . The previous conclusions about the limiting cases for $t = 0$ and $t \rightarrow \infty$ also apply here. The physical interpretation is as follows: when A varies, the consumption or production of M^{+z} causes the concentration of M^{+z} just outside the diffuse double layer to be different from the bulk value c_s ; since E is maintained potentiostatically at the equilibrium value corresponding to c_s , there is in fact an overvoltage which drives the separation or recombination process.

Determination of i_0 , q , and Γ_+ . The procedure for the determination of these quantities will be outlined to show that *a posteriori* separation of the various parameters is feasible. Thus, a plot of i against $t^{1/2}$ for $\lambda \ll 1$ has the slope $i_0(zFD^{1/2}c_s)^{-1}$ and yields i_0 provided D is known. The surface excess Γ_+ can then be computed from the intercept of this plot at $t = 0$ once i_0 is known (see eq 16). Conversely $q + zF\Gamma_+$ is obtained from the intercept at $t^{-1/2} = 0$ for a plot of i against $t^{-1/2}$ for $\lambda \gg 1$, and consequently q is obtained since Γ_+ is known from the previous plot. Thus, the transition in charging behavior from an ideal polarized electrode to an ideal reversible electrode allows complete analysis by extrapolation at $t = 0$ and $t \rightarrow \infty$.

(14) H. Gerischer and W. Vielstich, *Z. Physik. Chem. (Frankfurt)*, **3**, 16 (1955).

Conclusion

Faradaic and charging processes cannot be separated *a priori* in nonsteady-state electrode processes because of the phenomenon of charge separation or recombination at the electrode-electrolyte interface without flow of external current. Charging behaviors as ideal polarized or reversible electrode represent only two limiting cases of a more general case. Much of what has been done with relaxation and perturbation methods for fast electrode processes will have to be reexamined and possibly revised in the light of the present ideas. This task has already begun for impedance measurements⁴ and is being pursued. Some and perhaps most of the

glaring discrepancies on kinetic data obtained by different methods, as reported in the literature, may possibly be removed. (Other possible sources of discrepancies must, of course, be kept in mind.) Interpretation of double-layer phenomena for nonideal polarized conditions should also receive a new impetus from this work.

Acknowledgment. This investigation was supported by the National Science Foundation. The author thanks Drs. de Levie and G. Tessari for discussion of Sluyters' work and Dr. R. Parsons (University of Bristol), who kindly went over the initial draft of this paper.

Observations on Trapped Electrons and Allyl Radicals Formed in 2-Methylpentene-1 by γ Radiolysis at Low Temperature

by D. R. Smith and J. J. Pieroni

Research Chemistry Branch, Atomic Energy of Canada, Limited, Chalk River Nuclear Laboratories, Chalk River, Ontario, Canada (Received February 11, 1966)

The cobalt-60 γ radiolysis of 2-methylpentene-1 (2-MP-1) glass at 77°K has been studied by electron spin resonance (esr) methods. The esr spectra due to trapped electrons and an allyl-type radical are observed. When biphenyl is present, the esr spectrum of the biphenyl anion replaces that of trapped electrons. The results suggest that the allylic radical is formed *via* isomerization of the parent ion (2-MP-1)⁺ \rightarrow (2-MP-2)⁺. An interesting ultraviolet photoinduced conversion of the allylic radical to a different allylic radical is observed at 77°K. No free radicals resulting from hydrogen atom addition to olefin are detected.

Introduction

This work is part of a series of investigations¹⁻³ in which electrons and free radicals, trapped in organic glasses during γ radiolysis at low temperature, are studied by electron spin resonance (esr) spectroscopy. Our previous measurements, on trapped electrons and radicals or radical ions in irradiated 2-methyltetrahydrofuran (MTHF), demonstrated that esr data not only provide a check on data obtained by optical ab-

sorption spectrophotometry⁴ but also yield additional information. Hence, it was decided to study the radiolysis of an olefinic compound in which trapped electrons have been observed.

- (1) D. R. Smith and J. J. Pieroni, *Can. J. Chem.*, **42**, 2209 (1964).
- (2) D. R. Smith and J. J. Pieroni, *ibid.*, **43**, 876 (1965).
- (3) D. R. Smith and J. J. Pieroni, *ibid.*, **43**, 2141 (1965).
- (4) M. R. Ronayne, J. P. Guarino, and W. H. Hamill, *J. Am. Chem. Soc.*, **84**, 4230 (1962).

The system described in this paper, irradiated 2-methylpentene-1 (2-MP-1), has been studied by Guarino and Hamill⁵ by spectrophotometric methods. After γ irradiation of 2-MP-1 at 77°K, they observed that the absorption spectrum has a maximum at 18,000 Å and a shoulder at 6800 Å. Both features are removed by postirradiation photolysis with light of wavelength longer than about 7500 Å. The oscillator strength of the 18,000-Å absorption is about 0.8. Addition of a solute such as naphthalene or biphenyl prior to irradiation causes the optical spectrum of the solute anion to appear while the intensity of the 18,000-Å absorption is reduced and that of the 6800-Å absorption is enhanced. The presence of 0.13 mole % biphenyl is sufficient to eliminate completely the 18,000-Å band. Guarino and Hamill assign the 18,000-Å absorption to trapped electrons and the 6800-Å absorption to the 2-MP-1 cation. Since $G(\text{biphenyl anion}) \approx 0.7$ in 2-MP-1 containing 0.15 mole % biphenyl, one can make the reasonable assumption that $G(e^-_{\text{trapped}})$ is about 0.7 in pure 2-MP-1. (G is the quantity of the species indicated formed per 100 eV absorbed by the sample.) This type of assumption was shown by esr measurements to be valid for these species in irradiated MTHF.³

Other studies of 2-MP-1 which are relevant have been based on esr measurements. In γ -irradiated 2-MP-1 at 77°K Ayscough and Evans observed the esr spectrum of an allyl-type radical but did not detect any absorption due to trapped electrons.⁶ Aditya and Willard performed ultraviolet photolysis of hydrogen iodide (HI) in 2-MP-1 at 77°K and observed the esr spectrum of an allyl-type radical. They did not detect the formation of any radicals *via* hydrogen addition to the olefin.⁷

The purpose of the work reported in this paper was to attempt to detect trapped electrons, to study and identify the allyl-type radical which is formed, and to obtain any additional information by esr measurements on 2-MP-1 after γ radiolysis at 77°K.

Experimental Section

The various techniques of sample preparation, cobalt-60 γ irradiation, dosimetry, and esr measurements are the same as described earlier.¹⁻³ The accuracy of concentration measurements is estimated to be $\pm 15\%$.³ Phillips research grade 2-MP-1 was used after treatment under vacuum with a sodium mirror and distillation under vacuum. The esr absorption signal from the irradiated Spectrosil sample tube was eliminated from the spectra in Figures 1A, B, C, and 2 by the esr difference technique.¹ The sample tube signal had been bleached out by ultraviolet photolysis in Figure 1D. Postirradiation photolysis with visible or near-

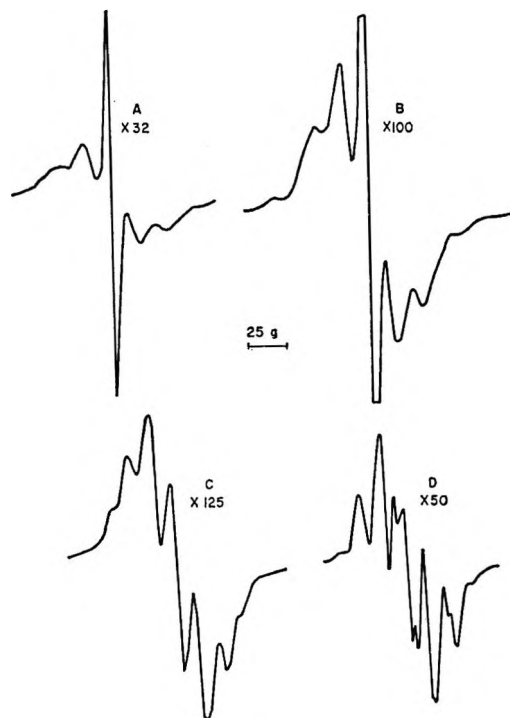


Figure 1. First-derivative esr spectra of irradiated 2-MP-1. The numbers are spectrometer gain settings: A and B, irradiated with a total dose of 6×10^{19} eV g⁻¹; C, after postirradiation illumination of the sample in A and B with visible light; D, after ultraviolet illumination of the sample in C.

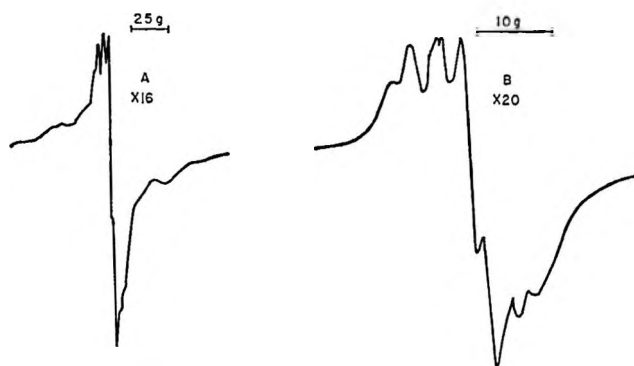


Figure 2. First-derivative esr spectra of irradiated 2-MP-1 containing 0.13 mole % biphenyl: A, total spectrum; B, spectrum of the biphenyl anion portion of A, obtained by the esr difference spectrum technique. Total dose 6×10^{19} eV g⁻¹.

infrared light was performed with light from a tungsten lamp transmitted by Corning filter 2-58 or 7-86. The former transmits above 6200 Å and the latter

(5) J. P. Guarino and W. H. Hamill, *J. Am. Chem. Soc.*, **86**, 777 (1964).

(6) P. B. Ayscough and H. E. Evans, *Trans. Faraday Soc.*, **60**, 801 (1964).

(7) S. Aditya and J. E. Willard, *J. Am. Chem. Soc.*, **88**, 229 (1966).

transmits between 13,000 and 28,000 Å. Post irradiation ultraviolet photolysis was performed by illuminating a sample for 15 min with light from a 4-w Mineralight Model SL 2537. The output of this lamp is predominantly the mercury resonance line at 2537 Å.

As an aid for interpretation of free-radical spectra, first-derivative esr spectra were calculated and printed by a Bendix G-20 computer using a modification of a program supplied by Snyder.⁸ Our allyl-type radical parameters for these calculations were based on the principles outlined by Poole and Anderson,⁹ Ayscough and Evans,⁶ and Symons.¹⁰

Results

At 77°K, 2-MP-1 forms a clear, colorless glass. After γ radiolysis the 2-MP-1 glass is colored blue. It exhibits an esr spectrum consisting of at least nine and possibly eleven partially resolved lines with a narrow, intense singlet superimposed on the central line. The average hyperfine splitting of the nine- or eleven-line spectrum is 14.7 gauss. This is illustrated at reduced sensitivity in Figure 1A to show the intensity of the singlet and at higher sensitivity in Figure 1B to show the details of the multiline spectrum more clearly. The intensities of both the singlet (corrected for postirradiation decay) and the multiline spectrum are proportional to dose up to 6×10^{19} ev g⁻¹ at a dose rate of 10^{18} ev g⁻¹ min⁻¹. At higher doses, decay during the irradiation period reduced the intensity of the singlet significantly.

Postirradiation photolysis of the sample at 77°K with visible or near-infrared light rapidly removes the blue color and the singlet esr absorption and leaves a pale green color. The esr spectrum remaining after photolysis with visible light is shown in Figure 1C. About 10% of the multiline absorption disappears during photolysis. The symmetry of the predominant multiline esr absorption suggests that there is mainly one free radical present, and we assume that its identity and concentration do not alter when the blue color and the esr singlet are eliminated by photolysis.

The intensity of the singlet esr line in 2-MP-1 was observed to decrease with time at 77°K. The decay kinetics are complex as in MTHF,² but the rate of decay is much more rapid. The line decreases in intensity by about 50% in 5 hr. The blue color diminishes, and the sample tends toward pale green at the same time as the singlet esr line is decaying. No significant change in the nature or intensity of the multiline spectrum was detected during this thermal decay.

This fairly rapid decay combined with the lower intensity of the singlet esr absorption (compared to

MTHF) renders it difficult to measure a precise microwave saturation curve. However, the microwave saturation curves of the singlet and multiline esr spectra in 2-MP-1 are qualitatively similar to those of the corresponding spectra in MTHF.² The esr singlet was resolved from the multiline spectrum by using the esr difference technique¹ and was found to be approximately gaussian as in MTHF.² The line was observed to be 4.0 gauss between derivative maxima, compared to 4.5 gauss in MTHF.²

At a dose of 6×10^{19} ev g⁻¹ in pure 2-MP-1, we observe that the yield of the species giving rise to the esr singlet is $G \simeq 0.7$ after correction for postirradiation decay. The yield of the free radical giving rise to the nine- or eleven-line esr spectrum is $G \simeq 0.8$.

One pure 2-MP-1 sample was γ irradiated, followed by photolysis with visible light. This left the esr spectrum of a radical as shown in Figure 1C. The sample was then illuminated for 15 min at 77°K with ultraviolet light. This caused the esr spectrum to alter to seven main lines having the same hyperfine splitting but somewhat better resolved as shown in Figure 1D. The integrated intensity of the esr spectrum was unchanged, and in a "blank" experiment no radicals were formed by 15-min ultraviolet photolysis (at 77°K) of 2-MP-1 which had not been γ irradiated.

In a 0.13 mole % biphenyl solution we observe that the esr singlet is completely replaced by the wider esr spectrum of the biphenyl anion as shown in Figure 2. Figure 2A is the observed spectrum. Figure 2B is the esr spectrum obtained as the difference between the spectra of two samples simultaneously present in the Varian TE₁₀₄ "dual" cavity.¹ One sample was the one containing biphenyl whose spectrum is shown in Figure 2A. The other was a sample of pure 2-MP-1 irradiated for the same length of time and then bleached with visible light. The difference spectrum is identical with the esr spectrum of the chemically prepared biphenyl anion.³ The yield of biphenyl anion was $G \simeq 0.7$, the same as $G(e^-_{\text{trapped}})$ in pure 2-MP-1.

Discussion and Conclusions

We have observed that the esr singlet is replaced by the spectrum of the biphenyl anion in the presence of biphenyl. Both are formed in a yield $G \simeq 0.7$ which agrees with the yield of trapped electrons measured by Guarino and Hamill.⁵ (The exact agreement is fortuitous since the inaccuracy of the esr method is at least $\pm 15\%$.) Photolysis with visible or near-in-

(8) S. H. Glarum and L. C. Snyder, *J. Chem. Phys.*, **36**, 2989 (1962).

(9) C. P. Poole, Jr., and R. S. Anderson, *ibid.*, **31**, 346 (1959).

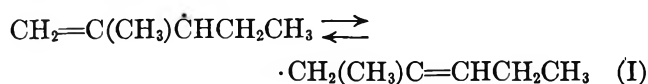
(10) M. C. R. Symons, *J. Chem. Soc.*, 277 (1959).

frared light removes the esr singlet and also the optical absorption assigned to trapped electrons. These results suggest that the narrow intense esr singlet is due to trapped electrons.

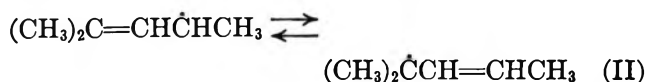
Ayscough and Evans⁶ did not observe the blue color or the esr singlet, possibly because of either decay before observation or microwave saturation of the singlet.

The observations on thermal decay, microwave saturation, and esr line width for electrons trapped in 2-MP-1 suggest similar conclusions to those derived for irradiated MTHF, *i.e.*, that electrons and free radicals are trapped in clusters or regions of relatively high local concentration.² The problem of measuring local unpaired electron concentrations has recently been discussed by Wyard,¹¹ Bullock and Sutcliffe,¹² and us.²

The spectrum of the predominant radical (Figure 1C) consists of at least nine and probably eleven lines (the outer lines being too weak to observe). The average hyperfine splitting of 14.7 gauss is typical of an allyl-type radical.^{6,13} It was found that the observed spectrum agreed well with a spectrum computed for a species in which the unpaired electron experiences equal hyperfine interaction with ten protons. On the basis of bond strengths, one would predict that allyl radical I would be formed from 2-MP-1.⁹



However, radical I would exhibit a seven-line spectrum due to equal hyperfine interaction with three α protons and one β proton and approximately double this hyperfine interaction with another β proton.^{6,9,10} Aside from the fact that we observe more than seven lines, the relative line intensities in the spectrum computed for radical I disagree with those observed. We suggest that the only allyl radical which could be formed from 2-MP-1 and which would give an esr spectrum involving equal hyperfine interaction with ten protons is II, possibly formed by isomerization of the positive ion (2-MP-1)⁺ to (2-MP-2)⁺ and subsequent loss of H⁺.



Ayscough and Evans⁶ also observed the esr spectrum of an allyl radical but assigned it to radical I. They measured a yield which agrees with our $G(\text{radical}) \simeq 0.8$.

From the change in the esr spectrum, it is apparent that ultraviolet photolysis induces a quantitative conversion from what we call radical II to a second allyl-type radical. The spectrum of this radical agrees

roughly with a computed spectrum using radical I as a model (except for partial resolution of lines in the observed spectrum). We suggest that either isomerization of II to I or formation of I *via* H abstraction from 2-MP-1 by II has been observed. Hydrogen abstraction by "hot" H atoms in 2-MP-1 results in an allyl radical esr spectrum similar to the one we have observed after ultraviolet photoinduced conversion of II to I. However, II may have been formed initially and then converted to I since ultraviolet photolysis of HI was being performed.⁷ Since radical I was observed to be thermally stable at 77°K, radical II must not have been formed by thermal isomerization of I. Hence, it may have been formed by isomerization of the primary cation as mentioned above. In support of this postulate, directly analogous observations and conclusions were obtained in irradiated 2-methylbutene-1 glass¹⁴ at 77°K.

It is interesting that there is no evidence of hydrogen atom addition to the double bond in 2-MP-1 irradiated at 77°K, or when HI is photolyzed in 2-MP-1 at 77°K.⁷ There are two radicals which might be formed by hydrogen atom addition, but the esr spectrum of the radical $\cdot\text{C}(\text{CH}_3)_2\text{CH}_2\text{R}$ would have ten lines separated by about 23 gauss and that of the radical $\cdot\text{CH}_2\text{CH}(\text{CH}_3)\text{R}$ would have five lines separated by about 20 gauss.¹⁵ There is no indication of either spectrum so no significant concentration of these species is formed. In contrast, irradiation of unsaturated carboxylic acids at room temperature¹⁶⁻¹⁹ and of vinyl monomers at low temperature²⁰ results in radical formation by hydrogen atom addition to the double bond.

Since $G(\text{II}) \simeq G(e^-_{\text{trapped}})$, it is possible that trapping has effected separation of most of the electrons from their parent ions and that no appreciable dissociation of excited molecules has occurred. Dissociation of an excited molecule to a radical and an $\cdot\text{H}$ atom result in $G(\text{radical}) > G(e^-_{\text{trapped}})$, especially since the $\cdot\text{H}$ atom

(11) S. J. Wyard, *Proc. Phys. Soc. (London)*, **86**, 587 (1965).

(12) A. T. Bullock and L. H. Sutcliffe, *Trans. Faraday Soc.*, **60**, 2112 (1964).

(13) B. Smaller and M. S. Matheson, *J. Chem. Phys.*, **28**, 1169 (1958).

(14) D. R. Smith and J. J. Pieroni, to be published.

(15) P. B. Ayscough and C. Thomson, *Trans. Faraday Soc.*, **58**, 1477 (1962).

(16) A. L. Kwiram and H. M. McConnell, *Proc. Natl. Acad. Sci. U. S.*, **48**, 499 (1962).

(17) O. H. Griffith and H. M. McConnell, *ibid.*, **48**, 1877 (1962).

(18) R. J. Cook, J. R. Rowlands, and D. H. Whiffen, *Mol. Phys.*, **7**, 57 (1963).

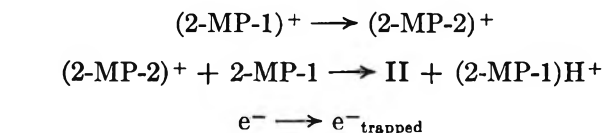
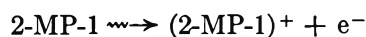
(19) M. Fujimoto, *J. Chem. Phys.*, **39**, 846 (1963).

(20) R. Marx, Thesis, Paris, 1963, quoted by R. Bensasson, M. Durup, A. Dworkin, M. Magat, R. Marx, and H. Szwarc, *Discussions Faraday Soc.*, **36**, 177 (1963).

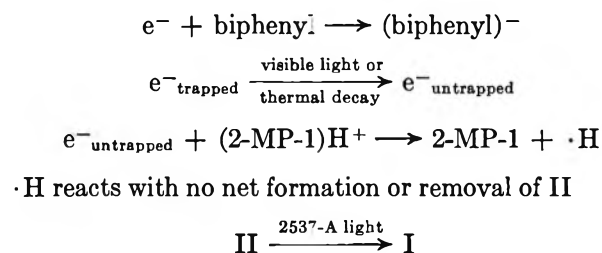
might form even more radicals by abstraction from a matrix molecule. However, the possibility cannot be ruled out that some excited molecules have dissociated and the enhanced radical yield canceled out *via* H atom combination with other radicals. There is no reason to believe that radical II is a cation so there must also be a similar yield of nonparamagnetic positive ions trapped in the matrix.

Ayscough and Evans have discussed the possible fate of the positive charge in irradiated solid olefins.⁶ The primary ion may transfer H⁺ to a neighboring olefin molecule to form the allyl radical and a nonparamagnetic cation. However, if this cation is neutralized when a trapped electron disappears (during photolysis or thermal decay) either (i) a saturated free radical or (ii) olefin + ·H would be formed.²¹ There is no evidence in favor of (i), and, if (ii) occurs, the ·H must disappear without net formation or destruction of allylic free radicals to be consistent with our observations.

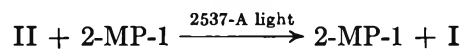
Our observations and tentative conclusions regarding the radiolysis of 2-MP-1 at 77°K are conveniently summarized by the reaction scheme²²



or



or



II and I are thermally stable at 77°K.

Acknowledgment. We wish to acknowledge a valuable discussion with Dr. B. Mile and Dr. J. Bennett at the Shell Research Centre, Thornton, U. K.

(21) F. Williams, *Quart. Rev.* (London), **17**, 101 (1963).

(22) \rightsquigarrow means "produces when subjected to ionizing radiation."

The Electrical Conductivity of Solutions of Metals in Their Molten Halides.

VIII. Alkaline Earth Metal Systems¹

by A. S. Dworkin, H. R. Bronstein, and M. A. Bredig

Chemistry Division, Oak Ridge National Laboratory, Oak Ridge, Tennessee (Received February 11, 1966)

In the alkaline earth metal-metal halide systems $\text{MX}_2\text{-M}$ ($\text{M} = \text{Ca}$ or Sr , $\text{X} = \text{Cl}$, Br , or I), the concentration dependence of the specific conductivity, κ , is similar to that in the sodium systems where the value of $d\kappa/dN_{\text{M}}$ decreases as the metal concentration increases. For explanation, an equilibrium $2\text{M}^{2+} + 2e \rightleftharpoons (\text{M}_2)^{2+}$ is assumed similar to $2\text{Na}^+ + 2e \rightleftharpoons \text{Na}_2$ for the sodium systems. The doubly charged alkaline earth molecule ions $(\text{M}_2)^{2+}$ contain M in a dimer of oxidation state I rather than zero (Na_2). The species $(\text{M}_2)^{2+}$ are analogous in electronic structure to the neutral Na_2 molecules. Their equilibrium with the F-center-like electrons is concentration dependent. The systems $\text{BaBr}_2\text{-Ba}$ and $\text{BaI}_2\text{-Ba}$, on the other hand, are similar to the potassium systems. They give an increasing slope of specific conductivity with increasing metal concentration. This is attributed to the much lower stability of the dimer traps K_2 and $(\text{Ba}_2)^{2+}$. As a result, electron orbital overlap occurs at lower metal concentration. Observed salt freezing point depressions agree with this interpretation if solubility of the metal in the solid is considered.

Introduction

The specific electrical conductivity κ of solutions of calcium in calcium chloride was found to increase as the metal concentration, N_{M} , is increased.² However, as in the sodium-sodium halide melts, $d\kappa/dN_{\text{M}}$ decreases as N_{M} increases. This was attributed to the gradual trapping, in pairs, of the single relatively mobile, probably F-center- or anion-like, electrons³ by the reaction $2e^- + 2\text{Ca}^{2+} \rightleftharpoons (\text{Ca}_2)^{2+}$, *i.e.*, through formation of molecule ions, $(\text{Ca}_2)^{2+}$ (*cf.* Hg_2^{2+} and Cd_2^{2+}). These represent the dimeric form of the otherwise uncommon oxidation state (I) of calcium. Their equilibrium with the mobile electrons and the normal cations Ca^{2+} depends on metal concentration. The explanation for the observed conductance behavior was thus analogous to that proposed earlier⁴ for solutions of sodium metal in molten sodium halides. There the "single bond" of the neutral group I metal molecules, Na_2 (oxidation state zero, M^0), presumably of similar electronic structure as the proposed group II metal molecule ions, $(\text{Ca}_2)^{2+}$, was proposed to represent the state in which the electrons are trapped in pairs. Preliminary measurements in the Sr-SrCl_2 solutions² indicated a situation intermediate between that of the Na-NaX and K-KX sys-

tems.⁴ The K-KX systems exhibit an accelerating rise in conductivity with increasing metal concentration. This is consistent with the assumption that in the solution K_2 molecules are less stable than Na_2 molecules as they are known to be in the vapor state. The conductivity of the Ba-BaX_2 systems, which like the K-KX systems exhibit far greater metal solubility than the Na-NaX and Ca-CaX_2 systems, was predicted² to behave similarly to that of the K-KX systems.

In the present study, we have measured the specific conductivity of solutions of Ca , Sr , and Ba in their respective bromides and iodides and made additional conductivity measurements in the Sr-SrCl_2 system. These measurements allow a comparison with the alkali and rare earth metal-halide systems.^{2,5,6} Freez-

(1) Research sponsored by the U. S. Atomic Energy Commission under contract with Union Carbide Corp.

(2) A. S. Dworkin, H. R. Bronstein, and M. A. Bredig, *Discussions Faraday Soc.*, **32**, 188 (1961); see also M. A. Bredig, *ibid.*, **32**, 257 (1961).

(3) (a) M. A. Bredig, J. W. Johnson, and W. T. Smith, Jr., *J. Am. Chem. Soc.*, **77**, 307 (1955); (b) K. S. Pitzer, *ibid.*, **84**, 2025 (1962).

(4) H. R. Bronstein and M. A. Bredig, *ibid.*, **80**, 2077 (1958); *J. Phys. Chem.*, **65**, 1220 (1961).

ing-point depression measurements were also made in an attempt to derive from the activity of the solvent salt thus obtained further information on the nature of the solute species. Previous data were incomplete and based mainly on gross phase diagrams of doubtful reliability.

Experimental Section

The molybdenum parallel electrode assembly used to measure the conductivity of the metal-metal halide solutions, the sapphire capillary cell used with the pure salts, and the experimental procedure have been described in detail previously.² The freezing-point depression measurements were made in a manner also reported earlier⁷ except that the solutions were held in tantalum metal capsules about 3 in. in length and 0.63 in. in diameter with a thermocouple well protruding about 0.75 in. into the solution. The capsules were filled and welded in a drybox under helium.

The salts were prepared from reagent alkaline earth carbonates or hydroxides which were dissolved in the appropriate aqueous acids. The hydrates were crystallized, crushed, and vacuum-desiccated at room temperature over P_2O_5 for 2 days after which they were dehydrated by gradual heating to about 400° over a period of 3 days. The chlorides and bromides were then melted in quartz in an atmosphere of their respective dry halogen gases, purged with Ar, and filtered into a quartz bulb. The iodides were melted under vacuum in a molybdenum boat. All of the salts and metals were free of foreign metals as determined spectrographically. The halides showed no alkalinity from pyrohydrolysis.

Results and Discussion

The specific conductivity of the pure salts as measured with the sapphire capillary cell agreed with the measurements of Bockris, *et al.*,⁸ to within $\pm 1\%$.

The results of the specific conductivity measurements for the solutions of the metal in the salt are given in Table I and Figure 1. Measurements were discontinued in the barium systems at metal concentrations far below saturation when the electrical resistance of the solution became so low that a large experimental error was introduced by the greatly increased relative contribution of the electrode resistance to the total resistance. (The Ba-BaCl₂ system could not be measured in the present apparatus because of the high melting temperature of BaCl₂, 960°). Saturation of the salt solution with metal was determined in samples taken from the liquid salt phase after excess metal had been added. This concentration agreed well in most cases

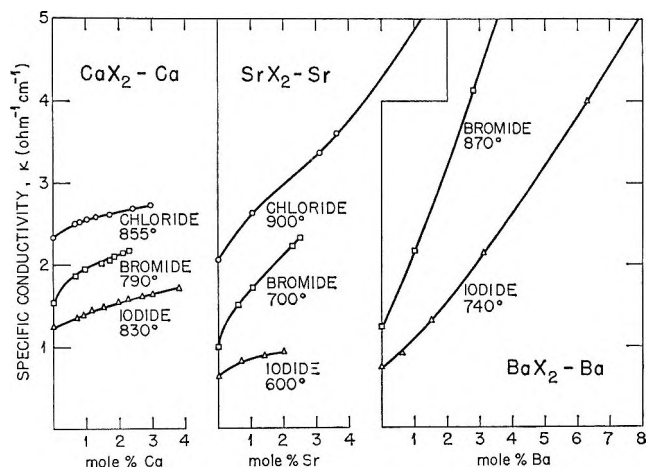


Figure 1. Specific conductivity in molten alkaline earth halides as a function of metal solute concentration. (For the SrCl₂-Sr and the barium systems, measurements extended beyond data shown, cf. Table I.)

Table I: Specific Conductivity, κ , in Alkaline Earth Metal-Halide Systems

Mole % metal	κ , ohms ⁻¹ cm ⁻¹	Mole % metal	κ , ohms ⁻¹ cm ⁻¹	Mole % metal	κ , ohms ⁻¹ cm ⁻¹
Ca-CaBr ₂ at 790°		Sr-SrCl ₂ at 900°		Ba-BaBr ₂ at 870°	
0	1.53	0	2.05	0	1.24
0.65	1.86	1.05	2.63	1.0	2.16
0.95	1.94	3.1	3.36	2.8	4.13
1.45	2.02	3.6	3.6	5.2	6.9
1.70	2.05	7.2 (satd)	5.4	24.0 (satd)	...
1.85	2.10				
2.1	2.14				
2.3 (satd)	2.16				
Ca-CaI ₂ at 830°		Sr-SrBr ₂ at 700°		Ba-BaI ₂ at 740°	
0	1.24	0	0.99	0	0.75
0.70	1.35	0.6	1.50	0.62	0.91
0.90	1.38	1.05	1.71	1.5	1.32
1.15	1.44	2.25	2.22	3.1	2.14
1.50	1.48	2.5 (satd)	2.32	6.3	4.0
1.95	1.54			11.6	9.2
2.25	1.57	Sr-SrI ₂ at 600°		16.2	18.8 ± 1
2.7	1.61	0	0.63	19.8	33.0 ± 3
3.0	1.64	0.7	0.82	22.0 (satd)	...
3.8 (satd)	1.71	1.4	0.89		
		2.0 (satd)	0.93		

(5) A. S. Dworkin, R. A. Sallah, H. R. Bronstein, M. A. Bredig, and J. D. Corbett, *J. Phys. Chem.*, **67**, 1145 (1963).

(6) A. S. Dworkin, H. R. Bronstein, and M. A. Bredig, *ibid.*, **67**, 2715 (1963).

(7) J. W. Johnson and M. A. Bredig, *ibid.*, **62**, 604 (1958).

(8) J. O'M. Bockris, E. H. Crook, H. Bloom, and N. E. Richards, *Proc. Roy. Soc. (London)*, **A255**, 558 (1960).

with that concentration at which the conductivity remained constant despite further additions of metal.

As can be seen in Figure 1, the rate of increase of the specific conductivity with increasing metal concentration decreases in the calcium and strontium systems. The conductivity in the barium systems shows an accelerating rise as predicted² which is thought to be caused by a relatively lower stability of $(\text{Ba}_2)^{2+}$ ions, leading to much higher concentrations of single, less localized mobile electrons and also slightly higher concentrations of metal ions, from the equilibrium $(\text{Ba}_2)^{2+} \rightleftharpoons 2\text{Ba}^{2+} + 2e^-$. The results for the Sr-SrCl₂ solutions are slightly different from the preliminary data² in that above 2 mole % metal a reversal in curvature is now observed, similar to that in the Na-NaBr and Na-NaI systems at similarly high metal concentrations and temperatures.⁴ This reversal was attributed to the increasing importance of the general orbital overlap of the metal electrons (beginning formation of a "conduction band") as compared with the trapping of electrons in localized two-electron bonds.

It is quite reasonable to assume that even the proposed alkaline earth molecule ions Ca_2^{2+} and Sr_2^{2+} are not very stable but in dilute solution dissociate into M^{2+} and two mobile, F-center-like electrons which are responsible for the conductivity increase. This type of electrons would be expected to behave thermodynamically as more or less distinctly separate particles.^{2,3b} As a result, measurements of the depression of the freezing points of the salts on the first additions of metal should yield a cryoscopic number n of 2, from $n = [(T_m - T)/N_{\text{metal}}](\Delta S_m/RT_m)$. With increasing N_{metal} , n should decrease from 2 toward 1 with a rate depending mainly on the equilibrium $2e^- + 2\text{M}^{2+} \rightleftharpoons (\text{M}_2)^{2+}$, *i.e.*, the liquids should be convex to the concentration axis. Unfortunately, much supercooling coupled with the short concentration range available for measurement weakened the reliability of the observed freezing-point lowering. This and the possibility of heat-of-mixing effects as well as of metal solubility in the solid salt prohibits a detailed quantitative evaluation of the liquidus curvature in terms of the equilibrium proposed above. However, as can be seen from the example shown in Figure 2, while the existence of this equilibrium as suggested by the conductivity results is not clearly supported, it is not contradicted by the cryoscopic measurements. For Sr-SrCl₂ ($\Delta S_m = 3.39$ eu/mole), n appeared to be slightly less than unity. (Earlier,² we had obtained $n = 2$ on the basis of $\Delta S_m = 7$ eu/mole, estimated previous to our calorimetric measurements⁹ and discovery of the solid-state transition.¹⁰ In this case, as in the system Ca-CaF₂,¹¹ high solubility of the metal in the solid salt SrCl₂¹² which also has the fluorite

type of crystal structure most likely interferes with the simple interpretation of the melting-point depression. On the basis of vapor pressure measurements for the systems M-MCl₂ (M = Ca, Sr, and Ba), van Westenburg and Peterson¹³ recently proposed that the dissociation (ionization) of the dissolved alkaline earth metal according to $\text{M} \rightarrow \text{M}^{2+} + 2e^-$ was complete. (Alternately but less likely,^{2,13} the oxidation-reduction reaction $\text{M} + \text{M}^{2+} \rightarrow 2\text{M}^+$ would also produce two "new" particles, *i.e.*, particles not present in the pure solvent salt.) This method has the great advantage of giving directly the activity of the solute and is of course not affected by the problem of solid solutions. No tendency to electron interaction such as formation of $(\text{M}_2)^{2+}$ is shown in these measurements below 3, 7, and 5 mole % metal in the Ca, Sr, and Ba systems, respectively. Our conductivity and cryoscopic measurements on the Ca and Sr chloride solutions do not seem to suggest much more electron interaction than might be compatible with a reasonably limited sensitivity of the vapor pressure measurements to such interaction. A comparison of the bromide systems which show intensive curvature of the conductivity *vs.* concentration curves (Figure 1), but for which vapor pressure measurements are not available as yet, will be more significant.

The eutectic compositions obtained from the freezing-point data are in good agreement with those derived from our conductivity and solubility measurements at slightly higher temperatures. Agreement is also good with available data reported by Staffansson¹⁴ and by Peterson and Hinkebein.¹⁵ On the other hand, various data of the older literature, and more recent phase diagrams proposed by Emons, *et al.*,¹⁶ and including the suggestions that ions such as Ca_3^{2+} and even Sr_4^{2+} occur, are totally at variance with our results as well as with those of the other investigators mentioned. The phase diagrams of the alkaline earth metal-metal

(9) A. S. Dworkin and M. A. Bredig, *J. Phys. Chem.*, **67**, 697 (1963).

(10) A. S. Dworkin and M. A. Bredig, *J. Chem. Eng. Data*, **8**, 416 (1963).

(11) B. D. Lichter and M. A. Bredig, *J. Electrochem. Soc.*, **112**, 506 (1965).

(12) E. Mollwo, *Nachr. Wissensch. Ges. Göttingen II*, **1** (6), 79 (1934).

(13) J. A. van Westenburg, Iowa State University of Science and Technology, Abstracts of Doctoral Theses, pp 1129-1130; University Microfilms, Inc., Ann Arbor, Mich., Order No. 64-9291.

(14) L. Staffansson, Ph.D. Thesis, London, 1960.

(15) D. Peterson and J. A. Hinkebein, *J. Phys. Chem.*, **63**, 1360 (1959); J. A. Hinkebein, Ph.D. Thesis, Iowa State College, *Dissertation Abstr.*, **19**, 1932 (1958), University Microfilms, Inc., Ann Arbor, Mich., Card No. 58-7557.

(16) H. H. Emons, *et al.*, *Z. Anorg. Allgem. Chem.*, **323**, 114 (1963); *Z. Chem.*, **2**, 313, 377 (1962).

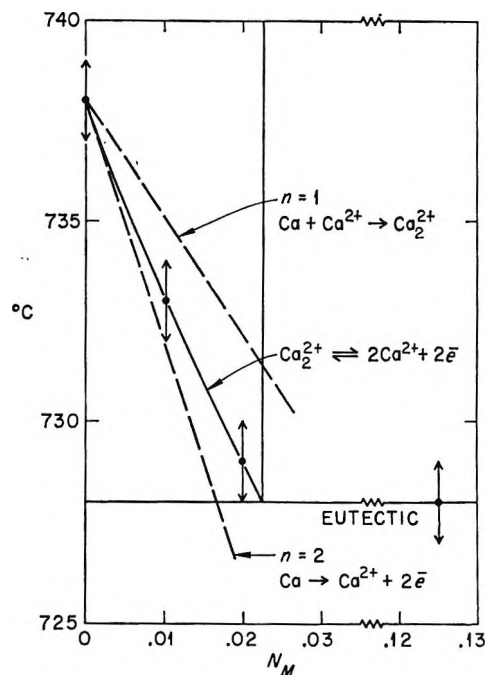


Figure 2. Salt melting point depression in the calcium-calcium bromide system.

halide systems will shortly be discussed by us in greater detail elsewhere on the basis of our own measurements.

It is of considerable interest to consider the behavior of the mobile electrons in the most dilute solutions where their mutual interaction is minimal. Figure 1 shows a steeper increase in conductivity on the addition of metal to the salt to occur in the bromide systems of calcium and strontium than in either the chloride or iodide systems. Table II shows this in a slightly different fashion, namely, through the values of the equivalent conductance of the solute metal Λ_M (or, at infinite dilution, Λ_M^∞). As first defined elsewhere,⁴ $\Lambda_M \equiv (\kappa_{\text{soln}} V_{\text{soln}} - (1 - N_M) \kappa_{\text{salt}} V_{\text{salt}}) / N_M$ (or $\Lambda_M^\infty \approx d\kappa/dN_M$ (lim $N_M \rightarrow 0$) $\times V_{\text{salt}}$), where V is the equivalent volume. The values of Λ_M^∞ for the bromide solutions far exceed those of both the corresponding chloride and iodide solutions. A much weaker but qualitatively somewhat similar effect had been found in the alkali metal systems also listed in Table II, the main difference being that for the alkali metals Λ_M^∞ in the iodide systems is still larger than Λ_M^∞ in the corresponding bromide systems.⁴ However, there the increase to the iodides is not nearly as large as the trend for the change from the fluoride to the bromide systems would lead one to expect (for NaI-Na: $\sim 16,000$ instead of an extrapolated value of at least 25,000 and for KBr-K: 8100 instead of at least 15,000 $\text{ohm}^{-1} \text{cm}^2 \text{equiv}^{-1}$).

Table II: Estimated Metal Solute Equivalent Conductance at Infinite Dilution, Λ_M^∞ (mho cm^2), in Molten Halide Solutions, M-MX₂ and M-MX

M	F	Cl	Br	I
Ca	...	890	4,200	860
Sr	...	1600	5,100	1,570
Ba	2,830	1,300
Na	...	6000	13,000	16,000
K	800	2800	6,500	8,100

The occurrence of the maximum of electron mobility in the bromide systems, or of the lag in the iodide systems, is probably of rather complex origin. Conceivably, it is mainly connected with the divergent influences, upon the electron mobility, of the size and of the polarizability of the halide ion. With increasing atomic number of the halide ion, its size is thought to inhibit increasingly the motion of electrons by increasing their jump distance, while its simultaneously increasing polarizability facilitates such motion. That the effect is so much stronger in the alkaline earth than in the alkali metal systems may be due to the much higher ratio of the number of halide ions to that of the metal ions.

Another effect is apparent from Table II and Figure 3. In the alkaline earth bromide and iodide systems, there is a drop of Λ_M^∞ in going from the strontium to the barium solutions after a rise in going from the calcium to the strontium systems. (A similar effect would probably have been observed for the barium chloride solutions, had they been accessible to measurement.) This behavior of the alkaline earth solutions may be considered similar to that of the alkali metal systems. Here Λ_M^∞ was also found to decrease in going from the Na (corresponding to Sr) to the K (corresponding to Ba) systems. However, the possible correspondence of the lithium to the calcium solutions with respect to a low Λ_M^∞ has not been accessible to measurement because of the low solubility of Li in its halides. As in the case of the effect of the halide ion above, a tentative explanation may be given. The size of the cation may influence the electron mobility in two opposing ways thus leading to the conductivity maximum at Na or Sr. For larger cations, the average distance for electron jumps from cation to cation is greater. Greater distance means smaller jump probability.¹⁷⁻¹⁹ On the other hand, the tighten-

(17) W. F. Libby, *J. Phys. Chem.*, **56**, 863 (1952).

(18) S. A. Rice, *Discussions Faraday Soc.*, **32**, 188 (1961).

(19) D. O. Raleigh, *J. Chem. Phys.*, **38**, 1677 (1963).

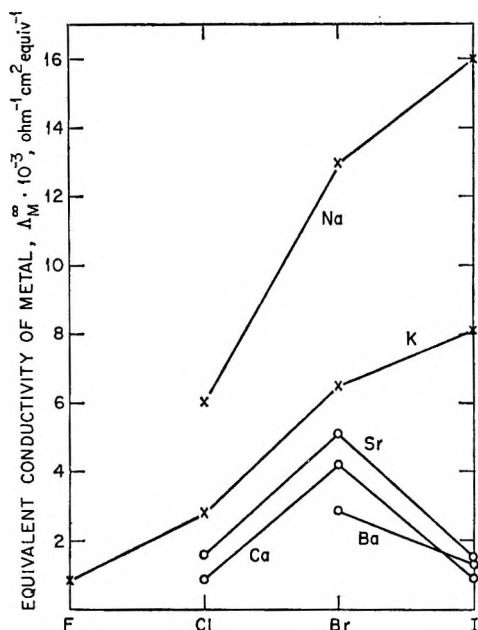


Figure 3. Estimated metal solute equivalent conductance at infinite dilution, Λ_M^∞ (mho cm^2), in molten halide solutions, M-MX_2 and M-MX .

ing of the electron shell of the anion in the field of the larger cations is smaller; *i.e.*, the anion polarizability

which controls the bridging action of the anion in electron transfer¹⁷ is greater.

Finally, a comparison of our results with a very recent attempt to study the electrical conductance of calcium solutions in molten calcium chloride by Emons and Richter²⁰ shows their results to be considerably different from ours, more so, in fact, than their Figure 4 which includes but misrepresents our early data² would seem to indicate. For instance, for $\Lambda_{\text{Ca}^\infty}$ one obtains from their data at 850° the value of only 200 $\text{mho cm}^2/\text{equiv}$ of calcium metal, not very much larger than some ionic equivalent conductances in molten salts, and only one-fifth of our value of nearly 1000 (Table II). Their apparatus did not permit sampling the solution during the measurements. The use of an inert gas flow from an inlet immediately above the crucible suggests that considerable losses of somewhat volatile calcium metal from the melt to colder parts of the apparatus may have occurred.

Acknowledgment. Our thanks are due to D. E. Lavalley for the preparation of the pure anhydrous salts used in our measurements.

(20) H. H. Emons and D. Richter, *Z. Anorg. Allgem. Chem.*, **339**, 91 (1965).

The Saturation Thermodynamic Functions for Bismuth Chloride

from 298°K to the Critical Point¹

by Daniel Cubicciotti, H. Eding, F. J. Keneshea, and J. W. Johnson

Stanford Research Institute, Menlo Park, California 94025 (Received February 14, 1966)

The saturation enthalpy increments above room temperature for BiCl_3 in its condensed phases were determined with a drop calorimeter to within 75° of the critical point. These were combined with previously determined enthalpies of vaporization to obtain values for the saturated vapor, and the data were extrapolated to the critical point. Saturation entropies for vapor and condensed phases were calculated from the enthalpies. The internal energy departures of the gas from ideal values were evaluated and compared with similar data for molecular fluids.

Introduction

Earlier reports from this laboratory have presented the vapor pressures² and the volume changes³ on vaporization for BiCl_3 up to its critical point and the enthalpies² of vaporization calculated from them. To extend this work, we have measured the heat evolved by samples of BiCl_3 when cooled from the liquid at high temperature to room temperature. From the heat evolved, the enthalpy and entropy increments above room temperature are calculated for the condensed phases under saturation conditions. From these and the enthalpies of vaporization, the functions for the saturated gas phase are derived.

Measured Heat Increments

Experimental Details

Samples of BiCl_3 sealed in quartz glass ampoules were heated to various temperatures, some as high as 1110°K , then dropped into a Parr calorimeter at room temperature to measure the heat evolved. The details of the calorimeter are described in an earlier paper.⁴

The samples were sealed in heavy-walled quartz glass ampoules to withstand the vapor pressure of the BiCl_3 , which reached as much as 70 atm in some of the measurements. Because of the large amount of glass required for strength, only a fraction of the heat liberated from the samples originated from the BiCl_3 ; the rest was from the quartz glass. Therefore, the accuracy of the measurements was limited. The

amounts of quartz glass and BiCl_3 in each of the six samples are given in Table I. A small part of the heat liberated by the sample was due to the condensation of BiCl_3 from the vapor. The amount of heat from that source was calculated for each drop from the known liquid and vapor densities, the volumes of the ampoules, and the known enthalpy of vaporization. It was assumed that all the vapor condensed at the drop temperature. Since the maximum correction was less than 0.5% of the total heat, the exact calculation using

Table I: Details of Samples Used

Sample no.	Wt of BiCl_3 , g	Wt of quartz, g	Internal vol. of ampoule, cc	Symbol used in Figure 1
1	3.8088	6.1521	1.7120	⊕
2	4.6110	5.9856	1.7224	●
3	4.7463	5.9236	1.6638	⊙
4	4.9224	6.1514	1.7688	⊕
5	4.8405	6.1879	1.7082	⊖
6	9.4603	3.8254	3.1743	○

(1) This work was made possible by financial support from the Research Division of the U. S. Atomic Energy Commission under Contract No. AT(04-3)-106.

(2) J. W. Johnson, W. Silva, and D. Cubicciotti, *J. Phys. Chem.*, **69**, 3916 (1965).

(3) J. W. Johnson and D. Cubicciotti, *ibid.*, **68**, 2235 (1964).

(4) D. Cubicciotti and H. Eding, *ibid.*, **69**, 2743 (1965).

the integrated heat of condensation was considered superfluous. For drops from temperatures below about 800°K this correction was negligible.

The heat liberated by the quartz ampoules was obtained from measurements on samples of quartz glass from the same batch of glass used to make the ampoules. The enthalpy increments measured for that quartz glass were very close to those obtained by Lucks, *et al.*⁵ An equation which fits both sets of data within about 1% from 290 to 1130°K is

$$(H_T - H_{298}) \text{ (cal/g)} = 0.2313T + 3.229 \times 10^{-5}T^2 + 7.619 + 10^3/T - 97.39$$

The material used was reagent grade BiCl₃ which was distilled into the ampoules in a stream of dry oxygen at 300°; the oxygen was removed by evacuation and the ampoules were sealed off under vacuum.

The resultant heat increments for BiCl₃ in condensed phases (*i.e.*, heat liberated when cooled from T to 298°K) are shown as circles in Figure 1. The different types of circles refer to different samples which are identified in Table I. The data obtained in the present work agree quite well with those reported by Topol, Mayer, and Ransom⁶ and those of Bredig.⁷ The results of Walden and Smith,⁸ however, are substantially lower. We feel that the purity of the material used by these last workers is questionable, as they used reagent grade BiCl₃ without purification. Since BiCl₃ is very hygroscopic, we suspect their values were low because of an impurity—possibly BiOCl.

Enthalpy Increments

The heat evolved by a sample in equilibrium with its vapor when cooled from T to 298°K is equal to the integral⁹

$$\int_{298}^T C_s dT = \int_{298}^T T \left(\frac{\partial S}{\partial T} \right)_s dT \quad (1)$$

The temperature derivative of that quantity gives C_s , the saturation heat capacity. The quantity C_s is related to the saturation enthalpy by

$$\left(\frac{\partial H}{\partial T} \right)_s = C_s + V \left(\frac{\partial P}{\partial T} \right)_s \quad (2)$$

$$= C_p + V \left[1 - \frac{T \left(\frac{\partial V}{\partial T} \right)_p}{V} \right] \left(\frac{\partial p}{\partial T} \right)_s \quad (3)$$

For ordinary liquids below the boiling point the last term is negligible and drop calorimeter measurements give the enthalpy increments at constant pressure as well as the saturation enthalpy increments. At temperatures well above the boiling point, the differ-

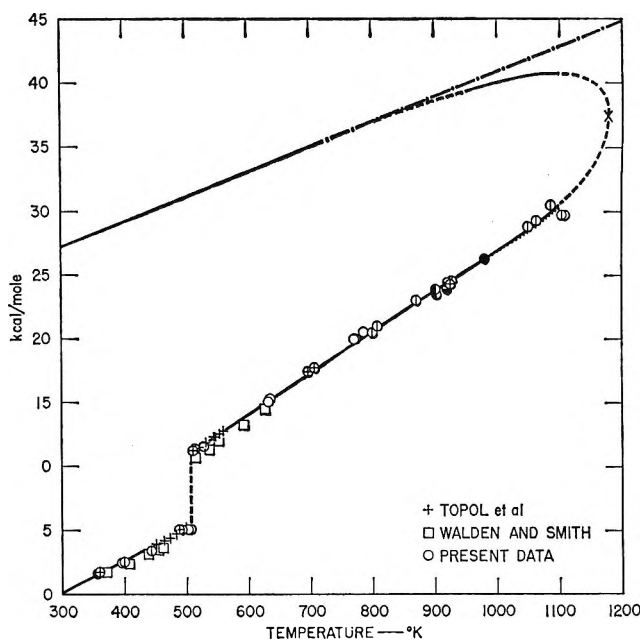


Figure 1. Enthalpy of BiCl₃ above 298°K. Data points are heats evolved in calorimeter. Different types of circles refer to different samples in present data (see Table I). Dotted curve and full curve at lower temperatures are smoothed representation of heats evolved. Full and dashed curve represents derived saturation enthalpies. Dot-dash curve represents calculated standard enthalpy of ideal gas. Reference state is solid BiCl₃ at 298°K. Critical point is shown by cross.

ences become significant, although small. Since we have no information about the compressibility of the liquid, we are not able to evaluate the constant pressure heat capacity or enthalpy increments. We can only evaluate the saturation quantities.

The heats evolved for drops from various temperatures are shown as data points in Figure 1. The enthalpy increments above 298°K, derived from the data, are given in Table II. Below 800°K the data were well represented by two straight lines (one for the solid and another for the liquid). In that range C_p and C_s are the same within an experimental error. The values obtained from our data for C_p (or C_s) were 25.6 eu

(5) C. F. Lucks, J. Matloch, and J. A. VanVelzor, U. S. Air Force Technical Report 6145, Part III, March 1954 (AD 95406).

(6) L. E. Topol, S. W. Mayer, and L. D. Ransom, *J. Phys. Chem.*, **64**, 862 (1960).

(7) M. A. Bredig, *ibid.*, **63**, 978 (1959).

(8) G. E. Walden and D. F. Smith, U. S. Bureau of Mines, Report of Investigations No. 5859, Mines Bureau, Pittsburgh, Pa., 1961.

(9) For a discussion of thermodynamics under saturation conditions see: E. A. Guggenheim, "Thermodynamics," 3rd ed, North-Holland Publishing Co., Amsterdam, 1957, p 149; or J. S. Rowlinson, "Liquid and Liquid Mixtures," Academic Press, Inc., New York, N. Y., 1959, p 16 ff.

for the solid and 32.6 eu for the liquid. Topol, Mayer, and Ransom found 26.1 and 34.3, respectively. The enthalpy of fusion obtained from our data was 5.71 ± 0.1 kcal/mole, in good agreement with 5.68 ± 0.08 reported by Topol, Mayer, and Ransom and 5.50 ± 0.15 reported by Bredig.

Table II: Standard Thermodynamic Functions of BiCl_3 in Condensed Phases below 800°K^a

T , $^\circ\text{K}$	$H^\circ_T - H^\circ_{298}$, kcal/mole ^b	S°_T , eu	$-(F^\circ_T - H^\circ_{298})/T$, eu ^b
298	...	41.70	41.70
350	1.33	45.82	42.01
400	2.61	49.24	42.70
450	3.89	52.25	43.59
500	5.17	54.95	44.60
506.7 (s)	5.34	55.30	44.74
506.7 (l)	11.05	66.57	44.74
550	12.47	69.25	46.56
600	14.10	72.08	48.57
650	15.73	74.68	50.48
700	17.36	77.10	52.26
750	18.99	79.35	54.03
800	20.62	81.45	55.67

^a Below 800°K the saturation values (*i.e.*, values for the substance under its own vapor pressure only) are the same, within experimental error, as the standard-state values (*i.e.*, under 1 atm pressure). The precision quoted in the table is greater than the accuracy of any one value but it is useful for differences between values. ^b The reference state for all values in the second and fourth columns is the solid at 298°K .

Above about 800°K , the heats evolved were better represented by a curved line, although the scatter of the data near 1100°K makes the curve difficult to draw. The curve is shown in Figure 1 as a full line from 800 to 950°K (where it is not sensibly different from the enthalpy curve) and as a dotted line from 950 to 1100°K . The slope of that curve at any temperature was taken as C_σ , the saturation heat capacity, according to the discussion above. The saturation enthalpy increment $(H_T - H^\circ_{298})_\sigma$ was obtained by a summation of eq 2. That is, for 10° intervals from 800 to 1100°K , the quantity $V(dp/dT)_\sigma$, evaluated from our earlier measurements of density and vapor pressure, was added to C_σ , and the sum was multiplied by 10 and added to the value of $(H_T - H^\circ_{298})$ for the preceding temperature. The resulting values of $(H_T - H^\circ_{298})_\sigma$ are shown as the full line in Figure 1 and for specific temperatures in Table III.

For the gas phase, the enthalpy was calculated relative to the solid at 298°K . At 298°K the quantity

$(H^\circ_T(\text{g}) - H^\circ_{298}(\text{s}))$ is equal to the enthalpy of evaporation and was taken from the evaluation of vaporization data¹⁰ as 27.3 kcal/mole. The enthalpy increments for the ideal gas, ϵ_s calculated by Kelley¹¹ and by Sundaram¹² from molecular constants, were used to establish the ideal standard-state curve for the gas shown in Figure 1. From 950 to 1100°K the enthalpies of evaporation, given by Johnson, *et al.*,² were added to the enthalpies of the liquid to give the saturation enthalpies of the gas (relative to the solid at 298°K), shown as a full curve in Figure 1. The curve was extended to join the ideal gas curve smoothly in the neighborhood of the boiling point because the vapor pressure data indicated that the gas was behaving ideally there. In that region the curve is shown dashed to indicate its interpolated nature.

A value of $(H_T - H^\circ_{298}(\text{s}))_\sigma$ at the critical point was estimated from data for other substances. To do this, a plot of reduced enthalpy increments for both liquid and vapor *vs.* reduced density was constructed for several¹³ substances: Ar, CO_2 , NH_3 , and H_2O . These formed a family of curves that were relatively close together for the liquid. Comparison of the values of $(H_T - H^\circ_{298})_\sigma$ and reduced density for BiCl_3 in the range 1000 to 1100°K with the family of curves led to a value of 37,500 cal/mole for $(H_T - H^\circ_{298})_\sigma$ for BiCl_3 at the critical point. The enthalpy increments for the saturated liquid and vapor from 1100°K to the critical point (1178°K) were then drawn so that they met at the critical value and so that their separation was equal to the enthalpy of vaporization given by Johnson, *et al.*² Values for the saturation quantities are given in Table III.

Entropies and Free Energy Functions

For the condensed phases, the absolute entropy at 298°K was taken from the evaluation by Cubicciotti.¹⁰ The heat capacities for the solid and the liquid up to 800°K were constant, as reported above, and the entropy increments above 298°K were calculated from the integral of C_p/T . These were added to the absolute entropy at 298°K and the resulting values are shown in Table II. Standard free energy functions were calculated from them and the enthalpy increments by the relation

(10) D. Cubicciotti, to be published.

(11) K. K. Kelley, U. S. Bureau of Mines Bulletin 584, U. S. Government Printing Office, Washington, D. C., 1960.

(12) S. Sundaram, *Z. Physik. Chem.*, **34**, 233 (1962).

(13) Data for these substances were taken from F. Din, "Thermodynamic Functions of Gases," Vols. 1-3, Butterworth and Co. Ltd., London, 1961-1962.

Table III: Thermodynamic Functions for BiCl₃ under Saturation Conditions to the Critical Point

T, °K	Liquid					Gas				
	$H_T - H^{\circ}_{298}$, kcal/mole ^a	S_T , eu	$-(F_T - H^{\circ}_{298})/T$, eu ^a	C_p , eu	V, cc/mole ^b	(dp/dT) , atm/deg ^c	$H_T - H^{\circ}_{298}$, kcal/mole ^a	S_T , eu	$-(F_T - H^{\circ}_{298})/T$, eu ^a	V, cc/mole ^b
800	20.62	81.45	55.67	32.5	97.8	0.050	9.65	101.7	89.6	...
850	22.25	83.43	57.25	32.5	102	0.084	10.56	101.6	89.2	10,300
900	23.86	85.26	58.75	31	107	0.132	11.68	101.6	88.6	5,360
950	25.40	86.92	60.18	30	112	0.195	12.10	101.6	88.9	3,220
1000	26.93	88.47	61.54	32	119	0.277	12.77	101.6	88.8	2,080
1050	28.62	89.93	62.67	35	128	0.378	13.40	101.4	88.6	1,380
1100	30.5	91.3	63.6	40	138	0.500	13.5	100.7	88.4	915
1150	33.3	93.7	64.7	78	165	0.648	12.9	99.7	88.5	558
1170	35.4	95.4	65.1	140	190	0.704	12.0	99.1	88.8	407
1178 (crit. pt.)	37.5	97.3	65.5	...	261	...	10.2	97.3	88.6	261

^a Reference state for second and fourth columns is the solid in its standard state at 298°K, and for eighth and tenth columns the gas in its standard state at 298°K. ^b Data in the sixth and eleventh columns calculated from the equations given in ref 3. ^c Data in this column calculated from the equations given in ref 2.

$$\left(\frac{F^{\circ}_T - H^{\circ}_{298}}{T}\right) = -S^{\circ}_T + \left(\frac{H^{\circ}_T - H^{\circ}_{298}}{T}\right) \quad (4)$$

These values are also given in Table II.

In the higher temperature range of these measurements, C_p and C_v are sensibly different. To evaluate the difference, data on the compressibility are required (see eq 3), and these are not available at present. Therefore, above 800°K, we report only the saturation values of the thermodynamic functions. Up to 1100°K, the saturation entropies were obtained by integrating the saturation heat capacity (*i.e.*, the slope of the curve of measured heat evolved in the calorimeter) divided by temperature. From 1100°K to the critical point, the slope of the enthalpy curve was reduced by the quantity $V(dp/dT)_s$ to evaluate C_p and this was integrated to give the entropy increments. The values obtained are reported in Table III and Figure 2.

For the vapor, the standard entropy for the ideal gas has been calculated by Kelley and by Sundaram from molecular constant data. This is shown as a broken line in Figure 2. The standard entropy refers to the gas in the hypothetical state of 1 atm pressure and equals the saturation entropy only at the normal boiling point (unlike the enthalpy increments which are essentially equal at all temperatures below the boiling point). Below the boiling point the saturation entropies were calculated by subtracting $R \ln p$ (vapor pressure in atmospheres) from the standard, ideal gas entropy.

The saturation entropy for the vapor above the boiling point was calculated from the value for the liquid plus the entropy of evaporation (equal to the

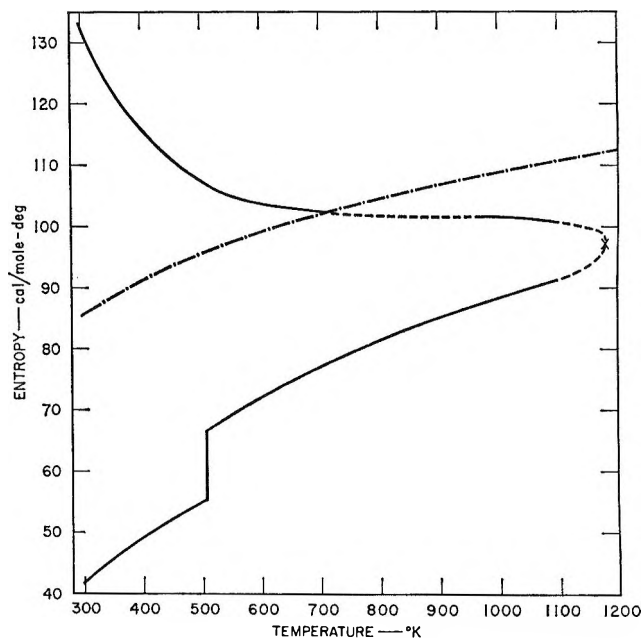


Figure 2. Absolute entropy of BiCl₃. Full and dashed curve represents saturation entropy of vapor (upper curve) and condensed (lower) phases. Dot and dash curve is standard entropy of ideal gas. Cross shows critical point.

enthalpy of evaporation divided by temperature). The resulting values are shown in Figure 2 as full lines, or dashed lines where extrapolations of the enthalpy data were involved.

The fact that the saturation entropy curves for the vapor above and below the boiling point join smoothly indicates consistency of the data because of the two different methods used for evaluating the curve. From

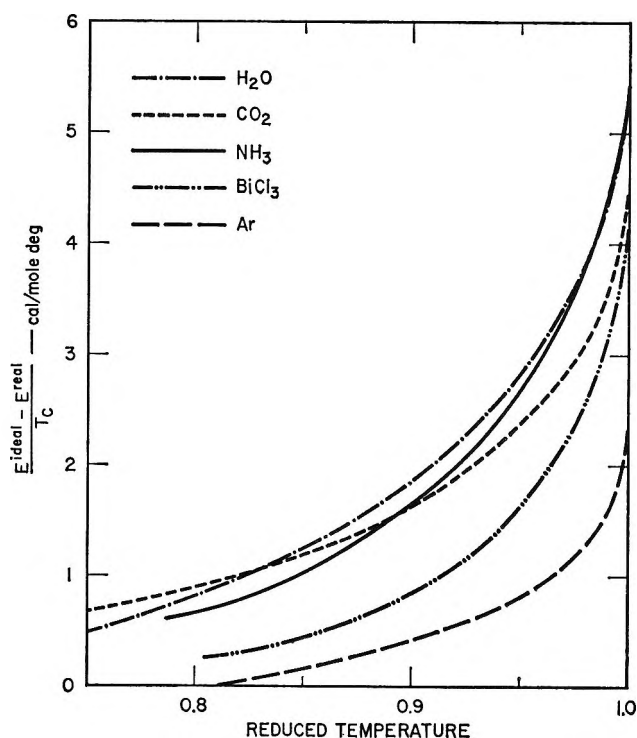


Figure 3. Energy departure from ideal gas values for several substances.

about 800 to 1000°K the saturation entropy of the vapor is almost independent of temperature. In that region there are two competing factors that influence the entropy. The increasing vapor pressure acts to decrease the entropy, and the increasing internal thermal motions of the molecules increases it. Apparently, these factors tend to balance one another with the result that the saturation entropy is essentially independent of temperature. Above about 1100°K, a factor that reduces the entropy becomes important and leads to the pronounced drop to the critical point. Presumably, this factor is a correlation of molecular positions and momenta over regions including several molecules (and might be considered as "clustering").

The saturation values for the free energy functions were calculated as for the condensed phases.

Gas Imperfection Energy. The difference between the internal energy of the ideal gas and that of the real gas ($E_T^{\text{ideal}} - E_T^{\text{real}}$) is approximately equal to the net average energy (of attraction) per mole between molecules. (There is a contribution to ($E_T^{\text{ideal}} - E_T^{\text{real}}$) from intramolecular energy differences between the ideal and real gas. This is assumed to be small and is neglected in the present discussion.) The quantity $E^{\text{ideal}} - E^{\text{real}}$ is, then, the gas imperfection energy and can be calculated from the enthalpies given above by the relation

$$\begin{aligned} (H_T^\circ - H_{298}^\circ)_{\text{ideal}} - (H_T - H_{298}^\circ)_\sigma = \\ H_T^{\text{ideal}} - H_T^{\text{real}} = E_T^{\text{ideal}} - E_T^{\text{real}} + \\ (PV)^{\text{ideal}} - (PV)^{\text{real}} \quad (5) \end{aligned}$$

The quantity $(PV)^{\text{ideal}}$ is equal to RT , and $(PV)^{\text{real}}$ was calculated from the saturation vapor pressures and volumes. The quantity $E_T^{\text{ideal}} - E_T^{\text{real}}$ can be converted to a function of reduced properties by dividing by the critical temperature.¹⁴

Comparison of $(E^{\text{ideal}} - E^{\text{real}})/T_c$ for several substances¹³ is made in Figure 3. The gas imperfection energy for BiCl₃ is seen to lie below those of H₂O, NH₃, and CO₂ and above that of Ar. Thus this property of BiCl₃ also falls among those of molecular fluids. It was shown earlier that the reduced density of the liquid fell between the values for H₂O and Ar. Examination of reduced vapor pressures shows that it also falls between H₂O and Ar. It appears, then, that in the thermodynamics of its vaporization BiCl₃ acts like a molecular fluid. This suggests either that the species that give rise to its ionic conductivity are of small concentration or that the thermodynamic quantities associated with their recombination to neutral, molecular species are small compared to the quantities associated with vaporization.

(14) See O. A. Hougen, K. M. Watson, and R. A. Ragatz, "Chemical Process Principles, Part II, Thermodynamics," 2nd ed, John Wiley and Sons, Inc., New York, N. Y., 1959, p 611.

Thermodynamic Properties of Gases in Propellants and Oxidizers. I.

Solubilities of He, N₂, O₂, Ar, and N₂O₃ in Liquid N₂O₄

by E. T. Chang and N. A. Gokcen

*Chemical Thermodynamics Section, Laboratories Division, Aerospace Corporation, El Segundo, California
(Received February 18, 1966)*

The solubilities of gaseous He, N₂, O₂, Ar, and N₂O₃ in liquid N₂O₄ have been measured over a wide range of pressure and temperature. The results show conclusively that Henry's law is obeyed for He, N₂, O₂, and Ar at all pressures at each temperature and for N₂O₃ at low pressures. The standard free energy, enthalpy, and entropy of solution for each gas have been obtained. Thermodynamic arguments are presented to show the absence of reactions of N₂ and O₂ with N₂O₄. A qualitative argument is presented to explain the negative heats of solutions as resulting from the dissociation of N₂O₄ into NO₂ in the liquid. The equilibrium between NO(g) and dissolved N₂O₃ has also been presented.

Introduction

Practical problems involved in storing, pumping, and pressurizing liquid propellants and oxidizers require reliable data on the solubilities of gases in such liquids. A program, therefore, was initiated to measure the solubilities of a number of gases in liquid propellants and oxidizers. The first part of this investigation consists of the solubilities of gases in liquid N₂O₄.

Available data^{1,2} on the solubilities of N₂ and He in N₂O₄ are inaccurate, and there appear to be no data on the solubilities of O₂ and Ar. Numerous investigations on systems containing NO, N₂O₄, NO₂, and N₂O₃ have been reported,³⁻⁶ but the results are incomplete and there are no results on the solubility of N₂O₃(g) in N₂O₄(l) and the related thermodynamic properties. A systematic and reliable investigation was therefore warranted.

Experimental Section

The apparatus for solubility measurements was all Pyrex construction with two capillary stopcocks lubricated with silicone grease and two Teflon O-ring joints. Three volumes connected by short capillary necks were calibrated to ± 0.0003 ml. They were connected to a bulb containing liquid N₂O₄ and to a precision bore manometer with 1-mm capillary tubings. The volumes of all connecting tubes were also calibrated to the same precision. The pressure measure-

ments were made with a barometer accurate to ± 0.02 mm, and the manometer readings were read to ± 0.01 mm with a micrometer slide-type cathetometer. The apparatus was located in a room thermostated to $\pm 0.1^\circ$. The calibrated volumes were thermostated to $\pm 0.03^\circ$.

The N₂O₄ bulb was attached to a connector with an O-ring joint. The connector had a stopcock and a second O-ring joint for attaching it to the calibrated volumes. The bulb was only 25 mm high, and it was calibrated to ± 0.0002 ml, having a capacity for 100 g of N₂O₄ with about 5 ml of space above fully exposed liquid surface.

The measurements were made as follows. The bulb was evacuated, the stopcock on the connector was closed, and the connector-bulb assembly was detached and weighed on an analytical balance. Research grade N₂O₄, 99.5% minimum purity, was oxidized to remove

(1) AFFTC, Edwards Air Force Base, "Storable Propellant Data for the Titan II Program," Quarterly Progress Report No. 1, AFFTC TR-60-62, Bell Aerosystems Co., Buffalo, N. Y., Oct 1960 (unclassified).

(2) R. R. Liberto, "Titan II Storable Propellant Handbook," Report No. 8111-933003, AFFTC TR-61-32, Bell Aerosystems Co., Buffalo, N. Y., June 1961 (unclassified).

(3) A. G. Whittaker, R. W. Sprague, S. Skolnik, and G. B. L. Smith, *J. Am. Chem. Soc.*, **74**, 4794 (1952).

(4) I. R. Beattie and S. W. Bell, *J. Chem. Soc.*, 1681 (1957).

(5) I. R. Beattie, S. W. Bell, and A. J. Vosper, *ibid.*, 4796 (1960).

(6) I. R. Beattie and A. J. Vosper, *ibid.*, 4799 (1960); 2106 (1961).

Table I: Solubilities of He, N₂, O₂, and Ar in Liquid N₂O₄^a

<i>T</i> , °K	He			N ₂			O ₂			Ar		
	<i>P</i>	10· <i>X</i>	10· <i>K</i>	<i>P</i>	10· <i>X</i>	10· <i>K</i>	<i>P</i>	10· <i>X</i>	10· <i>K</i>	<i>P</i>	10· <i>X</i>	10· <i>K</i>
262.02	0.5261	0.289	0.55	0.5916	3.28	5.54	0.6041	5.34	8.84	0.7110	6.18	8.69
	1.0149	0.599	0.59	0.6186	3.44	5.56	1.2017	10.58	8.80	1.2670	11.16	8.81
	1.2393	0.694	0.56	1.2964	7.38	5.69	1.3091	11.47	8.76	1.5162	13.28	8.76
	1.8346	1.12	0.61	1.3192	7.51	5.69	1.6119	14.23	8.83	1.8037	15.85	8.79
	1.9125	1.05	0.55	1.9440	10.91	5.61	1.9876	17.40	8.75	1.9080	16.83	8.82
			1.9500	11.08	5.68							
273.15	0.4951	0.361	0.73	0.3504	2.09	5.96	0.2643	2.43	9.19	0.3582	3.24	9.05
	0.6624 ^b	0.453	0.68	0.3811	2.32	6.09	0.6275	5.78	9.21	0.5702 ^b	5.15	9.03
	0.9566	0.698	0.73	0.4716 ^b	2.83	6.00	1.1241	10.30	9.16	0.6879	6.29	9.14
	1.2315 ^b	0.852	0.69	0.6830	4.06	5.94	1.7950	16.37	9.12	0.9366 ^b	8.50	9.08
	1.4186	0.950	0.67	0.8972	5.39	6.01				1.8425	16.76	9.10
	1.8770	1.30	0.69	0.9389 ^b	5.63	6.00						
				1.4283	8.60	6.02						
			1.5043	8.95	5.95							
			1.7951	10.77	6.00							
288.10	0.9773 ^b	0.870	0.89									
	1.3153 ^b	1.13	0.86									
298.15	0.3917	0.401	1.02	0.3801	2.47	6.50	0.3728	3.76	10.09	0.3801	3.77	9.92
	0.3963	0.404	1.02	0.5909	3.85	6.52	0.4989	5.16	10.34	0.4158	4.08	9.81
	0.7836	0.830	1.06	0.7222	4.82	6.67	0.5745	5.97	10.39	0.4897	4.80	9.80
	1.0192	1.00	0.98	0.7393	4.88	6.60	0.9963	10.08	10.12	0.6340	6.22	9.81
	1.1195	1.11	0.99	0.8457	5.54	6.55	1.0809	10.70	9.90	0.8037	7.94	9.88
	1.1455	1.23	1.07	1.1125	7.41	6.66				0.9912	9.72	9.81
			1.3032	8.59	6.59				1.1053	10.89	9.85	
303.16	0.5759 ^b	0.615	1.07	0.5604 ^b	3.81	6.80	0.4441 ^b	4.73	10.65	0.4470 ^b	4.42	9.89
	0.8867 ^b	0.909	1.03	0.8380 ^b	5.74	6.85	0.9189 ^b	9.47	10.31	0.5912 ^b	5.85	9.90

^a *P*, atm; *X*, mole fraction; *K* = *X*/*P*. ^b Data from a new apparatus having a greater degree of accuracy, but similar to that described in the Experimental Section. They are represented by the open points in Figure 1.

a trace of N₂O₃ by bubbling oxygen, degassed under vacuum, and then distilled into the bulb. The weight of N₂O₄ was obtained by reweighing, and the bulb was attached to the apparatus. The calibrated volumes and connections were then thoroughly flushed with the desired gas and evacuated after the bulb was attached. The bulb was immersed into a thermostat controlled to ±0.01°. A known amount of gas was obtained by reading pressure, *P*, and temperature, *T*, in a known volume, and the gas was forced over N₂O₄(l) with mercury from a leveling bulb after opening the stopcock in the connector. The stopcock was opened and closed intermittently to keep N₂O₄(g) in the bulb while the dissolution process was carried out by stirring N₂O₄(l) vigorously with a glass-coated magnet bar inside N₂O₄(l). Less than 10 min was sufficient to reach equilibrium, but usually 40 min was allowed to assure that there were no further changes in pressure readings. The measurements of *P*, *V*, and *T* of the gas above N₂O₄(l) and the remaining gas in the connecting tubes

yielded the necessary data for obtaining the dissolved gas in N₂O₄(l).

Accurate measurements of the volume over N₂O₄(l) in the bulb necessitated highly precise measurements of the density of the liquid. The results were represented by density (g/ml) = 1.4916 - 0.0022*t*(°C).

The experimental procedure was checked for the solubility of nitrogen in water, and the results agreed within 2% with the published data.⁷ The smallest solubility measurement in this investigation, *i.e.*, He in N₂O₄, is 10 times higher than the solubility of N₂ in water; hence the procedure appeared to be highly reliable.

The temperature range at which N₂O₄ exists in the liquid state under 1 atm is unfortunately too narrow, *i.e.*, -11.2 to 21.5°; hence the measurements were limited to -11.1 to 30°.

(7) R. C. Weast, S. M. Selby, and C. D. Hodgman, "Handbook of Chemistry and Physics," 45th ed, Chemical Rubber Publishing Co., Cleveland, Ohio, 1964, p B199.

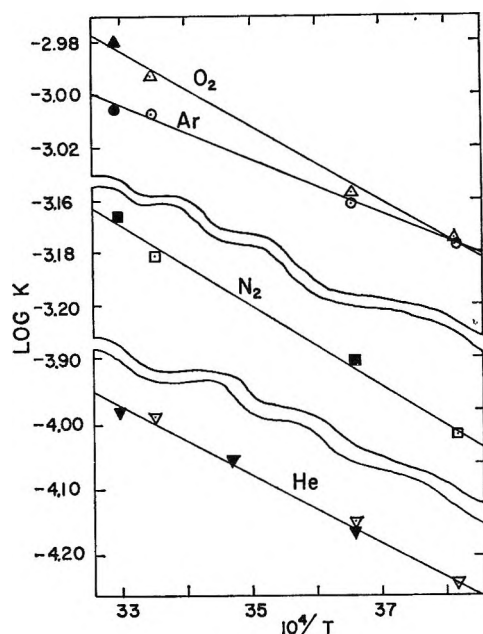
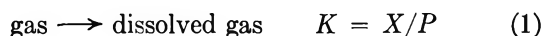


Figure 1. Solubilities of He, N₂, O₂, and Ar in N₂O₄(l); log (X/P) vs. 1/T(°K).

Results on He, N₂, O₂, and Ar

The results for He, N₂, O₂, and Ar are listed in Table I. In all cases Henry's law is obeyed; *i.e.*, the solubility is proportional to the partial pressure of gas dissolved by N₂O₄. This can be demonstrated either by plotting the concentration vs. the partial pressure, or by the constancy of *K* for the reaction



where *X* is the mole fraction and *P* is the partial pressure of the dissolved gas.

The average values for the solubilities of He, N₂, O₂, and Ar are represented in Figure 1. A small degree of scattering is well within the experimental errors. The equilibrium constant *K* also represents the value of solubility at 1 atm pressure of each gas. The equations representing the linear plots, expressed by $\Delta G^\circ = -RT \ln K$, are

$$\Delta G^\circ(\text{He}) = 2386 + 10.30T \quad (2)$$

$$\Delta G^\circ(\text{N}_2) = 699 + 12.19T \quad (3)$$

$$\Delta G^\circ(\text{O}_2) = 664 + 11.46T \quad (4)$$

$$\Delta G^\circ(\text{Ar}) = 475 + 12.18T \quad (5)$$

Discussion on He, N₂, O₂, and Ar

The dissolution process for nitrogen is represented by eq 1 and not by any other possible reactions, such as N₂(g) + 3N₂O₄(l) = 4N₂O₃(in liquid), N₂(g) + N₂O₄(l) = 4NO(in liquid), and N₂(g) + 1/3N₂O₄(l) =

4/3N₂O(in liquid). The equilibrium constant for the first of these reactions is (4*X*)⁴/*P*_{N₂}, where *X* is the mole fraction of nitrogen in a dilute solution which forms 4*X* mole fraction of N₂O₃. Therefore a plot of *X* vs. *P*_{N₂} would not yield a linear relationship if the dissolution process had followed this reaction. It can also be shown, similarly, that, for the remaining two reactions, a plot of *X* vs. *P*_{N₂} cannot be linear; hence these reactions do not take place when nitrogen is dissolved in liquid N₂O₄. Further evidence is the fact that $\Delta H^\circ = 699$ kcal/mole for nitrogen is not far from $\Delta H^\circ = 475$ kcal/mole for argon in N₂O₄. The endothermicity of any chemical reaction of N₂ with N₂O₄ is considerably greater than the preceding values for reaction 1. Similar arguments are also applicable to oxygen. In this case, however, there is only one possible reaction, *i.e.*, 1/2O₂(g) + N₂O₄(l) = N₂O₆(in liquid).

The foregoing results cannot be interpreted in terms of any simple energetic or molecular models of solution⁸⁻¹¹ because N₂O₄ is a polar solvent. A purely thermodynamic estimation of the order of magnitude of the solubilities can be made by using the equilibrium vapor pressures, *P*₁^v, of hypothetically existing liquid He, N₂, O₂, and Ar and by assuming that Raoult's law is obeyed. The solubility of each gas is then the ratio of its actual pressure *P*₁ to *P*₁^v. Such computations by Hildebrand and Scott⁸ are listed in Table II as *ideal* and are compared with the present results. The ideal value for He is not given by Hildebrand and Scott because of the very low boiling point for He which makes extrapolation to high temperatures unreliable, but the authors estimated a rough value of 1.6 × 10⁻⁴ mole fraction by assuming that the ratio of boiling points (°K) for He and H₂ is the same as the inverse of their vapor pressures at 298°K. It is noteworthy that the decrease in solubilities from ideal to actual values follows the increase in the dipole moment μ . However, this is not a strictly quantitative trend, having general applicability as evident from the listed values.

The ideal solubility calculations show that the solubility of a gas in a liquid should decrease with increasing temperature because the heat of condensa-

(8) J. H. Hildebrand and R. L. Scott, "The Solubility of Nonelectrolytes," 3rd ed, Reinhold Publishing Corp., New York, N. Y. 1950, p 243.

(9) J. H. Hildebrand and R. L. Scott, "Regular Solutions," Prentice-Hall, Inc., Englewood Cliffs, N. J., 1962.

(10) I. Prigogine, A. Bellemans, and V. Mathot, "The Molecular Theory of Solutions," Interscience Publishers, Inc., New York, N. Y., 1957.

(11) J. S. Rowlinson, "Liquids and Liquid Mixtures," Butterworth & Co., Ltd., London, 1959.

Table II: Comparison of Solubilities of He, N₂, O₂, and Ar in Liquid N₂O₄ and in Other Solvents at 25° and 1 Atm^a

Solvent	μ , D.	He	N ₂	O ₂	Ar
Ideal	...	1.6	10	13.2	16
<i>m</i> -Xylene	0.5	...	6.14
N ₂ O ₄	0.6	1.02	6.58	10.2	9.84
Water	1.9	0.07	0.12	0.23	0.25
Acetone	2.8	1.08	5.92	9.25	9.06
Nitrobenzene	4.1	...	2.63

^a Numbers represent mole fraction $\times 10^4$.

Table III: Comparison with Other Data on N₂ and He^a

	Temp, °C	This work	Liberto ²	Burns ¹⁴
N ₂	25	6.58 \pm 0.04	23 \pm 1 ^b	3.6 \pm 0.5 ^c
	0	6.00 \pm 0.04	11 \pm 1	4.6 \pm 0.7
He	25	1.25 \pm 0.04	41 \pm 10 ^b	...
	0	0.71 \pm 0.04	13.5 \pm 7	...

^a Numbers represent solubilities in mole fraction $\times 10^4$ at 1 atm. ^b The actual values at 70°F for N₂ and 73°F for He have been extrapolated a short distance to obtain the tabulated values at 77°F (25°C). ^c Deviations in this column (\pm) are approximate.

tion is a negative quantity. This is true of many gases and solvents having relatively small endothermic interaction energies with the solvent in comparison with the heat of condensation of the gas. For example, the solubilities of Ar, N₂, O₂, N₂O, and CO₂ in water follow this pattern; whereas, those of He, H₂, and CO in water do not. It may be possible to explain the increase in the solubilities of He, N₂, O₂, and Ar in N₂O₄, hence the endothermic heat effect, by assuming that each molecule of dissolved gas tends to break the NO₂-NO₂ bond which has a bond energy of about 3460 cal.¹² Thus ΔH° would be the sum of a fraction of the positive quantity 3460 and the negative quantity for the heat of condensation of each gas. If it is assumed that three molecules of solute are successful in breaking one bond, then all the ΔH° values in eq 2-5 fit the proposed pattern. Consequently, the difference between ΔH° (He) and ΔH° for N₂, O₂, or Ar, which is about 1.7 kcal, is very nearly due to the difference in their heats of condensation which is about 1.6 kcal. It was shown by Cundall¹³ that N₂O₄ dissociates into NO₂ in the liquid state by various solutes; hence this assumption is justified. Calculations show that such a small change in NO₂ in the liquid does not measurably affect the pressure of NO₂(g) + N₂O₄(g) over the liquid in the present investigation.

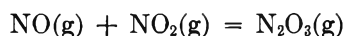
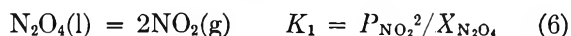
Comparison with Other Data on He and N₂

The results in this investigation are compared in Table III with those quoted by Liberto² and the recent values of Burns¹⁴ obtained by using a gas-solid partition chromatograph. The agreement with Burns' results for nitrogen is fair while the disagreement with the Titan II handbook² for nitrogen and helium is very large. There are no previous data on the solubilities of oxygen and argon.

Solubility of N₂O₃(g)

The reaction of NO(g) with N₂O₄ precludes the measurements of solubility of NO(g) in liquid N₂O₄. How-

ever, on the basis of data on the preceding gases and the fact that the boiling point of NO(l) is comparable to the boiling points of N₂, O₂, and Ar, the solubility of NO should be less than 0.002 mole fraction. Further, thermodynamic calculations from the available data^{12,15} show that the reaction NO(l) + $\frac{1}{2}$ N₂O₄(l) = N₂O₃(l) goes to completion; therefore when NO is present over the liquid, N₂O₃ is the overwhelmingly predominant dissolved species. It is therefore possible to investigate this system by admitting NO(g) over N₂O₄(l) and calculating the gas composition from the available thermodynamic data in order to compute the remaining gas over the liquid. For this purpose it is necessary to consider the following reactions.



$$K_3 = P_{\text{N}_2\text{O}_3}/P_{\text{NO}}P_{\text{NO}_2} \quad (8)$$

In the liquid state, N₂O₄ dissociates¹³ less than 0.05% into the monomer, and therefore it may safely be considered as entirely N₂O₄, although in the gas phase it dissociates markedly. The use of $X_{\text{N}_2\text{O}_4}$ instead of the activity in K_1 and K_2 was found to be justifiable because N₂O₃ and N₂O₄ form a eutectic system, and the present authors' calculation of the activity coefficient γ from the data of Beattie, Bell, and Vosper⁵ on the depression of freezing points showed that $\gamma_{\text{N}_2\text{O}_4}$ is 1.02 and 1.04 \pm 0.02 at 0.90 and 0.70, respectively,

(12) "JANAF Thermochemical Tables," The Dow Chemical Co., Midland, Mich., 1965.

(13) J. T. Cundall, *J. Chem. Soc.*, 59, 1076 (1895).

(14) E. A. Burns, "Direct Determination of the Solubility of Nitrogen in Nitrogen Tetroxide," TRW Space Technology Laboratories, Redondo Beach, Calif. (a preliminary report received by the authors).

(15) F. D. Rossini, *et al.*, "Selected Values of Chemical Thermodynamic Properties," National Bureau of Standards, Circular 500, U. S. Government Printing Office, Washington, D. C., 1952.

Table IV: Equilibrium Compositions of Liquid and Gas Phases for Mixtures of N_2O_4 , NO, and N_2O_3

T , °K	P_{total}	$P_{N_2O_4}$	P_{NO}	P_{NO}	$P_{N_2O_3}$	$X_{N_2O_3}$	K_4^a	K_5^b	y^c	y'^d
262.12	0.204	0.147	0.030	0.024	0.003	0.053	2.23	19.56	1.974	1.925
	0.260	0.127	0.028	0.095	0.010	0.186	2.18	18.26	1.907	1.735
	0.328	0.105	0.025	0.180	0.018	0.324	2.19	18.41	1.838	1.585
						Av	2.20	18.74		
273.15	0.410	0.253	0.067	0.080	0.010	0.084	1.10	8.56	1.958	1.86 ⁷
	0.549	0.208	0.061	0.252	0.028	0.248	1.13	8.79	1.876	1.64 ³
	0.753	0.159	0.053	0.493	0.048	0.425	1.14	8.81	1.788	1.43 ⁶
						Av	1.12	8.72		
298.15	1.272	0.819	0.346	0.093	0.014	0.031	0.339	2.28	1.984	1.949
	1.512	0.747	0.331	0.381	0.053	0.116	0.323	2.16	1.942	1.812
	1.780	0.670	0.313	0.703	0.094	0.206	0.329	2.21	1.897	1.687
	2.035	0.604	0.297	1.007	0.127	0.284	0.333	2.23	1.858	1.590
						Av	0.331	2.22		

^a $K_4 = X_{N_2O_3}/P_{NO}(X_{N_2O_4})^{1/2}$. ^b $K_5 = X_{N_2O_3}/P_{N_2O_4}$. ^c y is atomic ratio O/N in liquid. ^d y' is atomic ratio O/N in gas.

for $X_{N_2O_4}$; therefore in the region of our interest it was justified to assume $\gamma_{N_2O_4} = 1$ well within experimental errors. This assumption is also substantiated by our computation from the data of Beattie and Vosper.⁶ The total measured experimental pressure, P , is given by

$$P = P_{NO_2} + P_{N_2O_4} + P_{NO} + P_{N_2O_3} \quad (9)$$

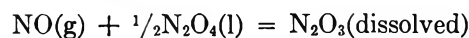
There are five unknowns in the four preceding equations, but $X_{N_2O_4}$ is obtained implicitly from the mass balance and the known volumes of liquid and gases by successive approximation. Equations 6–9 give

$$P_{NO} = \frac{P - K_2 X_{N_2O_4} - (K_1 X_{N_2O_4})^{1/2}}{1 + K_3 (K_1 X_{N_2O_4})^{1/2}} \quad (10)$$

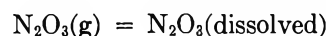
and similar relations for the remaining three gases. The equilibrium constants have been calculated from "JANAF Thermochemical Tables."¹² In order to obtain the first approximation for the partial pressures, $X_{N_2O_4}$ is set to unity, and P_{NO} and the remaining pressures were computed. These values and the known volume above the liquid and the mass of each constituent give $X_{N_2O_4}$. Substitution of this value in eq 10 and those for the other gases yield the second approximation and a new value of $X_{N_2O_4}$. The repetition of the procedure gives a third value of $X_{N_2O_4}$ which differs from the second by less than 0.1%. In an experimentally succeeding run, the previous composition is used as the first approximation. Various experiments with various ratios of gas volume to liquid weight differing by a factor of 5 showed no consistent change in the computation of $X_{N_2O_4}$. Further, the

agreement between the authors' extrapolated values to lower $X_{N_2O_4}$ and the published data⁶ shows that this procedure is reliable.

The results are listed in Table IV, columns 1–9, where the equilibrium constants and the corresponding reactions are



$$K_4 = X_{N_2O_3}/P_{NO}(X_{N_2O_4})^{1/2} \quad (11)$$



$$K_5 = X_{N_2O_3}/P_{N_2O_4} \quad (12)$$

The second relationship represents the solubility of $N_2O_3(g)$ in $N_2O_4(l)$. The reference state for dissolved N_2O_3 is the infinitely dilute solution. If the standard state for dissolved N_2O_3 is taken to be the pure liquid N_2O_3 , the activity coefficient $\gamma_{N_2O_3}$ becomes 0.127, 0.1124, and 0.117 at 262.12, 273.15, and 298.15°K, respectively. These values are obtained by combining $\Delta G^\circ = 9400 - 34.2T$ for $N_2O_3(l) = N_2O_3(g)$ from the available data¹⁵ with eq 12. A plot of the logarithm of K_4 and K_5 vs. $1/T$ is shown in Figure 2, where the deviations from the straight lines are remarkably small. The resulting relationships in terms of $\Delta G^\circ = -RT \ln K$ for K_4 and K_5 are

$$\Delta G_4^\circ = -8044 + 29.17T \quad (13)$$

$$\Delta G_5^\circ = -9051 + 28.77T \quad (14)$$

Discussion on the System $NO-N_2O_3-N_2O_4$

Previous investigators considered that the composition of liquid is unknown, and therefore they correlated

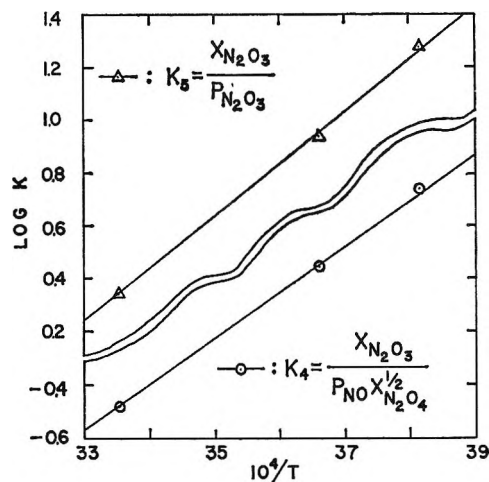


Figure 2. Variation of K_4 and K_5 with temperature.

the total pressure as a function of the atomic ratio of oxygen to nitrogen in liquid, y . They made no thermodynamic calculation, and the range of $X_{N_2O_3}$ investigated was about 0.8 and smaller. The authors' values for the atomic ratio O/N in the gas, y' , and that in the liquid, y , are listed in Table IV and represented in Figure 3 for comparison with the results of Beattie and Vosper. The agreement in the overlapping and extrapolated regions is excellent and substantiates the claim by Beattie, *et al.*, that y vs. y' is independent of temperature.

The measurements of total gas pressure by Beattie,

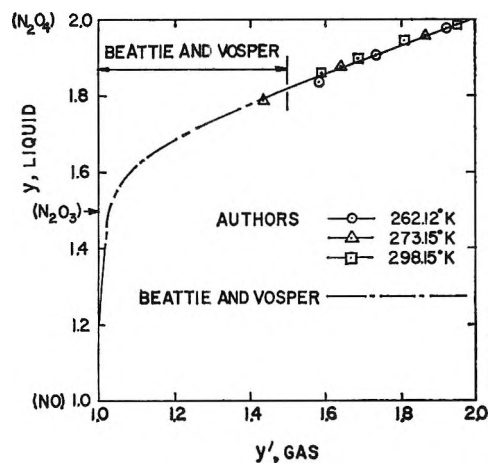


Figure 3. Variation of y in liquid with y' in gas in the system N_2O_4 - N_2O_3 - NO ; y and y' are in atomic ratios of oxygen to nitrogen in each phase.

et al.,⁴⁻⁶ and Whittaker, *et al.*,³ vs. $O/N = y$ in liquid can be expressed accurately by

$$\log P_{\text{total}} (\text{atm}) = 6.069 + \frac{1}{T} (1154 - 2652y + 593y^2)$$

The agreement of the data in Table IV with this equation is very good.

Acknowledgments. The authors wish to acknowledge the assistance of T. M. Poston and C. D. Robison of Aerospace Corp.

Mean Activity Coefficient of Polyelectrolytes. III. Measurements of

Hydrochlorides of Polyethylenimine and Its Low Molecular Weight Analogs¹

by Norio Ise and Tsuneo Okubo

Department of Polymer Chemistry, Kyoto University, Kyoto, Japan (Received February 18, 1966)

The mean activity coefficients of hydrochlorides of polyethylenimine and its low molecular weight analogs such as tetraethylenepentamine, triethylenetetramine, diethylenetriamine, and ethylenediamine have been measured, using a concentration cell with transference and silver-silver chloride electrodes. The single-ion activity coefficient of the gegenions (chloride ions) and the transference numbers of the macroions and low molecular weight polyvalent cations have also been determined. The results show that the mean activity coefficient of the polyelectrolyte cannot be equal to the single-ion activity coefficient of its gegenions. This agrees with the previous conclusion obtained with sodium salts of anionic polyelectrolytes. It is further demonstrated that the discrepancy between two coefficients can be small for the low molecular weight analogs. In the light of MacInnes' convention assuming the equality of the mean activity coefficient of potassium chloride and the single-ion activity coefficient of chloride (or potassium) ion, it is suggested that the discrepancy decreases continuously with decreasing charge numbers of electrolytes and therefore characterizes the transition from polyelectrolytes to simple electrolytes. The logarithm of the mean activity coefficient of the polyethylenimine salt decreases linearly with the cube root of concentration. The slope is -0.86 for this salt, not far from a value of -0.74 previously found for sodium polyacrylate. This cube-root rule is also found to be valid for the low molecular weight imine salts. The slope ranges from -0.60 to -1.10 , the magnitude increasing with rising valency.

Introduction

In previous papers,^{2,3} mean activity coefficients were measured on sodium polyacrylate (NaPAA) and sodium salts of polyvinyl alcohols partially acetalized with glyoxylic acid (NaPVAG). In the present paper, experimental data are reported on the hydrochlorides of polyethylenimine (PEI), tetraethylenepentamine (TP), triethylenetetramine (TT), diethylenetriamine (DT), and ethylenediamine (ED). These samples are of interest for three reasons. First, a concentration cell used for measurements of mean activity coefficients can be set up using silver-silver chloride electrodes, since the gegenion is Cl^- . This electrode has been studied much more intensively than the Na-glass electrodes used for NaPAA and NaPVAG.⁴ Second, the single-ion activity coefficients of the gegenions of $\text{PEI}(\text{HCl})_n$ and of its low molecular weight analogs have been studied earlier.⁵ Comparison of their data

and the mean activity data is a source of useful information. Third, by studying these hydrochlorides, the transition from simple electrolytes to polyelectrolytes can be investigated, as Lapanje, *et al.*, have asserted.⁵

Experimental Section

Principles. The method of the determination of mean activity coefficient adopted in this paper was described in the previous paper.² The galvanic cell with transference was as is shown in (I).

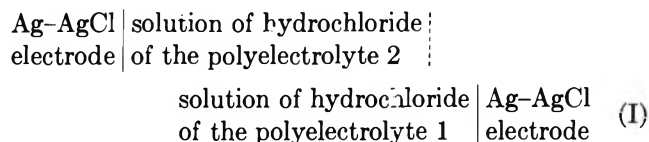
(1) Presented in part at the 14th Polymer Symposium, Kyoto, Japan, Oct 1965.

(2) N. Ise and T. Okubo, *J. Phys. Chem.*, **69**, 4102 (1965).

(3) N. Ise and T. Okubo, *ibid.*, **70**, 1930 (1966).

(4) R. G. Bates, "Determination of pH, Theory and Practice," 1st ed, John Wiley and Sons, Inc., New York, N. Y., 1964, Chapter 9.

(5) S. Lapanje, J. Haevig, H. T. Davis, and S. A. Rice, *J. Am. Chem. Soc.*, **83**, 1590 (1961).



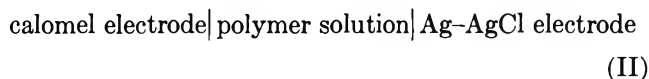
The emf of this concentration cell (E) can be given as

$$E = \frac{(1 + \alpha)RT}{\alpha F} \int_{a_2}^{a_1} t_{2p} d \ln a \quad (1)$$

where a_1 and a_2 are mean activities of the hydrochloride in the solutions 1 and 2, respectively, R is the gas constant, T the temperature, F the Faraday charge, t_{2p} the transference number of macroions, and α the number of free gegenions dissociated from one macroion.

The principle and detail of the transference experiments have been described in a previous paper.⁶ The polymer concentrations before and after the electrolysis were determined by conductometric titration. The chloride concentration was measured by a conductometric titration with AgNO_3 , using bright platinum electrodes.

The single-ion activity coefficient of gegenions γ_{2g}^* of the polyethylenimine salt was determined using the following cell.



The emf of this cell E_{2g} was assumed to be expressed as

$$E_{2g} = E_{2g_0} - (RT/F) \ln a_{\text{Cl}^-}$$

From this equation, we determined a_{Cl^-} , and hence γ_{2g}^* .

Electrodes. Ag-AgCl electrodes were prepared by electrodeposition of silver. The base for the electrodes was a spiral (2-mm diameter) of 4 or 5 turns of a platinum wire. On the base, a layer of silver was electrodeposited and then chloridized by anodizing in a dilute solution of hydrochloric acid.⁷ The standard potential of the silver-silver chloride electrodes (E_{00}) against the hydrogen electrode was estimated to be 222.6 mv when use was made of a standard potential value of the saturated calomel electrodes, 242.0 mv.⁸ On the other hand, Harned and Paxton⁹ reported 222.39 mv for E_{00} , with which our result is in good agreement. In the emf measurements, a pair of the Ag-AgCl electrodes was used for 10-15 pairs of solutions; the electrodes were discarded when they failed to show the potential values given by the calibration curve. The electrodes were equilibrated with the cell solutions for an hour or so in order to obtain reliable emf data.

Materials. Polyethylenimine used was a gift from the Sumitomo Chemical Co., Osaka. The sample was

a 50% aqueous solution. The molecular weight of the polyimine was estimated to be 4500 using a viscosity-molecular weight relationship.¹⁰ Purification of the sample was carried out by passing the diluted aqueous solution through columns containing cation- and anion-exchange resins in the hydrogen and hydroxide forms, respectively. Thereafter, hydrochloric acid was added quantitatively. The nitrogen content of the sample was determined by the Kjeldahl method, which agreed with the value from the conductivity method within the limit of experimental error. ED, DT, TT, and TP were commercially available. They were purified by distillation under reduced pressure of nitrogen and by recrystallization. These samples were analyzed with the results shown in Table I.

Table I

	Observed			Calculated		
	C	H	N	C	H	N
ED	40.3	13.9	46.0	40.0	13.4	46.6
DT	46.4	13.1	40.4	46.1	13.5	40.4
TT	50.4	12.5	37.1	49.3	12.3	38.4
TP	51.2	12.2	36.7	50.8	12.2	37.0

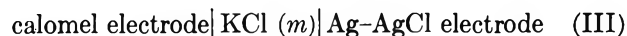
The degree of neutralization of these samples used for measurements were 0.86, 0.96, 0.98, 0.98, and 0.86 for PEI, TP, TT, DT, and ED, respectively.

The concentrations of all the solutions were determined by conductometry.

The emf and transference measurements were carried out at 25 ± 0.02 and $25 \pm 0.1^\circ$, respectively.

Results and Discussion

Calibration of the Ag-AgCl electrode was carried out using a cell shown by



For this type of cell, if the liquid junction potential can be assumed to be negligible, the emf (E) is given by

$$E = E_0 - \frac{RT}{F} \ln a_{\text{Cl}^-} \quad (2)$$

where E_0 is the standard value of the emf of the above

(6) T. Okubo, Y. Nishizaki, and N. Ise, *J. Phys. Chem.*, **69**, 3690 (1965).

(7) D. J. G. Ives and G. J. Janz, "Reference Electrodes, Theory and Practice," Academic Press Inc., London, 1961, Chapter 4.

(8) See ref 7, Chapter 3, p 159, Table V.

(9) H. S. Harned and T. R. Paxton, *J. Phys. Chem.*, **57**, 531 (1953).

(10) G. D. Jones, A. Langsjoen, M. M. C. Neumann, and J. Zomlefer, *J. Org. Chem.*, **9**, 125 (1944).

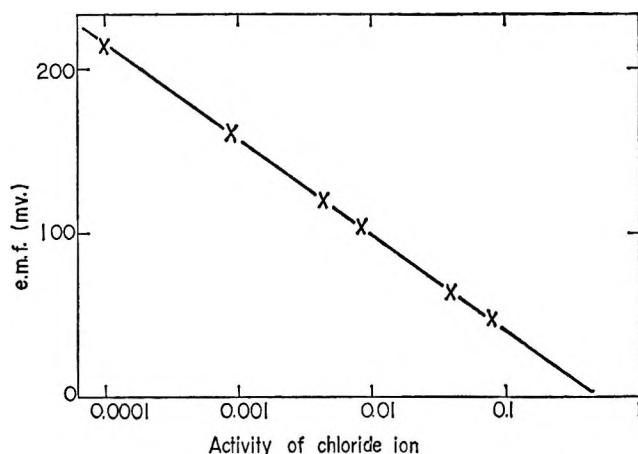


Figure 1. Calibration curve of silver-silver chloride electrode at 25°C: X, observed value; —, the Nernstian slope.

cell, and a_{Cl^-} is the single-ion activity of Cl^- . Using the value of the single-ion activity coefficient of Cl^- calculated by MacInnes' convention from the mean activity coefficient data of potassium chloride,¹¹ eq 2 was tested. As is shown in Figure 1, a linearity between E and $\log a_{\text{Cl}^-}$ was obtained over a wide range of a_{Cl^-} . The slope was 59.1 mv between $a_{\text{Cl}^-} = 1$ and $a_{\text{Cl}^-} = 10^{-4}$, which was in good agreement with the theoretical value, 59.157 mv at 25°C. The emf reading varied appreciably immediately after the electrodes were inserted into the solutions. It reached a limiting value which was constant within ± 0.1 mv over a 30-min period. The emf value given in this paper is this limiting value.

Important data of transference and activity coefficient data of $\text{PEI}(\text{HCl})_n$ are given in Table II. The first column gives the concentration of solution 2 (equiv/1000 g of water), that of solution 1 being 0.504. The emf's of the cells shown by (I) are given in the second column. The transference numbers, t_{2p} , are given in the third column. In the fourth column, the observed mean activity coefficients, γ^* , are given. These γ^* values were determined on the basis of a γ_{2g}^* value at $m = 0.01$ by the same convention as adopted in the preceding papers.^{2,3} Column 5 gives the single-ion activity coefficients of gegenions (Cl^-) in the same solution measured by the Ag-AgCl electrode and calomel electrode (cell II). In the last column the pH value of each solution is given. The degree of neutralization of the polymer was chosen so as to reduce hydrolysis to a negligible amount, at most 1.58% (at $m = 0.001$). In the present experiments using Ag-AgCl electrodes, the accuracy of the emf measurement can be claimed to be ± 0.1 mv, and the reproducibility was $\pm 1.5\%$. The error associated with the γ^*

Table II: Transference and Activity Coefficient Data of $\text{PEI}(\text{HCl})_n$ at 25°C^a

m , equiv/ 1000 g	E , ^b mv	t_{2p}	γ^*	γ_{2g}^*	pH
0.001	43.0	0.41	0.62	0.535	4.80
0.002	39.3	...	0.45	0.488	...
0.005	31.4	0.35	0.42	0.402	4.96
0.01	28.2	0.35	(0.302)	0.302	5.14
0.02	22.1	...	0.30	0.233	...
0.05	14.2	0.34	0.29	0.203	5.50
0.1	10.2	0.34	0.23	0.200	5.67
0.2	4.8	...	0.22	0.198	...
0.504	0	0.33	0.15	0.195	6.20

^a The degree of neutralization is 0.86. ^b The emf measurements were carried out with a reference concentration of 0.504 m .

value was smaller than $\pm 10\%$. The accuracy of the transference number is estimated to be $\pm 3\%$.

As is shown in Table II, the transference number, t_{2p} , decreased with increasing concentration. This observation is in agreement with the one on NaPVAG and in disagreement with the one on NaPAA. γ_{2g}^* of $\text{PEI}(\text{HCl})_n$ decreased with increasing concentration in the range covered. This is in contrast with γ_{2g}^* of NaPAA² and NaPVAG³ which was found to be almost independent of concentration. Though the reason for this disagreement is not clear, our finding on $\text{PEI}(\text{HCl})_n$ agrees with the one previously reported by Lapanje, *et al.*⁵ Table II also shows that the mean activity coefficient, γ^* , of $\text{PEI}(\text{HCl})_n$ decreased with increasing concentration, more sharply than γ_{2g}^* . In other words, γ^* cannot be always equal to γ_{2g}^* ; *i.e.*, we have

$$\gamma^* \neq \gamma_{2g}^* \quad (3)$$

This conclusion has also been obtained previously on NaPAA and NaPVAG^{2,3} and can now be asserted to be generally valid. The definition of γ^*

$$\gamma^{*1+\alpha} = \gamma_{2g}^*{}^\alpha \gamma_{2p}^* \quad (4)$$

indicates that the reason for this disagreement is the single-ion activity coefficient of macroions (γ_{2p}^*) being extremely large or extremely small. Thus the importance of the contribution of macroions to the thermodynamic solution properties is again clearly demonstrated.

In the previous paper,³ it was shown that the logarithm of the mean activity coefficient decreases

(11) For MacInnes' convention, see Chapter 3 in ref 4. The mean activity coefficient data of potassium chloride were taken from: H. S. Harned, *J. Am. Chem. Soc.*, 51, 416 (1929); H. S. Harned and M. A. Cook, *ibid.*, 59, 1290 (1937).

Table III: Transference and Activity Coefficient Data of TP(HCl)₅, TT(HCl)₄, DT(HCl)₃, and ED(HCl)₂ at 25°

Sample ^a	m , equiv/ 1000 g	E , ^b mv	t_p	γ^*	γ^*_{zg} ^c	pH
TP(HCl) ₅ $z = 5$ $\alpha = 3.88$	0.001	64.7	0.39	1.10	...	4.44
	0.002	56.9	...	1.02
	0.005	46.1	0.38	0.97	0.883	4.14
	0.01	39.6	0.38	(0.823)	0.823	4.12
	0.02	31.5	...	0.73	0.758	...
	0.05	22.7	0.38	0.66	0.655	4.26
	0.1	16.5	0.37	0.55	0.589	4.41
	0.2	9.1	...	0.51	0.528	...
	0.503	0	0.37	0.43	0.423	4.77
TT(HCl) ₄ $z = 4$ $\alpha = 3.72$	0.001	65.1	0.38	1.12	...	4.30
	0.002	57.5	...	1.04
	0.005	47.7	0.37	0.93	0.901	3.73
	0.01	40.5	0.37	(0.844)	0.844	3.51
	0.02	33.1	...	0.78	0.786	...
	0.05	23.5	0.36	0.71	0.685	3.28
	0.1	17.2	0.36	0.61	0.607	3.25
	0.2	10.0	...	0.56	0.538	...
	0.502	0	0.35	0.53	0.442	3.39
DT(HCl) ₃ $z = 3$ $\alpha = 2.94$	0.001	64.7	0.35	1.13	...	4.21
	0.002	57.3	...	1.06
	0.005	47.8	0.34	0.95	0.908	3.97
	0.01	40.7	0.34	(0.866)	0.866	3.94
	0.02	33.8	...	0.79	0.813	...
	0.05	23.6	0.33	0.76	0.727	4.06
	0.1	17.7	0.32	0.64	0.649	4.15
	0.2	10.1	...	0.62	0.566	...
	0.502	0	0.32	0.61	0.481	4.41
ED(HCl) ₂ $z = 2$ $\alpha = 1.72$	0.00095	104.7	0.50	1.06	...	6.18
	0.0019	92.6	...	0.96
	0.00475	73.6	0.50	0.98	0.904	6.32
	0.0095	62.0	0.50	(0.873)	0.873	6.38
	0.019	50.1	...	0.79	0.820	...
	0.0475	34.6	0.49	0.68	0.754	6.54
	0.095	24.0	0.48	0.58	0.683	6.64
	0.191	14.0	...	0.48	0.610	...
	0.476	0	0.47	0.40	0.497	6.87

^a The degrees of neutralization were 0.96, 0.98, 0.98, and 0.86 for TP, TT, DT, and ED, respectively. ^b In the emf measurements, the reference concentration was the highest one for each sample. ^c γ^*_{zg} values were cited from the results of Lapanje, *et al.*⁵

linearly with the cube root of concentration in the concentration range studied. It is interesting to see whether the cube-root rule also holds for PEI(HCl)_n. Thus log γ^* of this polyimine was plotted against the cube root of concentration, which is shown in Figure 2. Clearly the plot gives a linearity over a wide range of concentration with a slope of -0.86 . The slope of NaPAA was -0.74 and that of NaPVAG was in the range of -3.2 and -1.6 , varying with the degree of polymerization and the charge density.³ The data of NaPVAG's of various degrees of polymerization show that the magnitude of the slope decreases with increas-

ing degree of polymerization. This variation accounts for the difference in the slopes of NaPAA and PEI(HCl)_n of nearly equal charge densities, since the degree of the polymerization of the polyacid was 1640 and that of the polybase about 100.

In Table III, the essential data of activity coefficients and transference data of very low molecular weight analogs of the polyethylenimine salt, *i.e.*, TP(HCl)₅, TT(HCl)₄, DT(HCl)₃, and ED(HCl)₂, are shown. The number of free gegenions (α) is given in the first column, with the stoichiometric number of charges, z . In the second column, the concentrations in equiv/1000

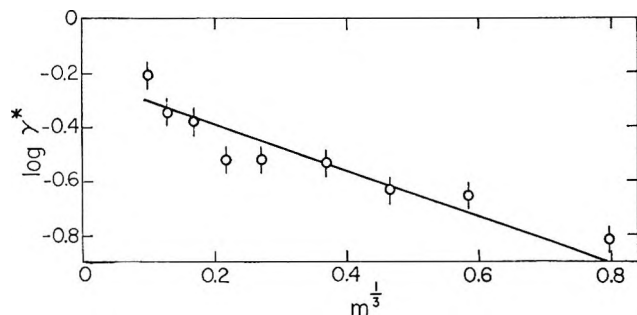


Figure 2. Concentration dependence of the mean activity coefficient of the hydrochloride of polyethylenimine (25°). Vertical bars represent an uncertainty of $\pm 10\%$.

g are given. The emf values of the concentration cells are given in the third column. The transference numbers of polyvalent cations (fourth column) at each concentration were obtained using the transference method described already.⁶ In column 5 the observed mean activity coefficients are given. Column 6 gives the single-ion activity coefficients of gegenions determined by Lapanje, *et al.*⁵ In the seventh column the pH values of each solution are given. The highest degree of hydrolysis of the imine salts was 4.2% in the case of TP at $m = 0.001$. The accuracy of the transference number data is estimated to be $\pm 3\%$. The error associated with the γ^* value was about $\pm 10\%$ for these imine salts. Table III shows that the transference number of polyvalent cation (t_{2p}) generally decreases with increasing concentration as was the case for polyethylenimine. As is readily seen from Table III, t_{2p} values of TT(HCl)₄ and DT(HCl)₃ are slightly smaller than those of TP(HCl)₅. This may be accounted for by the difference of the degree of neutralization: the degrees of neutralization of TT and DT were larger than that of TP, and the contribution of co-existing hydrogen ions to the conductivity was larger for TT and DT than for TP (compare the pH values of these three imines), though the experimental condition was always chosen such that the contribution of hydrogen ions was within 10% of the total conductivity. Table III shows that, in the case of ED, DT, TT, and TP, which are low molecular weight polyvalent electrolytes, γ^* can be nearly equal to γ^*_{2g} , *i.e.*

$$\gamma^* \approx \gamma^*_{2g} \quad (5)$$

According to the MacInnes convention,⁴ we have for potassium chloride

$$\gamma^* (= \gamma^*_{\pm KCl}) = \gamma^*_{2g} (= \gamma^*_{Cl^-} = \gamma^*_{K^+}) \quad (6)$$

Inspection of eq 3, 5, and 6 reveals that the discrepancy between γ^* and γ^*_{2g} becomes large as the valency of one ionic species (cationic one in the present case) in-

creases. This continuous change in the discrepancy appears to characterize the transition from simple electrolytes to polyelectrolytes and must be taken into consideration when thermodynamic properties of electrolyte solutions, polymeric and simple, are to be discussed from a unified standpoint.

In Figure 3, $\log \gamma^*$ of low molecular weight imine salts was plotted against the cube root of concentration. It is seen that the cube-root rule also holds for these salts. The upper limit of concentration, at which the cube-root rule begins to fail, and the slope are summarized in Table IV, together with the data for polyethylenimine salt. It would be plausible that the upper limit goes down at first with increasing charge

Table IV: The Constants of the Cube-Root Plot

	Upper limit, equiv/1000 g of water	Slope
ED(HCl) ₂	0.12	-0.60
DT(HCl) ₃	0.064	-0.86
TT(HCl) ₄	0.030	-0.94
TP(HCl) ₅	0.027	-1.10
PEI(HCl) _n	≈ 0.504	-0.86

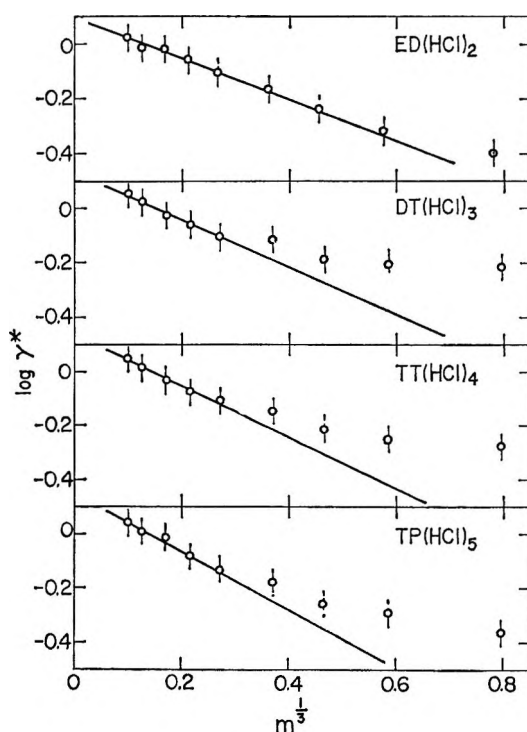


Figure 3. Concentration dependence of the mean activity coefficient of hydrochlorides of ED, DT, TT, and TP (25°). Vertical bars represent an uncertainty of $\pm 10\%$.

number and then, after passing through a minimum, increases. This tendency may be accounted for as follows. As the charge number of the cation increases, the repulsive force between the ionic species becomes large enough to break the local regular structure, which would have been present for electrolytes having a small number of charges and would be responsible for the linearity in the cube root. With a further increase in the charge number, however, the macromolecular properties of the cation become important, resulting in the intermacroion linkage mentioned in the previous paper,³ so that the upper limit goes up. The magnitude of the slope, as is seen from Table IV, appears to become large

at first, as the charge number increases, and then flattens out for the low molecular weight imines. The monotonic increase would be due to increasing electrical potential energy between ions. The comparatively small magnitude of the slope of polyethylenimine is due to the large volume effect of the cation, as was mentioned in the previous paper.³

Acknowledgments. The authors gratefully appreciate Professor Ichiro Sakurada's encouragement and useful comments. They also express their thanks to the Sumitomo Chemical Co., Osaka, for having kindly furnished the polyethylenimine.

Infrared Spectra of Ethylene Chemisorbed on Nickel and Platinum in Relation to the Activity of These Metals as Hydrogenation Catalysts

by B. A. Morrow

University Chemical Laboratory, Cambridge University, Cambridge, England

and N. Sheppard

School of Chemical Sciences, University of East Anglia, Norwich, England (Received December 29, 1965)

Platinum is considered to be better than nickel as a hydrogenation catalyst for converting ethylene to ethane.¹ The relatively poor performance of nickel is often attributed to the formation of surface complexes which are only slowly removed by hydrogen,^{2,3} and earlier infrared spectroscopic studies of the surface species by Eischens and Pliskin^{4,5} have thrown considerable light on the nature of these. We have now made a comparative study of the spectra obtained from the initial adsorption of ethylene and subsequent addition of hydrogen on both of these metals over a range of temperatures from -80 to 100° .

Many of our conclusions on Ni are similar to those derived from the earlier work,^{4,5} but one difference is that at all temperatures we consistently obtain very similar spectra under conditions ascribed previously to "hydrogen-covered" and "hydrogen-free" surfaces.⁵ A possibly significant difference in experimental technique is that our Cab-O-Sil (silica)-supported samples have been studied in the form of thin pressed disks, whereas in the previous work the metal was deposited on powdered Cab-O-Sil deposited on a CaF_2 plate.⁵

When ethylene was brought into contact with a Pt sample, a well-defined spectrum was obtained from the initially adsorbed species (Figure 1A); similar spectra are obtained with the same principal absorption bands throughout the temperature range -80 to 150° (Figure 1B). The absorption bands at 2795 and 2880 cm^{-1} and part of that at 2920 cm^{-1} are attributed to surface $\text{MCH}_2\text{-CH}_2\text{M}$ groups ($\text{M} = \text{metal}$). Admission of hydrogen to the reaction cell at 20° or below, after initial adsorption had been carried out at the same temperature, led to the removal of the original infrared absorption bands due to surface species and the production of much ethane either in the gas phase

or physically adsorbed at lower temperatures. Only at higher temperatures do moderate-strength spectra of chemisorbed surface species persist after the addition of hydrogen. Figure 1C shows such a spectrum obtained at 95° ; it is of a shape similar to that expected for an *n*-butyl group.⁵ At this temperature the gas-phase infrared spectrum indicated a relative hydrocarbon content of approximately 95% ethane and 5% *n*-butane, with more of the latter molecules in the gas phase than *n*-butyl groups on the surface. On evacuation for 5 min, the spectrum of the surface species decreased greatly in intensity (Figure 1D) but was nearly completely restored by readdition of hydrogen (Figure 1E); this behavior is very similar to that reported by Eischens and Pliskin for similar *n*-alkyl spectra obtained at 35° after hydrogenation of ethylene on nickel.

The spectrum of the initially adsorbed species from ethylene on Ni was found to vary considerably with

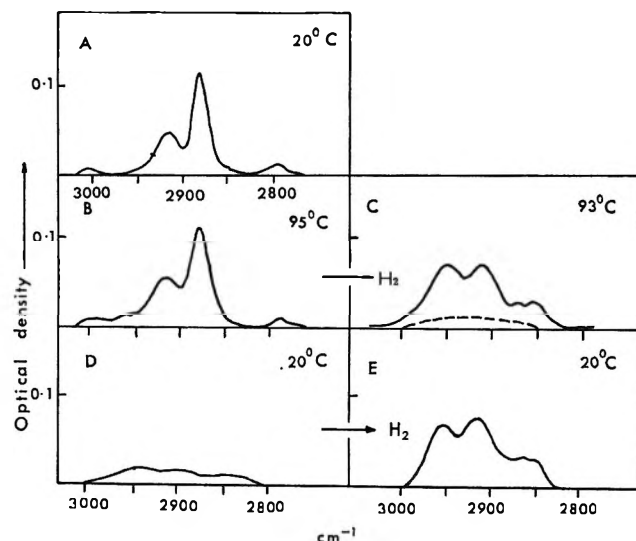


Figure 1. (A) The spectrum obtained at 20° on initial adsorption of ethylene on silica-supported platinum; (B) spectrum obtained on initial adsorption at 95° ; (C) spectrum after addition of gas-phase hydrogen (93°); dashed line denotes gas-phase spectrum; (D) spectrum obtained after cooling to 20° and evacuation of gas phase; (E) spectrum after readdition of hydrogen at 20° .

- (1) G. C. Bond, "Catalysis by Metals," Academic Press Inc., London, 1962, Chapter 11.
- (2) O. Beeck, *Discussions Faraday Soc.*, **8**, 118 (1950).
- (3) G. I. Jenkins and E. K. Rideal, *J. Chem. Soc.*, 2490 (1955).
- (4) W. A. Pliskin and R. P. Eischens, *J. Chem. Phys.*, **24**, 482 (1956).
- (5) R. P. Eischens and W. A. Pliskin, *Advan. Catalysis*, **10**, 1 (1958).

both the temperature and time of adsorption. Only the low-temperature spectrum (-78°) obtained after a short period of time was indicative of $MCH_2 \cdot CH_2M$ species in that it had considerable resemblance to that shown in Figure 1A for ethylene on Pt. On nickel a spectrum due to surface species of the *n*-butyl type was obtained after hydrogenation at -78° and this increased in intensity at room temperature. The gaseous or physically adsorbed hydrocarbons present after hydrogenation (which were always notably smaller in amount with Ni than with Pt) consisted largely of ethane with some butane at -78° , but almost entirely of *n*-butane at 20° .

The occurrence of considerable numbers of C_4 species in both the gaseous and adsorbed phases after hydrogenation in this case suggests that the time-dependent spectra on initial adsorption are caused by a polymerization process.

Although at room temperature comparable amounts of surface species are formed by adsorption of ethylene on both metals, hydrogenation brings about their conversion to a considerable proportion of surface butyl groups in the Ni case, but mostly to gas-phase ethane in the case of Pt. Only at considerably higher temperatures are surface alkyl groups formed on platinum. For the latter metal the surface therefore remains more accessible for the catalysis of the ethylene-hydrogen reaction. The spectra obtained in this work, and in work on higher olefins,⁶ will be published later in greater detail.

(6) M. Clark (1960), J. W. Ward (1962), and B. A. Morrow (1965), Ph.D. Theses, Cambridge University.

Concentration Dependence of Activity of a Macromolecular Component or Species

by Norio Ise and Tsuneo Okubo

Department of Polymer Chemistry, Kyoto University, Kyoto, Japan
(Received January 3, 1966)

The vapor pressure of macromolecules is too small to measure directly. Therefore, the activity of the macromolecular component or species in solution can be indirectly determined by measuring the activity of solvent using the Gibbs-Duhem equation. This method, however, can be replaced by a less indirect one if the macromolecule is a macroion. As reported previously,¹⁻³ the mean activity coefficients γ^* of poly-

electrolytes have been measured by the concentration cell method. The γ^* is defined as

$$\gamma^{*1+\alpha} = \gamma_{2g}^{*\alpha} \gamma_{2p}^* \quad (1)$$

where γ_{2g}^* and γ_{2p}^* are the (single-ion) activity coefficients of the gegenion and macroion, respectively, and α is the number of free gegenions dissociated from a polyelectrolyte molecule. Since α was determined using the transference method,⁴ the (single-ion) activity coefficient of the macroion, γ_{2p}^* , and hence the (single-ion) activity, a_{2p} , can be evaluated from γ^* and γ_{2g}^* . We must assume, however, that the well-known, but not exactly provable, assumption pertaining to the liquid junction potential is made, *viz.*, that the γ_{2g}^* value, which was determined electrochemically,⁴ may be regarded as correct.

In this note, we intend to comment on the dependence, thus determined, of the (single-ion) activity of a macromolecular species, or macroion, on concentration. In Figure 1, natural logarithms of a_{2p} of several polyelectrolytes having about the same degree of polymerization are shown against concentration (m) in a logarithmic scale. The a_{2p} was obtained from previous work on sodium polyacrylate (NaPAA)¹ and on sodium salts of polyvinyl alcohol partially acetalized with glyoxylic acid (NaPVAG).² It is readily seen from this figure that (1) a linear relation holds, (2) the slope is negative, and (3) the magnitude of the slope decreases with decreasing charge density. In Figure 2, $\ln a_{2p}$ of NaPVAG salts of various degrees of polymerization is presented, the ratio of charge z to degree of polymerization s being approximately constant (between 0.13 and 0.18). It is seen that a linear relation also holds with a negative slope; besides, (4) the magnitude of slope decreases with decreasing degree of polymerization. With respect to this finding, mention should be made of the fact that the slope is positive for very low molecular weight electrolytes, as is shown in Figure 3. In this figure the (single-ion) activity of polyvalent cations of the hydrochlorides of tetraethylenepentamine (TP) and diethylenetriamine (DT) and that of the potassium ion of potassium chloride are given.⁵ Thus, it is

(1) N. Ise and T. Okubo, *J. Phys. Chem.*, **69**, 4102 (1965).

(2) N. Ise and T. Okubo, *ibid.*, **70**, 1930 (1966).

(3) N. Ise and T. Okubo, *ibid.*, **70**, 2400 (1966).

(4) See, for example, T. Okubo, Y. Nishizaki, and N. Ise, *ibid.*, **69**, 3690 (1965). It should be noted that α was found to be insensitive toward concentration in the range covered.

(5) The activity of the polycations was calculated using the γ^* and γ_{2g}^* values mentioned in the ref 3. The activity of K^+ was calculated using MacInnes' convention and mean activity coefficient data reported earlier: T. Shedlovsky, *J. Am. Chem. Soc.*, **72**, 3680 (1950); H. S. Harned and B. B. Owen, *ibid.*, **59**, 1290 (1937). It should be further noted that the cation activities of the hydrochlorides of triethylenetetramine and ethylenediamine were also

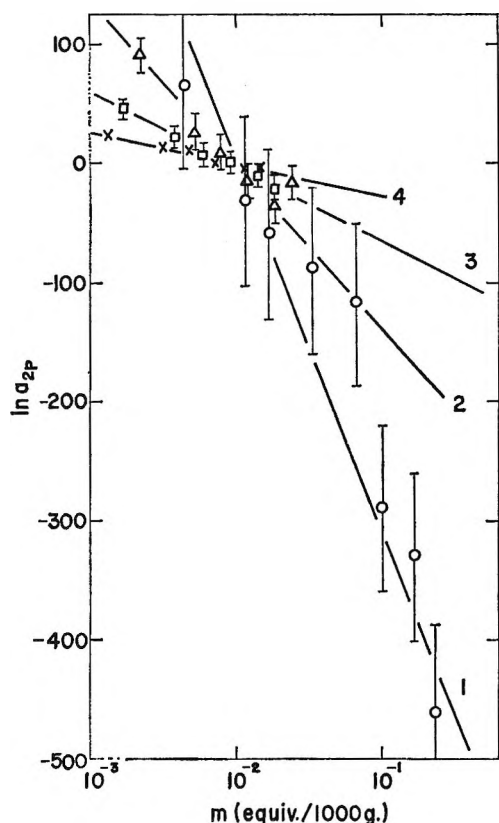


Figure 1. Concentration dependence of (single-ion) activity of macroions: (1) O, NaPAA (degree of polymerization $s = 1640$, degree of neutralization = 1.0); (2) Δ , NaPVAG-N3 ($s = 1700$, stoichiometric number of charge $z = 179$); (3) \square , NaPVAG-N2 ($s = 1700$, $z = 86$); (4) \times , NaPVAG-N1 ($s = 1700$, $z = 51$).

highly probable that the magnitude of the slope decreases with decreasing degree of polymerization, then passes through zero, and again increases with reversed sign.

According to the Flory-Huggins theory⁶ of neutral polymer solutions, the activity of solute polymer a_2 can be expressed as

$$\ln a_2 = \ln v_2 - (s - 1)(1 - v_2) + \chi_1 s(1 - v_2)^2 \quad (2)$$

where v_2 is the mole fraction of the solute, s is the degree of polymerization, and χ_1 is the interaction parameter.⁷ Equation 2 gives $\ln a_2$, which rises steeply with increasing concentration, when χ_1 can be assumed to be independent of concentration, as is often found⁸ to be approximately true. If the activity of the macromolecular component is taken to be comparable with the single-ion activity of macromolecular ionic species, we may say that this concentration dependence is in marked contrast to our second finding with macroions mentioned above.

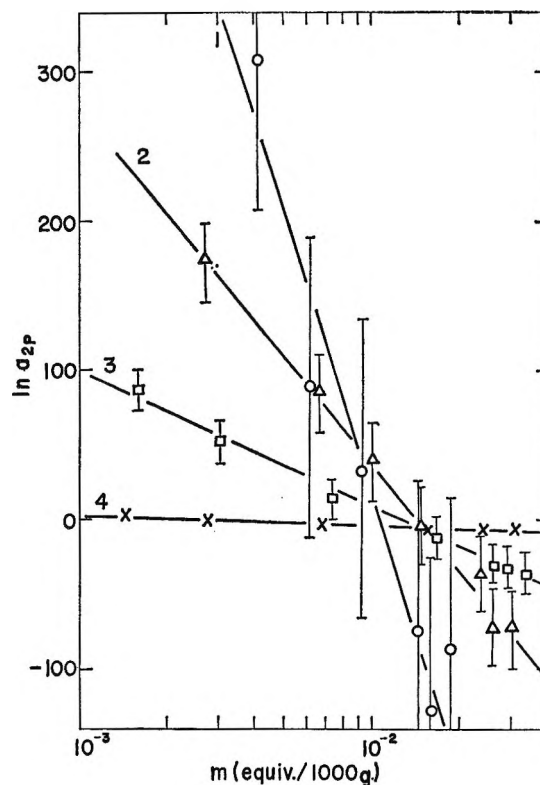


Figure 2. Concentration dependence of (single-ion) activity of macroions: (1) O, NaPVAG-27 ($s = 10,500$, $z = 1540$); (2) Δ , NaPVAG-24 ($s = 2490$, $z = 332$); (3) \square , NaPVAG-23 ($s = 1050$, $z = 164$); (4) \times , NaPVAG-21 ($s = 86$, $z = 15$).

By these comparisons with very low molecular weight electrolytes and neutral polymers in solution, the tendency for the activity to decrease with increasing concentration may be concluded to be characteristic of macroions. A large fraction of gegenions clusters around the macroions because of interionic attractive forces. If this force is strong enough, then the gegenions exert simultaneous attractive action on more than one macroion. The situation can be paraphrased by the statement that the macroions "attract" each other through the intermediary of the gegenions to inactivate

found to fall on the same line as shown in Figure 3. These data, however, were omitted for the sake of brevity.

(6) P. J. Flory, "Principles of Polymer Chemistry," Cornell University Press, Ithaca, N. Y., 1953, Chapter 12. This theory, as is well known, is not exactly applicable to the dilute solutions being discussed in this paper. Therefore, our argument in the text is not intended to be quantitative.

(7) The reference state of the activity in eq 2 is at $v_2 = 1$, whereas our reference state corresponds to a hypothetical infinite dilution of ionized groups. This difference does not matter in the present paper, since the concentration dependence of the activity is under consideration.

(8) See, for example, H. Tompa, "Polymer Solutions," Butterworth and Co. Ltd., London, 1956, p 96, 310. See also ref 6, Chapter 12.

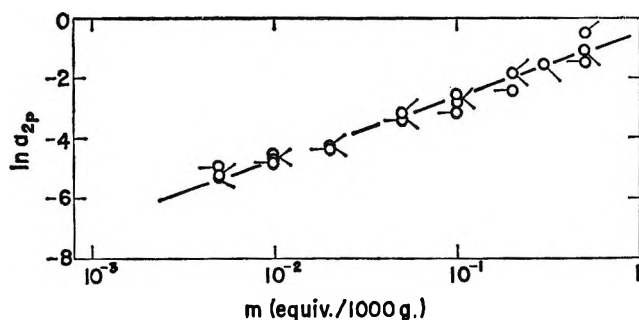


Figure 3. Concentration dependence of (single-ion) activity of very low molecular weight cations: \circ , $\text{TP}(\text{HCl})_6$; \square , $\text{DT}(\text{HCl})_3$; \triangle , KCl .

part of the macroions thermodynamically in spite of intermacroion repulsive force, so as to form an intermacroion "linkage."⁹ Thus, the (single-ion) activity of macroions decreases with increasing concentration, as was shown experimentally.

On the other hand, there exists no strong interaction such as the coulombic one in solutions of neutral polymers. Therefore, the intermacroion linkage would give rise to greater polymer association than would be expected between neutral polymer molecules.

Decreasing charge density or degree of polymerization clearly results in a decrease in the fraction of gegenions clustering around macroions and hence weakens the linkage. This would account for our third and fourth findings.

Acknowledgments. The authors gratefully acknowledge the criticisms and encouragements received from Professor Ichiro Sakurada. Their sincere thanks are due to Professor Michio Kurata for his stimulating discussion.

(9) This idea was earlier suggested (F. T. Wall and J. W. Drenan, *J. Polymer Sci.*, **7**, 83 (1951)) and theoretically treated (J. A. V. Butler, B. E. Conway, and D. W. F. James, *Trans. Faraday Soc.*, **50**, 612 (1954)). It is interesting to note that, as originally found in the case of the simple electrolyte solutions (H. S. Frank and P. T. Thompson, *J. Chem. Phys.*, **31**, 1086 (1959)), the cube-root rule of the concentration dependence of logarithm of mean activity coefficient was found to hold also for polyelectrolyte solutions in ref 2, and the rule was qualitatively accounted for by the intermacroion "linkage."

Absorption Spectrum of the Hydroxyl Radical¹

by J. K. Thomas, J. Rabani, M. S. Matheson, E. J. Hart, and S. Gordon

Chemistry Division, Argonne National Laboratory, Argonne, Illinois (Received January 20, 1966)

The discovery and identification of the absorption spectrum of the hydrated electron,² e_{aq}^- , has made

possible the measurement by means of the technique of pulse radiolysis of some 200 or more absolute rate constants for this species.³ It would also be advantageous to observe and identify the absorption spectra of the other primary transient species formed in the radiolysis of water. Reliable rate constants are known for the H atom;⁴ however, one would not expect the H atom in aqueous solution to absorb in an accessible region of the spectrum. On the other hand, the OH radical in the gas phase has groups of very narrow absorption lines belonging to a half-forbidden transition⁵ and, therefore, could exhibit a weak ultraviolet absorption in aqueous solution. In preliminary communications,^{6,7} we have suggested that there is indeed such a weak OH radical absorption below 3000 Å. In this paper this absorption is described and evidence for its identification presented.

Experimental Section

The pulse-radiolysis apparatus incorporating two light passes in the 4-cm cell, the high-pressure H_2 cell, and the dosimetry has already been described.⁸ At wavelengths below 2500 Å more than 10% of the photomultiplier signal was due to scattered light. However, by the use of interference filters (Baird Atomics Inc.) in conjunction with the Bausch and Lomb monochromator, the contribution of scattered light to the signal was reduced to less than 1%. It was then possible to observe absorptions down to 2200 Å precisely and probably to 2000 Å. Dosimetry was carried out by the direct observation of Fe^{3+} in a modified Fricke dosimeter (10 mM Fe^{2+} , 10^{-3} M O_2) where $G(\text{Fe}^{3+}) = 15.6$.

Results

Observation of the Spectrum. The points in Figure 1 are derived from initial optical densities, which were obtained by extrapolating optical density decay curves to the end of the 0.4- or 1.0- μsec pulse. For any given solution in Figure 1 pulses of equal intensity were used

(1) Based on work performed under the auspices of the U. S. Atomic Energy Commission.

(2) (a) E. J. Hart and J. W. Boag, *J. Am. Chem. Soc.*, **84**, 4090 (1962); (b) J. W. Boag and E. J. Hart, *Nature*, **197**, 45 (1963).

(3) See L. M. Dorfman and M. S. Matheson, *Progr. Reaction Kinetics*, **3**, 237 (1965), for a summary of work to May 1964.

(4) J. P. Sweet and J. K. Thomas, *J. Phys. Chem.*, **68**, 1363 (1964).

(5) O. Oldenberg and F. F. Rieke, *J. Chem. Phys.*, **6**, 439 (1938).

(6) J. Rabani and M. S. Matheson, *J. Am. Chem. Soc.*, **86**, 3175 (1964).

(7) J. K. Thomas, *Trans. Faraday Soc.*, **61**, 702 (1965).

(8) (a) L. M. Dorfman, I. A. Taub, and R. E. Buhler, *J. Chem. Phys.*, **36**, 3051 (1962); (b) S. Gordon, E. J. Hart, and J. K. Thomas, *J. Phys. Chem.*, **68**, 1262 (1964); (c) M. S. Matheson and J. Rabani, *ibid.*, **69**, 1324 (1965).

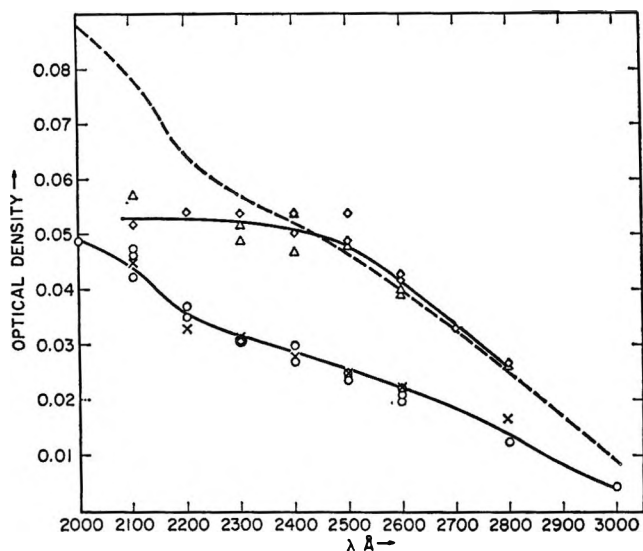


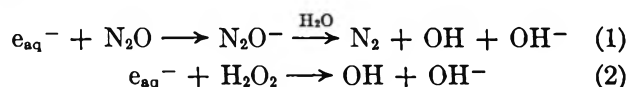
Figure 1. The absorption spectrum of the OH radical (optical path length, 8 cm; $0.76 \times 10^{-6} M$ OH radicals/pulse): O, 1 mN HClO₄, degassed; X, 1 mN H₂SO₄, degassed; ◇, 1 mM N₂O, neutral pH; Δ, $2 \times 10^{-4} M$ H₂O₂, neutral pH. In these results the optical density was corrected for the loss of H₂O₂ [$G(-H_2O_2) = 2.3$]; the extinction coefficients were taken from W. C. Schumb, C. N. Satterfield, and R. L. Wentworth in "Hydrogen Peroxide," A.C.S. Monograph Series No. 128, Reinhold Publishing Corp., New York, N. Y., 1955, p 287. The dashed line was obtained by multiplying the results in acid solution by 1.8. The molar extinction coefficient at 2600 Å is $370 M^{-1} cm^{-1}$.

on fresh solution at the various wavelengths indicated by the points. The molar extinction coefficient in $10^{-3} M$ HClO₄ at 2600 Å is $\epsilon_{OH}^{2600} = 370 M^{-1} cm^{-1}$; this is calculated from the dosimeter and using $G(OH) = 2.40$.

Identification of the Spectrum

Evidence supporting our assignment of this transient absorption band to the OH radical is derived from the effect of increased OH yields and from the effect of OH scavengers on the half-life.

Effect of Increased OH Radical Yields. Since $G_{OH} \approx G_{e_{aq}^-} = 2.6$,⁹ the replacement of e_{aq}^- by OH radicals should double the OH radical yield. The following reactions are commonly used for enhancing OH radical reactions



thereby doubling approximately $G(OH)$ since

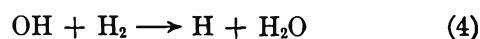


is the normal mode of e_{aq}^- removal in an acid solution. In the absence of N₂O and H₂O₂, reaction 3 is important since it removes the appreciable e_{aq}^- absorption in the spectral region where the OH band is found.

Note in Figure 1 that the approximate doubling of the optical density of the band takes place in the 1.0 mM N₂O and 0.2 mM H₂O₂ solutions at wavelengths between 2300 and 2800 Å.

Decay of the OH Radical Absorption

In the presence of high pressures of hydrogen, the OH radical absorption decays rapidly. In a typical experiment an initial optical density of 0.015 decays to a plateau level of 0.003. This residual absorption probably originates in the thick quartz window of the pressure cell. The rate of decay of the OH radical is first order and depends on the hydrogen gas pressure from 10 to 20 atm, giving $k_4 = (6.0 \pm 2.0) \times 10^7 M^{-1} sec^{-1}$.



The agreement with the literature values of $k_4 = 4.5 \times 10^7$ and 3.5×10^7 (ref 10 and 7, respectively) is satisfactory.

The decay of the OH radical absorption at 2600 Å *via* dimerization and *via* reaction with the H atoms is second order and has been reported.⁷ The value for $2k_{OH+OH}$ is $1.05 \times 10^{10} M^{-1} sec^{-1}$ and agrees with the values in the literature, 8×10^9 .¹⁰ The value for k_{H+OH} is $0.7 \times 10^{10} M^{-1} sec^{-1}$ and is lower than that reported by Fricke and Thomas.¹¹

The above data support the assignment of the absorption spectrum in Figure 1 to the OH radical. At wavelengths below 2300 Å, contrary to expectation, the spectrum in acid solution is larger than half that in the hydrogen peroxide and nitrous oxide solutions. This discrepancy from the predicted behavior might be attributed to another species, which is present only in the acidic solutions.

(9) J. Rabani, W. A. Mulac, and M. S. Matheson, *J. Phys. Chem.*, **69**, 53 (1965).

(10) H. A. Schwarz, *ibid.*, **66**, 255 (1962).

(11) H. Fricke and J. K. Thomas, *Radiation Res. Suppl.*, **4**, 25 (1964).

A New Σ -Plot Treatment of Equilibrium

Data and Its Application to the Vaporization of Bismuth Chloride¹

by Daniel Cubicciotti

Stanford Research Institute, Menlo Park, California 94025
(Received January 5, 1966)

The Σ -plot treatment of equilibrium data as ordinarily used² requires that the heat capacities of the sub-

stances involved be known as analytic functions of temperature. These are integrated in the Clausius-Clapeyron equation and Σ is defined as³

$$\Sigma = -R \ln K + \int \frac{1}{T^2} \int \Delta C_p dT dT \quad (1)$$

so that it will have linear dependence on $1/T$, *i.e.*

$$\Sigma = \Delta H_f/T + I \quad (2)$$

Many compilations provide thermodynamic data in tabular form at specific temperatures and not as analytic functions. This is particularly true of values calculated by statistical thermodynamics from molecular constant data since the electronic and vibrational contributions are obtained from tabulated data. As a result, the use of the ordinary Σ -plot method becomes difficult.

Principle of the Method

We have devised the following alternative Σ -plot procedure to use with tabular thermodynamic data. One can write

$$\frac{\Delta G^\circ_T}{T} = -R \ln K = \frac{\Delta H^\circ_T}{T} - \Delta S^\circ_T \quad (3)$$

$$\frac{\Delta G^\circ_T}{T} = \frac{\Delta H^\circ_{298}}{T} + \frac{\Delta(H^\circ_T - H^\circ_{298})}{T} - \Delta S^\circ_{298} - \Delta(S^\circ_T - S^\circ_{298}) \quad (4)$$

Define

$$\Sigma' = -R \ln K - \frac{\Delta(H^\circ_T - H^\circ_{298})}{T} + \Delta(S^\circ_T - S^\circ_{298}) \quad (5)$$

Therefore, also

$$\Sigma' = \frac{\Delta H^\circ_{298}}{T} - \Delta S^\circ_{298} \quad (6)$$

A plot of Σ' vs. $1/T$ should be a straight line whose slope gives ΔH°_{298} directly and whose intercept is ΔS°_{298} . (It is more precise, however, to obtain ΔS°_{298} by substituting values of Σ' and $1/T$ into eq 6, once ΔH°_{298} is known.) Alternately, the values of ΔH°_{298} and ΔS°_{298} can be obtained from a least-squares treatment of the data.

In practice, one adds to a measured value of $R \ln K$, at a given temperature, the quantity $\Delta(S^\circ_T - S^\circ_{298}) - \Delta(H^\circ_T - H^\circ_{298})/T$ obtained by interpolation from tabular data. When many values must be interpolated, it is more expedient to evaluate the quantity $\Delta(S^\circ_T - S^\circ_{298}) - \Delta(H^\circ_T - H^\circ_{298})/T$ at the temperatures tabulated and to plot the function for interpolation.

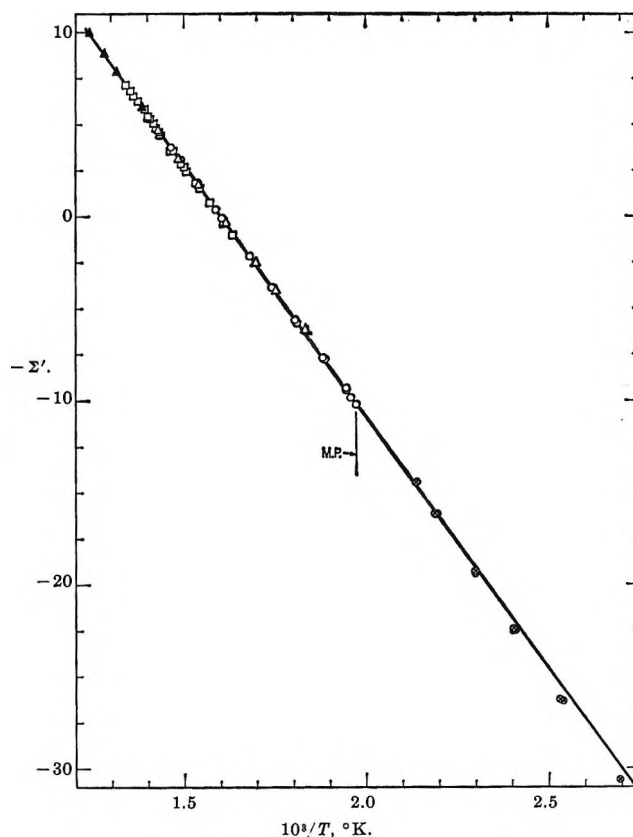


Figure 1. Σ' plot of BiCl_3 vapor pressure data: \square , Evnevich and Sukhodskii; Δ , Keneshea, *et al.*; \circ , Cubicciotti, *et al.*; \blacktriangle , Johnson, *et al.*; \otimes , Darnel and Yosim.

It is clear that the function $(S^\circ_T - S^\circ_{298}) - (H^\circ_T - H^\circ_{298})/T$ for a substance is simply the negative of the increment (at temperature T) of the free energy function above 298°K . We shall call this quantity the free energy function increment (fef incr). Thus

$$-\text{fef incr} = -\left(\frac{G^\circ_T - H^\circ_{298}}{T}\right)_T + \left(\frac{G^\circ_T - H^\circ_{298}}{T}\right)_{298} \quad (7)$$

$$-\text{fef incr} = (S^\circ_T - S^\circ_{298}) - \frac{(H^\circ_T - H^\circ_{298})}{T} \quad (8)$$

If tabular fef values are available, the calculation can be made through them. Once ΔH°_{298} and ΔS°_{298} are

(1) This work was made possible by the financial support from the Research Division of the U. S. Atomic Energy Commission under Contract AT(04-3)-106.

(2) For a discussion of the usual Σ -plot method see K. S. Pitzer and L. Brewer revision of G. N. Lewis and M. Randall, "Thermodynamics," McGraw-Hill Book Co., Inc., New York, N. Y., 1961, p 175.

(3) The symbols used in this paper have the same significance as in ref 2 except for modified Σ' .

Table I: Standard Thermodynamic Functions for BiCl₃

Gas			Condensed phases			
T_0 , °K	-fef, eu ^a	-fef incr, eu ^a	$H_T - H_{298}$, cal/mole ^b	$S_T - S_{298}$, eu ^b	-fef incr, eu ^c	-fef, eu ^c
298	85.24	41.70
400	90.88	0.74	2,610	7.53	1.00	42.70
500	95.23	2.18	5,170	13.24	2.90	44.60
506.7			(s) 5,340	13.58	3.04	44.74
506.7			(l) 11,050	24.85	3.04	44.74
600	98.81	3.79	14,100	30.36	6.87	48.57
700	101.84	5.41	17,360	35.35	10.56	52.26
800	104.48	6.97	20,620	39.74	13.97	55.67

^a Calculated from the data in K. K. Kelley, U. S. Department of Interior, Bureau of Mines Bulletin 594, U. S. Government Printing Office, Washington, D. C., 1960. ^b Calculated from values obtained in this laboratory, namely $C_p(s) = 25.6$ eu, $C_p(l) = 32.6$ eu, $\Delta H_f = 5.71$ kcal/mole, $T_f = 506.7^\circ\text{K}$. The experimental data will be published by D. Cubicciotti, H. Eding, F. J. Keneshea, and J. W. Johnson. ^c $\text{fef} = (G^\circ_T - H^\circ_{298})/T$, in which the reference state is *solid* BiCl₃ at 298°K.

determined from the experimental data, values of K can be calculated from them. From eq 4 one finds

$$R \ln K = \Delta S^\circ_{298} - \frac{\Delta H^\circ_{298}}{T} + \Delta(S^\circ_T - S^\circ_{298}) - \frac{\Delta(H^\circ_T - H^\circ_{298})}{T} \quad (9)$$

or alternatively

$$R \ln K = \Delta S^\circ_{298} - \frac{\Delta H^\circ_{298}}{T} - \Delta \text{fef incr} \quad (10)$$

The advantages of this method are the following. (a) It enables one to use tabular values of thermodynamic data without the labor of converting them to analytic form. (b) It gives the enthalpy and entropy changes for the reaction explicitly at the reference temperature—298°K for the form used above. (The usual Σ -plot treatment gives the enthalpy change in the temperature range of the measurements, while the entropy change is given indirectly in the integration constant.) (c) Perhaps the most important advantage is that data obtained *above and below* a transition should fall on the same straight line in this new Σ -plot method. Thus, for example, vapor pressures obtained above and below the melting point of a substance can be intercompared directly and values of ΔH°_{298} and ΔS°_{298} obtained that simultaneously weight liquid and solid data. (In the usual Σ -plot method a value of ΔH is obtained for one phase from one plot and another applicable to the second phase is obtained from another plot. Their difference is then compared with the heat of transition.)

Application to the Vaporization of BiCl₃

The vapor pressure of BiCl₃ has been measured for

the liquid and for the solid but these results have not been intercompared. The thermodynamic functions of the vapor have been calculated from molecular constant data.⁴ We have measured the enthalpy increments above 298°K for the condensed phases and so can evaluate the free energy function increments.

Values for the fef incr are given in Table I. For use in the above Σ -plot method, $\Delta \text{fef incr}$ (*i.e.*, the difference of fef incr between the vapor and condensed phases) was plotted as a function of temperature to give two smooth curves that intersect at the melting point. This plot was used to calculate Σ' for each vapor pressure measurement. Σ' was defined according to the above treatment as

$$-\Sigma' = R \ln p(\text{atm}) + \Delta \text{fef incr}$$

The Σ' plot for BiCl₃ is shown in Figure 1. For the liquid there are four sets of vapor pressure measurements in good agreement: Evnevich and Sukhodskii⁵ (by a boiling method), Keneshea, *et al.*⁶ (by a spiral gauge manometer), Cubicciotti, *et al.*⁷ (by transpiration), and Johnson, *et al.*⁸ (by boiling point). The higher pressure values of Maier⁹ are in agreement with the above data but his lower values are not; the results

(4) K. K. Kelley and E. G. King, U. S. Department of the Interior, Bureau of Mines Bulletin 592, U. S. Government Printing Office, Washington, D. C., 1961.

(5) E. V. Evnevich and V. A. Sukhodskii, *J. Russ. Phys. Chem. Soc.*, **61**, 1503 (1929).

(6) F. J. Keneshea, W. Wilson, and D. Cubicciotti, *J. Phys. Chem.*, **64**, 827 (1960).

(7) D. Cubicciotti, F. J. Keneshea, and C. M. Kelley, *ibid.*, **62**, 463 (1958).

(8) J. W. Johnson, W. J. Silva, and D. Cubicciotti, *ibid.*, **69**, 3916 (1965).

(9) C. G. Maier, U. S. Department of the Interior, Bureau of Mines Technical Paper No. 360, 1925.

of Tarasenkov and Afinogenov¹⁰ are too low in general. These last two sets of data were not considered in the present calculation.

The best straight line through the first four sets of data was drawn on a large-scale plot. Of the 71 data points for the liquid, 90% lie between two parallel straight lines of slope 27.3 kcal/mole and separated by 0.2 unit on the Σ' scale. The slope of the median line gives ΔH°_{298} (the standard enthalpy of sublimation at 298°K). Limits of uncertainty were taken from the lines of largest and smallest slope that could be put between these parallel lines in the range of the data. The resulting value of ΔH°_{298} was 27.3 ± 0.2 kcal/mole. ΔS°_{298} (the standard entropy of sublimation at 298°K) was taken from the value of Σ' at the midtemperature of the data through eq 6. Its uncertainty was evaluated from that associated with ΔH and the experimental uncertainty in Σ' . ΔS°_{298} was found to be 43.7 ± 0.4 eu.

A least-squares treatment of the data was obtained from the institute's computation group. The values and their standard deviations by this treatment were $\Delta H^\circ_{298} = 27.20 \pm 0.07$ kcal/mole and $\Delta S^\circ_{298} = 43.56 \pm 0.04$ eu. The differences between these and the graphical values are small. They occur because the higher temperature points were weighted somewhat more heavily than the midrange points in the graphical evaluation. This author prefers the graphical method of evaluation of data from different experimenters because of the convenience in weighting the data visually. Therefore, the data derived graphically are considered the more reliable and are used below in preference to the least-squares data.

For the solid there is only one set of vapor pressure data, those of Darnell and Yosim¹¹ by effusion. When Σ' is evaluated by the above method, the values above and below the melting point should fall on the same straight line. In the high-temperature region of their data, the values obtained by Darnell and Yosim fall close to the line defined by the liquid data; however, at the low-temperature end their data fall below the line by as much as 15% in pressure. The enthalpy and entropy of sublimation derived from the solid data alone (29.8 kcal/mole and 49.3 eu, respectively) are substantially different from the values derived from the liquid. The difference is presumed by this author to be due to some systematic error in the measurements over the solid.

The absolute entropy of $\text{BiCl}_3(\text{g})$ at 298°K is 85.4 ± 1.0 eu as calculated from molecular constants by Kelley.⁴ Using ΔS°_{298} , sublimation, of 43.7 ± 0.4 eu from above, one calculates the S°_{298} for solid BiCl_3 to be 41.7 ± 1.5 eu. With this value one can calculate

the free energy function for BiCl_3 in the condensed phases by subtracting it from the fef incr of Table I. Values of fef are given in the last column of the table.

The vapor pressure of BiCl_3 can be calculated at any temperature from (10). Thus $R \ln p(\text{atm}) = 43.7 - (27,300/T) - \Delta \text{fef}$ incr, with values of Δfef incr interpolated from the data in Table I.

(10) D. H. Tarasenkov and B. P. Afinogenov, *Zh. Fiz. Khim.*, **9**, 889 (1937).

(11) A. J. Darnell and S. J. Yosim, *J. Phys. Chem.*, **63**, 1813 (1959).

Transition Energies for a Merocyanine Dye in Aqueous Electrolyte Solutions. Solvent Polarity Indicator Transition Energy-Internal Pressure Relations¹

by John E. Gordon

Woods Hole Oceanographic Institution,
Woods Hole, Massachusetts 02543 (Received January 26, 1966)

Numerous compounds are known whose electronic transition energies, E_T , are more or less sensitive functions of the polarity of the solvent in which they are dissolved.²⁻⁴ That these transition energies measure a "microscopic" solvent polarity (in contrast to "macroscopic" measures such as the dielectric constant) and correlate better with chemical parameters representing solvent ionizing power, e.g., the Winstein-Grunwald Y values, than with functions of dielectric constant, e.g., $(D - 1)/(2D + 1)$, has been amply discussed.²⁻⁴ It is, however, instructive to extend these comparisons to include one further macroscopic quantity, namely, the cohesive energy density or internal pressure of the solvent, $\Delta E_v/V$ (ΔE_v = energy of vaporization, V = molar volume). Some such comparisons are made in Figures 1-3.

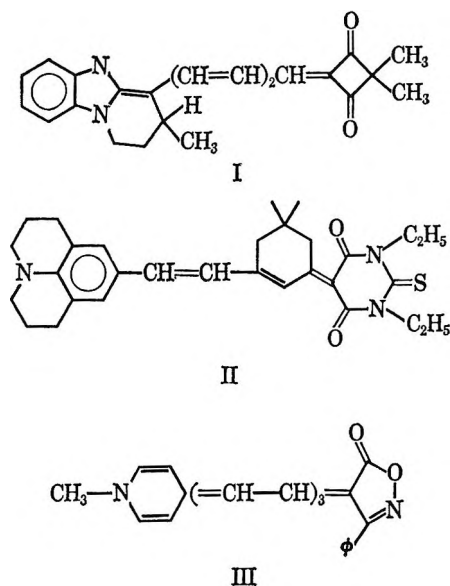
Figure 1 employs transition energies for the blue-shifting, polar merocyanine, I, given the symbol χ_B by Brooker, *et al.*^{2b} Figure 2 illustrates the analogous Z

(1) Contribution No. 1643 from the Woods Hole Oceanographic Institution; supported in part by the National Science Foundation, Grant No. GP 5110, and in part by the Office of Naval Research, Contract nonr 2196(00).

(2) (a) L. G. S. Brooker, *et al.*, *J. Am. Chem. Soc.*, **73**, 5332 (1951); (b) L. G. S. Brooker, A. C. Craig, D. W. Heseltine, P. W. Jenkins, and L. L. Lincoln, *ibid.*, **87**, 2443 (1965).

(3) E. M. Kosower, *ibid.*, **80**, 3253 (1958).

(4) K. Dimroth, C. Reichardt, T. Siepmann, and F. Bohlmann, *Ann.*, **661**, 1 (1963).



values measured by Kosower³ for 1-ethyl-4-carbomethoxypyridinium iodide. Two specially interesting families of solvents have been extracted from the more extensive compilation^{2b} of transition energies for the red-shifting dye II (χ_R values) to make up Figure 3.⁵

Consideration of the internal pressure at least provides an alternative view of this solvatochromism, for if one considers a dipolar solvent polarity indicator molecule comparable in dimensions and moment to the surrounding solvent dipoles, transition to a nonpolar electronic state ("blue-shifting" solute) is related to the creation of a hole in the solvent, and the transition

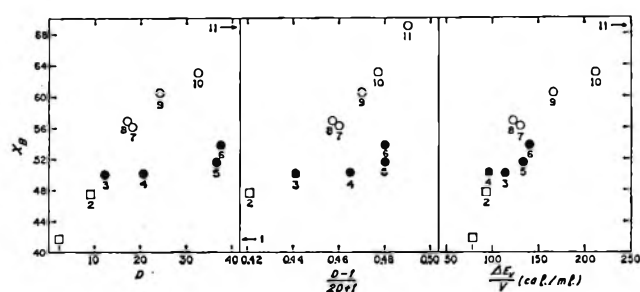


Figure 1. Plots of χ_B vs. D , $(D - 1)/(2D + 1)$, and $\Delta E_v/V$: O, hydroxylic solvents; ●, dipolar aprotic solvents; □, nonpolar and other solvents; 1, toluene; 2, dichloromethane; 3, pyridine; 4, acetone; 5, N,N-dimethylformamide; 6, acetonitrile; 7, 2-propanol; 8, 1-butanol; 9, ethanol; 10, methanol; 11, water. Heats of vaporization taken from: (a) "Landolt-Börnstein Physikalisch-Chemisch Tabellen," Springer, Berlin, 1929-1936; (b) A. Weissberger, E. S. Proskauer, J. A. Riddick, and E. E. Toops, Jr., "Organic Solvents," 2nd ed, Interscience Publishers, Inc., New York, N. Y., 1955; (c) J. H. Hildebrand and R. L. Scott, "The Solubility of Nonelectrolytes," 3rd ed, Dover Publications, Inc., New York, N. Y., 1964; (d) S. T. Preston, Jr., *J. Gas Chromatog.*, 1 (3), 8 (1963).

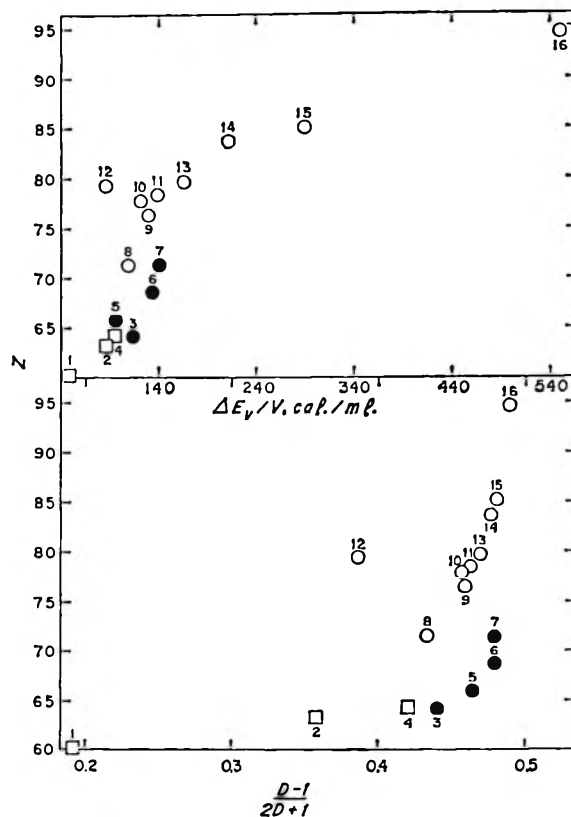


Figure 2. Plots of Z vs. $\Delta E_v/V$ and $(D - 1)/(2D + 1)$. Symbols are as in Figure 1: 1, 2,2,4-trimethylpentane; 2, chloroform; 3, pyridine; 4, dichloromethane; 5, acetone; 6, N,N-dimethylformamide; 7, acetonitrile; 8, *t*-butyl alcohol; 9, 2-propanol; 10, 1-butanol; 11, 1-propanol; 12, acetic acid; 13, ethanol; 14, methanol; 15, ethylene glycol; 16, water.

energy to the electrostatic component of the energy required to create the hole working against the cohesive forces of the liquid.⁶⁻⁸ (This qualitative model can be generalized from total to partial dipole annihilation, hence to any change in moment, and to inclusion of "red-shifting" indicators.) The transition energy should thus be a function of the internal pressure of the liquid, and its solvent sensitivity a function of the change in dipole. Ample opportunity exists, with complex indicators of the sort employed, for specific solute-solvent effects, for modification of the local cohesive energy density of the solvent by solute, and for modifi-

(5) Only with χ_R was a selection of data made to illustrate a specific point; the two foregoing cases include all compounds for which heat of vaporization data could be found. The remaining χ_R data behave similarly to those of Figures 1 and 2.

(6) N. C. Deno and H. E. Berkeimer, *J. Chem. Eng. Data*, 5, 1 (1960); *J. Org. Chem.*, 28, 2143 (1963).

(7) F. H. Stillinger, Jr., in "Molten Salt Chemistry," M. Blander, Ed., Interscience Publishers, Inc., New York, N. Y., 1964, pp 45, 102 ff.

(8) R. A. Pierotti, *J. Phys. Chem.*, 69, 281 (1965).

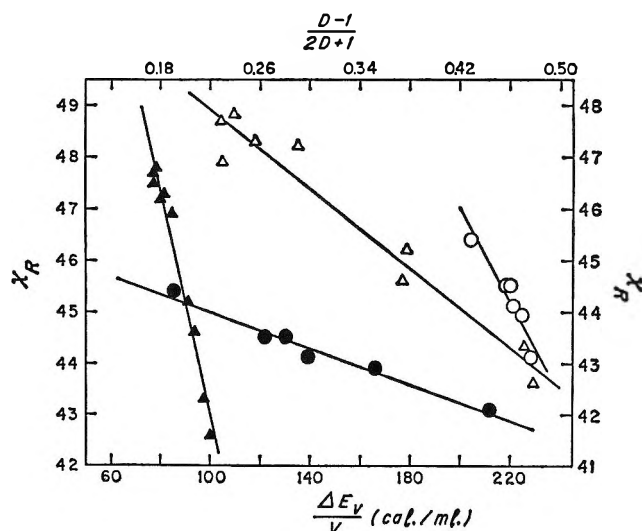


Figure 3. Plot of χ_R vs. $(D - 1)/(2D + 1)$ and $\Delta E_V/V$. Solid points ($\Delta E_V/V$): left ordinate, lower abscissa. Open points $(D - 1)/(2D + 1)$: right ordinate, upper abscissa. Δ , substituted benzenes, ArX, X = *m*-, *p*-, *o*-dimethyl, methyl, H, Cl, Br, CN, NO₂; O, alcohols, ROH, R = 1-octyl, 1-butyl, 2-propyl, 1-propyl, ethyl, methyl. Equations of least-squares lines and correlation coefficients: (1) for ArX, $\chi_R = 64.5 - 0.215\Delta E_V/V$, $r = 0.987$; (2) for ArX, $\chi_R = 52.1 - 19.1(D - 1)/(2D + 1)$, $r = 0.975$; (3) for ROH, $\chi_R = 46.7 - 0.0175\Delta E_V/V$, $r = 0.985$; (4) for ROH, $\chi_R = 64.4 - 43.9(D - 1)/(2D + 1)$, $r = 0.950$.

cation of the dipole moment change by electronic changes in solvent-indicator hydrogen bonds, where these exist.

According to Figures 1-3, correlation with the internal pressure diminishes the split of the transition energy data into hydroxylic-nonhydroxylic families⁴ as compared to correlation with functions of the dielectric constant; the dipolar aprotic solvents are universally better reconciled with the other liquids. The point of introducing the cohesive energy density is, however, not that it affords better correlations than the dielectric constant or that it supplants in any way the relations with chemical or microscopic solvent polarity measures, nor is it that the above model is more attractive or even very different from that offered by previous authors.³

The point of importance is that the cohesive energy density is a quantity of considerable importance, and any new source of information on it should be explored. Particularly in aqueous salt solutions and in the theory of salt-induced medium effects is the internal pressure a key variable.⁹⁻¹¹ Thus the first satisfactory theory¹² of nonelectrolyte salting relates salting-in or salting-out to the effect of the electrolyte on the cohesive energy density of the water by way of the energy required to create a hole for the nonelectrolyte. This effect of the electrolyte is measured independently by the quantity

$(V_s - \bar{V}_s^0)/\beta_0$, where $(V_s - \bar{V}_s^0)$ is the electrostriction of the salt and β_0 is the compressibility of water.¹³ Unfortunately, electrostrictions are not known for many salts of interest, and the ambiguity of estimating the intrinsic volume occupied by the ions in solution, V_s , has led to a number of electrostriction scales which, while generally agreeing in the order of the various salts, differ broadly in actual magnitude.^{9,11,14-16} Any readily measured quantity which can be shown to be quantitatively related to the electrostriction would thus be of value in, *e.g.*, the correlation of nonelectrolyte salting measurements, particularly in solutions of mixed or unfamiliar electrolytes. In the hope of finding such a property in the salt dependence of the transition energy of an appropriate solvent polarity indicator, we have made some preliminary measurements with aqueous electrolyte solutions of the merocyanine dye M88.^{2a}

Experimental Section

The inorganic salts employed were of analytical reagent quality. Distillation Products Industries tetra-*n*-propylammonium bromide and sodium benzenesulfonate were used as received and recrystallized three times from 90-95% ethanol, respectively. The dye was kindly furnished by Dr. L. G. S. Brooker, Eastman Kodak Co., and was used as received. A saturated methanol solution of the dye (8 μ l) was added to 3 ml of deionized water, or of a salt solution prepared therefrom, and the visible spectrum was immediately recorded on a Cary Model 14 spectrophotometer. This was found to be the most reproducible method of preparing the solutions, as the dye is very slow to dissolve in water and ultrasonic treatment resulted in chemical alteration. The solutions were stable during the time of measurement but decolorized on standing overnight. Salt solutions of low pH (*e.g.*, Al₂(SO₄)₃) decolorize the dye.

Results and Discussion

Observed wavelengths and computed transition energies for solutions of five salts are summarized in Table I and Figure 4. Unfortunately, the shifts are not

- (9) N. C. Deno and C. H. Spink, *J. Phys. Chem.*, **67**, 1347 (1963).
- (10) M. A. Paul, *J. Am. Chem. Soc.*, **74**, 5274 (1952).
- (11) F. A. Long and W. F. McDevit, *Chem. Rev.*, **51**, 119 (1952).
- (12) W. F. McDevit and F. A. Long, *J. Am. Chem. Soc.*, **74**, 1773 (1952).
- (13) Or alternatively by dP_e/dc_s where P_e is the effective pressure exerted by the salt in solution: R. E. Gibson, *J. Am. Chem. Soc.*, **56**, 4, 865 (1934); **57**, 284 (1935).
- (14) P. Mukerjee, *J. Phys. Chem.*, **65**, 740, 744 (1961).
- (15) J. Padova, *J. Chem. Phys.*, **40**, 691 (1964).
- (16) E. Glueckauf, *Trans. Faraday Soc.*, **61**, 914 (1965).

Table I: Wavelengths and Transition Energies of the Visible Absorption Band of the Dye M88 in Aqueous Salt Solutions

Salt concn, mole/l.	Na ₂ SO ₄		MgSO ₄		Salt NaCl		C ₆ H ₅ SO ₃ Na		Pr ₄ NBr	
	A	E _T ^a	A	E _T ^a	A	E _T ^a	A	E _T ^a	A	E _T ^a
0	4877 ^b	58.62								
0.25	4845	59.01	4854	58.90	4863	58.79	4908	58.25	4961	57.63
0.50	4833	59.16	4841	59.06	4852	58.92	4929	58.00	5012	57.04
1.00	4832	59.17	4828	59.22	4846	59.00	4972	57.50	5100	56.06
2.00			4817	59.35	4836	59.12				
4.00					4833	59.16				

^a $E_T(\text{kcal/mole}) = 28.59 \times 10^4/\lambda(\text{\AA})$. ^b Brooker, *et al.*,² report 4875 Å.

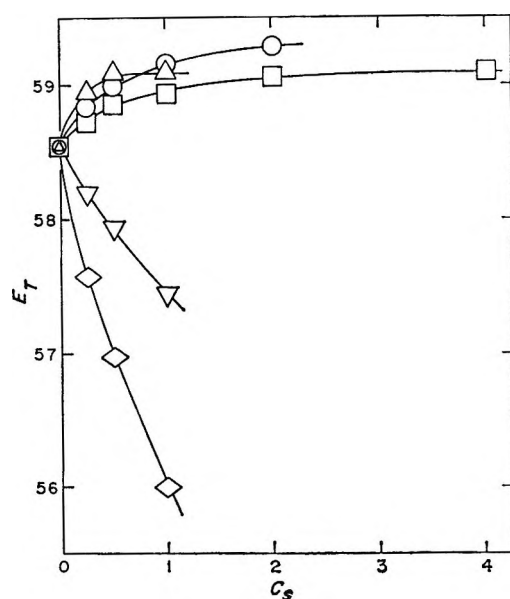


Figure 4. Transition energy, E_T (kcal/mole), of the merocyanine dye M88 in aqueous salt solutions vs. molarity of the salt: Δ , Na₂SO₄; \circ , MgSO₄; \square , NaCl; ∇ , NaC₆H₅SO₃; \diamond , (n-C₃H₇)₄NBr.

large relative to the precision of measurement of λ_{\max} for this broad band (± 3 –5 Å). More solvent-sensitive indicators are known,^{2b} however, and in the hope of making measurements with one of these at a later date, we did not attempt to determine quantitatively the limiting slopes dE_T/dc_s in the present system.

Qualitatively, the order of the limiting E_T vs. salt concentration slopes (Na₂SO₄ > MgSO₄ > NaCl > C₆H₅SO₃Na > Pr₄NBr) observed is the known order of

electrostrictions: Na₂SO₄, 53;⁹ MgSO₄, 46–65;¹⁴ NaCl, 12.8;⁹ C₆H₅SO₃Na, -9.0;⁹ Pr₄NBr, -32⁹ ml/mole. Correct also is the sign in each case; the salts with positive electrostrictions give blue shifts, those with negative electrostrictions red shifts, corresponding to non-electrolyte salting-out and salting-in, respectively.⁹

Kosower's model³ of the pyridinium iodide solvatochromism applied to the aqueous electrolyte systems would consist of a description of the effect of the various salts on the ability of the water to be organized into "cybotactic regions" about the indicator molecule, which could only follow from quantitative understanding of the effect of the ions on the water structure. This actively pursued goal of solution chemistry is, on the other hand, the key to prediction of the molal volumes of ions and the electrostriction,^{14–17} and the two views of the solvatochromism are thus closely related. It is doubtful that indicator E_T measurements will contribute appreciably to the underlying theory. The unknown role of possible local alteration of the native water structure by the large dye molecule itself has been pointed out earlier in this note and in the previous literature.^{2b,3} Nevertheless, the possibility of a useful empirical dE_T/dc_s -electrostriction-nonelectrolyte salting correlation appears real enough to justify the study of a greater variety of salts with a more sensitive indicator.

Acknowledgment. The author thanks Dr. L. G. S. Brooker for a gift of the merocyanine M88 and Mr. Robert L. Thorne for technical assistance.

(17) H. S. Frank and W.-Y. Wen, *Discussions Faraday Soc.*, **24**, 133 (1957).

COMMUNICATIONS TO THE EDITOR

The Thermodynamics of the System Pentafluorobenzene-Benzene

Sir: Much interest has recently been shown in the thermodynamic properties of binary systems of the type aromatic fluorocarbon-aromatic hydrocarbon. Hexafluorobenzene has been shown to form solid equimolar complexes with most aromatic hydrocarbons,^{1,2} and this is believed to be due to charge-transfer interaction with the fluorocarbon acting as the electron acceptor. From the experimental excess volumes of mixing,³ it appears that the extent of complexing increases as the electron-donating power of the hydrocarbon is increased.

The heats of mixing of the two systems hexafluorobenzene-benzene and pentafluorobenzene-benzene have been measured recently by Fenby, McLure, and Scott,⁴ who show that a reasonable interpretation of the results is that the specific interactions are much weaker in the system containing pentafluorobenzene. Our results presented here confirm that, in the solid state, this interpretation is correct.

The experimental phase diagram for the system pentafluorobenzene-benzene is shown in Figure 1 and was obtained using an apparatus previously described.² The system is seen to form two weak compounds

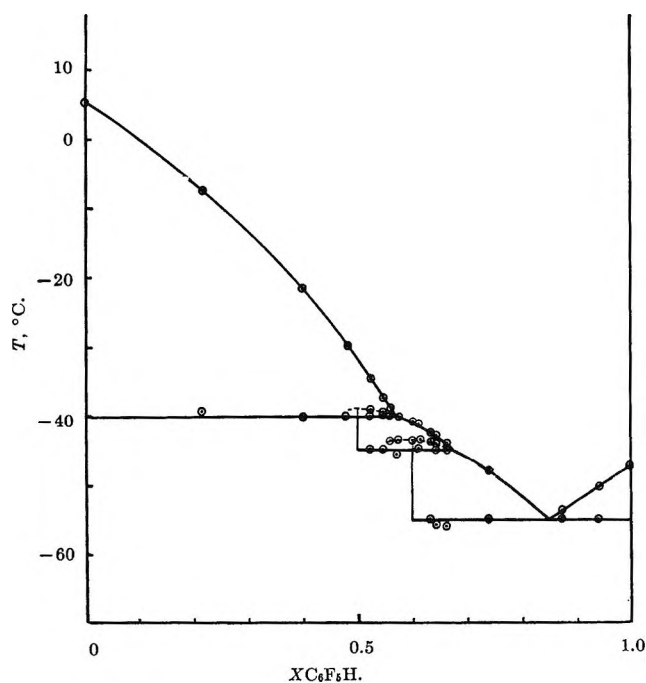


Figure 1. The phase diagram of the system pentafluorobenzene-benzene.

with incongruent melting points, the mole ratios of fluorocarbon to hydrocarbon being 1:1 and 3:2. The occurrence of an intermolecular complex of a molar ratio 3:2 appears to be unique among binary systems of organic substances. Our results do not agree with those of Patrick and Prosser,¹ who found no evidence for compound formation in this system. In contrast, hexafluorobenzene-benzene forms a strong 1:1 complex melting some 20° higher than the melting point of either pure component.

- (1) C. R. Patrick and G. S. Prosser, *Nature*, **187**, 1021 (1960).
- (2) W. A. Duncan and F. L. Swinton, *Trans. Faraday Soc.*, **62**, 1082 (1966).
- (3) W. A. Duncan, J. P. Sheridan, and F. L. Swinton, *ibid.*, **62**, 1090 (1966).
- (4) D. V. Fenby, I. A. McLure, and R. L. Scott, *J. Phys. Chem.*, **70**, 602 (1966).

DEPARTMENT OF PURE AND APPLIED
CHEMISTRY
UNIVERSITY OF STRATHCLYDE
GLASGOW C.1., SCOTLAND

WILLIAM A. DUNCAN
FINDLAY L. SWINTON

RECEIVED APRIL 18, 1966

Isomeric Transition Induced Reactions of Iodine-130 in Cyclohexane

Sir: Discovery of the $^{130}\text{I}^m$ (I.T.) ^{130}I nuclear reaction ($T_{1/2}$, 9.2 min)¹ has made it possible to compare isomeric transition induced reactions with reactions effected by other nuclear transformations in the iodine system. Several processes were reported to produce the same effects in several liquid alkyl halides.^{2,3} In the cyclohexane-iodine system, where iodine is not contained in the target molecule, the (n, 2n) reaction was reported to cause higher organic yields than the (n, γ) reaction due to its higher recoil energy.⁴ Since isomeric transition activated ^{130}I would be expected to have less kinetic energy than (n, γ)-activated ^{128}I , an isotope effect might be expected. None was found in the *n*-hexane-iodine system¹ within $\pm 5\%$.

Using the freeze-thaw technique developed in the study of $^{82}\text{Br}^m$ (I.T.) ^{82}Br reactions,⁵ we obtained the

- (1) D. D. Wilkey and J. E. Willard, *J. Chem. Phys.*, **44**, 970 (1966).
- (2) R. H. Schuler, *ibid.*, **22**, 2026 (1954).
- (3) G. Levey and J. E. Willard, *J. Am. Chem. Soc.*, **74**, 6161 (1952).
- (4) R. H. Schuler and C. E. McCauley, *J. Chem. Phys.*, **25**, 1080 (1956).
- (5) J. A. Merrigan, W. K. Ellgren, and E. P. Rack, *ibid.*, **44**, 174 (1966).

organic yields due to $^{130}\text{I}^{\text{m}}$ (I.T.) ^{130}I processes in liquid cyclohexane within $\pm 0.8\%$. Detailed experimental procedures and equipment used were described previously.^{5,6}

The organic yield of ^{130}I following neutron irradiation and decay of $^{130}\text{I}^{\text{m}}$ in the solid state was 2.8% in the 7.8×10^{-3} mole fraction $^{129}\text{I}_2$ system. This low yield was attributed to a phase separation between iodine and the cyclohexane (clumping) upon freezing, similar to that found in Br_2 -containing systems.^{5,7,8} When an identical sample was melted 20 sec after a 30-sec solid-state irradiation and $^{130}\text{I}^{\text{m}}$ allowed to decay in the liquid system, the yield was 21.7%. Allowing for the fraction of ^{130}I born by (I.T.) reactions (0.61),¹ and the fraction of $^{130}\text{I}^{\text{m}}$ which decayed while the sample was solid, the organic yield of ^{130}I due to (I.T.) was $1/(0.956 \times 0.61)$ times the ^{130}I yield observed after the $^{130}\text{I}^{\text{m}}$ decayed out in the liquid, minus 1.9%, i.e., 35.3%. The 1.9% is a correction for the organically combined ^{130}I as a result of solid-state reactions induced by (n, γ) processes and the fraction of $^{130}\text{I}^{\text{m}}$ which decayed while the sample was solid.

By resolidifying samples containing $^{130}\text{I}^{\text{m}}$, the high rate of increase in organic yield due to (I.T.) could be halted by the clumping of $^{129}\text{I}^{130}\text{I}^{\text{m}}$. Thus, growth in ^{130}I yield due to (I.T.) in the liquid state could be described by the equation,⁵ $R^t - R^0 = R^\infty - R^0(1 - e^{-\lambda t})$, where R^∞ is the yield due to (I.T.) after all $^{130}\text{I}^{\text{m}}$ had decayed, R^t is the yield due to (I.T.) at any time t , R^0 is the yield contribution of (n, γ) and the part of the (I.T.) processes occurring in the solid state, and λ is the decay constant for $^{130}\text{I}^{\text{m}}$. By analyzing a plot of ^{130}I organic yield due to (I.T.) vs. time after irradiation, as was done in the bromine system,⁵ a $^{130}\text{I}^{\text{m}}$ half-life of 8.9 ± 0.3 min was found. The values of organic yields of ^{130}I due to $^{130}\text{I}^{\text{m}}$ (I.T.) ^{130}I processes and those of ^{128}I produced by the ^{127}I (n, γ) ^{128}I process are compared with those due to $^{82}\text{Br}^{\text{m}}$ (I.T.) Br^{82} and ^{79}Br (n, γ) $^{80}\text{Br}^{\text{m}}$ in Table I.

Table I: Organic Yields of (I.T.)-Produced ^{130}I and ^{82}Br and (n, γ)-Produced ^{128}I and $^{80}\text{Br}^{\text{m}}$ in Cyclohexane at Room Temperature

Mole fraction of I_2	^{130}I	^{128}I	^{82}Br	$^{80}\text{Br}^{\text{m}}$
7.8×10^{-3}	35.3	36.1	35.3	22.5
5.2×10^{-3}	39.6	40.5	39.2	25.4

The similarity between ^{130}I and ^{128}I yields may indicate a similarity of reaction mechanisms independent of the initial kinetic energy of the activated atom. Their likeness to ^{82}Br yields would suggest that activated halogens may trace chemical processes which

result from a similarity of environmental activation and/or decomposition. These similarities were also found between ^{130}I , ^{128}I , and ^{80}Br formed by (I.T.), (n, γ), and (I.T.) processes, respectively, in *n*-hexane by Wilkey and Willard.¹ The Auger electron reaction hypothesis⁹ may explain these phenomena. The fact that radiative neutron capture induced yields of bromine were lower than (I.T.)-produced yields of ^{82}Br was found universal for the liquid C_8 alkanes.¹⁰ This may indicate that processes additional to Auger radiation induced reactions occur in iodine and (I.T.)-activated ^{82}Br , or possibly that internal conversion of (n, γ)-activated bromine occurs before the recoil energy has been dissipated; thus it would be carried away from the center of the pocket of fragments caused by radiolytic effects. The freeze-thaw technique,⁵ which lends itself to a high degree of precision, is a very valuable tool for studying isomeric transition induced reactions.

Acknowledgment. This is A.E.C. Document No. COO-1617-1.

- (6) J. A. Merrigan and E. P. Rack, *J. Phys. Chem.*, **69**, 2795 (1965).
 (7) R. M. A. Hahne and J. E. Willard, *ibid.*, **68**, 2582 (1964).
 (8) M. Milman, *J. Am. Chem. Soc.*, **80**, 5592 (1958).
 (9) P. R. Geissler and J. E. Willard, *J. Phys. Chem.*, **67**, 1675 (1963).
 (10) J. A. Merrigan, J. B. Nicholas, and E. P. Rack, *Radiochim. Acta*, in press.

DEPARTMENT OF CHEMISTRY
 UNIVERSITY OF NEBRASKA
 LINCOLN, NEBRASKA 68508

J. A. MERRIGAN
 J. B. NICHOLAS
 R. M. LAMBRECHT
 N. J. PARKS
 E. P. RACK

RECEIVED MAY 6, 1966

Anomalous Effect of Pressure on the Protolytic Dissociation of Excited States of Nitrophenols

Sir: In general, the ionic dissociation of a weak electrolyte in water involves a substantial contraction, and as a corollary the process is favored by an increase of hydrostatic pressure. The contraction arises because the free ions exert a powerful electrostatic attraction on the surrounding solvent and compress it to a greater density than normal. The phenomenon and its cause have been known for many years and were the subject of a review by the writer¹ in 1963. At that time, some 30 weak acids and bases had been examined under

(1) S. D. Hamann in "High Pressure Physics and Chemistry," R. S. Bradley, Ed., Academic Press Inc., New York, N. Y., 1963, Vol. 2, pp 146-156.

Table I: Spectral Shifts and Volume Changes for Some Nitrophenols in Water at 25°

Compound	$\partial\bar{\nu}_{\text{ROH}}/\partial P$	$\partial\bar{\nu}_{\text{RO}^-}/\partial P$	$\partial\Delta\bar{\nu}/\partial P$	$\Delta\bar{V}^* - \Delta\bar{V}$	$\Delta\bar{V}$	$\Delta\bar{V}^*$
	cm^{-1}	atm^{-1}				
2-Nitrophenol	-0.050 (25,910) ^a	0.015 (21,790) ^a	-0.065	7.7	-15.5	-8
2,5-Dinitrophenol	-0.060 (25,510)	-0.035 (20,960)	-0.025	3.0	-11.6	-9
3-Nitrophenol	-0.070 (27,170)	0.020 (22,680)	-0.090	10.6	-16.1	-5
4-Nitrophenol	-0.125 (28,570)	0.035 (23,090)	-0.160	18.9	-11.8	7
4-Nitro-2,6-dibromophenol	-0.125 (28,820)	0.030 (23,040)	-0.155	18.3	-10.9	7
4-Nitro-2-aminophenol	-0.090 (24,040)	0.020 (20,280)	-0.110	13.0	-8.9	4

^a The numbers in parentheses are the values of $\bar{\nu}$ (cm^{-1}) at the half-peak height.

pressure and, without exception, found to become stronger when the pressure was raised. However, it is apparent from the theory of the effect² that the trend might be reversed if, for some unusual reason, the parent molecules were more strongly solvated than their free ions. The writer has now obtained experimental evidence that this may be the case in the electronically excited states of some *p*-nitrophenols.

The results reported here were obtained as part of a wider investigation of the influence of pressure on the ionization equilibria of substituted phenols and anilines.³ Briefly, the molal dissociation constants ($K_m = m_{\text{RO}^-}m_{\text{H}^+}/m_{\text{ROH}}$) of nitrophenols in their ground states have been measured by standard spectroscopic methods⁴ and the behavior of the corresponding constants K_m^* for the excited states ROH* inferred from the shifts in the long-wavelength absorption spectra of ROH and RO⁻.⁵ In the notation of Weller⁶

$$RT \ln (K_m^*/K_m) \approx \Delta H - \Delta H^* = Nhc \times \Delta\bar{\nu}$$

where the approximation sign implies an assumption that the entropy change is the same for ionization of the excited state as for the ground state.⁷ From Planck's relationship⁸

$$\partial(RT \ln K_m)/\partial P = -\Delta\bar{V}$$

it follows that the changes of partial molar volume in the excited and ground states are related by the formula

$$\Delta\bar{V}^* - \Delta\bar{V} = -Nhc(\partial\Delta\bar{\nu}/\partial P)$$

In applying this formula to the experimental data, $\Delta\bar{\nu}$ has been taken to be the difference between the wavenumbers at half the maximum height⁹ of the long-wavelength absorption bands of ROH and RO⁻ (use of the wavenumbers for the peaks gives almost the same

result). The quantities $\Delta\bar{V}$ and $\partial\Delta\bar{\nu}/\partial P$ have been derived from measurements made between 1 and 2000 atm at 25° and at ionic strengths near 0.05 *M*. Their limiting values at low pressures are listed in Table I.

The estimated experimental errors in $\Delta\bar{V}$ are ± 1 cm^3 mole^{-1} , and in $\Delta\bar{V}^* - \Delta\bar{V}$ are ± 2 cm^3 mole^{-1} . Although $\Delta\bar{V}^*$ may therefore be uncertain to ± 3 cm^3 mole^{-1} , it is safe to draw the following conclusions: $\Delta\bar{V}$ is negative for all the phenols listed, as it is for many others;³ $\Delta\bar{V}^*$ is considerably more positive than $\Delta\bar{V}$, and although it is still negative for the *o*- and *m*-nitrophenols, it is positive for the last three *p*-nitrophenols.

The results imply that the excited state of a *p*-nitrophenol is abnormal in being more strongly solvated in its un-ionized than in its ionized form. The writer suggests that the reasons are as follows. Molecular orbital calculations¹⁰ show that the lowest excited

(2) J. Buchanan and S. D. Hamann, *Trans. Faraday Soc.*, **49**, 1425 (1953); S. D. Hamann, "Physico-Chemical Effects of Pressure," Academic Press Inc., New York, N. Y., 1957, p 152.

(3) S. D. Hamann, M. Linton, and A. J. Murphy, to be published.

(4) R. A. Robinson in "The Structure of Electrolyte Solutions," W. J. Hamer, Ed., John Wiley and Sons, Inc., New York, N. Y., 1959, p 253.

(5) Th. Förster, *Z. Elektrochem.*, **54**, 42 (1950).

(6) A. Weller in "Progress in Reaction Kinetics," Vol. 1, G. Porter, Ed., Pergamon Press, New York, N. Y., 1961, p 189.

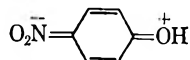
(7) In the present context, it is only necessary to assume that the pressure dependences of $T\Delta S$ and $T\Delta S^*$ are the same or are small in comparison with those of ΔH and ΔH^* . The latter assumption is valid for thermodynamic solvation functions calculated from Born's formula,³ and it is likely that solvation is the main factor governing the entropy changes of the present reactions.

(8) M. Planck, *Ann. Phys. Chem.*, **32**, 462 (1887).

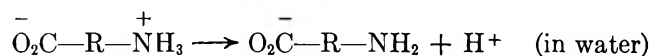
(9) See ref 6, pp 197-199.

(10) S. Nagakura, *J. Chem. Phys.*, **23**, 1441 (1955); J. N. Murrell, "The Theory of the Electronic Spectra of Organic Molecules," John Wiley and Sons, Inc., New York, N. Y., 1963, Chapter 10.

state is a highly polar charge-transfer one resembling the valence bond structure



and this conclusion is supported by experimental evidence that the analogous excited state of *p*-nitroaniline has a very large dipole moment.¹¹ The charges are far enough apart to act independently on the solvent. When protolytic dissociation occurs, the charge on the anion RO^- becomes delocalized and some bound solvent is released. It is worth remarking that density data¹² show that the electrically analogous dissociation of zwitterions of amino acids



also involves a small increase of volume.

(11) J. Czekalla and G. Wick, *Z. Elektrochem.*, **65**, 727 (1961).

(12) H. H. Weber, *Biochem. Z.*, **218**, 1 (1930).

DIVISION OF PHYSICAL CHEMISTRY
COMMONWEALTH SCIENTIFIC AND INDUSTRIAL
RESEARCH ORGANIZATION
MELBOURNE, AUSTRALIA

S. D. HAMANN

RECEIVED MAY 9, 1966

Carbon Dioxide Adsorbed on

Linde X and Y Zeolites

Sir: In a recent article,¹ Ward and Habgood reported on carbon dioxide adsorbed on Linde X zeolites. They found that in the alkali earth metal cation substituted zeolites the asymmetric stretching vibration of the adsorbed carbon dioxide was at a higher frequency than in the gas phase and dependent on the cation present. They attributed this shift to an ion-dipole interaction resulting in a linear adsorption of the CO_2 molecule. This phenomenon is very similar to our observation² on the cation dependence of the vibration of adsorbed carbon monoxide, which we explained as due to a polarization of the carbon monoxide molecule in the electrostatic field of the cation. We also observed a frequency shift in the case of CO_2 adsorbed on Linde Y zeolites, and we were able to put the field dependence on a semiquantitative basis. The method of calculating the electrostatic field in the neighborhood of the cation has been described previously.^{2,3}

Figure 1 shows the frequency of the asymmetric stretching vibration of adsorbed CO_2 plotted against the calculated field strength (filled circles represent our values, and open circles represent values from

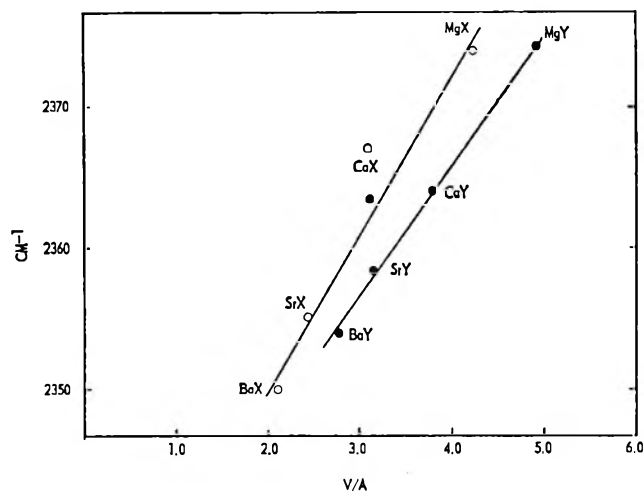


Figure 1.

Ward and Habgood¹). The linear relation confirms the suggestion^{1,2} that the adsorption of carbon dioxide (like that of carbon monoxide) is essentially a polarization effect caused by the electrostatic field due to the cations in the zeolite. The X and Y series give separate lines indicating that the field strength calculations have not fully taken into account the differences between the X- and Y-type zeolites. It is interesting to note that in the case of transition metal cation Y zeolites, the CO_2 frequency is practically unchanged from the gas-phase value, although the electric field was calculated to be very close to that in Mg^{2+} -containing zeolites.

(1) J. W. Ward and H. W. Habgood, *J. Phys. Chem.*, **70**, 1178 (1966).

(2) C. L. Angell and P. C. Schaffer, *ibid.*, **70**, 1413 (1966).

(3) P. E. Pickert, J. A. Rabo, E. Dempsey, and V. Schomaker, *Actes Congr. Intern. Catalyse, 3^e, Amsterdam, 1964*, 714 (1965). Actual values of the field strength based on an improved model were kindly made available by Dr. E. Dempsey.

UNION CARBIDE RESEARCH INSTITUTE
UNION CARBIDE CORPORATION
TARRYTOWN, NEW YORK

C. L. ANGELL

RECEIVED MAY 19, 1966

The Reactions of Thermal Hydrogen Atoms with Ethanol and Ethanol Free Radicals at 77°K

Sir: The reactions of hydrogen atoms and trapped free radicals in alcohol glasses at 77°K have been the subject of considerable speculation.¹⁻⁵ As a result

(1) R. S. Alger, *et al.*, *J. Chem. Phys.*, **30**, 695 (1959).

(2) R. H. Johnsen, *J. Phys. Chem.*, **65**, 2144 (1961); **67**, 831 (1963).

(3) P. J. Sullivan and W. S. Koski, *J. Am. Chem. Soc.*, **86**, 159 (1964).

of a series of investigations involving the reactions of thermal hydrogen atoms with a variety of organic solids, as well as with irradiated ethanol glass, in the manner of Klein and Sheer,⁶ we have made the following observations. (1) Thermal hydrogen atoms under these conditions undergo no appreciable reaction with solid ethanol. This is based on the observation that there is no pressure change observed during H atom bombardment and that no products detectable by flame ionization gas chromatography were observed. (2) When a sample of solid ethanol at 77°K which has previously received a total dose of 4.2×10^{20} ev/g of 3-Mev-peak X-rays was subjected, before melting, to H atom bombardment, $G(\text{glycol})$ was reduced from 0.94 to 0.02 while $G(\text{aldehyde})$ was increased from 2.64 to 4.70. Assuming that two α -ethanol radicals are required to produce one glycol molecule, this corresponds to a loss of $2 \times 0.92 = 1.84$ radicals, which is nearly equivalent to the increase in $G(\text{aldehyde})$.

These observations suggest that the following processes are significant in the radiolysis of ethanol glasses. Those H atoms which are thermalized diffuse freely through the matrix, but can react only by combination or with species other than the substrate ethanol; thus cyclic photochemical reactions resulting from the reaction of hydrogen atoms produced by the photolysis of trapped free radicals as suggested by Dainton⁷ are possible only when the radiation employed is energetic enough to produce hot hydrogen atoms. This point is currently under investigation, and preliminary results suggest that in methanol, light of wavelengths less than 3300 Å is necessary to achieve this type of cyclic process, while light of wavelengths as long as 5400 Å is capable of photolyzing certain of these trapped radicals.

Glycols are produced by the combination of α -ethanol radicals subsequent to the softening of the matrix rather than by radical diffusion at 77°K. Otherwise, the bombardment by H atoms would not be likely to affect the glycol yield so drastically.

H atoms react with α -ethanol radicals mainly by disproportionation rather than combination, which is attested to by the appearance of acetaldehyde in an amount essentially equivalent to the reduction in the glycol yield.

The aldehyde which is produced directly by the radiation ($G = 2.64$) is not affected by the thermal H atoms at this low temperature. This suggests that this yield of aldehyde does not result from the disproportionation of ethanol free radicals but is rather the result of an ionic reaction or a unimolecular dissociation. This is in agreement with the observations of Myron and Freeman⁸ that scavengers do not lower the yield of aldehyde in the liquid state.

These observations are a part of a general study of the reactions of thermal hydrogen atoms with the aliphatic alcohols which will be reported on in the near future.

Acknowledgment. This work was supported in part by the U. S. Atomic Energy Commission under Contract AT-(40-1)-2001.

(4) J. Tepy, A. Habersbergerova, and K. Vacek, *Collection Czech. Chem. Commun.*, **30**, 793 (1965).

(5) J. A. Leone and W. Koski, *J. Am. Chem. Soc.*, **88**, 224 (1966).

(6) R. Klein and M. D. Sheer, *ibid.*, **80**, 1007 (1958).

(7) F. S. Dainton, G. A. Salmon, and J. Tepy, *Trans. Faraday Soc.*, **61**, 27 (1965).

(8) J. J. J. Myron and G. R. Freeman, *Can. J. Chem.*, **43**, 381 (1965).

DEPARTMENT OF CHEMISTRY
FLORIDA STATE UNIVERSITY
TALLAHASSEE, FLORIDA 32306

R. H. JOHNSEN
A. K. E. HAGOPIAN
H. B. YUN

RECEIVED MAY 25, 1966

The Radiolysis of Pure Decaborane-14¹

Sir: Preliminary results are herewith reported on the Co^{60} γ -ray radiolysis of pure decaborane in the solid state. This work was carried out using standard vacuum² and gas chromatographic techniques.^{3,4} The results of this study indicate that the products of the radiolysis are hydrogen, diborane, pentaborane-9, and a polymeric substance. The polymeric substance has not yet been identified except that it is not the icosaborane-26 reported by Hall and Koski⁴ in their deuteron irradiation of decaborane-14.

The yields of the gaseous products at 35° as a function of total dose are shown in Figure 1. The initial product yields in the linear region of these curves have G values for hydrogen, diborane, and pentaborane of 0.84, 1.70, and 0.15, respectively. The results shown in Figure 1 are typically what is to be expected from radiolysis as a function of dose except in the case of the diborane yield. It is felt that this unusual behavior of the diborane yield may be due to either radiolysis of the polymer produced or interconversion reactions between the diborane and unstable boranes such as tetraborane between the time of radiolysis and analysis of the samples.⁵

(1) This research was supported in part by the Oak Ridge Associated Universities Inc.

(2) S. Dushman, "Scientific Foundations of Vacuum Techniques," John Wiley and Sons, Inc., New York, N. Y., 1962.

(3) G. F. Shipman, *Anal. Chem.*, **34**, 877 (1962).

(4) L. H. Hall and W. S. Koski, *J. Am. Chem. Soc.*, **84**, 4205 (1962).

(5) The time here was of the order of 3-5 days at a temperature of about 30°.

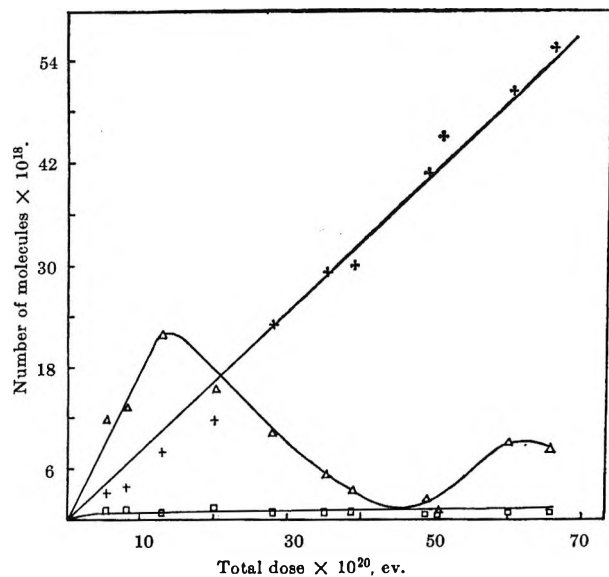


Figure 1. Radiolysis of $B_{10}H_{14}$ at 35° as a function of total dose. Product yields: +, H_2 ; Δ , B_2H_6 ; \square , B_5H_9 .

The radiolysis of decaborane-14 was also carried out as a function of temperature at total doses which were in the linear region of all of the curves shown in Figure 1. The results are shown in Figure 2. It appears from these data that hydrogen, diborane, and pentaborane-9 are produced in the region between -196 and -80° by a temperature-independent mechanism, such as molecular detachment or hot radicals. The observed G values at -196° are 0.59, 0.15, and 0.05 for hydrogen, diborane, and pentaborane, respectively.

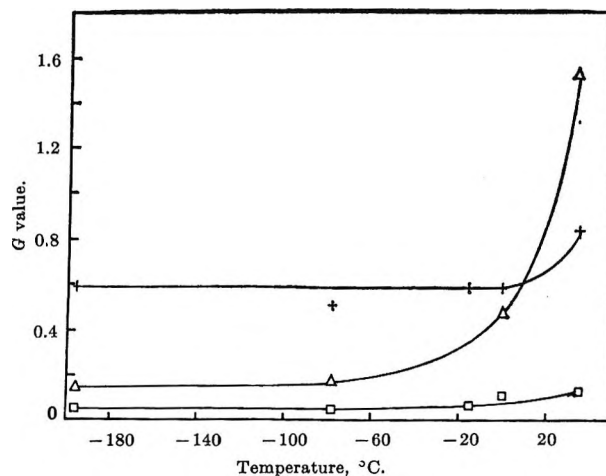


Figure 2. Radiolysis of $B_{10}H_{14}$ as a function of temperature. Product yields: +, H_2 ; Δ , B_2H_6 ; and \square , B_5H_9 .

It appears from the data in Figure 2 that there is the onset of a temperature-dependent set of reactions in the temperature range between -80 and 0° which gives rise to only diborane and pentaborane as gaseous products. At 0° the yield of hydrogen begins to rise rapidly, indicating the onset of a second set of temperature-dependent reactions producing all three observed gaseous products. The polymeric solid is observed over the entire temperature range.

DEPARTMENT OF CHEMISTRY
THE UNIVERSITY OF MISSISSIPPI
UNIVERSITY, MISSISSIPPI 38677

T. J. KLINGEN
J. M. O'NEAL

RECEIVED MAY 31, 1966